Teilnehmerliste

Name	Vorname	Institution und Ort
Abu Ghazleh	Shahrazad	United Arab Emirates University, Al-Ain
Alawi	Mashal	Deutsches GeoForschungsZentrum Potsdam
Almeev	Renat	Universität Hannover
Andreev	Andrej	Universität Köln
Arslan	Arzu	Göttingen
Bahr	André	Universität Frankfurt
Banning	Denise	Universität Münster
Batenburg	Sietske	Universität Frankfurt
Bauersachs	Thorsten	Universität Kiel
Baumgarten	Henrike	LIAG Hannover
Becker	Harry	Freie Universität Berlin
Beermannn	Oliver	Universität Kiel
Behrmann	Jan	GEOMAR, Kiel
Berner	Ulrich	Bundesanstalt für Geowissenschaften und Rohstoffe, Hannover
Berthold	Susann	Dresdner Grundwasserforschungszentrum e.V.
Biber	Jani	Universität Frankfurt
Bleibinhaus	Florian	Universität Jena
Blöthe	Marco	Bundesanstalt für Geowissenschaften und Rohstoffe, Hannover
Böhm	Florian	GEOMAR, Kiel
Bohnhoff	Marco	Deutsches GeoForschungsZentrum Potsdam
Bolte	Torsten	Universität Hannover
Bornemann	André	Universität Leipzig
Bosch	Frank	RWTH Aachen
Brachert	Thomas	Universität Leipzig
Brandl	Philipp	Universität Erlangen-Nürnberg
Brauer	Achim	Deutsches GeoForschungsZentrum Potsdam
Bräuer	Karin	Helmholtz-Zentrum für Umweltforschung – UFZ, Leipzig
Breitkreuz	Christoph	TU Bergakademie Freiberg
Buske	Stefan	TU Bergakademie Freiberg
Contreras	Lineth	Universität Frankfurt
Conze	Ronald	ICDP International, Deutsches GeoForschungsZentrum Potsdam
Cukur	Deniz	GEOMAR, Kiel
De Campos	Cristina	Universität München
Deutsch	Alex	Universität Münster
Diester-Haaß	Liselotte	Universität des Saarlandes, Saarbrücken
Drath	Gabriela	IODP, Bundesanstalt für Geowissenschaften und Rohstoffe, Hannover
Dullo	Christian	GEOMAR, Kiel
Dultz	Stefan	Universität Hannover
Dupont	Lydie	MARUM, Universität Bremen
Ehmann	Sebastian	TU Braunschweig
Engelen	Bert	ICBM, Universität Oldenburg
Erbacher	Jochen	IODP, Bundesanstalt für Geowissenschaften und Rohstoffe, Hannover
Erzinger	Jörg	Deutsches GeoForschungsZentrum, Potsdam
Fallahi	Mohammad	Universität Leipzig
Fanara	Sara	Universität Hannover
Ferdelman	Timothy	MPI für Marine Mikrobiologie, Bremen
Flechsig	Christina	Universität Leipzig
Förster	Verena	Universität Köln
Frank	Martin	GEOMAR, Kiel
Friedrich	Oliver	Universität Frankfurt
Fritz	Jörg	Museum für Naturkunde, Humboldt-Universität zu Berlin
Gabriel	Gerald	LIAG Hannover
Gaedicke	Christoph	Bundesanstalt für Geowissenschaften und Rohstoffe, Hannover
Geldmacher	Jörg	GEOMAR, Kiel
Giehl	Christopher	Universität Tübingen
Gischler	Eberhard	Universität Frankfurt
Glasmacher	Ulrich	Universität Heidelberg
Glomb	Vera	TU Bergakademie Freiberg
Gohl	Karsten	Alfred-Wegener-Institut für Polar- und Meeresforschung, Bremerhaven
Görsch	Janine	Deutsches GeoForschungsZentrum Potsdam
Grunert	Patrick	Universität Graz, Österreich
Grützner	Jens	Alfred-Wegener-Institut für Polar- und Meeresforschung, Bremerhaven
Gutjahr	Stine	Freie Universität Berlin
Hammerschmidt	Sebastian	MARUM, Universität Bremen
Harms	Ulrich	ICDP International, Deutsches GeoForschungsZentrum Potsdam
Hathorne	Edmund	GEOMAR, Kiel
Heldt	Matthias	IODP, Bundesanstalt für Geowissenschaften und Rohstoffe, Hannover
Hess	Kai-Uwe	Universität München
Heuer	Verena	MARUM, Universität Bremen
Heydolph	Ken	GEOMAR, Kiel
Hinrichs	Kai-Uwe	MARUM, Universität Bremen
Hockun	Katja	MARUM, Universität Bremen

Höfig	Tobias	TU Bergakademie Freiberg
Hofmann	Peter	Universität Köln
Holtz	François	Universität Hannover
Holzheid	Astrid	Universität Kiel
Hoerdt	Andreas	TU Braunschweig
Horsfield	Brian	ICDP International, Deutsches GeoForschungsZentrum Potsdam
Hüpers	Andre	MARUM, Universität Bremen
Inoue	Mayuri	Universität Münster
Jehle	Sofie	Universität Leipzig
Kallmeyer	Jens	Deutsches GeoForschungsZentrum Potsdam
Kämpf	Horst	Deutsches GeoForschungsZentrum Potsdam
Karas	Cyrus	Universität Frankfurt
Kenzler	Michael	Universität Greifswald
Khélifi	Nabil	GEOMAR, Kiel
Klügel	Andreas	Universität Bremen
Knebel	Carola	GESEP, Deutsches GeoForschungsZentrum Potsdam
Knorr	Gregor	Alfred-Wegener-Institut für Polar- und Meeresforschung, Bremerhaven
Koch	Mirjam	Universität Frankfurt
Koepke	Jürgen	Universität Hannover
Kolaei	Mohammad	Universität Kiel
Kollaske	Tina	Bundesanstalt für Geowissenschaften und Rohstoffe, Berlin-Spandau
Korn	Michael	Universität Leipzig
Kotthoff	Ulrich	Universität Hamburg
Krastel	Sebastian	Universität Kiel
Krawczyk	Charlotte	LIAG Hannover
Küchler	Rony	MARUM, Universität Bremen
Kukowski	Nina	Universität Jena
Kunze	Sabine	IODP, Bundesanstalt für Geowissenschaften und Rohstoffe, Hannover
Kwiecien	Ola	Ruhr-Universität Bochum
Landmann	Günther	TU Darmstadt
Lazarus	David	Museum für Naturkunde, Leibniz-Institut für Evolutions- und Biodiversitätsforschung, Berlin
Lehnert	Oliver	Universität Erlangen-Nürnberg
Lembke-Jene	Lester	Alfred-Wegener-Institut für Polar- und Meeresforschung, Bremerhaven
Lindhorst	Katja	Universität Kiel
Lippold	Jörg	Universität Heidelberg
Litt	Thomas	Universität Bonn
Lückge	Andreas	Bundesanstalt für Geowissenschaften und Rohstoffe, Hannover
Lüniger	Guido	Deutsche Forschungsgemeinschaft DFG
Mangelsdorf	Kai	Deutsches GeoForschungsZentrum Potsdam
Maronde	Dietrich	Universität Bonn
Marxer	Holger	Universität Tübingen
März	Christian	Universität Oldenburg
Meinhardt	Ann-Katrin	Universität Oldenburg
Meinhold	Guido	Universität Göttingen
Meister	Patrick	MPI for Marine Microbiology, Bremen
Meschede	Martin	Universität Greifswald
Meyers	Philip	University of Michigan, Ann Arbor, U.S.A.
Möbius	Iris	Universität Frankfurt
Mohnke	Oliver	RWTH Aachen
Montinaro	Alice	Universität Münster
Müller	Juliane	Alfred-Wegener-Institut für Polar- und Meeresforschung, Bremerhaven
Müller	Tim	Universität Hannover
Mueller-Michaelis	Antje	Alfred-Wegener-Institut für Polar- und Meeresforschung, Bremerhaven
Mullick	Nirjhar	TU Bergakademie Freiberg
Naafs	David	School of Chemistry, University of Bristol
Neugebauer	Ina	Deutsches GeoForschungsZentrum Potsdam
Nowak	Marcus	Universität Tübingen
Oberhänsli	Roland	ICDP, Universität Potsdam
Oeser	Martin	Universität Hannover
Osborne	Anne	GEOMAR, Kiel
Pabich	Stephanie	Universität Münster
Pälike	Heiko	MARUM, Universität Bremen
Pickarski	Nadine	Universität Bonn
Preuss	Franziska	ICBM, Universität Oldenburg
Preuß	Oliver	Universität Tübingen
Pross	Jörg	Universität Frankfurt
Rammensee	Philipp	Universität Frankfurt
Raschke	Ulli	Museum für Naturkunde, Leibniz-Institut für Evolutions- und Biodiversitätsforschung, Berlin
Rausch	Svenja	Universität Bremen
Reich	Mike	Universität Göttingen
Renaudie	Johan	Museum für Naturkunde, Leibniz-Institut für Evolutions- und Biodiversitätsforschung, Berlin
Rocholl	Alexander	Universität München
Röhl	Ursula	MARUM, Universität Bremen
Sarnthein	Michael	Universität Kiel
Sauerbrey (geb. Kukkonen)	Maaret	Universität Köln
Schlüter	Nils	Universität Göttingen
Schmincke	Hans-Ulrich	GEOMAR, Kiel

Schmitt	Ralf Thomas	Museum für Naturkunde, Leibniz-Institut für Evolutions- und Biodiversitätsforschung, Berlin
Schulz	Hartmut	Universität Tübingen
Schwamborn	Georg	Alfred-Wegener-Institut für Polar- und Meeresforschung, Potsdam
Schwenk	Tilmann	Universität Bremen
Smolka	Peter	Universität Münster
Sprenk	Daniela	Universität Köln
Stadler	Susanne	Bundesanstalt für Geowissenschaften und Rohstoffe, Hannover
Stein	Rüdiger	Alfred-Wegener-Institut für Polar- und Meeresforschung, Bremerhaven
Strack	Dieter	International Oil & Gas Consultant, Ratingen
Strauch	Gerhard	Helmholtz-Zentrum für Umweltforschung – UFZ, Leipzig
Strauss	Harald	Universität Münster
Sumita	Mari	GEOMAR, Kiel
Tauber	Elisabeth	LIAG Hannover
Thiede	Jörn	GEOMAR, Kiel
Timmerman	Martin	ICDP, Universität Potsdam
Ulmer	Sarah	Universität Tübingen
Uenzelmann-Neben	Gabriele	Alfred-Wegener-Institut für Polar- und Meeresforschung, Bremerhaven
Vallé	Francesca	MARUM, Universität Bremen
van de Schootbrugge	Bas	Universität Frankfurt
Virgil	Christopher	TU Braunschweig
Voigt	Janett	GEOMAR, Kiel
Voigt	Silke	Universität Frankfurt
Wagner	Dirk	Deutsches GeoForschungsZentrum Potsdam
Wagner	Thomas	Newcastle University, Newcastle upon Tyne, United Kingdom
Weber	Michael E.	Universität Köln
Wefer	Gerold	MARUM, Universität Bremen
Wellmer	Friedrich	Bundesanstalt für Geowissenschaften und Rohstoffe, Hannover, Präsident a.D.
Wennrich	Volker	Universität Köln
Westerhold	Thomas	MARUM, Universität Bremen
Weyer	Stefan	Universität Hannover
Wiersberg	Thomas	ICDP International, Deutsches GeoForschungsZentrum Potsdam
Wiesmaier	Sebastian	Universität München
Wigger	Peter	Freie Universität Berlin
Wonik	Thomas	LIAG Hannover
Wörner	Gerhard	Universität Göttingen
Zhang	Chao	Universität Hannover
Zhu	Jiayun	Forschungszentrum Jülich
Zirkel	Jessica	Universität Frankfurt
Zolitschka	Bernd	Universität Bremen

Koch, M.C., Friedrich, O., Wilson, P., Cooper, M.	Early Pleistocene glacial-interglacial changes of North Atlantic intermediate-water masses	IODP	109
Koepke, J., Faak, K. and the Expedition 345 Scientists	Cruise Report: IODP Expedition 345: Fast-spreading Lower Crust at the Hess Deep Rift	IODP	24
Kotthoff, U., McCarthy, F.M.G., Greenwood, D.R., Hesselbo, S.P.	Oligocene, Miocene, and Pleistocene vegetation and climate development on the Atlantic Coastal Plain (IODP Expedition 313)	IODP	111
Kuechler, R.R., Dupont, L., Schefuß, E.	NW African vegetation and climate variability: Plant-wax signals during the Pliocene-Pleistocene	IODP	112
Kukowski, N., Totsche, K.U., Abratis, M., Augustsson, C., Goepel, A., Habisreuther, A., Ward, T. & Influins-Working Group	Tiefbohrung zur Untersuchung der Wechselwirkung tiefer und flacher Fluidströme in Sedimentbecken	ICDP	115
Landmann, G., Kempe, S.	Paleoclimate of the Lake Van region (Eastern Anatolia) in the period 20-15 ka BP	ICDP	115
Lazarus, D., Barron, J., Renaudie, J., Türke, A., Diver, P.	Cenozoic marine planktic diatom evolution controlled by climate change: implications for future extinction risk	IODP	118
Lehnert, O., Meinhold, G., Arslan, A., Berner, U., Calner, M., Huff, W.D., Ebbestad, J.O., Joachimski, M.M., Juhlin, C., Maletz, J.	The Siljan impact structure of central Sweden: an unique window into the geologic history of western Baltoscandia	ICDP	121
Lindhorst, K., Krastel, S., Schwenk, T., Wagner, B.	Tectono-stratigraphic interpretation of sediments within Lake Ohrid (Albania/Macedonia) for the SCOPSCO ICDP campaign	ICDP	124
Lippold, J., Luo, Y., Francois, R., Allen, S.E., Gherardi, J., Pichat, S., Hickey, B., Schulz, H.	Reconstruction of the Atlantic Meridional Overturning Circulation applying sediment 231Pa/230Th	IODP	127
Lippold,J., Frank, N., Blaser, P., Gutjahr, M., Luo, Y., Rempfer, J., Schulz, H.	New Proposal: Ocean circulation modes of the Glacial-Interglacial cycle - high resolution measurements of neodymium isotopes	IODP	128
Marshall, J., Brunner, B., Goldhammer, T., Murray, R., Spivack, A., Ziebis, W., Hoppie, B., Inagaki, F., D'Hondt, S.E. and Ferdelman, T.G.	Biogeochemistry of Phosphorus in Ultra-oligotrophic South Pacific Gyre Seafloor and Sub-seafloor Sediments (IODP Expedition 329)	IODP	129
Marxer, H., Bellucci, P., Ulmer, S., Nowak, M.	Simulating magma ascent: An experimental challenge	ICDP	130
März, C., Poulton, S.W., Wagner, T., Schnetger, B., Brumsack, H.-J.	Four million years of phosphorus burial and diagenesis in the Bering Sea (IODP Site U1341, Bowers Ridge): Implications for the marine P cycle	IODP	131
Meinhardt, A.-K., Mandytsch, T., März, C., Brumsack, H.-J.	Regional differences in the chemical composition of surface sediments across the central Arctic Ocean	IODP	134
Meister, P., Liu, B., Khalili, A., Ferdelman, T.G., Jørgensen, B.B.	How kinetics of organic matter degradation controls the distribution of sulphate and methane in the deep biosphere	IODP	135
Meister, P., Chapligin, B., Picard, A., Meyer, H., Fischer, C., Amthauer, G., Aiello, I.W.	Early diagenetic quartz formation at a deep iron oxidation front in the Eastern Equatorial Pacific	IODP	136
Moebius, I., Friedrich, O., Edgar, K.M., Sexton, P.F.	Episodes of intensified biological productivity during the termination of the Middle Eocene Climatic Optimum	IODP	138

Fahrtberichte

Short Report on IODP Expedition 343/343T (JFAST): Drilling and instrumenting the Tohoku-OKI 2011 earthquake rupture zone

JAN H. BEHRMANN[1] AND MATT IKARI[2]

[1] GEOMAR Helmholtz Centre for Ocean Research Kiel, Wischhofstr, 24148 Kiel, Germany
[2] MARUM, University of Bremen, Leobener Str., 28359 Bremen, Germany

The main science goal of the Japan Trench Fast Drilling Project (JFAST) was to understand the physical mechanisms and dynamics of large slip earthquakes. This understanding is fundamental to explain the huge exceptionally large tsunami following the 2011 Tohoku earthquake. The first objective of JFAST was to locate the fault that ruptured during the Tohoku event using logging while drilling (LWD). Second objective was to characterize the composition, architecture, and fundamental mechanisms of dynamic frictional slip and healing processes along the fault by retrieving core samples. Thirdly a temperature measurement observatory across the fault was to be installed to be able to estimate the frictional heat and stress within and around the fault zone in a long-term geophysical experiment.

The main JFAST expedition (Integrated Ocean Drilling Program Expedition 343 was carried out between 1st April and 24th May 2012. First, logging while drilling (LDW) at Site C0019 was completed in a borehole drilled to 850.5 meters below seafloor (mbsf) in 6924 m water depth. Second, a coring hole was drilled at the same Site to 844.5 mbsf. 21 cores were successfully recovered that spanned the two main fault targets previously defined by the LDW hole. Because of delays associated with severe weather, and the general challenges of operating in such great water depths in a zone of active forearc deformation, installation of the observatories for temperature and pressure measurements was not completed, and deferred to July 2012. A string of temperature sensors, however, was then successfully deployed during a technical extension of JFAST, IODP Expedition 343T.

Principal results of Expedition 343/343T are as follows:

1. The overall structure at the drill site consists of a prism of faulted and folded clayey to silty mudstones above, and in fault contact (at ~820 mbsf) with an largely undeformed, relatively thin sequence of pelagic clays and cherts on top of the incoming Pacific plate. The the mudstones of the accretionary prism consist of silt and clay, vitric ash, and biogenic silica. The fault contact, interpreted as the plate boundary décollement, is defined by a subhorizontal zone of highly sheared clay that displays penetrative scaly fabric and localized slip surfaces. This zone is about 5 m thick.

2. Faults and bedding are variable in dip magnitude, but faults and bedding at all depths in the prism show a preferred NE strike. Fault geometries reflect downskope xtension at shallow levels in the prism, and horizontal contraction at greater depths approximately parallel to the plate convergence vector.

3. Borehole breakouts in the LWD hole indicate changing in situ stress domains along the borehole. At shallow depths (from <200 to ~500 mbsf), the maximum horizontal compressive stress (SHmax) is very variable. At deeper levels in the prism (537–820 mbsf), SHmax has a clear preferred orientation approximately 20° clockwise from the plate convergence direction.

4. Major fault slip during the 2011 Tohoku-Oki event and other past earthquakes likely occurred on the plate boundary décollement. Slip on other faults at higher structural level in the prism cmay have also occurred during the Tohoku event. One possible location of recent fault slip was identified at ~700 mbsf on the basis of a local H2, methane, and chlorinity anomaly. Several core samples from a fractured and brecciated zone at ~720 mbsf contain faults, the largest of which is a high-angle reverse fault that occurs at the same depth as a low-resistivity feature identified in image logs.

5. Successful recovery of a core containing about one meter of highly sheared clay from the plate boundary décollement, and less deformed wall rock, provided material for mechanical and physical properties testing, as well as for geochemical, mineralogical, and microstructural analyses. Three structural whole-round community samples from the sheared clay, and two other structural whole rounds capturing secondary faults, provide material for coordinated nondestructive and destructive investigations of structure, chemistry, and mineralogy.

6. An observatory made up of 55 temperature sensors and data loggers was successfully installed across the two fault targets at Site C0019 (720 mbsf, 820 mbsf) during IODP Exp. 343T. These instruments are monitoring the temperature distribution across the lower portion of the borehole to estimate the amount of frictional heat dissipated and the dynamic frictional strength along the slip zones.

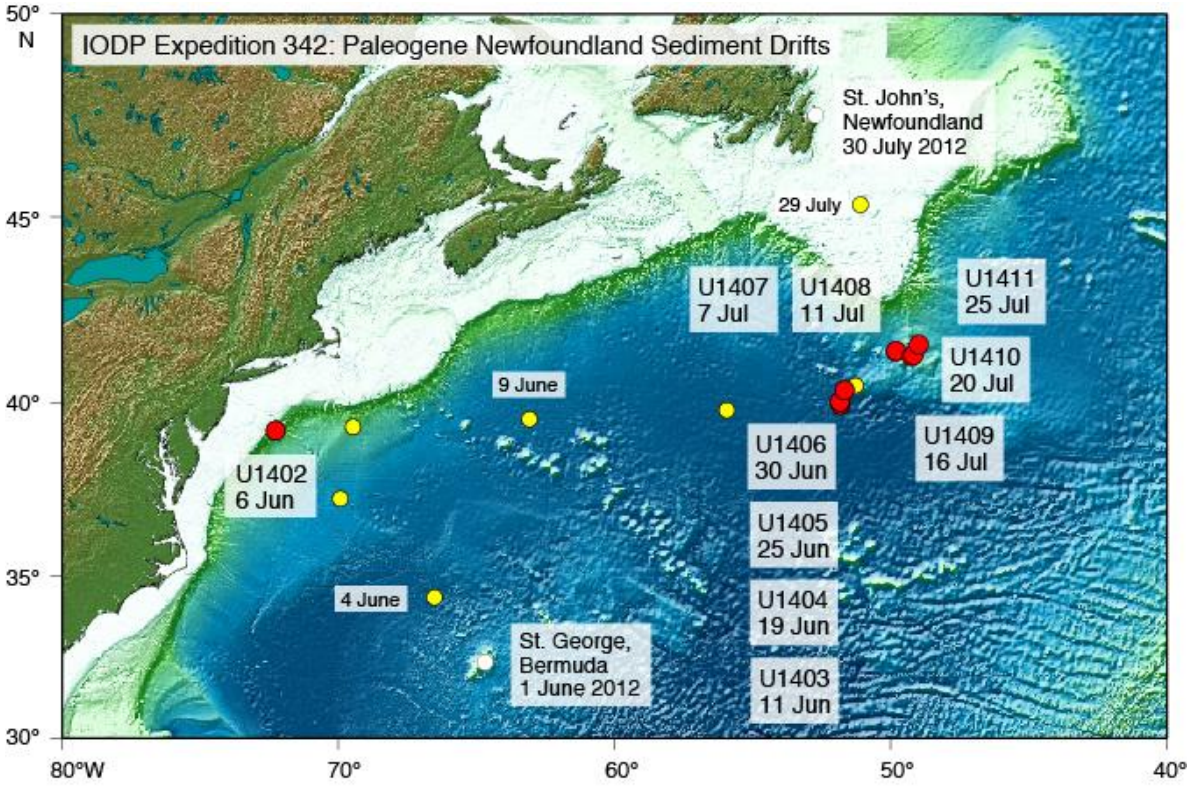

Figure 1: Operational area of Expedition 342. Red circles show the Expedition 342 drill sites. The expedition left from Bermuda and ended in St. Johns, Newfoundland (white circles) (Expedition 342 Scientists, 2012).

Report: IODP Expedition 342 – „Paleogene Newfoundland Sediment Drifts“

A. BORNEMANN[1], O. FRIEDRICH[2], R.D. NORRIS[3], P.A. WILSON[4], P. BLUM[5], SHIPBOARD SCIENTIFIC PARTY

[1] Institut für Geophysik und Geologie, Universität Leipzig, Germany
[2] Institut für Geowissenschaften, Goethe-Universität Frankfurt, Germany
[3] Scripps Institution of Oceanography – University of California San Diego, USA
[4] National Oceanography Centre Southampton, University of Southampton, UK
[5] Integrated Ocean Drilling Program, Texas A&M University, USA

The principal objective of IODP Expedition 342 (1 June – 30 July 2012, St George, Bermuda – St John's, Canada) was to recover sediment cores to study paleoclimate events like the onset and development of Cenozoic glaciations and hyperthermals recorded in drift sediments of Paleogene age along depth transects east off Newfoundland. The expedition was also targeted at reconstructing the Paleogene carbonate compensation depth (CCD) changes in the North Atlantic for reference to recently published CCD records from the equatorial Pacific (IODP Expedition 320; Pälike et al., 2012).

Prior to the main leg of Expedition 342, two operational days were spent on a sea trial of the Motion Decoupled Hydraulic Delivery System developmental tool (MDHDS) with the temperature-dual-pressure probe (T2P). These trials included drilling of Site U1402 on the New Jersey margin (Fig. 1). The second of two deployments of this system successfully acquired in situ pressure measurements confirming indirect pressure estimates.

During the main leg of this expedition, nine sites were drilled along two depth transects: four on J-Anomaly Ridge (J-A, U1403-U1406) and five on the South-Eastern Newfoundland Ridge (SENR, U1407-U1411; Fig. 1) situated about 250 km northeast of the J-A sites. The first site drilled on the J-A was U1403 at a water depth of about 4944 mbsl (~4500 mbsl at 50 Ma according to Tucholke and Vogt,1979), representing the deep end of the depth transect and, thus, ideal to record CCD changes during the Paleogene and to improve the stratigraphic control on both the seismic reflectors and the sediments drilled on J-Anomaly Ridge due to the condensed nature of this site. At Site U1403 a sedimentary sequence of Holocene/Pleistocene to Campanian age was recovered, including key intervals like the well-developed Cretaceous-Paleogene (K-Pg) boundary, early Eocene hyperthermals (Paleocene-Eocene Thermal Maximum, PETM; Eocene Thermal Maximum 2, ETM-2) and the late Eocene Chesapeak Bay impact. Most of the Paleogene consists of carbonate poor sediments relatively rich in siliceous microfossils and punctuated by usually poorly recovered chert layers. Intervals marking a shallow CCD position in the North Atlantic include the Early Eocene Climatic Optimum, the late Eocene, and the middle Oligocene.

Site U1404 is the second deepest site drilled (4743 mbsl). Principal objectives included the recovery of a Paleogene record of the position of the North Atlantic CCD and a more expanded sedimentary succession compared to the condensed, sub-CCD record at Site U1403. Another goal was to discover the types of sediments that make up the thick acoustically transparent sediment packages that are prominent on J-A. The recovered sediments span the Pleistocene to Eocene interval with a very expanded Miocene to Oligocene comprising sedimentation rates of

up to 7 cm/ky, whereas the Eocene-Oligocene transition (EOT) is more condensed with sedimentation rates between 0.5 and 1 cm/ky.

Site U1405 is a mid-depth site (today 4280 mbsl) on J-A and comprises sediments of Pleistocene to Oligocene age. Here, a very thick sedimentary package of the Oligocene-Miocene transition (OMT) has been recovered containing excellently preserved calcareous microfossils. Shipboard startigraphy suggests sedimentation rates of up to 10 cm/ky; ideal to study environmental changes on suborbital timescales during this key interval of Cenozoic climate history.

Site U1406 (today 3814 mbsl, ~3300 mbsl at 50 Ma, Tucholke and Vogt, 1979) has been drilled close to DSDP Site 384 and was positioned to capture a sedimentary record ~1 km shallower than Site U1403. Pleistocene to middle Eocene sediments have been drilled with the main scientific objectives to reconstruct the mid-depth CCD, and to obtain records of both the OMT and EOT.

Sites U1407 (3073 mbsl; ~2600 mbsl at 50 Ma; Tucholke and Vogt, 1979) and U1408 (~3022 mbsl; ~2575 mbsl at 50 Ma; Tucholke and Vogt, 1979) are mid-depth sites at SENR representing the shallow end of the depth transect. The location of both sites is well above the average late Paleogene CCD and should be sensitive to changes in carbonate burial, whether caused by dissolution related to CCD shallowing, carbonate production, or supply of fine-grained siliciclastics. At U1407 a thick sequence of Pleistocene to Lower Cretaceous age was recovered, including a well-developed middle Paleocene, and a nearly complete Upper Cretaceous sequence including the Oceanic Anoxic Event (OAE) 2 at the Cenomanian-Turonian boundary, a possible Albian OAE 1d and the top of the reef complex forming the basement in this area. At U1408 Pleistocene to upper Paleocene sediments have been recovered. All critical stratigraphic boundaries (Oligocene-Miocene, Eocene-Oligocene, Paleocene-Eocene), however, are represented by hiati at this site.

Sites U1409 (~3500 mbsl; ~3050 mbsl at 50 Ma, Tucholke and Vogt, 1979), U1410 (~3400 mbsl; ~2950 mbsl at 50 Ma, Tucholke and Vogt, 1979) and U1411 (~3300 mbsl; ~2850 mbsl at 50 Ma, Tucholke and Vogt, 1979) are located east of U1407 and U1408 and represent the upper mid-depth of the transect. The main aim of these sites was again to record changes of carbonate burial and to drill expanded middle Eocene drift sediments covering Eocene hyperthermals, specifically the Middle Eocene Climatic Optimum (MECO). Site U1411 also aimed at drilling an expanded EOT sequence. Overall, expanded Eocene sequences, including the EOT and the MECO, have been recovered by sites U1409 to U1411.

In summary, the following highlights for future research efforts have been recovered during Expedition 342:

- the drilled depth transect will allow for a more detailed reconstruction of the CCD in the North Atlantic during the last 65 Ma,
- thick sediment drifts with well-preserved microfossils will provide more insights into key intervals of the Cenozoic climate history (MECO, EOT, and OMT), the evolution of the Western Boundary Current and biological evolution,
- the high sedimentation drift deposits will allow climate reconstructions on suborbital time scales during the Oligocene to Miocene and partly the middle Eocene,
- the unexpectedly recovered Cretaceous-Paleogene and Cenomanian-Turonian boundaries will provide more detailed information from the deep-sea concerning the paleoenvironmental changes triggered by these events.

References:

Expedition 342 Scientists, 2012. Paleogene Newfoundland sediment drifts. IODP Prel. Rept., 342. doi:10.2204/iodp.pr.342.2012.

Pälike, H., Lyle, M.W., Nishi, H., Raffi, I., Ridgwell, A., Gamage, K., Klaus, A., Acton, G., Anderson, L., Backman, J., Baldauf, J., Beltran, C., Bohaty, S.M., Bown, P., Busch, W., Channell, J.E., Chun, C.O., Delaney, M., Dewangan, P., Dunkley Jones, T., Edgar, K.M., Evans, H., Fitch, P., Foster, G.L., Gussone, N., Hasegawa, H., Hathorne, E.C., Hayashi, H., Herrle, J.O., Holbourn, A., Hovan, S., Hyeong, K., Iijima, K., Ito, T., Kamikuri, S., Kimoto, K., Kuroda, J., Leon-Rodriguez, L., Malinverno, A., Moore, T.C., Jr., Murphy, B.H., Murphy, D.P., Nakamura, H., Ogane, K., Ohneiser, C., Richter, C., Robinson, R., Rohling, E.J., Romero, O., Sawada, K., Scher, H., Schneider, L., Sluijs, A., Takata, H., Tian, J., Tsujimoto, A., Wade, B.S., Westerhold, T., Wilkens, R., Williams, T., Wilson, P.A., Yamamoto, Y., Yamamoto, S., Yamazaki, T., Zeebe, R.E., 2012. A Cenozoic record of the equatorial Pacific carbonate compensation depth. Nature 488, 609-614.

Tucholke, B.E., and Vogt, P.R., 1979. Western North Atlantic: sedimentary evolution and aspects of tectonic history. In Tucholke, B.E., Vogt, P.R., et al., Init. Repts. DSDP, 43: Washington, D.C. (U.S. Govt. Printing Office), 791–825.

IODP 340: Lesser Antilles volcanism and landslides - Implications for hazard assessment and long-term magmatic evolution of the arc (Cruise report)

C. BREITKREUZ[1], IODP 340 SCIENCE PARTY[2]

[1] Institut für Geologie und Paläontologie, TU Bergakademie Freiberg, Bernhard-von-Cotta-Str. 2, 09599 Freiberg, cbreit@geo.tu-freiberg.de

[2] http://iodp.tamu.edu/scienceops/precruise/lesserantilles/participants.html

The IODP cruise 340 on the JOIDES Resolution took place from March 2nd to April 17th, 2012, and was prepared and led by the co-chief scientists Anne Le Friant (Institut de Physique du Globe de Paris) and Osamu Ishizuka (Geological Survey of Japan). Precursory studies (bathymetry, 2d seismics, piston coring) revealed that the submarine aprons of Lesser Antilles volcanic islands such as Montserrat, Dominica and Martinique are characterized by large mass flow fans presumably related to volcanic eruptions and collapse of volcanic edifice (Le Friant et al. 2003, Lebas et al. 2011). The principal goals of IODP 340 are to reach a better understanding of the constructive and destructive processes occurring along the Lesser Antilles volcanic arc (Expedition 340 Scientists, 2012).

During cruise 340, a total of 2400 m of core has been recovered from 22 holes at sites U1993 to U1401 located south and west of Montserrat, and west of Dominica and Martinique (Fig. 1). Down hole logging was successful on four sites. E.g. at site U1399, logging included the triple combo instrument, FMS-sonic and VSI tool strings. The sedimentation record for site U1396, located on a submarine ridge west of Montserrat, reaches as far back as ~4.62 Ma, as indicated by magnetostratigraphy and micropaleontology. However, despite a maximum penetration depth of 436 m (DSF), the other drill sites did not reach sediments older than Upper Pleistocene. This is due to high sedimentation rates in the studied submarine fan systems.

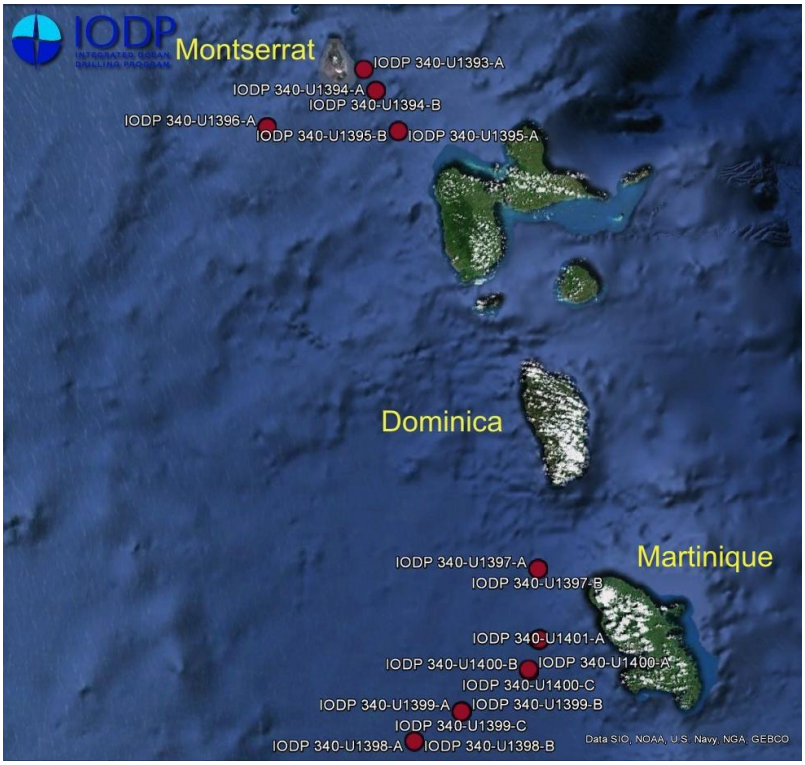

Fig. 1: Google Earth map depicting the IODP 340 drill sites near Montserrat and west of Dominica and Martinique.

The main lithologies encountered comprise hemipelagic calcareous sediments (with variable amounts of clay such as glauconite), volcaniclastic and mixed volcaniclastic-bioclastic turbidites, debris flow deposits and other debrites (deformed by creeping, sliding or slumping). In addition, a wealth of tephra layers (water-lain fallout from Lesser Antilles subaerial volcanoes) and clay horizons (detritus presumably derived from the Orinoco and/or Amazonas delta systems) have been recovered. Drilling and core recovery of abundant loose turbiditic sands and gravels, and in particular sandy to cobbly debrites was challenging, however, the amount of less disturbed units of turbidites gained is satisfying.

The principal author of this contribution formed part of the physical property team during Cruise 340. As a first result, Manga et al. (2012) documented the heat flow variation in the Lesser Antilles arc and back arc basin (i.e. the Grenada Basin) ranging from < 0.07 to 1.0 W/m². A granulometric, XRD- and isotope geochemistry study on clay samples supervized by the principal author is in progress. A proposal is under review for a PhD project on Pleistocene volcaniclastic turbidites drilled to the west of Dominica and Martinique.

References:

Expedition 340 Scientists (2012): Lesser Antilles volcanism and landslides: implications for hazard assessment and long-term magmatic evolution of the arc.- IODP Prel. Rept., 340. doi:10.2204/iodp.pr.340.2012

Lebas, E., Le Friant, A., Boudon, G., Watt, S.F.L., Talling, P.J., Feuillet, N., Deplus, C., Berndt, C., and Vardy, M.E. (2011): Multiple widespread landslides during the long-term evolution of a volcanic island: insights from high-resolution seismic data, Montserrat, Lesser Antilles.- Geochem., Geophys., Geosyst., 12: Q05006–Q05025.

Le Friant, A., Boudon, G., Deplus C., and Villemant B. (2003): Large-scale flank collapse events during the activity of Montagne Pelée, Martinique, Lesser Antilles. J. Geophys. Res., [Solid Earth], 108(B1): 2055.

Manga, M., M. J. Hornbach, A. Le Friant, O. Ishizuka, N. Stroncik, T. Adachi, M. Aljahdali, G. Boudon, C. Breitkreuz, et al. (2012): Heat flow in the Lesser Antilles island arc and adjacent back arc Grenada basin.- Geochem. Geophys. Geosyst., 13, Q08007, doi:10.1029/2012GC004260, 19 pp

IODP Exp. 344 CRISP2: Costa Rica Seismogenesis Project – Preliminary Results

K. HEYDOLPH[1], S. KUTTEROLF[1] AND EXP. 344 SCIENCE PARTY

[1] GEOMAR, Helmholtz Centre for Ocean Research Kiel, Wischhofstr. 1-3, 24148 Kiel, Germany

IODP Expedition 344 CRISP2 is the continuation of the Costa Rica Seismogenesis Project A, which started with IODP Expedition 334 (CRISP1) in 2011. A second part, CRISP Project B, is planned to be conducted with the Japanese deep-sea drilling ship Chikyu in the near future.

In general, the Costa Rica Seismogenesis Project researches the processes, which control nucleation and rupture of large earthquakes at erosional subduction zones especially offshore Osa Peninsula (Costa Rica, Fig. 1). Additionally it is designed to generate data to solve longstanding tectonic problems of this area. This includes a better understanding of relationship between the Cocos Ridge subduction to the tectonics of the upper plate and evolution of the Central American volcanic arc.

More specifically, the main objectives of both cruises, Leg 334 and 344, are:

1) Estimate the composition, texture and physical properties of the decollement zone and upper plate material.
2) Assess rates of sediment accumulation and margin subsidence/ uplift in slope sediment.
3) Evaluate fluid/ rock interaction, the hydrologic system and the geochemical processes (indicated

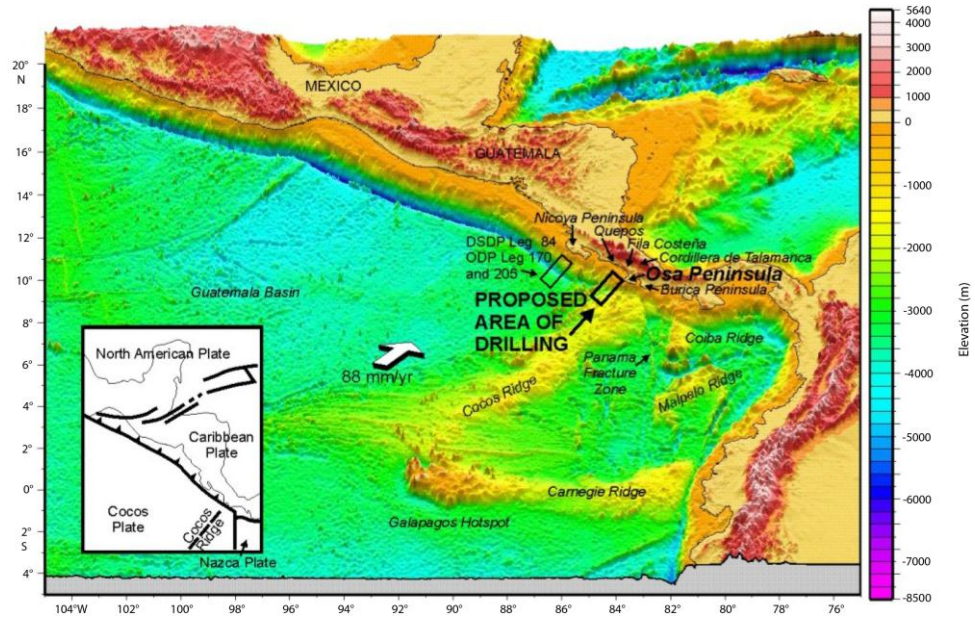

Figure 1. Topographic and bathymetric map of the CRISP2 drilling area offshore Costa Rica. Seafloor bathymetry is based on satelite gravimetry and swath mapping (Barckhausen et al., 2001; Fisher et al., 2003; von Huene et al., 2000). Inset shows tectonic plates and setting of Central America.

by composition and volume of fluids) active within the upper plate.

4) Measure the stress field across the updip limit of the seismogenic zone.

Characteristic for this drilling area is a very shallow seismogenic zone (i.e. just a few hundred meters below seafloor), resulting from the subduction of the Cocos Ridge. Generally, the west coast of Costa Rica is a characteristic erosive margin consisting of continental basement built up by thickened oceanic crust in an oceanic island arc setting and a small frontal sediment wedge. Material from the overriding continental plate is eroded at the front and from below by the subducting oceanic plate. This subduction erosion and the related extensional tectonics cause a continuous thinning of the forearc and an upward and landward migration of the plate boundary. The eroded upper plate material represents much of the filling of the subduction channel between the two plates and explains the shallow trench in this region.

During IODP expedition 344 five sites on the incoming plate (Sites U1381, Hole C and U1414), the toe of the margin (Site U1412, Hole A to D), the midslope region (Site U1380, Hole C) and the upper slope region (Site U1413, Hole A to C) have been successfully drilled (Fig. 2). While the recovery was good at the midslope and upperslope sites (122 cores with 75% recovery), it was very good (76 cores with 86%) at the incoming plate sites and poor (55 cores with 54%) at the toe sites.

Preliminary results concerning the main objectives from this cruise include: (1) New results of upper plate material from the midslope site U1380 indicating the origin from forearc basin material, consisting of lithic sedimentary units and lacking igneous basement components, opposing the previously supposed mélange of oceanic material or the offshore extension of the Caribbean large igneous complex. (2) Recovered slope sediments from Sites U1380 and U1413 will help to assess margin subsidence and evolution, which are supposed to be quite

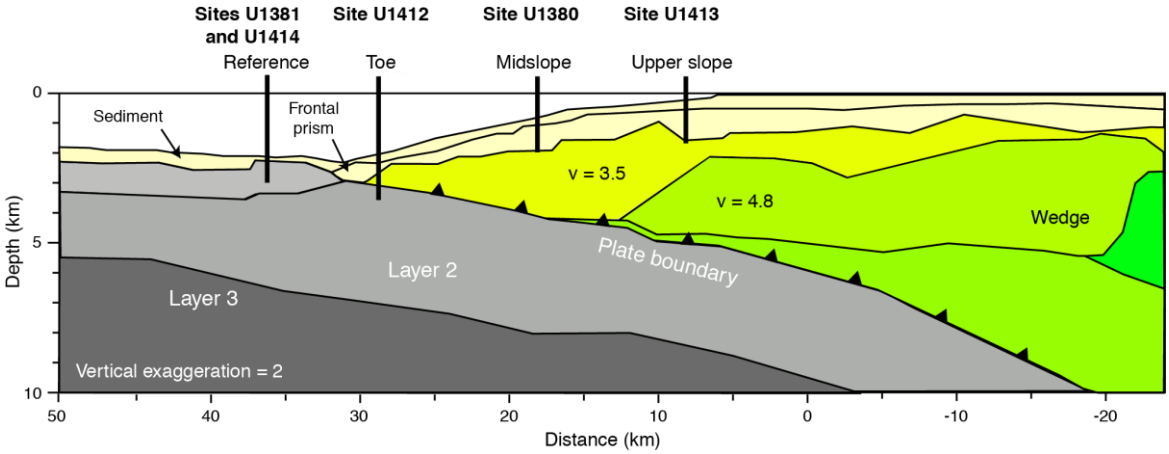

Figure 2: Interpreted wide-angleseismic section from Stavenhagen et al. (1998). Schematic figure through the Osa Peninsula margin showing drill Sites U1381, U1414, U1412, U1380 and U1413. Note that sites U1414 and U1413 are located on a different seismic line ca. 10km offset further to the NW.

high based on shipboard data. (3) On board pore fluid measurements in the uppermost 50m at all drilled margin sites indicate dominant organic carbon cycling influences. The uppermost 50m of the slope sites show pore fluid chemistry with active sulfate reduction, biogenic methane production and precipitation of authigenic carbonates. The depth of the sulfate methane transition zone (SMT) varies from site to site, with the shallowest (12 mbsf) occurring at Site U1412. The input Sites U1381 and U1414 show no methane activity and sulfate contents result from organic matter catabolic reactions. (4) Borehole breakout related stress field assessments indicate a minimum compressive stress north-south oriented. This stress orientation corresponds to an upper slope extensional stress regime and is consistent with earlier results from Expedition 334.

Additionally to the main objectives, drilling the two incoming plate sites provide a complete sedimentary input succession from Holocene to Early Miocene favoring any kind of modeling the seismogenic zone. Furthermore, the recovered sediments from these Sites will provide insights into the evolution of the Costa Rican explosive volcanism as well as how and to what extent the hiatus, discovered during Expedition 334, has been generated.

Therefore, except the failure in drilling the decollement, the results from CRISP2 expedition have generally, exceeded the expectations, by far.

References:

Barckhausen, U., Ranero, C.R., von Huene, R., Cande, S.C., and Roeser, H.A., 2001. Revised tectonic boundaries in the Cocos plate off Costa Rica: implications for the segmentation of the convergent margin and for plate tectonic models. *J. Geophys. Res., Solid Earth*, 106(B9):19207-19220.

Fisher, A.T., Stein, C.A., Harris, R.N., Wang, K., Silver, E.A., Pfender, M., Hutnak, M., Cherkaoui, A., Bodzin, R., and Villinger, H., 2003. Abrupt thermal transition reveals hydrothermal boundary and role of seamounts within the Cocos Plate. *Geophys. Res. Lett.*, 30(11), 1550-1553.

Stavenhagen, A.U., Flueh, E.R., Ranero, C., McIntosh, K.D., Shipley, T., Leandro, G., Shulze, A., and Danobeitia, J.J., 1998. Seismic wide-angle investigations in Costa Rica: a crustal velocity model from the Pacific to the Caribbean coast. *Zb. Geol. Paläontol.*, 1997(3-6): 393-408.

Von Huene, R., Ranero, C.R., Weinrebe, W., and Hinz, K., 2000. Quaternary convergent margin tectonics of Costa Rica, segmentation of the Cocos plate and Central American volcanism. Tectonics, 19(2):314-334.

Preliminary results from IODP Expedition 337 (Deep Coalbed Biosphere off Shimokita)

K.-U. HINRICHS[1,2], M.W. BOWLES[1], C. GLOMBITZA[3#], V.B. HEUER[1,2], Y.-S. LIN[1*], AND THE IODP EXPEDITION 337 SCIENTISTS

[1]MARUM – Center for Marine Environmental Sciences & Department of, Universtiy of Bremen, 28334 Bremen. Germany
[2] Department of Geosciences, University of Bremen, 28334 Bremen, Germany
[3] Potsdam University – Institute for Earth and Environmental Sciences, Karl-Liebknecht-Str. 24, 14467 Potsdam, Germany
[#] New address: Department of Bioscience - Center for Geomicrobiology, Ny Munkegade 116, 8000 Aarhus C, Denmark
[*] New address: Institute of Marine Geology and Chemistry, National Sun Yat-Sen University, Kaohsiung, Taiwan

IODP Expedition 337 (25 July - 30 September, 2012) was the first scientific expedition dedicated to subseafloor geomicrobiology that used riser-drilling technology. Our primary objectives were to study the relationship between the deep microbial biosphere and the subseafloor coalbeds that are widespread in the NW Pacific, and to explore the limits of life at depths that have never been reached before by scientific ocean drilling.

Marine subsurface hydrocarbon reservoirs are among the most frequently exploited but least characterized Earth systems. So far, their scientific investigation has been limited due to the fact that drilling into hydrocarbon reservoirs requires riser-technology. While such technology has long been used by the oil and gas industry, it only became available for scientific ocean drilling with the implementation of DV Chikyu. The availability of this technology paved the way for a number of important research questions regarding subseafloor hydrocarbon systems to be addressed. For example: What role does subsurface microbial activity play in the formation of hydrocarbon reservoirs? Do deeply buried hydrocarbon reservoirs such as natural gas and coalbeds act as geobiological reactors that sustain subsurface life by releasing nutrients and carbon substrates? Do the conversion and transport of hydrocarbons and other reduced compounds influence biomass, diversity, activity and functionality of deep subseafloor microbial populations? What are the fluxes of both thermogenically and biologically produced organic compounds and what role do they play in carbon budgets in the shallower subsurface and the ocean?

To address these questions, Expedition 337 drilled and investigated Site C0020 off the Shimokita Peninsula of Japan (Inagaki et al., 2010) (Fig. 1). The site is located at a water depth of 1,180 meters in a forearc basin formed by the subduction of the Pacific Plate beneath northeastern Honshu, where seismic profiles strongly suggested the presence of deep coal-bearing horizons at about 2 km subseafloor depth (Taira and Curewits, 2005) and previous scientific and commercial drilling expeditions had revealed a strong upward flux of free hydrocarbon gases and the presence of coal formations (Inagaki et al., 2010; Osawa et al., 2002). Site C0020 is the extension of Site C9001 Hole D which was drilled as a pilot hole down to 647 meters below seafloor (mbsf) during the Chikyu shakedown cruise CK06-06 in 2006 (Aoike, 2007). During Expedition 337, we reentered the pilot hole, renamed it, and drilled and spot-cored it as Hole C0020A to a total depth of 2466 mbsf using the riser-drilling system of DV Chikyu. We found a series of coal layers at around 2 km below the seafloor. Based on a thermal gradient of 22.5°C km^{-1} (Osawa et al., 2002), the coal-bearing horizons have temperatures around 50°C and thus provide comfortable conditions, temperature-wise, for many microbes. Hole C0020A is currently the deepest hole in the history of scientific ocean drilling. It extends the previous maximum penetration depth in scientific ocean drilling by 355 meters and provides the chance that our post-cruise research will extend the current evidence of deepest subseafloor life by up to 800 meters. From an operational point of view, this expedition was extremely successful: we carried out nearly all operations, we drilled and sampled several coalbed layers, and were able to drill 266 meters deeper than our initial target depth. The core recovery through riser drilling was remarkably high, often close to 100%, even at great burial depths of 2,000 mbsf and deeper.

The use of riser-drilling technology in very deeply buried sediments creates both unique opportunities and

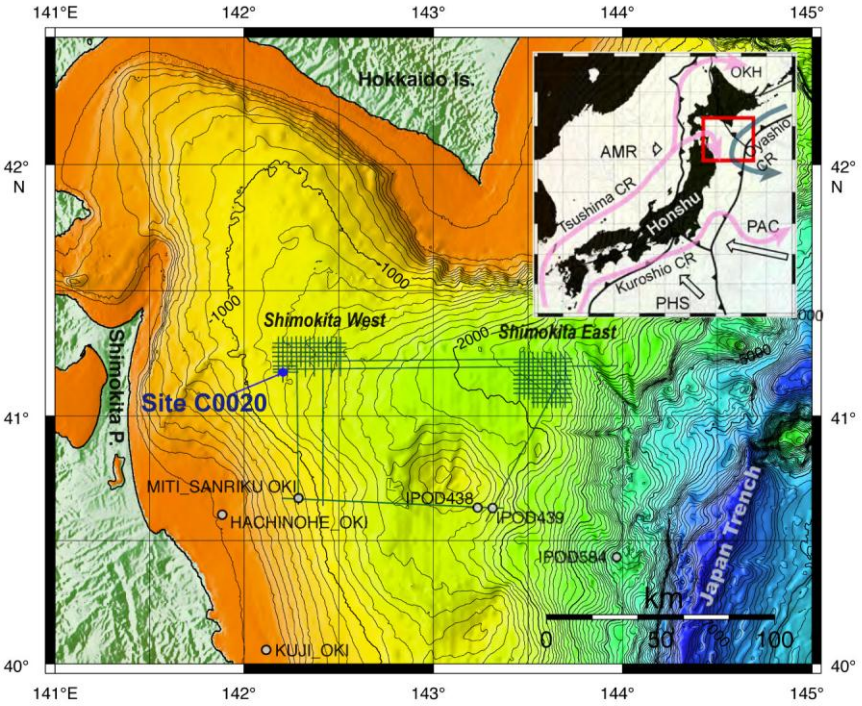

Fig.1 Index map of Site C0020 off Shimokita Peninsula of Japan with bathymetry, seismic survey track lines, and locations of existing drill holes. Inset map exhibits plate configuration around Japanese Islands and the location of the index map (red square) (Figure from Inagaki et al., 2012).

new challenges for the science party. While riser-drilling allows the retrieval of sediment cores from sediment depths that have never been reached before by scientific ocean drilling, budget and thus time constraints require fast drilling without coring and limit the recovery of intact sediment cores to selected horizons. Alternative approaches are needed to characterize the drilled formation, such as analysis of cuttings and mud-gas, which are sampled from the circulating drilling mud, and advanced wireline logging techniques for in-situ analysis of geophysical and geochemical properties. During Expedition 337, we employed a newly installed mud-gas monitoring laboratory for on-line analysis of biogeochemically relevant gases, including carbon isotope analysis of methane. Wireline logging benefitted greatly from the excellent conditions in the riser-drilled hole and yielded data of unprecedented quality. Moreover, we used wireline logging to conduct downhole fluid analysis and sampling in selected depth intervals for the first time in scientific ocean drilling. At the same time, the drilling technology, in particular the use of drilling mud created substantial obstacles that pose considerable threats to the scientific success of Expedition 337. Riser-drilling mud is saline, alkaline, contains a multitude of organic compounds, and most importantly also high concentrations of microbes. While contamination control has already become an integral part of quality assurance in ODP/IODP expeditions with focus on subseafloor life (Smith et al. 2000a, 2000b, House et al. 2003, Lever et al. 2006), the riser drilling procedure requires an even more rigorous program of quality assessment and quality control (QA/QC). Strategies to detect, quantify, and minimize contamination as well as to deal with residual levels thereof have consequently played an important role during shipboard work. Our QA/QC program included routine monitoring of the integrity of samples selected for interstitial water and microbiology analysis by X-ray CT scanning. Heavily disturbed or fractured samples were returned into the normal core flow before processing and alternative samples with lower risk of contamination were selected. The outer layers of samples that had been in contact with drilling mud were thoroughly removed prior to further processing. A combination of both chemical and microbial contamination tracers was applied. A perfluorocarbon (PFC) compound was added daily as a chemical tracer to drilling mud tanks. Detailed sampling and analyses of drilling mud, sediment cuttings, and core samples provided valuable quantitative estimates of the volume of drilling mud and number of cells introduced into samples during riser drilling. PFC measurements within cores show that the majority of core samples have low to non-detectable levels of contamination at the core center in spite of high contamination levels near the core liner. DNA analysis was successfully conducted shipboard for the first time, and DNA-based contamination tests targeting organisms associated with surface seawater, drilling mud viscosifiers, and sewage revealed drilling mud viscosifiers as the main source of drilling-induced microbial/DNA contamination. This data provides the framework for differentiating signals of indigenous microbes from those of contaminants. In addition, lipid analysis was included into the shipboard program and revealed molecular signatures of the asphalt-based drilling additive ASTEX (trade name; also known as sulfonated asphalt sodium salt – SAS) in cuttings and some core samples. While contamination control is of utmost importance for microbiological and geochemical investigations, other disciplines were affected by contamination as well. In particular, micropaleontological analysis suffered from the riser-drilling technology due to a memory effect that

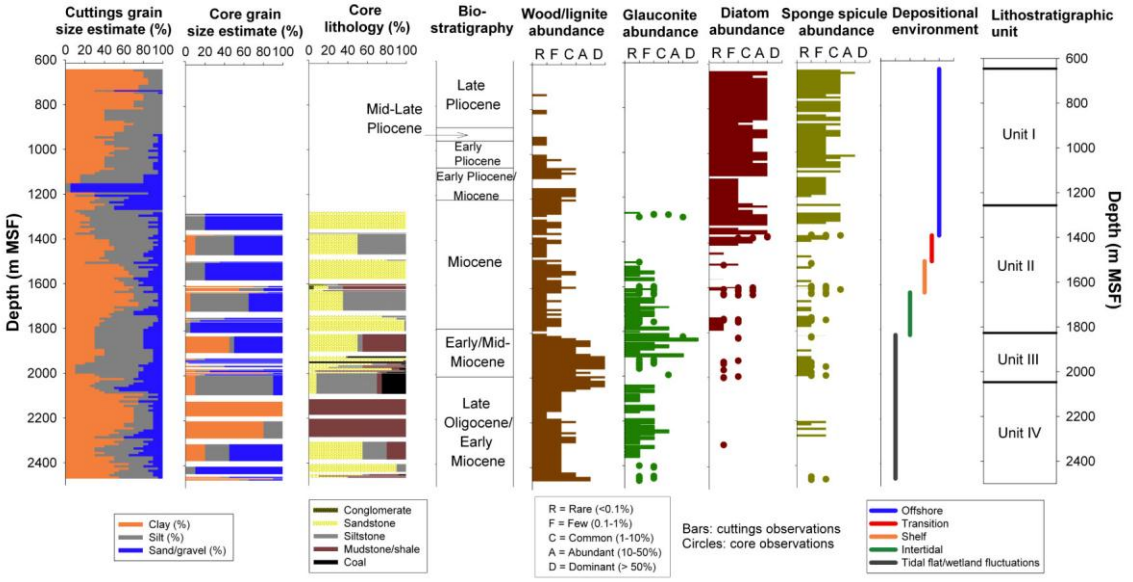

Fig.2 Lithostratigraphic profiles derived from macroscopic observation of cuttings samples and cores in Hole C0020A with ages, its wood/lignite, glauconite, diatom, and sponge spicules relative abundance, depositional environment, and the subdivision into different units (Figure from Inagaki et al., 2012).

resulted from the admixture of younger assemblages within the drilling mud. For example, relatively young diatom assemblages representative of shallower, late Miocene and Pliocene strata were abundant in drilling mud and complicated the use of cuttings for diatom-based chronostratigraphy. Focus on undisturbed core samples eliminated this problem but also substantially lowered the resolution in our analysis of age-relevant marker fossils.

Expedition 337 identified four lithologic units at Site C0020 that range from warm-temperate coastal back-swamps to cool water continental shelf and revealed the dynamically changing depositional environments in the former forearc basin off the Shimokita Peninsula during the late Oligocene and Miocene (Fig. 2): Unit I (647 to 1,256.5 mbsf) consists primarily of diatom-bearing silty clay and resulted from sedimentation in an offshore marine environment. Unit II (1,256.5 to 1,826.5 mbsf) consists mostly of silty shale with some interspersed intervals of sandstone and siltstone. While the upper part of Unit II represents an offshore environment, with increasing depth the paleoenvironment gradually changes into a shallow marine setting so that the bottom part of Unit II is situated in the intertidal zone. Unit III (1,826.5 to 2,046.5 mbsf) is dominated by several coal horizons. It represents a terrestrial to coastal shallow marine sediments and the presence of siderite bands at the bottom of this unit suggests a back barrier marine environment in combination with wetlands (e.g., salt marsh, swamp). Based on correlations of log data and visual core descriptions, seven coal layers including the thickest two were acquired by coring, from a total of 13 identified layers with thicknesses greater than 1 meter. The depositional environment of Unit IV (2,046.5 to 2,466 mbsf) resembles that of Unit III, except that the former contains only one thin coal bed. Physical property measurements show a gradual decrease of porosity with a progression of siltstone, sandstone and shale with increasing depth. Interestingly the porosity of coal does not deviate from the major trend of the other lithologies. Due to low porosity and permeability, only 24 of 48 processed whole-round cores yielded interstitial fluids through squeezing, with low volumes between 0.2 and 33.5 mL despite large sub-samples (up to 70 cm of whole-round core for selected segments). Low recovery of fluids and contamination with drilling mud severely hampered the investigation of interstitial water geochemistry. Shipboard solid phase suggested that organic matter from predominantly terrigenous sources is available for the deep biosphere not only in coals (40.9±9.9 wt%) but also in TOC-rich clays (1.4±1.0 wt%). The organic matter is apparently thermally relatively immature down to 2466 mbsf. High C_1/C_2 ratios in mud-gas and core samples point unambiguously to the predominance of biogenic methane sources throughout the recovered depth profile.

Expedition 337 incorporated extensive onboard microbiological and molecular biological analyses. These were performed with state-of-the-art equipment in the designated microbiology laboratory aboard the DV Chikyu. Both microbial activity and cellular concentrations are expected to decrease with sediment depth and age (e.g., Parkes et al., 2000). In deeply buried horizons below 1,000 mbsf, microbial cell numbers approach the detection limits of most established protocols. Even if our samples were uncontaminated, the detection and examination of such deep life would not be trivial and would require both state-of-the-art methodology and utmost scientific scrutiny. Therefore, various cell-counting methods, partly in combination with techniques for separation and concentration of cells, were applied (e.g., manual cell count, image-based cell count, high-spec flow cytometry, and density gradient cell separation). To implement these ultra-sensitive assays for the detection of deep life, QA/QC is extremely important. With the added difficulty of contamination due to riser-drilling, IODP 337 scientists will need to build a case that integrates various lines of biological and chemical evidence for the presence and activity of microbes and the nature of microbially mediated processes. Preliminary results of cell detection and

enumeration show that extremely small cells are present at very low concentrations in deep samples below 1,000 mbsf. These cells potentially represent the deepest subseafloor life that has ever been studied through scientific ocean drilling. In order to verify shipboard findings and fully address the primary scientific objectives, over 1,700 sub-samples were prepared for shore-based microbiological and biogeochemical studies, including stable-isotope-probing combined with nano-scale secondary ion mass spectrometry (SIP-NanoSIMS) experiments, quantitative functional gene surveys, metagenomics and single cell genomics, batch-type and bio-reactor cultivation experiments.

Expedition 337 has begun to assemble preliminary lines of evidence that are suggestive of microbial life associated with the coalbed and provide first answers to some of our scientific questions. The most compelling evidence for microbially mediated methanogenesis is found in our gas compositional and isotopic data.

Expedition 337 also provided a test ground for the use of riser drilling technology to address geobiological and biogeochemical objectives and was therefore a crucial step toward the next phase of deep scientific ocean drilling. Since the riser system has originally been developed by the petroleum industry, the DV Chikyu is equipped with a mature technology. However, the adaptation of this technology to the needs of basic science will be an important challenge that needs to be addressed as integral component in plans for the next riser missions.

References:

Aoike K (ed.) (2007) CK06-06 D/V Chikyu shakedown cruise offshore Shimokita. Laboratory Operation Report, CDEX-JAMSTEC, pp. 40-43.

House CH, Cragg BA, Teske A, Leg 201 Scientific Party. 2003. 2. Drilling contamination tests during ODP Leg 201 using chemical and particulate tracers. Proc Ocean Drilling Prog Init Rept 201:1–18.

Inagaki, F, Hinrichs, KU, Kubo, Y, and the Expedition 337 Scientists, 2012. Deep coalbed biosphere off Shimokita: microbial processes and hydrocarbon system associated with deeply buried coalbed in the ocean. IODP Prel. Rept., 337. doi:10.2204/iodp.pr.337.2012

Inagaki F., Hinrichs K.-U., Kubo Y., and the Expedition 337 Project Team (2010) Deep coalbed biosphere off Shimokita: microbial processes and hydrocarbon system associated with deeply buried coalbed in the ocean. Integrated Ocean Drilling Program Scientific Prospectus, 337. doi:10.2204/iodp.sp.337.2010.

Lever MA, Alperin MJ, Engelen B, Inagaki F, Nakagawa S, Steinsbu BO & Teske A (2006) Trends in basalt and sediment core contamination during IODP Expedition 301. Geomicrobiol J 23: 517-530.

Osawa M, Nakanishi S, Tanahashi M, Oda H (2002) Structure, tectonic evolution and gas exploration potential of offshore Sanriku and Hidaka provinces, Pacific Ocean, off northern Honshu and Hokkaido, Japan. Journal of the Japanese Association for Petroleum Technology 67: 37-51. (In Japanese with English abstract and figures)

Parkes RJ, Cragg BA, Wellsbury P (2000) Recent studies on bacterial populations and processes in subseafloor sediments: A review. Hydrogeology Journal 8: 11-28.

Smith DC, Spivack AJ, Fisk MR, Haveman SA, Staudigel H. 2000a. Tracerbased estimates of drilling-induced microbial contamination of deep sea crust. Geomicrobiol J 17:207–219.

Smith DC, Spivack AJ, Fisk MR, Haveman SA, Staudigel H, and Leg 185 Shipboard Scientific Party. 2000b. Methods for quantifying potential microbial contamination during deep ocean coring. ODP Tech Note 28.

Taira A, Curewitz D (eds.) (2005) Shimokita area site survey: Northern Japan Trench seismic survey, offshore northern Honshu, Japan. CDEX Technical Report 2: 1-155, ISSN 1880-0875, JAMSTEC-CDEX, Yokohama.

Report from IODP Expedition 338: Nankai Trough Seismogenic Zone Experiment Stage 3 - Plate Boundary Deep Riser

A. HÜPERS[1], S. HAMMERSCHMIDT[1], AND THE IODP EXPEDITION 338 SCIENTISTS

[1] MARUM - Center for Marine Environmental Sciences, University of Bremen, P.O. Box 330440, 28334 Bremen, Germany.

The Nankai Trough Seismogenic Zone Experiment (NanTroSEIZE) is a multistage drilling project of the Integrated Ocean Drilling Program (IODP). NanTroSEIZE comprises interdisciplinary approaches including direct sampling, *in situ* measurements, and long-term monitoring of the Nankai subduction system off Kii peninsula (SW Japan) to investigate fault mechanics and seismogenesis along a subduction megathrust. The offshore expeditions and associated core and log data are complemented by shore-based research such as laboratory experiments and numerical modeling. The primary goals of IODP Expedition 338 with D/V *Chikyu* (1 October 2012 - 13 January 2013) were to deepen Site C0002 above the presumably locked portion of the megathrust from 856 meters below the sea floor (mbsf) with riser drilling, analyse cuttings and limited cores (100 m from 2300 to 2400 mbsf), conduct logging-while-drilling (LWD), and eventually case the hole to the target depth of 3600 mbsf. However, rough sea conditions along with the strong Kuroshio Current on November 17 caused damage to part of the riser pipe. As a result further riser drilling operations were abandoned and the hole was suspended at 2005 mbsf but left for future re-entry. Drilling operations were revised to LWD and coring with riserless drilling at important sites for NanTroSEIZE. The aim of the contingency plan included a comprehensive characterization of the alteration stage of the oceanic basement seaward of the subduction zone (Site C0012), investigation of the early stage evolution of the Kumano Basin (Site C0002), assessment of recent activity of the shallow megasplay fault zone system (Site C0022), and mechanics of submarine landslides (Sites C0018 and C0021).

At Site C0002, Expedition 338 successfully conducted LWD, mud gas monitoring, and cuttings analyses while riser drilling to 2005 mbsf (Hole C0002F) and also recovered cores from 200-505 mbsf (C0002K, C0002L), 900-920 mbsf (C0002H) and 1100-1120 mbsf (C0002J) during riserless operation. Preliminary results give evidence for syn-depositonal erosional processes in the lower part of Kumano forearc basin (Unit III) and provide new insights on the debatable unconformity between forearc basin sediments and the accretionary prism. The lithology of the accretionary prism sediments is composed of silty claystone with sandstone as a minor lithology. Two lithological units (Unit IV and V) can be distinguished in the wedge that are separated by a major fault zone at 1640 mbsf. The upper section of Unit IV is composed of accreted slope basin sediments while the underlying sediments represent probably deposits from the trench, accretionary prism slope basin or Shikoku Basin submarine fan. Unit V is dominanted by a greenish-gray silty claystone. Downhole increase of thermogenically formed gas and evidence for mechanical compaction and cementation provide constraints on physical properties and insights in processes in the unknown deeper part of the accretionary prism.

Results from riserless drilling at Site C0012 include a comprehensive LWD characterization and allow a detailed core-log-seismic integration of the subduction inputs. The sediment/basement contact was penetrated at ~530msbf. The underlying oceanic crust consists of a 100 m thick zone of altered pillow basalts and sheet flow deposits. Fluctuations in gamma ray values may reflect a changing volume of sediment within the basement. Below 626 mbsf logging data suggests a less altered basement without evidence for interlayered sediment horizons. The hole was abandonded when the target depth of 709 mbsf was reached.

Expedition 338 collected LWD logs in Holes C0018B and C0021A and cores in C0021B in the slope basin seaward of the megasplay fault. Maximum target depth for these holes was 420 mbsf. The LWD data provides new constraints to characterize *in situ* internal structures and properties of mass-transport deposits and to improve our understanding of submarine landslides in the slope basins seaward of the splay fault. In addition, low angle faults identified in X-ray Computed Tomography scans of cores from Site C0021 suggest a splay-fault-related, out-of-sequence thrust within slope basin sediments and shed new light on recent activity of the megasplay. At Site C0022B the megasplay fault is probably located within an interval of 100-101 mbsf. Several observations are in favor for this interval which is characterized by an increase in bedding dips in the vicinity of this interval, a higher density of minor faults 15-20 m above the interval and the presence of three 2 cm-thick intervals of claystone showing planar fabrics never encountered elsewhere at Hole C0022B. The hole was terminated at 416 mbsf.

In conclusion, Expedition 338 results provide new insights into the Nankai subduction system. Numerous whole-round and cuttings samples were taken for further on-shore laboratory investigations of composition, microstructures, frictional properties, and porosity/permeability.

Cruise Report: IODP Expedition 345: Fast-spreading Lower Crust at the Hess Deep Rift

J. KOEPKE[1], K. FAAK[2], AND THE EXPEDITION 345 SCIENTISTS

[1] Institut fuer Mineralogie, Universitaet Hannover
koepke@mineralogie.uni-hannover.de

[2] Institut GMG, Ruhr-Universitaet Bochum
kathrin.faak@ruhr-uni-bochum.de

Expedition 345, Hess Deep, started at the 12.12.2012 in Puntarenas (Costa Rica) and ended at 12.02.2013 in Balboa (Panama). The principal objective for drilling at the Hess Deep Rift located in the equatorial Pacific was, to test competing hypotheses of magmatic accretion and hydrothermal processes in the lower ocean crust formed at the fast-spreading East Pacific Rise (EPR). These hypotheses make predictions that can only be tested by drilling, i.e., the presence or absence of systematic variations with depth in mineral and bulk rock compositions, presence or absence of modally layered gabbro, and the extent and nature of hydrothermal alteration and deformation.

The Hess Deep Rift is a complex region that was formed by extension as a consequence of the westward propagating Cocos-Nazca spreading center. The surface expression of rifting is first evident ~30 km from the EPR, where two 5 km wide, east–west grabens expose ~0.5 Ma crust.

The drilling was carried out in ~4850 m water depth under quite challenging borehole conditions. We recovered primitive (Mg# 73-89) plutonic lithologies including gabbro, olivine gabbro, troctolite, and orthopyroxene-bearing gabbroic rocks. The recovered rocks exhibit cumulate textures similar to those found in layered mafic intrusions and some ophiolite complexes. Details of their mineralogical and petrologic evolution, however, are novel on the ocean floor. Additionally, they were deformed primarily in a partly molten regime expressed by the abundance of magmatic foliation. After that, nor or only minor sub-solidus crystal plastic deformation took place. Typical late-stage magmatic features, like abundant crystallization of a late, evolved melt producing interstitial mineral assemblages composed of amphibole, oxides, ± apatite ± zircon, which are well-known from gabbroic rocks from slow-spreading ridges (e.g. from ODP drillings at the KANE area at the Mid-Atlantic Ridge or at Atlantis bank at the Southwest Indian Ridge) were not observed.

Metamorphism at amphibolite facies is evident in tremolite-chlorite replacements of olivine + plagioclase, but at low concentrations. Metamorphism is dominated by background sub-greenschist facies alteration to prehnite + chlorite assemblages associated with cataclastic deformation, likely the result of Cocos-Nazca rifting. Penetrative amphibolite facies assemblages indicative of pervasive and intense high-temperature hydrothermal alteration of the lower crust were not observed.

Abstracts

ICDP

Water level changes of Lake Lisan, the glacial precursor of the Dead Sea: implications for palaeoclimatic changes of the Jordan Valley

S. ABU GHAZLEH[1], S. KEMPE[2]

[1] United Arab Emirate University, Al Ain, United Arab Emirate. Email: shahrazad@geo.tu-darmstadt.de
[2] Technische *Universität* Darmstadt, Darmstadt, Germany. Email: kempe@geo.tu-darmstadt.de

Lake Lisan, the glacial precursor of the Dead Sea, was one of several lakes that occupied the Jordan Valley during the Last Glacial period (70-14 ka BP*). It extended for ~ 300 km from Lake Tiberias in the north to > 60 km south of the current Dead Sea (DS). Prominent sequences of shoreline terraces and deep water deposits of aragonite and gypsum were left behind by the lake regression, now exposed on the Lisan Peninsula and along the shores of the DS (Landmann et al., 2002; Abu Ghazleh and Kempe, 2009). The ability to determine shoreline elevations and to date them offers excellent possibilities to evaluate hydrologic changes, paleoclimatic conditions and tectonic activity of the lake basin during the Last Glacial.

High-level terraces on the Jordanian side of the valley were surveyed for the first time using DGPS techniques. Terrace levels range between -370 m and -130 m, implying that the highest stand of Lake Lisan was at least 50 m higher than the previously reported one. Comparison of several terrace profiles and correlation of their altitudes show no evidences of tectonic subsidence, demonstrating that the lake level drop was entirely climatic.

In-situ stromatolites, most probably of cyanobacterial origin, were found on most of the terraces, reflecting a shallow, highly $CaCO_3$-supersaturated water environment. U/Th dating of stromatolites shows that Lake Lisan stood at a high level of -137 m at 31.99 ± 0.21 ka BP. Afterward, the lake dropped to -148 m at 30.55 ± 0.22 ka BP, consistent with the Heinrich event 3 and Dansgaard Oeschger Stadial 5, the coldest period in the North Greenland Ice Core record (NGRIP). The lake continued to drop to -152 m at 27.38 ± 0.16 ka BP and to -154 m at 22.9 ± 0.29 ka BP, corresponding with Heinrich event 2 and the cold stadial 2C, the final phase of the Last Glacial Maximum (LGM). OSL dating of Lisan sand in Wadi Dahel -south east of the Dead Sea- shows that Lake Lisan receded to lower than -200 m at ~11 ka BP induced by cold dry climate during the Younger Dryas.

Although Lake Lisan experienced high water stands during the cold stadials, it is quiet clear from our dates that the lake level was dropping. This implies cold dry climatic conditions of the Jordan Valley during the N-Hemispheric cold periods.

* ka BP: 1000 years ago.

References

Abu Ghazleh, S., & Kempe, S., 2009: Geomorphology of Lake Lisan terraces along the eastern coast of the Dead Sea, Jordan. Geomorphology 108:246–263.

Landmann, G., Abu Qudaira, G.M., Shawabkeh, K., Wrede, V., Kempe, S., 2002: Geochemistry of Lisan and Damya Formation in Jordan and implications on palaeoclimate. Quaternary International 89:45–57.

IODP

New procedure for recovering extra- and intracellular DNA from marine sediment samples

M. ALAWI[1], J. KALLMEYER[1]

[1] Helmholtz Centre Potsdam, GFZ German Research Centre for Geosciences, Geomicrobiology, Brandenburg, Germany

Extracellular DNA (eDNA) is a ubiquitous biological compound in aquatic sediment and soil. Despite major methodological advances, analysis of DNA from sediment is still technically challenging, not just because of the co-elution of inhibitory substances, but also due to co-elution of extracellular DNA, which potentially leads to an overestimate of the actual diversity. Previous studies suggested that eDNA might play an important role in biogeochemical element cycling, horizontal gene transfer and stabilization of biofilm structures. Several protocols based on the precipitation of eDNA e.g. with CTAB and ethanol have already been published. However, using these methods we did not succeed in quantifying very low amounts of eDNA (e.g. <1µg eDNA/g dry wt) in marine sediment even when using DNA carriers like glycogen. Since the recovery of eDNA by precipitation strongly depends on its concentration, these previously published procedures are not adequate for deep biosphere sediment due to the low eDNA content. We have focused on the question whether eDNA could be a source of nitrogen and phosphorus for microbes in the subseafloor biosphere. Therefore we developed a new method for the (semi)-quantitative extraction of eDNA from sediment. The new extraction procedure is based on sequential washing of the sediment to remove simultaneously eDNA and microbial cells without lysing them. After separation of the cells by centrifugation, the eDNA was extracted from the supernatant and purified by adsorption onto a solid phase (silica particles), followed by removal of the solids and subsequent elution of the pure eDNA. Intracellular DNA (iDNA) was extracted and purified from the cell pellet using a commercial DNA extraction kit. Additional to a very low detection limit and reproducible quantification, this new method allows separation and purification of both extracellular and intracellular DNA to an extent that inhibitors are removed and downstream applications like PCR can be performed. To evaluate the new extraction method two sediments with rather opposing composition were analyzed. Sediment from the South Pacific Gyre (IODP Exp. 329), the most oligotrophic oceanic region on Earth and organic-rich Baltic Sea sediment (Northern Germany) were processed. Using this new procedure, high purity genomic iDNA and eDNA with a molecular size range between 20 bp and 50k bp can be simultaneously recovered, even from very oligotrophic sediment with very low cell abundances. The recovered eDNA was suitable for downstream applications like PCR and had a molecular size range that indicates minimal shearing. The results show only a weak correlation between cell counts, iDNA and eDNA content. However, a link between eDNA contentration and cells is obvious. The eDNA amount in the investigated sediment is up to 48 times higher compared to the co-extracted iDNA. Comparative sequence analysis of extracted iDNA and eDNA will provide deeper insights into the origin and turnover of eDNA and the apparent microbial community composition in the deep biosphere.

ICDP

Petrological and geochemical investigations on the pseudotachylytes of the Alpine Fault, New Zealand

ALTENBERGER, U.[1], OBERHÄNSLI, R.[1], TIMMERMAN, M.J.[1], GÜNTHER, C.[1], TOY, V.[2]

[1] Institute of Earth and Environmental Sciences, University of Potsdam, Germany
[2] Department of Geology, University of Otago, Dunedin, New Zealand

Pseudotachylytes of the Alpine Fault Zone, New Zealand represent fossil frictional melts of upper crustal origin. They are formed during seismic pulses in different protoliths. Toy (2008) and others presented detailed investigations on structural and PT-evolution evolution. However, based on the current knowledge we have started to examine the fluid-friction-melt interaction and the disequilibrium melting processes on surface samples and samples from the ICDP drill core DFDP-1B.

Petrological, microstructural and geochemical analyses show, that the central veins, at which dislocation and frictional melt as well as the injection veins have initiated show significant and complex compositional layering (Fig. 1). In addition to chilled margins, different vein-parallel layers are formed. In some cases, pseudotachylytes reworked older generations, i.e. seismic slip reactivated older slip planes. Some samples show pseudotachylytes crosscutting as liquids. The different layers indicate chemical differences, as proven by electron microscopy and electron-microprobe analyses. Some of these results are used as a tool to determine the sequence of non-equilibrium melting of the different phases as well as determining changes in the rheological parameters, such as viscosity and density.

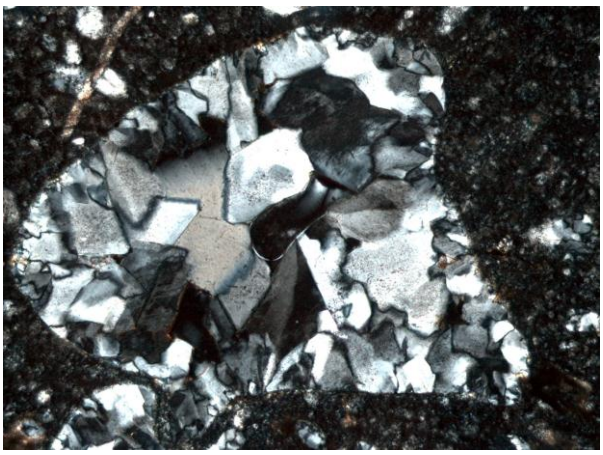

Figure 2: Pseudotachylyte with amygdule, filled by K-feldspar and quartz. Thin section photomicrograph. Crossed nicols. Long side of the image 1.2 mm.

A remarkable phenomenon of the pseudotachylytes of the Alpine Fault is the frequency of vesicles, open or filled, representing gas or fluid bubbles (Fig.2). The calculation of the cavities reveals the influence of the high water content of the protolithes and in some cases additional external water.

References:
Toy, V.G., Prior, D.J., Norris, R.J. 2008. Quartz fabrics in the Alpine Fault mylonites: Influence of pre-existing preferred orientations on fabric development during progressive uplift. Journal of Structural Geology 30, 602-621.

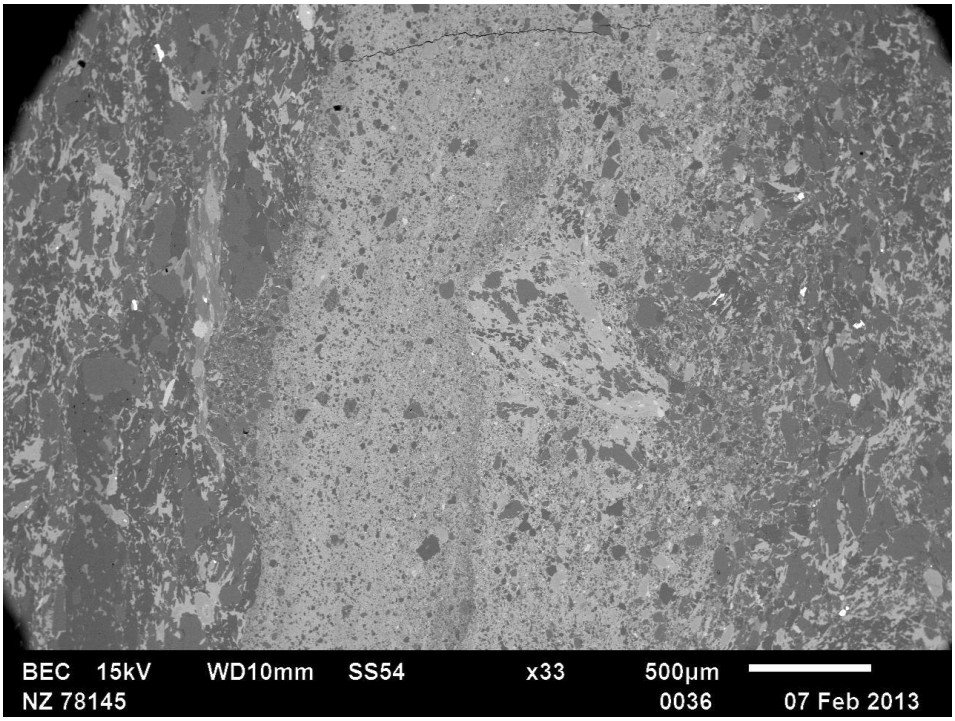

Figure 1: Back-scattered electron image of pseudotachylyte with vein-parallel layers of different composition.

ICDP

Late Pliocene/Early Pleistocene environments inferred from Lake El'gygytgyn pollen record

A.A. ANDREEV[1], V. WENNRICH[1], P.E. TARASOV[2], J. BRIGHAM-GRETTE[3], N.R. NOWACZYK[4], M. MELLES[1]

[1] Institute of Geology and Mineralogy, University of Cologne, Germany
[2] Free University Berlin, Institute of Geological Sciences, Palaeontology Branch, Berlin, Germany
[3] Department of Geosciences, University of Massachusetts, Amherst, USA
[4] Helmholtz-Zentrum Potsdam, Deutsches GeoForschungsZentrum, Potsdam, Germany

The Arctic is known to play a crucial, but not yet completely understood, role within the global climate system. The Middle Pliocene (3-3.5 Ma) is considered to be the most probable scenario of the future climate changes. Therefore, the development of possible scenarios of future climate changes in the Arctic is a major scientific challenge. However, reliable climate and environmental projections are hampered by the complexity of the underlying natural variability and feedback mechanisms. An important prerequisite for the validation and improvement of the future projections is a better understanding of the long-term environmental history of the Arctic. Unfortunately, formation of continuous, non-interrupted paleoenvironmental records in the Arctic was widely restricted due to repeated glaciations, limiting information predominantly to the Holocene and in a few cases to the last glacial/interglacial cycles (e.g. Andreev et al., 2011 and references therein). Continuous sequences that penetrates the entire Quaternary and further into the Pliocene, with a temporal resolution at least as good as the marine record, are highly desired from the terrestrial Arctic and would enable to validate the absolute temperature rise during the mid-Pliocene that was proposed by former studies. Such a record has now become available from Lake El´gygytgyn (67º30'N, 172º05E') located in a meteorite impact crater in north-eastern Siberia (Melles et al., 2011).

The crater was created nearly 3.6 Ma ago in volcanic target rocks. The impact formed an 18 km wide hole in the ground that then filled with water. The modern lake is 170 m deep and has a roughly circular shape with a diameter of 12 km. The retrieved lake sediments are trapped pollen from a several thousand square-kilometer source area providing reliable insights into regional and over-regional millennial-scale vegetation and climate changes of the Arctic since the Pliocene (for details see Melles et al., 2011, 2012 and references therein).

The German-Russian-American ''El´gygytgyn Drilling Project" of ICDP has completed three holes in the center of the lake between October 2008 and May 2009, penetrating about 318 m thick lake sediments and about 200 m of the impact rocks below. Because of its unusual origin and high-latitude setting in western Beringia, scientific drilling at Lake El´gygytgyn offered unique opportunities for paleoclimate research, allowing the time-continuous reconstruction of the climatic and environmental history of the terrestrial Arctic back into the Pliocene for the first time (Melles et al., 2012; Brigham-Grette et al 2013). We received the first pollen record reflecting paleoenvironmental and paleoclimate changes during the Late Pliocene and transition to the Early Pleistocene inferred from the lower 200 m of Lake El'gygytgyn lacustrine sediments (Andreev et al., 2013).

Revealed pollen assemblages can be subdivided into 50 main pollen zones and a number of subzones, which reflect the main environmental fluctuations in the region during the Late Pliocene and Early Pleistocene, approximately 3.55-2.15 Ma BP. Pollen-based climate reconstructions show that conditions in the study area were the warmest about 3.55-3.4 Ma BP when spruce-pine-fir-hemlock-larch-*Pseudotsuga* forests dominated in nowadays treeless tundra area. After ca. 3.4 Ma BP dark coniferous taxa gradually disappeared from the vegetation cover. Very pronounced environmental changes are revealed about ca. 3.35-3.275 Ma BP when treeless tundra and steppe habitats dominated. Large amounts of coprophilous fungi spores point to a permanent presence of numerous grazing herds around the lake. It is interesting that this episode occurred at the so-called Mammoth subchron (M2).

Since ca. 3.05 Myr BP (ca. 163 m of the sediment core) extremely numerous, small (ca. 12 μm), round and transparent cysts occur in many sampled intervals. The origin of these cysts is unclear. According to Dr. T. Leya (personal communication), it is very likely that these cysts were produced by the so-called snow-algae (genera of *Haematococcus* (*Sphaerella*), *Chlamydomonas*, and *Chloromonas*).

Treeless and shrubby environments are also indicative for the beginning of the Pleistocene, ca. 2.6 Ma. Dry and cold climate conditions were similar to those during the Late Pleistocene. The Early Pleistocene sediments contain pollen assemblages reflecting alternation of treeless intervals with cold and dry climate and warmer intervals when larch forests with stone pines, shrub alders and birches were also common in the region. Very dry environments are revealed after ca. 2.175 Ma BP. High amounts of green algae colonies (*Botryococcus*) in the studied sediments point to a shallow water conditions ca. 2.55, 2.45, and ca. 2.175 Ma BP.

Our pollen studies show that lacustrine sediments accumulated in Lake El´gygytgyn are an excellent archive of vegetation and climate changes since ca. 3.55 Myr BP (Andreev et al., 2013). The record well reflects main paleoenvironmental fluctuations in the region. The further high-resolution palynological study of the sediment core will reveal climate fluctuations inside the main glacial/interglacial intervals and will give the first continuous and detailed scheme of environmental changes for a whole Arctic.

References:

Andreev, A., Schirrmeister, L., Tarasov, P., Ganopolski, A., Brovkin, V., Siegert, C., Hubberten, H.-W. Vegetation and climate history in the Laptev Sea region (arctic Siberia) during Late Quaternary inferred from pollen records. Quaternary Science Reviews 30, 2011. 2182-2199.

Andreev, A.A., Wennrich, V., Tarasov, P.E., Brigham-Grette, J., Nowaczyk, N.R., Melles, M., El'gygytgyn Scientific Party. 2013. Late Pliocene/Early Pleistocene environments of the north-eastern Siberian Arctic inferred from Lake El'gygytgyn pollen record. Climate of the Past. (in preparation).

Melles, M., Brigham-Grette, J., Minyuk, P., Koeberl, C., Andreev, A., Cook, T., Gebhardt, C, Haltia-Hovi, E., Kukkonen, M., Nowaczyk, N., Schwamborn, G., Wennrich, V., El'gygytgyn Scientific Party. 2011. The Lake El'gygytgyn Scientific Drilling Project - Conquering Arctic Challenges in Continental Drilling. Scientific Drilling 11, 29-40.

Melles, M., Brigham-Grette, J., Minyuk, P.S., Nowaczyk, N.R., Wennrich, V., DeConto, R.M. Anderson, P.M., Andreev, A.A., Coletti, A., Cook, T.L., Haltia-Hovi, E., Kukkonen, M., Lozhkin, A.V., Rosén, P., Tarasov, P., Vogel, H., Wagner, B. 2.8 Million. 2012. Years of Arctic

Climate Change from Lake El'gygytgyn, NE Russia. Science 337, 315-320.
Brigham-Grette, J., Melles, M., Minyuk, P., Andreev, A., Tarasov, P., DeConto, R., Koenig, S., Nowaczyk, N., Wennrich, V., Rosén, P., Haltia-Hovi, E., Cook, T., Gebhardt, C., Meyer-Jacob, C., Snyder, J., Herzschuh, U. 2013. Pliocene Warmth, extreme Polar Amplification, and Stepped Pleistocene Cooling recorded in NE Russia. Science (under review).

IODP

The 2002 Osa (Costa Rica) earthquake sequence revisited: Will CRISP deep drilling reach the seismogenic coupling zone?

I.G. ARROYO[1], I. GREVEMEYER[1], J. BEHRMANN[1], E.R. FLUEH[1]

[1] GEOMAR Helmholtz Zentrum für Ozeanforschung Kiel, Wischhofstraße 1-3. 24148 Kiel, Germany (iarroyo@geomar.de)

On March 11, 2011 the Magnitude 9.0 Tohoku earthquake hit NE Japan offnorthern Honshu. In contrast to the evidence from seismology and GPS-derived slip models, maximum (> 50 m) coseismic slip occurred near the trench axis, an area in forearcs generally believed to be characterized by stable sliding rather than seismic coupling and locking. This concept holds at least for accretionary subduction zones. However, after the Tohoku earthquake it must be challenged for erosive margins. Offshore of Central America, IODP may help to answer some of the questions, as the Costa Rica Seismogenesis Project (CRISP) is designed to explore the processes involved in the nucleation of large interplate earthquakes at tectonically erosive subduction zones. CRISP is a three-stage drilling project. CRISP-A was drilled in 2011 and CRISP-B successfully extended key holes to greater depth in late 2012. However, will CRISP-C ever be able to reach the seismogenic zone? The June 16, 2002 magnitude Mw=6.4 earthquake and its aftershocks may point towards an answer.

Unfortunately, global event locations present uncertainties too large to prove that the event actually occurred at a location and depth accessible by riser drilling. We have compiled a database including foreshocks, the mainshock, and ~400 aftershocks, with phase arrival times from all the seismological networks that recorded the 2002 Osa sequence locally. This includes a temporal network of ocean-bottom hydrophones (OBH) that happened to be installed close to the area at the time of the earthquake. The coverage provided by the marine network enabled us to better constrain hypocentral parameters. Moreover, teleseismic waveform inversion provided additional constraints on the centroid depth of the 2002 Osa earthquake, allowing us to study the focal mechanism.

Along the central portion of the Costa Rican subduction zone, the 2002 Osa sequence is the most recent large offshore event. It nucleated in the SE region of the forearc where this erosional margin is underthrust by seamounts covering the incoming oceanic plate. A Mw=6.9 earthquake sequence occurred in 1999, co-located with a subducted ridge and associated seamounts. The Osa main shock and first hours of aftershocks nucleated in the CRISP drilling area, ~30 km seaward of the 1999 sequence. In the following two weeks, aftershocks migrated into the 1999 aftershock area and also clustered in an area updip from the 1999 main shock. The updip seismicity in the area of CRIP drilling near the Osa peninsula, however, apparently occurred where interplate temperatures are ~100°C or less. These temperature estimates are based on surface heat flow and thermal modelling. CRISP-A drilling confirmed the low temperatures, thus challenging previous concepts of seismogenesis at erosive margins.

Deutsche Forschungsgemeinschaft funded project CRISP-EQ started in October 2012 to yield precise hypocentral parameters for the Osa mainshock and its aftershocks. We have updated location precision replacing a 1-D reference model with a so called 2.5-D velocitiy model that incoroporates strong lateral changes in the structure of the active continental margin of Costa Rica. The resulting hypocentre occurs to the NW of the epicentre obtained from the 1-D model, and several kilometres seaward with respect to global location estimates. While the global Centroid Moment Tension inversion procedure of Lamont Earth Observatory of Columbia University found a centroid depth (i.e., location of main moment release) of 16 km, our estimates now suggest a nucleation and centroid depth of 6 km. Thus, our results support the notion that CRISP-C will be able to reach the seismogenic zone. In the future, we plan to derive a full 3-D velocity field for SE Costa Rica and its Pacific margin from a unique dataset of several temporary deployments of OBS and land stations, that will provide much lower error bounds for the location of the Osa seismic sequence. Further, along with constraints from CRISP-A and B drilling we will survey the properties controlling earthquake nucleation and rupture propagation at erosive continetal margins.

ICDP

Tectonic structures in the Stumsnäs 1 core of the southern Siljan Ring, central Sweden

A. ARSLAN[1], G. MEINHOLD[2], O. LEHNERT[3,4]

[1] Ulmenweg 2, D-37077 Göttingen, Germany; arzuarsl@gmail.com
[2] Geowissenschaftliches Zentrum der Universität Göttingen, Abt. Sedimentologie/ Umweltgeologie, Goldschmidtstr. 3, D-37077 Göttingen, Germany; variscides@gmail.com
[3] GeoZentrum Nordbayern, Universität Erlangen, Schloßgarten 5, D-91054 Erlangen, Germany; lehnert@geol.uni-erlangen.de
[4] Department of Geology, Lund University, Sölvegatan 12, SE-223 62 Lund, Sweden

The Stumsnäs 1 core represents a structurally highly complex section and provides new insights into the regional structure of the southern part of the Siljan Ring in central Sweden. The Siljan Ring was formed around the central uplift of a huge meteorite crater in the Late Devonian which represents the largest known impact structure in Europe. Our work contributes to the "Concentric Impact Structures in the Palaeozoic" project (CISP) that is integrated in the "Swedish Deep Drilling Program" (SDDP; http://www.sddp.se/CISP). The lower ~261 m thick interval in Stumsnäs 1 is composed of Proterozoic igneous rocks in which several, meter-scale cataclastic zones occur. The overlying ~88 m thick interval comprises a Tremadocian to Katian (Lower to Upper

Ordovician) sedimentary sequence which is tectonically disturbed in its upper parts with some units cut out or repeated. The sedimentary sequence is tectonically overlain by a ~192 m thick section of Proterozoic igneous rocks. The tectonic contact is a few meters thick complex fault zone with alternating thrust slices of highly disturbed sedimentary and granitic rocks, fault breccia and gouge. The major fault zones throughout the core section have large damage zones with intense fracture networks and veins along which alteration and mineralization took place likely impact related. Furthermore, small scale faults and fractures are common throughout the core and are critical for fluid migration and hence for ongoing exploration of hydrocarbons and geothermal energy reservoirs in the Siljan impact structure

IODP

Preliminary results from XRF scanning of contourite deposits in the Gulf of Cadiz (IODP Exp. 339)

A. BAHR[1], F. JIMENEZ-ESPEJO[2], N. KOLASINAC[1], S. AUSCHILL[1], U. RÖHL[3], J. HERNÁNDEZ-MOLINA[4], D.A.V. STOW[5], D. HODELL[6], C. ALVAREZ-ZARIKIAN[7], AND IODP EXPEDITION 339 SCIENTISTS[8]

[1] Institute of Geosciences, University Frankfurt, Altenhöferallee 1, 60438 Frankfurt, Germany
[2] Institute of Biogeosciences, Japan Agency for Marine-Earth Science and Technology, Yokosuka 237-0061, Japan.
[3] MARUM, University of Bremen, Leobener Str., 28359 Bremen, Germany
[4] Facultad de Ciencias del Mar, Universidad de Vigo, 36310 Vigo, Spain
[5] Institute of Petroleum Engineering, Heriot-Watt University, Edinburgh, EH13 4AS, UK
[6] Department of Earth Sciences, University of Cambridge, Downing Street, Cambridge, Cambridgeshire, CB2 3EQ, UK
[7] Department of Oceanography, Texas A&M University, 1000 Discovery Dr. College Station, TX 77845-9547, USA
[8] IODP Expedition 339 Scientists: Acton, G., Balestra, B., Ducassou. E., Flood, R., Flores, J.A., Furota, S., Grunert, P., Kim, J. K., Krissek, L., Kuroda, J., Li, B., Llave, E., Lofi, J., Lourens, L., Miller, M., Nanayama, F., Nishida, N., Richter, C., Roque, C., Sanchez Goñi, M., Sierro Sanchez, F., Singh, A., Sloss, C., Takashimizu, Y., Tzanova, A., Voelker, A., Williams, T., Xuan, C.

During IODP Expedition 339 complete sequences of Pliocene and Quaternary contourite deposits were drilled in the Gulf of Cádiz. Since the build-up of these contourites is tightly linked to the Mediterranean Outflow Water (MOW) they provide a unique archive of MOW variability and its influence on global circulation and climate. We performed high-resolution XRF scanning on spliced sections of two sites: 1) U1387, located on Faro Drift in 559.1 m water depth, and 2) U1389, in 644 m water depth on Huelva Drift ~90 km W of Cádiz, located more proximal to the Gibraltar Gateway. Site U1387 provides a mostly continuous succession of Holocene and Plio-Pleistocene deposits with an average sedimentation rate of 25 cm/kyr. Below a significant hiatus (1.8–3.2 Ma), event beds become dominant, while the lowermost unit is composed of hemipelagic sediments most probably of Late Miocene (Messinian) age. Here, XRF Scanning focused on the sediments younger than 1.8 Ma and the Miocene deposits. Site U1389 cores were scanned down to 125 mcd, recovering late Pleistocene (<250 ka) contourite sediments with high sedimentation rates (up to 50 cm/kyr).

The results from XRF scanning show a tight link between lithological (grain size) changes and elemental composition. Elements associated with heavy minerals (e.g. Fe, Ti and Zr) are typically enriched in coarse-grained intervals by gravitational sorting related to bottom current strength. The bigradational grain size pattern typical for contourites is closely reflected in the elemental distribution. Despite such sorting variations paleoceanographic/stratigraphic information does not appear to be compromised. Particularly useful for these purposes appears to be the Br record, which relates to the organic matter content of the sediment. High frequent changes in Br content closely resemble millennial-scale variations recorded e.g. in Greenland ice core records and, thus, represents a valuable stratigraphic tool. Additionally, the XRF data enables a precise stratigraphic correlation between both sites. These preliminary results will be highly useful to reconstruct the evolution of the MOW.

ICDP

Resolving sedimentary sulfur cycling during the Shunga Event (early Palaeoproterozoic) with sulfur isotopes

D. BANNING[1], H. STRAUSS[1], V.A. MELEZHIK[2,3], A. LEPLAND[2], M.J. WHITEHOUSE[4]

[1] Westfälische Wilhelms-Universität Münster, Institut für Geologie und Paläontologie, Münster, Germany
[2] Geological Survey of Norway (NGU), Trondheim, Norway
[3] University of Bergen, Centre of Geobiology, Bergen, Norway
[4] Swedish Museum of Natural History, Box 50007, SE-104 05 Stockholm, Sweden

Early Earth's ocean - atmosphere system experienced fundamental global events during the early Palaeoproterozoic including the unprecedented accumulation of organic matter during the Shunga event in the aftermath of the Lomagundi-Jatuli Event (e.g. Melezhik et al., 1999a, b) ~2.05 billion years ago (Hannah, 2008) and the Great Oxidation Event (GOE, 2.3 Ga) (Holland, 1999) causing enhanced terrestrial sulfide weathering and subsequent delivery of sulfate to the ocean (Reuschel et al., 2012). The enhanced input of sulfate into the ocean water most likely resulted in an increased role of sulfate reducing bacteria in the microbial turnover of sedimentary organic matter which is archived in the isotopic signature of sulfur bearing minerals embedded in the Palaeoproterozoic sediments.

The data presented here are based on analyses of drillcore material from the Fennoscandia Arctic Russia – Drilling Early Earth Project (FAR DEEP). The drilling location is situated near Shunga, which is north of Petrozavodsk near the Onega Lake in NW Russia (Fig. 1). Some 744 m of "shungite" drillcore from three drillholes within the c. 2.05 Ga old Zaonega Formation (ZF) were recovered. Results focus on samples from drillcores 12A, 12B and 13A. Drillcore 13A ranges in depth from 0 to 240 m below surface and 12A and 12B belong to the same lithological profile with 12A covering the uppermost core meters to a depth of ~95 m and 12B covering the core from a depth of 95 m to 500 m below surface. The main

Fig. 1: Map of the study area (modified after Melezhik et al. 1999a).

objective of this project is to resolve sedimentary sulfur cycling during the early Palaeoproterozoic with sulfur isotopes and related geochemical markers.

It was suggested that rhythmically bedded sedimentary rocks of the ZF were deposited in a low-energy, non-euxinic environment (Melezhik et al., 1999a). They are of typically black to grey colour due to the great amount of organic matter which is most likely of algal or bacterial origin (Melezhik et al., 1999a). The rocks deposited during the Shunga Event underwent metamorphic alteration under greenschist facies conditions during the 1.8 Ga Svecofennian orogeny (Melezhik et al., 1999a). Iron sulfides are very common in these sedimentary rocks and show a high variability in their habitus (Fig. 2) with pyrite being the most prevalent iron sulfide. The complex pattern of the iron sulfide morphologies (cf. Fig. 2, 5) and their geochemical characteristics relate to the nature of marine sulfur cycling, to different sulfide or sulfate generation stages, late-diagenetic processes (e.g. migration of solutes) and organic matter degradation accompanying the generation and migration of bitumen within the sediments of the ZF (Melezhik et al., 2009; Strauss et al., 2013) as a result of postdepositional processes. The migrated hydrocarbons, now petrified (locally termed as shungite) complicate the interpretation of the collected dataset in terms of primary versus secondary pyrite formation. Therefore, it is of major interest to assess the different aforementioned processes.

Initially, sulfur and carbon contents were measured, in the following expressed as total sulfur (TS), total carbon (TC) and total inorganic carbon (TIC) abundances in bulk rock samples (Figs. 3, 4) with a CS MAT 5500 in Münster.

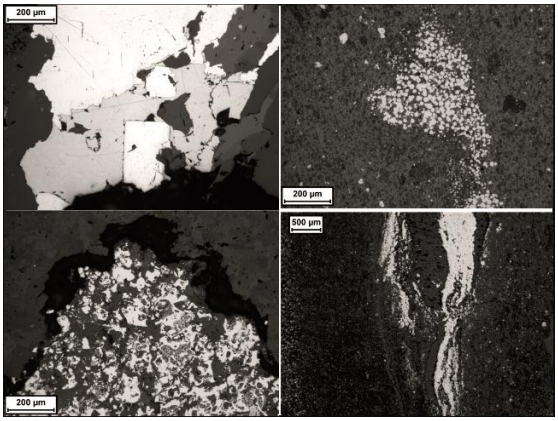

Fig. 2: Some polished section images of different iron sulfide morphologies in drillcores 12A, 12B and 13A.

Sedimentary rocks with an increased total sulfur content (TS) usually (but not always) show an enrichment in the total organic content (TOC). They interbed with high-TIC/TC-dominated rocks in a relatively close pattern. A first attempt was made to separate types of different geochemical characteristics by correlating TIC versus TC content. Three data populations can be distinguished: carbonate dominated rocks (TIC/TC 0.5-1), organic carbon (C_{org}) dominated rocks (TIC/TC <0.15 and a third population with transitional TIC/TC ratios. Mean values for TS (wt.%) are 1.47 for carbonate dominated rocks, 1.77 for the transition zone and 2.31 for organic carbon dominated rocks.

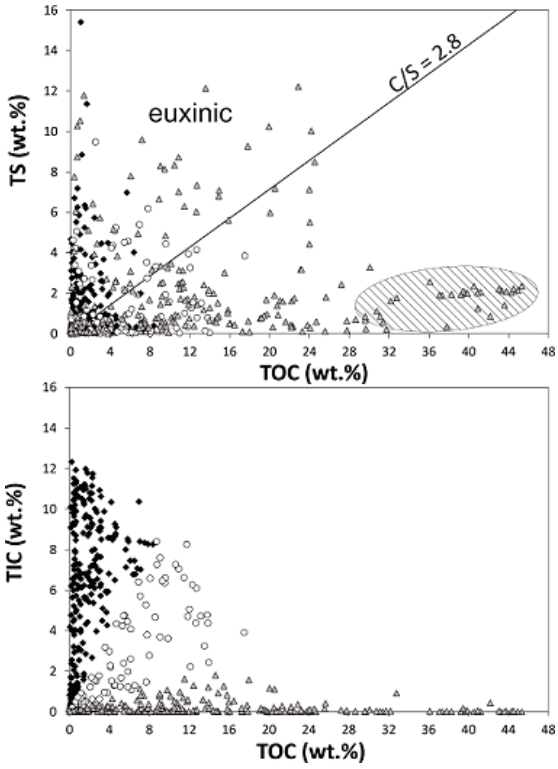

Fig. 3: Scatter plot of TS versus TOC and TIC versus TOC. Upper diagramm: line marks Holocene normal marine $C_{org}/S_{sulfide}$ ratio. The hatched field marks samples where bitumen migration is suggested. Carbonate dominated samples are displayed in dark grey/diamonds, organic dominated samples in light grey/triangles and transitional samples in white/circles.

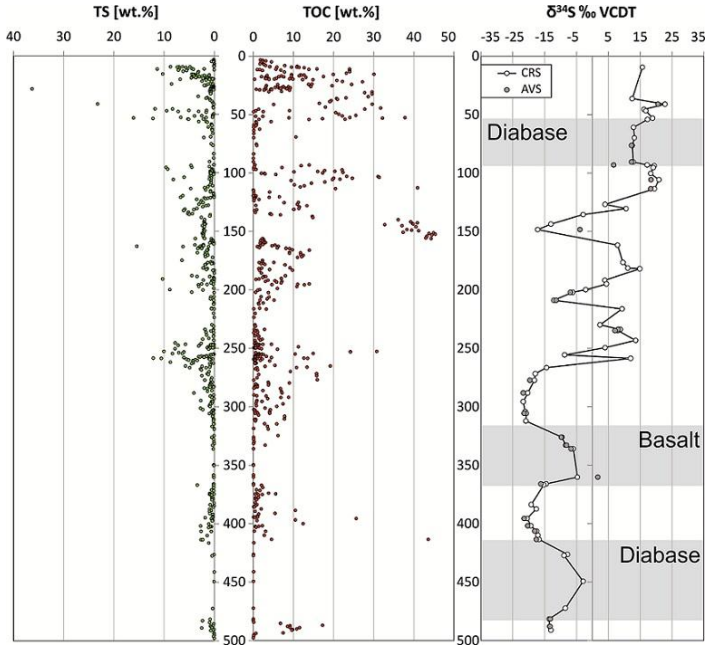

Fig. 4: Profiles of drillcore 12A and 12B. From left to right: TS, TOC and $\delta^{34}S$ values against depth.

Stable sulfur isotopic data were obtained by a sequential extraction method after Canfield et al. (1986). Based on highly variable $\delta^{34}S$ values of the chromium reducible fraction (CRS; disulfides; mainly pyrite) with -21.7 to +33.9 ‰ VCDT and of the acid volatile fraction (AVS; monosulfides) within the same range, differences in microbial sulfur cycling can be deduced. Although no clear correlation between $\delta^{34}S$ values and TOC or TIC contents could be observed, samples displaying the highest values for TOC (32.77 to 43.59 wt.%) show preferentially negative $\delta^{34}S$ signals, which is consistent with bacterial sulfate reduction (-13.0 and -17.2 ‰ VCDT). In figure 4 the depthprofile of $\delta^{34}S$ data from drillcores 12A and 12B together with the TS and TC content are shown. Up-section a general positive shift of $\delta^{34}S$ is discernible, which can be interpreted as a change towards a limited sulfate supply and subsequently, successively heavier $\delta^{34}S$ signatures of the residue. A positive correlation between $\delta^{34}S$ and total sulfur content (R^2=0.81) in the uppermost massive organic matter rich rocks could be observed, whereas the deeper ones show negative signatures (-13.0 ‰ to -17.5‰ VCDT) with relatively constant TS values of 2 wt.% on average. Below 315 m in drillcore 12B two magmatic rock members occur whose bulk rock samples show a less negative isotopic signature of sulfur than for the intercalated greywacke siltstones and organic matter-rich rocks. Mean values for $\delta^{34}S$ of -9.1 ‰ for the magmatic rocks can be ascertained in contrast to a mean value of -18.3 ‰ for the greywacke siltstones and organic matter-rich sediments.

High-spatial in situ isotopic measurements on single sulfide grain scale were conducted on the Nordsim facility in Stockholm and yielded extreme values for $\delta^{34}S$ of -40.10 ‰ to +84.76 ‰ and for $\Delta^{33}S$ of -0.81 ‰ to +0.53 ‰

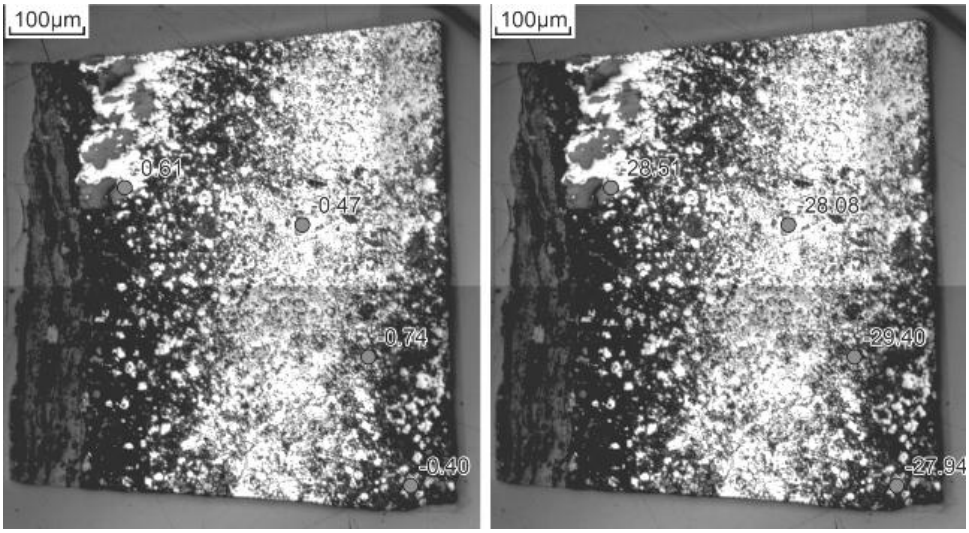

Fig. 5: Polished section images of a conglomerate sample from drillcore 12B. Isotopic values for $\delta^{34}S$ on the right side and for $\Delta^{33}S$ on the left side.

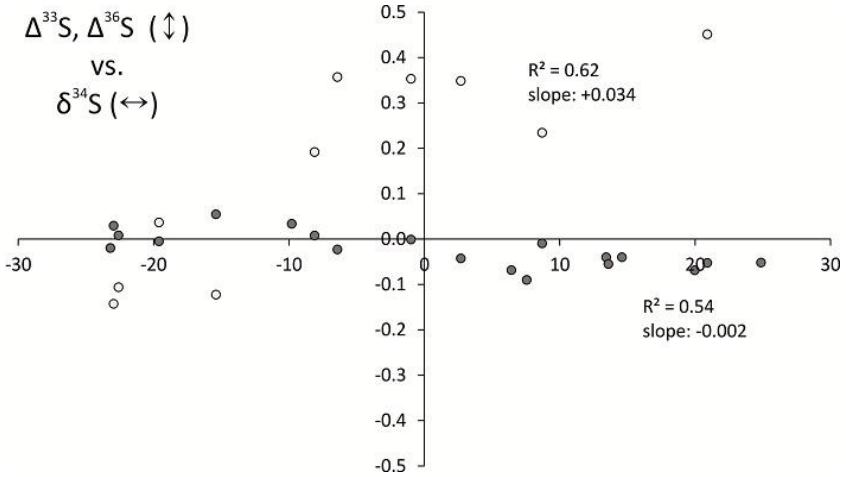

Fig. 6: Multiple sulfur isotope data for some bulk rock samples of drillcores 12A, 12B and 13A. $\Delta^{33}S$ is shown in grey circles and $\Delta^{36}S$ in white circles.

VCDT. A maximum fractionation within one sample of 82.23 ‰ for $\delta^{34}S$ and 0.98 ‰ for $\Delta^{33}S$ could be determined. Mass independent fractionation (MIF) of stable sulfur isotopes is commonly accepted as a proxy for a oxygen free atmosphere (Farquhar et al., 2000). The slight MIF signature in $\Delta^{33}S$ of -0.34 ‰ to -0.81 ‰ in the conglomerates (cf. figure 5) and of -0.53 ‰ to -0.63 ‰ in the greywacke are interpreted as inherited signal of older source rocks deposited in a pre-GOE atmosphere. Additional in situ measurements will have to be conducted to approve this hypothesis.

Moreover, multiple sulfur isotope analysis ($\Delta^{33}S$ and $\Delta^{36}S$) on some first bulk rock CRS samples have been performed (Fig. 6). In general the samples show an average $\Delta^{33}S$ value of 0.023 ‰ with a maximum range from -0.090 to +0.055 ‰. $\Delta^{36}S$ values range between -0.775 and +0.896‰ with an average of 0.342 ‰. These results are in good agreement with literature data for other post-GOE sediments.

The abundant sulfides and their different generations and diverse sulfur isotope characteristics point to a complex (dia)genetic history.

Acknowledgements: Financial support through the Deutsche Forschungsgemeinschaft (STR281/35) is gratefully acknowledged.

References:

Canfield, D.E., Raiswell, R., Westrich, J.T., Reaves, Berner, R.A. (1986). The use of chromium reduction in the analysis of reduced inorganic sulfur in sediments and shales. Chemical Geology 54: 149-155.

Farquhar, J.; Bao, H.; Thiemens, M. (2000). Atmospheric influence of Earth's earliest sulphur cycle. Science 289:756-758.

Hannah, J.L. (2008). Re-Os geochronology of a 2.05 Ga fossil oil field near Shunga, Karelia, NW Russia. Abstract, 33rd International Geological Congress, Oslo, 2008, 6-14 August

Holland, H.D. (1999). When did the Earth's atmosphere become oxic? The Geochemical News 100: 20-22.

Melezhik, V.A., Fallick, A.E, Filippov, M. M. Larsen, O. (1999a). Karelian shungite - an indication of 2.0-Ga-old metamorphosed oil-shale and generation of petroleum: geology, lithology and geochemistry. Earth-Science Reviews 47: 1-40.

Melezhik, V.A., Fallick, A.E., Medvedev, P.V., Makarikhin, V.V. (1999b). Extreme 13Ccarb enrichment in ca. 2.0 Ga magnesite-stromatolite-dolomite-`red beds´ association in a global context: A case for the world-wide signal enhanced by a local environment: Earth-Science Reviews 48: 71–120.

Melezhik, V.A., Fallick, A.E, Filippov, M.M., Lepland, A., Rychanchik, D.V., Deines, Y.E., Medvedev, P.V., Romashkin, A.E., Strauss, H. (2009). Petroleum surface oil seeps from a Palaeoproterozoic petrified giant oilfield. Terra Nova 21: 119–126.

Strauss, H.; Melezhik, V.A.; Lepland, A.; Fallik, A.E.;.Hanski, E.J.; Filippov, M.M.; Deines, Y.E.; Illing, C.J.; Črne, A.E.; Brasier, A.T. (2013) Enhanced accumulation of organic matter: The Shunga Event. In: Reading the archive of Earth´s oxygenation, Vol.3, pp. 1195-1273.

IODP

Orbitally calibrated carbon-isotope stratigraphy of the Maastrichtian of U1403, IODP Expedition 342, Newfoundland

S. BATENBURG[1], O. FRIEDRICH[1], K. MORIYA[2], S. VOIGT[1], T. HASEGAWA[2], IODP EXPEDITION 342 SCIENTISTS

[1] Intitute of Geosciences, Goethe-University Frankfurt, Altenhöferallee 1, 60438 Frankfurt, Germany
[2] Division of Earth and Environmental Sciences, Kanazawa University, Ishikawa 920-1192, Japan

The mode of ocean circulation during latest Cretaceous to Paleocene times (75-55 Ma) is poorly understood and the location of deep-water formation relative to the opening of the Atlantic Ocean is debated. This project aims to investigate the conditions of intermediate- and deep-water formation and exchange in the individual sub-basins of the North and South Atlantic Ocean. It is planned to perform Nd-isotope analyses of sediment coatings from a series of DSDP-/ODP-/IODP-Sites in different sub-basins and at different water depths in the North and South Atlantic Ocean. This approach allows the identification of different intermediate and deep-water masses by recognizing their potential source region and revealing time intervals of established deep-water connections between the oceanic sub-basins. Robust stratigraphic integration of new and available data will provide answers to the following questions: 1) when did the individual sub-basins of the deep Atlantic Ocean fully integrat into the global thermohaline circulation, 2) how do sub-oceanic volcanic plateaus become barriers to deep water circulation, and 3) to what extent was the Caribbean Sea an equatorial gateway for deep-water exchange between the Atlantic and the Pacific oceans.

Here, we present the first stratigraphic results from the North Atlantic Site U1403 drilled last year during IODP Expedition 342 at Newfoundland. Site U1403 recovered

about 50 m of Maastrichtian sediments comprising mainly of nannofossil chalk. The succession was studied in high resolution (10-cm spacing) to generate a $\delta^{13}C$ record which is biostratigraphically calibrated to calcareous nannofossil events (Expedition 342 Scientists 2012). Recently, Maastrichtian carbon-isotope stratigraphy has proven to be a powerful tool in global correlation (Voigt et al. 2012, Thibault et al. 2012). Significant high-frequency $\delta^{13}C$ variations occur superimposed on prominent Maastrichtian events, namely the the Campanian–Maastrichtian Boundary Event (CMBE), the mid-Maastrichtian Event (MME), and the Cretaceous-Paleogene transition (KPgE).

The observed $\delta^{13}C$ pattern at Site U1403 allows a detailed correlation with $\delta^{13}C$ variations at ODP-Site 1210 (Jung et al. 2012) and the orbitally-tuned $\delta^{13}C$ record of Zumaia-Sopelana, northern Spain (Batenburg et al. 2012). Consequently, the new $\delta^{13}C$ record of Site U1403 can be tied into the recently developed floating astronomical timescales of the Maastrichtian. Lithologic cyclicity recorded at Zumaia-Sopelana and ODP-Site 762 provides ages for bioevents, magnetic reversals and carbon isotope excursions and resolves thirteen 405 kyr eccentricity cycles in the Maastrichtian (Husson et al. 2012, Batenburg et al. 2012). The $\delta^{13}C$ record at Zumaia exposes large amplitude shifts in $\delta^{13}C$ on the 405-kyr and 1.2-Myr scales, which can also be identified at Site U1403. In particular, the interval between the MME and the KPgE is recorded in unprecedented detail. Such high-resolution correlation will allow us to test recent hypotheses concerning nannofossil datum diachroneity.

The comparison of orbitally-tuned $\delta^{13}C$ records of Gubbio, Zumaia-Sopelana, ODP Site 120 and IODP Site U1403 with the astronomical solution La2011 (Laskar et al. 2011 and unpublished data) clearly show the Cenozoic pattern of 405 kyr cycle insolation maxima corresponding to carbon isotope minima. Furthermore, amplitudes of $\delta^{13}C$ minima are particularily pronounced during the terminal CMBE, the MME and the KPgE representing intervals of minima in the very long 2 Myr eccentricity. Future work in the project will focus on Nd-isotope analyses of sediment coatings to show how ocean circulation evolved in the Atlantic ocean in particular in relation to the orbital pacing of Maastrichtian climate change.

References:

Batenburg, S., et al. 2012. Cyclostratigraphy and astronomical tuning of the Late Maastrichtian at Zumaia (Basque country, Northern Spain). Earth and Planetary Science Letters, http://dx.doi.org/10.1016/j.epsl.2012.09.054.

Expedition 342 Scientists, 2012. Paleogene Newfoundland sediment drifts. IODP Prel. Rept., 342. doi:10.2204/iodp.pr.342.2012.

Husson, D., Galbrun, B., Laskar, J., Hinnov, L.A., Thibault, N., Gardin, S., and Locklair, R.E., 2011. Astronomical calibration of the Maastrichtian (Late Cretaceous). Earth and Planetary Science Letters 305, 328-340.

Jung, C., Voigt, S., and Friedrich, O., 2012. High-resolution carbon-isotope stratigraphy across the Campanian-Maastrichtian boundary at Shatsky Rise (tropical Pacific). Cretaceous Research 37, 177-185.

Laskar, J., Gastineau, M., Delisle, J.-B., Farrés, A., Fienga, A., 2011. Strong chaos induced by close encounters with Ceres and Vesta. Astronomy and Astrophysics 532, L4.doi: 10.1051/0004-6361/201117504.

Thibault, N., et al. 2012. Astronomical calibration of upper Campanian-Maastrichtian carbon isotope events and calcareous plankton biostratigraphy in the Indian Ocean (ODP Hole 762C): Implication for the age of the Campanian-Maastrichtian boundary. Palaeogeography Palaeoclimatology Palaeoecology 337, 52-71.

Voigt, S., Gale, A.S., Jung, C., and Jenkyns, H.C., 2012. Global correlation of Upper Campanian - Maastrichtian successions using carbon-isotope stratigraphy: development of a new Maastrichtian timescale. Newsletters on Stratigraphy 45, 25-53.

IODP

Palaeoceanography and climate variability of the NW Pacific over the last 8 Myr

T. BAUERSACHS[1], A.S. JONAS[1], L. SCHWARK[1,2] AND IODP EXPEDITION 333 SCIENTISTS

[1] Department of Organic Geochemistry, Institute of Geosciences, Christian-Albrechts-University, Kiel, Germany
[2] WA-OIGC, Curtin University, Perth, Australia

The Kuroshio Current (KC) is the western boundary current of the subtropical North Pacific Ocean and essential for the meridional transport of heat from the Western Pacific Warm Pool to the northern mid-latitudes. Off the coast of Japan (presently at 36°N), the KC is diverted eastwards to form the Kuroshio extension as it encounters the subarctic Oyashio Current (OC), which is part of the western subarctic gyre and transports cold waters from the North Pacific Ocean to the south. Variation in the strength and migration pattern of both ocean currents are considered to control much of the climate of the NW Pacific Ocean with particular impact on Japan and the East Asian continent. Previous studies addressing the variability of the Kuroshio Current and the Oyashio Current off Japan mainly focused on the transition from the last glacial maximum to the Holcene (Sawada and Handa 1998) and information on the migration of the Kuroshio-Oyashio front over longer time scales is currently lacking.

In this study, we reconstructed sea surface temperature changes of the Kuroshio and Oyashio Currents over the last 8.1 Myr by studying the lipid inventory of deep-sea sediments recovered from the Nankai Trough area (SE Japan) during IODP Expedition 333. Results of this investigation showed that TEX_{86}-derived sea surface temperatures (SSTs) were warmest during the late Miocene with subsequent cooling over the length of the record. SST declined by ca. 5 °C between 7.4 and 5.5 Myr ago, and cooled an additional 8 °C from the early Pliocene warm period, about 3.7 Myr ago, into the recent Pleistocene ice ages. Similar trends in the SST variation, although somewhat different in magnitude, were also obtained from the distributions of C_{37} di- and triunsaturated alkenones ($U^{K'}_{37}$) and long chain diols (LDI) in the Nankai Trough deep-sea sediments. Our record is thus consistent with other sea surface temperature data reported from the central NW Pacific (LaRiviere et al. 2012), which also show a general warming trend from the early Pleistocene to the late Miocene. When viewed in concert with previous SST estimates from the Western Pacific Warm Pool (Nathan and Leckie 2009; LaRiviere et al. 2012), our new SST record of the NW Pacific also reveals that late Miocene meridional SST gradients were reduced relative to those of the Pliocene and that the cooling trend in SST starting in the late Pliocene may be related to the closing of the Indonesian Seaway, which resulted in the reorganization of ocean current circulations in the NW Pacific.

Despite the overall similarity in the long-term cooling trend for the NW Pacific, our record differed significantly from other palaeotemperature records in that it repeatedly showed periods characterized by short-lived and severe drops in sea surface temperatures by 5-7 °C. We interpret these periods as the results of the southward migration of the Kuroshio-Oyashio mixing front, leading to a stronger

influence of subarctic waters and a subsequent decline in sea surface temperatures at our study site. This agrees with an increase in the concentration of nonacosan-10-ol, a specific biological marker for members of the Pinaceae such as *Pinus* and *Picea* (Jetter et al. 2006), which have been reported to proliferate in the north of Honshu and Hokkaido during the last glacial periods (Inagaki et al. 2009). We also observed an increase in the relative proportion of C_{32} *n*-alcohols during glacial periods. The presence of this component is considered to indicate an aeolian input of C_4 plant material, known to contain high concentrations of the C_{32} homologue (Schwark et al. 2002) and which have been reported to expand in East Asia during the Pleistocene (Collatz et al. 1998).

Our SST record of the Nankai Trough deep-sea sediments provides first evidence that late Miocene SSTs off Japan were significantly warmer than present (by 5–6 °C), and that there was nearly unidirectional cooling over the past 8 Myr. Our results also show that variation in the strength and flow pattern of the Kuroshio and Oyashio Currents excerted a major control on the climate of the NW Pacific and associated vegetation changes on Japan and the East Asian continent.

References:

Collatz, G.J., Berry, J.A., Clark, J.S. (1998) Effects of climate and atmospheric CO_2 partial pressure on the global distribution of C_4 grasses: present, past, and future. Oecologia 114, 441-454.

Inagaki, M., Yamamoto, M., Igarashi, Y., Ikehara, K. (2009). Biomarker records from Core GH02-1030 off Tokachi in the northwestern Pacific over the last 230,000 years: Environmental changes during the last deglaciation. Journal of Oceanography 65, 847-858.

Jetter, R., Kunst, L., Samuels, A.L. (2006). Composition of plant cuticular waxes. In: Riederer, M., Müller, C. (eds.) Annual plant reviews, biology of the plant cuticle. Blackwell Publishing Ltd, Oxford, pp. 145-181.

LaRiviere, J.P., Ravelo, A.C., Crimmins, A., Dekens, P.S., Ford, H.L., Lyle, M., Wara, M.W. (2012). Late Miocene decoupling of oceanic warmth and atmospheric carbon dioxide forcing. Nature 486, 97-100.

Nathan, S.A., Leckie, R.M. (2009). Early history of the Western Pacific Warm Pool during the middle to late Miocene (similar 13.2-5.8 Ma): Role of sea-level change and implications for equatorial circulation. Palaeogeography Palaeoclimatology Palaeoecology 274, 140-159.

Sawada, K., Handa, N. (1998).Variability of the path of the Kuroshio ocean current over the past 25,000 years. Nature 392, 592-595.

Schwark, L., Zink, K., Lechterbeck, J. (2002). Reconstruction of postglacial to early Holocene vegetation history in terrestrial Central Europe via cuticular lipid biomarkers and pollen records from lake sediments. Geology 30, 463-466.

IODP

Fractionation of highly siderophile and chalcogen elements in the lower oceanic crust at Site 735B

H. BECKER[1], C. MEYER[1]

[1] Institut für Geologische Wissenschaften, Freie Universität Berlin, Malteserstrasse 74-100, 12249 Berlin. E-Mail: hbecker@zedat.fu-berlin.de

Introduction. The processes that lead to the strong fractionation of the platinum group elements, Re and Au (collectively known as highly siderophile elements, HSE) in the crust are not well understood. Compared to the mantle, abundances of Os and Ir in gabbroic oceanic crust and ocean ridge basalts (a few pg/g) are lower by a factor of 1000 or more, whereas Re is mildly enriched in the crust (factor 1.5 to 3). Likewise, the causes of the large variability of some HSE ratios (e. g., Os/Ir) in crustal rocks also remain enigmatic. Most of the variability of the HSE in crustal rocks may reflect crustal fractionation processes or reaction processes during transport in the mantle. Because most erupting basalts are sulphide saturated it has been suggested that the highly variable abundances of the HSE in basalts may reflect sulfide fractionation in the oceanic crust (e.g. Hertogen et al. 1980). Because of the limited availability of HSE data on lower crustal rocks, the detailed processes of magmatic fractionation of the HSE in different lithologies are poorly constrained (Blustajn et al., 2000; Peucker-Ehrenbrink et al., 2012). The scarcity of data also results from the difficulties in analyzing these elements at the low-pg/g level.

Among the few sections of lower oceanic crust that have been sampled, ODP Site 735b (legs 118 and 176) at the SW Indian Ridge stands out for its detailed sampling and study of a 1500 m section of tectonically exhumed middle to lower oceanic crust (e. g., Hart et al., 1999; Dick et al., 2000). Previous work indicates that the lower crust drilled at 735b is a complex lithological assemblage comprised of several major intrusive events and many secondary intrusions, with different lithologies, reflecting cumulates that formed during different stages of fractional crystallization. The data indicates a gradual change from relatively evolved lithologies near the top of the section, to more primitive compositions (mostly olivine gabbros) at depth. The deepest parts of the crust at this site have not been drilled. The primary goal of the present work was to determine the abundances of HSE and the Os isotopic composition of major lithologies (olivine gabbro, different Fe-Ti oxide gabbros, leucogabbro and various troctolitic rocks) at different depth levels of Hole 735b to study magmatic fractionation of the HSE in the deeper oceanic crust. Hypotheses and questions to be tested include: (1) Primitive gabbros may show fractionated or unfractionated HSE patterns and variable initial $^{187}Os/^{188}Os$ may reflect the influence of seawater, or, alternatively, isotopic heterogeneity of the underlying mantle. (2) Sulfides are the main control on HSE abundance distribution in the crust, but some HSE ratios, such as Os/Ir may reflect processes in the mantle. (3) Are troctolithes early cumulates or hybrid mantle rocks produced by reactive infiltration of basic melts in upper mantle dunites and harzburgites?

Analytical methods. About 60 samples were selected on the basis of previously published data to include different lithologies, samples from different depth levels, and, least altered samples. Sawn and broken pieces provided by the core repository were abraded with carborundum to remove potential surface contamination, crushed and ground to powder in an agate disk mill. About 2.5 g of powder was digested in inverse aqua regia in a high pressure asher at 320 °C. HSE separation and analytical methods (mostly isotope dilution for concentration determination) of the HSE and Os isotopes follow those established previously in our lab (Fischer-Gödde et al. 2011; Gleißner et al. 2012). Because the direct comparison with chalcogen element abundances in the analyzed sample aliquot will provide constraints on the role of early and late sulfide fractionation, we have developed isotope dilution techniques to determine the abundances of S, Se and Te in the same sample aliquot as the HSE (this work and Wang et al., 2013). Total chemistry blanks (± 1 σ) are 1.7±0.9 (recently improved to 0.4±0.3) pg Os, 16±10 pg Re, 2.3±1.9 pg Ir, 49±34 pg Pt, 14±6 pg Pd, 5±2 pg Ru,

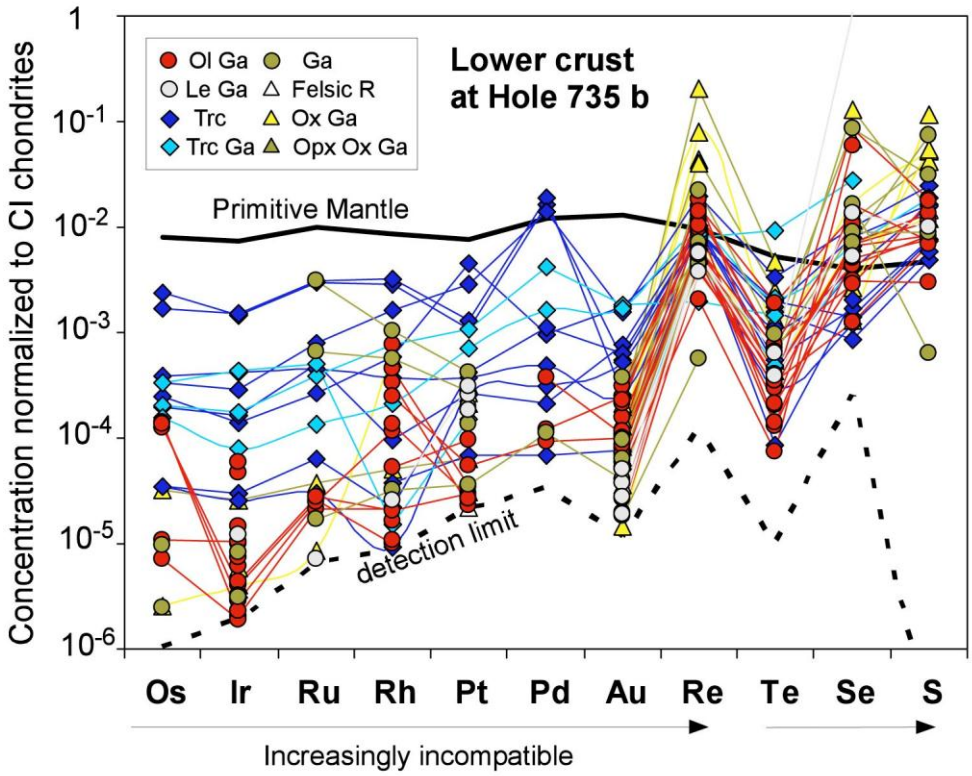

Fig. 1. Overview of abundance systematics of HSE and chalcogens in Hole 735 b. Ol, olivine, Ga, gabbro, Ox, oxide, Le, leuco, Opx, orthopyroxene, Trc, troctolite, R, rocks.

1.1±0.8 pg Rh,4±4 pg Au, 14±11 ng S, 24±13 ng Se and 9±4 pg Te. Element abundances and $^{187}Os/^{188}Os$ have been corrected for blank contributions, which range from negligible to substantial, depending on element and rock type. In chemically evolved samples, Os, Ir, Pt and Pd are often below the limit of detection (assuming 3 * 1 σ uncertainty of the total chemistry blank, Fig. 1).

General results. CI-chondrite normalized abundances of HSE in the lower crustal rocks cover a wide range of abundances (at the most extreme 10^{-3} to $<10^{-6}$ x CI chondrite for Os, the lower level reflecting a conservative estimate of the limit of detection, Fig. 1). Of note are the following features of the data: 1) Some oxide gabbros and differentiated gabbros contain more abundant sulfide than the typical olivine gabbros. In the latter individual large sulfide grains occur, which may result from coagulation of smaller sulfide droplets. 2) Troctolitic rocks tend to have higher abundances of the PGE and less fractionated HSE patterns, compared to olivine gabbros and more differentiated rocks. 3) Abundances of the PGE and Re in olivine gabbros and differentiates tend to be lower than in typical MORB, perhaps by a factor of 2 or more (Schiano et al., 1997; Bezos et al., 2005), although rare samples with high Re abundances of up to 8 ng/g may occur. The relatively low abundances of Re are consistent with previous Re concentration data obtained by HF-HNO_3 digestion on integrated strip samples from 735b (Hart et al., 1999; Blusztajn et al. 2000). 4). In the troctolites. PGE abundances decrease with decreasing Ni abundance or decreasing Mg# (Fig. 2), whereas Au, Re and the chalcogens increase or do not vary systematically. In contrast, olivine gabbros and differentiates show no clear variations of the PGE with S, Ni or Mg#, although PGE abundances in differentiated rocks are often below detection limits. S abundances in these rocks increase with Mg #. 5) Abundances of S, Se and Te range from values similar to mantle rocks (troctolites and olivine gabbros) to concentrations similar or higher than in typical MORB (Fig. 1, Hertogen et al. 1980, Yi et al., 2000). 6) Measured $^{187}Os/^{188}Os$ range from 0.129 (= chondritic) in some troctolites to > 20, reflecting the extremely large range in $^{187}Re/^{188}Os$ (1.5 in troctolites to $>10^4$ in some oxide gabbros) and radiogenic growth since 11 Ma. Initial $^{187}Os/^{188}Os$ (calculated at 11 Ma) of samples with $^{187}Re/^{188}Os < 70$ show no correlation with 1/Os, but the range of $^{187}Os/^{188}Os_i$ from 0.128 to 0.24 suggests substantial initial isotopic heterogeneity in all lithologies.

Olivine gabbro and differentiated lithologies. Relatively high concentrations of the chalcogens occur in differentiated gabbros and oxide gabbros, correlate with enhanced Re and Fe, and likely reflect enrichment of these elements in oxidized and highly fractionated late stage melts. Some olivine gabbros have S/Re, S/Se and Se/Te relatively close, but still higher than mantle rocks (Wang et al., 2013). Differentiated rocks such as oxide gabbros with enhanced S and Se concentrations display a dramatic increase of these ratios. These changes reflect changing sulfide-silicate melt partition coefficients in the course of differentiation ($D_{Te} > D_{Se} > D_{Re} > D_S$). The enrichments of the chalcogens in late stage differentiates contrasts with the low abundances of the PGE in most rocks of the series, even for some olivine gabbros with high Mg# that formed from relatively unfractionated magmas (Fig. 2). This suggests that even the primitive magmas were already quite

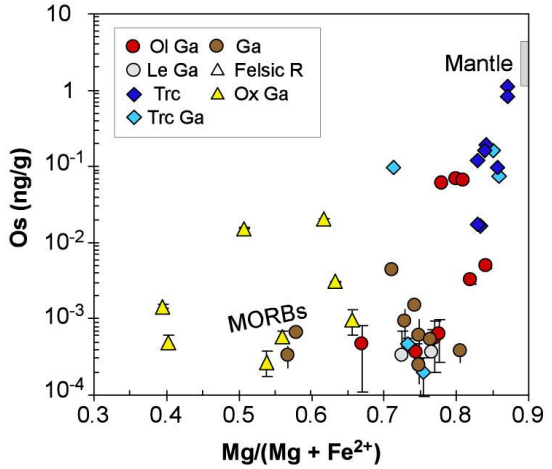

Fig. 2. Os abundances and Mg# in rocks from Hole 735b. Detection limit of Os is close to 10-4 ng/g and many samples, also "primitive" ones are at or below this value (not shown). Low Os in gabbro with high Mg# suggests that parent melts have undergone early sulfide fractionation processes.

depleted in the PGE, because the high sulfide-silicate partition coefficients of the PGE result in near-quantitative transfer of these elements into the cumulates. Accordingly, significant early PGE and sulfide fractionation likely occurred either near the crust-mantle boundary or during melt transport and reaction in the upper mantle (e. g., Hanghoj et al., 2010; Wang et al., 2013). Because of the lithological heterogeneity and large differences in the abundances of the HSE between specific lithologies, it is difficult to obtain a precise and accurate estimate of the HSE in the bulk composition of such sections (Peucker-Ehrenbrink 2012). The relatively low Re concentrations calculated in previous composites, and the very low Os concentrations of olivine gabbros and their differentiates indicate that HSE concentrations of the section may be lower than in average MORB. In particular the moderate depletion of Re (an incompatible element) in 735b contrasts with estimates for the integrated abundances of lithophile incompatible elements that suggest a more enriched composition of this drilled section compared to average MORB (Hart et al., 1999; Dick et al., 2000).

Origin of troctolitic rocks in the lower oceanic crust. Recent studies provide textural and geochemical evidence that some troctolites (s. l.) in drilled lower oceanic crust and in ophiolite sequences have formed by reactive infiltration of basic melt into olivine rocks (e. g., Suhr et al., 2008, Dick et al., 2008, Renna and Tribuzio 2011). The origin of the ultrabasic protolith of the troctolites is still debated, and could have been either olivine rich cumulates or replacive upper mantle dunites with a history of previous reactive infiltration (e. g., Kelemen et al., 1997a). In element variation diagrams, troctolites and troctolitic gabbros from hole 735b lie compositionally in-between mantle rocks on one side and gabbro compositions on the other side (Fig. 2). The relatively high abundances of the PGE in the troctolites, the decrease of PGE abundances with decreasing Ni abundance, but at the same time constant or increasing chalcogens are most easily explained by reactive infiltration of Re and chalcogen enriched basic melts in dunitic or harzburgitic mantle rocks. Initial $^{187}Os/^{188}Os$ of troctolites and troctolitic gabbros range from chondritic mantle like values to moderately suprachondritic and correlate positively with S and other chalcogen element abundances. These data also support the origin of these rocks by variable melt infiltration in chalcogen depleted upper mantle rocks (Fig. 3). The moderately radiogenic $^{187}Os/^{188}Os_i$ of chalcogen element enriched troctolites and olivine gabbros may either reflect interaction of the magma with seawater (or rocks altered by seawater), or, may be inherited from melting of enriched domains in the mantle underneath the SW Indian ridge.

Conclusions. The data on 735b and published data on a lower crustal section in the Oman ophiolite indicate that primitive Mg rich lithologies hold the key to understanding fractionation of the HSE in the oceanic crust. Low abundances of the PGE, and also Re in the most abundant lithologies at 735b hint that most of the fractionation of these elements occurs either near the Moho, or below. Both HSE patterns and abundances in the lower crust drilled at 735b and at the S part of the Oman ophiolite differ substantially. The cause and controls on these differences are not clear (spreading rate, mantle composition). The peridotite like composition of some troctolites found at relatively high stratigraphic levels in the 735b crust supports the sill model for the formation of layer 3 of very slow spreading oceanic crust (Kelemen et al., 1997b).

Outlook. Several open questions that result from the present study and comparison with MORB data and the lower crustal data from Oman can be addressed by further study of cumulates from the deepest level of the oceanic crust and troctolites and dunites that have formed in faster spreading oceanic crust: What are the compositions, processes and fractionation of HSE in cumulates near the base of the oceanic crust? Are there significant differences in HSE and chalcogen element composition between very slow, slow and fast spreading lower crust? Which geodynamic processes control these differences? Is the radiogenic initial Os isotopic composition of lower crustal gabbros and troctolites caused by contamination of magma

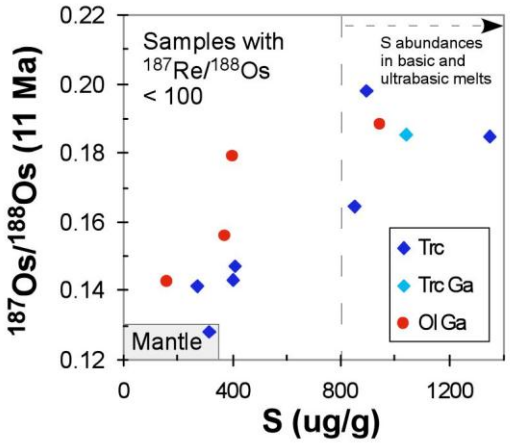

Fig. 3. Initial $^{187}Os/^{188}Os$ correlate with sulfur abundances. This data array reflects mixing of basaltic magma with radiogenic Os with mantle like Os in the troctolites, and presumably also in the olivine gabbros. Note: samples with Re/Os > 100 are not used because of uncertainties imposed by age and blank corrections.

with seawater in the lower crust, or are these signatures inherited from enriched mantle reservoirs?

References:
Bezos A. et al., 2005, Geochim. Cosmochim. Acta 69, 2613–2627.
Blusztajn et al., 2000, Chemical Geology, 168, 113 – 122.
Dick, H.J.B. et al., 2000, Earth Planet. Sci. Lett., 179, 31-51.
Fischer-Gödde et al., 2011, Chem. Geol., 280, 365 – 383.
Gleißner et al., 2012 Chem. Geol., 302-303, 33-47.
Hanghoj, K. et al., 2010, J. Petrol., 51, 201-227.
Hart, S. R. et al., 1999, Geochim. Cosmochim. Acta, 63, 4059-4080.
Hertogen, J. et al. 1980: Geochim. Cosmochim. Acta, 44, 2125 – 2143.
Kelemen, P. B. et al., 1997a, Phil. Trans. R. Soc. London, A 355, 283-318.
Kelemen, P. B. et al. , 1997b, Earth Planet. Sci. Lett, 146, 475-488.
Peucker-Ehrenbrink, B. et al. 2012, Geology, doi:10.1130/G32431.1
Renna, M. R. and Tribuzio, R., 2011, J. Petrol., 52, 1763 – 1790.
Schiano et al. 1997, Earth Planet. Sci. Lett., 150, 363 – 379.
Suhr et al. 2008, Geochem Geophys Geosyst 9, Q10007. doi:101029/2008GC002012
Wang et al.2013, Geochim. Cosmochim. Acta, in press.
Yi, W., et al., 2000, J. Geophys. Res. Solid Earth, 105, 18927-18948.

Acknowledgements: This work has been supported by DFG-SPP 527 funding (Be 1820/9-1)

IODP

Reaction of seawater with fresh oceanic gabbro generates high REE fluid fluxes and atypical REE pattern: Experiments at 425°C, 400bar

O. BEERMANN[1], D. GARBE-SCHÖNBERG[1], A. HOLZHEID[1]

[1] Institut für Geowissenschaften (IFG), Christian-Albrechts-Universität zu Kiel (CAU)

High-temperature submarine hydrothermalism along mid-oceanic ridges (MOR) creates high elemental fluxes into, and out of, oceanic lithosphere significantly affecting ocean chemistry. The hydrothermal system at 5° S on the slow-spreading Mid-Atlantic Ridge (MAR) has recently been discovered and it is suggested, that hydrothermal venting intensified after a volcanic eruptive event in 2002 [1]. The Sisters Peak and Turtle Pits vents are hosted in young lava flows at water depths of ~3000 m (~300 bar) and emanate extremely hot fluids (> 400°C) [2] containing high concentrations of dissolved gases (e.g., H_2), transition metals, and rare earth elements (REE). The normalised [3] REE pattern of these 'ultrahot' fluids are uncommon as they exhibit depletions of LREE and no Eu-anomaly ('special' REE-signature in [4]), which is in contrast to the "typical" LREE enrichment and pronounced positive Eu-anomaly known from many Mid-Ocean Ridge (MOR) vent fluids observed world-wide [e.g., 5] (Fig. 1).

Although hydrothermal fluid REE-signatures may play a key role in understanding processes during water-rock interaction, only few experimental data have been published on REE distribution in seawater-like fluids reacted with variably altered rocks from the ocean crust [e.g., 6, 7]. Besides temperature, the seawater-to-rock ratio (w/r ratio) strongly affects water-rock reaction processes and, thus, has significant control on the fluid chemistry [e.g., 8, 9].

To understand how vent fluid REE-signatures are generated during water-rock interaction processes along MOR we followed two experimental strategies investigating (i) the effect of fluid composition, and (ii) the effect of seawater-to-rock ratio on the REE distribution between reacted fluid and gabbroic rock. These strategies

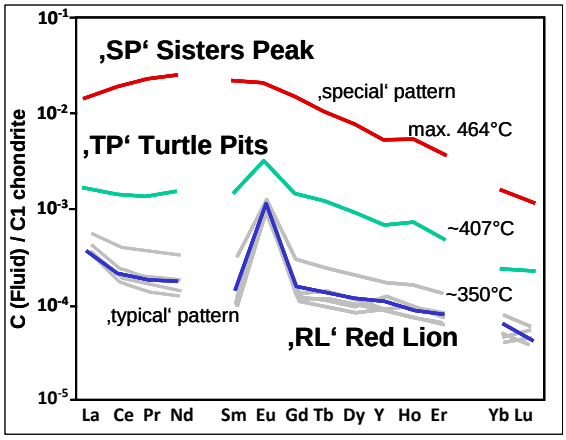

Fig. 1: C1-normalized [3] REE-pattern of hydrothermal vent fluids emanating at MAR 5°S. Fluids from the Red Lion vent field exhibit REE pattern that are typical for MOR vent fluids world-wide [e.g., 5]. The 'special' REE signature of Sisters Peak fluids displays LREE depletion and no Eu-anomaly.

have been implemented by using common high p-T autoclaves, so called cold seal pressure vessels (CSPV) that allow fluid sampling after cooling down to room temperature and decompression.

A series of experiments was conducted with mineral assemblages from fresh, unaltered gabbro (Atlantis Massif, 30°N MAR, Site U1309D, IODP expedition 305) that reacted in gold capsules with different fluid types - natural bottom seawater collected at MAR 5°S, and synthetic 3.2 wt.% $NaCl_{(aq)}$ fluid. Mixtures of 125-500 µm-sized hand-picked clinopyroxene (Cpx) and plagioclase (Plag) grains reacted with the fluids. Subsequently, fluids were extracted from the Au-capsules after cooling and analysed by ICP-OES and ICP-MS.

Cpx and Plag mixtures with a Cpx/Plag mass proportion of 1 (in the following denoted as gabbro) reacted at 425°C and 400 bar with both fluid types. In the seawater experiments the w/r ratio varied from 1-100 and the run duration was 3 d. In the NaCl(aq) experiments the w/r ratio was fixed at 10 and the run duration was 3, 10, and 30 d. Only in the seawater experiments, the gabbro reacted considerably with the liquid resulting in a strong REE enrichment relative to the original seawater (Fig. 2a). Increasing w/r ratios gave rise to decreasing pH of the quench fluid (Fig. 2b) and enforced the enrichment of HREE in the fluid with relative depletions of LREE and no Eu-anomaly (Fig. 2a). The 'special' REE-signatures observed in Sisters Peak vent fluids at 5°S MAR could be reproduced in our seawater experiments at a w/r ratio of 5 (pH = ~6.2), whereas the fluid exhibited the "typical" REE pattern with a positive Eu-anomaly at a w/r ratio of 1 (pH = ~6.3). Fluids from experiments with w/r ratios ≥10 (pH ~5.7 to ~2) showed higher HREE enrichment than observed in natural MOR vent fluids so far. Although the REE concentrations in the reacted NaCl(aq) fluids were in many cases close to the detection limit, a clear trend of increasing REE mobility in the fluid with decreasing quench pH was observed (Fig. 2c), except for Eu (not shown). Mass balance calculations revealed, that in the seawater experiments at high w/r ratio (50-100) the gabbro lost ~10-25 rel.wt.% of HREE to the fluid, whereas at low w/r ratios (≤ 5) the general loss of REE was below 1 rel.wt.% (Fig. 2d).

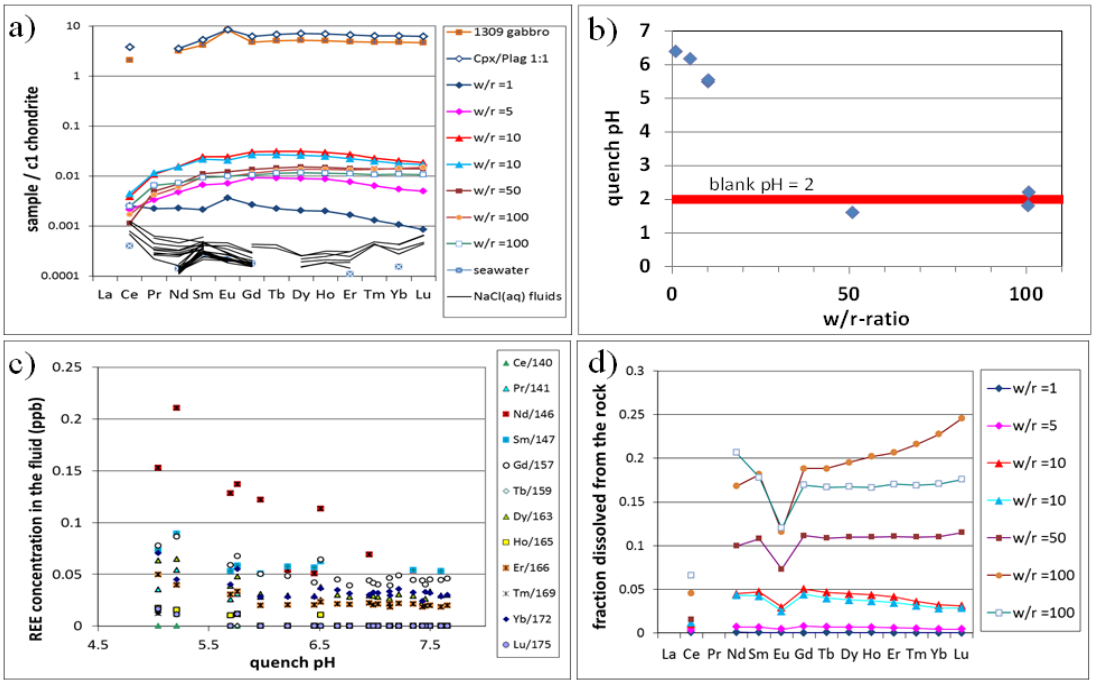

Fig. 2: Results of the expetriments carried out at 425°C, 400 bar and a run duration of 3 d: (a) C1-normalized REE-pattern [3] of the seawater- and NaCl(aq) fluids reacted with gabbro; (b) pH of the quenched seawater fluids (quench pH) reacted with gabbro. The red bar assignes the quench pH of the "blank" experiments with seawater only; (c) the REE concentration vs. quench pH of NaCl(aq) fluids reacted with gabbro; (d) the fraction of REE dissolved from the fresh gabbro into the seawater fluid, calculated by mass balance. (Note: La is not shown due to contamination during the experiments, and Pr was below detection limit in the rock.)

However, these losses of REE did not significantly change the bulk gabbro REE pattern. It is noteworthy, that heated seawater fluids from "blank" experiments with no mineral charge were extremely acidic and had a quench pH of 2 (Fig. 2b), which is distinctly different from bottom seawater (pH ~8). Thus, an important mechanism for enhanced REE mobilisation from oceanic crustal rocks is the decrease of pH during (magmatic) heating of seawater producing a highly reactive hydrothermal fluid. This will be "titrated" by the host rock during water-rock interaction processes. The drop in seawater pH during its downward flow through the crust is temperature-dependent, and this might define the conditions that are required to develop a hydrothermal fluid-recharge/rock-leaching zone (generally referred to as "recharge zone").

The product of w/r ratio and duration of water rock-reaction processes can be considered as the fluid flux. This in turn controls the reaction rate of fluid-recharge and rock-leaching processes in hydrothermal MOR recharge zones. The relatively low pH of Sisters Peak- (pH ~3), Turtle Pits- (pH ~5) [2], and many other seafloor hydrothermal fluids (pH ~2.5 to 6.6) [10] suggest incomplete titration of the acidic fluid by the host rock that may result from either the reaction of with already altered and REE depleted rocks at a variable fluid flux, or from the reaction of seawater with partly altered rocks at high fluid flux, corresponding to short term reactions at high w/r ratios. Both low pH and high REE concentrations of Turtle Pits and, in particular, Sisters Peak fluids suggest that seawater reacted with relatively unaltered rock at high fluid fluxes.

Based on our experimental results at 425°C and 400 bar we modeled the time- and w/r ratio-dependent changes in REE pattern of rock and fluid during leaching processes ocurring in hydrothermal recharge zones. We applied incremental time steps of 3 days assuming that REE partitioning between fluid and rock is constant and follows Henry's Law behavior. Each time-step represents a closed system water-rock interaction process with fresh seawater reacting with progressively leached gabbro. Figure 3 illustrates that leaching of gabbro by a hydrothermal seawater fluid produces a positive Eu-anomaly in both, the gabbro and the fluid. Our results support the assumption that the evolution of U-shaped REE pattern with a positive Eu-anomaly as observed in altered natural gabbro and serpentinites from 15°20'N MAR and interpreted to result from "fluid-dominated serpentinization" [11] should be indeed indicative for water-rock interaction processes at high w/r ratios, lasting e.g., for 0.5-2 years at w/r ~10, or for 2-10 years at w/r ~5. However, those U-shaped pattern with HREE enrichment of the corresponding fluids have not yet been observed in MOR hydrothermal vent fluids. This discrepancy may result from the faster dissolution kinetics of LREE relative to HREE, being more relevant for leaching processes during continuous percolation of heated seawater.

Although relative differences in LREE and HREE concentrations are obvious in natural and experimental fluids (Turtle Pits vs. experimental fluid at w/r = 5, and Sisters Peak vs. experimental fluid at w/r = 10) their ∑REE contents are similar within one order of magnitude. Time-resolved calculations of the changes in ∑REE fluid and rock contents (Sum REE* in Fig. 4a,b where REE* refers to REE excluding La) as well as calculations of REE* fluid flux (Fig.4c) and cumulative REE* discharge, yield estimates of the temporal evolution of element-discharge and element discharge-rates, respectively, during the initial phase of MOR hydrothermalism (Fig.4). This scenario might be suggested for the Sisters Peak and Turtle Pits

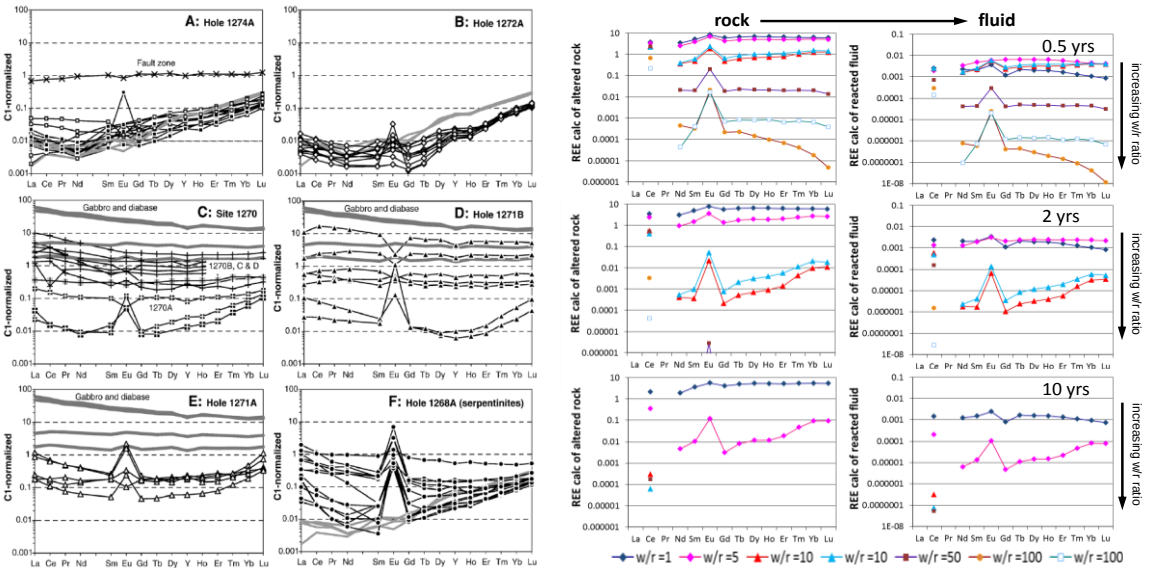

Fig. 3: (left) C1-normalized REE pattern of variably altered rocks from 15°20'N MAR [11]: (A) Harzburgite and Dunite, (B) iowaite-bearing serpentinites, (C, D, E) gabbro and diabas, and (F) serpentinites with strong Eu-anomaly and pronounced U-shaped pattern, formed during high-temperature "fluid-dominated serpentinization" [11]. (right) The modeled time-dependent evolution of REE pattern over 0.5, 2, and 10 years for progressively altered gabbro ("rock") and corresponding reacted "fluid" caused by incremental leaching with seawater at 425°C, 400 bar and variable water-to-rock ratios (w/r = 1-100). The duration of leaching process in "yrs" correspond to cumulative 3-day time steps (which is the experimental duration; further explanation is given in the text). The REE pattern calculated for the altered gabbro at w/r = 5 and w/r = 10 are strikingly similar to those of the altered rocks from 15°20'N MAR. The calculated REE signatures of the fluids and corresponding gabbro are nearly identical. However, such U-shaped REE pattern are not yet observed in MOR hydrothermal fluids and may represent equilibration of seawater and rock. (*Note*: La is not shown due to contamination during the experiments, and Pr was below detection limit in the rock.)

fluids. The ΣREE* of fluid and progressively altered gabbro rapidly decrease at w/r ≥ 5 (Fig. 4a,b). Starting the reaction with fresh rock at w/r ≥ 10 fluid composition drops to 50 %rel. of its "initial REE*" already after ~20-60 d, and after ~1 yr at w/r = 5, but only after more than 10 yrs at w/r = 1 (where "initial REE*" means the experimentally obtained REE concentration in fluids reacted for 3 d with the fresh, unaltered gabbro mineral assemblage).

The timescale for a 50 %rel. REE* loss from the rock would be quite similiar to that of the fluids, except for low w/r = 1 where it would take ~20 yrs. These estimates are supported by observations of dramatic changes in vent fluid chemistry from 9°-10°N East Pacific Rise within the first weeks after emplacement of new dike intrusions [12]. Even if fluids contain low total REE* at high w/r ratios the resulting high fluid flux will result in a high total REE* discharge rate, here defined as the REE* fluid flux (in ppb/d, Fig. 4c). Very high fluid REE* discharge rates within the first ~30 d after seawater started to react with fresh unaltered gabbro can in particular occur at w/r ratios ≥ 10 (Fig. 4c). The time-integrated cumulative REE* discharge from fluids (Fig. 4d) illustrates that, if seawater has no access to fresh rock, almost all REE* from the rock will be rapidly transferred by the fluid, in particular at w/r ≥ 5. The total hydrothermal element mass transfer to the ocean floor is strongly controlled by the fluid access to fresh rock, delivered either by crustal faulting or by subvolcanic intrusions. At slow-spreading ridges (e.g., the MAR) focused hydrothermal fluid-flow occurs along e.g., detachment faults [13] resulting in high fluid fluxes. Both, fluid access to fresh unaltered rock and focused fluid-flow along a faulting system might define the conditions of the Sisters Peak and Turtle Pits hydrothermal system, with slightly weaker fluid flux of Turtle Pits fluids as inferred from lower water-to-rock ratios of the experimentally reproduced REE-pattern.

Our experimental results and numerical simulations suggest that REE-signatures of mafic-hosted MOR hydrothermal fluids allow some constraints on water-to-rock ratio, time period of rock-leaching, and fluid recharge processes and can be used for time-resolved quantification of fluid elemental fluxes into the ocean. Although our similations currently follow a relatively simple approach without considering the effect of e.g., temperature, pressure, physical fluid properties, and lithology on fluid chemistry it can be demonstrated that elemental fluxes from high-temperature MOR hydrothermalism into the ocean can be extremely high if seawater fluid reacts with fresh unaltered rock. However, other geochemical approaches for determining the chemical fluxes of MOR hydrothermalism [e.g., 14, 15] may have overlooked the effect of hydrothermal interaction with "fresh-rock" as it is evident for e.g., the Sisters Peak and Turtle Pits hydrothermal systems. Such systems are expected to be not uncommon along slow-spreading oceanic ridges [15].

References:

[1] German C. R., Bennett S. A., Connelly D. P., Evans A. J., Murton B. J., Parson L. M., Prien R. D., Ramirez-Llodra E., Jakuba M., Shank T. M., Yoerger D. R., Baker E. T., Walker S. L., and Nakamura K. (2008) *EPSL* **273**, 332-344.
[2] Koschinsky A., Garbe-Schönberg D., Sander S., Schmidt K., Gennerich H.-H., and Strauss H. (2008) *Geology* **36**, 615-618.
[3] McDonough W. F. and Sun S.-s. (1995) *Chem. Geol.* **120**, 223-253.
[4] Schmidt K., Garbe-Schönberg D., Bau M., and Koschinsky A. (2010) *GCA* **74**, 4058–4077.
[5] Douville E., Bienvenu P., Charlou J. L., Donval J. P., Fouquet Y., Appriou P., and Gamo T. (1999). *GCA* **63**, 627-643.
[6] You C.-F., Castillo P. R., Gieskes J. M., Chan L. H., and Spivak A. J. (1996) *EPSL* **140**, 41-52.
[7] Allen D. E. and Seyfried [Jr.] W. E. (2005) *GCA* **69**, 675-683.
[8] Seyfried [Jr.] W. E. and Bischoff J. L. (1977) *EPSL* **34**, 71-77.

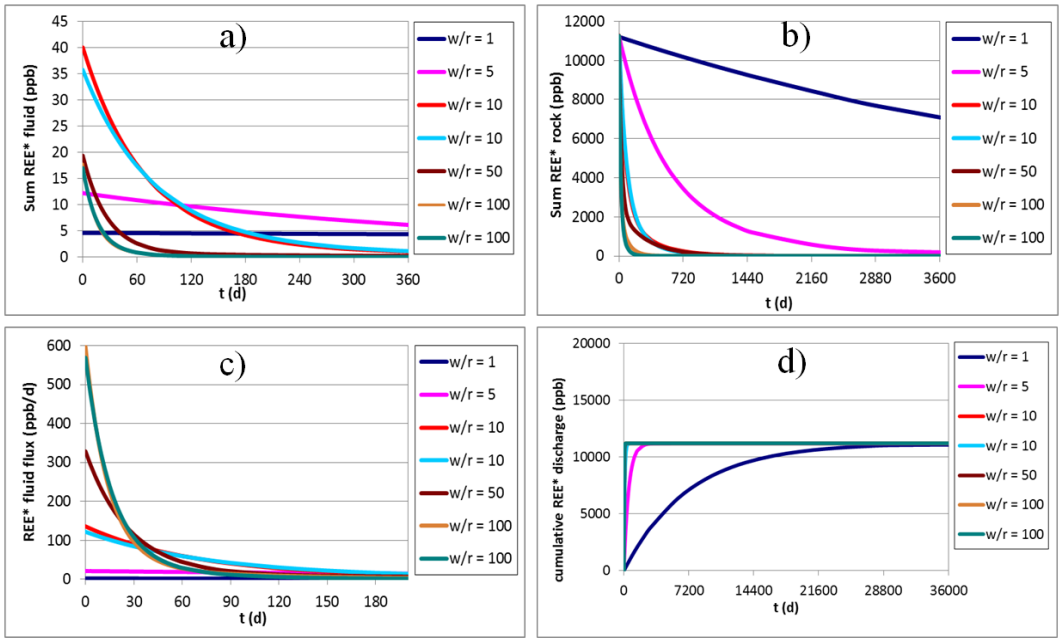

Fig. 4: Calculated time-resolved simulations based on our experimental results for seawater fluid reacted with gabbro at 425°C and 400 bar for a duration of 3d; REE* is the sum of REE without La, explanation is given in the text; (a) the time-dependent concentration of REE* in the fluids reacting with step-wise progressively leached gabbro; (b) the REE* content of gabbro,continuously leached over time by reactive seawater fluid; (c) the REE* discharge rate from the fluid (REE* fluid flux) in ppb/d deriving from (a); (d) the time integrated cumulative REE* discharge from seawater fluid reacted with progressively leached gabbro.

[9] Hajash A. and Chandler G. W. (1981) *Contrib Mineral Petrol* 78, 240-254.
[10] German C. R. and Von Damm K. L. (2003) In: Holland H. D. and Turekian K. K. (Eds.) Treatise on Geochemistry. Vol. 6. Elsevier - Pergamon, Oxford, 181-222.
[11] Paulick H., Bach W., Godard M., De Hoog J. C. M., Suhr G., and Harvey J. (2006) *Chem. Geol*. 234, 179-210.
[12] Von Damm K. L. (2000) *JGR* 105, 11203-11222.
[13] McCaig A. M. and Harris M. (2012) *Geology* 40, 367-370.
[14] German C. R., Thurnherr A. M., Knoery J., Charlou J.-L., Jean-Baptiste P., and Edmonds H. N. (2010) *Deap Sea Res*. 157, 518-527.
[15] Coogan L. A. and Dosso S. (2012) *EPSL* 323-324, 92-101.

ICDP

Core on Deck to Core Repository

Work in Progress – Status Report

V. BENDER[2], R. CONZE[1], C. KNEBEL[1], F. KRYSIAK[3], J. PÄTZOLD[2], H.-J. WALLRABE-ADAMS[2]

[1] GFZ German Research Centre for Geosciences, Potsdam
[2] MARUM, University of Bremen
[3] smartcube GmbH, Berlin

The German Scientific Earth Probing Consortium GESEP e.V.* is currently coordinating a DFG-funded project that aims for a comprehensive IT-supported infrastructure for the storage, documentation and curation of sample material gained during geoscientific expeditions on land, lakes, oceans or ice. The opportunity has been seized to test a new Drilling Information System (DIS) based on requirements of the MARUM GeoB Core Repository, University Bremen in Germany on six German expeditions performed from February to June 2012. A next cruise will follow in March 2013. The previous DIS applied by ICDP (International Continental Scientific Drilling Program) and ECORD (European Consortium for Ocean Drilling Research) used a common but specific naming convention for samples. The new DIS has been extended to allow various free formats without changing the legacy DIS data model in general. Two iterations of customization have been done so far to adjust the ExpeditionDIS used on the vessels and the CurationDIS used in the MARUM GeoB Core Repository Bremen according to the achieved feedback from the tests.

The DIS is made up of two major components: the ExpeditionDIS and the CurationDIS. While the ExpeditionDIS is designed to collect the sample data of a distinct expedition or cruise, the CurationDIS is developed to bring together the maintained data and sample collections from many expeditions in a single core repository. The intention is that geoscientific samples taken and lifted up on deck are documented and prepared for on board and later on subsampling using the ExpeditionDIS. On arriving ‘on shore’, the data is transferred from the ExpeditionDIS into the CurationDIS of the corresponding core repository while the physical sample materials are ready to be stored in appropriate ways. This includes the assignment of IGSNs (International Geo Sample Numbers) as worldwide unique sample identifiers both offshore and onshore. The CurationDIS itself shall serve as source for sample metadata that will be made available to the community at the overarching GESEP Core Repository Portal which will be online in 2014.

*)GESEP e.V.: In order to pool the existing potential and expertise while preserving the dispersed local activities, the German Scientific Earth Probing Consortium (GESEP) was found in 2008 as a non-profit association, primarily composed of 11 institutions, universities and other German research institutes. The number of members has meanwhile increased to 15.

ICDP

Fluid Migration in Ordovician and Silurian Rocks of the Siljan Impact Structure (Sweden) – Insights from Geochemistry

U. BERNER[1], O. LEHNERT[2,3], G. MEINHOLD[4]

[1] Bundesanstalt für Geowissenschaften und Rohstoffe, Hannover, Stilleweg 2, Germany; ulrich.berner@bgr.de
[2] GeoZentrum Nordbayern, Lithosphere Dynamics, University of Erlangen-Nürnberg, Schloßgarten 5, D-91054, Erlangen, Germany; lehnert@geol.uni-erlangen.de
[3] Department of Geology, Lund University, Sölvegatan 12, SE-223 62 Lund, Sweden
[4] Department of Sedimentology & Environmental Geology, Geoscience Centre, University of Göttingen, Goldschmidtstrasse 3, D-37077 Göttingen, Germany, variscides@gmail.com

Geochemical investigations in the vicinity of Europe’s largest impact structure (Siljan, Central Sweden) focussed for years on abiogenic concepts and largely neglected state of the art inorganic and organic geochemistry to explain the presence of oil seeps and gas reservoirs in the subsurface. In our study we analyze sedimentary rocks obtained from three drill sites (Mora001, Stumsnäs 1 & Solberga 1) of the ring structure around the central uplift to investigate the hydrocarbon potential of Ordovician and Silurian strata.

Elemental analyses provided information on concentrations of carbonate and organic carbon, total sulfur as well as on the composition of major and minor elements of the sediments. The data has been used to evaluate the depositional environment and possible diagenetic alterations of the organic matter. RockEval pyrolysis and solvent hydrocarbon extraction gave insight into the hydrocarbon generation potential and the type and thermal maturity of the sediments as well as of the extent of hydrocarbon migration.

From the geochemistry data of the studied wells it is obvious that changes of depositional environments (lacustrine – marine) have occurred during Ordovician and Silurian times. Although, the quality of the organic matter has been influenced in marine and brackish environments through sulfate reduction, we observe for a number of marine and lacustrine sediments a good to excellent preservation of the biological precursors which qualify the sediments as hydrocarbon source rocks (Type II kerogens). Lacustrine source rocks show a higher remaining hydrocarbon potential (up to ~550 mg HC per g C_{org}) than those of marine or brackish environments. Our investigations indicate that the thermal maturity of organic matter of the drill sites has reached only the initial stage of oil generation.

At Mora001 and Solberga 1 a significant number of sediment samples were impregnated with oil indicating hydrocarbon migration. We do not observe any indication of an overall vertical hydrocarbon migration trend in both wells but present evidence of strata bound hydrocarbon displacement, which strongly contradicts vertical migration of abiotic hydrocarbons assumed by others to be associated with the impact event. We see evidence for an internal concentration driven primary redistribution within the Upper Ordovician Fjäcka Formation compatible with an early stage of thermal hydrocarbon generation. However, the abnormal hydrocarbon concentrations within the Lower Silurian sediments likely result from a pressure induced migration through which hydrocarbons from more mature

Lower Silurian sediment sources of the Siljan structure were forced into the marginally mature sediments of the drill sites. A scenario which would explain our observations involves a heating of the source rocks through the impact event with pressure built-up and subsequent release of fluids into the adjacent environment, which is largely compatible with observations of thermal hydrocarbon generation and redistribution at sill intrusions around the world.

IODP

Early Pleistocene sea level and millennial-scale climate fluctuations: a view from the tropical Pacific

J.L. BIBER[1], O. FRIEDRICH[1], J. PROSS[1]

[1] Institut für Geowissenschaften, Goethe-Universität Frankfurt, Altenhöferallee 1, 60438 Frankfurt/Main, Germany

This project aims at deciphering the rate of sea-level variability and its effect on millennial-scale climate fluctuations during the final phase of the intensification of northern hemisphere glaciation (NHG).

Millennial-scale climate fluctuations have increasingly become recognized as a persistent feature of the warmer climates of the latest Pliocene to early Pleistocene (e.g., Becker et al. 2006; Bolton et al., 2010). However, when compared to the well-known millennial-scale fluctuations of the late Pleistocene, the millennial-scale fluctuations under a warmer climate show markedly lower amplitudes. One hypothesis to explain this difference is an ice-volume/sea-level threshold that amplifies millennial-scale climate fluctuations and that was not reached prior to the Mid-Pleistocene Transition (MPT). However, high-resolution datasets that recently have become available (Bolton et al., 2010; Friedrich et al., unpublished data) raise concerns regarding the existence of an "ice-volume/sea-level threshold" as previously postulated. In addition, unpublished data from a pilot study covering MIS 100 from the North Atlantic (IODP Site U1313) also contradict this hypothesis, showing that the proposed threshold value was clearly reached and even surpassed during several glaciations around 2.5 Ma (i.e., 700 kyr before the MPT) without an amplification of millennial-scale climate fluctuations.

Besides questioning the proposed threshold value altogether, these data indicate that either the amplification of millennial-scale climate fluctuations before the MPT required a higher ice-volume threshold than in the late Pleistocene, that ice volume had no significant effect on the amplitude of these climate fluctuations, and/or that the available modeling-based sea-level estimates for the early Pleistocene are inaccurate.

In this project, we will study material from the tropical Pacific Ocean (ODP Site 849) for the time interval from 2.6 to 2.4 Ma (marine isotope stages 104 to 96).

For the first week of this project (starting February 2013), sampling at the IODP Gulf Coast Resporitory (GCR, College Station, Texas) was arranged. Adjacent, the first aim is the development of a high-resolution benthic forminiferal δ18O stratigraphy (using Cibicidoides wuellerstorfi), the comparison of these data with the former low-resolution δ18O stratigraphy from Site 849 of Mix et al. (1995) and tuning to the LR04 benthic isotope stack (Lisiecki & Raymo, 2005). Subsequently, a high-resolution (~700 years) benthic foraminiferal Mg/Ca and $\delta^{18}O$ dataset (using Oridorsalis umbonatus) will be generated and compared to data from the North Atlantic (IODP Site U1313) and to the well-known late Pleistocene glacial intervals.

This combined geochemical approach using oxygen isotopes and Mg/Ca of benthic foraminifera will be used to provide the following main deliverables: (1) Quantification of sea-level change during the time interval from 2.6 to 2.4 Ma; (2) Test of the hypothesis that an ice-volume threshold existed for the amplification of millennial-scale climate oscillations during the early Pleistocene (and if it did, what its value was); (3) Indepth comparison with late Pleistocene glacials; (4) Model-data comparison to assess the fidelity of modelbased sea-level estimates; and (5) Expansion and verification/falsification of already existing high-resolution sea-level estimates from the North Atlantic (IODP Site U1313).

References:

Becker, J., Lourens, L. J., and Raymo, M., 2006, High-frequency climate linkages between the North Atlantic and the Mediterranean during marine oxygen isotope stage 100 (MIS100): Paleoceanography, v. 21, no. 3, p. PA3002.

Bolton, C. T., Wilson, P. A., Bailey, I., Friedrich, O., Beer, C. J., Becker, J., Baranwal, S., and Schiebel, R., 2010, Millennial-scale climate variability in the subpolar North Atlantic Ocean during the late Pliocene: Paleoceanography, v. 25, no. 4, p. PA4218.

Lisiecki, L. E., and Raymo, M. E., 2005, A Pliocene-Pleistocene stack of 57 globally distributed benthic δ18O records: Paleoceanography, v. 20, no. 1, p. PA1003.

Mix, A. C., Pisias, N. G., Rugh, W., Wilson, J., Morey, A., and Hagelberg, T., 1995, Benthic foraminifer stable isotope record from Site 849 (0-5 Ma): local and global climate changes1995, Proceedings of the Ocean Drilling Program, Scientific Results.

IODP

Characterization of metabolically active bacteria in hydrothermal active field in the Okinawa Trough

MARCO BLÖTHE[1], ANJA BREUKER[1], AXEL SCHIPPERS[1]

[1] Federal Institute for Geosciences and Natural Resources (BGR), Stilleweg 2, 30655 Hannover, Germany

The BGR project, as part of the post-cruise research of IODP Expedition 331, Deep Hot Biosphere, shall test the hypothesis that the quantitative microbial community composition and the cultivable microorganisms in hydrothermally influenced deeply-buried marine sediments are significantly different from those in cold and temperate deeply-buried marine sediments. The previously successfully applied molecular techniques real-time PCR (qPCR) and catalyzed reporter deposition - fluorescence in situ hybridisation (CARD - FISH) shall be used as well as cultivation and stable isotope-probing to proof the existence of a deep hot biosphere, to describe it and to isolate novel microorganisms. The domains *Archaea*, *Bacteria* and *Eukarya* as well as the JS1 candidate group, *Chloroflexi*, *Geobacteraceae*, Crenarchaeota and the functional genes dsrA, mcrA, aprA, and Rubisco (cbbL) have been quantified for 20 samples so far. All genes have been detected in different copy numbers. The overall order of abundance is Archaea > Bacteria > Eukarya. Directly after IODP Expedition 331 in October 2010, culture media

were inoculated with IODP samples and the enrichment cultures are maintained since then. Growth is continuously checked about every three months and in case of growth, colonies are picked and transferred to fresh media. Several aerobic and anaerobic enrichments have been obtained so far. To explore microbial activity in the original samples microcalorimetric measurements showed a considerable activity at 90°C which was partly attributed to microbial activity. The microcalorimetric measurements revealed activity of thermophilic microorganisms in the IODP Exp. 331 samples.

IODP

Strontium Isotope Fractionation of Low Temperature Alteration Calcite in the Ocean Crust

F. Böhm[1], A. Eisenhauer[1], S. Rausch[2], W. Bach[2], A. Klügel[2], A. Niedermayr[3], J. Tang[4], M. Dietzel[5]

[1] GEOMAR, Helmholtz-Zentrum für Ozeanforschung Kiel, Germany
[2] Geoscience Department, University of Bremen, Germany
[3] Institut für Geologie, Mineralogie und Geophysik, Ruhr-Universität Bochum, Germany
[4] Department of Earth & Environmental Sciences, Tulane University, New Orleans, USA
[5] Institute of Applied Geosciences, Graz University of Technology, Graz, Austria

The calcium carbonate minerals calcite and aragonite frequently form during low temperature alteration (LTA) of ocean crust basalts (Staudigel et al., 1981). LTA carbonates represent a sink for carbon and calcium that plays a significant role in global budgets (Alt & Teagle, 1999). They further can provide records of the chemical composition of seawater (Sr/Ca, Mg/Ca ratios) on multi-million year timescales (Coggon et al., 2010; Rausch et al. 2013). However, the latter application is still debated (Creech et al., 2010; Broecker & Yu, 2011; Coggon et al., 2011).

Stable isotopes of calcium and strontium in LTA carbonate minerals may allow to evaluate the quality of the seawater chemistry records. Kinetic processes during mineral formation and diagenetic alteration during deep burial in the ocean crust can modify the composition of the LTA carbonates. These processes are expected to influence both element and isotope ratios. We therefore investigated radiogenic strontium isotopes ($^{87}Sr/^{86}Sr$), stable strontium isotopes ($\delta^{88/86}Sr$) and calcium isotopes ($\delta^{44/40}Ca$) of LTA calcites and aragonites from DSDP and ODP cores of the Atlantic and Pacific Ocean.

Isotope Fractionation Experiments

Studies of paired strontium and calcium isotope analyses of calcite and aragonite grown in laboratory experiments (5, 25, 40°C) using CO_2 diffusion techniques (Tang et al., 2008; Niedermayr, 2011) provide a baseline for interpretation of isotope effects observed in the LTA samples. Experimental precipitation studies of **calcite** revealed a strong positive correlation of $\delta^{88/86}Sr$ and $\delta^{44/40}Ca$ (R^2=0.98, n=11) resulting from kinetic isotope fractionation controlled by precipitation rate (Böhm et al., 2012). Temperature has a weak influence on both isotope systems. Temperature and precipitation rate controls on isotope fractionation are inter-dependent: rate effects are largest at low temperatures; temperature effects are largest at high precipitation rates (Tang et al. 2008).

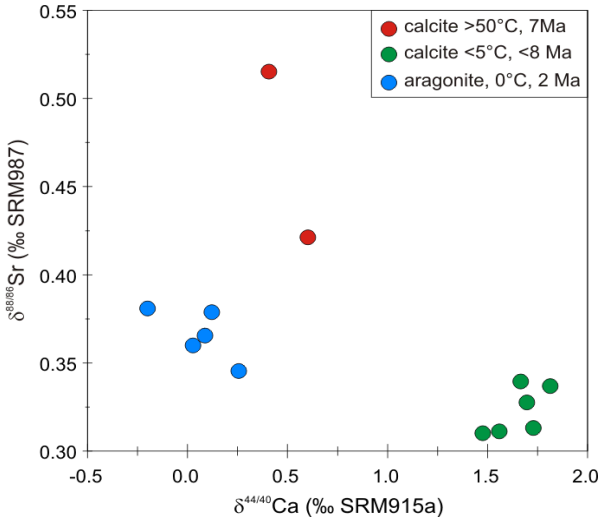

Fig. 1: Calcium and strontium isotope values of aragonite and calcite samples from young sites.

Aragonite, in contrast, displays rate dependent fractionation for calcium isotopes (Gussone et al., 2005; Niedermayr, 2011), but probably not for strontium isotopes. A temperature control on calcium isotopes was observed by Gussone et al. (2005). Strontium isotope fractionation of aragonite appears not significantly controled by temperature. No significant difference was detected in $\delta^{88/86}Sr$ of aragonite precipitated with high rates at 6, 25 and 40°C (unpublished data).

LTA Aragonite

Pure aragonite was found only at Site 409 (Reykjanes Ridge) in 2.3 Ma old basement. Carbonate precipitation ages were derived from the SIS curve of McArthur & Howarth (2004). SIS ages of 2 ± 0.2 Ma ($^{87}Sr/^{86}Sr$ = 0.70908) are in good agreement with rapid growth from unaltered seawater soon after emplacement of the basalt. The formation temperatures derived from measured $\delta^{18}O$ values between 4.2 and 4.5 ‰ (V-PDB) point to

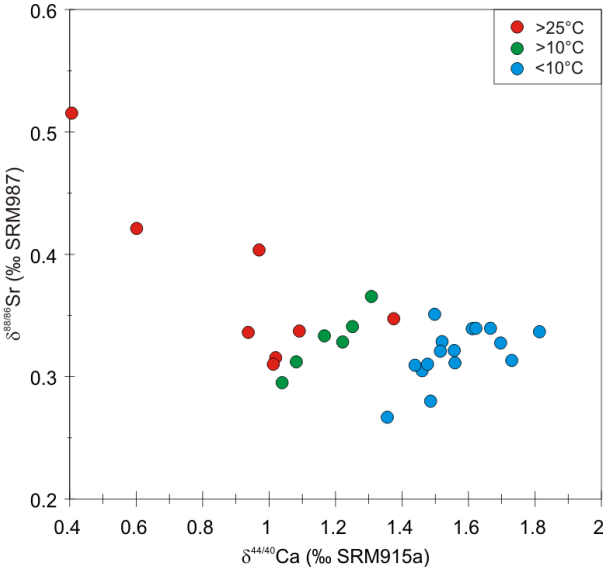

Fig. 2: Crossplot of strontium and calcium isotopes of LTA calcites.

precipitation in cold deep-water of about 0°C. Basement depths of the samples range from 13 to 168 m. The aragonites are characterized by high Sr/Ca ratios (13-14 mmol/mol) and very low $MgCO_3$ contents (<0.5 mol%).

Calcium isotopes are strongly fractionated with respect to seawater with $\Delta^{44/40}$Ca ranging from -1.6 to -2.0 ‰ ($\delta^{44/40}$Ca between -0.2 and +0.3 ‰ SRM915a). Strontium isotopes show values only slightly lighter than seawater with $\Delta^{88/86}$Sr between -0.04 and -0.01 ‰ ($\delta^{88/86}$Sr between 0.35 and 0.38 ‰ SRM987). The sample from 168 m basement depth shows slightly lighter $\delta^{44/40}$Ca and heavier $\delta^{88/86}$Sr compared to the shallower samples. However the differences are only slightly greater than the precision of ±0.13‰ and ±0.02‰ for $\delta^{44/40}$Ca and $\delta^{88/86}$Sr, respectively. Compared to young cold sites with calcite precipitation the aragonite site shows lighter $\delta^{44/40}$Ca and heavier $\delta^{88/86}$Sr values (Fig. 1).

With the very slow precipitation rates expected for these cold deep-water settings we expect isotope fractionation close to equilibrium values. Kinetic fractionation should be of minor importance. The high Sr/Ca ratios of the aragonites largely exclude Rayleigh fractionation as an explanation for the heavy $\delta^{88/86}$Sr values. The $^{87}Sr/^{86}Sr$ values close to seawater exclude significant isotope exchange between pore fluids and basalt. This suggests that the oberved differences between aragonite and calcite reflect different equilibrium fractionation of the two mineral polymorphs.

LTA Calcite

The LTA calcites samples are characterized by low Sr/Ca ratios ranging from 0.01 to 0.9 mmol/mol. Mg contents range from 1 to 26 mol% $MgCO_3$. Sites of different basement ages were sampled. Samples show SIS ages from 1 to 35 Ma. For older samples (basement ages from 57 to 165 Ma) $^{87}Sr/^{86}Sr$-dating is not possible. Basement depths of the samples ranged from 4 to 470 m. Precipitation temperatures derived from $\delta^{18}O$ values (-9.5 to +4.0 ‰, V-PDB) ranged from 0 to 60°C.

In contrast to the kinetically controlled experimental calcites, which show a very strong correlation between $\delta^{44/40}$Ca and $\delta^{88/86}$Sr, the two isotope systems appear uncorrelated in the LTA calcites. While $\delta^{44/40}$Ca shows significant variability, ranging from 0.4 to 1.8 ‰ (SRM915a), there is little variation of $\delta^{88/86}$Sr (0.27 to 0.52 ‰, SRM987), except for three samples that formed in warm fluids (Fig. 2). The lack of correlation excludes kinetic fractionation as a significant source of variability of the two isotope systems. LTA calcites probably formed in isotopic equilibrium with respect to calcium and strontium.

Calcites that grew in waters warmer than 25°C show lighter $\delta^{44/40}$Ca values than calcites grown in cold waters (Fig. 2). This is opposite to the temperature effect observed in precipitation experiments, which leads to heavier isotope values at higher temperatures (Tang et al. 2008). Most likely it reflects increased fluid-rock interaction at higher temperatures. Calcium released from basalt ($\delta^{44/40}$Ca ca. 0.8 ‰) is significantly lighter than seawater calcium (1.9 ‰) (Amini et al., 2008). The same is true for strontium, however the difference is smaller, with basalt $\delta^{88/86}$Sr=0.30 ‰ (Charlier et al. 2012) and seawater $\delta^{88/86}$Sr=0.39 ‰ (Krabbenhöft et al., 2010). Therefore the basaltic strontium has little effect on the composition of the LTA calcites. Even at sites where $^{87}Sr/^{86}Sr$ values indicate the presence of basaltic Sr in the fluid there is little variation of $\delta^{88/86}$Sr except for Site 896 (Fig. 3).

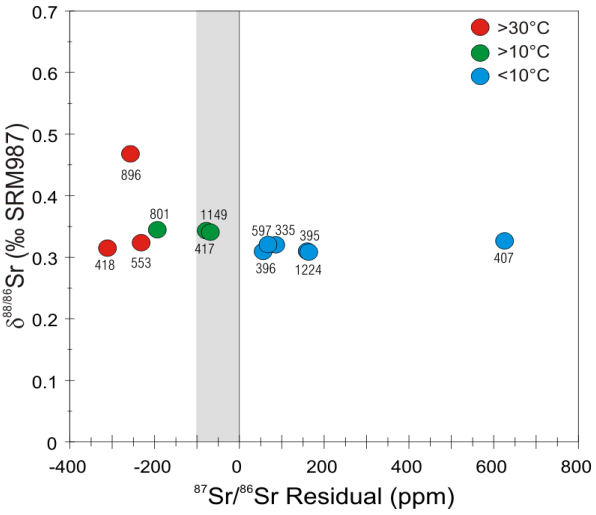

Fig, 3: Difference between measured and seawater $^{87}Sr/^{86}Sr$ values at time of basement formation. Site means of LTA calcites with average temperatures. Grey bar: isotope variation during Cretaceous.

Surprisingly at this site $\delta^{88/86}$Sr is strongly elevated with respect to basalt and seawater. Other processes than just dissolution of Sr from the basement rocks must play a role here. Site 896 is quite young (basement age 6.7 Ma) and hot (average oxygen isotope temperature 54°C). Expectedly the average $\delta^{44/40}$Ca (0.6 ‰) is much lower than for cold young sites (1.7 ‰, see Fig. 1). This indicates a strong influence of fluid-rock interaction, which is also reflected in the $^{87}Sr/^{86}Sr$ of 260 ppm lower than contemporaneous seawater Sr. Either incongruential dissolution of heavy Sr or Rayleigh fractionation increased the the fluid $\delta^{88/86}$Sr at this site. Rayleigh fractionation of Sr is however rather unlikely as the average Sr/Ca ratio of the Site 896 calcites is 0.4 mmol/mol, pointing rather to a Sr-rich than Sr-poor fluid.

Strontium isotopes of most LTA samples plot in a very narrow range slightly lighter than the modern seawater value. LTA aragonite is slightly heavier than LTA calcite and is significantly heavier than experimental aragonite. LTA calcites are slightly enriched in heavy Sr compared to experimental calcite, probably because of slower precipitation. There is no correlation between Ca and Sr isotopes of the LTA calcites, which is in obvious contrast to the experimental calcite results. The lack of correlation largely excludes rate effects as an explanation for the light Ca isotope signatures of the LTA calcites that formed in warm basement fluids (Fig. 2). More likely light basaltic Ca was enriched in these warm fluids. Some unknown process led to enrichment of heavy strontium isotopes in the same warm fluids, probably by incongruential dissolution of basalt.

Using average $\delta^{88/86}$Sr values of Sites that show no indication of basaltic strontium (data points above or within 100 ppm of the 0 residual line in Fig. 3) we can estimate variations of seawater $\delta^{88/86}$Sr through time (Fig. 4). Apparently there was little variation during the last 40 Ma. Cretaceous seawater may have been slightly enriched in $\delta^{88/86}$Sr compared to modern seawater.

Calcium and strontium isotopes show different behaviour in LTA systems, partly due to the strong isotopic

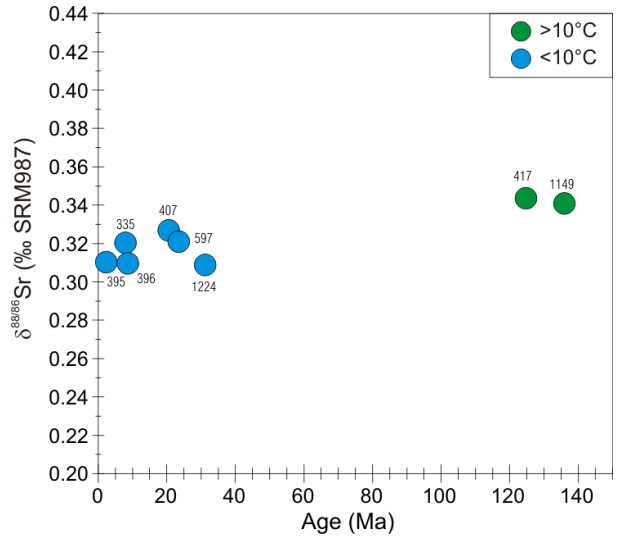

Fig. 4: Strontium isotope values of Sites with little fluid-rock interaction.

difference between basaltic and seawater calcium that is not observed for stable strontium isotopes. The data largely exclude kinetic processes during LTA calcite precipitation. Isotope exchange between basalt and calcite is indicated for some sites by the calcium isotope composition and $^{87}Sr/^{86}Sr$ of the calcites. LTA carbonates represent a sink for heavy strontium in the oceans.

References:

Alt J.C., Teagle D.A.H. (1999) The uptake of carbon during alteration of ocean crust. *Geochimica et Cosmochimica Acta* **63**, 1527-1535.

Amini, M., Eisenhauer, A., Böhm, F., Fietzke, J., Bach, W., Garbe-Schönberg, D., Rosner, M., Bock, B., Lackschewitz, K.S., Hauff, F. (2008). Calcium isotope ($\delta^{44/40}$Ca) fractionation along hydrothermal pathways, Logatchev field (Mid-Atlantic Ridge, 14°45′N). *Geochimica et Cosmochimica Acta* **72**, 4107–4122.

Böhm, F., Eisenhauer A., Tang J., Dietzel M., Krabbenhöft A., Kisakürek B., Horn C. (2012) Strontium isotope fractionation of planktic foraminifera and inorganic calcite. *Geochimica et Cosmochimica Acta* **93**, 300–314.

Broecker W.S., Yu J. (2011) What do we know about the evolution of Mg to Ca ratios in seawater? *Paleoceanography* **26**, doi:10.1029/2011PA002120.

Charlier, B.L.A., Nowell, G.M., Parkinson, I.J., Kelley, S.P., Pearson, D.G., Burton, K.W. (2012) High temperature strontium stable isotope behaviour in the early solar system and planetary bodies. *Earth and Planetary Science Letters* **329-330**, 31–40.

Coggon, R.M., Teagle, D.A.H., Smith-Duque, C.E., Alt, J.C., Cooper, M.J. (2010), Reconstructing past seawater Mg/Ca and Sr/Ca from mid-ocean ridge flank calcium carbonate veins. *Science* **327**, 1114-1117.

Coggon R.M., Teagle D. A. H., Dunkley Jones T. (2011) Comment on "What do we know about the evolution of Mg to Ca ratios in seawater?" by Wally Broecker and Jimin Yu. *Paleoceanography* **26**: doi:10.1029/2011PA002186

Creech J.B., Baker J.A., Hollis C.J., Morgans H.E.G., Smith E.G.C. (2010) Eocene sea temperatures for the mid-latitude southwest Pacific from Mg/Ca ratios in planktonic and benthic foraminifera. *Earth and Planetary Science Letters* **299**: 483-495.

Gussone, N., Böhm, F., Eisenhauer, A., Dietzel, M., Heuser, A., Teichert, B.M.A., Reitner, J., Worheide, G., Dullo, W.-C., 2005. Calcium isotope fractionation in calcite and aragonite. *Geochimica et Cosmochimica Acta* **69**, 4485–4494.

Krabbenhöft, A., Eisenhauer, A., Böhm, F., Vollstaedt, H., Fietzke, J., Liebetrau, V., Augustin, N., Peucker-Ehrenbrink, B., Müller, M.N., Horn, C., Hansen, B.T., Nolte, N., Wallmann, K. (2010) Constraining the marine strontium budget with natural strontium isotope fractionations (87Sr/86Sr*, δ88/86Sr) of carbonates, hydrothermal solutions and river waters. *Geochimica et Cosmochimica Acta* **74**, 4097–4109.

McArthur, J.M., Howarth, R.J. (2004) Strontium isotope stratigraphy. In: Gradstein, F., Ogg, J., Smith, A. (eds.), A Geologic Time Scale. Cambridge University Press, Cambridge, pp.96–105.

Niedermayr, A. (2011) Effects of magnesium, polyaspartic acid, carbonate accumulation rate and temperature on the crystallization, morphology, elemental incorporation and isotopic fractionation of calcium carbonate phases. Doctoral Thesis, 158pp., Graz University of Technology, Graz.

Rausch, S., Böhm, F., Bach, W., Klügel, A., Eisenhauer, A., 2013. Calcium carbonate veins in ocean crust record a threefold increase of seawater Mg/Ca in the past 30 million years. *Earth and Planetary Science Letters* **362**, 215–224.

Staudigel H., Hart S., Richardson S. (1981) Alteration of the oceanic crust: Processes and timing. *Earth and Planetary Science Letters* **52**, 311-327.

Tang J., Dietzel M., Böhm F., Köhler S. J., Eisenhauer A. (2008) Sr^{2+}/Ca^{2+} and $^{44}Ca/^{40}Ca$ fractionation during inorganic calcite formation: II. Ca isotopes. *Geochimica et Cosmochimica Acta* **72**, 3733-3745.

ICDP

GONAF: A borehole-based Geophysical Observatory at the North Anatolian Fault zone in NW Turkey

MARCO BOHNHOFF[1,2], GEORG DRESEN[1], FATIH BULUT[1], CHRISTINA RAUB[1], PETER MALIN[3] , HISAO ITO[4], TUGBAY KILIC[5], MURAT NURLU[5]

[1] GFZ German Research Center for Geosciences, Helmholtz-Centre Potsdam, Germany
[2] Freie Universität Berlin, Department of Earth Sciences, Germany.
[3] Institute of Earth Science and Engineering, University of Auckland, Auckland, New Zealand.
[4] Jamstec, Center for Deep Earth Exploration (CDEX), Japan Agency for Marine-Earth Science and Technology (JAMSTEC), Kanagawa, Japan.
[5] AFAD, Disaster and Emergency Management Presidency, Earthquake Department, Ankara, Turkey.

The North Anatolian Fault Zone (NAFZ) below the Sea of Marmara represents a 'seismic gap' where a major earthquake is expected to occur in the near future. The Marmara segment of the NAFZ is located between the 1912 Ganos and 1999 Izmit ruptures and is the only segment that has not ruptured since 1766. The GONAF project (Geophysical Observatory at the North Anatolian Fault; www.gonaf.de) involves the installation of a high-resolution borehole seismic observatory at the NAFZ consisting of up to eight 300m deep vertical boreholes around the eastern Sea of Marmara to monitor the NAFZ segment at the transition to the recent 1999 Izmit rupture. GONAF is an international collaboration and co-funded by the International Continental Scientific Drilling Programme (ICDP), GFZ Potsdam and the Disaster and Emergency Management Presidency in Ankara/Turkey (AFAD). Further principal partners are MIT and UNAVCO/both US, IESE/New Zealand and JAMSTEC/Japan. The principal scientific objective of GONAF is to study physical processes acting before, during and after the expected M>7 earthquake along the Princes Islands segment of the NAFZ by monitoring microseismic activity at significantly reduced magnitude detection threshold and improved hypocentral resolution. In October 2012 the first GONAF borehole was successfully drilled in Istanbul on the Tuzla peninsula and an array of borehole seismometers was installed for permanent operation. In addition a surface station at the same site was installed consisting of short period, broadband and strong motions sensors.

ICDP

Evolution of magma storage conditions along the Yellowstone Hotspot track, an experimental study on volcanic rocks from the Snake River Plain. (DFG project HO1337/22)

T. BOLTE[1], F. HOLTZ[1], R. ALMEEV[1], B. NASH[2]

[1] Institute of Mineralogy, Leibniz University of Hannover
[2] Department of Geology and Geophysics, University of Utah

The main targets of the scientific drilling project in the Snake River Plain (SRP) are the characterization of the chemical and isotopic composition of the recovered basalts and rhyolites to constrain the role of magma fractionation, recharge, and assimilation, the effects of the underlying lithosphere on magma compositions, and the temporal evolution of these magmatic processes. Information of ages and compositions of rhyolitic caldera complexes that underlie the eastern SRP is useful to determine their origin (crustal melts, mantle fractionates) and to constrain the timing of eruption and rate of mantle plume movement.

Among the general questions mentioned above, this drilling project focuses on the evolution of magma storage conditions of rhyolites and basalts in space and time. In this report we present results obtained in the first 26 months of the project. Analytical and experimental work has been conducted to trace the temporal evolution of magma storage conditions, by using natural samples from different eruptive centers along the Snake River plain. The ages of the collected natural rhyolite samples vary from 10.5 Ma to 0.6 Ma. In a first stage, particular attention is given to 12.7 to10.5 Ma rhyolitic eruptive events (Bruneau Jarbidge eruptive center) and 6.6 to 4.4 Ma events (Heise eruptive center). The natural rhyolites of all sample locations range from low to high silica, medium to high K_2O and display classical characteristics of A-type granites.

Analytical work.

Bulk rock and microprobe analyses of glasses, glass inclusions and of the main mineral phases (Pl+San+Aug+Pig+Mt+Ilm+Qtz±Fa) have been used to determine crystallization temperatures using various geothermometers (two-pyroxene and two-feldspar thermometer; ilmenite-magnetite geothermometer; Ti-in-quartz; zircon and apatite saturation thermometer). Our new results obtained from two-pyroxene thermometry for the Bruneau Jarbidge eruptive center (975°C to 994°C) confirm the temperatures determined previously by Cathey and Nash (2004). The calculated temperatures obtained for the different collected, natural eruptive units are also in a good agreement with previous published observations (Nash & Perkins, 2005; Nash *et al*, 2006; Christiansen & McCurry, 2008; Watts, 2010). Our measurements of Ti concentration in quartz (using the recent Ti-in-quartz thermo-barometer of Huang & Audetat, 2011)) indicate similar temperature range of 975 to 995°C. Pressure estimates using the Ti-in-quartz method are in the range of 315 – 375MPa for Bruneau Jarbidge eruptive center. For Heise eruptive center and other younger rhyolites magma storage pressures and temperatures are lower for younger units (up to 100 MPa and ~ 825 °C). However intermediate units of the Twin Falls eruptive center again exhibit higher pressures and temperatures (up to 500 MPa and ~ 950-1050 °C).

To complement our recently published experiments on the *oldest* rhyolites from Bruneau Jarbidge eruptive center (Almeev et al., 2012, see below), we performed second experimental study on two rhyolitic samples from the *younger* (6.63 – 4.45 Ma) Heise volcanic eruptive center. The extended analytical and petrographic work with natural samples from the Heise eruptive center was prerequisite to choose an appropriate sample for high pressure experiments. The 6.63 Ma Blacktail Creek Tuff (BCT) is a high evolved, re-welded ash-fall tuff with a relatively high crystal amount of up to 20% and the SRPY typical, anhydrous mineral assemblage. The containing minerals are rich in melt inclusions in nearly all mineral phases and the calculated temperatures are overlapping in a narrow range of 803 – 869°C over all 5 used geothermometers. The 4.43 Ma Kilgore Tuff is a nearly mineral free (<5%) high welded ignimbrite, without any melt inclusions in minerals, additionally single mafic glass chips are observable. The calculated temperature range for these samples is slightly higher than BCT and is varying over a wide range from 815 – 980°C. The results of experiments on a 6,63Ma Blacktail Creek Tuff (BCT) are summarized below and shown in Figure 1. Experiments on a 4.45 Ma Kilgore Tuff (KT) are still in progress.

Experimental work.

A. Experiments with BJR and IBR compositions (Almeev et al., 2012). A first experimental study on dry and high-temperature SRPY rhyolites was carried out to constrain phase relations representative for the old (10-12.5 Ma) Bruneau Jarbidge eruptive center (BJ). Two different samples were selected as representatives of explosive and effusive stages of silicic volcanism (Cathey & Nash, 2004). The explosive, high evolved Bruneau Jarbidge Rhyolite (BJR) sample is ~ 10.5 Ma old, crystal poor (5-15%) and characterized by the anhydrous phenocryst assemblage including Pl, San, Aug, Pig, Qtz, Mt, Ilm, fayalite (Fa), and accessory zircon (Zir) and apatite (Ap). These sample is selected from Unit 9j of the Cougar Point Tuff (Cathey and Nash, 2004). The effusive, less evolved Indian Batt rhyolite (IBR) sample is ~ 9.8 Ma old and contains the same ammount of crystalls and mineral assemblage than BJR(Cathey and Nash, 2009). Crystallization experiments were performed at 200 MPa in cold-seal pressure vessels (CSPV) at 800-850°C, and at 50, 200 and 500 MPa in internally-heated pressure vessels (IHPV) at 850-1025°C. The run duration varied from 7 to 40 days. The water activity (aH_2O) of the experimental charges was varied by adding a fluid composed of a mixture of H_2O and CO_2. In CSPV the oxygen fugacity was monitored by adding a solid Ni-NiO oxygen buffer, whereas in IHPV experiments were conducted at intrinsic oxygen conditions, corresponding to NNO+2.6 under H_2O-saturated and to

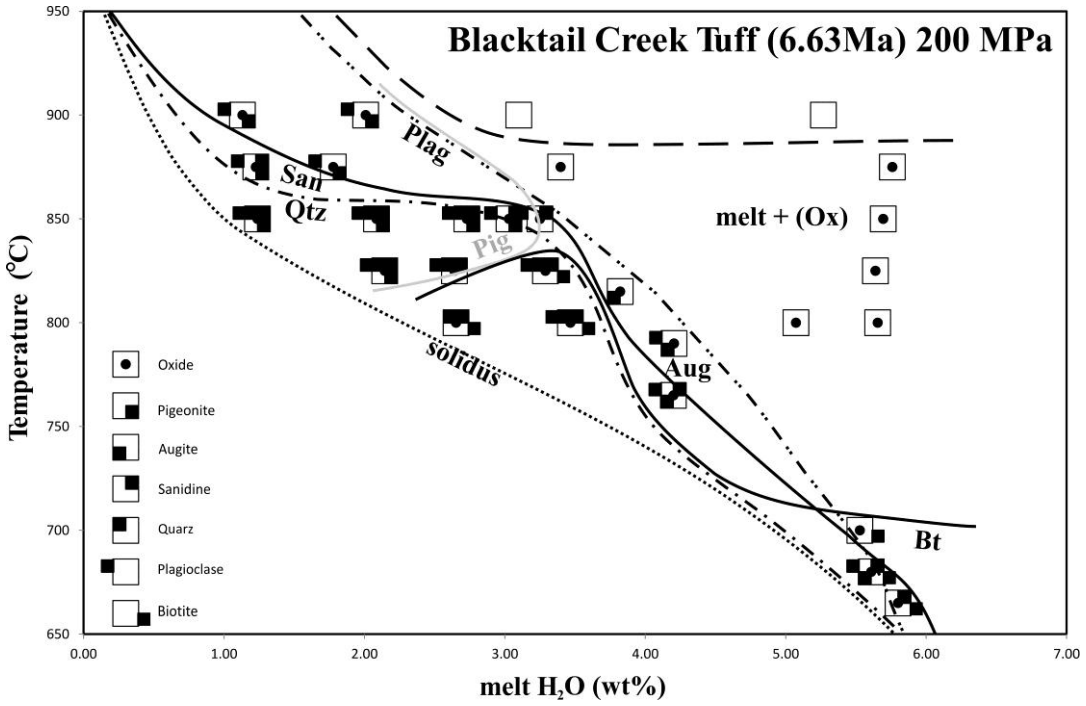

Figure 1. Phase diagram with phase stability fields for the experimental run of BCT composition at 200MPa. Lines show estimated stability fields as a function of temperature and water content in the melt. Note that Augite is always present in the natural rocks but not in the best fitting stability field of the natural sample assemblage. The pre-eruptive conditions are within the stability field of 825 - 850°C (H_2O content 1 - 3 wt%).
Abbreviations of phase symbols: Plag = plagioclase, Aug = augite, Pig = pigeonite, San = sanidine, Qtz = quartz, Bt = Biotite. Ox = Titanomagnetite/Ilmenite.

~QFM at nominally dry conditions. Additional experiments were conducted at reduced oxygen conditions down to QFM -4.5 by adding Hydrogen into the IHPV. Partial Hydrogen pressure was monitored by Shaw membrane technique to calculate oxygen fugacity. Water concentrations in most of the experimental glasses were determined using infrared spectroscopy (FTIR) or Karl Fischer Titration (KFT) (Holtz *et al*, 2001).

B. Experiments with BCT composition.

Crystallization experiments were performed at 200 MPa in cold-seal pressure vessels (CSPV) at 665 - 875°C, and at 100, 300 and 500MPa in internally-heated pressure vessels (IHPV) at 900°C for both Heise samples. These experiments were conducted without adding CO_2 as fluid phase to perform experiments near to the natural system without detectable CO_2 contents. The experimental results for BCT at 200 MPa are shown in the phase diagram in Fig. 1. The observed natural phase assemblage of BCT composition is reproduced experimentally and fits best to the natural BCT at water contents of 1 – 2.8 wt% at 850°C. For slightly lower temperatures at 825°C a water content of 2 wt% is necessary to crystallize the natural phase assemblage. At temperatures of 825°C and water contents of more than ~3 wt% the crystallization of Biotite initiates. It has to be mentioned that the crystallization of Augite is not observed over the whole range of experiments, except 3 experiments with added CO_2 fluid phase at 765, 790 and 815°C. The presence of CO_2 as a fluid phase seems to be crucial for this experiments to buffer the water activity to lower units and near to the solidus. However, the results of BCT experiments are proving again the anhydrous, near solidus character of these magmas. An additional observation is the significant shift of crystallization degree: the experiments performed at very low water contents (< 1 wt%) reach crystal cotents of >90%. Experiments with high water contents are charcterized by lower crystal abundance, e.g. run with 3 wt% H_2O has crystallinity <1%.

In the course of this experimental study a set of pre-hydrated glasses from natural Blacktail Creek Tuff samples was produced in IHPV with different melt water contents (0.2 – 10.8 wt% H_2O; H_2O determinations by FTIR and KFT). These samples were used as internal standards for determination of water contents in experimental glasses (a conventional "by difference" technique was implemented during each microprobe measurement session). The measurement of H_2O in melt inclusions with this technique is still in progress.

How hot and dry is high-T anhydrous SRPY rhyolite?

In general, our crystallization experiments support that crystal fractionation is the dominating mechanism responsible for chemical variations in rhyolite from the Bruneau-Jarbidge eruptive center, whereas for the Heise volcanic field melting of old granitic crust is the main magma producing factor. This is illustrated by the good overlap of natural petrochemical trends (lava flows, ignimbrites, air fall glasses) with experimentally determined liquid lines of descent. Furthermore the anhydrous character of the magmas from the Bruneau Jarbidge eruptive center, published by previous investigations (e.g. Honjo et al., 1992; Perkins & Nash, 2002), is verified by our experiments. Water contents of less than 1.5wt% H_2O are necessary to reproduce natural

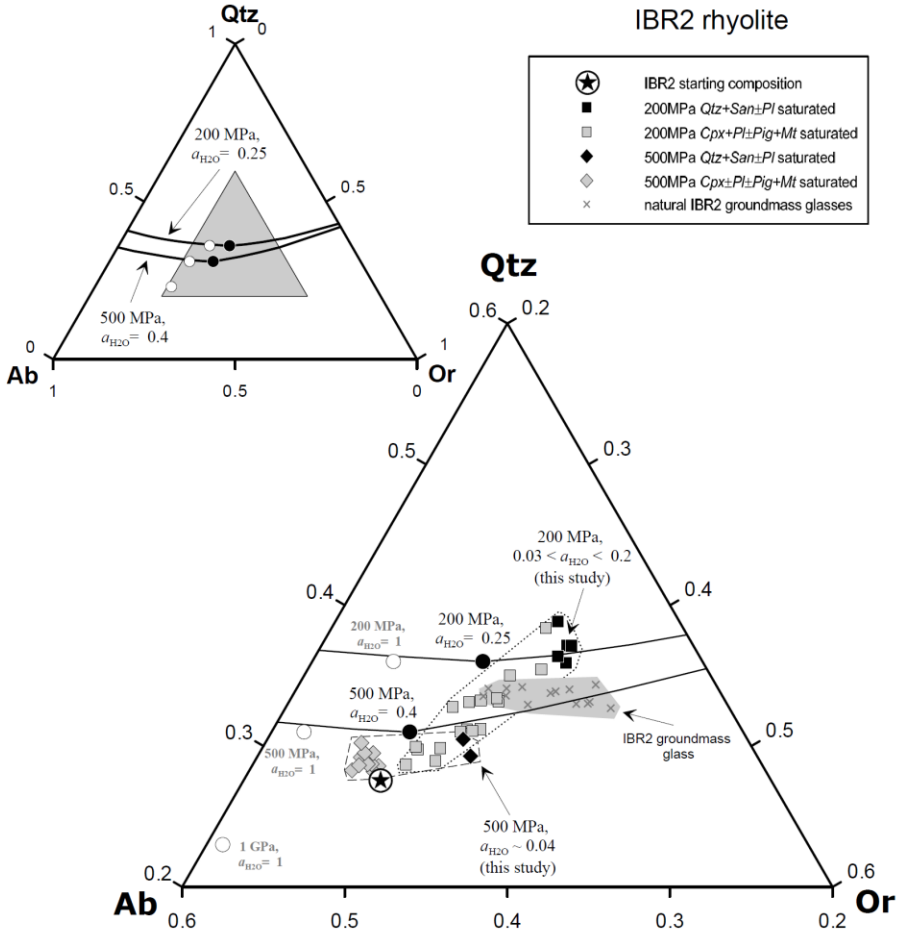

Figure 2. Ternary Qz-Ab-Or diagram with selected glass compositons of IBR experiments compared to natural glasses. Plotted are 200 and 500MPa experiments in addition to experimentally determined cotectic lines of the synthetic haplogranitic system (Holtz et al, 1992). The circles are minimum und eutectic compositions for water-saturated conditions; the black dots are minimum compositions for reduced water activities. The grey field and crosses display the range of natural matrix glass compositions.
The Qz-Ab-Or contents have been corrected for Ca using the calculation method of Cashman and Blundy (2000).

phase assemblage. The occurrence of iron-phases (magnetite, ilmenite) in the system is strongly dependent on oxygen fugacity; however, changes in oxygen fugacity do not affect significantly LLDs and the stability of phases because of the low Fe content of the systems.

The comparison of the composition of natural and experimentally synthesized phases confirms that high temperatures (> 900 °C) and extremely low melt water contents (less than 1.5 wt% H_2O) are required to reproduce the natural mineral assemblages. In melts containing ~ 0.5 to 1.5 wt% H_2O, the liquidus temperature of the more evolved composition BJR is ~940 – 1000°C and is at least 30°C lower than that of the IBR sample (970-1030°C). At 200 and 500 MPa, a minimum temperature of 920°C is necessary to reproduce the main phases in IBR. At 200 MPa, the pre-eruptive water content of the melt for IBR is constrained in the range 0.7 – 1.3 wt% at 950°C and 0.3 – 1.0 wt% at 1000°C, assuming a pressure of 200 MPa. For the same ranges of water concentration, at 500 MPa, the respective pre-eruptive temperatures are slightly higher (by ~ 30 to 50°C). It was difficult to constrain pre-eruptive conditions for BJR because one of the main natural phases, plagioclase, could only be synthesized at conditions close to the solidus. However, the compositions of natural and synthetic glasses indicate that the pre-eruptive temperature of plagioclase-free rhyolite is at least 900°C. The composition of the clinopyroxene and pigeonite pairs can only be reproduced for water contents below 1.5 wt% H_2O at 900°C, or even lower water contents if the temperature is higher. The results of experiments on BCT confirm the general relationship of temperature and water content in the melt. The natural phase assemblage of BCT is reproduced in these experiments at lower temperatures (825 - 850°C) for 200 MPa, but higher water contents in the melt (1 – 3 wt% H_2O). In this case, it was possible to synthesize plagioclase in this high evolved rhyolite but the crystallization of augite is just observable in experiments with reduced wateractivity (aH_2O) and an additional fluid (CO_2). Further work on this results is still in progress.

Depths of SRPY magma storage

The experimental results are used to explore possible proxies to constrain the depth of magma storage. The crystallization sequence of tectosilicates is strongly dependent on pressure between 200 and 500 MPa. In addition, normative Qtz-Ab-Or contents of glasses

quenched from melts coexisting with quartz, sanidine and plagioclase depend on pressure and melt water content, assuming that the normative Qtz and Ab/Or content of such melts is mainly dependent on pressure and water activity, respectively (Holtz et al. 1992). The composition of experimental glasses (melts) obtained in experiments at 200 and 500 MPa and the position of cotectic lines for the haplogranite system are reported in Fig. 2, together with the composition of natural groundmass glasses. Clearly, the experimental melts coexisting with Pl+San+Qtz have normative Qz-contents close to those of the cotectic lines at the corresponding pressure (black diamonds at 500 MPa; black squares at 200 MPa), indicating that the synthetic Qz-Ab-Or system can be used to interpret the composition of the natural rhyolitic systems.

Since the composition of the natural matrix glasses from IBR are between the cotectic lines for 200 and 500 MPa (Fig. 2), a pre-eruptive pressure of ~ 300-400 MPa can be estimated from the glass composition. This pressure estimations are in good agreement with the Ti-in-quartz method indicating a quartz crystallization pressure of ~350 MPa (assuming a temperature of 980°C). Using the same approach for BJR composition, a pre-eruptive pressure of 200-300 MPa can be deduced. Finally, it is emphasized that the petrological approach to determine pressure from the composition of glasses coexisting with cotectic assemblages (feldspar +Qtz) and which has been tested for the Snake River Plain rhyolites using experimental data may be useful for a variety of rhyolitic magmas, considering that it is extremely difficult to use geobarometers in amphibole-free rhyolitic systems.

Further objectives

The method based on projecting natural rhyolitic glasses onto ternary Qz-Ab-Or system and comparison of their compositions with cotectis experimentally derived in the range of P-aH_2O is a promisiing barometric tool. However, it still needs to be very accurately calibrated. These experiments are planned in the frame of the project HO 1337/31-1 ("*Determination of the depth of rhyolitic magma chambers in the Snake River Plain province, USA,: an experimental calibration* ") initiated in 2013.

The recently proposed Ti-in-quartz thermometer of Huang & Audetat (2011) will be verified on the basis of run products from the dataset produced on SRPY rhyolites. Additional experiments are planed to be conducted to re-calibrate/improve the thermobarometer for the investigated compositions.

Petrological investigations of basaltic and rhyolitic rocks cored at Kimama and Kimberly Sites of the Snake River plain are planed in a close collaboration with research groups of J. Shervais (Utah State University) and E. Christainsen (Brigham Young University). Core samples with no or very little alteration have been already selected for future studies during short field campaign in 2012. The geochemical characterization of selected samples was recently finished. Experimental investigations will be focused on representative samples at only selected P-T-aH_2O conditions, since systematic phase equilibria studies with completed phase diagrams have been already performed for both rhyolites (Ameev et al., 2012; Bolte et al. 2012) and basalts (Whitaker et al., 2007).

References:

Almeev, R. R., Bolte, T., Nash, B.P., Holtz, F., Erdmann, M., & Cathey, H.E. (2012): Journal of Petrology 53(9), 1837-1866.
Bolte, T. (2012): EMPG conference abstract.
Camp, V. E. and M. E. Ross (2004): Journal of Geophysical Research, 109 (B8).
Cashman, K. and J. Blundy (2000): Philosophical Transactions: Mathematical, Physical and Engineering Sciences 358(1770): 1487-1513.
Cathey, H.E., & Nash, B.P. (2009): Journal of Volcanology and Geothermal Research 188, 173–185
Cathey, H.E., & Nash, B.P. (2004): Journal of Petrology, 45, 27-58.
Christiansen, R. L., Foulger, G. R. & Evans, J. R. (2002): Geological Society of America Bulletin 114, 1245-1256.
Christiansen, E. & McCurry, M., (2008): Bulletin of Volcanology, 70(3): 251-267.
Holtz, F., Johannes W., Tamic N. & Behrens H. (2001): Lithos 56: 1-14.
Holtz, F., H. Behrens, et al. (1992): Chemical Geology 3-4: 289-302.
Honjo, N., Bonnichsen, B., Leeman, W.P., and Stormer, J.C. (1992): Bulletin of Volcanology, 54(3), 220-237.
Huang, R. & Audetat, A. (2012): Geochimica et Cosmochimica Acta, 84, 75 -89
Morgan, L.A. & McIntosh, C.M. (2005): GSA Bulletin, 117, 3/4, 288 - 306.
Nash, B. P. & Perkins, M. E. (2005): Geochimica et Cosmochimica Acta 69, A142.
Nash, B.P., Perkins, M.E., Christensen, J.N., Der-Chuen Lee, Halliday, A.N. (2006): Earth and Planetary Science Letters 247, 143-156.
Perkins, M.E., & Nash, B.P. (2002): Geological Society of America Bulletin, 114(3), 367-381.
Shervais, J. W., Kauffman, J. D., Gillerman, V. S., Othberg, K. L., Vetter, S. K., Hobson, V. R., Zarnetske, M., Cooke, M. F., Matthews, S. H. & Hanan, B. B. (2005): In: Pederson, J. & Dehler, C. M. (eds.) Interior Western United States, 1-26, doi: 10.1130/2005.fl d1006(1102).
Watts, K. E., Bindeman, I. N. et al. (2010): Journal of Petrology 52(5), 857-890.
Whitaker, M.L., Nekvasil, H., Lindsley, D.H. and Difrancesco, N.J., (2007). Journal of Petrology, 48(2): 365-393.

IODP

High mantle temperatures recorded in post-breakup MORB

P. A. BRANDL[1*], M. REGELOUS[1], C. BEIER[1], K. M. HAASE[1]

[1] LEG | Lehrstuhl für Endogene Geodynamik, GeoZentrum Nordbayern, Friedrich-Alexander-Universität Erlangen-Nürnberg, Schloßgarten 5, D-91054 Erlangen, Germany, *correspondence: philipp.brandl@fau.de

Previous studies of the geochemical composition of ancient mid-ocean ridge basalt (MORB) have shown that the upper mantle was about 50-60°C warmer in the time prior to about 80 Ma compared to zero-age (Humler et al., 1999). Possible explanations for this change in mantle potential temperature comprise a Cretaceous mantle avalanche (Machetel & Humler, 2003) or mantle temperature as a function of distance from MOR to a continent (Humler & Besse, 2002). However, previous studies used mixed geochemical data of glasses and whole-rocks with variable alteration and phenocryst content and did not investigate a possible link to the presence of a supercontinent.

Nevertheless, formation and breakup of supercontinents have a major influence on the climate, eustatic sealevel and in consequence the biosphere on timescales of 10-100 Ma. The role of a supercontinent in regard to mantle convection and thus spreading in the ocean basins has been recently addressed by various studies, focused on numerical modelling. These studies predict higher mantle temperatures on the order of 100°C higher due to the effect of 'continental insulation' (e.g., Coltice et al., 2007; Whittaker et al., 2008; Rolf et al., 2012). This temperature difference would amplify the effects on sealevel and volcanic CO_2 output associated with creation of new spreading centres. However, there is as yet no direct geochemical evidence that could confirm or quantify the continental insulation effect.

We have sampled 340 fresh glasses from 30 different sites drilled into old oceanic crust (6-170 Ma; Figure 1) and determined their chemical composition using electron microprobe and ICP-MS techniques. A zero-age MORB database has been compiled as a reference dataset including more than 9,500 glass analyses from PetDB and the Smithsonian Abyssal Volcanic Glass Data File. Our data as well as the reference dataset have been screened for the effects of alteration and inter-laboratory bias (where possible, all data have been normalised to a common preferred VG-2 glass standard). Using these two datasets of zero-age and ancient MORB, we were able to rule out regional chemical variations, a preferential sampling of off-axial lava flows by ocean drilling or biased sampling along hotspots margins as possible origin for the observed differences in geochemistry (Brandl et al., in press).

Klein and Langmuir (1987) were the first who found a clear correlation between mid-ocean ridge depth (as a function of degree of partial melting) and the geochemistry of MORB. When corrected for the effects of fractional crystallisation, Na_2O is an indicator for the overall degree of partial melting and FeO^T indicate the average pressure of melting. These two oxides can thus be used to directly estimate mantle potential temperatures from geochemical observations. Today, the methods to correct for fractional crystallisation have improved significantly. We followed the method of Kelley et al. (2006) and recalculated the primitive magma composition in a three step model combining linear and incremental methods. In the first two steps, the chemical composition is being tracked back along a slope of the liquid line of descent typical for a three phase fractionation of olv±plag±cpx. In a third step, when olivine is assumed to be the only phase fractionating from the liquid, olivine with a modal composition that is in equilibrium with the liquid is added to the melt composition incrementally (0.1% steps) until the glass composition is in equilibrium with mantle olivine (Fo=90).

The oldest MORB recovered from the Atlantic and Indian Oceans have lower Na_8, higher Fe_8 than zero-age MORB. This implies that during the early stage of ocean spreading in these two oceans, the degree of partial melting and the average pressure of melting has been greater. If interpreted as the effects of mantle potential temperature, this chemical difference indicates a mantle source hotter by 50-150°C depending on the method of calculating a primary melt composition and applied chemical thermometry for mantle potential temperatures (Figure 2).

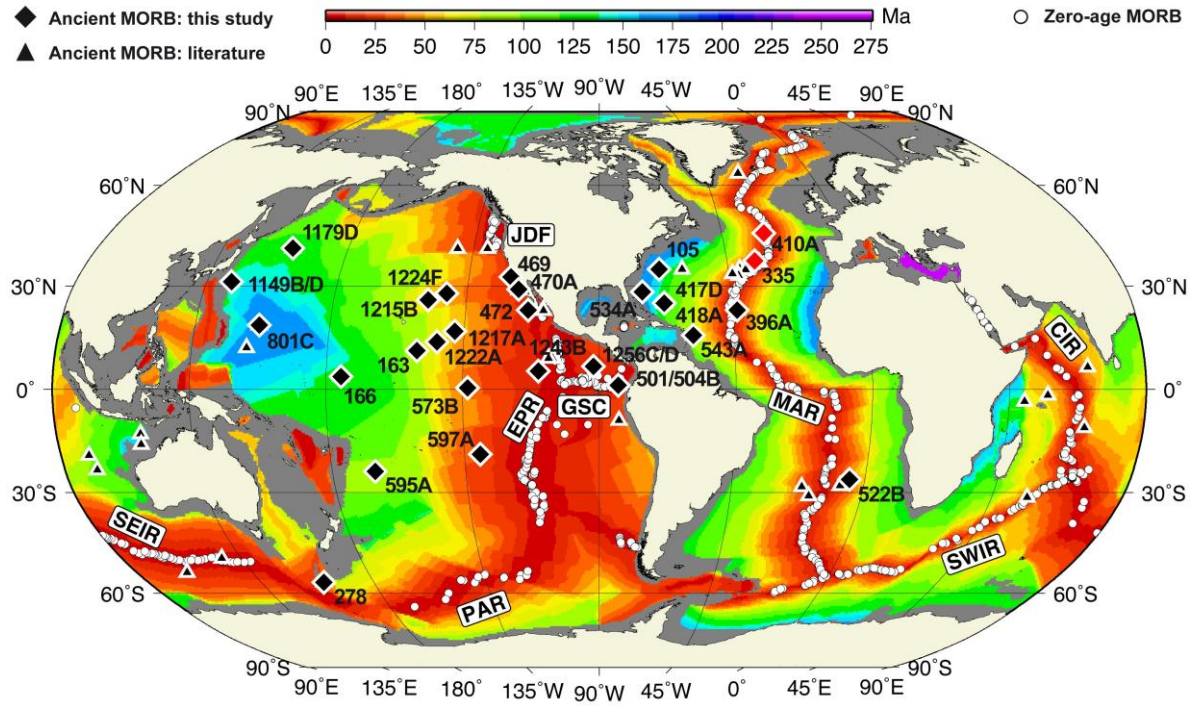

Figure 1 (modified from Brandl et al., in press): Global map showing the locations of DSDP-ODP-IODP sites sampled in our study. Colours correspond to the age of the oceanic crust as inferred from magnetic lineations (Müller et al., 2008a, b). Black diamonds represent sites located on 'normal' oceanic crust, and red diamonds represent sites that are influenced by mantle material distinct from normal MORB mantle (Azores, MAR at 45°N). Location of previously analysed samples of ancient MORB are shown by black triangles. White circles show locations of zero-age MORB samples. Abbreviations: JdF – Juan de Fuca Ridge, EPR – East Pacific Rise, GSC – Galapagos Spreading Centre, PAR – Pacific-Antarctic Ridge, MAR – Mid-Atlantic Ridge, CIR – Central Indian Ridge, SWIR – Southwest Indian Ridge, SEIR – Southeast Indian Ridge.

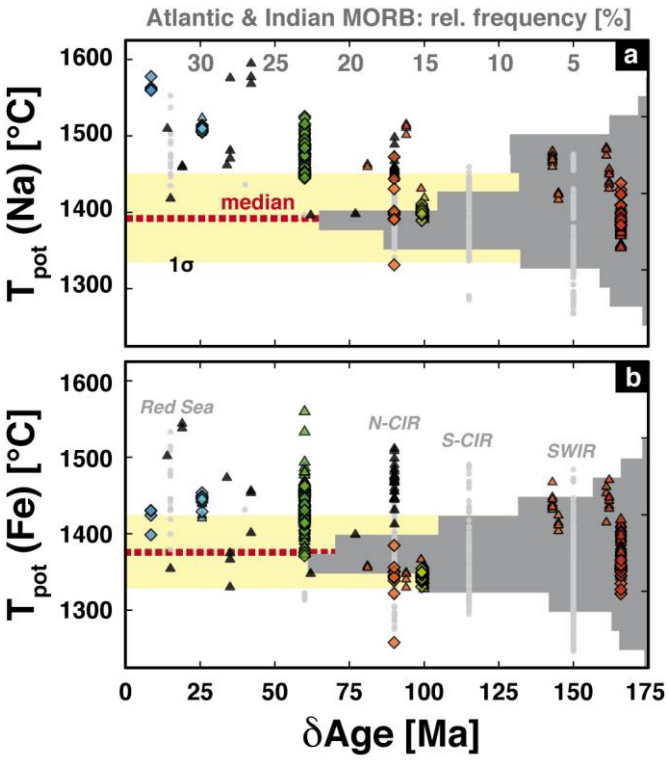

Figure 2 (modified from Brandl et al., in press): Evolution of mantle temperature with time following continental breakup. Variation of mantle potential temperature (T_{pot}) estimated using a) Na and b) Fe (Kelley et al., 2006), with the difference between eruption age and the time of local continental breakup (δAge). Black triangles; ancient Indian Ocean MORB (PetDB). Temperatures inferred from ancient and zero-age MORB erupted at spreading ridges soon after their initial development following continental rifting and breakup are 50-150°C higher than the median for zero-age Atlantic and Indian Ocean MORB (yellow field represents one standard deviation) for spreading ridges which have been in existence since continental breakup in the Mesozoic (histogram).

In contrast to previous studies, we argue that higher mantle potential temperatures during the Mesozoic are not a global phenomena but instead restricted to the proto-Atlantic and Indian Ocean. Zero-age MORB from the juvenile Red Sea-Gulf of Aden-Central Indian Ridge region (excluding those clearly influenced by the Afar hotspot) have similar major element compositions, indicating that higher mantle temperatures beneath young ocean basins result from continental insulation (Brandl et al., in press).

A subset of about 120 samples has also been analysed for trace element composition using laser ablation and solution ICPMS techniques. These samples are representative for our ancient MORB database in terms of age and geological setting. Trace element ratios sensitive to the degree of partial melting or source fertility such as La/Sm, Sm/Yb, La/Yb or $(Dy/Yb)_N$ are positively correlated with fractionation corrected Na_2O and negatively correlated with fractionation corrected FeO^T. The results from trace element analyses and modelling are currently in preparation for publication.

We show that thermal insulation of large continents influences the thermal structure of the upper mantle. These thermal anomalies persist for at least 60-70 Ma after the initiation of spreading, and would influence oceanic crust thickness, ridge depth and eustatic sealevel and the climate (by enhanced CO_2 output). Our ancient MORB database provides probably the first systematic insight into mantle temperature, source heterogeneity and melting processes affecting the petrogenesis of MORB during the lifespan of an ocean basin. Our results have important implications not only to the chemical composition of MORB but also to mantle convection and magmatism related to plate tectonic processes. The potential of continental insulation as a driving force for plate tectonics (e.g. rifting/breakup) and melting in the mantle as suggested e.g. by Anderson (1982) and Coltice et al. (2009) has to be discussed in further detail.

A related manuscript discussing the effects of continental insulation on the chemical composition of ancient MORB and the thermal structure of the mantle is currently in press for publication in Nature Geosciene and another manuscript discussing the trace element composition of ancient MORB is in preparation. This study is funded through grants RE3020/1-1 and 1-2 within SPP 527 (IODP/ODP) of Deutsche Forschungsgemeinschaft.

References:

Anderson, D. L. Hotspots, polar wander, Mesozoic convection and the geoid. *Nature* **297**, 391–393 (1982).

Brandl, P.A., Regelous, M., Beier, C. & Haase, K.M. High mantle temperatures following rifting caused by continental insulation. *Nature Geoscience* (in press).

Coltice, N., Betrand, H., Rey, P., Jourdan, F., Phillips, B.R. & Ricard, Y. Global warming of the mantle beneath continents back to the Archaean. *Gondwana Research* **15**, 254–266 (2009).

Coltice, N., Phillips, B. R., Bertrand, H., Ricard, Y. & Rey, P. Global warming of the mantle at the origin of flood basalts over supercontinents. *Geology* **35**, 391-394 (2007).

Humler, E. & Besse, J. A correlation between mid-ocean-ridge basalt chemistry and distance to continents. *Nature* **419**, 607-609 (2002).

Humler, E., Langmuir, C. & Daux, V. Depth versus age: new perspectives from the chemical compositions of ancient crust. *Earth Planet. Sci. Lett.* **173**, 7-23 (1999).

Kelley, K. A., Plank, T, Grove, T. L., Stolper, E. M., Newman, S. & Hauri, E. Mantle melting as a function of water content beneath back-arc basins. *J. Geophys. Res.* **111**, B09208 (2006).

Klein, E. M. & Langmuir, C. H. Global correlations of ocean ridge basalt chemistry and axial depth and crustal thickness. *J. Geophys. Res.* **92**, 8089-8115 (1987).
Machetel, P. & Humler, E. High mantle temperature during Cretaceous avalanche. *Earth Planet. Sci. Lett.* **208**, 125-133 (2003).
Müller, R., Sdrolias, M., Gaina, C., Steinberger, B. & Heine, C. Long-term sea-level fluctuations driven by ocean basin dynamics. *Science* **319**, 1357 (2008a).
Müller, R., Sdrolias, M., Gaina, C. & Roest, W. Age, spreading rates, and spreading asymmetry of the world's ocean crust. *Geochemistry Geophysics Geosystems* **9**, (2008b).
Rolf, T., Coltice, N. & Tackley, P. J. Linking continental drift, plate tectonics and the thermal state of the Earth's mantle. *Earth Planet. Sci. Lett.* **351-352**, 134-146 (2012).
Whittaker, J. M., Müller, R. D., Roest, W. R., Wessel, P. & Smith, W. H. F. How supercontinents and superoceans affect seafloor roughness. *Nature* **456**, 938-941 (2008).

ICDP

Bewertung von Fluidprozessen im westlichen Eger Rift

K. BRÄUER[1], H. KÄMPF[2], G. STRAUCH[3]

[1] HELMHOLTZ CENTRE FOR ENVIRONMENTAL RESEARCH – UFZ, Department Catchment Hydrology, Theodor-Lieser-Str.4, 06120 Halle, karin.braeuer@ufz.de
[2] HELMHOLTZ CENTRE POTSDAM Deutsches Geoforschungszentrum – GFZ, Department Organic Geochemistry, Telegrafenberg, 14473 Potsdam, kaempf@gfz-potsdam.de
[3] HELMHOLTZ CENTRE FOR ENVIRONMENTAL RESEARCH – UFZ, Department Hydrogeology, Permoserstraße 15,04118 Leipzig, gerhard.strauch@ufz.de

Das Eger Rift (ER) ist Teil des Europäischen Känozoischen Riftsystems. Der westliche Teil dieser ENE-WSW streichenden Struktur wird von der N-S streichenden Regensburg-Leipzig-Rostock Zone (RLRZ) gekreuzt. Zwischen Leipzig und Marienbad, mit dem Vogtland im Zentrum, ist die RLRZ seismisch aktiv. Das Vogtland ist locus typicus für den Begriff „Erdbebenschwarm", wobei Erdbebenschwärme international meist in Vulkan- oder magmatisch aktiven Gebieten auftreten. Schwärme mittlerer und hoher Intensität wurden im westlichen Eger Rift in den vergangenen 30 Jahren gehäuft aufgezeichnet (1985/86, 1997, 2000, 2008, 2011). Im Kreuzungsbereich von ER und RLRZ (Cheb Becken) und entlang der RLRZ nach Norden (Vogtland) treten Gase an der Oberfläche in Mineralquellen und Mofetten aus.

Seit 1992 wurden zur Bewertung von Fluidprozessen umfangreiche Untersuchungen der Gaszusammensetzung und der Isotopie (CO_2, He) dieser Entgasungen in der Region begonnen und mit drei, jeweils mehrjährigen Monitoringstudien an ausgewählten Entgasungsstellen mit wöchentlicher bis monatlicher Beprobung durchgeführt.

Durch Kombination von gas- und isotopenchemischer Charakterisierung mit Gasflussmessungen konnten Entgasungsstrukturen abgegrenzt und durch das detailierte Fluidmonitoring geodynamische Prozesse beleuchtet werden.

Die detaillierten Langzeituntersuchungen führten zu folgenden grundlegenden Erkenntnissen:

(1) *Regionale Verteilung der Mantelentgasungen im Vogtland und dem westlichen Eger Rift*

Im Untersuchungsgebiet konnten drei Entgasungszentren unterschieden werden – das Cheb Becken, der Marienbader Raum sowie Karlsbad und Umgebung. Alle Entgasungszentren zeichnen sich durch hohen Gasfluss und hohe CO_2-Konzentrationen im freien Gas aus. Die Isotopenverhältnisse (CO_2, He) zeigen Unterschiede, die auf Existenz mehrerer getrennter Magmenreservoire im oberen Erdmantel schließen lässt. Ganz allgemein gilt: Von den Entgasungszentren zur Peripherie nimmt der Einfluss des Mantelgasanteils jeweils ab.

(2) *Seismisch bedingte Änderungen der Isotopensignaturen*

Seismisch bedingte und zeitlich begrenzte Änderungen der Isotopensignatur der Gase wurden zuerst nach einem kleinen Schwarmbeben im Dezember 1994 beobachtet. Dabei konnte die Beeinflussung der Signatur noch in ca. 40 km Entfernung vom Epizentralgebiet in Schönbrunn (südlich Plauen) nachgewiesen werden. Es konnte gezeigt werden, dass die Änderung der Isotopensignatur durch seismisch induzierte Freisetzung von Krustenfluiden erfolgt.

Das 2000-Schwarmbeben wurde von einem detaillierten gas- und isotopenchemischen Monitoring begleitet, dass im Mai 2000 also ca. 4 Monate vor dem Beginn der seismisch aktiven Periode begonnen wurde. Ein Abfall der $^3He/^4He$-Verhältnisse wurde vor dem Schwarmbeben an allen Monitoringstellen beobachtet und als Anzeichen für Änderung des Spannungszustandes vor dem Beben interpretiert, der zur Mobilisierung kleiner Moleküle (He, H_2) führt. Nach den Beginn des Schwarmbebens traten etwa zwei Jahre lang an allen Monitoringstellen wiederholt durch Krustenfluide veranlasste Anomalien auf.

(3) *Anstieg von Mantelhelium im Cheb Becken*

Die im Mai 2000 begonnenen Untersuchungen zeigten einen im Vergleich zu den Ergebnissen der regionalen Kartierung höheren Anteil an Mantelhelium an Entgasungsstellen des Cheb Beckens und erbrachten damit erstmals den Hinweis für einen aktiven magmatischen Prozess im oberen Erdmantel unter der Region. Weiterführende vergleichende Untersuchungen unter Einbeziehung von Entgassungsstellen im Marienbader und Karlsbader Raum führten zu der Erkenntnis, dass der in der Tiefe stattfindende magmatische Prozess auf den Ostteil des Cheb Beckens in der der Nähe des Schwarmbeben-Epizentralgebietes Nový Kostel begrenzt und offensichtlich mit den wiederholt auftretenden Schwarmbeben verknüpft ist.

(4) *Detalierte Charakterisierung des Entgasungsverhaltens entlang der N-S streichenden Počatký Plesná Störungszone (PPZ)*

Von 2000 bis 2008, im Ergebnis der Charakterisierung weiterer Entgasungsstellen entlang der PPZ im östlichen Teil des Cheb Beckens zwischen Bublák und Hartoušov war ein progressiver Anstieg an Mantelhelium zu verzeichnen. Im Jahr 2000 wurden nur im Bublák-Gas $^3He/^4He$ Verhältnisse gemessen, die der Signatur des subkontinentalen Mantels entsprechen während 2005 auch im Gas der südlich von Bublák gelegenen Mofette Hartoušov die Heliumisotopenverhältnisse der Signatur des subkontinentalen Mantels entsprachen. Ausgehend von den Ergebnissen der regionalen Charakterisierung der Entgasungsstellen im westlichen Eger Rift Anfang der Neunziger Jahre korreliert der Anstieg von Mantelhelium

an der Hauptmofette in Bublák mit einem Anstieg des CO_2-Flusses um etwa 40%. Die Charakterisierung weiterer Mofetten zwischen 2005 und 2008 führte zu der Erkenntnis, dass das Gas aller untersuchten Mofetten zwischen Bublák und Hartoušov die Heliumisotopensignatur des subcontinentalen Mantels und $\delta^{13}C$-Werte von -2 ‰ aufweist.

Der hohe Gasfluss und die Mantelsignatur des Gases sprechen dafür, daß unter dem westlichen Eger Rift bis in den lithosphärischen Mantel hinabreichende hochpermeable Fluidkanäle (conduits) existieren.

(5) *Anzeichen für Magmabewegung unter dem Cheb Becken und störungsgebundene Charakterisierung seismisch bedingter geochemischer Anomalien.*

Das monantliche Monitoring zwischen 2005 und 2008 an den Lokationen, die dem Epizentralgebiet Nový Kostel am nächsten liegen zeigte, dass auch Mikroschwärme isotopenchemische Anomalien hervorrufen, wenn auch das Ausmaß der Beeinflussung wesentlich geringer als bei starken Schwärmen ist. Überraschenderweise wurde 2006 auch ein drei Monate andauernder weiterer Anstieg von Mantelhelium an den untersuchten Entgasungsstellen der PPZ und auch im Kreuzungsbereich von PPZ und MLF registriert. Dieser Anstieg wurde als Anzeichen für die Zufuhr von Magma aus einem nicht bzw. weniger entgasten Reservoir gedeutet – ein Prozess der möglicherweise den Oktoberschwarm 2008 im Epizentralgebiet Nový Kostel getriggert hat. Seit 2007 wurde auch Dolni Častkov – eine gasreiche Mofette, die am östlichen Rand des Cheb Beckens auf der MLF liegt, in die monatlichen Untersuchungen einbezogen. So konnte nach dem Oktoberschwarm 2008 das Auftreten seismisch induzierter stofflicher Anomalien entlang der PPZ und der MLF bewertet werden. Dabei zeigte sich, dass die Anomalien an Probenahmestellen entlang der MLF schneller und häufiger auftraten, als die an Probenahmestellen auf der PPZ. Das kann ein Anzeichen für das Vorhandensein unterschiedlich permeabler Migrationspfade auf den tiefreichenden, wenige Kilometer voneinander entfernt liegenden Bruchstörungszonen und/oder ein Hinweis darauf sein, dass die Hypozentralgebiet Nový Kostel näher an der MLF als an der PPZ liegt.

Im Ergebnis der vor 20 Jahren im Vogtland und dem westlichen Eger Rift begonnenen Fluiduntersuchungen ist, obwohl im Detail noch viele Fragen zu klären sind, die Wechselbeziehung zwischen Mantelentgasung/aktiven magmatischen Prozessen und den in der Oberkruste auftretenden Erdbebenschwärmen unbestritten. Obwohl mehrjährige isotopengeochemische Zeitreihenstudien mit wöchentlicher bis monatlicher Beprobung an jeweils mehreren Entgasungsstellen sehr zeit- und arbeitsaufwendig sind, bietet der Forschungsansatz ein bisher nicht ausgeschöpftes Potential, um neue Einsichten in gegenwärtig verdeckt ablaufende Fluidfreisetzungs- und -transportprozesse zu gewinnen. Die rezente, durch magmatische Intrusionsprozesse getriggerte geodynamische Aktivität im Untersuchungsgebiet ist gegenwärtig einzigartig für den Gesamtbereich des Europäischen Känozoischen Riftsystems und sollte durch eine ICDP-Initiative umfassend untersucht zu werden.

Die wichtigsten Publikationen zur den Fluiduntersuchungen im Untersuchungsgebiet :

Bräuer K., Kämpf H., Strauch G. Weise S. (2003) Isotopic evidence ($^3He/^4He$, $^{13}C_{CO2}$) of fluid-triggered intraplate seismicity. J.Geophys. Res. 108, doi:10.1029/2002JB002077.

Bräuer K., Kämpf H., Niedermann S., Strauch G. (2005) Evidence for ascending upper mantle-derived melt beneath the Cheb basin, central Europe. Geophys. Res. Lett. 32, doi:10.1029/2004GL022205.

Bräuer K., Kämpf H., Koch U., Niedermann S., Strauch G.(2007) Seismically induced changes of the fluid signature detected by a multi-isotope approach (He, CO_2, CH_4, N_2) at the Wettinquelle, Bad Brambach (central Europe). J.Geophys. Res. 112, doi:10.1029/2006JB004404.

Bräuer K., Kämpf H., Niedermann S., Strauch G. Tesař T. (2008) Natural laboratory NW Bohemia: Comprehensive fluid studies between 1992 and 2005 used to trace geodynamic processes. Geochem. Geophys. Geosys. 9, doi:10.1029/2007GC001921.

Bräuer K., Kämpf H., Strauch G. (2009) Earthquake swarms in non-volcanic regions: What fluids have to say. Geophys. Res. Lett. 36, doi:10.1029/2009GL039615.

Bräuer K., Kämpf H., Koch U., Strauch G. (2011) Monthly monitoring of gas and isotope compositions in the free gas phase at degassing locations close to the Nový Kostel focal zone in the western Eger Rift¸ Czech Republic. Chem. Geol. 290, 163-176.

Kämpf H., Bräuer K., Schumann J., Hahne K., Strauch G. (2012) CO2 discharge in an active, non-volcanic continental rift area (Czech Republic): Characterisation ($\delta^{13}C$, $^3He/^4He$) and quantification of diffuse and vent CO_2 emissions. Chem. Geol. http://dx.doi.org/10.1016/j.chemgeo.2012.08.005.

Weinlich F.H., Bräuer K., Kämpf H., Strauch G., Tesar J., Weise S.M.(1999) An active subcontinental mantle volatile system in the western Eger rift, Central Europe: Gas flux, isotopic (He, C, and N) and compositional fingerprints. Geochim. Cosmochim. Acta 63, 3653-3671.

ICDP

"Drilling the Eger Rift":

An initiative to probe intracontinental magmatic activity

S. BUSKE[1], T. DAHM[2], M. KORN[3], J. HORALEK[4], P. HRUBCOVÁ[4], B. RŮŽEK[4], T. FISCHER[5]

[1] TU Bergakademie Freiberg, Institute of Geophysics and Geoinformatics, 09596 Freiberg, buske@geophysik.tu-freiberg.de

[2] GFZ Potsdam, 14467 Potsdam

[3] Universität Leipzig, Institute of Geophysics and Geology, 04103 Leipzig

[4] Institute of Geophysics of the Academy of Sciences of the Czech Republic, 141 31 Prague, CZ

[5] Institute of Hydrogeology, Engineering Geology and Applied Geophysics, Charles University, 128 43 Praha, CZ

The western Eger rift area is dominated by ongoing magmatic processes in the intra-continental lithospheric mantle. These processes take place in absence of any presently active volcanism at the surface. However, they are expressed by a series of phenomena distributed over a relatively large area, like occurrence of repeated earthquake swarms, surface exhalation of mantle-derived and CO_2-enriched fluids, mofettes, mineral springs and enhanced heat flow, among others. At present this is the only known intra-continental region where such deep-seated, active lithospheric processes currently occur. The geodynamic nature and the implications of these processes are far from being understood, and a series of open questions remain: Is magmatic activity taking place in the upper mantle or in the lower crust ? Is it a developing large-scale fault zone or a zone of developing volcanism ? What is the geodynamic role of fluids in general and of CO_2 in particular ? What is the geodynamic relationship between geophysical and geochemical signatures of these magmatic processes ?

On the other hand, continuous seismic monitoring, active seismic surveys, fluid and groundwater level monitoring as well as GPS measurements have been carried out in this region for many years. In particular the seismic and seismological investigations performed during the last 2-3 years (see abstracts by Fallahi et al., Mousavi et al., Mullick et al.) with their focus on the topic of "fluids triggering lithospheric activity" have resulted in an increased understanding of the related phenomena. In turn this has led to the conclusion that this area is an excellent location for an ICDP drilling project targeted to a better understanding of the crust-mantle interaction in such an area of active magmatic underplating.

Our initiative of "Drilling the Eger Rift" has been established to address these questions, to create a common geophysical and geochemical frame between the former KTB site and Eger Rift, bounded at its Western and Eastern endings by scientific drilling data, and in that way to significantly contribute to understanding the intra-continental mantle-crust interaction in a broader scale.

This poster gives an overview about the objectives and goals of this drilling project and summarizes the general framework for further investigations (network of shallow boreholes, new reflection seismic profiles, etc.). The final goal will be to develop a Czech-German observatory at depth consisting of an array of several drill holes suitable for long-term monitoring experiments, accompanied by several other geoscientific studies from various disciplines, with the final aim to shed light on the ongoing geodynamic processes in that area as a whole and to yield the structural and petrophysical framework for a future ICDP drilling project.

ICDP

"Drilling the Eger Rift":

Reflection seismic imaging of the Novy-Kostel swarm earthquake area and geomechanical interpretation of related seismogenic processes

S. BUSKE[1], F. BLEIBINHAUS[2], S. SHAPIRO[3], P. WIGGER[3], B. RŮŽEK[4], P. HRUBCOVÁ[4], T. FISCHER[5]

[1] TU Bergakademie Freiberg, Institute of Geophysics and Geoinformatics, 09596 Freiberg, buske@geophysik.tu-freiberg.de
[2] FSU Jena, Institute of Geosciences, 07749 Jena
[3] FU Berlin, Department of Geophysics, 12249 Berlin
[4] Institute of Geophysics of the Academy of Sciences of the Czech Republic, 141 31 Prague, CZ
[5] Institute of Hydrogeology, Engineering Geology and Applied Geophysics, Charles University, 128 43 Praha, CZ

This project comprises a reflection seismic investigation of the Novy-Kostel swarm earthquake region as a preparatory step for a future ICDP drilling project in that region, including numerical modeling and geomechanical interpretation of the related microseismic processes.

A key to understand the general geological setting of a selected drilling target and to obtain the best possible drilling location is to derive a high-resolution seismic image of the investigation area. For that reason a new reflection seismic survey is proposed to directly illuminate and image the fault plane system of the Novy-Kostel swarm earthqakes, including a high-resolution sub-survey for characterizing the crustal structure between the swarm earthquakes and the surface. The key aspect of this research is the detection of the detailed fault zone geometry (one dominant/single fault versus a number of similar faults; strike and dip of fault planes; depth extent; etc.) as well as fluid traps in the crust and potential fluid ascent paths. Modern imaging and inversion techniques (Fresnel-Volume-Migration, Full-Waveform-Inversion) will be applied to the acquired multi-component data set and will yield a multi-scale/multi-parameter image of the crustal swarm earthquake environment. Additionally, new approaches designed to exploit secondary arrivals within earthquake recordings will be further developed and applied to swarm earthquake data provided by the WEBNET seismic network.

Furthermore, geomechanic modeling of the swarm seismicity will be performed with respect to its possible forcing by tectonic stresses and intrusions of magmatic fluids. Both, the modeling and imaging approaches will use common calibrated elastic models.

The results of these approaches will foster the understanding of the ongoing magmatic processes that lead to earthquake swarm activity in that region and will finally yield the structural and petrophysical framework for a future ICDP drilling project in that area.

ICDP

Seismic site characterization in and around the COSC-1 drillhole

S. BUSKE[1], R. GIESE[2], C. JUHLIN[3], C. SCHMELZBACH[4], H. MAURER[4], J. ROBERTSSON[4]

[1] TU Bergakademie Freiberg, Institute of Geophysics and Geoinformatics, 09596 Freiberg, buske@geophysik.tu-freiberg.de
[2] GFZ Potsdam, 14473 Potsdam
[3] U Uppsala, Department of Earth Sciences, 75236 Uppsala, Sweden
[4] ETH Zürich, Institut für Geophysik, 8092 Zürich, Switzerland

The project COSC (Collisional Orogeny in the Scandinavian Caledonides) focuses on the mid Paleozoic Caledonide Orogen in Scandinavia in order to better understand orogenic processes, both in the past and in recent active mountain belts (Gee et al., 2010). The Scandinavian Caledonides provide a well preserved example of Paleozoic plate collision, where the surface geology in combination with geophysical data provide control of the geometry of the Caledonian structure, both of the allochthon and the underlying autochthon, including a shallow W-dipping décollement surface on a thin skin of Cambrian black shales beneath the Caledonian thrust sheets. The structure of the basement underneath the décollement is highly reflective and apparently dominated by mafic sheets intruded into either late Paleoproterozoic granites or Mesoproterozoic volcanics and sandstones. The COSC project will examine the structure and physical conditions of these units, in particular the Caledonian nappes ("hot" allochthon) and the underlying basement, with two approximately 2.5 km deep drillholes, located near Åre and Mörsil in western Jämtland (http://www.sddp.se/COSC). In addition to that, the drillholes will provide unique information about the present

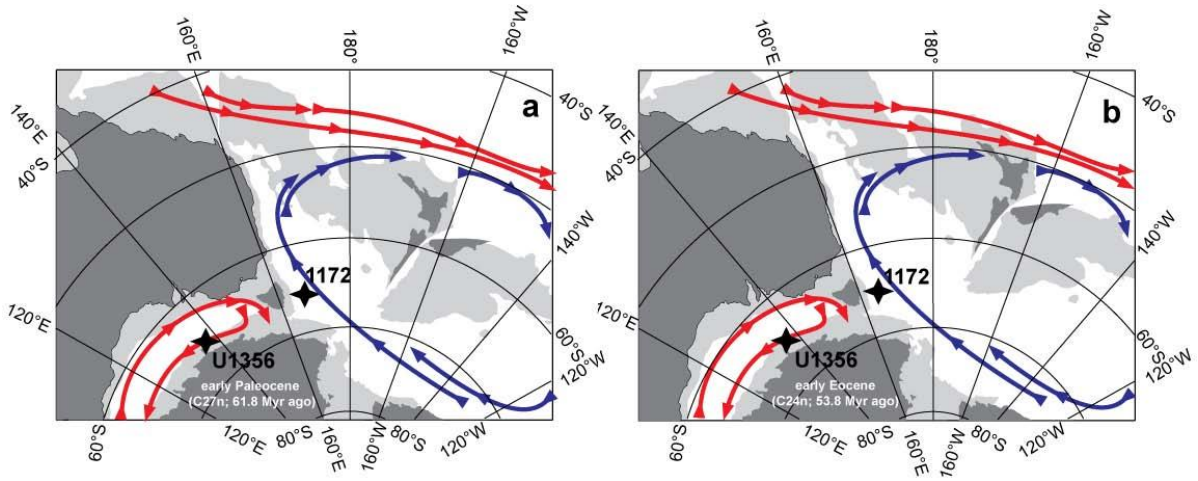

Fig. 1. Paleogeographic reconstructions of the East Antarctic/Australian sector of the Southern Ocean for the early Paleocene (left) and the early Eocene (right). Warm and cold surface-water currents are marked by red and blue arrows, respectively. Positions of IODP Site U1356 and ODP Site 1172 are indicated by asterisks. Dark grey areas indicate present-day land, light grey areas are submerged continental blocks above 300 m [after Bijl (2011), with paleogeographic reconstructions modified from Cande and Stock (2004)].

temperature gradient in the Caledonides, the porosity and permeability of the rock formations, and the petrophysical properties of the rocks at depth.

Existing regional seismic and magnetotelluric data have imaged the geometry of the upper crust, and pre-site seismic reflection survey were preformed in 2010 and 2011 to better define the exact drill site locations (Hedin et al., 2012). This project is dedicated to complement these surface seismic measurements by drillhole-based investigations to better resolve and define the small-scale structures (including lithological boundaries, steeply dipping fault segments, fracture sets, etc.) around the drillhole COSC-1. This will be achieved by a combination of seismic transmission and reflection experiments using a 3C borehole geophone system and complemented by 3C geophones at the surface, where sources and surface receivers will be aligned at different azimuths and centred around the borehole location. The data processing will employ recently developed advanced imaging techniques and will focus on, amongst other things, the analysis of anisotropic effects caused by aligned fractures and faults and their relation to the stress regime.

The results of our investigations will be high-resolution images of the fine-scale structure of faults and fractures around the borehole. This information is vital not only for a reliable spatial extrapolation of the structural and petrophysical properties observed in the borehole, but also for a thorough understanding of the tectonic and geodynamic setting, including, but not limited to, the past and present stress regime.

IODP

Paleocene to Eocene climate and vegetation dynamics in the high southern latitudes: Insights from IODP Site U1356 and ODP Site 1172

L. CONTRERAS[1], J. PROSS[1], P.K. BIJL[2], U. RÖHL[3], S.M. BOHATY[4], L. TAUXE[5], S. SCHOUTEN[6], B. VAN DE SCHOOTBRUGGE[1], A. KOUTSODENDRIS[1], H. BRINKHUIS[2,6]

[1] University of Frankfurt, Germany
[2] Utrecht University, Utrecht, The Netherlands
[3] MARUM - Center for Marine Environmental Sciences, University of Bremen, Bremen, Germany
[4] Ocean and Earth Science,, University of Southampton, UK
[5] Scripps Institution of Oceanography, La Jolla, USA
[6] NIOZ Royal Netherlands Institute of Sea Research, Den Burg, The Netherlands

The ‘Greenhouse World’ of the Early Cenozoic (65–34 million years ago, Ma) was characterized globally by warm climates and markedly higher greenhouse-gas concentrations than today (e.g., Zachos et al., 2008). Warming reached a broad maximum between 56 and 50 Ma during the late Paleocene through the Early Eocene Climatic Optimum (EECO; 53–51 Ma). Superimposed on this long-term warming trend are transient, warming events such as the Paleocene Eocene Thermal Maximum (PETM, ~56 Ma), which is characterized by a negative carbon isotope excursion (CIE) of 3–8 ‰ (e.g., Sluijs et al., 2011). The warmer conditions of the early Eocene are followed by high-latitude cooling through the middle and late Eocene. The final step of this cooling trend occurred during the Eocene-Oligocene transition when continental ice sheets rapidly expanded across Antarctica and global icehouse conditions started to develop (e.g., Zachos et al., 2008).

Considering that the Antarctic margin is presumed to have been the dominant deep-water source during the Paleogene (Thomas et al., 2003), detailed climate proxy records from the high southern latitudes are required to better understand the paleoclimate dynamics during the ‘Greenhouse World’. However, paleoclimate datasets from the circum-Antarctic region spanning this time interval are relatively sparse. For the Antarctic continent, the climate

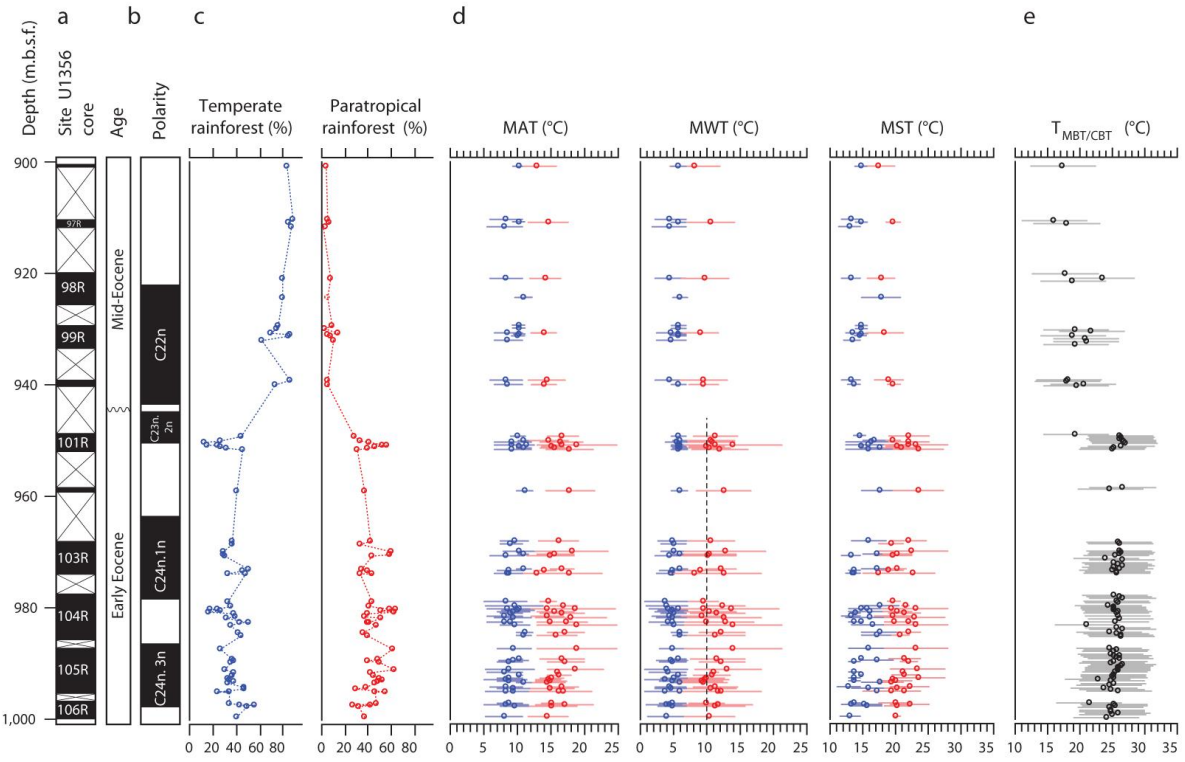

Fig. 2. Climate reconstruction for the Wilkes Land margin of East Antarctica during the early and mid-Eocene derived from Site U1356 sediments. (a) Core recovery; (b) Age model; (c) Relative abundances of sporomorphs representing temperate and paratropical rainforest biomes; (d) Estimates of Mean Annual Temperature, Mean Winter Temperature and Mean Summer Temperature for temperate (blue) and paratropical (red) rainforest biomes based on the methodology of (Greenwood et al., 2005). (e) Temperatures derived from MBT/CBT index with horizontal error bars indicating analytical error [from Pross et al., (2012)].

and ecosystem evolution through the Paleogene is still incompletely known due to the erosional obliteration and coverage of sedimentary archives by ice sheets. Hence, our current knowledge is based on reconstructions from a relatively small number of stratigraphically discontinuous records with poor age control from around the Antarctic margin.

In order to further elucidate high-latidue climates of the Early Cenozoic, we applied terrestrial palynology and MBT/CBT paleothermometry to two well-dated deep-marine sediment cores of Paleocene and early Eocene age: IODP Hole U1356A (Wilkes Land margin, East Antarctica) and ODP Hole 1172D (East Tasman Plateau, southwest Pacific Ocean) (Figure 1).

The analysis of pollen and spores combined with the MBT/CBT data from IODP Hole U1356A provides the first terrestrial climate reconstructions for the early Eocene of Antarctica. The cores from Hole U1356A comprise mid-shelfal sediments representing early Eocene (53.9–51.9 Ma) greenhouse conditions and, separated by a ~2 myr-long hiatus, an interval of presumed cooling during the latest early Eocene to middle Eocene interval (49.3–46 Ma; here informally referred to as 'mid Eocene') (Pross et al., 2012). Analyses of Paleogene pollen and spore assemblages from ODP Hole 1172D are currently in progress, with the aim of unravelling the terrestrial climate and ecosystem evolution of the East Tasman Plateau during the middle Paleocene to early Eocene (~60 to ~54 Ma). The Paleocene to lower Eocene succession of Hole 1172D is interpreted to reflect very shallow water to restricted marine conditions with marked runoff from the hinterland (e.g., Shipboard Scientific Party, 2001).

The early and mid Eocene palynological assemblages from Site U1356 represent two main biomes (Pross et al., 2012, Contreras et al., submitted.). A paratropical rainforest biome, which prevailed during the early Eocene, is interpreted to have occupied the lowlands of the Wilkes Land margin. This assemblage includes mesothermal to megathermal taxa characteristic of modern subtropical to tropical settings in Australia, New Guinea and New Caledonia. In addition to ferns and tree ferns (*Lygodium*, Cyatheaceae), it is characterized by the presence of palms (Arecaceae), Bombacoideae (Malvaceae), *Strasburgeria* (Strasburgeriaceae), *Beauprea* (Proteaceae), *Anacolosa* (Olacaceae), and *Spathiphyllum* (Araceae). The palm and Bombacoideae pollen not only represent the southernmost documented occurrences for both taxa, but, importantly, imply that winter temperatures must have remained substantially above freezing. Extant palms occur naturally only in regions with a cold-month mean temperature (CMMT) ≥5 °C (Greenwood and Wing, 1995). Because their cold-season temperature requirements increase further when growing under high atmospheric pCO_2, the CMMT inferred from the presence of palms during the early Eocene was at least 8°C (Royer et al., 2002). Even warmer conditions are suggested by the record of Bombacoideae, which today occur where CMMT >10°C. Since even winter-hardy extant palms are damaged by short-term freezing, winters must have been essentially frost-free.

Sporomorphs representing a temperate rainforest biome, with taxa typical of extant forests in montane settings of Australia, New Caledonia, New Guinea, and New Zealand, typically account for ~30 % of all sporomorphs at Site U1356A during the early Eocene.

Prominent taxa within the intepreted temperate rainforest biome include Araucariaceae and *Nothofagus*. Based on the floral composition, this biome likely occupied cooler environments of Wilkes Land located further inland and/or at higher elevations. A markedly different vegetation pattern emerges for the mid Eocene interval (49.3–46 Ma), with a strong increase of taxa attributable to the *Nothofagus*-dominated temperate rainforest biome and an almost complete disappearance of the paratropical rainforest biome (Fig. 2). Hence, the temperate rainforest biome became dominant over the entire catchment area of Site U1356, and extended into the coastal regions, with relict mesothermal components of the paratropical rainforest biome present only in localized pockets along the Wilkes Land margin. These shifts in dominance and floral composition indicate a strong cooling, which in light of the cold-season sensitivity of meso- to megathermal taxa was particularly pronounced during the winter months.

To further quantify the sporomorph-derived paleoclimatic information, bioclimatic analyses using the nearest living relative concept were carried to reconstruct the mean annual temperature (MAT), and the mean winter (MWT) and summer (MST) temperatures (Fig. 2).

Because the two biomes documented at Site U1356 represent distinct environments with different climatic conditions, our approach allows a spatiotemporally differentiated view of the climate evolution of the Wilkes Land margin from early Eocene peak warmth through the onset of mid-Eocene cooling. Our temperature estimates for the paratropical rainforest biome show that climates were generally warm until at least 51.9 Ma, with most samples indicating temperatures of 16±5 °C for MAT, 11±5 °C for MWT and 21±5 °C for MST. A significantly cooler climate emerges for the temperate rainforest biome, in particular for MAT and MWT, for which most samples yield values of 9±3 °C and 5±2 °C, respectively. For MST, the data show a strong scatter between 14±1 °C and 18±3 °C, and the calculated values overlap partially with those for the paratropical rainforest biome. This suggests that the seasonal temperature contrast between the habitats of both biomes was skewed towards the polar winter. For the mid-Eocene interval, our reconstructions suggest a pronounced cooling. Estimates for MAT are 14±3 °C, representing a decline of ~2 °C between the early Eocene and mid-Eocene.

Independent support for a warm terrestrial climate during the early Eocene and marked cooling during the mid-Eocene is supplied by MBT/CBT paleothermometry data (Fig. 3). Soil temperatures of ~24–27 °C are estimated for the early Eocene and ~17–20 °C for the mid-Eocene intervals at Site U1356. These temperatures fall close to the MSTs derived for the paratropical rainforest biome. Hence, besides suggesting an origin of terrestrial biomarkers from the coastal lowlands of the Wilkes Land sector of Antarctica, they also provide evidence for a potential bias of this proxy towards summer temperatures when applied to high-latitude settings. These data further indicate that paratropical conditions persisted in the lowlands of the Wilkes Land margin of Antarctica from at least 53.9 to 51.9 Ma. The CMMT and MWT estimates of ≥10 °C and 11±5 °C, respectively, compare favourably with deep-water temperatures of ~11 °C in the marine realm at this time (Lear, 2000; Zachos et al., 2008). Because early Eocene deep waters originated from the downwelling of surface waters off Antarctica (Thomas et al., 2003), winter temperatures in these regions cannot have dropped much below 11 °C. Although our MWT estimates are not representative of the Antarctic continent as a whole, they bear implications for the current debates on the general ability of climate models to reproduce extreme greenhouse conditions and the response of polar ecosystems to increased CO_2 forcing.

Preliminary palynological results from ODP Hole 1172D indicate that the middle Paleocene to early Eocene sporomorph assemblages are dominated by Araucaceae, Cyatheaceae and Podocarpaceae. *Nothofagus* pollen only reaches percentages of (<11%) in both the Paleocene and Eocene assemblages. During the early Paleogene, Hole 1172D was located at a paleolatitude of ~65°S, which makes it the southernmost record of the PETM (Sluijs et al., 2011). Based on our preliminary results, the PETM interval at Hole 1172D is characterized by a transient presence of the thermophilous mangrove palm *Nypa*. Extant members of this genus are restricted to areas with a MAT >21.7°C, a mean temperature of the coldest month >15.2°C, and mean temperature of the warmest month >27.5°C. Due to the fact that temperature and paleoecological data from marginal marine PETM sections from the Southern Hemisphere are currently rare (Sluijs et al., 2011), our sporomorph-based data will provide new insights into the response of terrestrial ecosystems in the high southern latitudes to PETM warming.

References:

Bijl, P.K., 2011. Environmental and climatological evolution of the early Paleogene Southern Ocean. Utrecht, the Netherlands: LPP Contribution Series No. 34, Utrecht University. 213 pp.

Cande, S.C., Stock, J.M., 2004. Cenozoic Reconstruction of the Australia-New Zealand-South Pacific Sector of Antarctica. In: Exon, N.F., Kennett, J.P., Malone, M. (Eds.), Geophysical Monograph Series. American Geophysical Union, 5-18.

Contreras, L., Pross, J., van de Schootbrugge, B., Bijl, P.K., Raine, J.I., Koutsodendris, A., Brinkhuis, H., subm. Early to Middle Eocene vegetation dynamics at the Wilkes Land Margin (Antarctica).

Greenwood, D.R., Archibald, S.B., Mathewes, R.W., Moss, P.T., 2005. Fossil biotas from the Okanagan Highlands, southern British Columbia and northeastern Washington State: climates and ecosystems across an Eocene landscape. Canadian Journal of Earth Sciences 42, 167-185.

Greenwood, D.R., Wing, S.L., 1995. Eocene continental climates and latitudinal temperature gradients. Geology 23, 1044-1048.

Lear, C.H., 2000. Cenozoic Deep-Sea Temperatures and Global Ice Volumes from Mg/Ca in Benthic Foraminiferal Calcite. Science 287, 269-272.

Pross, J., Contreras, L., Bijl, P.K., Greenwood, D.R., Bohaty, S.M., Schouten, S., Bendle, J.A., Röhl, U., Tauxe, L., Raine, J.I., Huck, C.E., van de Flierdt, T., Jamieson, S.S.R., Stickley, C.E., van de Schootbrugge, B., Escutia, C., Brinkhuis, H., IODP Expedition 318 Scientists, 2012. Persistent near-tropical warmth on the Antarctic continent during the early Eocene epoch. Nature 488, 73-77.

Royer, D.L., Osborne, C.P., Beerling, D.J., 2002. High CO_2 increases the freezing sensitivity of plants: Implications for paleoclimatic reconstructions from fossil floras. Geology 30, 963-966.

Shipboard Scientific Party, 2001. Site 1172. In Exon, N.F., Kennett, J.P., Malone, M.J., et al. Proceedings of the Ocean Drilling Program, Initial Reports, 189, 1-149.

Sluijs, A., Bijl, P.K., Schouten, S., Röhl, U., Reichart, G.J., Brinkhuis, H., 2011. Southern ocean warming, sea level and hydrological change during the Paleocene-Eocene thermal maximum. Climate of the Past 7, 47-61.

Thomas, D.J., Bralower, T.J., Jones, C.E., 2003. Neodymium isotopic reconstruction of late Paleocene-early Eocene thermohaline circulation. Earth and Planetary Science Letters 209, 309-322.

Zachos, J.C., Dickens, G.R., Zeebe, R.E., 2008. An early Cenozoic perspective on greenhouse warming and carbon-cycle dynamics. Nature 451, 279-283.

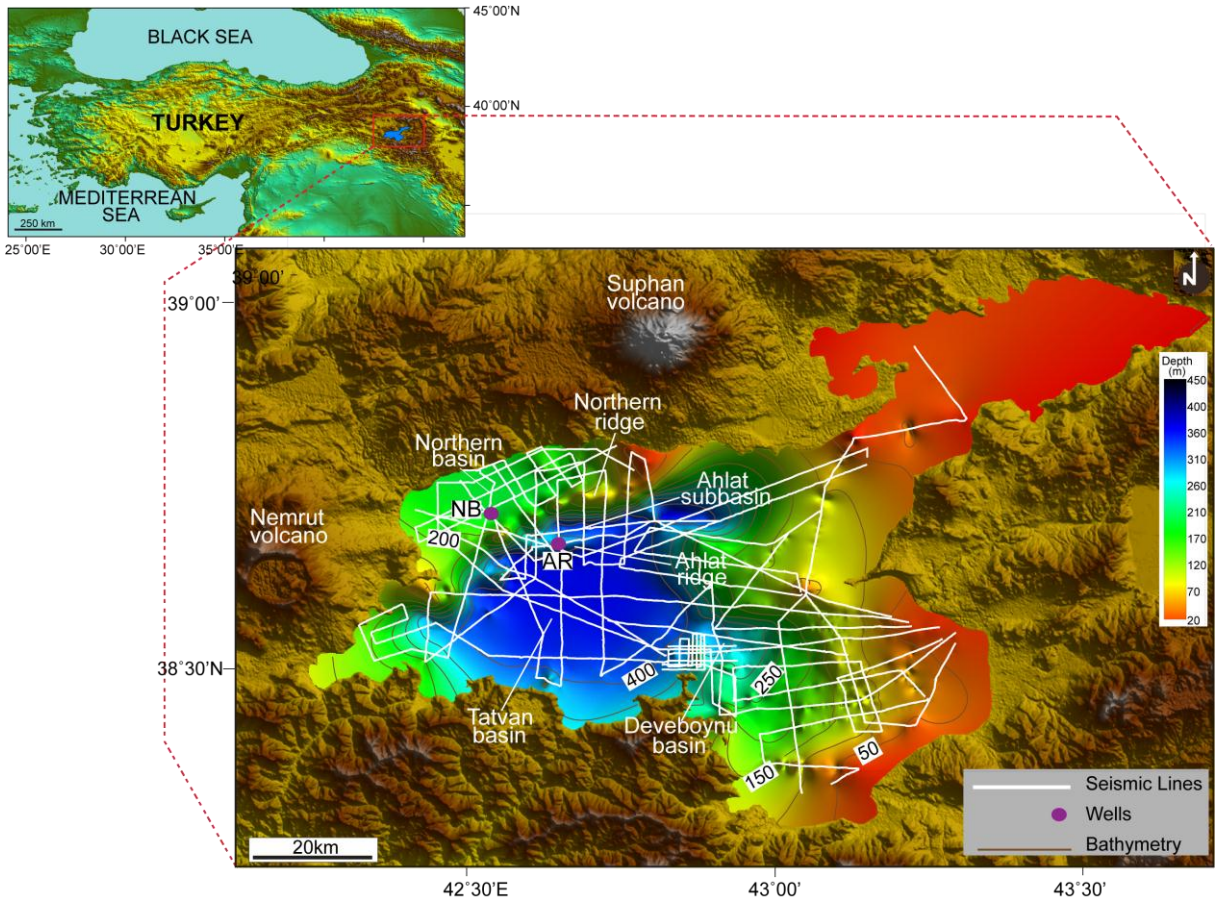

Fig. 1. Location of Lake Van as well as seismic reflection profiles and drilled wells.

ICDP

New insights in the evolution of Lake Van: A joint analysis of seismic, hydroacoustic, and drill data

D. CUKUR[1], S. KRASTEL[2], H.-U. SCHMINCKE[1], M. SUMITA[1], D. WINKELMANN[1] AND PALEOVAN SCIENTIFIC TEAM

[1] GEOMAR | Helmholtz Centre for Ocean Research Kiel, Wischhofstr.1-3, 24148 Kiel, Germany
[2] Institute of Geosciences, Christian-Albrechts-Universität zu Kiel, Otto-Hahn-Platz 1, 24118 Kiel, Germany

Lake Van in Eastern Anatolia (Turkey) is the fourth largest terminal lake in the world with a surface area of 3,574 km², a volume of 607 km³, a maximum depth of 450 m, and a maximal length of 130 km WSW-ENE (Wong and Degens, 1978) (Fig. 1). Over 1500 km of multi-channel seismic reflection profiles in combination with ICDP drilling and bathymetric data from Lake Van, eastern Turkey, allow to reconstruct stratigraphic evolution of the lake basin. Three major basins (Tatvan, Deveboynu and the Northern basin) are separated from each other by Ahlat and Northern ridges. The sedimentary history of the lake was subdivided into19 distinct phases reflecting major environmental and depositional changes (Fig. 2). Five major regressive and fourteen transgressive phases have been identified. Five lake lowstands have been dated as follows: (Phase 1) ~580 ka; (Phase 5) ~ 355-341 ka; (Phase 7) ~ 320-210 ka; (Phase 12) ~ 170-140 ka; and (Phase 18) ~ 30-16 ka. Estimated paleolake levels (below present lake level) at the end of each phase are; 610 m for Phase 1, 560 m for Phase 5, 470 m for Phase 7, 310 m for Phase 12, and 210 m for Phase 18. The sediment infill history of Lake Van over the ~580 ka is characterized five types of sedimentary facies. (a) Uniform 'well-stratified' lacustrine deposits (alternating organic muds and fine grained turbidites and tephra) formed under quiescent lake level conditions characterize the deeper parts of the basin. (b) Chaotic 'mass-transport' deposits characteristics of the southern parts of the lake have likely resulted from mass-transport process possibly triggered by ongoing tectonic activity along the lake margins. (c) Oblique or complex-oblique shaped 'deltaic' deposits have formed on the eastern/southeastern shelf and slope areas most likely due to accumulation of large volumes of clastic material derived from adjacent rivers. (d) Non-uniform 'fluvial' deposits characterizing the shelves are interpreted to have mainly deposited by fluvial processes when the shelf was subaerially exposed. (e) Chaotic 'volcaniclastic' deposits that fill local basins (Northern basin) are probably due to volcanic mass flows such as pyroclastic flows. In summary, our data show that sedimentation in the basins was mainly controlled by tectonic, climatic, and volcanic factors. The effect of climate was more pronounced in sedimentary phases rather than other factors as suggested by repeated patterns of lake level fluctuations. Such lake level fluctuations which reflected in clinoforms in seismic data are also documented as morphological features (channels, terraces) in bathymetric data (Fig. 3).

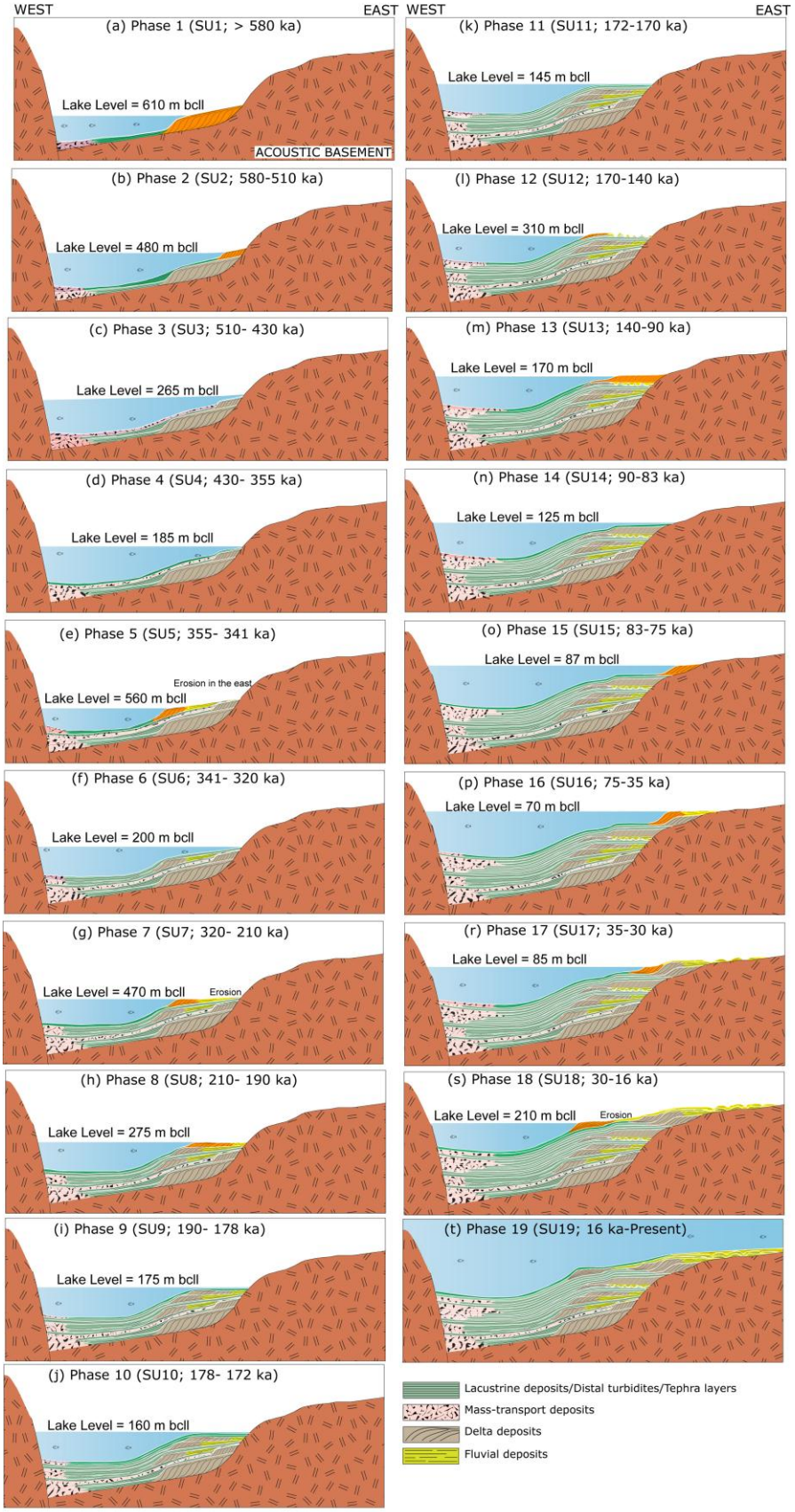

Fig. 2. Schematic E-W cross-sections illustrating sedimentary and lake level history of Lake Van.

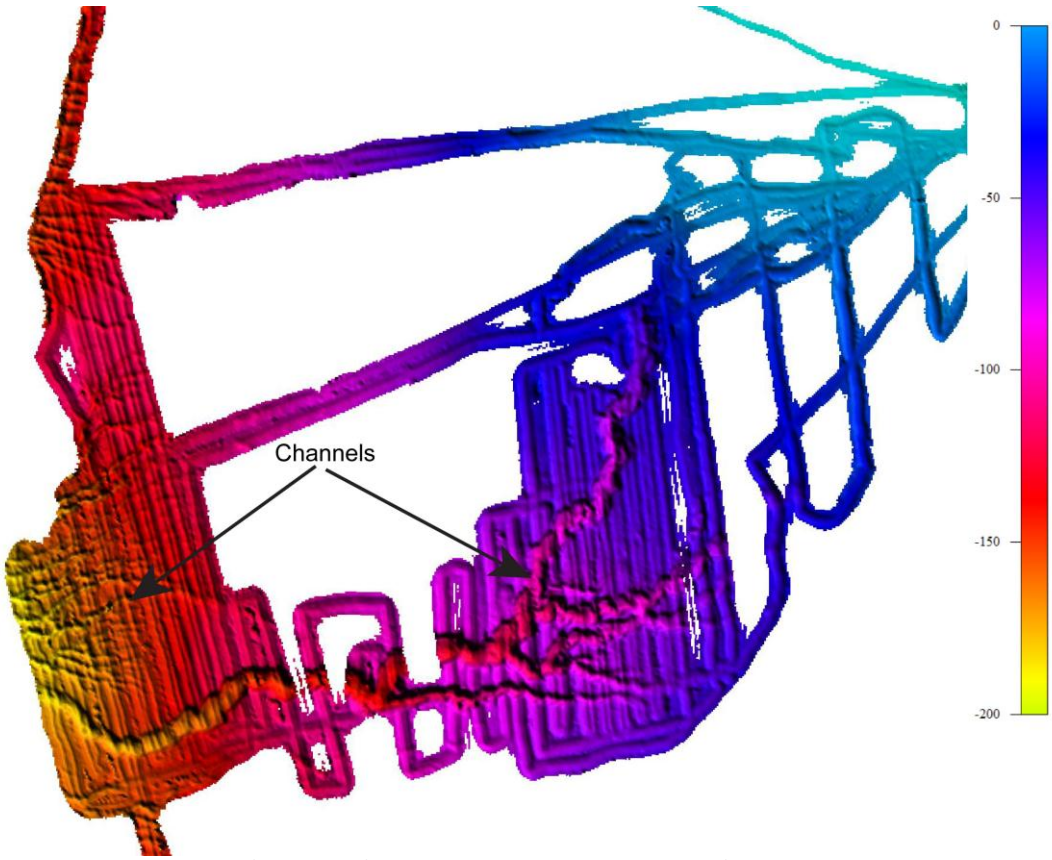

Fig. 3. Multibeam bathymetry map of eastern shelf showing numerous channels on the lake floor.

On average channels are V-shaped, 5-25 m deep, 40-500 m wide, and extending water depth of 200 m where approximately the shelf breaks occur (Fig. 3). Previous studies describe these morphological depressions as a karst-like morphology, braided channel system, and pockmarks. Mapping the spatial distribution of these depressions using multibeam bathymetry leaves us no doubt that they represent channels.

References:

Wong, H. K., and E. T. Degens (1978), The bathymetry of Lake Van; A preliminary report, in Geology of Lake,vol. 169, edited by E. T. Degens, F. Kurtman, M.T.A. press, Ankara, Turkey.2524-2546.

ICDP

Magma Mixing: from nature to lab

C. P. DE CAMPOS[1], D. MORGAVI[1], , S. WIESMAIER[1], W. ERTEL-INGRISCH[1], K. U. HESS[1], Y. LAVALLÉE[3], D. PERUGINI[2], D. DINGWELL[1]

[1] Ludwig-Maximilians-Universität München, Earth and Environmental Sciences, Munich, Germany (campos@min.uni-muenchen.de)
[2] Department of Earth Sciences, University of Perugia, Perugia, Italy
[3] School of Environmental Sciences, University of Liverpool, Liverpool, UK

Magma diversity in the Snake River Plain and Yellowstone (SRP-Y) volcanic fields presents a unique opportunity to study the interaction of a hot-spot-related thermal anomaly with the continental crust and the subsequent development of magma reservoirs. As a reservoir forms, primitive magma batches induce crustal melting and, therefore assimilation, and mixing. Mixing caused by a recharge of a more primitive magma is expected to be accompanied by heating of the reservoir which may obstruct fractionation and thus to precede it. The SRP-Y holds the tale of this chemical process and may provide essencial pieces of the puzzle portraying the evolution of magmas.

We performed a series of experiments to systematically characterize the evolution of mixing using as end-members the most contrasting magmas involved in magmatic systems: basalt and rhyolite. Our results are divided into two different kinds of experiments: i) those using analogue silicate melts at high temperature (Anorthite-Diopside and Haplogranite); and, ii) those using natural SRP-Y end-member candidates, basalt and rhyolite. Following experimental results will be resumed and discussed:

i) with Anorthite-Diopside and Haplogranite

a) how mixing can be enhanced by chaotic dynamics [1];

b) how complex can be the space and time interaction of chaotic mixing silicate melts [2];

c) the study and application of a new experimental parameter to measure chemical element mobility during mixing of magmas [3, 4];

ii) with natural SRP-Y end-members (basalt and rhyolite):

a) how natural rhyolite and basalt may physically and chemically interact during chaotic mixing [4, 6]; these studies focus on changes in the differential mobilities of major, minor and trace elements in space and time;

b) how the morphochemistry of rhyolite and basalt interactions may change in space and time, during chaotic mixing natural melts [5];

The continuation of another series of experiments to investigate the influence of crystals on magma mixing aims an even more complex and realistic scenario to further constrain the nature and timescales of mixing under different crystal and/or volatile contents [7], and will be reported by Wiesmaier et al. [8] in this meeting.

Evidence of natural magma mixing, especially in the Yellowstone system, has already been observed and studied from natural outcrops by means of geochemical and isotopic data [8], with on-going experimental studies [9].

We are confident that the results of our research will contribute towards providing new tools for unravelling, even very subtle, mixing processes in magmatic systems, constraining changes in the timescale of replenishment, assimilation and mixing, not only for the SRP-Y volcanic fields, but also with a broader application for different magma reservoirs.

References:

[1] De Campos, C., D. Perugini, W. Ertel-Ingrisch, D. Dingwell, and G. Poli (2011), Enhancement of magma mixing efficiency by chaotic dynamics: an experimental study, Contrib. Mineral. Petrol. , 161(6), 863-881.

[2] Perugini D., De Campos C.P., Ertel-Ingrisch W., Dingwell D.B. (2012) - The space and time complexity of chaotic mixing of silicate melts: Implications for igneous petrology, Lithos, 155, 326-340.

[3] Perugini D., De Campos C.P., Dingwell D.B., Dorfman A. (2013) Relaxation of concentration variance: A new tool to measure chemical element mobility during mixing of magmas, Chemical Geology, 335, 8-23.

[4] Morgavi D., Perugini D., De Campos C.P., Ertel-Ingrisch w., Lavallée Y., Morgan L. Dingwell D.B. (in press) Interactions Between Rhyolitic and Basaltic Melts Unraveled by Chaotic Magma Mixing Experiments, Chemical Geology. http://dx.doi.org/10.1016/j.chemgeo.2012.10.003.CHEMGE-16697.

[5] Morgavi D., Perugini D., De Campos C.P., Ertel-Ingrisch W., Dingwell, D.B. (2013) Morphochemistry of Patterns Produced by Mixing of Rhyolitic and Basaltic Melts, Journal of Volcanology and Geothermal Research, 253: 87–96.

[6] Morgavi D., Perugini D., De Campos C.P., Ertel-Ingrisch W., Dingwell, D.B.- Time Evolution of Chemical Exchanges During Mixing Between Rhyolitic and Basaltic Natural Melts. Submitted to Contributions to Mineralogy and Petrology. In review.

[7] Wiesmaier S., Morgavi D., Perugini D., De Campos C.P., Hess K., Lavallee Y., Dingwell D. B. (2012) - Magma mixing enhanced by bubble ascent, AGU 2012 Fall Meeting, Abstract V11B-2748.

[8] Wiesmaier S., Morgavi D., Perugini D., De Campos C.P., Hess K., Lavallee Y., Dingwell D. B. - The role of bubble ascent in magma mixing. Submitted to be presented during the next 2013 ICDP/IODP Kolloquium, Freiberg, Germany.

[9] Pritchard, C. J. and Larson, P.B. (2012) Genesis of the post-caldera eastern Upper Basin Member rhyolites, Yellowstone, WY: from volcanic stratigraphy, geochemistry, and radiogenic isotope modeling. Contrib Mineral Petrol (2012) 164:205–228 DOI 10.1007/s00410-012-0733-9.

[10] Morgavi D, Perugini D, Pritchard C J, De Campos C P, Larson P, Dingwell D B - Experimental constraints on mixing between basaltic and rhyolitic magmas along the Norris-Mammoth Corridor in the Yellowstone National Park (USA). Submitted to IVCEI 2013, Kagoshima, Japan.

IODP

The Mid Pleistocene transition: did marine biological productivity lead to pCO_2 changes? (New project)

L. DIESTER-HAASS[1], K. BILLUPS[2]

[1] l haass@mx.uni-saarland.de
[2] kbillups@udel.edu

The Mid Pleistocene transition (MPT), the period between about 1200-500 ky (Head and Gibbard, 2005) marks the transition from the “40 ky to a 100 ky world”, and the development of thicker ice sheets without any change in the mode of orbital forcing, and a decrease in atmospheric pCO_2 by about 30 ppm (Lüthi et al., 2008; Wolff et al., 2010,). The pCO_2 atm in glacial as well as in interglacial periods was lower during the MPT (800-450 ky) compared to the post-MPT period (op.cit.). In the marine realm, the $\delta^{13}C$ values in shells of benthic foraminifera display a pronounced minimum (Raymo et al., 1997).On land, the MPT is marked by a global increase in aridity (de Menocal, 1995). There is evidence for a transient transfer of dust and terrestrial organic particles, as well as transfer of organic matter from shelf and upper slope areas to the deep ocean. (Clarke et al., 2006); Martinez-Garcia et al., 2009; 2011).

Here we investigate whether or not a global increase occurred in sequestration of carbon in marine sediments due to enhanced export productivity. We will reconstruct export production using benthic foraminiferal accumulation rates (Herguera, 2000) measured in sediments from ODP sites along a S-N profile in the Atlantic Ocean.

First results from ODP Site 607, located in a modern low productivity area at the northern end of the subtropical gyre, show that paleoproductivity increases sharply at about 1.05 Ma and decreases in parallel with the decrease in benthic foraminiferal $\delta^{13}C$ values. Individual maxima, however, apparent at 1.05 Ma, 0.9 Ma and 0.8 Ma correspond to minima in $\delta^{13}C$ values and to maxima in dust and alkenone accumulation at Southern Ocean Site 1090 (Martinez-Garcia et al., 2009). This finding suggests that productivity increases are not only a regional, high southern latitude signal, but may be a basin-wide phenomenon supporting hypotheses calling for global climate forcing mechanisms such as greenhouse gases.

Ref.erences

Clarke, P.U., Archer, D. et al.,(2006). The middle Pleistocene transition: characteristics, mechanisms, and implications for long-term changes in atmospheric pCO_2. Quat.Sc.Rev., 25, 3150-3184

de Menocal,P.B. (1995). Plio-Pleistocene African climate. Science, 270, 53-59.

Head,M.J. and Gibbard,P.L., (1995).Early Middle Pleistocene transitions: an overview and recommendation for the defining boundary. In: Early Middle Pleistocene transitions: the land-ocean evidence, ed. by M.J.Head and P.L.Gibbard, p 1-18, Geol.Soc.London.

Herguera,J. C., (2000), Last glacial paleoproductivity patterns in the eastern equatorial Pacific: benthic foraminifera records, Mar. Micropal., 40, 259–275.

Lüthi, et al., (2008).High-resolution carbon dioxide concentration record 650.000-800.000 years before present. Nature, 453, 379-382, doi:10.1039/nature06949.

Martinez-Garcia, A., Rosell-Mele,A., Geibert, W., Gersonde, R., Masque, P., Gaspari,V., and Barbante,C., (2009). Links between iron supply, marine productivity, sea surface temperature, and CO2 over the last 1.1 Ma. Paleoceanography, vol. 24, PA1207, doi:10.1029/2008PA001657, 2009

Martinez-Garcia, A., Rosell-Mele,A., Jaccard, S.L., Geibert, W., Sigman, D.M., and Haug, G. (2011). Southern Ocean dust-climate coupling

over the past four million years. Nature, 476, 312-316. doi: 10.1038/nature10310
Raymo, M.E., Oppo,D.W., and Curry, W., (1997). The mid-Pleistocene climate transition: a deep sea carbon isotopic perspective. Paleoceanography, 12/4, 546-559.
Wolff,E.W. et al.(2010). Changes in environment over the last 800.000 years from chemical analysis of the EPICA Dome C ice core. Quat.Sc.Rev. 29, 285-295. doi:10.1016/jquascirev.2009.06013.

ICDP

Passivating properties of the palagonite layer on subsurface basaltic and rhyolithic glass alteration from ICDP sites Hawaii and Snake River Plain

S. DULTZ[1], H. BEHRENS[1], M. PLÖTZE[2]

[1] Institute of Mineralogy, Leibniz University Hannover, Callinstr. 3, D-30167 Hannover
[2] Institute for Geotechnical Engineering, ETH Zürich, 8093 Zürich, Switzerland

Palagonite forms an alteration layer on pristine glass which may constitute a diffusion barrier that slows down or even inhibit glass alteration. The effect of such a barrier is not constant over time, as constituents react among eachother and with solute compounds. Recondensation and precipitation can affect porosity and in consequence passivating properties. Microorganisms forming pits and tubes in basaltic glass surfaces at the boundary to palagonite may provide routes which enhance abiotic glass alteration too. Findings on porosity and non-equilibrium textures in glass alteration layers, and a new model on an interface-coupled dissolution reprecipitation mechanism (Geisler et al., 2010) encouraged us to use altered glass samples in combination with experimental work to determine the dependency of glass alteration from palagonite properties, in particular effects of porosity of layers and solution chemistry on glass weathering rate. Chemically different basaltic and rhyolitic glasses available from ICDP drilling cores Hawai and Snake River Plain exposed to saline and different groundwaters in a temperature range allowing microbial colonization (Walton, 2008) were included. For understanding and prediction of interdependencies of palagonite formation, glass alteration rates, solution composition and biochemical factors (i) petrographical investigation of glass alteration, (ii) characterization of pore system (iii) determination of transport, (iv) analysis of ionic effects on glass dissolution, and (v) fluid-glass experiments at conditions relevant to the drilling sites are carried out.

For analysis of electrolyte effects on glass weathering reactions, the zeta potential, which is a key electrochemical property of the pore water/solid interface, is determined for powdered basaltic and rhyolitic glass samples in different solutions at 4, 20, and 60°C. In course of time a shift of zeta potential from negative to positive values was observed for basaltic glass powders in diluted synthetic sea water, typically after 120 h at 20 and 60°C. This charge reversal can most probably be assigned to increasing amounts of Fe on the outer rim of the leached layer, highly affecting sorption propertities. The observed generation of positive charge is important in many ways, e.g. for the attachment of microorganisms and sorption of dissolved organic matter and is determined in currently running experiments with solutions of different cations (Na^+, K^+, Mg^{2+}, Ca^{2+}, Ba^{2+}, Zn^{2+} and Al^{3+}) in the concentration range from 0.1-5.0 mmol L-1. Analysis of textures in glass alteration products in Hawaiin drill cores revealed the presence of cracks within the palagonite layer, which are sealed only to a part by the formation of zeolite. According to first results from Hg-porosimetry, the pore volume in palagonite samples from Hawaii is 27-34 %, with high shares of fine pores with radii less than 10 nm indicating that transport in the matrix of palagonite is diffusion controlled. The presence of these cracks might increase the mobility of water in palagonite and is thought to ease the reaction of the glass with fluids. The modes of formation of these cracks and the degree of filling with zeolite will be analyzed by their micromorphology using tomography combined with image analysis and impregantion of samples with a molten alloy. Voids observed in vicinity of the outer rim of bioaltered glass with formation of microtubules give some indication for a dissolution-reprecipitation mechanism during glass alteration mediated by microorganisms.

References:

Geisler, T., Janssen, A., Scheiter, D., Stephan, T., Berndt, J., Putnis, A. (2010) Aqueous corrosion of borosilicate glass under acidic conditions: A new corrosion mechanism. Journal of Non-Crystalline Solids 356, 1458-1465.
Walton, A.W. (2008) Microtubules in basalt glass from Hawaii Scientific Drilling Project #2 phase 1 core and Hilina slope, Hawaii: evidence of the occurrence and behavior of endolithic microorganisms. Geobiology 6, 351–364.

IODP

Rock magnetization from three component magnetic logging data measured on the Louisville Hotspot trail during IODP Expedition 330

S. EHMANN[1], L. ANDERSON[2], A. HÖRDT[1], M. LEVEN[3], C. VIRGIL[1]

[1] Institut für Geophysik und Extraterrestrische Physik, TU Braunschweig, Braunschweig, Germany
[2] Department of Geology, University of Leicester, United Kingdom
[3] Institut für Geophysik, Universität Göttingen, Göttingen, Germany

One of the main results of ODP Leg 197 was that the hotspot that creates the Hawaiian-Emperor Seamount Chain has moved southward by about 15° in the time between about 80 and 50 MA. The Louisville Seamount Chain has been formed during the last 80 million years by a different hotspot underlying the Pacific Plate. A comparison of both seamount chains allows to determine whether the hotspots moved congruently or independently. Either result can give information about the scale and magnitude of mantle convection currents, as they affect the trajectories of the ascending mantle plumes.

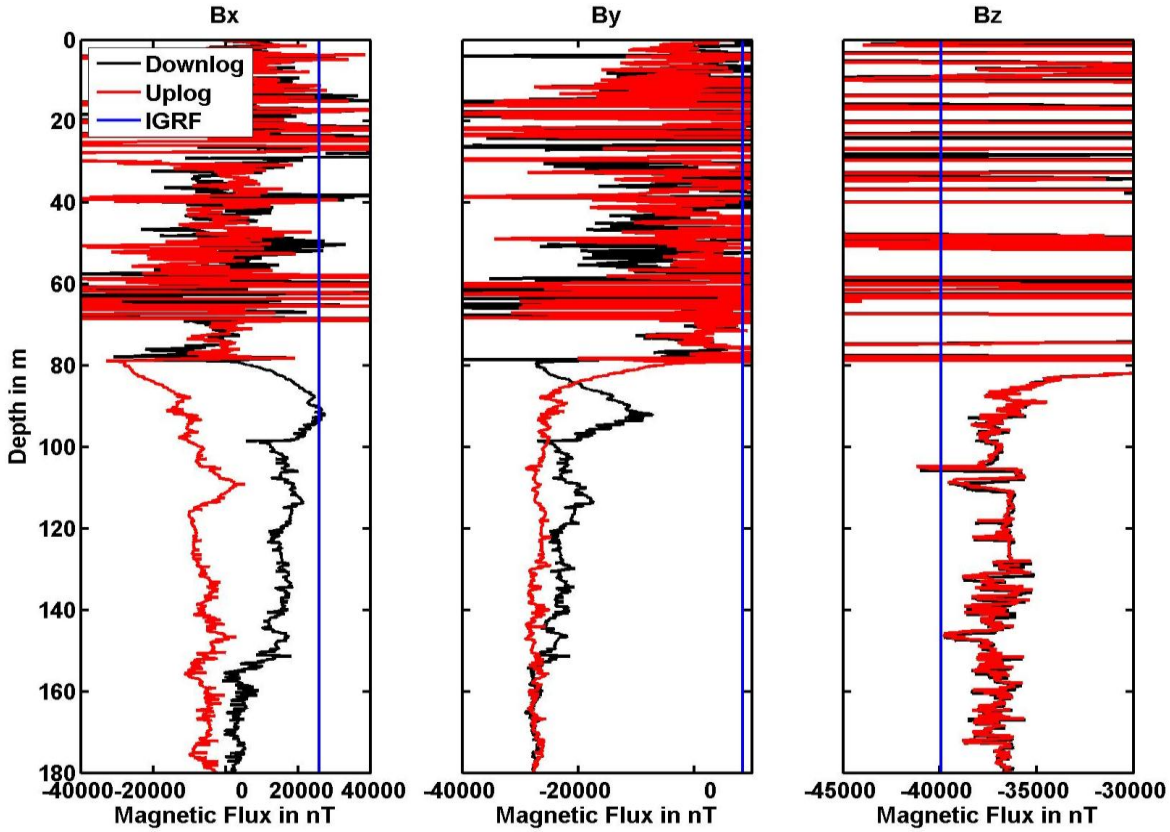

Figure 1: Unoriented magnetic field data. The upper 80 are distorted by ferromagnetic casing. X- and y-component are distorted by the tool's rotations, as can be seen by large differences between down- and uplog. On the contrary, the z-component already gives some information about the vertical field, as it is only affected by small variations in the tilt of the tool. For comparison, the expected magnetic field as given by the IGRF is shown in blue.

During IODP Leg 197, six sites on five different seamounts of ages comparable to those examined in ODP Leg 197 were drilled. The main goals of the expedition were exact dating and determination of the paleolatitude of each seamount as well as determination of their geochemical composition.

First results of paleomagnetic measurements on the drill cores collected during our Expedition suggest that the Louisville hotspot has remained more or less stationary in the same period while the Hawaiian hotspot has moved considerably, which suggests independent hotspot motion (Koppers et al. 2012).

A problem of paleomagnetic measurement on drill cores is that only the inclination and the total strength of the magnetization of the drilled rocks can be determined. As the cores rotate uncontrollably during removal, the declination of the magnetization is unknown. The declination of the magnetization can help characterizing the spatial and temporal motion of the hotspot. For that purpose, the Göttinger Bohrloch Magnetometer (GBM) was run three times in two of the sites of Expedition 330. The instrument comprises three orthogonal fibre optical gyros (FOGs), three orthogonal fluxgate magnetometers and two inclinometers. The FOGs record the angular rate of the GBM with a high accuracy of up to $9*10^{-5}$°/s. This allows to calculate the orientation of the GBM during measurements and thus to reorient the recorded magnetic field vector from the tool's internal reference frame to a geographic reference frame. Using appropriate models, the reoriented magnetic field can be used to calculate the rock magnetization, in particular its declination.

Data preparation

Several steps lie between the measurement of the magnetic field, its reorientation and the calculation of the magnetization, of which the most important ones will be explained in the following (further detail can be found in Virgil, 2012).

First of all, the magnetic field data and the FOG data are corrected for errors in the sensors like offsets, scale factors and errors in orthogonality. Also, the effect of the rotation of the Earth on the FOG signal has to be removed during data processing. To make this possible, the initial orientation of the tool relative to the geographic reference frame has to be known as exactly as possible. During Expedition 330, the GBM was aligned to the axis of the ship using a sight mounted to the GBM and a marker set up on the heli pad in the back of the ship. The orientation of the ship itself is determined using the ship's navigational gyro. The output of the ship's gyros is regularly compared to celestial navigation data and known landmarks and has a mean deviation of about 0.2°.

To check and compensate for any errors in the initial orientation of the GBM, its inclinometers can be used. Their accuracy is limited to about 0.3° and they are affected by shocks and vibrations, thus they are not regularly used to reorient the data. However, their advantadge over the FOGs is that they give the true tilt of the GBM and not incremental changes in tilt. Any drift left

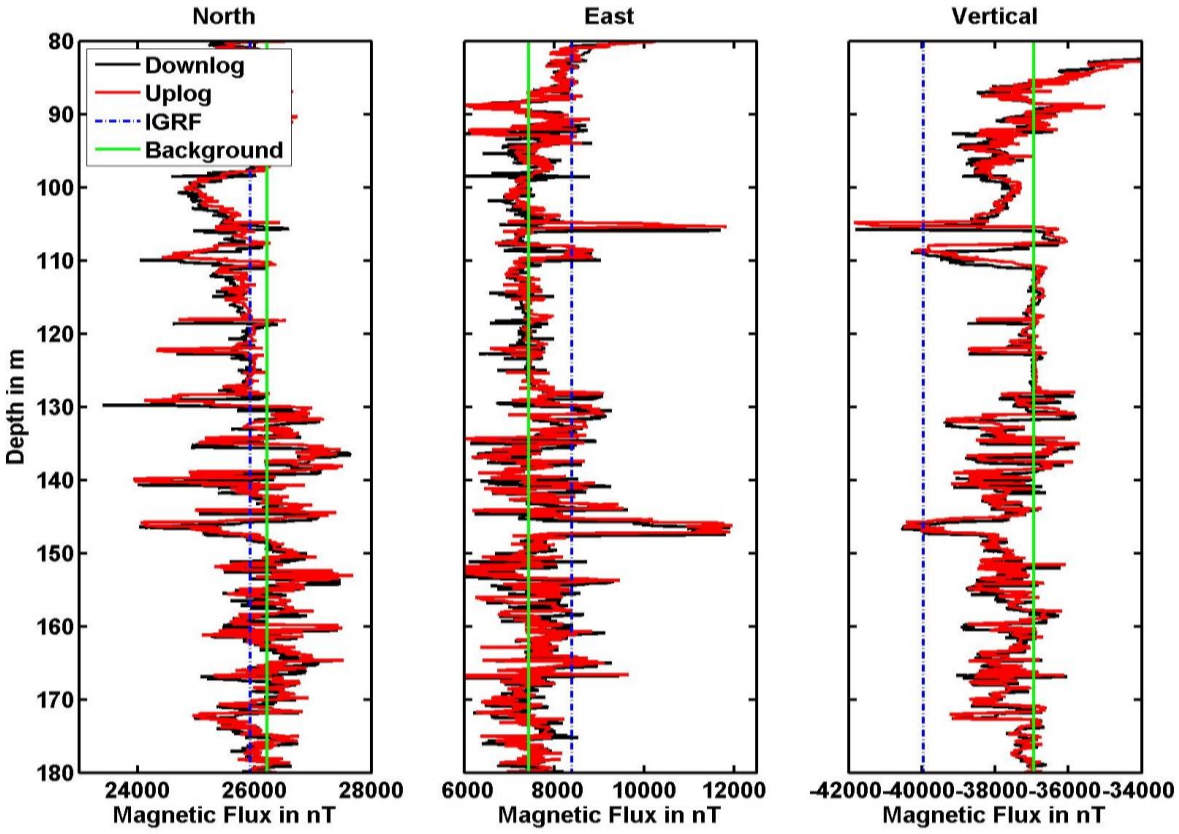

Figure 2: Reoriented magnetic fields given in the geographic reference frame. Down- and Uplog agree well. The green lines give the magnetic background field values used for further modeling. Differences to the IGRF values can be attributed to an offset due to ferromagnetic parts in the tool string (Vertical component) and a remaining error in orientation of about 2.1° , which is accounted for by an equivalent rotation of the background field (North and East component).

in the data of the gyros after data processing expresses itself by a growing difference between the tilt measured by the inclinometers and the tilt calculated from gyro data. These differences can be minimized by determining an optimal offset to the initial orientation and adding an optimal constant drift to the FOG data. In the last step, the misalignment between the coordinate system of the FOGs and the coordinate system of the magnetometers is corrected and the magnetic field data is reoriented into the geographic reference frame.

Figure 1 shows the unoriented magnetic field in the tool's internal x-y and z-reference frame. The black lines denote the downlog, the red lines the uplog, the agreement of which is the most important quality control available. The expected magnetic field value as given by the IGRF is shown in blue. The x- and y-component are heavily influenced by the rotations of the tool and don't give any valuable information, as can be easily seen by the large differences of down- and uplog . Only the z-component is close to the true magnetic field in the borehole, as it is only influenced by small variations in the tilt of the tool and not by rotations about its symmetry axis. The magnetic field above 80 meters below sea floor is distorted by the casing that remained in the upper part of the borehole.

Figure 2 shows the fully corrected magnetic field (the distorted upper part is omitted here). Down- and Uplog now agree well in all three components. The green lines give the field values that are used as background field for the different magnetization models. The difference to the IGRF can be easily explained: The vertical component of the magnetic field is still influenced by ferromagnetic parts in the tool string and the cable, which causes a (constant) offset that can be fully removed by chosing an appropriate value for the background field. The differences in the North- and East-component can be attributed to a remaining error in the determination of the orientation of the GBM: the background field used for modeling is equivalent to the IGRF field rotated by 2.1 degrees about the vertical axis.

Magnetization models

A first approximation for the magnetization of the drilled rock layers can be found by using a model of horizontal layers of infinite lateral extent (Bosum et al, 1988). The diameter of the borehole (assumed to be circular) was measured by a different toolstring. For the inversion, the magnetic field data is interpolated to a fixed sampling interval of 0.1m and one layer is fitted to each data point. The initial model does not take neighbouring layers into account and is improved iteratively by first calculating the combined magnetic field of all layers and then adding corrections to each individual layer. Figure 3 shows the result of the infinite horizontal layer model, the magnetization as measured on the drill cores (Gee, personal communication) and the lithology of the drill site. Only the horizontal and vertical component of the magnetization is shown, to allow for a better comparison with the core data. The magnetizations correlate well with the lithology, but

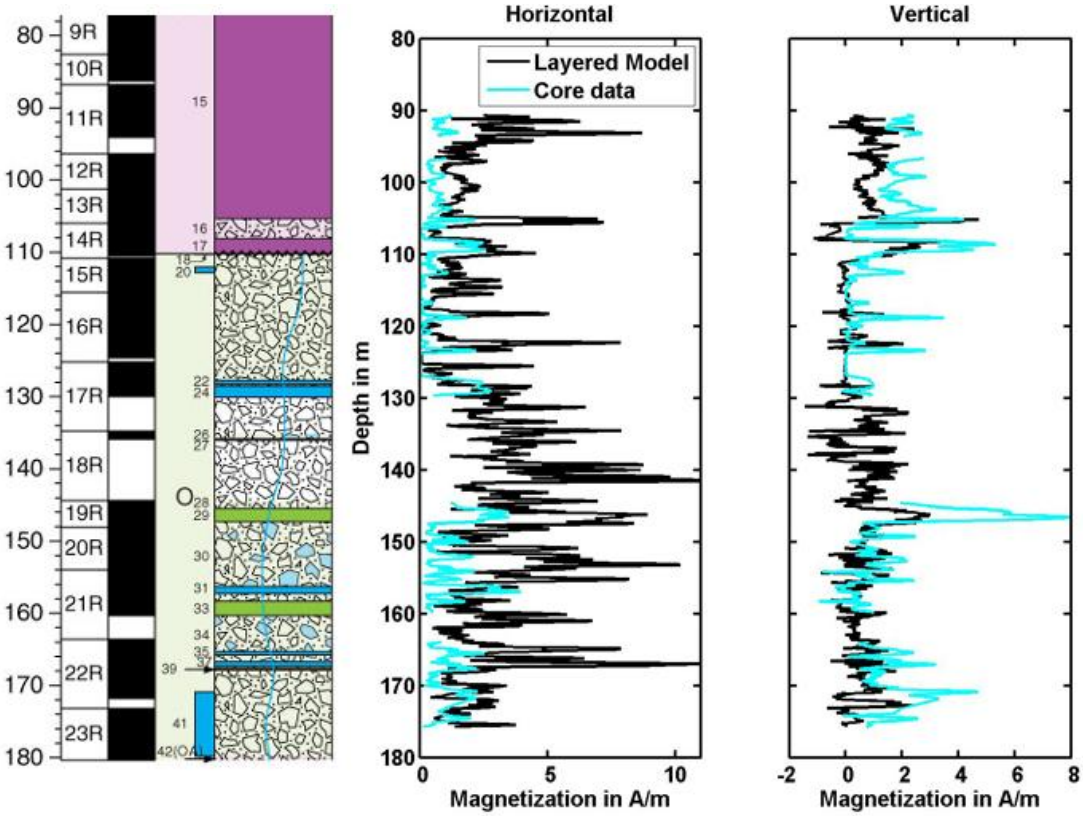

Figure 3: Comparison of the lithology of Site U1376 (Exp. 330 Scientists, 2011) to the magnetization calculated using horizontal layers (black lines) to the magnetization measured on the drill cores. The black and white columns mark cored and non-cored parts of the borehole. The lithology shows massive flow units (solid colors) intersected by brecciated sections and dikes. Both magnetizations correlate well with the lithology, but the calculated magnetization is either much higher (horizontal component) or lower (vertical component) than the directly measured calculation. This means that a horizontal layer model is insufficent to explain the data.

the infinite horizontal layer model overestimates the horizontal component and underestimates the vertical component. Thus, a different model is needed to explain the data.

Borehole imager data suggests that the drilled layers are in fact not horizontal but inclined. The magnetic field in a borehole that intersects inclined layers can be calculated using formulas given by Gallet and Courtillot (1989). The disadvantadge here is that the calculation of inclined layers involves solving integrals numerically, which is much more computationally expensive than the analytical formulas used in the horizontal case. Also, there is no obvious way to implement an iterative, additive improvement of an initial model.

To overcome this and to allow a fast assesment of whether a model using tilted layers can explain our data, we developed an empirical approximation of the Gallet and Courtillot model. We calculated the magnetic field caused by layers of different strikes and dips and then fitted a horizontal layer to the data to obtain a relationship between our (wrong) horizontal layer model and the magnetization measured on the cores. Then we empirically derived a formula to approximate this relationship, which now can be used to check whether a strike and dip can be found that, together with the known horizontal and vertical magnetization measured on the cores, explains the magnetizations calculated with horizontal infinite layers.

Figure 4 shows the result of calculations using the empirical formula. The interpretation is not as straight forward as in the other case. The black line again shows the result of the horizontal layer model. The green line shows the empirical model that uses the core data and tries to calculate strike, dip and declination in a way that the resulting magnetic field would be (wrongly) intepreted by a horizontal model in the same way our previous horizontal model explains the data. Gaps in the data are in sections where no core was retrieved. The good agreement of both models means that a tilted model can be used to explain both our three component magnetic field data as well as the magnetizations measured on the drill cores.The angles (strike, dip and declination of magnetization) are not shown, as they cannot be unambiguously determined; neither by the empirical model nor by the complete semi-analytical model of Gallet and Courtillot. Additional information in form of a more detailed interpretation of borehole imager data is necessary, as this can give information about possible strikes and dips and thus significantly limit the number of possible models.

References

Bosum,W., Eberle,D. & Rehli,H.-J.; A gyro-oriented 3-component borehole magnetometer for mineral prospecting, with examples of its application; Geophysical Prospecting, 1988, 36, 933-961

Expedition 330 Scientists, Expedition 330 Preliminary Report - Louisville Seamount Trail - Implications for geodynamic mantle flow models and the geochemical evolution of primary hotspots, Integrated Ocean Drilling Program, 2011

Gallet,Y. & Courtillot,V.; Modeling magnetostratigraphy in a borehole; Geophysics, 1989, 54, 973-983

Koppers, A.A.P., Yamazaki, T., Geldmacher, J., Gee, J.S., Pressling, N., Hoshi, H., Anderson, L., Beier, C., Buchs, D.M., Chen, L.-H., Cohen,

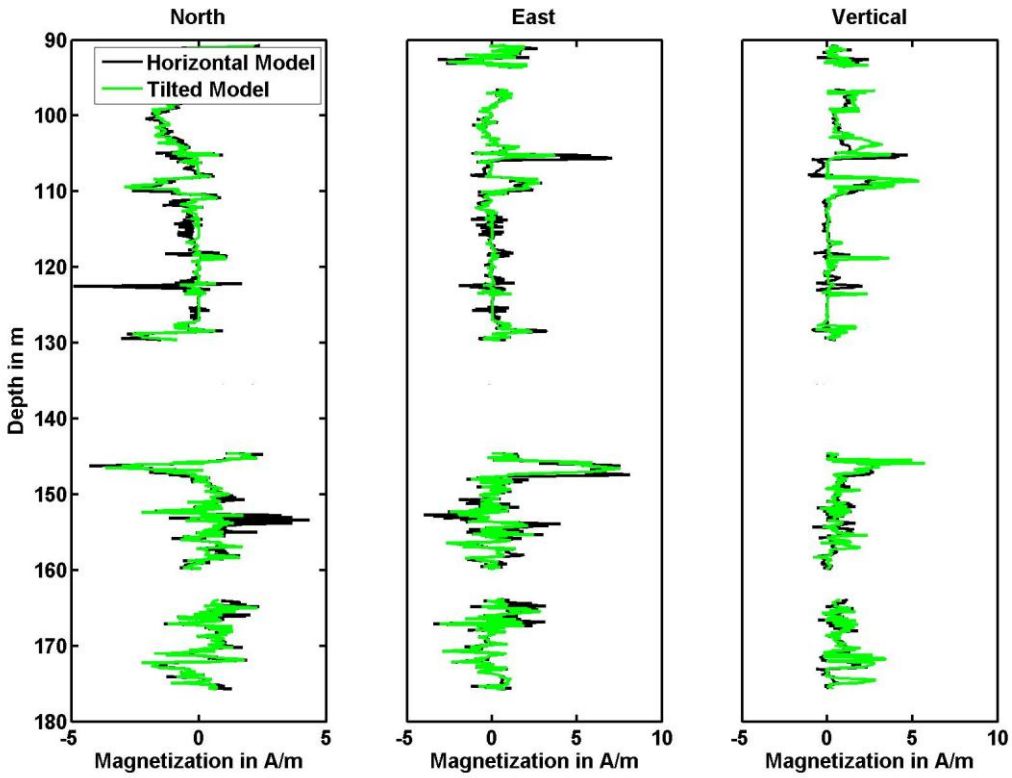

Figure 4: Results of using the empirical formula to explain the differences between the horizontal layer magnetization model and the magnetization of the drill cores. With suitable angles for dip, strike and magnetic declination, the drill core magnetization can be brought into agreement with the horizontal layer model. Without further information, the necessary angles cannot be determined unambiguously.

B.E., Deschamps, F., Dorais, M.J., Ebuna, D., Ehmann, S., Fitton, J.G., Fulton, P.M., Ganbat, E., Hamelin, C., Hanyu, T., Kalnins, L., Kell, J., MacHida, S., Mahoney, J.J., Moriya, K., Nichols, A.R.L., Rausch, S., Sano, S.-I., Sylvan, J.B., Williams,R.; Limited latitudinal mantle plume motion for the Louisville hotspot; Nature Geoscience,Volume 5, Issue 12, December 2012, 911-917

Virgil, C.; Vorbereitung und Durchführung von dreikomponentigen Magnetfeldmessungen mit dem Göttinger Bohrloch Magnetometer; PhD Thesis, TU Braunschweig, 2012

ICDP

Rayleigh and Love wave tomography in NW Bohemia/Vogtland from seismic ambient noise

M. FALLAHI[1], M. KORN[1], C. SENS-SCHOENFELDER[2]

[1] Institut für Geophysik und Geologie, Universität Leipzig, Talstraße 25, 04103 Leipzig
[2] Deutsches Geoforschungszentrum Helmholtz-Zentrum Potsdam

The W-Bohemia/Vogtland region at the border between Germany and Czech republic is a place of presently ongoing geodynamic processes in the intra-continental lithosphere, which result in the occurrence of repeated earthquake swarms, mantle-derived fluid exhalations, mofettes, mineral springs and enhanced heat flow. It is a key site to study the mantle-crust interaction in an active magmatic environment, and has been proposed as a site for scientific drilling. Fluid reservoirs have been proposed for the upper crust as well as for the crust-mantle transition zone, but their direct observation is still missing.

Using the vertical and transverse component ambient noise data, we estimate both Rayleigh and Love waves from ambient noise cross-correlation waveforms to investigate the crustal seismic structure of W-Bohemia/Vogtland.

More than 2000 Rayleigh and Love group-velocity dispersion curves are obtained by time-frequency analysis of stacked ambient noise cross-correlation functions between station pairs using the data between 2002 and 2004 recorded at 43 seismic stations from BOHEMA experiment and between 2006 and 2008 recorded at 79 seismic stations from permanent station networks of Germany, Czech Academy of Sciences (WEBNET) and PASSEQ experiments.

At each period between 1 and 10 s, group velocity maps are constructed, all corresponding to different sampling depths, and thus together giving an indication of the 3D shear wave velocity structure extending to a depth of about 15 km.

ICDP

Understanding pre-eruptive conditions of the Campanian Ignimbrite eruption combining solubility and phase equilibria experiments and natural rocks analyses

S. FANARA[1], R.E. BOTCHARNIKOV[1], D.M. PALLADINO[2], H. BEHRENS[1]

[1] Institut of Mineralogy, Leibniz University of Hannover, Callinstr. 3, 30167 Hannover, Germany
[2] Dipartimento di Scienze della Terra, Universitá "La Sapienza" di Roma, Piazzale Aldo Moro 5, 00185 Roma, Italy

The Campanian Ignimbrite (CI) is the most powerful eruption of the Campi Flegrei Volcanic District (CFVD), located in southern Italy, immediately north-west of the city of Naples. For more than 300 ka, this volcano was characterized by a predominantly explosive volcanic activity (Pappalardo et al., 2002). Nowadays this area, characterized by fumarolic and hydrothermal activity coupled with bradisismic activity and seismic swarms, still lies under volcanic unrest conditions and is listed among those with the highest volcanic risk worldwide (Todesco 2009, Chiodini et al., 2011).

The CI yielded around 200 km^3 dense rock equivalent (DRE) with trachytic-phonolitic composition circa 39 ka ago (e.g. Civetta et al. 1997; Pappalardo et al. 2002; Arienzo et al. 2009; Di Renzo et al., 2011), synchronous with significant climatic change (Fedele et al., 2003). Although the CI eruption has been largely investigated for hundreds of years, being still the object of study today, the vent location, the stratigraphic sequence as well as the shape and depth of the magma chamber(s) of the CI are still under debate. Such informations are crucial for the interpretation of drilling products and observations at the planned drilling site at Campi Flegrei (CFDDP).

Natural samples were collected during three field excursions in 2010 and 2012 organised by the University of Hannover in collaboration with the University La Sapienza of Rome (Prof. Danilo M. Palladino) and The University Federico II of Naples (Prof. Benedetto De Vivo). Samples collected during the field trip in Procida were investigated with optical microscope and electron microprobe analyses in three bachelor theses (Güttler 2010, Krull 2010, Mozar 2010). The sampling was aimed to record and successively compare the whole sequence of the CI as it outcrops in the Neapolitan area, NE of the hypothetic vent of CI, and on the Procida Island, in the SW sector. The Basal Pumice Fallout was collected in the Taurano Valley, about 30 km E of the city of Naples and circa 40 km E from the hypothetic vent of the CI, since the pumice fallout is SE distributed. Samples from the higher part of the CI sequence were collected around Naples in the areas of Ponti Rossi, Soccavo, Acquamorta, Zaccaria and Spinelli. These locations are close to the reconstructed boundary of the CI caldera (Rosi and Sbrana, 1987). A complete record of samples from the CI sequence was collected also on Procida, at the outcrops of Punta della Lingua, Scotto di Carlo and Spiaggia del Postino. Products from the juvenile parts of the deposit (obsidian clasts, sputter clasts, white crystal-rich pumices and gray crystal-rich pumices) as well as the pyroclastic flow matrix from the CI were collected,

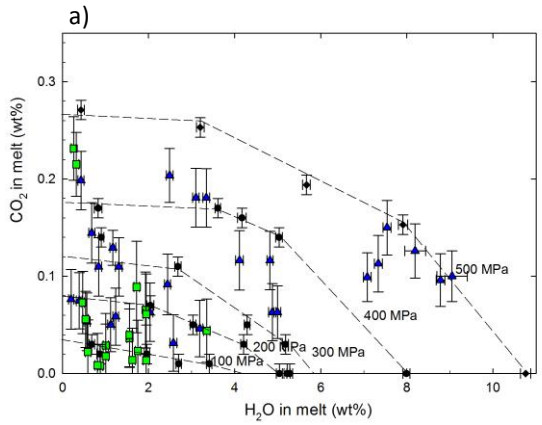

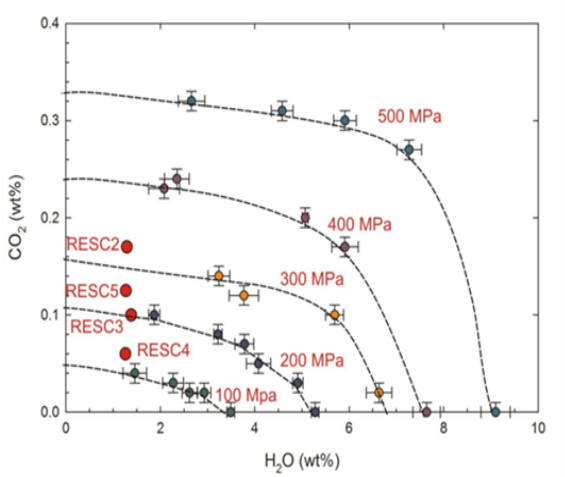

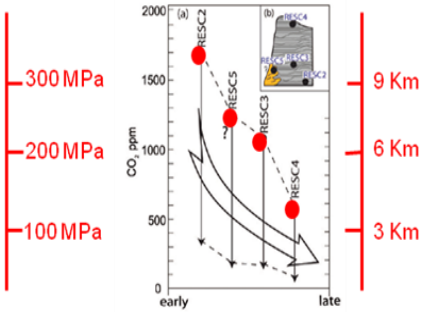

Fig. 1a – (left) H_2O and CO_2 solubility plot for CI trachytic melt – black dots refer to experimental samples and dashed lines represent the reconstructed isobars. Blue triangles are data from the natural samples collected on-land, around the city of Neaples. Green squares refer to natural samples from the Procida island.
Fig. 1b – (down) H_2O and CO_2 solubility plot for CI trachybasaltic Solchiaro melt. Red dots refer to the H_2O and CO_2 contents in melt inclusions from Esposito et al. (2011). Fig.1c - variations in CO_2 abundances with eruptive sequence in Solchiaro melt inclusions from Esposito et al. (2011). Red lines with labels show P and depth estimated from the solubility data.

being the CI the most-evolved member of the PVD (Arienzo et al., 2009). To collect further informations on the source of the most evolved magmas, the youngest products of Procida island coming from the Solchiaro eruption were also sampled, being the least evolved of the PVD area and considered as the mafic end-member for the Campi Flegrei magmatism (De Astis et al., 2004; Mormone et al., 2011).

The natural samples were analysed under the microscope and electron microprobe to investigate the chemical compositions and the mineral associations, as well as using Karl-Fisher Titration (KFT) and Carbon-Sulfur Analyser (CS) to determine the concentrations of H_2O and CO_2 in the glasses. The data collected on the natural samples were used for comparison with the experimental ones.

A synthetic trachyte (Triflisco OF17c1; Civetta et al., 1997) and a synthetic trachybasalt reproducing the least evolved composition of the entire CFVD (De Astis et al., 2004) were prepared by melting of mixtures of oxides and carbonates at 1600°C in Pt crucibles for 10 h in a conventional muffle furnace. Bulk compositions and homogeneity of the produced glasses were tested by electron microprobe CAMECA SX100.

H_2O and CO_2 solubilities were investigated in the trachyte at 1100°C and at pressure from 100 to 500 MPa for approx. 24 h in an Internally Heated Pressure Vessel (IHPV) (Fig.1) (master project F. Adams, 2012). The experimental data are reported in comparison with natural data in Fig.1a. It was found that solubility of water increases with pressure in a range from 4.2 wt% at 100 MPa to 10.80 wt% at 500 MPa with XH2O=1. The solubility of CO_2 increases with increasing pressure as well from 350 ppm at 100 MPa to 2700 ppm at 500 MPa with nominal XH2O=0. The concentrations of H_2O and CO_2 analysed in the glass matrix of the natural samples show maximum values comparable with the isobar of 500 MPa defined on the basis of the experimental data. The samples from Procida show lower amount of water compared to the samples collected around the city of Naples. Volatile concentration data from melt inclusions are particularly scarce in the case of the CI. For instance, Mangiacapra et al. (2008) estimated that the melt inclusion were trapped in clinopyroxene phynocrysts at pressure between 100 and 20 0 MPa.

The solubilities of H_2O and CO_2 in the melt were investigated also for the trachybasaltic composition of Solchiaro eruption. The experiments were run at 1200°C and at pressure from 100 to 500 MPa for approx. 24 h in IHPV (Fig.1b) (diploma thesis Buddensiek, 2010). It was found that solubility of water increases with pressure in a range from 3.49 wt% at 100 MPa to 9.15 wt% at 500 MPa with XH_2O=1 and shows a non linear dependence on XH_2O in the whole pressure range. The solubility of CO_2 increases with increasing pressure as well from 400 ppm at 100 MPa to 3200 ppm at 500 MPa with XH_2O=0.8, showing a linear dependence at pressure up to 200 MPa but deviating from linearity for higher pressures. Esposito et al. (2011) reported analyses of H_2O and CO_2 in melt inclusions of Solchiaro trachybasalt and found a correlation between volatile composition of the magma and eruptive sequence in Solchiaro deposits. In Fig.1b the data from the melt inclusions are reported in red in comparison with the experimental data, showing a range of pressures of the

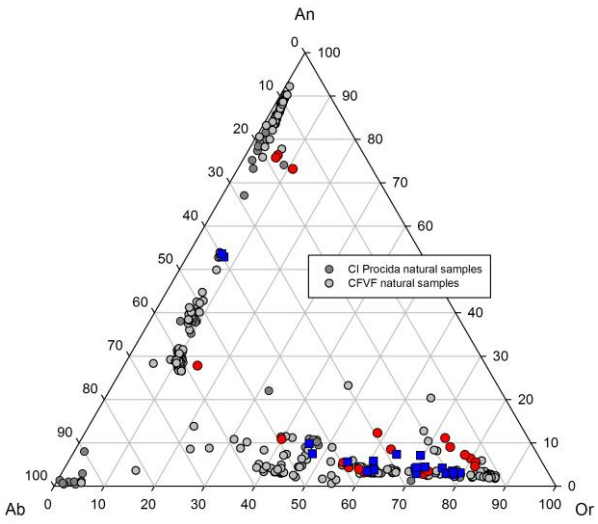

Fig.2 - feldspar ternary diagram: natural samples are shown in gray, samples at 100 MPa and 300 MPa are shown in blue and red respectively.

magma storage conditions between 130 and 330 MPa. Solubility experiments are of fundamental importance in relating pressure and depth of the stored magma. Based on our experimental data we can conclude that the depth for the trachybasaltic eruption of Solchiaro was underestimated by about 100 MPa in the study of Esposito et al. (2011) because their estimations were based on another composition.

To investigate the differentiation of the magma, tracing the evolution of the melt composition, and to shed light on the temperature of the magma at the storage conditions, the different mineral phases and their stability field of the less evolved end-member of the CI were investigated experimentally. Furthermore, natural samples from the CI were melted at 1600°C and ambient pressure in a muffle oven and then analysed by electron microprobe to better estimate the contribution from magma differentiation via fractional crystallization. Phase equilibria experiments were run at 100, 200 and 300 MPa (master thesis G. Macchi Ceccarani (in preparation), A. Husen (2010) and S.Righi (in preparation), respectively) and at temperatures from 850 to 1050°C with XH_2O fluid between 1 and 0.5 in Cold Seal Pressure Vessel (CSPV) and IHPV. Run products were analysed by microscope, electron microprobe and, if possible, spectroscopic techniques.

The compositions of the feldspars from experimental samples were compared with those of the natural ones (Fig.2) and with the results of the two-feldspar geothermometry from a previous work of Fuliginati et al. (2004). The trend of the natural samples from Procida and Naples is similar to that of experimental samples in the temperature range from 850°C to 1000°C, and the pressure plays a minor role. This results are in agreement with those of Fuliginati et al. (2004), indicating a range of temperature between 860°C and 980°C.

The phase relationships at 200 MPa pressure under relatively oxidizing conditions are shown in Fig. 3. The liquidus for the investigated system lies between 1050°C and 1000°C with magnetite as the first crystallising phase and pyroxene as second phase appearing between 1050°C and 950°C. Biotite crystallizes between 1000°C and 950°C and plagioclase between 900°C and 850°C. The last phase

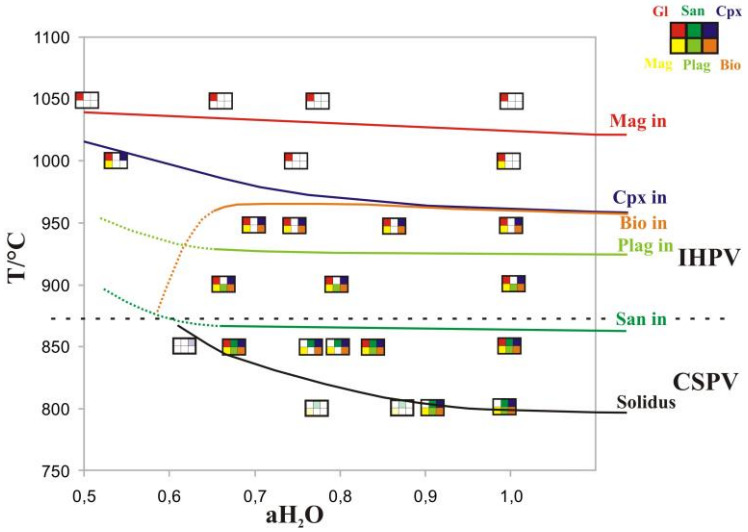

Fig.3 - Phase diagram with estimated stability fields of the mineral phases for CI trachytic melts at 200 MPa. Filled squares show presence of the phase.

is the sanidine which appears below 900°C. In general, the phase relationships at 100 MPa and 300 MPa are similar to those at 200 MPa but small differences can be noticed, for istance at 300 MPa the biotite crystallizes already at 1000°C.

In Fig. 4 a-b the melt evolution of the experimental samples is plotted in Harker diagrams and compared with the natural whole rock composition from this study and from previous ones. Black dots represent the bulk composition of natural samples from this study (obtained by the analysis of melted rock).

The diagrams SiO_2 vs MgO and SiO_2 vs CaO may shed light on the presence of crystal differentiation processes and on crustal assimilation processes, respectively. In both cases, the trends of the experimental samples are reproducing the trend of the natural samples, in particular those of the bulk analyses.

The glasses analysed in the natural samples show often a wide range in MgO concentration (about 1 wt%) for the same SiO_2 content. This range is strongly narrowed (about 0.2 wt%) if the bulk composition of natural samples is considered (melted rock). Therefore it is suggested that the crystal fractionation via differentiation plays a major role during the evolution of the magma prior to the CI eruption.

The natural glasses show a wide range in CaO concentration (about 2 wt%) too. Also in this case that range is narrowed in the bulk analyses. The presence of carbonate rocks at a depth of 6 km is anyway inferred from previous studies (Fedele et al., 2008), therefore assimilation processes from the wall of the magma chamber(s) are supposed, even if they do not play a major role in the magma prior to the CI eruption.

In conclusion, considering our results on H_2O and CO_2 solubility experiments compared with analyses on natural samples, we support the idea of a multi stage magma chamber (Arienzo et al., 2009; 2011; Di Renzo et al., 2011), where a magmatic storage region, probably formed by several magma chambers, is located between 2 and 10 km depth. The comparison of the compositions of feldspars from experimental and natural samples together with the two-feldspar geothermometry of Fuliginati et al. (2004) suggests a temperature range for the magma storage prior to the CI eruption between 850°C and 1000°C. Comparing the paragenesis of the natural samples with those from the phase equilibria experiment, the temperature range may be further restricted to below 900°C.

It is difficult to estimate the shape of the magma chamber(s) from the data we have, anyway it is clear that the Procida samples show higher values of CO_2 possibly due to assimilation processes from the sorrounding carbonatic rocks. Instead, the samples that show higher H_2O values are those from the Basal Pumice Fall Unit, that is, the first magma emitted during the CI eruption.

Further phase equilibria studies are planned on the trachybasaltic magma of Solchiaro to provide more informations about the role of crystal separation during magma differentiation.

In addition to equilibria with H_2O-CO_2 fluids we plan to study selectively the influence of other volatiles (Cl and S) that turned out to be of larger importance (Webster et al., 2011). Furthermore, H_2O-undersaturated experiments, where the same water content in the melt will be adjusted as in experiments with mixed H_2O-X fluids (X = CO_2, Cl or S), will be performed. Comparison of both types of experiments will allow us to distinguish the effect of changing water fugacity from specific effects of other fluid components. The experiments will be carried out at relatively oxidizing conditions. Such conditions are consistent with suggested relatively high oxygen fugacities in the CI magma chamber.

References:

Arienzo, I., Civetta, L., Heumann, A., Wörner, G., and Orsi, G. (2009) Isotopic evidence for open system processes within the Campanian Ignimbrite (Campi Flegrei-Italy) magma chamber. Bull Volcanol 71: 285-300.

Arienzo, I., Heumann, A., Civetta, L., Wörner, G., and Orsi, G. (2011) Processes and timescales of magma evolution prior to the Campanian Ignimbrite eruption (Campi Flegrei, Italy). Earth and Planet. Sc. Lett. 306: 217-228.

Chiodini, G., Avino, R., Caliro, S., and Minopoli, C. (2011) Temperature and pressure gas geoindicators at the Solfatara fumaroles (Campi Flegrei) Annals of Geoph. 54, 2; doi: 10.4401/ag-5002.

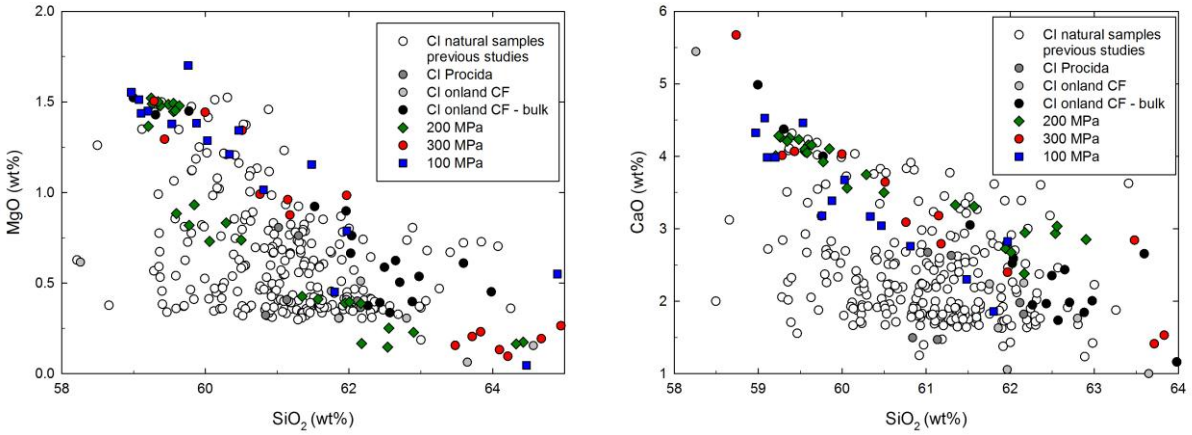

Fig.4 a-b: SiO_2 vs MgO plot(a – left) and SiO_2 vs CaO plot (b – right) of natural CI glasses (gray), bulk CI compositions (black) and experimental glasses at pressure of 100 MPa (blue), 200 MPa (green) and 300 MPa (red). Analyses of CI glasses from previous studies are shown in white.

Civetta. L., Orsi, G., Pappalardo, L., Fisher, R.V., Heiken, G., and Ort, M. (1997) Geochemical zoning, mingling, eruptive dynamics and depositional processes - The Campanian Ignimbrite, Campi Flegrei caldera, Italy. J Volcanol Geotherm Res 75:183–219.

De Astis, G., Pappalardo, L., and Piochi, M. (2004) Procida volcanic history: new insights into the evolution of the Phlegrean Volcanic District (Campania region, Italy). Bull. Volcanol. 66, 622-641.

Di Renzo, V., Arienzo, I., Civetta, L., D´Antonio, M., Tonarini, S., Di Vito, M.A., and Orsi, G. (2011) The magmatic feeding system of the Campi Flegrei caldera: Architecture and temporal evolution. Chem. Geol. 281, 3-4, 227-241.

Esposito, R., Bodnar, R.J., Danyushevsky, L.V., De Vivo, B., Fedele, L., Hunter, J., Lima, A., and Shimizu, N. (2011) Volatile Evolution of Magma Associated with the Solchiaro Eruption in the Phlegrean Volcanic District (Italy). J. Petr., 52, 2431-2460.

Fedele, F., Giaccio, B., Isaia, R., and Orsi, G. (2003) The Campanian Ignimbrite eruption, Heinrich 4 event, and Palaeolithic change in Europe: a high resolution investigation. In: Robock, A and Oppenheimer C. (eds) Volcanism and the Earth's Atmosphere. Washington, DC: American Geophysical Union: 301-325.

Fedele, L., Scarpati, C., Lanphere, M., Melluso, L., Morra, V., Perrotta, A., and Ricci, G. (2008) The Breccia Museo formation, Campi Flegrei, southern Italy: geochronology, chemostratigraphy and relationship with the Campanian Ignimbrite eruption. Bull. Volcanol. 70, 1189-1219.

Fulignati P, Marianelli P, Proto M, Sbrana A (2004) Evidences for disruption of a crystallizing front in a magma chamber during caldera collapse: an example from the Breccia Museo unit (Campanian Ignimbrite eruption, Italy). J Volcanol Geotherm Res 133: 141-155.

Mangiacapra, A., Moretti, R., Rutherford, M., Civetta, L., Orsi, G., and Papale P. (2008) The deep magmatic system of the Campi Flegrei caldera (Italy): Geophys. Res. Lett., 35, 21.

Mormone, A., Piochi, M., Bellatreccia, F., De Astis, G., Moretti, R., Della Ventura, G., Cavallo, A., and Mangiacapra, A. (2011) A CO_2-rich magma source beneath the Phlegrean Volcanic District (Southern Italy): Evidence from a melt inclusion study. Chem. Geol. 287, 1-2, 66-80.

Pappalardo, L., Civetta, L., De Vita, S., Di Vito, M., Orsi, G., Carandente, A., and Fisher, R.V. (2002) Timing of magma extraction during the Campanian Ignimbrite eruption (Campi Flegrei Caldera). J Volcanol Geotherm Res 114: 479-497.

Rosi, M., and Sbrana, A. (1987) Phlegrean Fields. CNR, ''Quaderni de La Ricerca Scientifica'' 114:1-175

Todesco, M. (2009), Signals from the Campi Flegrei hydrothermal system: Role of a "magmatic" source of fluids, J Geophys Res 114: B05201, doi:10.1029/2008JB006134.

Webster, J.D. (2011) Distribution of Sulfur between melt and fluid in S-O-H-C-Cl- bearing magmatic systems at shallow crustal pressures and temperatures. Rev. Mineral. Geoch. 73, 247-283.

ICDP

The Chew Bahir Drilling Project, southern Ethiopia: Towards a reconstruction of Quaternary climate shifts in the cradle of humankind

V.FOERSTER[1], A. JUNGINGER[2], A. ASRAT[3], M. UMER[†], H.F. LAMB[4], T. KASSA[1], V. WENNRICH[6], M. WEBER[6], J. RETHEMEYER[6], N. NOWACZYK[5], U. FRANK[5], M. C. BROWN[5], M.H. TRAUTH[2], F. SCHAEBITZ[1]

[1] University of Cologne, Seminar for Geography and Education; Gronewaldstrasse 2; 50931 Cologne; Germany
[2] University of Potsdam, Institute of Earth and Environmental Science; Germany
[3] Addis Ababa University, Department of Earth Sciences; P. O. Box 1176, Addis Ababa, Ethiopia
[4] Aberystwyth University, Institute of Geography and Earth Sciences, Aberystwyth SY23 3DB, U.K.
[5] Helmholtz-Zentrum Potsdam, Deutsches GeoForschungsZentrum – GFZ, 14473 Potsdam; Germany
[6] University of Cologne, Institute of Geology and Mineralogy; Zülpicher Str.49A; 50674 Cologne; Germany

Chew Bahir, today a saline mudflat in a tectonically-bounded basin in southern Ethiopia is situated in a biogeographically highly sensitive transition zone between the Main Ethiopian Rift and the Omo-Turkana basin, where the fossils of the oldest known anatomically modern human were found. Thus the lacustrine sediment infill of Chew Bahir represents a unique archive to reconstruct Late Quaternary environments in the source region of *Homo sapiens.* The study site, Chew Bahir, is a key part of the ‚Hominid Sites and Paleolakes Drilling Project' (HSPDP) which involves similar scientific drilling at four other sites in East Africa, all being lacustrine sedimentary archives close to globally- significant fossil hominin sites (Cohen et al., 2010). Furthermore, the project is part of the CRC-806 programme "Our Way to Europe".

Aim of the Chew Bahir pilot project is twofold: On the one hand to infer past variability in moisture like the youngest and hence best to be studied insolation controlled wet phase, the so-called African Humid Period (AHP; ca.15-5 ka BP) in the southern Ethiopian Rift, thus gaining insights into similar but older variations that have potentially important implications for the evolution and dispersal of *Homo sapiens* from Africa into Eurasia. On the

other hand, this pilot study targets at determining the necessary information about the type and character of the estimated 5 km sediment infill of the Chew Bahir basin to test for the optimal drilling site to recover a longer sediment core (400m) within the ICDP programme.

The recently desiccated lake floor was cored in two consecutive drilling campaigns in 2009 and 2010 in a NW-SE transect across the basin to provide fundamental data from this site, including the type and character of the deposits as well as sedimentation rates and their variability within the basin itself. In December 2009 the pilot core CB-01-2009 was recovered from the western margin of Chew Bahir (N04° 50'6; E36° 46'8) close to an extensive alluvial fan east of the Hammar Range, using a rotary single tube drill provided by Addis Geosystems Ltd. The record covers the uppermost 18.86 m of the deposits with a recovery rate of 81%. Coring was carried out in 19 drives without overlap. In November 2010, five more continuous cores were cored in the transect through the playa (Figure 1) with a percussion corer and an electrical operated hammer. CB-02 to CB-06 are ranging between 9 and 11m oring depth without overlap and a recovery rate of more than 97 %.

Multiproxy analysis, including geochemical, geophysical, biological, paleomagnetic and sedimentological analyses, combined with AMS radiocarbon dates, has been applied to all 6 cores. The results from the pilot core CB-01-2009 have been published (Foerster et al., 2012), showing that the pilot core has recorded the past 45 ka of the climatically highly variable Late Quaternary reflecting partly abruptly shifts in moisture availability. Chew Bahir responds sensitively to even minor climatic fluctuations on millennial to centennial timescales including Dansgaard-Oeschger cycles and Heinrich events. The data correlate with both high-latitude and tropical climatic records. The core lithology of CB-01 comprises lacustrine silty clays, intercalated with sandy coarse detrital layers, interpreted as resulting from erosional input by strong rainfall events from an arid, sparsely vegetated catchment. Carbonate layers towards the base of the core indicate past lacustrine environments with enhanced evaporation. Six horizons with high abundances of the gastropod *Melanoides tuberculata* occur in various matrixes from silty clay to sandy gravel. Diatoms and ostracods are present, mostly in discrete layers of the core profile; pollen and spore concentrations are low. Diatoms gradual increase to higher abundances dominated by *Aulacoseira* and *Cyclotella* spp. at ~6.20 m to ~5.45 m, but the low absolute numbers and low diversity do not allow quantitative estimation of past ecological conditions in the former lake. No saline/alkaline indicator taxa were found in the core, possibly because of lack of preservation. The few microfossils and molluscs present in the core support the geochemical results obtained by high-resolution XRF scanning, MSCL logging and XRD analyses.

Age control and sedimentation rates were determined by a series of calibrated radiocarbon ages. The radiocarbon

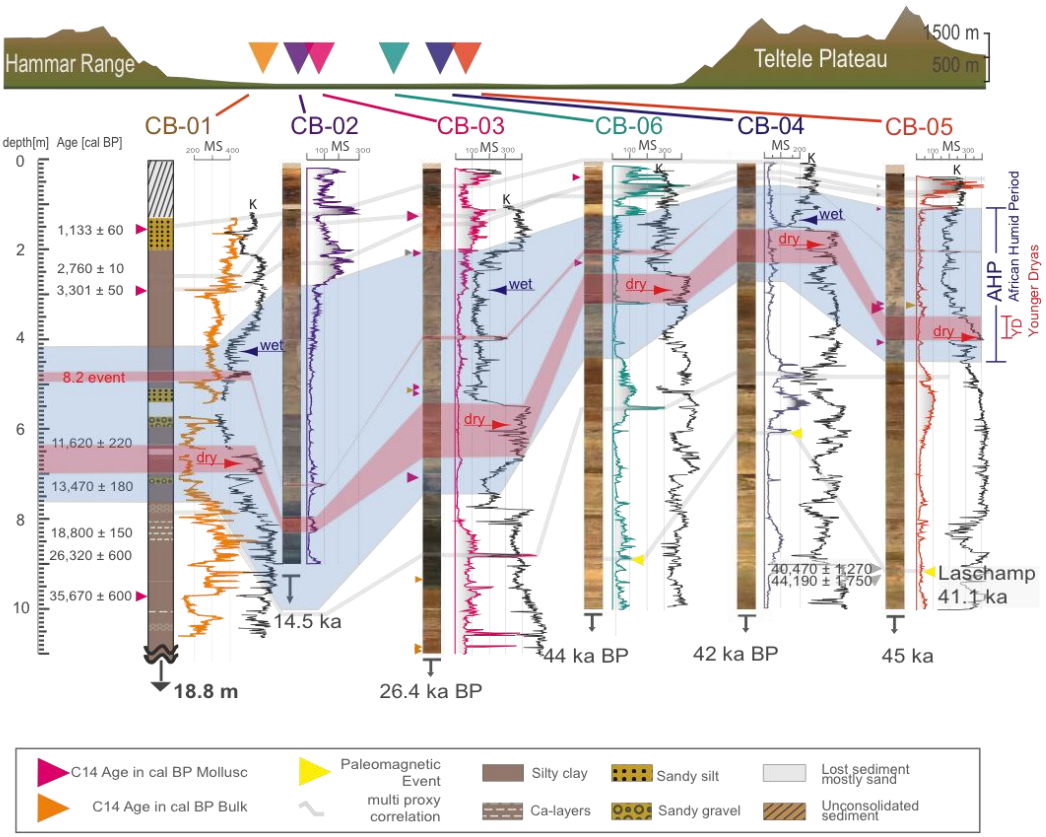

Figure 1: Profile of the Chew Bahir NW-SE transect of 6 cores through basin, showing correlation with the pilot core CB-01, the upper part of the lithology of CB-01, core pictures of CB-02 to CB-06. The correlation is based on a multi proxy approach. Sedimentation rates are generally decreasing towards the center of the basin. Magnetic susceptibility (MS) and potassium (K) records show sensitive reaction towards moisture shifts like LGM, AHP, YD and the 8.2 ka event. High K values indicate dry conditions.

ages of biogenic carbonates (shells of the abundant *Melanoides tuberculata*) and bulk sediment samples are consistent, showing no reversals. However, charcoal samples (fossil wood) were picked to approach an estimation of a possible reservoir effect in the basin and its variation through time. The age model, combined with a paleomagnetic chronology, indicates that CB-01 records the environmental history of Chew Bahir from ~45 to 1.0 ka BP, including the Last Glacial Maximum (23-18 ka BP), the African Humid Period (15-5 ka BP) and the onset of the Medieval Warm Period (700-1,000 BP/950-1,250 AD). The mean sediment accumulation rate (SAR) determined from the pilot core is 0.7 mm/a, but the rate varies, with a relatively high value of 1.3 mm/a from 45 to 40 ka BP. After 40 ka BP sedimentation rates decreased to 0.6 mm/a until ~35 ka BP), and then to 0.1 mm/a until 13 ka BP. The sedimentation rate then increased in two steps, from 0.4 mm/a between 13 and 3 ka BP, to 0.7 mm/a between 3 and 1 ka BP, reaching 1.3 mm/a during the last millennium. Inferred wetter conditions coincide with increased deposition rates, due to enhanced fluvial input with more continuous deposition of generally finer material. Consequently, the inferred dry-wet-dry cycles are also evident in the distinct sedimentation rate changes. At the onset of the AHP, 15 ka ago, the sedimentation rate increased six or seven-fold until 13 ka BP.

Besides the other measured chemical elements such as Ti, Fe, Ca, Sr, and Mn, the most striking paleoenvironmental indicator seems to be potassium (K) as a proxy for aridity in the catchment of the Chew Bahir. Following the potassium curve of our pilot record (Foerster et al., 2012) but also of CB-03, CB-04, CB-05, CB-06 as shown in Figure 1, demonstrating humidity with decreasing values, it becomes clear that during the time interval between ~15-5 ka the basin has been subdued to humid conditions. These resulted in an enlarged lake with fresh water diatoms and a dominance of fluvial fine-grained input (also expressed in the magnetic susceptibility curve of all cores), outlining a prominent and clearly defined wetter period, known as the insolation controlled AHP with a remarkable abrupt onset and a rather gradual termination. The AHP frames a sharply defined arid phase (12.8-11.6 ka cal BP) that has been associated with the Younger Dryas chronozone and is followed by a marked drought around 8.2 ka ago, most likely induced by the sudden decrease in global temperatures that is known as the 8.2 ka event and has resulted in a drastic drop of moisture over large parts of East Africa. Under generally arid conditions with sparse vegetation cover, the gneisses (e.g., the potassium-rich orthoclase feldspar biotite muscovite- gneisses) as well as two-mica granites with conspicuous orthoclase phases constituting the Hammar range are eroded more easily, and then washed into the basin via alluvial fans. These events are expressed by sharp increases of K in the record, reflecting the onset of dry conditions. Increased sediment supply from the alluvial fans of Hammar range during dry conditions into a shallow or even dried out lake also is reflected by coarser material (like sandy silt and sandy gravel), which is washed in during strong rain events. The K in the record can be attributed exclusively to terrigenous and allochthonous input; and once deposited, no further processes change or enrich the amount of K. Thus, the K record potentially provides a clear aridity signal, as the provenance and transport mechanisms of the element are rather constrained.

CB-02 to CB-06 have a similar lithology as described for the pilot core CB-01, with fine silts and clays intercalated by few coarser layers that largely correlate with drier phases as also suggested by geochemical results. Changes of grainsize and material composition are reflected in the MS signal that was moreover used for correlation of the transect cores. Fine silts and clays predominate towards the centre of the basin with increasing influence of fluvial inwash. During the sections that have been associated with the AHP, the fresh water diatom assemblages that were described for the pilot core can be also found in CB-06 and with an even wider spectrum of taxa in CB-03 and CB-05. Furthermore, a sharply defined horizon with densely packed fossilized fish-bones and vertebrates in three of the cores documents the presence of a lake whereas horizons with abundances of up to 2 mm in diameter big calcites indicate arid phases with enhanced evaporation in a shallow or even dried out lake bed.

So far, results from the cores CB-02 to CB-06 have also shown fluctuating sedimentation rates corresponding to moisture shifts as well as a change of the sedimentation rate within the basin itself. Generally the sedimentation rate is decreasing towards the center of the basin as Figure 1 illustrates. Eighteen radiocarbon dates have been determined from CB-03, CB-05 and CB-06, that have been correlated incorporating the age model of the pilot core, all geochemical, geophysical and foremost paleomagnetic results. At 9.17 m in CB-05, the proposed deep drilling site in the center of the basin, the Laschamp event (41 ka BP) has been identified, suggesting an age of ~ 45 ka BP for the maximal depth of the 10 m long core. Also in CB-04 at 6.11 m and in CB-06 at 8.93 m the Laschamp event could be found, outlining that the 10 m long CB-04 covers the last 42 ka and CB-06 the last 44 ka with merely 10 m SB depth. Consequently this implies that the 400 m long cores (field campaign scheduled for October to December 2013) will extend the record to 750 ka BP, and thus span the time frame of Homo diversification, the emergence of anatomically modern humans at 195 ka, their recent dispersal from Africa at ca. 60 ka, the Middle Stone Age, and the age of habitual use of fire.

References:

Cohen, A., Arrowsmith, R., Behrensmeyer, A.K., Campisano, C., Feibel, C., Fisseha, S., Johnson, R., Kubsa Bedaso, Z., Lockwood,C., Mbua, E., Olago, D., Potts, R., Reed, K., Renaut, R., Tiercelin, J.-J., Umer, M., 2010. The Hominin Sites And Paleolakes Drilling Project (HSPDP): Using Scientific Drilling To Understand The Paleoclimate Context Of Human Evolution.doi:10.2204/iodp.sd.8.10.2009.

Foerster, V., Junginger, A., Langkamp, O., Gebru, T., Asrat, A., Umer, M., Lamb, H., Wennrich, V., Rethemeyer, J., Nowaczyk, N., Trauth, M.H., Schäbitz, F. (2012). Climatic change recorded in the sediments of the Chew Bahir basin, southern Ethiopia, during the last 45,000 years, Quaternary International, 274, 25-37.

ICDP

SCOPSCO: Late Glacial to Holocene sedimentation at lakes Ohrid (Macedonia, Albania) and Dojran (Macedonia, Greece)

A. FRANCKE[1], B. WAGNER[1], M. LENG[2,3], K. LINDHORST[4], S. KRASTEL[4,5], R. SULPIZIO[6], G. ZANCHETTA[7]

[1] University of Cologne, Institute for Geology and Mineralogy, Cologne, Germany
[2] University of Leicester, Department of Geology, Leicester, UK
[3] NERC Isotope Geosciences Laboratory, British Geological Survey, Nottingham, UK
[4] Helmholtz Centre for Ocean Research, GEOMAR, Kiel, Germany
[5] Institute of Geosciences, University of Kiel, Germany
[6] Dipartimento di Scienze della Terra e Geoambientali, University of Bari, Italy
[7] Dipartimento di Scienze della Terra, University of Pisa, Italy

Although lakes Ohrid and Dojran in the Balkans are considered to have been formed by tectonic activity and to be of Tertiary age, they may have archived different environmental histories due to differing geographical settings and hydrological regimes. Lake Dojran is located at an altitude of 144 m asl at the border of the Former Yugoslav Republic of Macedonia (FYROM) and Greece (Fig. 1). The lake has a surface area of ca 40 km^2 and a maximum water depth of 7 m. In contrast, Lake Ohrid is located ca 160 km to the west at an altitude of 693 m asl at the border between FYROM and Albania. The lake has a surface area of 360 km^2 and is 289 m deep. Several studies have shown that smaller and shallower lakes often react more sensitive to environmental change (Leng et al., 2010; Wagner et al., 2010), so a comparison of sediment records from both lakes is useful to better understand local and regional effects on environmental change.

From the deepest part of Lake Dojran, a ca. 7 m long sediment record (Co1260) was recovered in summer 2011. At the coring location, the hydro-acoustic survey indicated horizontally bedded and undisturbed deposits for the uppermost few meters. A strong, somewhat undulated reflector was observed at ca. 7 m sediment depth in the hydro-acoustic data. This reflector corresponded to a stiff sediment layer, which hampered deeper penetration during coring. A robust age-model was established for core Co1260 from 13 radiocarbon ages, and indicates a basal age of ca. 12,500 cal yr BP. The sedimentological properties (TOC, $CaCO_3$, TC, N, S, grain-size, XRF, $\delta^{18}O_{carb}$, $\delta^{13}C_{carb}$, $\delta^{13}C_{org}$) of core Co1260 were linked to the hydro-acoustic data and suggest that the core base was deposited when the lake-level and temperatures were low. This overall cold and dry period lasted until around 11,500 cal yr BP and likely corresponds to the Younger Dryas. Our data suggest that the Younger Dryas at Lake Dojran can be separated into a first cooler and dryer, and a second, slightly warmer and more humid period. During the Holocene, the sediment record exhibits distinct environmental changes, including the 8.2 ka and 4.2 cooling events and longer-term changes, such as the Medieval Warm Period and the Little Ice Age. Human induced erosion processes in the catchment of Lake Dojran intensified after 2,800 cal yr BP.

Lake Ohrid is considered to be the oldest lake of Europe and probably provides the longest continuous paleoclimate record in the Mediterranean region. This forms the backbone for the ICDP drilling project SCOPSCO (Scientific Collaboration on Past Speciation Conditions in Ohrid), which aims (1) to reveal a precise age and origin of Lake Ohrid, (2) to unravel the seismotectonic history of the lake area including effects of major earthquakes and associated mass wasting events, (3) to obtain a continuous record containing information on volcanic activities and climate changes in the central northern Mediterranean region, and (4) to better understand the impact of major geological/environmental events on general evolutionary patterns and shaping an extraordinary

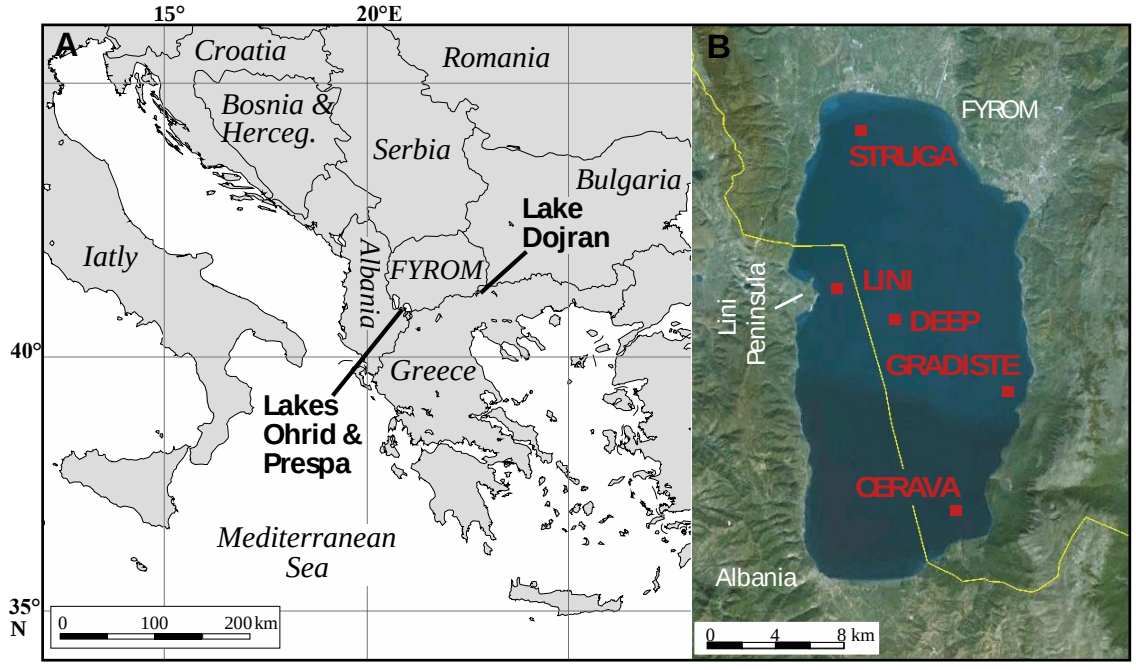

Fig. 1: A: Locations of lakes Ohrid, Prespa, and Dojran in the northeastern Mediterranean region. B: Lake Ohrid, located at the border (yellow line) of the Former Yugoslav Republic of Macedonia (FYROM) and Albania. The red squares mark the 5 proposed drill sites.

degree of endemic biodiversity as a matter of global significance. Based on the results of pre-site surveys including sedimentological studies of limnic sediments from the lake, detailed hydro-acoustic surveys, and tectonic mapping in the catchment, 5 drill sites at Lake Ohrid were selected (Fig. 1B). The deep drilling with the main aim to recover a 700 m long sediment core from the central basin of Lake Ohrid (ICDP site "DEEP") is now scheduled for spring 2013.

As part of the ICDP SCOPSCO project, the "LINI" site was drilled already in summer 2011. The recovered sediment core (Co1262) is 10.8 m long (Fig. 2). Overall, core Co1262 is mainly formed by relatively homogenous clayey to silty mud of greyish to olive color. The sediments appear massive, probably as a result of bioturbation, as it was also observed in other sediment sequences from Lake Ohrid at least throughout the Holocene (Wagner et al., 2009; Vogel et al., 2010a). Some gravel grains in the lowermost meter of core Co1262 are interpreted as ice-rafted debris and indicate that the sediment core reaches back into the Late Glacial (Wagner et al., 2009; Vogel et al., 2010a). A chronological control of the recovered sediments is based on tephrostratigraphy, radiocarbon dating and cross correlation with existing records from lakes Ohrid, Prespa, and Dojran (Fig. 2). Three crypothepra layers at 709 cm, 517 cm and 320 were identified by XRF scanning and by microscopical and geochemical analyses. The cryptotephras could be assigned to the Mercato (8890 cal yr BP), to the FL (3370 cal yr BP) and to a mixture of the AD 512 and AD 472 Somma-Vesuvius tephras, respectively. In addition, the age model of core Co1262 was improved by five radiocarbon ages from terrestrial plant material fragments (Fig. 2). Terrestrial plant material is considered to provide reliable ages, as it is not affected by reservoir effects. However, reservoir effects of up to 1500 years have been reported for bulk organic material dating from Lake Ohrid sediments (Wagner et al., 2008; Vogel et al., 2010b) and may have also influenced the radiocarbon age of a fish bone at 754 cm. To improve the age model in the lower sections of core Co1262, cross correlation to existing records from lakes Ohrid and Prespa was carried out. The increase of TOC and the end of ice-rafted debris deposition at ca. 900 cm in core Co1262 was correlated with the onset of the Holocene. Furthermore, peaks in TIC and Ca and the minimum in TOC around 800 cm depth in core Co1262 were correlated with the period 10,500–9,500 cal yr BP, when similar fluctuations are observed at Lake Prespa (Aufgebauer et al., 2012), and when a minimum in winter precipitation is reconstructed from a record at nearby Lake Maliq (Bordon et al., 2009). The minima in TIC content and Ca counts around 650 cm most likely correspond to the 8.2-cooling event, as comparable patterns in biogeochemical proxies are also reported from other cores from lakes Ohrid, Prespa and Dojran (Wagner et al., 2009; Vogel et al., 2010a; Aufgebauer et al., 2012; Francke et al., 2012). Based on the chronological tie points, the established age depth model using a smooth spline function yields sedimentation rates between 0.02 and 0.2 cm*yr^{-1} and a basal age of 12,250 cal yr BP for core Co1262.

The most prominent horizon in core Co1262 occurs between 320 and 121 cm depth. This horizon is characterized by a 1 to 2 cm thick sandy horizon at the base and very homogenous sediments without major variations in most sediment proxies above. The coarse grained base and the overall homogenous facies identifies this horizon

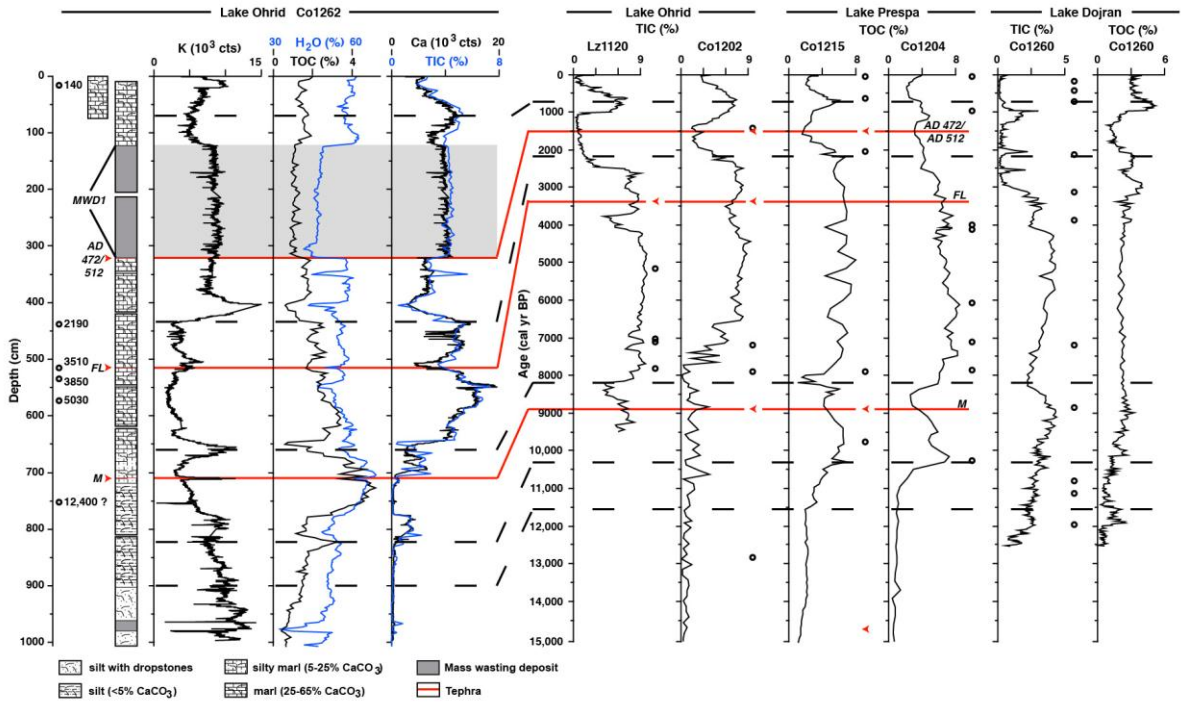

Fig. 2: Lithology, water content, and geochemical composition of core Co1262 from Lake Ohrid. Note that the entire sediment succession appears massive due to bioturbation. The gaps in XRF scanning data (Sr, K, and Ca counts) are due to non-overlapping cores. These gaps are smaller in water content, TIC, and TOC, as core catcher samples are included. The cross correlation with cores Lz1120 and Co1202 from Lake Ohrid, cores Co1215 and Co1204 from Lake Prespa, and core Co1260 from Lake Dojran (black dashed lines) can be used for an age estimation of core Co1262. Red arrows and lines indicate tephras and cryptotephras (AD 472/512, FL eruption, and M= Mercato). Black circles indicate radiocarbon dated horizons in cores from lakes Ohrid, Prespa and Dojran.

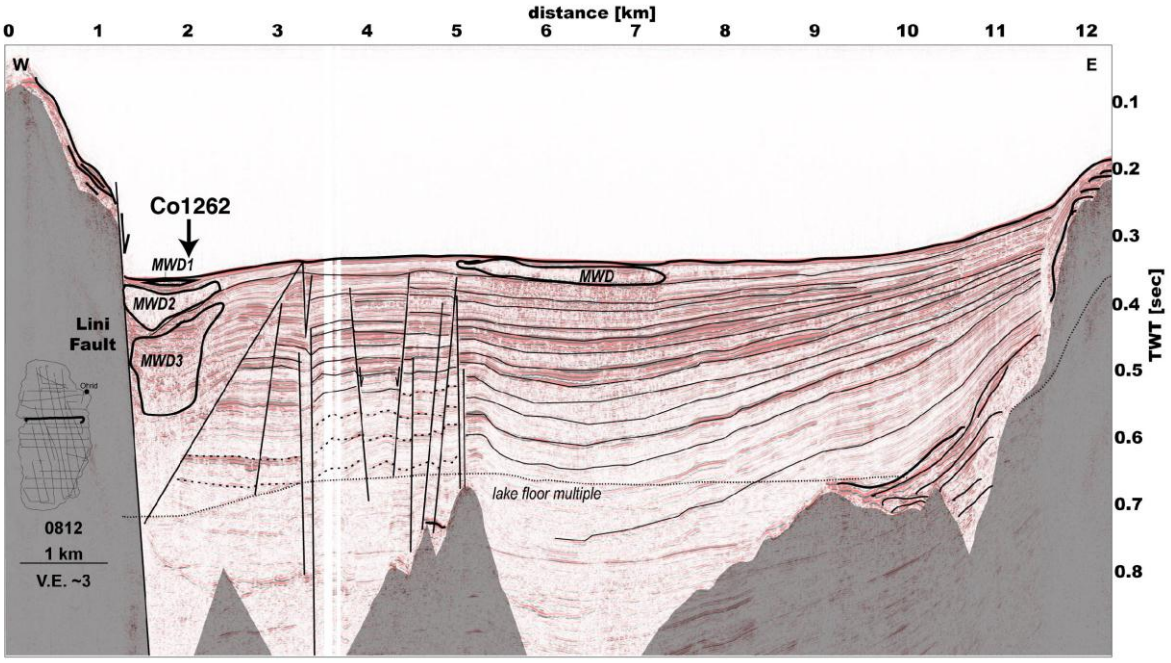

Fig. 3: Interpreted multichannel seismic profile taken by a Mini GI Gun across Lake Ohrid with the Lini Fault in the west. Grey parts indicate bedrock. The arrow indicates coring location Co1262 (ICDP site "LINI"). Transparent sediment bodies indicated mass wasting deposits (MWD1-3).

as a mass wasting deposit. This mass wasting deposit is also visible in the hydro-acoustic data and corresponds to MWD1 (Fig. 3). In addition to MWD1, a 15 cm thick turbidite from 980 cm to 965 cm as well as several < 4 cm thick wasting deposits were identified by variations in water content and grain-size composition, but these events are too small to be visible in the hydro-acoustic data. The established age model for core Co1262 can be used to determine the age of MWD1. MWD1 directly overlays the 1mm thick greyish band, which was identified as the AD 472/512 tephra. According to the established age model, the sedimentation rate during the 6th century was about 0.1 $cm*yr^{-1}$. This implies that the mass movement occurred less than 20 years after the deposition of the AD 472/512 tephra. Potential triggers for a mass movement include delta collapses, rockfalls, lake level changes, or earthquakes. A delta collapse can be excluded, as there is no inlet close to the coring location and deltaic deposits cannot be observed in the hydro-acoustic data. The steep subaquatic slopes close to the Lini Peninsula could have promoted rockfalls, but typical rockfall structures, such as relatively fresh scarps onshore or subaquatic basin-marginal cones cannot be observed. The existing records from lakes Ohrid and Prespa or paleoclimatic reconstructions from the region do not indicate that the early 6th century AD was characterized by significant changes in lake level and hydrology (Wagner et al., 2009; Vogel et al., 2010a; Aufgebauer et al., 2012). However, historical documents indicate that an earthquake destroyed the city of Lychnidus (Ohrid) in the early 6th century AD. Potential candidates for such an earthquake are the 518 AD earthquake, which according to some authors more affected the city of Scupi (Skopje, Aliaj et al., 2004, Ambraseys et al., 2009), or the 526 or 527 AD earthquake, which concentrated more on the Ohrid region (Ambraseys et al., 2009, Reicherter et al., 2011). Although the bioturbated structure of the sediment core and the impossible differentiation between the AD 472 and AD 512 tephra do not allow a chronological discrimination between the two (or three) earthquakes, it is evident that the MWD1 must have occurred during the early 6th century AD and is likely related to one of these earthquakes. Seismic activity probably also induced the Udenisht Slide Complex in the southwestern part of the lake (Lindhorst et al., 2012), which is one of the largest mass wasting events in the younger history of Lake Ohrid and clearly visible in a multi-beam dataset from the lake floor. The chronological control of this slide is difficult, but extrapolation of sedimentation rates of overlying sediment indicates that this slide is younger than 1500 yr and also probably associated with an early 6th century AD earthquake (Lindhorst et al., 2012). These observations strongly suggest that major earthquakes in Lake Ohrid triggered lacustrine slides and are confirmed by onshore information, which indicate that the morphology of the Ohrid basin is formed by frequent earthquakes of magnitudes between M 6.0 and 7.0 (Reicherter et al., 2011).

In the hydro-acoustic dataset, similar mass wasting deposits (MWD2 and MWD3) are indicated below the recovered sediment sequence Co1262 and reflect that the western part of Lake Ohrid in front of Lini Peninsula is characterized by one of the most active faults (Reicherter et al., 2011). The thickness of these mass wasting events exceeds 10 m. MWD2, which underlies core sequence Co1262, could originate from an older, Late Pleistocene earthquake. Most existing sediment records from Lake Ohrid spanning into the last glacial cycle have disturbed sedimentation at the Late Pleistocene/Holocene transition (Wagner et al., 2009; Vogel et al., 2010a), which might be related to high seismic activity. There are a number of other slides indicated in multichannel seismic sections from other parts of the lake (Lindhorst et al. 2012), which suggest that a long paleoseismic record will become available once a long core from Lake Ohrid will be recovered and studied.

References:
Aliaj, S., Adams, J., Halchuk, S., Sulstarova, E., Peci, V., and Muco, B.: Probabilistic Seismic Hazard Maps for Albania, 13th World Conference on Earthquake Engineering, Vancouver, BC, Canada, 2004.
Ambraseys, N.: Earthquakes in the Mediterranean and Middle East, Cambridge University Press, New York, 2009.
Aufgebauer, A., Panagiotopoulos, K., Wagner, B., Schaebitz, F., Viehberg, F. A., Vogel, H., Zanchetta, G., Sulpizio, R., Leng, M. J., and Damaschke, M.: Climate and environmental change in the Balkans over the last 17 ka recorded in sediments from Lake Prespa (Albania/F.Y.R. of Macedonia/Greece), Quaternary International, 274, 122-135, 10.1016/j.quaint.2012.02.015, 2012.
Bordon, A., Peyron, O., Lézine, A.-M., Brewer, S., and Fouache, E.: Pollen-inferred Late-Glacial and Holocene climate in southern Balkans (Lake Maliq), Quaternary International, 200, 19-30, 10.1016/j.quaint.2008.05.014, 2009.
Francke, A., Wagner, B., Leng, M. J., and Rethemeyer, J.: A Late Glacial to Holocene record of environmental change from Lake Dojran (Macedonia, Greece), Clim. Past Discuss., 8, 5743-5785, 10.5194/cpd-8-5743-2012, 2012.
Leng, M. J., Baneschi, I., Zanchetta, G., Jex, C. N., Wagner, B., and Vogel, H.: Late Quaternary palaeoenvironmental reconstruction from Lakes Ohrid and Prespa (Macedonia/Albania border) using stable isotopes, Biogeosciences, 7, 3109-3122, 10.5194/bg-7-3109-2010, 2010.
Lindhorst, K., Gruen, M., Krastel, S., and Schwenk, T.: Hydroa- coustic Analysis of Mass Wasting Deposits in Lake Ohrid (FYR Macedonia/Albania), Submarine Mass Movements and Their Consequences, 245–253, 2012.
Reicherter, K., Hoffmann, N., Lindhorst, K., Krastel, S., Fernandez- Steeger, T., Grützner, C., and Wiatr, T.: Active basins and neotectonics: morphotectonics of the Lake Ohrid Basin (FYROM and Albania), Zeitschrift der Deutschen Gesellschaft für Geowissenschaften, 162, 217-234, 10.1127/1860-1804/2011/0162-0217, 2011.
Vogel, H., Wagner, B., Zanchetta, G., Sulpizio, R., and Rosén, P.: A paleoclimate record with tephrochronological age control for the last glacial-interglacial cycle from Lake Ohrid, Albania and Macedonia, Journal of Paleolimnology, 44, 295-310, 10.1007/s10933-009-9404-x, 2010a.
Vogel, H., Zanchetta, G., Sulpizio, R., Wagner, B., and Nowaczyk, N.: A tephrostratigraphic record for the last glacial-interglacial cycle from Lake Ohrid, Albania and Macedonia, Journal of Quaternary Science, 25, 320-338, 10.1002/jqs.1311, 2010b.
Wagner, B., Reicherter, K., Daut, G., Wessels, M., Matzinger, A., Schwalb, A., Spirkovski, Z., and Sanxhaku, M.: The potential of Lake Ohrid for long-term palaeoenvironmental reconstructions, Palaeogeography, Palaeoclimatology, Palaeoecology, 259, 341-356, 10.1016/j.palaeo.2007.10.015, 2008.
Wagner, B., Lotter, A. F., Nowaczyk, N., Reed, J. M., Schwalb, A., Sulpizio, R., Valsecchi, V., Wessels, M., and Zanchetta, G.: A 40,000-year record of environmental change from ancient Lake Ohrid (Albania and Macedonia), Journal of Paleolimnology, 41, 407-430, 10.1007/s10933-008-9234-2, 2009.
Wagner, B., Vogel, H., Zanchetta, G., and Sulpizio, R.: Environmental change within the Balkan region during the past ca. 50 ka recorded in the sediments from lakes Prespa and Ohrid, Biogeosciences, 7, 3187-3198, 10.5194/bg-7-3187-2010, 2010.

ICDP

The Early Terrestrial Impact Record from the ICDP Drilling “Barberton Mountain Land”.

J. FRITZ[1], W.U. REIMOLD[1,2], R. T. SCHMITT[1], C. KOEBERL[3], I. MCDONALD[4], A. HOFMANN[5]

[1] Museum für Naturkunde, Invalidenstrasse 43 10115 Berlin, Germany
[2] Humboldt Universoity zu Berlin, Unter den Linden 6, 10099 Berlin, Germany
[3] University of Vienna, Alservorstadt, 1090 Wien, Austria
[4] School of Earth and Ocean Sciences, University of Cardiff, Park Place, Cardiff CF10 3AT Wales, UK
[5] University of Johannesburg, Siemert Rd, Johannesburg 2028 South Africa

Late Archean volcanic and sedimentary rocks will be available from the 2012-2013 ICDP drilling “Barberton Mountain Land”. These marine metasedimentary sections include spherule layers that are considered to represent the oldest known impact ejecta layers on Earth [1]. The Archean spherule layers have been interpreted as products of large impacts by 20 to >100 km diameter objects [2,3], because the ejecta contain millimeter-sized spherules that are larger and form thicker layers compared to any impact ejecta layer known from Phanerozoic sediments, including the global ejecta layer of the Chicxulub impact cratering event[4]. For comparison, the 180-km-diameter Chicxulub impact structure with a Cretaceous-Paleogene boundary age was formed by a projectile “only” 10 to 15 km size [5]. The estimated large sizes of the Archean impactors mainly account for the observation that, compared to any Phanerozoic spherule layer, the Archean spherule layers are composed of substantially larger spherules that form thicker layers, with some showing extremely high enrichments in projectile component (as indicated by high Ir concentrations [6]). However, estimates regarding size of the impact event and correlations between the different outcrops in the Barberton mountain land are complicated by post-depositional alterations of the tectonically deformed sediments [7,8].

The current ICDP project provides relatively fresh samples that were drilled from below the water table, and thus offers the opportunity to investigate / discriminate primary and secondary features of these rare rocks. Therefore, the spherule layers, as well as the hanging and footwall lithologies, will be characterized petrologically and geochemically by: 1) bulk chemical analyses of major and trace elements, 2) petrographic, micro-chemical, isotopic, and mineralogical characterization of the impact ejecta layers, and 3) LA-ICP-MS elemental mapping of platinum group element (PGE) distributions and elemental analyses of moderately siderophile elements. This aims at 1) characterization of the ejecta layers, 2) identification of the phases hosting the extraterrestrial PGE signature, 3) discrimination of the primary geological evidence of the impact event from those characteristics that resulted from syn- and post-sedimentary alteration.

Investigating the post depositional alteration will allow to identify those mineral phases that retained a chemical and mineralogic record of spherule formation. In addition, the identification of the PGE host phases and their distribution between matrix and spherules is key for understanding the delivery process of the extraterrestrial component and the post depositional alterations. So far the spherules are interpreted as condensates from a vapor plume and might serve as “flight recorders” [7,9], potentially documenting differences in thickness and chemistry between the Phanerozoic and the Archean atmosphere [10,11] Alternatively, the spherules represent a massive amount of ejected particles that (re)melted during re-entry into Earth’s atmosphere [12]. Applying the lessons learned from the Chicxulub impact event [13] to the Archean spherule layers [12] can improve our understanding of processes during large meteorite impacts onto Earth.

Identifying traces of mega-impacts in Earth’s ancient history could be of relevance for the evolution of atmosphere, biosphere, and parts of the Earth’s crust during that time. Such changes might be documented in the hanging and footwall lithologies of the spherule layers.

Recognizing global stratigraphic marker horizons is highly valuable for inter-correlating sedimentary successions between Archean cratons [3,14]. In addition clusters of spherule layers were identified in Paleoarchean and Neoarchean sediments. Hassler et al. [15] raise the question if the apparent clustering is an artifact of preservation, or alternatively hints to fluctuations in the rate of large impacts during the Archean, possibly as a response to long-term variations in the frequency of bolide-producing collisions in space. We will address this question by investigating the PGE and isotopic "fingerprint" of the Paleoarchean spherule layers.

Acknowledgement: Financially supported by the DFG -RE 528/14-1

References: [1] Lowe D. R. et al. (2003) Astrobiology 3, 7-47. [2] Lowe, D. R. and Byerly, G. R. (1986) Geology 14, 83–86. [3] Melosh H. J. and Vickery A. M. (1991) Nature 350, 494–497. [4] Simonson B. M., Harnik P. (2000) Geology 28, 975-978. [5] Morgan J., the Chicxulub Working Group (1997) Nature 390, 472–476. [6] Simonson, B. M. and B. P. Glass (2004) Annual Review of Earth and Planetary Sciences 32, 329-361. [7] Reimold W. U., et al. (2000) Impacts and the Early Earth. Eds.: Gilmour I., Koeberl C. Lecture Notes in Earth Sciences 91, Springer-Verlag, Berlin, pp.117-180. [8] Hofmann A. et al. (2006) GSA Special Paper 405, 33 - 56. [9] Krull-Davatzes A. E., Byerly G. R., Lowe D. R. (2010) Earth and Planetary Science Letters 296, 319-328. [10] Kasting J. F. (1993) Science 257, 920-926. [11] Zerkle A. L. et al. (2012) Nature Geoscience, doi:10.1038/ngeo1425. [12]Artemieva N. A. and Simonson, B. M. (2012) 43rd LPSC #1372. [13] Johnson B. C. and Melosh H. J. (2012) Icarus 217, 416-430. [14] Byerly G. R. et al. (2002) Science 297, 1325-1327. [15] Hassler C. W. et al. (2010) *Geology*, 39, 307-310.

ICDP

Geophysical characterisation of facies changes in overdeepened alpine valleys - a contribution to DOVE

G. GABRIEL[1], C.M. KRAWCZYK[1], U. POLOM[1], T. GÜNTHER[1]

[1] Leibniz Institute for Applied Geophysics (LIAG), Stilleweg 2, 30655 Hannover, Germany

DOVE – drilling of overdeepened Alpine valleys – is a new ICDP initiative that aims to investigate overdeepened Alpine valleys (Fig. 1) along various drilling transects, i) along the northern alpine margin (CH, D, A), ii) in inner-alpine areas (CH, A), and iii) along the southern alpine margin (I, SLO). The several hundred meter deep core drillings will contribute to a significant increase in our knowledge about A) the timing and extent of past Alpine glaciations, B) the impact of atmospheric circulation patterns on the ice build-up along and across the Alps, and C) the effect of repetitive glaciations on the shape of mountain ranges and their foreland. Secondary scientific objectives are related to the role of overdeepened structures as groundwater reservoirs, seismic microzonation and site effects, and geothermal applications.

A major challenge will be the selection and characterisation of the final drilling sites. Although important information can be provided by existing gravity data and reflection / refraction seismic data as well as by existing boreholes, this information is still limited to single Alpine valleys and to specific parts of these valleys. Hence, for some drilling locations additional pre-site surveys are required and for a detailed, spatial characterisation of the valley fills modern and complementing datasets must be collected. After Preusser et al. (2010) and references therein, geophysical data imply a complex history of erosion and infilling of valleys. However, some relevant discrepancies between seismic interpretations and drillholes, especially with respect to the differentiation between Quaternary and pre-Quaternary rocks, indicate the importance of integrated studies combining geophysical methods and borehole/core investigations.

Pre-site surveys will focus on the estimation of the basement depth, i.e. the thickness of the sedimentary fill (e.g. de Franco et al., 2009), and on contrasts in rock physical properties within the sediments. The variation of rock physical properties in combination with the imaged structures can subsequently be interpreted in terms of facies changes; this must be done based on experiences gained from existing geophysical surveys across Alpine valleys and the available geological knowledge of the valley. As lateral and vertical structures need to be resolved both, a combination of reflection seismics and gravimetry is planned, that turned out to be an appropriate combination in the past (e.g. Brückl et al., 2010), possibly complemented by electrical sounding methods and magnetics. The combined interpretation shall be based on an improved constrained inversion scheme that needs to be developed within the project. Because the start of the drilling campaign is already envisaged for 2015/2016, possible pre-site surveys must be performed and finished within a short time; the location of the pre-site surveys will be defined by the overall requirements of the DOVE project.

Beyond the pre-site surveys, further geophysical exploration is mandatorily required in combination with the new drilling results for a detailed, spatial characterization of the internal structure of the valleys sediments. Detailed information about the 3D sedimentary architecture is a basic requirement for the more applied goals of the project that are related to sedimentological, hydrogeological, and geothermal aspects. A detailed (seismic) facies analysis, constrained by the information from the new boreholes and complementing geophysical surveys will help to unravel the glacial history and the corresponding sedimentological processes of the different valleys. To tackle the challenges of imaging steeply dipping structures and horizontal structures, both characterized by small vertical and lateral variations in the petrophysical properties (i.e. information from downhole logging experiments is not necessarily representative for the entire valley fill), the combined inversion of different geophysical datasets must be extended to 3D.

The geophysical datasets can be used for a systematic comparison between different Alpine valleys. The overall aim is a more general characterization of the facies types of the sedimentary fill in terms of different geophysical properties,glacial advances, and the identification of marker horizons that can be related to specific glacial cycles. In addition to the newly acquired data, existing information should also be considered (e.g. Bücker et al., 1998; Reitner et al., 2010; Dehnert et al., 2012). If such an attempt would be successful, the value of geophysical data for applied investigations, e.g. hydrogeological studies, would increase significantly and the interpretation of the geophysical data does not mandatorily require borehole information as constraints in future. In this context also a comparison between inner-alpine valleys and foreland valleys is envisaged that are typically expected to have

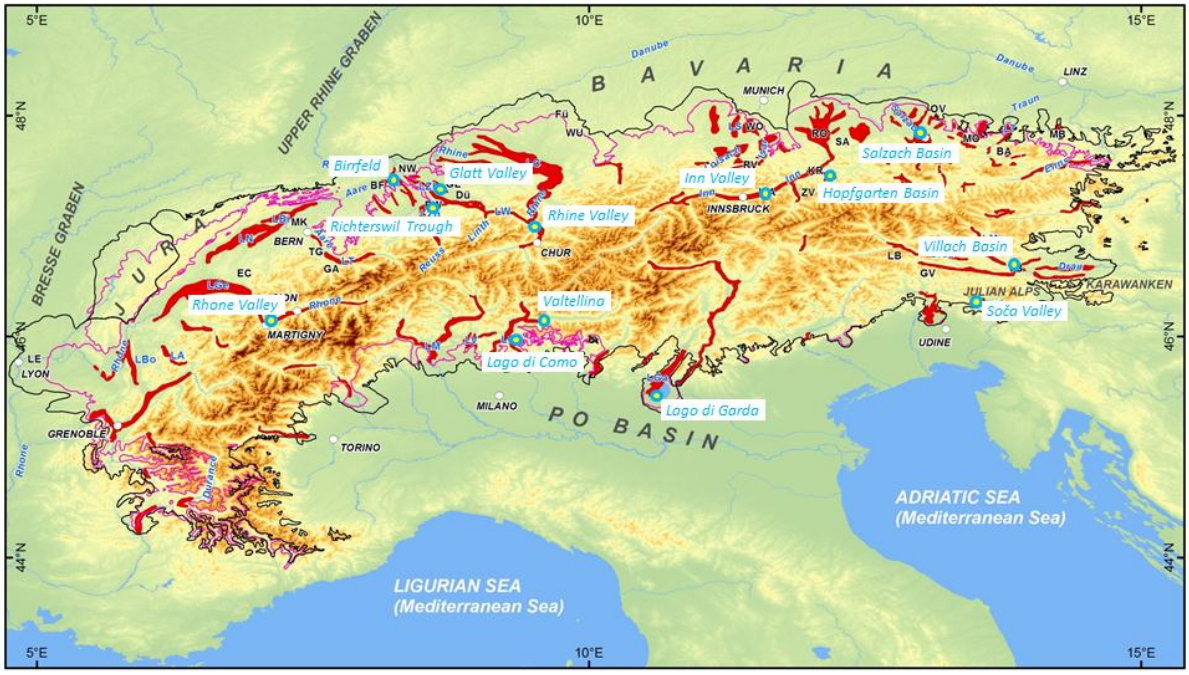

Fig. 1: Relief map of the alpine region with the limit of the Last Glacial Maximum (pink line), the maximum limit of Pleistocene glaciation (black line), and the location of overdeepened valleys and basins (red) (from Anselmetti et al., 2012; modified after Preusser et al., 2010).

quite different characters. Whereas for the inner-alpine valleys typically a complete excavation and refilling of the sediments between two glacial advances is expected, the filling of the foreland basins is considered to be generated from several, sequential glacial advances.

To achieve these goals methodological improvements in geophysical data acquisition, processing, and interpretation are required. Seismic data acquisition should make use of both P- and S-wave surveys so that the determination of Vp/Vs, elastic properties or geotechnical parameters is possible (Krawczyk et al., 2013). The latter is especially accounted for by shear-wave seismics, so that site effects and microzonation could also be analysed (c.f. Havenith et al., 2007; Polom et al., 2008). A better understanding and areal distribution of these valuables stabilises process models and long-term predictions. The high resolution of shear-wave data in comparison to P-wave data also enables delineating sedimentary sequences in more detail and deriving sedimentation directions, a first order parameter to understand valley development.

Another, integrative topic will be constrained and joint inversion of different geophysical datasets, especially reflection seismic data and gravity anomalies. Complementing information from electrical sounding or magnetics might be used to improve the accuracy of the estimation of the valley depth and the identification of different facies. The joint inversion of the data can be integrated into a more complex process that helps to improve the interpretation of the geophysical data: (1) interpretation of individual datasets by specific modelling, the results are used as input information for the inversion; (2) constrained and joint inversion of the data, the result is the spatial distribution of different physical properties (p- and s-wave velocities, densities, resistivities) and a misfit between observations and models; (3) seismic wavefield modelling based on the inversion results (input Vp, Vs, ρ); (4) discussion of the misfits between the modelled and observed wavefields in terms of geological information; (5) feedback to the joint inversion in terms of a refinement of the models.

The proposed geophysical studies will be discussed and focussed at the international ICDP-Workshop "Drilling Overdeepened Alpine Valleys" to be held in Como in early April 2013.

References:

Anselmetti, F., Bavec, M., Gabriel, G., Preusser, F., Ravazzi, C., Reitner, J. (2012): Drilling Overdeepened Alpine Valleys. – ICDP workshop proposal (unpublished).

Brückl, E., Brückl, J., Chwatal, W., Ullrich, C. (2010): Deep alpine valleys: examples of geophysical explorations in Austria. – Swiss Journal of Geosciences, 103: 329-344.

Büker, F., Green, A., Horstmeyer, H. (1998): Shallow seismic reflection study of a glaciated valley. – Geophysics, 63(4): 1395-1407.

de Franco, R., Biella, G., Caielli, G., Berra, F., Guglielmin, M., Lozej, A., Piccin, A., Sciunnach, D. (2009): Overview of high resolution seismic prospecting in pre-Alpine and Alpine basins. – Quaternary International, 204: 65-75.

Dehnert, A., Lowick, S.E., Preusser, F., Anselmetti, F.S., Drescher-Schneider, R., Graf, H.R., Heller, F., Horstmeyer, H., Kemna, H.A., Nowaczyk, N.R., Züger, A., Furrer, H. (2012): Evolution of an overdeepened trough in the northern Alpine Foreland at Niederweningen, Switzerland. – Quaternary Science Reviews, 34: 127–145.

Havenith, H.-B., Fäh, D., Polom, U., Roulle, A. (2007): S-wave velocity measurements applied to the seismic microzonation of Basel, Upper Rhine Graben. – Geophysical Journal International, 170 (1), 346-358.

Krawczyk, C.M., Polom, U., Beilecke, T. (2013): Shear-wave reflection seismics as valuable tool for near-surface urban applications. – The Leading Edge, accepted.

Peusser, F., Reithner. J.M., Schlüchter, C. (2010): Distribution, geometry, age and origin of overdeepened valleys and basins in the Alps and their foreland. – Swiss Journal of Geosciences, 103: 407–426.

Polom, U., Arsyad, I., Kümpel, H.-J. (2008): Shallow shear-wave reflection seismics in the tsunami struck Krueng Aceh river basin, Sumatra. – Advances in Geosciences (ADGEO), 14, 135-140.

Reitner, J.M., Gruber, W., Römer, A., Morawetz, R. (2010): Alpine overdeepenings and paleo-ice flow changes: an integrated geophysical-sedimentological case study from Tyrol (Austria). – Swiss Journal of Geosciences, 103: 385–405.

ANDRILL

ANDRILL – Wissenschaftliches Bohren in der Antarktis: Das Coulman-High-Projekt

C. GAEDICKE[1], G. KUHN[2], A. LÄUFER[1], F. NIESSEN[2] & D-ANDRILL GRUPPE

[1] Bundesanstalt für Geowissenschaften und Rohstoffe, Stilleweg 2, 30655 Hannover
[2] Alfred-Wegener-Institut für Polar- und Meeresforschung, Am Alten Hafen 26, 27568 Bremerhaven

ANDRILL (Antarctic Geological Drilling Program) ist ein langfristig ausgelegtes internationales Forschungsprogramm, in seiner Struktur ähnlich organisiert wie IODP oder ICDP, unter bisheriger Federführung der National Science Foundation (NSF) der USA. ANDRILL untersucht die bedeutende Rolle der Antarktis bei den während der jüngeren Erdgeschichte (<60 Ma) bis heute ablaufenden globalen Umweltveränderungen durch die Rekonstruktion des klimatischen, tektonischen und glazialen wechselhaften Geschehens aus hochauflösenden Sedimentkernen mit herausragenden Kerngewinnen von 98%. Das Programm wird von den USA, Neuseeland, Italien, Großbritanien, Brasilien Südkorea und Deutschland getragen. In den vorangegangenen ANDRILL Bohrungen lieferten (1) das McMurdo Ice Shelf (MIS) Projekt mit dem bisher längsten Sedimentkern aus der Antarktis von 1285 mbsf einen detailierten Klimarecord der Westantarktis über die letzten ca. 14 Ma, während (2) das Southern McMurdo Sound (SMS) Projekt einen 1139 m langen Kern erbohrte, der die Geschichte des Westantarktischen Eisschildes bis vor etwa 20 Ma widerspiegelt und in dem das Mittelmiozäne Klimaoptimum enthalten ist.

Das Coulman-High-Projekt (CHP) hat jetzt zum Ziel, Sedimente des Paläogens bis untersten Miozäns des westlichen Rossmeers von einer auf dem Schelfeis stehenden Plattform aus zu erbohren. Diese Zeitspanne beinhaltet wesentliche klimatische und tektonische Veränderungen in der Antarktis sowie weltweit, wie z.B. den Übergang von einem Treibhaus- zu einem Kühlhaus-Klima an der Eozän-Oligizän-Grenze. Die Lokation liegt auf dem Coulman High zwischen dem Victoria Land Basin und dem Central Trough des Westantarktischen Riftsystems, etwa 125 km nordöstlich der US-Antarktisstation McMurdo. Das Ross-Schelfeis hat dort eine Dicke von etwa 270 m über einer Wassertiefe um 850 m und bewegt sich relativ schnell mit etwa 2 m am Tag nordwärts.

Wesentliche Ziele des Projektes sind:

(1) Marine und terrestrische Umwelt- und Klimabedingungen in hohen Breiten im Eozän, vor dem Einsetzen einer kontinentweiten Vereisung,
(2) der Übergang zur kontinentweiten antarktischen Vereisung,
(3) der Einfluß von Klima- und tektonischen Veränderungen der Westantarktis auf die frühe Entwicklung und Variabiltät der antarktischen Kryosphäre,
(4) Größe und Frequenz der Eisvolumen-Änderungen unter moderaten bis geringen atmosphärischen CO_2 Gehalten und Auswirkungen auf den globalen und regionalen Meeresspiegel,
(5) die Entwicklung polarer Land- und Meeresoberflächen-Temperaturen und die Größenordung polarer Verstärkung (polar ampflification) während vergangener Warmzeiten,
(6) Datierung antarktischer tektonischer Episoden und die Entwicklung des Rossmeer-Sedimentbeckens.

Hierzu sollen durch das sich schnell bewegende Schelfeis zwei Bohrungen abgeteuft werden, die auf ca. 800 m stratigraphisch vom unteren frühen Miozän bis zum mittlerem Eozän und evtl. bis in kreidezeitliche frühe Sedimente im Untergrund reichen. Damit soll die in den vorhergehenden Kampagnen erbohrten Sedimentarchive um die fehlenden Einheiten komplettiert werden. Das voranschreitende Schelfeis stellt eine große Herausforderung an die Logistik die Bohrtechnik dar: Das größte Problem ist hier der sich zunehmend verbiegende Bohrstrang, nachdem er in den Meeresboden eingedrungen ist, während sich das Schelfeis mit 2 m am Tag nach Norden schiebt. Unter mehreren Möglichkeiten wurde hier die den besonderen Bedingungen und den gegebenen technischen Voraussetzungen der „downstream spud-in drilling“-Methode der Vorzug gegeben. Hierbei wird der Riser durch ein mit einem Gewicht beschwertes Kabel von der momentanen Position der Bohranlage stromabwärts gezogen, um dann an einer der Eisbewegungsrichtung vorausliegenden Stelle im Meeresboden verankert zu werden.

IODP

The origin of Shatsky Rise: What we have learned from IODP Exp. 324

J.GELDMACHER[1], T. SANO[2], W.W. SAGER[3], K.HEYDOLPH[1], R. ALMEEV[4] AND EXP. 324 SCIENTISTS

[1] GEOMAR Helmholtz-Zentrum für Ozeanforschung Kiel, Wischhofstr. 1-3, 24148 Kiel, Germany,
[2] Department of Geology and Paleontology, National Museum of Nature and Science, Tsukuba, Japan
[3] Department of Oceanography, Texas A&M University, College Station, TX, USA
[4] Institut für Mineralogie, Leibniz Universität Hannover, Germany

In fall 2009, Integrated Ocean Drilling Program (IODP) Expedition 324 drilled at five sites (U1346-U1350) into the igneous plateau of Shatsky Rise, one of the large igneous provinces (LIP) of the Pacific Ocean (Sager et al., 2010). Since we are now three years post-cruise and seeing more results of post-expedition studies come to light, we here present what we have learned about Shatsky Rise.

Introduction and scientific question

The submarine Shatsky Rise plateau is a unique large igneous province (LIP) situated in the northwest Pacific Ocean ca. 1500 km east of Japan. In contrast to other large oceanic LIP's (e.g., Ontong-Java, Manihiki and Hess Rise), which formed during the Cretaceous normal superchrone (122-84 Ma), it is the only large intraoceanic plateau that formed during the Late Jurassic to Early Cretaceous during a time period with frequent reversals of the Earth's magnetic field. The magnetic reversals, combined with bathymetric data, allow a reconstruction of the original tectonic setting and temporal evolution (e.g. Nakanishi et al., 1999). Accordingly, Shatsky's three main volcanic edifice Tamu, Ori, and Shirshov massives, formed by massive volcanism during a short time span along a southwest - northeast trending, rapidly spreading triple junction. On the other hand, the decreasing volume of the three edifice with decreasing age, indicate that the initially voluminous volcanism, which created the Tamu massif, waned to less voluminous phases creating the Ori and then the youngest Shirshov massif. This temporal evolution could represent the transition from a plume head to tail. However, drill and dredge samples from former cruises to Shatsky Rise, show trace element and isotopic characteristics similar to Pacific mid-ocean-ridge basalt (MORB) (e.g. Tatsumi et al., 1998; Mahoney et al., 2005). Therefore, Shatsky Rise shows characteristics of both, ridge-control and involvement of a plume-head. Accordingly, Nakanishi et al. (1999) and Sager et al. (1999) suggest that Shatsky Rise formed through the interaction of a mantle plume head with a spreading center. Consequently one main objective of Expedition 324 was to test both hypotheses (plume head versus ridge-control).

Initial drilling results

During the expedition five sites on the three different massives were drilled and successfully sampled, with one site (U1346) on the summit of Shirshov Massif and two sites on Ori (U1349 and U1350) and on Tamu (U1347 and U1348) respectively (Fig.1a). All sites (except for site U1348) revealed basaltic lava flows, which occur as packages of pillow basalt and massive inflation units, frequently interbedded with volcaniclastic sediments (Sager et al., 2010). The largest massive inflation flows

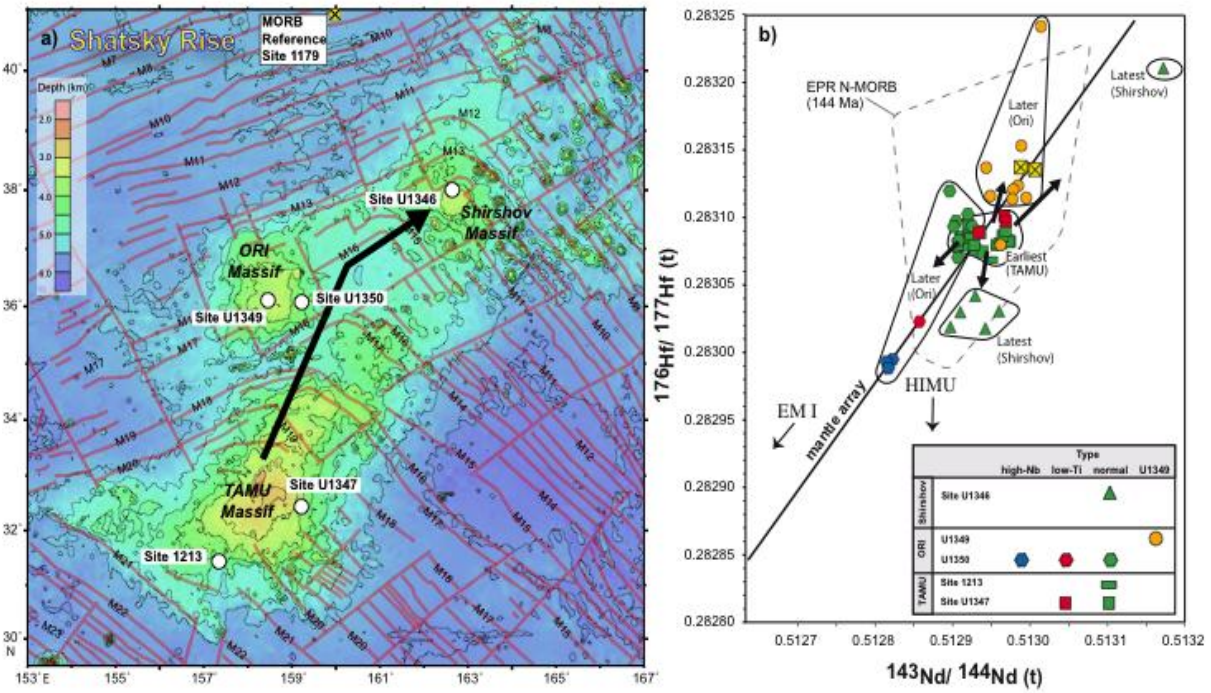

Figure 1. (a) Overview map of the Shatsky Rise plateau with magnetic lineations (M); depth contours are in kilometer (after Sager, 2010). Drill sites that reached igneous basement are marked by white circles (including ODP Site 1213). Contemporaneous MORB reference site is shown by a yellow square in both figures. Thick black arrow indicate path of the triple junction (increasing age); (b) $^{143}Nd/^{144}Nd$ vs. $^{178}Hf/^{177}Hf$ composition of drilled lava rocks classified according to the geochemical groups of Sano et al. 2012. Thick arrows and solid-contoured fields indicate increasing geochemical heterogeneity with time. Stipelled line marks (age-corrceted) N-MORB (normal mid ocean ridge basalt) from todays East Pacifc Rise (EPR) from the PetDB database (http://www.petdb.org/).

have a maximum thickness ~ 23m and the thickest occur on Tamu Massif, comparable to massive flows cored on Ontong Java Plateau during ODP Leg 192. Massive flows are also found at Sites U1349 and U1350, on Ori Massif summit and flank, respectively, though an entire ~50 m succession of igneous rocks from Site U1346 (Shirshov Massif summit) consists of pillow lavas (Fig.1b). Ori Massif flow units are generally thinner than on Tamu Massif, presumably indicating that the average eruptions became smaller and less effusive from Tamu to Ori to Shirshov massives. Cores from site U1348 contain a thick sequence (~120 m) of highly altered volcaniclastic sediments with shallow-water carbonaceous sandstones on top (Fig.1b). The cored basaltic lava flows range from relatively fresh (Sites U1347 and U1350) to moderately to highly altered (Sites U1346 and U1349). Additional recovered basement rocks from two summit sites (U1346 and U1349) show the most severe alteration, whereas rocks from Sites U1347 and U1359 are apparently less affected by alteration.

Post-cruise reserach

Timing of volcanism

Preliminary $^{40}Ar/^{39}Ar$ age determinations on groundmass and plagioclase separates yield ages between 144-140 Ma (Tamu Massif) and 134 Ma (Ori Massif) (Koppers, pers. com.) consistent with an earlier published age of 144.6 Ma from Tamu Massif (Mahoney et al. 2005) and supporting the proposed age progression from the SW to the NE as inferred by the magnetic lineations. More age determinations are currently carried out at Oregon State University and at GEOMAR. The analysis of downhole magnetic field measurements conducted at Site U1347 revealed negative paleoinclination directions for the lower part (Units VI and VII, see Fig.1) and positive inclination for the upper part (Units I-V) of the hole (Tominaga et al., 2012). Proposing that the magnetic remanence of all lavas at this site was acquired during normal polarity, Tominga et al. interpret this inversion to record the crossing of the paleoequator of the rapidly northward moving Pacific-Farallon-Izanagi triple junction, during the build-up of Tamu Massif. This result can provide new constraints for refining Pacific plate reconstruction models.

Magma chamber processes

New petrological data obtained by the Hannover Group for the Site 1347 complements previous data from Sager et al. (2010) and Sano et al. (2012) and shows that basaltic magmas from Tamu Massif are located within the compositional range of global MORB, and also follow the trend defined by the Ontong Java Plateau basalts. Our new data demonstrate that fractionation-corrected low Na_8 (~1.6) and high Fe_8 (~10.5) parameters of Tamu magmas indicate high melt fractions in the source produced at depth within the garnet stability field. This is in agreement with data of Sano et al., (2012) who demonstrated high $(Ce/Yb)^N$ and $(Sm/Yb)^N$ in normal type basalts and proposed that the melting beneath Shatsky Rise may have started in the deep garnet stability field and stopped at the base of the lithosphere (see below). However, our low Na_8 (which is similar to OJP) may even suggest higher degrees of partial melting (> 20%) than those proposed in the previous study (~15% , Sano et al., 2012). In Tamu Massif cores, several magmatic events have been identified which may be evenly related to a small scale source variability or/and differences in melting conditions. However the subsequent evolution of different magma batches is mostly controlled by fractional crystallization processes. The calculated pressure (*P*) - temperature (*T*) conditions at which the natural glasses represent cotectic olivine-plagioclase-clinopyroxene compositions range from 0.1 to 210 MPa and from 1110 to 1170°C. Based on the glass, mineral and bulk rock compositions and on the modeled *P-T* conditions, five different magmatic groups can be discriminated along the profile. Within each magmatic pulse we distinguished changes in magma storage conditions which can be attributed to the polybaric crystallization in the course of magma ascend en route to the surface. The ongoing experimental study of phase equilibria in Shatsky Rise representative magma compositions prinicipally confirms the low crystallization pressures (below 200 MPa) and results of phase equilibria modeling (see details in Husen et al., 2013, this volume).

Trace element geochemistry

Using alteration-immobile incompatible race element ratios (Zr/Ti, Nb/Sc, Nb/Ti), Sano et al. (2012) divided the recovered Shatsky lavas in four groups: Normal, Low-Ti, High-Nb and U1349 types, with the Normal type group being the most abundant. According to Sano et al (2012), the Normal type lavas were formed by 15% melting of a relatively depleted mantle source in presence of garnet and the low-Ti group could be derived from the Normal group by different degrees of melting. Formation of the High-Nb group lavas, however, requires a distinct and more enriched source. The U1349 group is proposed to have formed by highly depleted mantle material that has already experienced the extraction of large amounts of the Normal type magma. The Normal type constitute to ca. 94% of the TAMU massif (the oldest edifice of Shatsky) while the other types comprise ca. 57% of drilled lavas from the younger Ori Massif and implying that the Shatsky's geochemical composition may have become more heterogeneous with time.

Sr, Nd, Pb, Hf and He isotope geochemistry

Sr, Nd, Pb, and Hf isotope ratios of the Normal and Low-Ti groups are identical (consistent with Sano et al.'s interpretation of the trace element data) and most data overlap with (age-corrected) Pacific MORB compositions (Heydolph et al., in prep.). U1349 group lavas yield the most depleted isotope composition and overlap with contemporary MORB samples from ODP site 1179 obtained from regular sea floor basement north of Shatsky. Therefore, U1349 samples could represent the local, upper mantle MORB source (Geldmacher et al., 2012). The High-Nb type lavas show isotopically slightly more enriched compositions indicating recycled (EM I and HIMU) source components. Interestingly, the Normal and Low-Ti lavas possess Nd, Pb and Hf isotope compositions similar to the primitive, early depleted (non-chondritic) mantle reservoir recently proposed by Jackson and Carlson (2011) as source of most flood basalt events. However, a slight contamination with the enriched (HIMU) material is required to explain the observed trace element and isotopic systematics. This model is supported by $^3He/^4He$ ratios of

the Normal type lavas slightly lower than MORB (Hanyu et al., submitted).

Whereas lavas from three drill sites on the oldest edifice, Tamu Massif, yield fairly uniform compositions, a wider isotopic spread is found for lavas erupted on the younger edifice, Ori and Shirshov (with all four groups present), suggesting that the Shatsky source has become more heterogeneous with time (consistent with the trace element data of Sano et al. (2012). This variation could reflect a decreasing degree of melting (and therefore less homogenization of inherent plume heterogeneities) or less effective stirring and mixing during the interaction of the spreading center with a waning plume head.

References:

Geldmacher J., Heydolph K., Murphy D., Romanova I., Mahoney J., Hoernle K. (2012) Combined Sr, Nd, Pb and Hf isotopic constraints on the origin of Shatsky Rise (NW Pacific). *AGU Fall Meeting*, DI51A-2339

Hanyu, T., Shimizu, K., Sano, T. Noble gas evidence for the presence of recycled material in magma sources of the Shatsky Rise. *Geol. Soc. Am. Spec. Paper*, submitted

Jackson M.G., Carlson, R.W. (2011) An ancient recipe for flood-basalt genesis. *Nature* 476, 316-318

Mahoney, J.J., Duncan, R.A., Tejada, M.L.G., Sager, W.W., and Bralower, T.J. (2005) Jurassic-Cretaceous boundary age and mid-ocean-ridge-type mantle source for Shatsky Rise. *Geology* 33, p. 185-188

Nakanishi, M., Sager, W. W., and Klaus, A. (1999) Magnetic lineations within Shatsky Rise, northwest Pacific Ocean: Implications for hot spot-triple junction interaction and oceanic plateau formation. *J. Geophys. Res*. 104

Sager, W. W., Kim, J., Klaus, A., Nakanishi, M., and Khankishieva, L. M. (1999) Bathymetry of Shatsky Rise, northwest Pacific Ocean: Implications for ocean plateau development at a triple junction. *J. Geophys. Res*. 104

Sager, W.W., Sano, T., Geldmacher, J. and the Expedition 324 Scientists (2010) *Proc. IODP 324: Tokyo (IODP-MI, Inc.)* doi:10.2204/iodp.proc324.2010

Sano, T., Shimizu, K., Ishikawa, A., Senda, R., Chang, Q., Kimura, J.-I., Widdowson, M., Sager, W.W. (2012) Variety and origin of magmas on Shatsky Rise, northwestern Pacific Ocean. *Geochem. Geophys. Geosyst.* 13, Q08010, doi:10.1029/2012GC004235

Tatsumi, Y., Shinjoe, H., Ishizuka, H., Sager, W.W., and Klaus, A., (1998) Geochemical evidence for a mid-Cretaceous superplume: *Geology* 26, p. 151-154

Tominaga, M., Evans, H.E., Iturrino, G. (2012) "Equator crossing" of Shatsky Rise?: New insights on Shatsky Rise tectonic motion from downhole magnetic architecture of the uppermost lava sequences at Tamu Massif. *Geophs. Res. Lett.* 39, L21301, doi:10.1029/2012GL052967.

IODP

Microfacies and diagenesis of older Pleistocene (pre-LGM) reef deposits, Great Barrier Reef, Australia (IODP Expedition 325): a quantitative approach

EBERHARD GISCHLER[1], ALEX L. THOMAS[2], ANDRÉ W. DROXLER[3], JODY M. WEBSTER[4], YUSUKE YOKOYAMA[5], BERND R. SCHÖNE[6]

[1] Institut für Geowissenschaften, Goethe-Universität, 60438 Frankfurt am Main, Germany
[2] Department of Earth Sciences, University of Oxford, South Parks Road, Oxford OX1 3AN, U.K.
[3] Department of Earth Science, Rice University, Houston TX 77251, USA
[4] Geocoastal Research Group, School of Geosciences, University of Sydney, Sydney NSW 2006, Australia
[5] Atmosphere and Ocean Research Institute, University of Tokyo, Kashiwa Chiba 277-8564, Japan
[6] Institut für Geowissenschaften, Gutenberg-Universität, 55128 Mainz, Germany

During IODP Expedition 325, thirty-four holes were drilled along five transects in front of the Great Barrier Reef of Australia penetrating some 700 m of late Pleistocene reef deposits (postglacial; largely 20-10 kyrs BP) in water depths of 42-127 m. In seven holes, drilled in water depths of 42-92 m on three transects, older Pleistocene (pre-LGM, >20 kyrs BP) reef deposits were recovered from lower core sections. In this study, facies, diagenetic features, mineralogy and stable isotope geochemistry of 100 samples from six of the latter holes were investigated and quantified. Lithologies are dominated by grain-supported textures, and were to a large part deposited in high-energy, reef or reef slope environments. Quantitative analyses allow eleven microfacies to be defined including mixed skeletal packstone and grainstone, mudstone-wackestone, coral packstone, coral grainstone, coralline algal grainstone, coral-algal packstone, coralline algal packstone, Halimeda grainstone, microbialite and caliche. Microbialites, that are common in cavities of younger, postglacial deposits, are rare in pre-last glacial maximum core sections, possibly due to a lack of open framework suitable for colonization by microbes. In pre-LGM deposits of holes M0032A and M0033A (>20 kyrs BP), marine diagenetic features are dominant; samples consist largely of aragonite and high-magnesium calcite. Holes M0042A and M0057A, which contain the oldest rocks (>169 kyrs BP), are characterized by meteoric diagenesis and samples mostly consist of low-magnesium calcite. Holes M0042A, M0055A and M0056A (>30 kyrs BP), and a horizon in the upper part of hole M0057A, contain both marine and meteoric diagenetic features However, only one change from marine to meteoric pore water is recorded in contrast to the changes in diagenetic environment that might be inferred from sea-level history. Values of stable isotopes of oxygen and carbon are consistent with these findings. Samples from holes M0032A and M0033A reflect largely positive values $\delta^{18}O$: -1 to +1‰ and $\delta^{13}C$: +1 to +4‰), whereas those from holes M0042A and M0057A are negative ($\delta^{18}O$: -4 to +2‰ and $\delta^{13}C$: -8 to +2‰). Holes M0055A and M0056A provide intermediate values, with slightly positive $\delta^{13}C$, and negative $\delta^{18}O$ values. The type and intensity of meteroric diagenesis appears to have been controlled both by age and depth, i.e., the time available for diagenetic alteration, and reflects the relationship between reef deposition and sea-level change.

IODP/ICDP

Calcite as a new thermochronological archive

U.A. GLASMACHER[1], S. DEDERA[1], M. BURCHARD[1] C. TRAUTMANN[2,3]

[1] Institute of Earth Sciences, University Heidelberg, Neuenheimer Feld 234, 69120 Heidelberg;
[2] Gesellschaft für Schwerionenforschung mbH, Darmstadt, Germany
[3] TU Darmstadt, Germany

Carbonate minerals such as calcite ($CaCO_3$) are abundant in carbonate rocks in nature. Radiometric dating of calcite is still a matter of formation age and covers only the last 400.000 years, in general. Nevertheless, calcite can bear uranium concentration in the range of 10 to 168 µg/g (Hoffmann et al. 2009). Uranium concentrations in this range should allow to use calcite as an radiometric dating archive for longer time scales by applying the (U-Th-Sm)/He and fission-track technique. First published analytical data for the (U-Th-Sm)/He technique by Copeland et al. (2007) provided insight into the calcite as a thermochronological archive. The fission-track dating is based on visualization of spontaneous fission tracks by etching techniques. First etching of calcite has been performed by Hones and Jones (1937) and Boos (1941) to reveal the crystal structure od calcite. Keith and Gilmann (1960) tested various etching solutions and indicated clearly the possibility to reveal localized etch pits. Sippel and Glover (1964) described the first successful etching experiments to reveal etch pits of spontaneous and induced fission tracks. As MacDougall and Price (1974) declared that total annealing occurs above 20 °C no significant thermochronological research was published afterwards.

Over the last three years we followed the old studies and performed heavy ion accelerater experiments to create arifical ion tracks. The artifical ion tracks were used to define the etching solution and the etching conditions. In addition, we performed first annealing experiments to understand the total annealing temperature of ion tracks in calcite. Results of these experiments will be presented and combined with first etching and dating experiments of natural fission tracks in calcite from various locations.

References:

Boos, A., 1941. Ätzversuche an Calcit, Rhodochrosit und Siderit, N. Jahrbuch f. Mineralogie, 89-130.

Copeland P., Watson, E.B., Urizar, S.C., Patterson, D., Lapen T.J., 2008. Alpha thermochronology of carbonates. Geoch. Cosmoch. Ac. 71, 4488–4511

Hoffmann, D., Spötl C., Mangini, A., 2009. Micromill and in situ laser ablation sampling techniques for high spatial resolution MC-ICPMS U-Th dating of carbonates. Chem. Geol. 259, 253-261.

Hones, A.P., Jones, J.R., 1937. Etch figure investigations with optically active solvents. Bull. Geol. Soc. Am. 48, 667-722.

Keith, R.E. & Gilman, J.J, 1960. Dislocation Etch Pits and Plastic Deformation in Calcite“, Acta Metallurgica 8,

MacDougall, D., Price, P.B., 1974. Attempt to Date Early South African Hominids by using Fission Tracks in Calcite. Science 185, 943-944.

Sippel, R.F., Glover, E.D. 1964. Fission Damage in Calcite and the Dating of Carbonates. Sciences 144, 409-411.

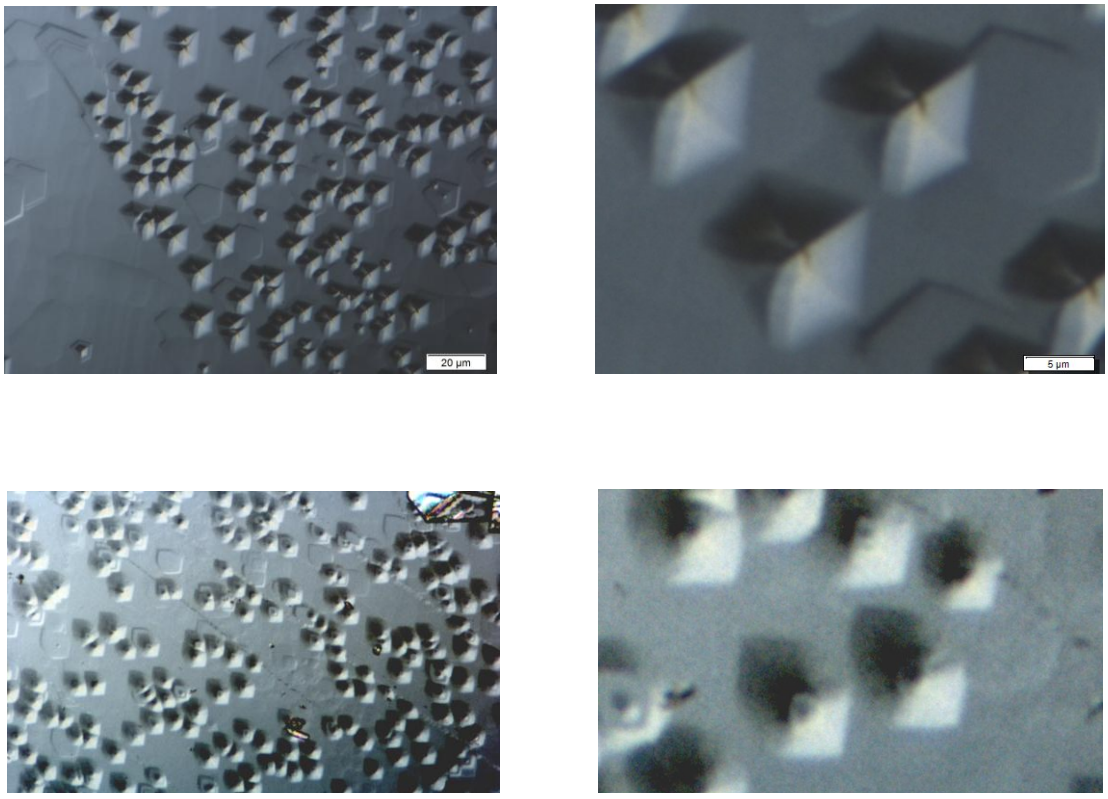

Fig.1: Top two: Calcite crystal etched with 0,091% HNO_3 for 4s. The etch pits have a more pentagonal shape. (all images optical microscope with attached Nomarski Interference Contrast, DIC). Bottom two: Calcite crystal etched with EDTA + 5% acetic acid for 20s. The etch pits have a pseudohexagonal shape.

ICDP

Seismic site characterization for the Deep-Fault-Drilling-Project Alpine Fault

V.GLOMB[1], S.BUSKE[1], A. KOVACS[2], A. GORMAN[2]

[1] TU Bergakademie Freiberg, Institute of Geophysics and Geoinformatics, 09596 Freiberg, vera.glomb@geophysik.tu-freiberg.de

[2] University of Otago, Department of Geology, Dunedin 9054, New Zealand

The Alpine Fault in New Zealand (South Island) is one of the largest active plate-bounding continental fault zones on earth with earthquakes of magnitude 7.9 occuring every 200-400 years. Due to the surface exposure and the shallow depth of mechanical and chemical transitions it is a globally significant natural laboratory. Within the ICDP Deep-Fault-Drilling-Project Alpine Fault (DFDP-AF; https://wiki.gns.cri.nz/DFDP) a drill hole shall give insight into the geological structure of the fault zone and its evolution to understand the related deformation and earthquake processes.

With the help of advanced seismic imaging techniques, the shallow structure of the Alpine Fault is imaged to find the most suitable drill site location. A new seismic reflection profile has been acquired in 2011 by the WhataDUSIE project team consisting of partners from the University of Otago (New Zealand), TU Bergakademie Freiberg (Germany) and the University of Alberta (Canada). The reflection profile, located in the Whataroa river valley, has a total length of about 5 km. Up to 643 geophones with spacings between 4-8 m recorded 182 shots at approximately 100 shot point locations along the profile line (Figure 1).

The obtained data quality was in general very good. Nevertheless, extensive preprocessing of the data had to be performed to obtain shot gathers usable for imaging. Due to the field conditions the profile was divided into 5 parts (stations in Figure 1) with different features concerning geophone spacing and eigenfrequency of the geophones. To combine the single stations to one shot gather, we used overlapping geophones to derive the relative time

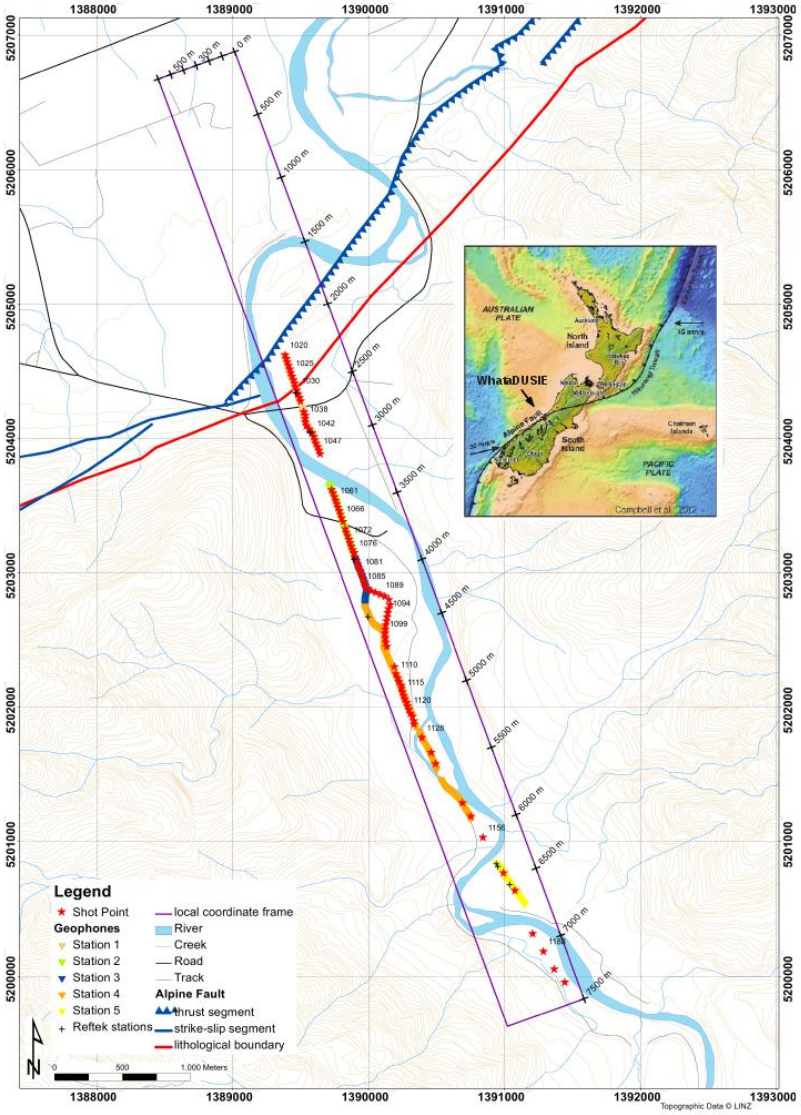

Fig. 1: Field layout of WhatDUSIE experiment. The 2D profile consists of five seperate parts where geophones have been laid out independently (coloured triangles). Shotpoints are donated by stars. The local coordinate system is indicated by the magenta rectangle (x positive to SE). The approximate position of the expected surface trace of the Alpine Fault is highlighted in red.

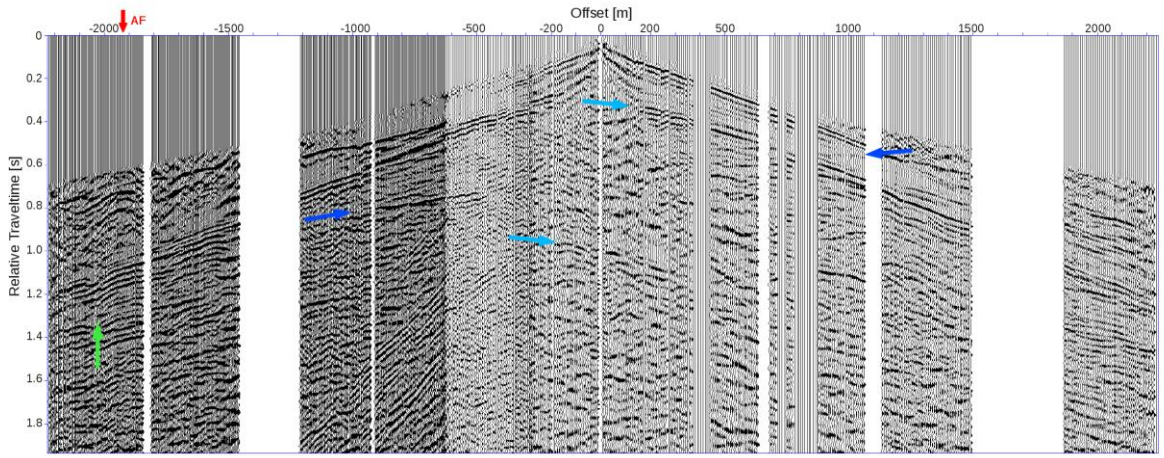

Fig. 2: Shot gather from shot point 1100 (at ca. x=4.6 km in local coordinate system). The data processing includes trace editing, bandpass filtering, trace equalization, FK-filtering and AGC as well as a mute of noise before the first break arrivals. Blue arrows indicate strong reflections and possibly reflected refractions (dark blue). A region with distorted wavefields (green arrow) lies directly in the vicinity of the expected surface trace of the Alpine Fault (red arrow).

corrections by crosscorrelating these particular traces. Additionally three Reftek 130 stations were recording continuously. By correlating the absolute Reftek time and the adjacent geophone trace we extracted the absolute shot time and applied the resulting time-shift to the corresponding traces. Finally the merged single shot gathers (Figure 2) were further processed, including basic trace editing, bandpass filtering, trace equalization, FK-filtering and automatic gain control.

Single shot gathers as well as preliminary imaging results show various indicators of the Alpine Fault and the surrounding geology. Strong reflections and distorted first-arrival wavefields are clearly visible already in single shot gathers (see Figure 2). Up to now, 3D Kirchhoff pre-stack depth migration has been applied to the data set. The obtained images (see example in Figure 3) show several reflectors with varying dips (20° - 55°) in a depth range of 0.5-3.5 km. Three bands of high reflectivity indicate major

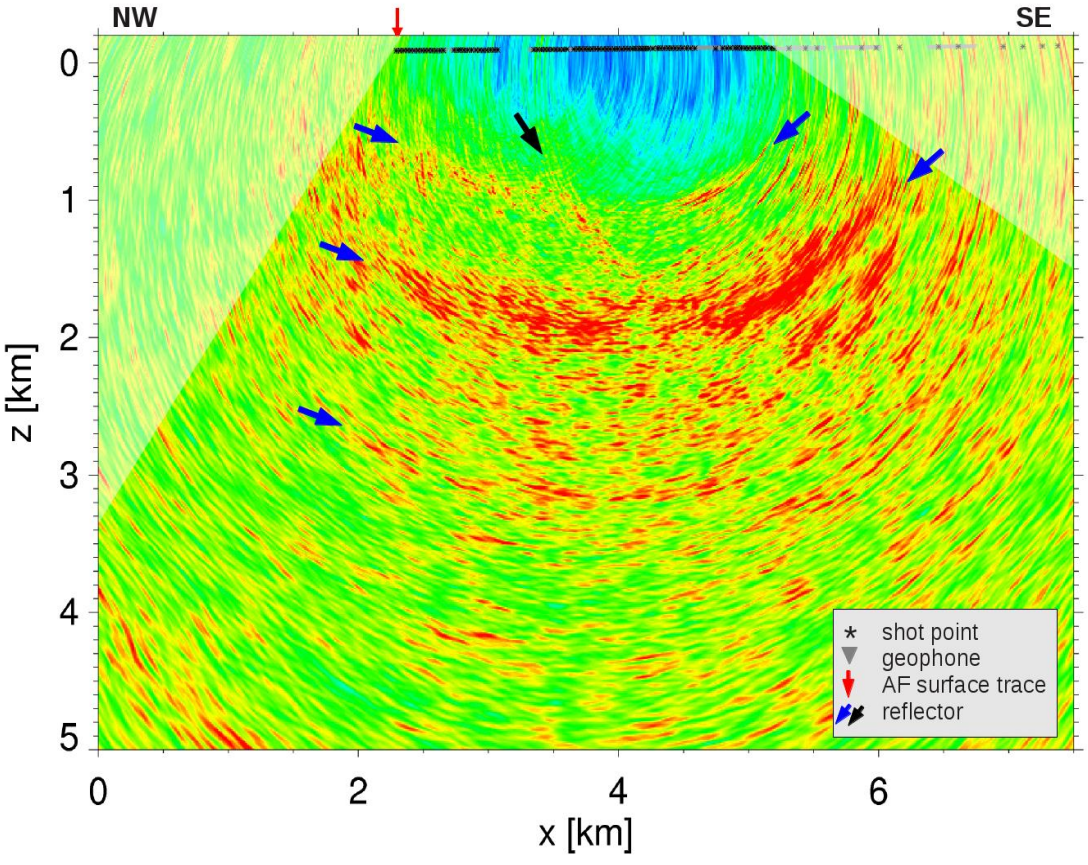

Fig. 3: Seismic reflection image obtained by Kirchhoff pre-stack depth migration and stacking of 46 shot gathers along the profile.

geological boundaries. Of particular interest is the reflector which starts at x=3.5 km and z=1 km and which dips at an angle of about 55 degrees to the SW (black arrow), because the prolongation of this reflector to the surface ends at the major mapped surface trace of the Alpine Fault (red arrow). This reflector is supposed to be the main drilling target.

Further work will concentrate on a detailed velocity analysis and the shallow (< 1 km) subsurface. In particular for the latter but also for increasing the general image quality and resolution, we will apply focussing migration techniques. Consequently, further processing and intensive interpretative work will enable a seismic site characterization providing important information for the selection of the borehole location. Additionally, the high resolution seismic images themselves allow a better understanding of the tectonic and geodynamic settings.

ICDP

Phylogenetic and physiological characterization of deep-biosphere microorganisms in sediments of the El'gygytgyn Crater Lake, Far East Russia

J. GÖRSCH[1], K. MANGELSDORF[2], D. WAGNER[1]

[1] Helmholtz Centre Potsdam, GFZ German Research Centre for Geosciences, Section 4.5 Geomicrobiology, Telegrafenberg, 14473 Potsdam, Germany.
[2] Helmholtz Centre Potsdam, GFZ German Research Centre for Geosciences, Section 4.3 Organic Geochemistry, Telegrafenberg, 14473 Potsdam, Germany

Despite apparent diverse and active microbial ecosystems in the deep subsurface [1; 2], the research of the deep biosphere in arctic environments is still limited. Molecular investigations of sediment material of the El'gygytgyn Crater Lake, Chukotka, Far East Russian Arctic, give us a unique view into the past of the last 3.6 million years of microbial life. Since its formation, the lake has not been covered by a glacier and thus an accumulation of continuously deposition of lake sediments was possible. These chronological layers contain information about how arctic microorganisms have responded to the various glacial/interglacial periods of the past millennia. To investigate this climate archive, the El'gygytgyn Crater Lake sediments were drilled in 2009 in the framework of the ICDP project Scientific Drilling in El'gygytgyn Crater Lake [3].

In an initial investigation of the microbial composition in up to 470 ka old sediment deposits we showed the existence of a diverse archaeal community along the chronosequence. Furthermore we examined a strong correlation between the amount of organic carbon and the microbial abundance and diversity. Additionally our group determined an indirect response of archaeal and bacterial microorganisms to glacial/interglacial periods. This indirect response can be explained by the improved nutrient supply in course of related algal bloom within warmer periods [4].

Our further analyses of the entire sediments down to 317 m with an age of up to 3.6 million years should provide detailed knowledge about the pioneering microorganisms of the El'gygytgyn Crater Lake after the meteorite impact. In addition we will examine the changes of the composition and abundance of the microbial community along the chronosequence. Another goal is to verify the existence of metabolically active microorganisms in this ancient sediment material and to analyse their function within the carbon cycling. Therefore we will perform a propidium monoazide (PMA) protocol optimized for sediment material to distinguish between free DNA and intact cells.

Thereby our planned combination of analytical methods (including ribosomal DNA gene based approach, high throughput sequencing, cultivation and fluorescence in situ hybridization), biogeochemical techniques and phylogenetical analyses should increase the knowledge about the development of microbial life and provide information about the limitations of microbial activity.

References:
[1] J. Kallmeyer, R. Pockalny, R. R. Adhikari, D. C. Smith, S. D'Hondt, PNAS (2012), 10.1073/pnas.1203849109.
[2] B.A. Lomstein, A. T. Langerhuus, S. D´Hondt, B: B: Jørgensen, A. J. Spivack, Nature 484 (2012), p. 101-104.
[3] M. Melles, J. Brigham-Grette, P. Minyuk, C. Koeberl, A. Andreev, T. Cook, G. Fedorov, C. Gebhardt, E. Haltia-Hovi, M. Kukkonen, N. Nowaczyk, G. Schwamborn, V. Wennrich, Scientific Drilling 11 (2011), p. 29-40.
[4] J. Bischoff, K. Mangelsdorf, J. Görsch, P. Lam, P. Rosen, D. Wagner, in prep. (2012)

IODP

Recent benthic foraminiferal assemblages in the Gulf of Cádiz and W off Portugal: a key to the history of the Mediterranean Outflow Water (IOPD Expedition 339)

PATRICK GRUNERT[1], BARBARA BALESTRA[2], DAVID HODELL[3], JOSÉ-ABEL FLORES[4], CARLOS ALVAREZ-ZARIKIAN[5], F. JAVIER HERNÁNDEZ-MOLINA[6], DORRIK A.V. STOW[7], AND IODP EXPEDITION 339 SCIENTISTS*

[1] Institute for Earth Sciences, University of Graz, Austria; patrick.grunert@uni-graz.at
[2] Department of Earth and Environmental Sciences, Queens College, New York, USA
[3] Department of Earth Sciences, University of Cambridge, United Kingdom
[4] Department of Geology, University of Salamanca, Spain
[5] Integrated Ocean Drilling Program, Texas A&M University, College Station, Texas, USA
[6] Departmento Geociencias Marinas, Universidad de Vigo, Facultad de Ciencias del Mar, Vigo, Spain
[7] Institute of Petroleum Engineering, Heriot-Watt University, Edinburgh, Scotland, United Kingdom

IODP Expedition 339 recently drilled 5 sites in the Gulf of Cádiz and 2 west off Portugal, and recovered 5.5 km of core. The Gulf of Cádiz was targeted for drilling 1) to investigate the Mediterranean Outflow Water (MOW) and its influence on global circulation and climate, and 2) to understand the effects of tectonic activity and eustatic changes on evolution of the Gibraltar Gateway and margin sedimentation. During the expedition samples from surface-waters and the seafloor were collected to evaluate recent communities of foraminifers, ostracods and calcareous nannoplankton. The results will serve as an important reference for future paleoceanographic work based on the actualistic approach in the Upper Miocene-Pleistocene deposits drilled during IODP Expedition 339.

Over 400 foraminiferal taxa have been identified in size fractions >125µm at six sites of IODP Expedition 339. The preliminary results show that living specimens are rare (1-5% of the assemblages), which is most likely related to deep-sea patchiness; loss during the drilling process cannot be excluded for some samples. The composition of live and dead assemblages strongly depends on water depth and position along the pathway of MOW. Statistical analysis indicates the distinction of three groups of foraminiferal assemblages that reflect the influence of the upper and lower cores of MOW, and North Atlantic Deep Water.

Combined with ostracod and nannoplankton assemblages the results will provide insights into the effect of spatial and vertical fluctuation of North Atlantic Deep Water, Antarctic Intermediate Water and MOW circulation on the microfauna and –flora. Moreover, $\delta^{13}C$, $\delta^{18}O$, Mg/Ca and Sr/Ca of foraminifers, ostracods and coccoliths will be determined and compared to seawater geochemistry to evaluate "vital effects".

* IODP Expedition 339 Scientists: Acton, G., Bahr, A., Ducassou. E., Flood, R., Furota, S., Jimenez-Espejo, F., Kim, J. K., Krissek, L., Kuroda, J., Li, B., Llave, E., Lofi, J., Lourens, L., Miller, M., Nanayama, F., Nishida, N., Richter, C., Roque, C., Sanchez Goñi, M., Sierro Sanchez, F., Singh, A., Sloss, C., Takashimizu, Y., Tzanova, A., Voelker, A., Williams, T., Xuan, C.

IODP

Potential drilling locations at the Argentine continental margin to investigate the Cenozoic history of South Atlantic deep water circulation

J. GRUETZNER[1], G. UENZELMANN-NEBEN[1], D. FRANKE[2]

[1] Alfred-Wegener-Institut für Polar- und Meeresforschung, Bremerhaven, Germany
[2] Bundesanstalt für Geowissenschaften und Rohstoffe, Hannover, Germany

Persistent geostrophic currents interacting with sea-floor topography and available sediment sources are capable of eroding, transporting and depositing fine-grained particles into mounded and elongated sediment drifts. These drifts show enhanced accumulation rates when compared to pure pelagic sequences and are thus attractive targets for high resolution paleoceanographic studies (Knutz, 2008). Several expeditions of the IODP/ODP (e.g. 162, 172, 303, 306, 339, 342) therefore have successfully targeted giant contourite drifts. An unexplored area in this context is a prominent contourite depositional system (CDS) located in the southernmost sector of the extensional Argentine margin (Hernández-Molina et al., 2009). Here the thermohaline circulation is characterized by the interaction of northwardflowing Antarctic water masses (Antarctic Intermediate Water, AAIW; Circumpolar Deep Water, CDW; Antarctic Bottom Water, AABW) and southward-flowing North Atlantic Deep Water (NADW) (Carter et al., 2008). The transfer of heat and energy via these water masses constitutes an important component in maintaining the global ocean conveyor belt.

We investigate an extensive set of high quality seismic reflection profiles from the Argentine continental margin to detect, characterize and map sedimentary features related to bottom current activity and to reconstruct past changes in the abyssal circulation. Typical margin-parallel morphosedimentary features such as (1) a set of four terraces on the slope and rise, (2) channels separating the terraces, (3) a giant buried sediment drift, and (4) sheeted drifts on the abyssal plain indicate that along slope (contour current) transport dominates over downslope (turbiditic) processes at the southern Argentine margin (Gruetzner et al., 2011; Hernández-Molina et al., 2010). Along the central Argentine margin the relative importance of the permanent, steady bottom currents and the shorter-duration, unsteady mass wasting processes on sediment deposition was variable in time and space (Gruetzner et al., 2012). Based on a detailed investigation of a continental slope terrace at the southern margin and the mapping of depocenter geometries of four major seismic units at the central margin a chronology of the depositional processes during the Cenozoic was derived:

While the Paleocene/Eocene (~65 – 34 Ma) is characterized by hemipelagic sedimentation under relatively sluggish bottom water conditions, strong AABW circulation led to widespread erosion on the slope and growth of a large detached sediment drift during the Oligocene and early Miocene (~34 – 17 Ma). After deposition of an aggradational seismic unit interpreted to represent low bottom current activity during the Mid-Miocene climatic optimum (~17 – 14 Ma), a current reorganization through the emergence of Lower CDW took place at approx. 14–12 Ma when the Valentin Feilberg Terrace started growing. Current controlled sedimentation under moderate flow speed commenced at the southern Argentine margin during the middle to late Miocene (~12 – 6 Ma) but at the same time gravitational down-slope sediment transport increased at the central Argentine margin possibly related to tectonic uplift in South America. The Pliocene to Holocene unit at the southern Argentine margin indicates strengthening of bottom flow after 6 Ma possibly due to a general change in deep water mass organization following the closure of the Panamanian gateway. At the central Argentine margin this unit is very heterogeneous and formed by interactions of down-slope and along-slope sediment transport processes as indicated by the evolution of canyons, slope plastered drifts and channels.

The available multichannel seismic profiles constitute a high-quality site survey and the results from our project may be used as background information for future ocean drilling in the region which would reveal important aspects of the deep water history and provide better age constraints. We here suggest a transect of drill sites on continental slope terraces in different water depths at the southern Argentine margin. Inferred sedimentations rate of >8 cm/1,000 years would make these drill sites suitable for high-resolution paleoclimatic studies of the Cenozoic.

References:

Carter, L., I. N. McCave, and M. J. M. Williams (2008), Circulation and Water Masses of the Southern Ocean: A Review, in *Antarctic Climate Evolution*, edited by F. Florindo and M. Siegert, pp. 85-114, Elsevier B.V., Amsterdam.

Gruetzner, J., G. Uenzelmann-Neben, and D. Franke (2011), Variations in bottom water activity at the southern Argentine margin: indications from a seismic analysis of a continental slope terrace, *Geo-Mar. Lett.*, *31*(5), 405-417.

Gruetzner, J., G. Uenzelmann-Neben, and D. Franke (2012), Variations in sediment transport at the central Argentine continental margin during the Cenozoic, *Geochem. Geophys. Geosyst., 13*, Q10003.

Hernández-Molina, F. J., M. Paterlini, R. Violante, P. Marshall, M. de Isasi, L. Somoza, and M. Rebesco (2009), Contourite depositional system on the Argentine Slope: An exceptional record of the influence of Antarctic water masses, *Geology*, *37*(6), 507-510.

Hernández-Molina, F. J., M. Paterlini, L. Somoza, R. Violante, M. A. Arecco, M. de Isasi, M. Rebesco, G. Uenzelmann-Neben, S. Neben, and P. Marshall (2010), Giant mounded drifts in the Argentine Continental Margin: Origins, and global implications for the history of thermohaline circulation, *Mar. Petrol. Geol.*, *27*(7), 1508-1530.

Knutz, P. C. (2008), Paleoceanographic Significance of Contourite Drifts, in *Contourites*, edited by M. Rebesco and A. Camerlenghi, pp. 511-535, Elsevier, Amsterdam.

ICDP

Reflection Seismic Images Across the San Andreas Fault Zone near Cholame, California

S. GUTJAHR[1], S. BUSKE[2]

[1] Freie Universität Berlin, Department of Geophysics, Malteserstrasse 74-100, 12249 Berlin, stine@geophysik.fu-berlin.de

[2] TU Bergakademie Freiberg, Institute of Geophysics and Geoinformatics, 09596 Freiberg, buske@geophysik.tu-freiberg.de

We applied a modern seismic imaging technique to old industry seismic reflection data. This data was recorded in south central California in order to obtain further information on the crustal structures beneath the California Coast Ranges and the Great Valley. These structures include the San Andreas fault zone and other fault zones.

The industry seismic reflection data set „SJ-6“ was acquired in 1981 and purchased by the USGS in 1983. The acquisition line extends from the Pacific Coast at Morro Bay eastward to the foothills of the Sierra Nevada. So far, this seismic profile is the only one crossing the non-volcanic tremor region near Cholame which is situated between the creeping segment of the San Andreas fault to the northwest and the locked segment to the southeast.

We reprocessed the original 6 second field records to approx. 26 second two-way traveltime and applied the so-called Fresnel Volume migration approach. The latter is an extension to standard Kirchhoff Prestack Depth migration in which the migration operator is restricted to the region around the actual reflection point using the concept of Fresnel Volumes. A 3D tomographic velocity model derived from local earthquake data was used and the imaging technique was implemented in 3D in order to account for the true source and receiver positions along the crooked profile line.

The resulting images illustrate the reflectivity down to approx. 30 km depth beneath the entire line. Within the Salinian Block situated between the Nacimiento-Rinconada fault zone and the San Andreas fault zone subhorizontal reflectors in the shallow crust represent sedimentary layer sequences that thickens northeastward. The latter cannot be observed in the vicinity of the San Andreas fault zone. The lower crust of the Salinian Block consists of very strong northeast dipping reflectors at depths between 17 km and 25 km. It can be assumed that they represent the transition zone from the lower crust to the upper mantle with a thickness of approx. 5 km.

At the northeastern border of the Salinian Block the San Andreas fault appears as a near vertical zone of approx. 4 km width. This zone is characterized by a lack of reflections and the cut off of coherent reflectors at both sides. Microseismic events have been located within this zone at depths not deeper than 15 km. Below this depth the reflection-free area widens and non-volcanic tremor are located there. This correlation of the change in seismicity and reflection character, respectively, indicates the brittle-ductile transition at approx. 15 km depth within the San Andreas fault zone.

Comparable observations have been made during a reflection seismic experiment across the San Andreas fault farther north near Parkfield as described by McBride and Brown in 1986. Farther east in the Great Valley west dipping reflectors appear beneath sedimentary layer sequences down to depths of 17 km. These may represent Great Valley ophiolite formations as suggested by Godfrey et al., 1998.

The application of the so-called Fresnel Volume migration approach combined with a modern 3D velocity model resulted in considerably improved seismic images. Especially in the region of the San Andreas fault and the

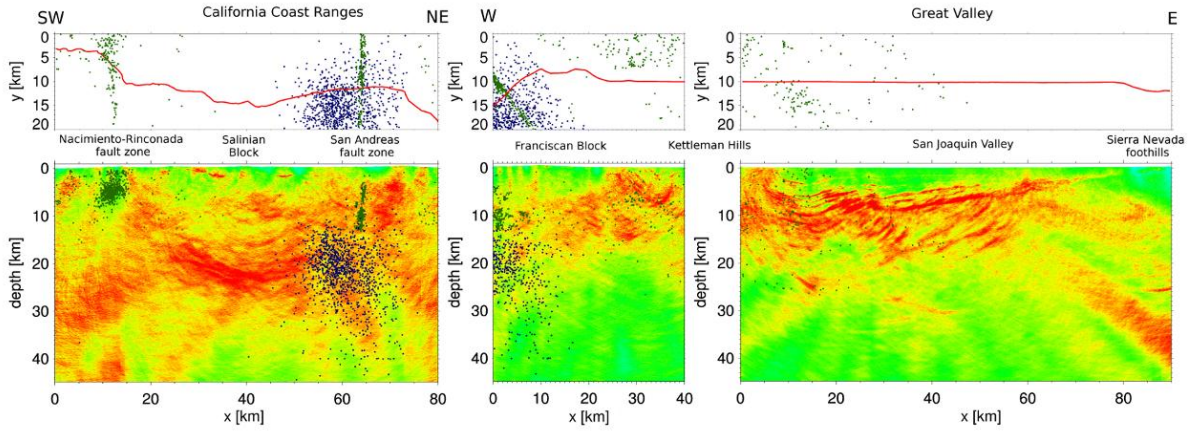

Figure 1: In order to account for the significant kink in the profile line the imaging was performed separately within three subvolumes. Figures on top show to respective map views of the receiver line (red lines) according to the depth sections below. Green dots are microseimic event locations from Waldhauser et al., 2008 and blue dots represent non-volcanic tremor locations from Nadeau et al., 2009, respectively. Note that the perspective changes from SW-NE in the left figure to W-E in the middle and right figure. Red colors in the depth sections represent high reflectivity values and green colors low reflectivity values.

lower crust beneath the Great Valley the resolution of the imaged structures could be increased compared to previous studies made by Trehu and Wheeler, 1987, as well as Walter et al., 1987 and others.

References:
Buske, S., S. Gutjahr, C. Sick (2009), Fresnel Volume Migration of single-component seismic data, Geophysics, Vol.74, No.6, WCA47—WCA55.
Godfey, N. J., S. L. Klemperer (1998), Ophiolitic basement to a forearc basin and implications for continental growth: The Coast Range / Great Valley ophiolite, California, Tectonics, Vol. 17, No. 4, Pages 558-570.
Lin, G., C. H. Thurber, H. Zhang, E. Hauksson, P. M. Shearer, F. Waldhauser, T. M. Brocher, J. Hardebeck (2010), California statewide three-dimensional seismic velocity model from both absolute and differential times, Bull. Seism. Soc. Am., 100, pp.225--240.
Mc Bride, J. H., L. D. Brown (1986), Reanalysis of the COCORP deep Seismic Reflection Profile Across the San Andreas fault,Parkfield, California, Bull. Seism. Soc. Am., Vol.76, No.6, pp. 1668-1686.
Nadeau, R. M., and A. Guilhem (2009), Nonvolcanic tremor evolution and the San Simeon and Parkfield, California earthquakes, Science, 325, 191-193, doi:10.1126/science.1174155.
Thurber, C., H. Zhang, F. Waldhauser, J. Hardebeck, A. Michael, D. Eberhart-Phillips (2006), Three-dimensional compressional wavespeed model, earthquake relocations, and focal mechanisms for the Parkfield, California region, Bull. Seism. Soc. Am., 96, S38—S49.
Trehu, A., and W. H. Wheeler (1987), Possible evidence in the seismic data of profile SJ-6 for subducted sediments beneath the Coast Ranges of California, USA, Interpretations of the SJ-6 seismic Reflection/Refraction Profile, South Central California, Open-File Report 87-73.
Waldhauser, F., and D.P. Schaff (2008), Large-scale relocation of two decades of Northern California seismicity using cross-correlation and double-difference methods, J. Geophys. Res., 113, B08311, doi: 10.1029/2007JB005479.
Walter, A. W., W. D. Mooney, C. M. Wentworth (1987), An interpretation of seismic reflection and refraction data recorded between Cholame Valley and the Sierra Nevada, California, USA, Interpretations of the SJ-6 seismic Reflection/Refraction Profile, South Central California, Open-File Report 87-73.

ICDP

Nationales Bohrkernlager für kontinentale Proben

U. HARMS[1], J. ERBACHER[2], U. RÖHL[3], G. WEFER[3], T. KOLLASKE[4], C. KNEBEL[1]

[1] Deutsches GeoForschungsZentrum GFZ, Potsdam
[2] Bundesanstalt für Geowissenschaften und Rohstoffe, Hannover
[3] MARUM – Zentrum für Marine Umweltwissenschaften, Universität Bremen
[4] Bundesanstalt für Geowissenschaften und Rohstoffe, Berlin-Spandau

Proben, Daten und Veröffentlichungen von wissenschaftlichen Bohrungen sind in den Geowissenschaften die wichtigsten „Produkte“ wissenschaftlicher Arbeit. Für Publikationen ist durch Bibliotheken und Datenbanken ein dauerhaft gesicherter Zugang etabliert, doch für Proben wie Bohrkerne und daraus gewonnene Daten gibt es bisher wenig Vergleichbares. Im internationalen Rahmen sind Bohrkerne der Ozeanbohrprogramme DSDP, ODP und IODP unter anderem in Bremen langfristig zugänglich. Für Landbohrungen gab es eine solche zentrale Einrichtung bisher nicht. Aus diesem Grund hat sich das Deutsche Forschungsbohrkonsortium GESEP e.V. für den Aufbau eines nationalen Bohrkernlagers für kontinentale Forschungsbohrungen eingesetzt.

Das MARUM – Zentrum für Marine Umweltwissenschaften an der Universität Bremen und die Bundesanstalt für Geowissenschaften und Rohstoffe (BGR) in Hannover haben hierzu gemeinsam ein Konzept entwickelt, um sowohl gekühlte terrestrische Kerne wie aus Seesedimenten, als auch ungekühlte Festgesteinsproben professionell zentral zu lagern und das Kernmaterial zugänglich zu machen. In Bremen ist bereits seit 1994 im Europahafen und seit 2005 auf dem Campus der Universität eine einzigartige Infrastruktur zur Lagerung und Auswertung von marinen Kernen etabliert. Zu mehr als 152 km Bohrkernen aus dem Atlantischen Ozean, dem Mittelmeer, dem Arktischen Ozean und dem Schwarzen Meer der Ozeanbohrprogramme DSDP, ODP, und IODP, kommen nun auch Kerne aus Seebohrungen des International Continental Scientific Drilling Program (ICDP): Kerne aus dem Vansee (Türkei, 800 m) und dem Toten Meer (Israel, Jordanien, Palästina, 460 m) sind bereits archiviert. Die Lagerung der Kerne in 1.5 m langen D-Tubes erfolgt in 5.5 m hohen Spezialregalen bei +4°C. Zusätzlich besteht die Möglichkeit, ausgewählte Proben bei -20°C oder -80°C zu gefrieren bzw. tiefstgefrieren. Die BGR hat an ihrem Standort in Berlin-Spandau eine neue Lagerhalle für Festgesteinsproben, die nicht der Kühlung bedürfen, errichtet. Diese Halle bietet auf 800 m² Grundfläche in 5 m hohen Schwerlastregalen Platz für bis zu 34 km Kernmaterial.

Beide Kernlagerstandorte verfügen, neben den Lagermöglichkeiten und der Expertise vor Ort, über Räumlichkeiten zur Kernbeschreibung und professionellen, effizienten Probennahme sowie über modernste Technik zur zerstörungsfreien Bohrkernanalyse wie petro-physikalische und Röntgenfluoreszenz-Scanner. Für umfangreichere Beprobungskampagnen (Sampling Parties) stehen an beiden Standorten Laborplätze und Computerausstattung zur Verfügung. Das eingelagerte Probenmaterial wird mit dem DrillingInformationSystem (DIS) nach einheitlichem Standard dokumentiert und beschrieben. Zusätzlich wird jede Probe durch eine International Geo Sample Nummer (IGSN) eindeutig identifizierbar, analytisch nachvollziehbar sowie zitierbar gemacht - ähnlich den DOIs für Publikationen. Das Kernlagerinventar (Informationen und Daten inklusive der Metadaten sowie der IGSNs) in Bremen und Berlin werden über ein für 2014 geplantes Webportal digital zugänglich sein. Zusätzlich sollen mittels des Daten-informationssystems PANGAEA des Alfred-Wegener-Instituts /MARUM die an Proben gewonnenen Analysedaten mit ihren Ursprungskernen und Publikationen verknüpft werden.

Die Definition und Einhaltung von Kernlager-Statuten zur Sicherung von Qualitätsstandards inklusive der Aufnahmebedingungen von Bohrkernen an den beiden Standorten wird durch ein Kuratorium sicher gestellt.

IODP

History of the Indian Monsoon recorded in Andaman Sea sediments

E.C. HATHORNE[1], D.G. YIRGAW[1], L. GIOSAN[2], T.S. COLLETT[3]

[1] Helmholtz-Zentrum für Ozeanforschung Kiel (GEOMAR), Wischhofstr. 1-3, 24148 Kiel, Germany
[2] Woods Hole Oceanographic Institution, 360 Woods Hole Rd., Woods Hole, MA 02543, USA
[3] U.S. Geological Survey, Box 25046, MS-939 Denver, Colorado 80225, USA

Over 3 billion people live in the area influenced by the Asian monsoon, the rains of which provide vital water resources while posing a risk to human life through flooding. Despite the importance to so many the monsoon is difficult to predict and model, making its future development in a changing global climate uncertain. To help improve models and predictions, histories of monsoon variability beyond the instrumental record are required. Many records of the East Asian monsoon have been generated from China and the South China Sea while past variability of the Indian Monsoon is mostly known from records of monsoon wind strength over the Arabian Sea. This study uses a unique long sediment core obtained by the IODP vessel *JOIDES Resolution* in the Andaman Sea to examine the past variability of Indian Monsoon precipitation on the Indian sub-continent and directly over the ocean. Our multi-proxy approach will reveal changes in continental weathering, runoff and direct precipitation on orbital timescales for the last 2 million years, filling a fundamental gap in our understanding of the Indian Monsoon in the past. Here we present initial data examining variations on millennial timescales for the last glacial and deglaciation.

The monsoon related influx of freshwater to the Bay of Bengal and Andaman Sea leads to a low salinity surface layer and a strong stratification of the upper 200 meters. Ocean atlas data (Antonov et al., 2010) indicates this stratification is remarkably stable throughout the year while the salinity of the surface layer changes with the monsoon. A sediment trap study in the region suggests that the abundance of mixed layer dwelling planktonic foraminifera *G. ruber* and *G. sacculifer* are not biased towards a particular season (Guptha et al., 1997). The thermocline dwelling *N. dutertrei* was also found throughout the year but exhibited a broad peak at the initiation and during the summer monsoon (Guptha et al., 1997). Core top studies have suggested the abundance of *N. dutertrei* is directly related to the low surface salinities associated with the monsoon (Cullen 1981). We utilize these ecological preferences to investigate the freshwater induced stratification with *N. dutertrei* abundance data and paired Mg/Ca and $\delta^{18}O$ analyses of both *G. sacculifer* and *N. dutertrei* for the last glacial and deglaciation. Preliminary measurements of Mg/Ca ratios from many individual shells of *N. dutertrei* from a Holocene sample and also an last glacial maximum (LGM) sample suggest little change in the range of calcification temperatures experienced by *N. dutertrei*. Individual *N. dutertrei* $\delta^{18}O$ measurements reveal a large contrast between the LGM and Holocene with the LGM samples exhibiting a normal distribution and a relatively small range. The Holocene individuals have a greater range of $\delta^{18}O$ values and a large skew toward more negative values indicating the greater influence of fresh water. These data demonstrate the usefulness of individual shell analyses for the reconstruction of monsoon variability for intervals in the past.

References:
Antonov, J. I., D. Seidov, T. P. Boyer, R. A. Locarnini, A. V. Mishonov, and H. E. Garcia (2010). World Ocean Atlas 2009 Volume 2: Salinity. S. Levitus, Ed., NOAA Atlas NESDIS 69, U.S. Government Printing Office, Washington, D.C., 184 pp.
Cullen, J. L. (1981), Microfossil Evidence for Changing Salinity Patterns in the Bay of Bengal Over the Last 20, 000 Years, Palaeogeography, Palaeoclimatology, Palaeoecology, 35, 315-356.
Guptha, M. V. S., W. B. Curry, V. Ittekkot, and A. S. Muralinath (1997), Seasonal variation in the flux of planktic Foraminifera; sediment trap results from the Bay of Bengal, northern Indian Ocean, The Journal of Foraminiferal Research, 27(1), 5-19.

IODP

Realtime mudgas monitoring during riser drilling - first results from a new technique applied during IODP Expedition 337 *Deep Coalbed Biosphere off Shimokita*.

V.B. HEUER[1], W.-L. HONG[2], M. BOWLES[1], A. IJIRI[3], Y. KUBO[4], F. INAGAKI[3], K.-U. HINRICHS[1] AND THE EXPEDITION 337 SCIENTISTS

[1] MARUM – Zentrum für marine Umweltwissenschaften & Fachbereich Geowissenschaften, Universität Bremen, 28334 Bremen
[2] College of Earth, Ocean, and Atmospheric Sciences, Oregon State University, Corvallis, OR, USA
[3] Kochi Institute for Core Sample Research, Japan Agency for Marine-Earth Science and Technology (JAMSTEC), Kochi, Japan
[4] Center for Deep Earth Exploration (CDEX), Japan Agency for Marine-Earth Science and Technology (JAMSTEC), Yokohama Kanagawa, Japan

Marine subsurface hydrocarbon systems are among the most frequently exploited but least characterized Earth systems. This is partly due to the fact that drilling into hydrocarbon reservoirs requires riser-technology. While such technology has long been used in commercial drilling operations, it only became available for scientific ocean drilling with *DV Chikyu* in 2005. IODP Expedition 337 (26 July - 30 September, 2012) was the first scientific expedition that used riser-technology to study the microbial ecology and biogeochemistry associated with a subseafloor hydrocarbon system. With Site C0020, the expedition targeted a natural gas field in the tectonically active forearc basin offshore the Shimokita Peninsula of Japan, where three deep thick coal layers were known to exist (Inagaki et al., 2010). Expedition 337 drilled and spot-cored Hole C0020A down to a total depth of 2466 meters below seafloor (mbsf) and recovered samples from a series of coal layers at around 2000 mbsf, where in situ temperatures were around 50°C (Inagaki et al., 2012). The recovered materials will help to elucidate the role of subsurface microbial activity in the formation of hydrocarbons in subseafloor coalbeds that are widespread in the NW Pacific.

The use of riser-drilling technology in very deep sediments creates both unique opportunities and new challenges. While riser-drilling allows the retrieval of sediment cores from sediment depths that have never been reached before by scientific ocean drilling, budget and time constraints require fast drilling without coring and limit the

recovery of intact sediment cores to selected horizons. Alternative approaches are needed to characterize the drilled formation, such as analysis of cuttings and mud-gas, which are sampled from the circulating drilling mud. During Expedition 337, we employed a newly installed mud-gas monitoring laboratory for online analysis of biogeochemically relevant gases. Mud gas was separated from the circulating drilling mud by gas separator and sent online to a laboratory unit equipped with methane carbon isotope analyzer (using cavity ring-down spectroscopy), mass spectrometer and gas chromatograph. Real-time analysis of both hydrocarbon gas contents and carbon isotopic compositions of methane revealed high C_1/C_2 ratios and low $^{13}C/^{12}C$ ratios as typically found in biogenic methane. In this manner, on-line mud-gas monitoring provided first indications for an important role of biogenic methane sources while Hole C0020A was still being drilled.

Mud-gas monitoring onboard *DV Chikyu* is a promising new technique in the context of riser-drilling operations and therefore it requires careful evaluation. In particular the following questions need to be addressed by post-cruise investigations: (1) Does on-line cavity ring-down spectroscopy yield accurate carbon isotope data for methane in the presence of other, potentially interfering mud gas components? In order to verify the novel shipboard data, we have analyzed the carbon isotopic composition of methane in mud gas samples shore-based by a well established method, i.e. isotope-ratio-monitoring gas chromatography/mass spectrometry. (2) How representative is the carbon isotopic composition of mud-gas methane? In order to address this question, we compare the carbon isotopic compositions of methane in gas samples taken from cuttings, sediment cores, and formation fluids. (3) To which extent is the recovery and composition of mud-gas influenced by drilling parameters (e.g. rate of penetration, mud weight)? We address this question through careful inspection of mud-gas monitoring data in the context of drilling operations. In this presentation, we will report our initial results for Site C0020 and discuss our data in the context of method evaluation.

References:

Inagaki F., Hinrichs K.-U., Kubo Y., and the Expedition 337 Project Team (2010) Deep coalbed biosphere off Shimokita: microbial processes and hydrocarbon system associated with deeply buried coalbed in the ocean. Integrated Ocean Drilling Program Scientific Prospectus, 337. doi:10.2204/iodp.sp.337.2010.

Inagaki F., Hinrichs K.-U., Kubo Y., and the Expedition 337 Scientists (2012) Deep coalbed biosphere off Shimokita: microbial processes and hydrocarbon system associated with deeply buried coalbed in the ocean. Integrated Ocean Drilling Program Preliminary Report, 337. doi:10.2204/iodp.pr.337.2012.

IODP

Gaining crucial new insights into understanding the geochemical zonation of the Galapagos hotspot track from IODP Exp. 344 (CRISP2) basement drilling and characterization of the overlying sedimentary cover

K. HEYDOLPH[1], J.GELDMACHER[1], K. HOERNLE[1] AND EXP. 344 SCIENCE PARTY

[1] GEOMAR Helmholtz-Zentrum für Ozeanforschung Kiel, Wischhofstr. 1-3, 24148 Kiel

We here present a newly proposed project based on igneous basement and sediment samples from the Cocos Plate drilled during Costa Rica Seismogenesis Project (CRISP) Expedition 344 (CRISP2) combined with additional igneous and sediment samples from CRISP1.

During CRISP 2 Expedition 344, which aimed to investigate the processes controlling nucleation and rupture of large megathrust earthquakes at erosional subduction zones, a total of five sites were drilled including two sites on the subducting Cocos plate (Sites U1381 and U1414). Igneous basement, belonging to the Galápagos hotspot track, was recovered from both Cocos Plate drill sites. These new samples provide the opportunity to gain valuable insights into the composition, structure and evolution of the Galápagos hotspot, one of the few primary hotspots worldwide (Courtillot et al., 2003).

The projects first main objective is it to measure the geochemical composition (including Sr, Nd, Pb, Hf and He isotope ratios) and age (Ar/Ar radiometric dating) of the hotspot track lavas, which will help to constrain the lateral and temporal (downhole) variation of the four distinct Galápagos hotspot geochemical domains (e.g. Hoernle et al., 2000) and to test proposed Galápagos plume-ridge interaction models. The expected results will be important to address the suggested specific geochemical zonation of Galápagos mantle plume with implications for currently discussed zoned plume models in general. In addition, a few samples from older Galápagos hotspot material, accreted to the midslope of the Costa Rica forearc (recovered during CRISP 1 Expedition 334) will also be analyzed to fill a crucial gap in the reconstruction of the earlier history of the Galápagos hotspot and its geochemical evolution.

The second main objective of this project is to analyze the composition of the sedimentary cover overlying the igneous basement at Sites U1381 and U1414 on the subducting Cocos Plate. The Pb isotope composition of central East Pacific sediments can be used to constrain the source of the deposited material (Höfig et al. revised for Geology). Expected downhole variation especially in Pb and Nd isotope ratios will be used to constrain different source contributions and the possible influence of the closure of the Panamanian gateway and climate change in Mexico and Central America.

References:
Expedition 334 Scientists, (2011) Costa Rica Seismogenesis Project (CRISP): sampling and quantifying input to the seismogenic zone and fluid output. IODP Prel. Rept., 334. doi:10.2204/iodp.pr.334.2011
Expedition 344 Scientists, (2013) Costa Rica Seismogenesis Project (CRISP-A2): sampling and quantifying lithological inputs and fluid inputs and outputs of the seismogenic zone. IODP Prel. Rept., 344. doi:10.2204/iodp.pr.344.
Hoernle K., Werner, R., Morgan, J.P., Garbe-Schönberg, D., Bryce, J., Mrazek, J. (2000) Existence of complex spatial zonation in the Galápagos plume. Geology 28, 435-438, doi:10.1130/0091-7613(2000)28.
Höfig, T.W., Hoernle, K., Hauff, F., Frank, M. Hydrothermal versus cratonic sediment supply to the eastern equatorial Pacific over the past 23 Ma and Central American Seaway closure. Geology (revised)
Werner, R., Hoernle, K., Barckhausen, Hauff, F. (2003) Geodynamic evolution of the Galapagos hot spot system (Central East Pacific) over the past 20 m.y.: Constraints from morphology, geochemistry, and magnetic anomalies. Geochem. Geophys. Geosyst. 4(12): 1108, doi:10.1029/2003GC000576.

ICDP

'PASADO Lipids'– evaluating lipid biomarkers and their compound-specific isotopes as proxies for paleoenvironmental reconstruction in Southern Patagonia

K. HOCKUN[1], G. MOLLENHAUER[1,2], E. SCHEFUß[1] AND THE PASADO SCIENCE TEAM

[1] MARUM – Zentrum für Marine Umweltwissenschaften, Universität Bremen, Leobener Straße, 28359 Bremen
[2] Alfred Wegener Institut Helmholtz- Zentrum für Polar- und Meeresforschung, Am Handelshafen 12, 27570 Bremerhaven

Southern Patagonia is a key region, in particular for paleoclimatic reconstruction in the Southern Hemisphere as it is the only landmass located in the Southern Hemisphere westerly wind (SHW) region. Most paleoclimatic studies focused on the Chilean side of the Andes or the Andean region (Kilian and Lamy, 2012). Only a few promising sedimentary archives exist in the southeastern part of Argentina. In 2007, the PASADO core was drilled in a volcanic maar situated in the Pali Aike volcanic field in Southern Patagonia. A high resolution sedimentary record was taken within the framework of an ICDP PASADO drilling campaign from Laguna Potrok Aike (51°58´S, 70°23´W). At present, the climate in our study area is mainly influenced by the SHW and the topography of the landmass (Mayr et al., 2007a,b).

Extensive studies with the focus on multiproxy approaches have been carried out within the PASADO project framework. Previous work was conducted to establish regional calibrations for pollen, diatom and chironomid associations in order to reconstruct temperature and precipitation changes in Southern Patagonia. In addition, several approaches have been taken to infer paleo-hydrological changes and associated lake-level variations (Haberzettl et al., 2007a; Haberzettl et al., 2005; Haberzettl et al., 2008), yielding, however, inconclusive results in comparison with the reconstructions based on archives in the Andean region. Furthermore, so far no quantitative paleoclimatic reconstructions exist for temperature and hydrological changes for Laguna Potrok Aike.

Therefore, the PASADO ("Potrok Aike Maar Lake Sediment Archive Drilling Project") Lipids project started in 2011 aiming to provide new insights into the climate history of southern South America by using organic-geochemical proxies based on lipid biomarkers. We study abundances and compound-specific isotope compositions (δD, $\delta^{13}C$) of biomarkers derived from terrestrial and aquatic plants including *n*-alkanes and *n*-fatty acids as well as temperature- and pH-sensitive abundance ratios of membrane lipids of archaea and bacteria (glycerol dialkyl glycerol tetraethers, GDGTs). Based on the GDGTs it was aimed to infer lake temperature changes using TEX_{86} (TetraEther index of GDGTs with 86 carbon atoms), as well as soil temperature and pH changes using the MBT/CBT indices (methylation ratio/cyclization ratio of branched tetraethers). Compound-specific δD values of biomarkers from aquatic and terrestrial sources are expected to reflect the local hydrology and changes in the lake water balance in particular. Combining all datasets will allow to develop an improved mechanistic understanding of terrestrial climatic conditions in the Southern Hemisphere.

We characterized the lipid biomarker signatures of terrestrial plants, cyanobacterial matter, aquatic mosses and macrophytes, soils and lake surface sediments from Laguna Potrok Aike to identify suitable tracers for paleo-reconstructions. These results will help us to identify hydrologic signals in lipids of the various organic matter sources which adequately describe the modern hydro-climatic balance of Laguna Potrok Aike.

To investigate the isotope signal in wax lipids derived from higher terrestrial plants in relation to moisture sources and fractionation effects during evaporation and transpiration we analysed 16 top-soil samples along a W-E transect along the same latitude of Laguna Potrok Aike. Long-chain *n*-alkanes (*n*-C_{29} & *n*-C_{31}) in the top soils show similar ranges of compound-specific δD and $\delta^{13}C$ compositions as in investigated sediment samples of Laguna Potrok Aike. The δD values of the *n*-C_{31} alkane vary from -225‰ to -195‰ and show an increase from W to E which might indicate the higher relative influence of the Atlantic (isotopically enriched) moisture over south-east Patagonia. The compound-specific $\delta^{13}C$ values of the *n*-C_{31} alkane (range: -34.9‰ to -32.7‰) also show an increase from W to E which is interpreted as higher water-use-efficiency of the C_3 plants in the east due to higher aridity, i.e., lower mean annual precipitation amounts. The positive correlation of $\delta^{13}C$ and δD signals suggests that fractionation effects due to higher evapo-transpiration in the east partly cause the observed trend in long-chain *n*-alkane δD values. To strengthen our hypothesis we target analyses of additional samples provided by the cooperation partners in Argentina. The first down core data show high variability in the abundance of the *n*-alkyl lipids. The dominance of long-chain n-alkanes (*n*-C_{29} & *n*-C_{31}, terrestrial origin) during the late glacial shifted to a higher abundance of *n*-C_{20} and *n*-C_{23} (of aquatic origin) after the Antarctic Cold Reserval, which seem to be related to lake level changes.

Results of GDGT distributions in the top soil samples as well as a series of lake surface samples confirm a correlation between GDGT index parameters (MBT/CBT indices) and soil temperature and pH in the study area. The predicted temperatures based on the global calibration (Weijers et al., 2007) are, however, lower than measured temperatures. For this reason we developed a new calibration for the use of GDGT-based proxies in southern Patagonia based on the published MBT/CBT indices. The MBT-based reconstructed temperature values, however,

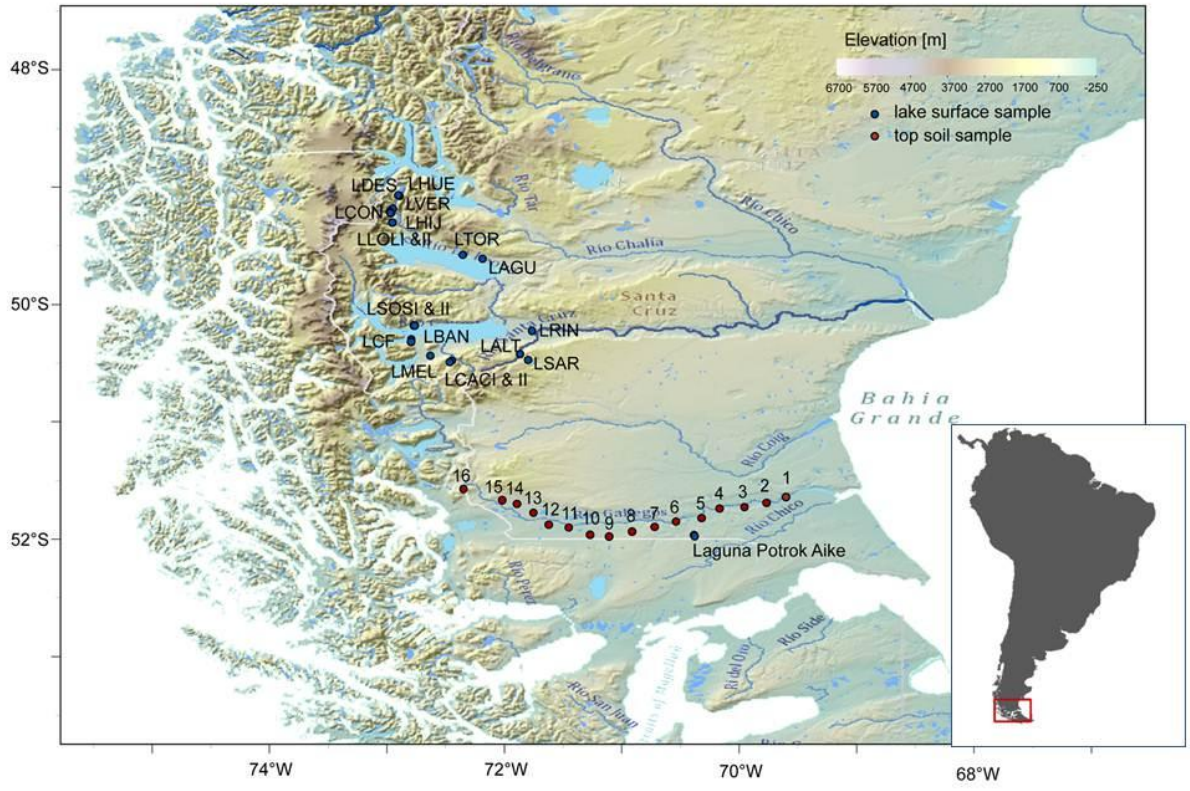

Figure 1: Map of study area including the locations of the W-E top soil transect and the lake surface sediments.

differ (+/-2°C) from the measured mean annual temperatures in our study area (Fig. 2). The temperature estimates from the analysed lake surface sediments overestimate regional mean annual air temperatures by almost 10°C (Fig. 3). I*n situ* production of a couple of GDGTs used in the calibration appears to compromise the signals. For that reason, we are trying to avoid the questionable components for the new regional calibration. Therefore, additional samples covering a wider temperature range will be analysed to identify suitable temperature sensitive components and thus develop a calibration appropriate for Southern Patagonia. 60 additional top soil samples from a north-south transect and a few samples from the Andean region are provided for this purpose from our cooperation partners from Argentina involved in the PASADO project.

110 PASADO core samples are currently being processed to measure abundance and compound-specific isotope compositions (δD, $\delta^{13}C$) of *n*-alkanes and *n*-fatty acids as well as temperature- and pH-sensitive abundance ratios of GDGTs covering a period of 20,000 years. The first results of the PASADO core will be available for the colloquium.

References:
Haberzettl, T. et al., 2007a. Lateglacial and Holocene wet-dry cycles in southern Patagonia: chronology, sedimentology and geochemistry of a lacustrine record from Laguna Potrok Aike, Argentina. Holocene, 17: 297-310.
Haberzettl, T. et al., 2005. Climatically induced lake level changes during the last two millennia as reflected in sediments of Laguna Potrok Aike, southern Patagonia (Santa Cruz, Argentina). Journal of Paleolimnology, 33: 283-302.
Haberzettl, T. et al., 2008. Hydrological variability in southeastern Patagonia and explosive volcanic activity in the southern Andean Cordillera during Oxygen Isotope Stage 3 and the Holocene inferred from lake sediments of Laguna Potrok Aike, Argentina. Palaeogeography Palaeoclimatology Palaeoecology, 259: 213-229.
Kilian, R. and F. Lamy (2012). "A review of Glacial and Holocene paleoclimate records from southernmost Patagonia (49-55˚S)."

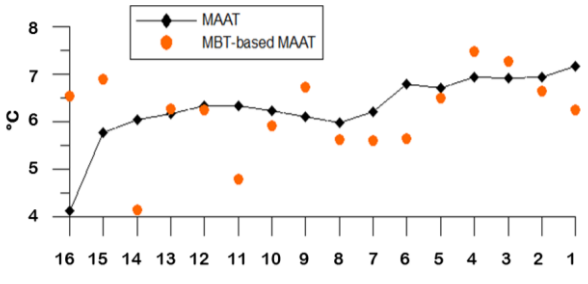

Figure 2: Comparison of measured mean annual air temperature (MAAT) with estimated MAAT values from MBT reconstruction

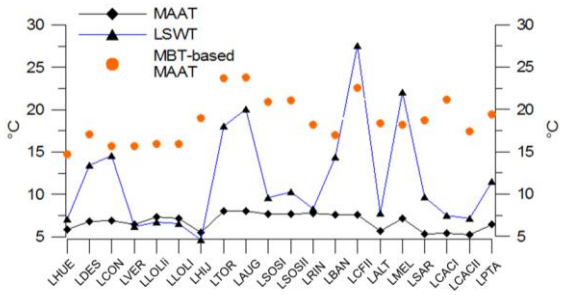

Figure 3: Comparison of mean annual air temperature (MAAT), lake surface water temperature (LSWT) and estimated MAAT values from MBT reconstruction. LSWT of the N-S lake transect were measured on the day of sample collection.

Quaternary Science Reviews 53: 1-23.
Mayr, C., Wille, M., Haberzettl, T., Fey, M., Janssen, S., Lücke, A., Ohlendorf, C., Oliva, G., Schäbitz, F., Schleser, G., Zolitschka, B., 2007a. Holocene variability of the Southern Hemisphere westerlies in Argentinean Patagonia (52_S). Quat. Sci. Rev., 26, 579–584.
Mayr, C., Lücke, A., Stichler, W., Trimborn, P., Ercolano, B., Oliva, G., Ohlendorf, C., Soto, J., Fey, M., Haberzettl, T., Janssen, S., Schäbitz, F., Schleser, G.H., Wille, M., Zolitschka, B., 2007b. Precipitation origin and evaporation of lakes in semi-arid Patagonia (Argentina) inferred from stable isotopes ($\delta^{18}O$, $\delta^{2}H$). Journal of Hydrology, 334, 53-63.
Weijers, J.W.H., Schouten, S., van den Donker, J.C., Hopmans, E.C. and Damste, J.S.S., 2007a. Environmental controls on bacterial tetraether membrane lipid distribution in soils. Geochimica et Cosmochimica Acta, 71: 703-713.

IODP

Hydrothermal versus cratonic sediment supply to the eastern equatorial Pacific over the past 23 Ma and Central American Seaway closure

T.W. HÖFIG[1,2], K. HOERNLE[1], F. HAUFF[1], M. FRANK[1]

[1] GEOMAR | Helmholtz Centre for Ocean Research, Wischhofstr. 1-3, D-24148 Kiel, Germany
[2] Department of Mineralogy, TU Bergakademie Freiberg, Brennhausgasse 14, D-09596 Freiberg, Germany

The source areas of oceanic sediments can be tracked by the three-isotope lead (Pb) radiogenic system, since it enables the reconstruction of mixing relationships between different endmembers within one isotopic system (cf. Frank, 2002). Potential sources include tephras from intraplate and subduction zone volcanoes, particulate matter originating from hydrothermal fluids associated with areas of active submarine volcanism, such as mid-ocean ridges, and erosional inputs from the continents. The low mean oceanic residence time of Pb of 50 (Atlantic) to 200–400 (Pacific) years in dissolved form gives rise to its importance as an oceanographic tracer (Frank, 2002). Variations in the Pb isotope composition of marine sediments thus provide an important archive for reconstructing both changes in the sources of the sediments and of the water masses transporting the sediment particles or dissolved Pb through time.

The present study combines down-core records of bulk sediment and sediment leachate high-precision Pb isotopes from two eastern equatorial Pacific (EEP) seafloor sites, namely Deep Sea Drilling Project (DSDP) Site 495 and Ocean Drilling Program/Integrated Ocean Drilling Program (ODP/IODP) Site 1256. Both sites are located on the Cocos Plate. They provide the first continuous Pb isotope evolution of the dissolved and detrital fraction of eastern Pacific sediments over the past 23 Ma. The main goal of this study was to determine the major sources of the sediments and to reconstruct past changes in deep water mixing at the two DSDP/IODP sites in the EEP, spanning the entire succession from the formation of the underlying seafloor at the East Pacific Rise (EPR) to present-day pelagic sedimentation close to the Central American subduction zone.

Detrital Pb isotope compositions ($^{206}Pb/^{204}Pb_{in}$ = 18.28–18.80, $^{207}Pb/^{204}Pb_{in}$ = 15.56–15.63, $^{208}Pb/^{204}Pb_{in}$ = 37.93–38.71) became systematically more radiogenic from ~23 Ma at Site 495 and from ~14 Ma at Site 1256 until ~4 Ma, as a consequence of plate tectonic movements of the core locations (Fig. 1). The data from both cores form well-defined correlations of uranogenic and thorogenic Pb isotopes, which can be explained by mixing of an unradiogenic hydrothermal component carrying an East Pacific Rise mid-ocean ridge basalt composition and a radiogenic continental component from the Maya (southeastern Mexico) and Chortís (northwestern Central America) Blocks. Central Asian dust, which is widely deposited in the central Northern Pacific (e.g., Pettke et al., 2002), cannot serve as the radiogenic endmember, since its $^{208}Pb/^{204}Pb$ is too high for the associated $^{206}Pb/^{204}Pb$ ratios (Fig. 2).

The Pb at the base of the sediment sequence deposited close to the spreading center is primarily hydrothermal in origin, whereas the sediments from the upper part of the sequences were deposited far from the spreading center and were primarily sourced from older continental terranes. The decreasing Pb isotope ratios after 4 Ma (Fig. 1) most likely relate to the closure of the Central American Seaway, which led to reorganization of the EEP ocean circulation pattern and caused mountain uplift in Central America (Retallack and Kirby, 2007; Schmidt, 2007; Montes et al., 2012). The modified ocean circulation could have implied a provenance change by strengthening of a westward directed current system increasing the contribution of the Central American Volcanic Arc (CAVA) at the expense of southward directed cratonic Maya-Chortís sediment supply. Contemporaneously, consistent with the global late Cenozoic cooling trend,

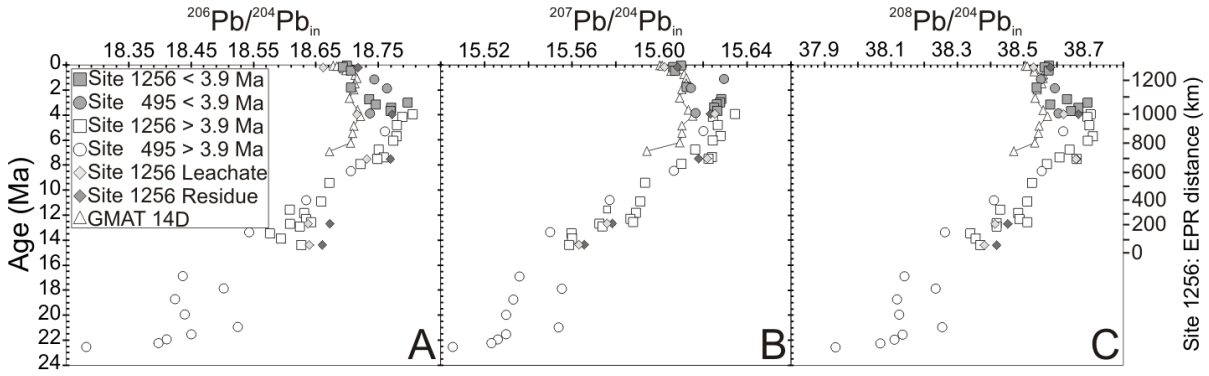

Figure 1: Initial A) $^{206}Pb/^{204}Pb_{in}$, B) $^{207}Pb/^{204}Pb_{in}$, and C) $^{208}Pb/^{204}Pb_{in}$ isotope ratios versus age (and distance between Site 1256 and the EPR). Eastern equatorial Pacific (EEP) Fe-Mn crust GMAT 14D (Frank et al., 1999) is displayed, too. EPR distances calculated with the software GPlates. Errors are within symbol size. Note that leachate and residue Pb isotope ratios refer to measured values.

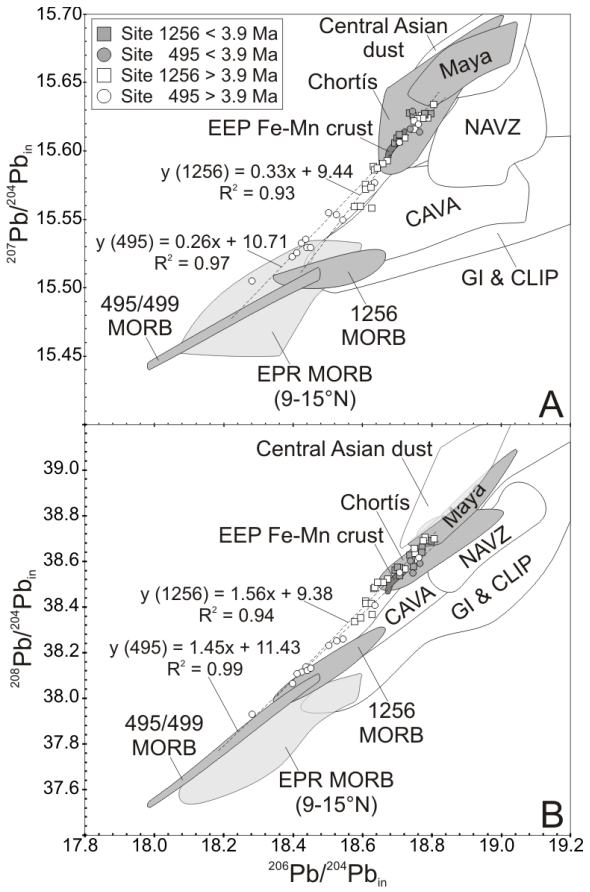

Figure 2: $^{206}Pb/^{204}Pb_{in}$ versus $^{207}Pb/^{204}Pb_{in}$ (A) and $^{208}Pb/^{204}Pb_{in}$ (B), respectively, defining linear two-component isotopic mixing arrays (initial ratios) between East Pacific Rise (EPR) mid-ocean ridge basalt (MORB) and the Maya (SE Mexico) and Chortís (NW Central America) Blocks. Site 1256 MORB (age-corrected) (Geldmacher et al., 2013). Site 495/499 MORB (age-corrected) (Geldmacher et al., 2008, 2013; Heydolph et al., 2012). EPR MORB (9–15°N) (Castillo et al., 2000; Sims et al., 2002; Waters et al., 2011). Maya and Chortís Block data (Cumming and Kesler, 1976; Cumming et al., 1981; Heydolph et al., 2012) include the range of Pb isotope compositions of Central American mineral deposits. Central Asian dust: Pettke et al., 2000, 2002. GMAT 14D: Frank et al., 1999. Central American Volcanic Arc (CAVA): Hoernle et al., 2008; Heydolph et al., 2012. Galápagos Islands (GI): White et al., 1993; Hoernle et al., 2000; Werner et al., 2003. Caribbean Large Igneous Province (CLIP): Hauff et al., 2000a, 2000b; Hoernle et al., 2002. Northern Andean Volcanic Zone (NAVZ): Chiaradia et al., 2004, 2009; Bryant et al., 2006. Errors are smaller than size of the symbols.

aridification migrated from north (Mexico) to south (Central America), promoted by landmass emergence (Graham, 1999; Retallack and Kirby, 2007). This probably gave rise to reduced runoff from the Maya-Chortís area, while southwestern Central America simultaneously maintained its less radiogenic CAVA-dominated riverine Pb input.

In conclusion, the present Pb isotopic record provides clear evidence for a significant tectonic, paleogeographic, and climatic change in the central East Pacific by drilling core coverage of hydrothermal and detrital sources in that part of the global ocean.

References:

Bryant, J.A., Yogodzinski, G.M., Hall, M.L., Lewicki, J.L., and Bailey, D.G., 2006, Geochemical constraints on the origin of volcanic rocks from the Andean Northern Volcanic Zone, Ecuador: Journal of Petrology, v. 47, p. 1147–1175.

Castillo, P.R., Klein, E., Bender, J., Langmuir, C., Shirey, S., Batiza, R., and White, W., 2000, Petrology and Sr, Nd, and Pb isotope geochemistry of mid-ocean ridge basalt glasses from the 11°45'N to 15°00'N segment of the East Pacific Rise: Geochemistry, Geophysics, Geosystems, v. 1, 1011, doi: 10.1029/1999GC000024.

Chiaradia, M., Fontboté, L., and Beate, B., 2004, Cenozoic continental arc magmatism and associated mineralization in Ecuador: Mineralium Deposita, v. 39, p. 204–222.

Chiaradia, M., Müntener, O., Beate, B., and Fontignie, D., 2009, Adakite-like volcanism of Ecuador: lower crust magmatic evolution and recycling: Contributions to Mineralogy and Petrology, v. 158, p. 563–588.

Cumming, G.L., and Kesler, G.E., 1976, Source of lead in Central American and Caribbean mineralization: Earth and Planetary Science Letters, v. 31, p. 262–268.

Cumming, G.L., Kesler, S.E., and Krstic, D., 1981, Source of lead in Central American and Caribbean mineralization: II. Lead isotope provinces: Earth and Planetary Science Letters, v. 56, p. 199–209.

Frank, M., 2002, Radiogenic isotopes: Tracers of past ocean circulation and erosional input, Reviews of Geophysics, v. 40, 1001, doi: 10.1029/2000RG000094.

Frank, M., Reynolds, B.C., and O'Nions, R.K., 1999, Nd and Pb isotopes in Atlantic and Pacific water masses before and after closure of the Panama gateway: Geology, v. 27, p. 1147–1150.

Geldmacher, J., Hoernle, K., van den Bogaard, P., Hauff, F., and Klügel, A., 2008, Age and geochemistry of the central American forearc basement (DSDP Leg 67 and 84): Insights into Mesozoic arc volcanism and seamount accretion on the fringe of the Caribbean LIP: Journal of Petrology, v. 49, p. 1781–1815.

Geldmacher, J., Höfig, T.W., Hauff, F., Hoernle, K., Garbe-Schönberg, D., and Wilson, D.S., 2013, Influence of the Galápagos hotspot on the East Pacific Rise during Miocene superfast spreading: Geology, v. 41, p. 183–186.

Graham, A., 1999, The Tertiary history of the northern temperate element in the northern Latin American biota: American Journal of Botany, v. 86, p. 32–38.

Hauff, F., Hoernle, K., Tilton, G., Graham, D.W., and Kerr, A.C., 2000a, Large volume recycling of oceanic lithosphere over short time scales: geochemical constraints from the Caribbean Large Igneous Province: Earth and Planetary Science Letters, v. 174, p. 247–263.

Hauff, F., Hoernle, K., van den Bogaard, P., Alvarado, G., and Garbe-Schönberg, D., 2000b, Age and geochemistry of basaltic complexes in western Costa Rica: Contributions to the geotectonic evolution of Central America: Geochemistry, Geophysics, Geosystems, v. 1, 1009, doi: 10.1029/1999GC000020.

Heydolph, K., Hoernle, K., Hauff, F., van den Bogaard, P., Portnyagin, M., Bindeman, I., and Garbe-Schönberg, D., 2012, Along and across arc geochemical variations in NW Central America: Evidence for involvement of lithospheric pyroxenite: Geochimica et Cosmochimica Acta, v. 84, p. 459–491.

Hoernle, K., Abt, D.L., Fischer, K.M., Nichols, H., Hauff, F., Abers, G.A., van den Bogaard, P., Heydolph, K., Alvarado, G., Protti, M., and Strauch, W., 2008, Arc-parallel flow in the mantle wedge beneath Costa Rica and Nicaragua: Nature, v. 451, p. 1094–1098.

Hoernle, K., van den Bogaard, P., Werner, R., Lissinna, B., Hauff, F., Alvarado, G., and Garbe-Schönberg, D., 2002, Missing history (16–71 Ma) of the Galápagos hotspot: Implications for the tectonic and biological evolution of the Americas: Geology, v. 30, p. 795–798.

Hoernle, K., Werner, R., Morgan, J.P., Garbe-Schönberg, D., Bryce, J., and Mrazek, J., 2000, Existence of complex spatial zonation in the Galápagos plume: Geology, v. 28, p. 435–438.

Montes, C., Bayona, G., Cardona, A., Buchs, D.M., Silva, C.A., Moron, S., Hoyos, N., Ramirez, D.A., Jaramillo, C.A.,Valencia, V., 2012, Arc-continent collision and orocline formation: Closing of the Central American seaway: Journal of Geophysical Research, v. 117, B04105, doi: 10.1029/2011jb008959.

Pettke, T., Halliday, A.N., Hall, C.M., and Rea, D.K., 2000, Dust production and deposition in Asia and the north Pacific Ocean over the past 12 Myr: Earth and Planetary Science Letters, v. 178, p. 397–413.

Pettke, T., Halliday, A.N., and Rea, D.K., 2002, Cenozoic evolution of Asian climate and sources of Pacific seawater Pb and Nd derived from eolian dust of sediment core LL44-GPC3: Paleoceanography, v. 17, 1031, doi: 10.1029/2001PA000673.

Retallack, G.J., and Kirby, M.X., 2007, Middle Miocene global change and paleogeography of Panama: Palaios, v. 22, p. 667–679.

Schmidt, D.N., 2007, The closure history of the Central American seaway: evidence from isotopes and fossils to models and molecules, in Williams, M., Haywood, A.M., Gregory, F.J., Schmidt, D.N., eds., Deep-time perspectives on climate change - marrying the signal from computer models and biological proxies.: The Micropalaeontological Society, Special Publications: London, Geological Society of London, p. 427–442.

Sims, K.W.W., Goldstein, S.J., Blichert-Toft, J., Perfit, M.R., Kelemen, P., Fornari, D.J., Michael, P., Murrell, M.T., Hart, S.R., DePaolo, D.J., Layne, G., Ball, L., Jull, M., and Bender, J., 2002, Chemical and isotopic constraints on the generation and transport of magma beneath

the East Pacific Rise: Geochimica et Cosmochimica Acta, v. 66, p. 3481–3504.
Waters, C.L., Sims, K.W.W., Perfit, M.R., Blichert-Toft, J., and Blusztajn, J., 2011, Perspective on the Genesis of E-MORB from Chemical and Isotopic Heterogeneity at 9-10 degrees N East Pacific Rise: Journal of Petrology, v. 52, p. 565–602.
Werner, R., Hoernle, K., Barckhausen, U., and Hauff, F., 2003, Geodynamic evolution of the Galápagos hostspot system (Central East Pacific) over the past 20 m.y.: Constraints from morphology, geochemistry and magnetic anomalies: Geochemistry, Geophysics, Geosystems, v. 4, 1108, doi: 10.1029/2003GC000576.
White, W.M., McBlirney, A.R., and Duncan, R.A., 1993, Petrology and geochemistry

IODP

African drift, million-year cooling and marine biotic crises in the Cretaceous greenhouse

P. HOFMANN[1], A. MCANENA[1,2], T. WAGNER[3], A. GRIESAND[4], J.O. HERRLE[4,5], J. PROSS[4], H.M. TALBOT[3], S. FLÖGEL[6]

[1] Universität zu Köln, Institut für Geologie und Mineralogie, Köln, Germany
[2] IMCS, Rutgers University, NJ, USA
[3] School of Civil engineering and Geosciences, Newcastle University, UK
[4] Goethe-Universität Frankfurt, Frankfurt, Germany
[5] Biodiversity and Climate Research Center (BIK-F), Frankfurt, Germany
[6] GEOMAR, Kiel, Germany

Marine biotic crises in the Cretaceous greenhouse have been often associated with episodes of extreme global warming, often associated with widespread ocean anoxia (e.g. Leckie et al., 2002). There is, however, circumstantial evidence that cooling may also have caused similar biotic crisis in the mid-Cretaceous (e.g. Mutterlose et al., 2009; Iba et al., 2011). Convincing support for such a mechanism is still pending as continuous temperature and carbon isotope records are rare and often not sufficiently detailed to confirm relationships with biotic change (figure 1).

Our study of Deep Sea Drilling Program (DSDP) Site 545 sediments provides high-resolution, multi-proxy records from the eastern North Atlantic (Mazagan Plateau, NW Africa) that constrain the internal structure and magnitude of a pronounced cooling cycle that allows us to discuss the connections between plate tectonics, climate, marine carbon burial and marine biota. Our high-resolution records to constrain the timing and magnitude of late Aptian climate change and associated biotic crises for the subtropical eastern North Atlantic, combining detailed records of TEX86-derived sea surface temperature estimates (SSTe), $\delta^{13}C$ isotopes, element geochemistry, and calcareous nannofossil studies.

The lower part of the studied succession is marked by low carbon isotope values and warm sea surface water temperatures (SST) (*G. ferreolensis*-Zone – upper *H. trocoidea*-Zone). The deep dwelling nannoconids are marked by fluctuating values, suggesting short-term changes in surface water stratification and surface water productivity at the Mazagan Plateau. Changing surface water productivity is also indicated by the nutrient index.

Following the onset of the main positive carbon isotope excursion of >1.5 ‰ SST decrease of about 3°C within the middle part of the *T. bejaouaensis*-Zone. The onset of the cold snap is accompanied by pronounced biotic changes (Fig. 2). Major mid-Cretaceous carbonate producing organisms such as nannoconids, planktic foraminifera, and reef building organisms are marked by a crisis whereas the boreal cold water taxon *R. parvidentatum* as well as siliceous organisms occur in higher abundances (see summary figure 1). In addition, the nutrient-index indicate higher surface waters compared to the lower part of the studied succession.Our results show a million-year ~5 °C cooling period with superimposed climate instability in the late Aptian. This cooling coincided with a significant decline in calcareous nannoconids and an extinction of planktic foraminifera suggesting a causal link. We also observe a broad positive ~1.5 - 2 ‰ carbon isotope excursion of organic and inorganic carbon that mirrors SST with the most positive isotopic signatures occurring during the coolest period.

To explore the underlying mechanisms controlling the positive carbon excursion and global cooling we invoke two mechanisms, both related to the Cretaceous drift of Africa. These are (1) enhanced organic carbon burial in the South Atlantic as the basin widened but was not yet connected to the North Atlantic and (2) variations in the inflow of warm surface waters into the eastern North Atlantic via the western Tethys Gibraltar Gateway. Modelling results suggest, within limitations of model parameterisation, that up to around of 30% of the global carbon isotope excursion can be explained by organic carbon sequestration in the North and South Atlantic, emphasizing Atlantic as a major carbon sink during that period. The turning point in global cooling was probably related to fundamental global re-organisations, including S-Atlantic ocean circulation, leading to more oxygenated conditions, as supported by the presence of oxic sediments. This study supports that tectonic induced long-term cooling during past greenhouse conditions were capable of triggering critical periods for global evolutionary and biogeochemical change.

References:

Bralower, T.J., et al. (1997): Mid-Cretaceous strontium-isotope stratigraphy of deep-sea sections. Geological Society of America Bulletin 109, 1421-1442.
Haq, B., et al. (1987): Chronology of fluctuating sea levels since the Triassic (250 million years ago to present). Science 23, 1156-1167.
Herrle, J.O. et al. (2003): Forcing mechanisms for mid-Cretaceous black shale formation: Evidence from the Upper Aptian and Lower Albian of the Vocontian Basin (SE France). Palaeogeography, Palaeoclimatology, Palaeoecology 190, 399–426.
Herrle, J.O., et al. (2004): High-resolution carbon isotope records of the Aptian to Lower Albian from SE France and the Mazagan Plateau (DSDP Site 545): a stratigraphic tool for paleoceanographic and paleobiologic reconstruction. Earth and Planetary Science Letters, 218, 149-161.
Hong, S. K.; Lee, Y. I. (2012): Evaluation of atmospheric carbon dioxide concentrations during the Cretaceous. Earth and Planetary Science Letters, 327–328, 23–28.
Huber, B.T., Leckie, R. M. (2011) Planktic foraminiferal species turnover across deep-sea Aptian/Albian boundary sections, Journal of Foraminiferal Research, 41, 53-95.
Iba, Y., Mutterlose, J., Tanabe, K., Sano, S., Misaki, A., Terabe, (2011): K. Belemnite extinction and the origin of modern cephalopods 35 m.y. prior to the Cretaceous-Paleogene event. Geology 39, 483-486
Johnson, C.C. et al. (1996): Middle Cretaceous reef collapse linked to ocean heat transport. Geology 24, S. 376–380.
Kauffman, E.G.; Johnson, C.C. (1988): The Morphological and Ecological Evolution of Middle and Upper Cretaceous Reef-Building Rudistids. Ancient Reef Ecosystems. Palaios 3, 194–216.
Kim, J. H. et al. (2010): New indices and calibrations derived from the distribution of crenarchaeal isoprenoid tetraether lipids: Implications for past sea surface temperature reconstructions. Geochimica et Cosmochimica Acta 74, 4639–4654.
Larson, R.L. (1991): Latest pulse of the Earth: evidence for a mid-Cretaceous super plume. Geology 19, 547-550.
Leckie, R. M., Bralower, T. J. & Cashman, R. (2002): Oceanic anoxic events and plankton evolution: biotic response to tectonic forcing during the mid-Cretaceous. Paleoceanography 17, 1-29.

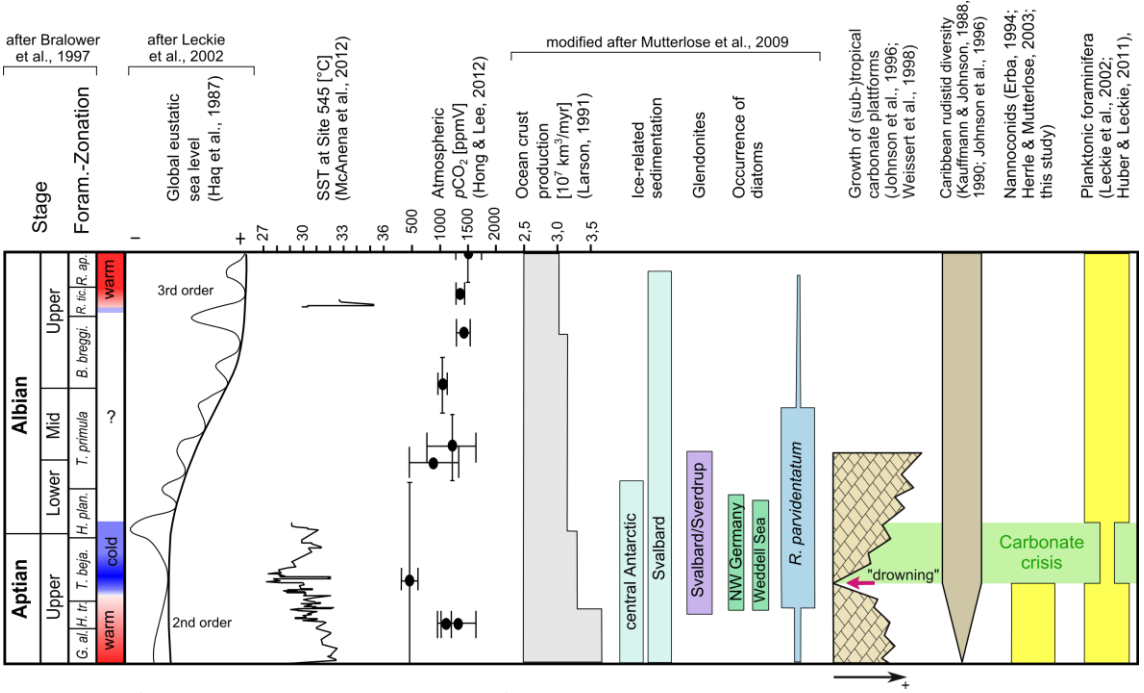

Fig. 1: Overview of sedimentological and biological changes from the Upper Aptian to Upper Albian (modified by Mutterlose et al., 2009). Global eustatic sea level was low in the Aptian and began to rise during the Albian. SST at Site 545 decreased from ~32°C to a minimum of 27°C within the *T. bejaouaensis*-Zone. Atmospheric pCO_2 decreased from about 1000 ppmV in the Lower Aptian to 400 ppmV in the Upper Aptian. Sedimentological proxies such as ice-rafted sediments and glendonites from the high latitudes also suggest cooler temperatures. Diatoms and the boreal cold-water calcareous nannofossil *R. parvidentatum* became widespread during this interval. Carbonate producing organisms (reef builders, nannoconids, planktic foraminifera) are characterized by a crisis in the uppermost Aptian associated with the cold snap. In contrast, rudist reefs became widespread in the Caribbean region.

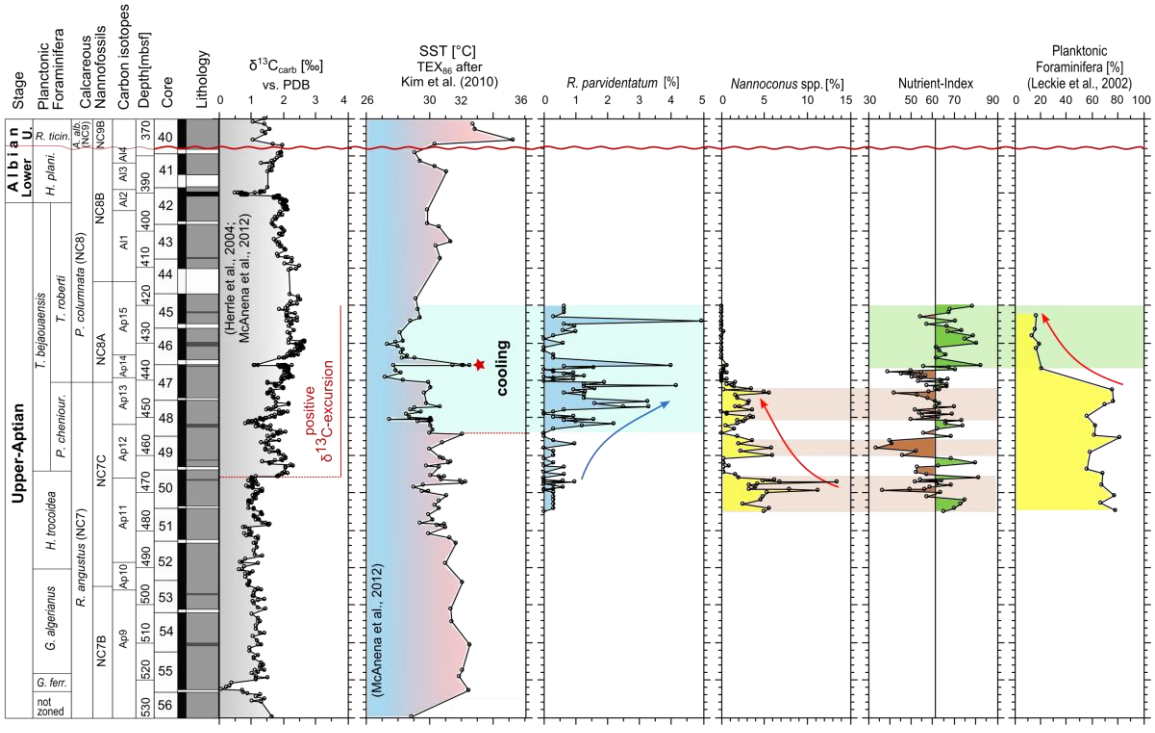

Fig 2. High resolution records of carbon isotopes, sea surface temperature (based on TEX_{86}), *Repagulum parvidentatum*, *Nannoconus spp*., Nutrient-Index and planktic foraminifera percentages. High percentages of *nannoconids* correspond to low values of the nutrient index indicating an increased surface water stratification and decreased surface water productivity and vice versa. High percentages of the cold water taxon *R. parvidentatum* are accompanied by cooler surface water as indicated by lower TEX_{86} values. The decrease in nannoconid percentages is accompanied by a decrease in planktic foraminifera indicating a major change within the marine calcifying organisms.

McAnena, A. et al. (2012): Evidence for long term cooling and short punctuated climate events at the Aptian-Albian boundary in the sub-tropical eastern Atlantic (Mazagan Plateau, DSDP Site 545). Geophysical Research Abstracts, 14, EGU2012-6257-1.

Mutterlose, J., Bornemann, A. & Herrle, J. O. (2009): The Aptian – Albian cold snap: Evidence for "mid" Cretaceous icehouse interludes. Neues Jahrbuch Geologisch Paläontologische Abhandlungen 232, 217–225.

Weissert, H. et al. (1998): Correlation of Early Cretaceous carbon isotope stratigraphy and platform drowning events: a possible link? Palaeogeography, Palaeoclimatology, Palaeoecology 137, 189–203.

IODP

Implications of clay dehydration processes on pore water geochemistry constrained by laboratory experiments

A. HÜPERS[1] AND A.J.KOPF[1]

[1] MARUM - Center for Marine Environmental Sciences, University of Bremen, P.O. Box 330440, 28334 Bremen, Germany.

Incoming sediments on the downgoing plate at convergent margins are initially water-rich. The greatest water mass is stored as interstitial water. Additional water is stored within the structure of hydrous minerals such as smectite or opal-A. Within the first few kilometers of subduction much of the interstitial water is expelled by mechanical compaction while mineral-bond water is carried to greater depth. With progressive subduction the increasing temperature and pressure eventually drive diagenetic and low-T metamorphic reactions. Several low-T reactions (>50 °C) such as clay dehydration reactions are thought to be of special importance because the released fluids facilitate excess pore pressure and reduce the shear strength of faults and the effective stress of the surrounding wall rock. Clay minerals contain numerous trace elements (e.g. boron, lithium, nitrogen, rubidium, cesium, and barium) which may provide the source for the exotic composition of fluids along convergent margins at shallow depth. Freshened fluid and other specific geochemical signals are therefore considered as evidence for long-distance fluid flow. However, the relation between geochemical fingerprints and clay dehydration is not well constraint. Here we present results from laboratory experiments under controlled pressure and temperature conditions up 100°C and 100MPa to shed light on characteristic pore water signatures of clay dehydration in subduction sediments from the Nankai and Costa Rica subduction zones. Fluids expelled during the experiments were analyzed for major and minor element content. The fluids are characterized by fluid-freshening that can be correlated to the increasing effective stress in the experiment. Clay dehydration begins at ~1.3 MPa effective stress and the smectite interlayer water content decreases continuously from 27 wt-% to 20 wt-% with increasing stress. The low chlorinity of the sampled pore water suggests that up to 17% of the fluid derives from clay dehydration. In addition, clay dehydration is characterized by the release of volatile elements such as boron, lithium or silicium. The release of these elements shows a first order relation to the increasing temperature, which suggests that they are not necessarily linked to clay dehydration. Further research is therefore needed to constrain the application of volatile elements as fingerprints for deep fluids.

IODP

Petrological and experimental study of Basalts from Tamu Massif, Shatsky Rise Oceanic Plateau (IODP Expedition 324)

A. HUSEN[1], R. ALMEEV[1], F. HOLTZ[1], J. KOEPKE[1], K. MENGEL[2], T. SANO[3]

[1] Institute of Mineralogy, Leibniz University of Hannover, Germany (* a.husen@mineralogie.uni-hannover.de)
[2] Institute of Disposal Research, TU Clausthal, Adolph-Roemer-Straße 2a, 38678 Clausthal, Germany
[3] National Museum of Nature and Science, 3-23-1 Hyakunin-cho, Shinjyku-ku Tokyo 169-0073, Japan

Shatsky Rise – Expedition 324

Large igneous provinces (LIPs) are large emplacements of magmatic rocks, caused by ernormous magma production in the mantle. They represent products of fundamental processes of mantle convection and dynamics. Thus the knowledge of their formation mechanisms contribute to the understanding of the whole earth system. The high magma production is mostly explained by the arrival of a mantle plume in the lithosphere. An other model compeeting to the previous, proposes decompression melting of an unusually fuisable mantle beneath fast spreading ridges.

The Shatsky Rise oceanic plateau is a unique representative of those LIPs, because its tectonic history is well known. The detailed reconstruction of the tectonic evolution is based on the magnetic reversals preserved in the oceanic floor, which is not possible for other plateaus, because they formed during a time without reversals of the earth magnetic field. Shatsky Rise formed along the path of the Pacific-Farallon-Izanagi triple junction. Sager et al. (1999) and Nakanishi et al. (1999) proposed the arrival of a mantle plume interacting with the spreading center. Contradictory to this, Mahoney et al. (2005) described MORB –like signatures in isotipic and trace elment geochemical data for basalts of the Tamu Massif. To enable further investigations on the age, physical volcanology, geochemistry, and tectonic evolution of the plateau, the Integrated Oceanic Drilling Program Expedition 324 was conducted and drilled five cores of the igneous rocks of Shatsky Rise (Sager et al., 2010, 2011).

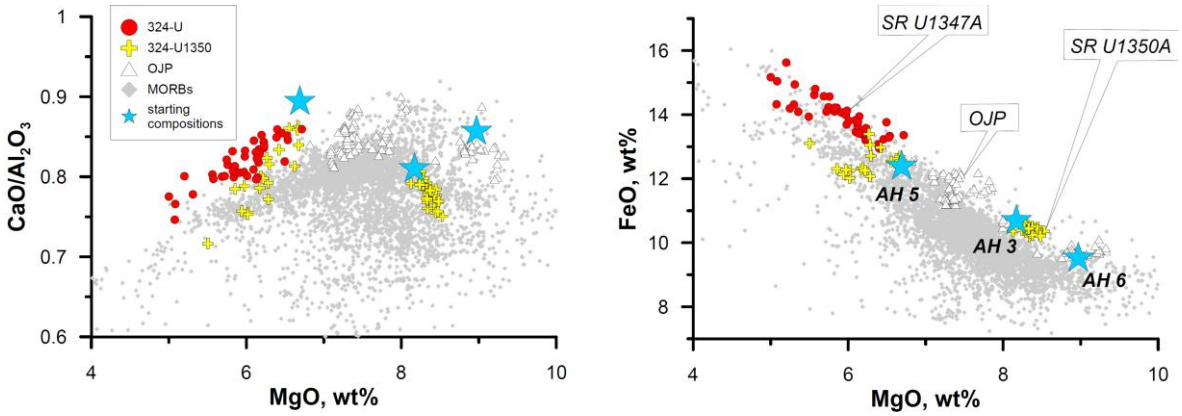

Figure 1: Glas compositions recovered on Shatsky Rise (U1347A – red dots and U1350A – yellow crosses) are shown in comparison to Ontong Java Plateau basalts (white triangles) and the whole range of natural MORBs (grey points). Additionally the blue stars mark the starting compositions used for the experimental simulation of magma differentiation.

Shatsky Rise consists of three distinct massifs (Tamu, Ori and Shirshov Massif), which are mostly constructed by massive flows and pillow lava basalts, with intercalated sedimentary layers. These three massifs formed during different stages of Shatsky Rise evolution accompanied by the northeastwards propagation of the triple junction. The most voluminous and the oldest massif is the Tamu Massif. Age and eruption volume are decreasing in the other massifs to the Northeast. Nakanishi et al. (1999) assumes an initial volcanism at the southwestern flank of the Tamu Massif. The younger (between M16 and M15) Ori Massif is located to the north of the Tamu Massif at the western side near the triple junction. The youngest (M16 - M15) and smallest Shishov Massif is located in the northeast of the Ori Massif. The northernmost Papanian Ridge further propagates to the Northeast, building an elongated extension of the Shatsky Rise and correspond to a waning of magmatic activity.

Recent post-cruise geochemical investigations of Shatsky Rise fresh glass samples (Sano et al., 2012) from four sites (U1346, U1347, U1348, U1350) revealed an existence of *tholeiitic basalts* broadly clustered into three geochemical magma groups - normal, low-Ti and high-K. The chemical compositions of the normal group are similar to those of N-MORB with slight depletion in HREE. The low-Ti group has slightly lower Ti, Fe, and Mn contents at a given MgO. The high-K basalts are characterized by distinctively high contents in K, Nb, and REEs, indicating that they are likely affected by enriched source mantle components (Sano et al., 2012).

Petrography and thermobarometry of Tamu Massif (U1347A)

The samples from Shatsky Rise oceanic plateau rocks range compositionally from picritic basalts (15.6 wt% MgO) to more differentiated tholeiitic basalts (4.9-8 wt% MgO) located within the compositional field of East Pacific Rise MORBs (Expedition 324 Scientists, 2010). The glass compositions from Site U1347 and U1350 are shown in Fig. 1, where they are compared to the range of natural MORBs and basaltic compositions of the Ontong Java Plateau. The rocks recovered in these drill cores are the least affected by alteration. The basalts from Site U1347 are more evolved (5.3-6.7 wt% MgO), whereas basalts from Site U1350 exhibit two compostional groups (first is similar to those from U1347 and found in basalts of the upper part of the column, the second in the lower part of the core is more primitive having 8.1-8.5 wt% MgO). The higher-MgO rocks from U1350 have elevated FeO and low Na_2O contents with decreasing MgO. The CaO/Al_2O_3 ratio increases in all basalts, indicating the melt evolution along Ol+Pl cotectic. The glass compositions from the more evolved rocks from both sites display depletion of FeO (Fig. 1), CaO and Al_2O_3 concentrations with decreasing MgO. This results in a CaO/Al_2O_3 (Fig. 1) decrease, indicating the fractionation along Ol+Pl+Cpx cotectics.

In the course of our study we focused mainly on samples from the Site U1347 at TAMU Massif (77 thin sections, containing 41 quenched glasses). Here we present the results obtained after petrographical characterization of the cored samples and the chemical analyses of the glass rinds (for major elements and H_2O-CO_2). The chemical data was used to estimate pre-eruptive conditions of the basaltic magmas and to compare geochemical characteristics (obtained by other groups). Additionally an experimental study contributed to the characterization of the basalts regarding phase stabilities and their isobaric differentiation.

Methods

The major element compositions of the mineral phases and glasses were measured with the electron probe micro analyzer (EPMA) at the Institute of Mineralogy in Hannover (Cameca SX100). For mineral analyses a beam current of 15nA was used for a focused beam. The peak counting time was 10s for all elements (Si, Ti, Al, Fe, Mn, Mg, Ca, Na, K, Ni). Glasses were measured also with 10nA, using defocused beam size (5-10 µm). The counting times were 10 seconds for all major elements (Si, Ti, Al, Fe, Mn, Mg, Ca, Na, K). Cl and S were measured with 40nA for 60s.

Glass H_2O and CO_2 determinations were performed by Fourier Transformation IR (FTIR) spectroscopy (Bruker IFS88 FTIR, University of Hannover). For these measurements doubly polished glass fragments with a size of approximately 1mm³ from the natural chilled margins were used. For each core sample chips of 145-150 and 40-50 µm thickness were used. The thicknesses were measured with a digital micrometer (Mitutoyo, precision:

≤2µm). The spectrometer was coupled together with an IR-Scope II optical microscope. Before measuring, the quality of the measured glass volume was controlled whether scratches, crystals or pores are present. (Operation conditions: MCT narrow range detector, globar light source and KBr beamsplitter)

The H_2O concentration was measured at the peak which is attributed to the OH stretch vibration (3550 cm^{-1}) with a typical molar absorptivity of 67 l/mol-cm for basaltic glasses (Stolper, 1982). On each sample three spectra with a spot size of 100 x 100 µm were taken, every spectrum was the average of 50 scans. The density was assumed to be a typical value for basalic glasses, 2815 g/l. The calculation of the H_2O concentrations was calculated depending on the peak height, which was determined referring a straight tangential base line.

Petrography

The samples cored at Site U1347 delivered mostly differentiated tholeiitic basalts from both massive flow and pillow units. In general, the rocks form Site U1347 are less altered, though sometimes the glasses show altered relicts. Some samples have veins with higher degree of alteration with calcite, zeolites or chlorite as alteration minerals. The textures and mineral assemblages are very similar in all lava flows. They are bordered by glassy rims, followed by a zone of transition, where crystallites form spherulitic bodies around phenocrysts. The inner parts are holocrystalline with increasing crystal sizes to the core. The basalts show phenocrysts of Pl and Cpx within a matrix of intergranular textrure. Some samples show calcite pseudomorphs after Ol. There are three different groups of mineral associations: (1) coarse grained Pl phenocrysts/ glomerocrysts (up to 0.5 mm, discontinuously normal or multiple zoned) with many inclusions, (2) fine grained Pl and Cpx subphenocrysts which show evidence of undercooling (embayments, inclusions, skeletal growth) and form sometimes clots of radiate intergrowth (skeletal, columnar, discontinuously normal and/or sector zoned), (3) crypto- to microcrystalline groundmass, containing Mt, Pl, Cpx (dendritic and skeletal).

In the quenched glasses volatiles (H_2O, CO_2) were determined by FTIR spectroscopy. H_2O concentrations vary between 0.18 and 0.6 wt%. CO_2 concentrations are below the detection limit of the FTIR method (<50 ppm) indicating the degassing depths corresponding to pressures (<50MPa) (Shishkina et al. 2010). As shown in Fig. 1, the basaltic glasses from Site U1347 are evolved tholeiitic basalts (5.2-6.8 wt% MgO), corresponding in composition to typical East Pacific Rise (EPR) MORBs. Compared to the compositions of basalts found on the Ontong Java **Plateau (OJP), the basalts show similarities, especially in** the lower MgO compositions. However, they have very distinct high FeO and low SiO_2 and Al_2O_3 concentrations. Their CaO/Al_2O_3 ratios are amongst the highest known for MORBs, which may be related to their very low pressures of partial crystallization.

Geothermobarometry

We used the COMGAMAT model (Ariskin, 1999) to simulate differentiation processes in the Shatsky Rise basaltic glasses in order to prove the assumption of low pressure fractionation. Therfore we applied the model in two different approaches. In the first, we calculated the glass evolution during fractionatioal crystallization applying different pressures and initial H_2O contents. For those calculations we used one of the most primitive compositions found on Ori Massif (U1350A 24R2 31-33). By comparison of those calculated Liquid Lines of Descent (LLDs) with the range of natural Shatsky Rise glass compositions we tried to find the conditions, which reproduce best the natural differentiation trend. In the second approach we assumed that the Shatsky Rise basalts diffentiated along Ol+Pl+Cpx cotectics. Using the COMGMAT model we calculated P-T conditions at which each individual glass composition is in equilibrium with the three mineral phases at given (measured) H_2O contents.

The calculations of LLDs for fractional crystallization led to the best reproduction of the natural glass compositions at 200 MPa and 0.2 wt% H_2O. It should be noted that this pressure is an approxymate value, which is strongly controlled by the H_2O content. The results of the calculation of multiple saturation of the melts with Ol+Pl+Cpx are displayed in figure 2. They range between 1 atm and 200 MPa and 1100 and 1160 °C.

Based on the observation of characeristic variiations along the profile rearding major elment composition, H_2O concentrations and the results of the P-T conditions of multiple saturation, we defined five different groups. Those groups are bordered by discontinuities in the lithology, which appear as sedimentary layers or a change in eruption style. Although the calculated temperatures and pressures vary in a relatively small range compared to the error of the COMAGMAT model (±15°C, ±100MPa, discussed below), a clear trend for thermodynamic conditions is produced for the individual groups. Within these groups, we identified at least three individual magmatic events, which are characterized by differentiaiton and upwards movement of the magma reservoir (Group I,III,V – see figure 2). Basaltic glasses are rare in group I, II and IV which caused very few data representing those groups.

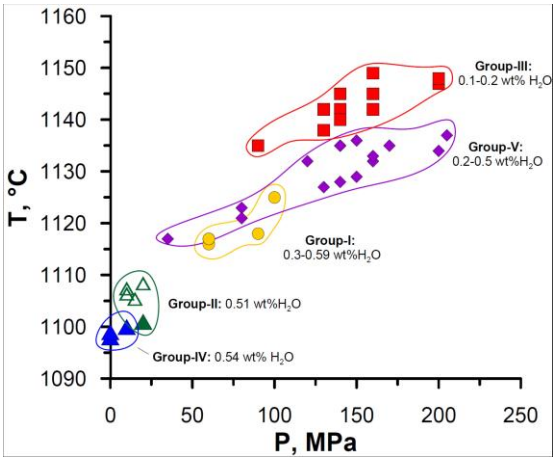

Figure 2: Calculated pressures and temperatures for Tamu Massif glasses (U1347A) using the COMAGMAT model. Compositional groups along the Profile (distigushed by different symbols) have different pressures and temperautres of magma storage. Additionally water concentration of the melts are given for each group, indicating a progressive compositional differentiation from higher to lower pressures. Group I, III and V show a trend which shows a positive corellation of pressure and temperature. Filled symbols show calculations based on compositions determined in this study, open symbols represent calculations based on data from Sano et al. (2012).

However, group 2 and 4 led to extremely low pre-eruptive pressures, which is accompanied a higher degree of differentiation (lowest MgO and highest H_2O).

Experimental study of phase equilibia and melt evolution in Shatsky Rise magmas

In order to investigate the phase equilibria in the Shatsky Rise basaltic compositions we conducted a set of experiments with three different starting materials (light-blue stars in Fig 1). The experimental products were used to construct *P-T* phase diagrams. The experimental glass compositions were compared to the natural Shatsky Rise galss compositions to prove the data obtained by thermobarometry. In addition, experimental data were used to evaluate the accuracy of the method applied during thermobarometric calculations.

Preconditions and Experimental Method

The three starting materials are synthetic analogues to natural compositions found in the Shatsky Rise basalts of Tamu and Ori Massif representing different stages of evolution. Their compositions are displayed in figure 1. The most primitive starting material (AH6, 8.97 wt% MgO) is based on a melt inclusion found in fresh olivines from Site U1349 (Ori Massif), which has compositional similarities to the primitive basalts found on the OJP. The intermediate (AH3, 8.17 wt% MgO) composition is an anlaogue to a glass composition from Site U1350 (Ori Massif) and the most evolved (AH5, 6.69 wt% MgO) represents one of the lowest MgO compositions found on Tamu Massif (Site U1347). All three compositions were run simultaneously in internally heated pressure vessels (IHPV) at the Institute of Mineralogy, Leibniz University of Hannover. The experimental pressures were 100, 200, 400 and 700 MPa and the temperatures ranged between 1225 and 1125°C. To obtain conditions close to the natural system, the H_2O concentrations were controlled at very low values (~0.1 wt%) by using C-Pt double capsules representing the minimum values of the natural basalts.

Observations and Implications

The natural phase assemblage was reproduced for all investigated starting materials. However, in the most evolved starting material, olivine crystallization was found only at the lowest pressures (100, 200 MPa). A severe effect of pressure on clinopyroxene stability was observed in all starting materials, beeing also accompanied by the lowering of the olivine liquidus at high pressures. This correlation of pressure and clinopyroxene liquidus temperature has also a significant influence on the isobaric differentiation which is showm in figure 3. Thus the natural glass compositions could not be reproduced in experiments at 700 MPa and 100 MPa for the intermediate starting material. Staring from the most primitive composition, at 100 MPa, the experimental galsses show significant discrepancies to the natural basaltic galsses. At 200 MPa, the experimental LLD is close to the more evolved group of basalts recovered at U1347 and U1350, whereas those compositions, which are less evolved and found only in the core of Site U1350 (Ori Massif) were intersected by the experimental LLDs produced at 400 and 700 MPa. Regarding the most evolved starting material, the experimental glasses are all in the field of the natural Shatsky Rise basalts. It should be noted, that those compositions recovered at Tamu Massif (U1347) have slightly higher $CaO/Al2O_3$ ratios, which were reproduced mainly by the low pressure (100, 200 MPa) experiments, whereas the higher pressures (400, 700 MPa) led to experimental glass compositions close to those of Ori Massif (U1350).

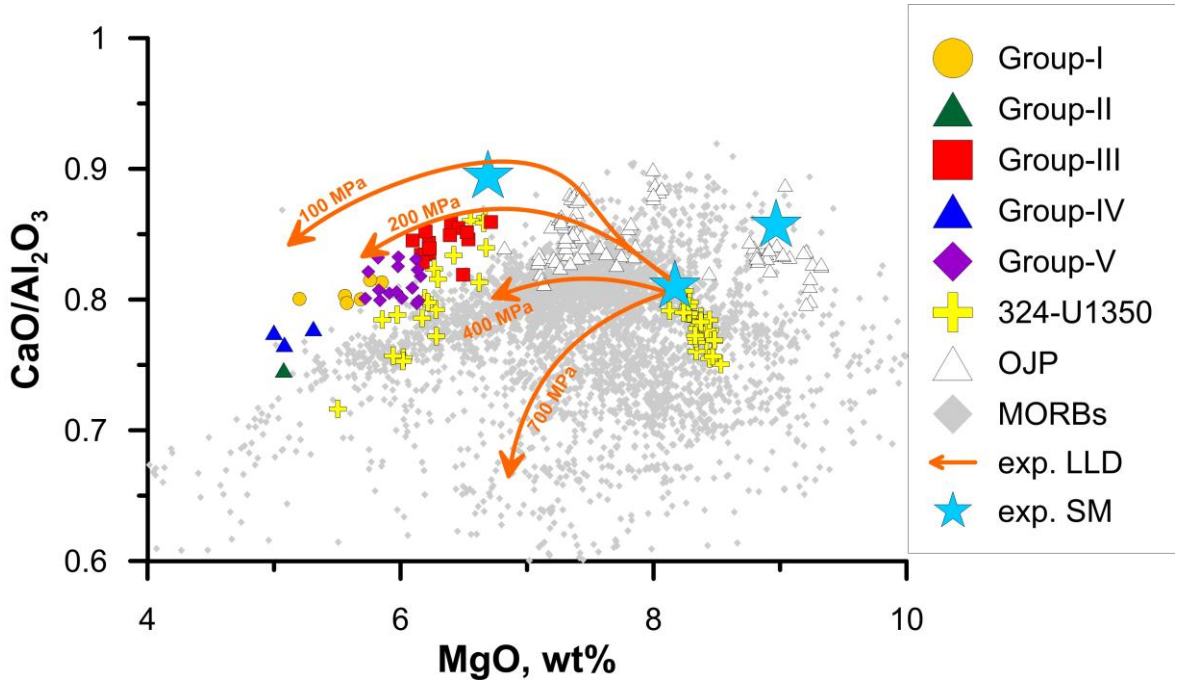

Figure 3: Experimentally produced Liquid Lines of Descent (exp. LLD - orange arrows) and the three starting materials (exp. SM – blue stars) are displayed in comparison to natural Shatsky Rise glasses. Also shown are Ontong Java Plateau basaltic compositions and the whole range of natural MORBs. Experimental glass compositions obtained at 200 MPa reproduce best the natural galsses of Shatsky Rise.

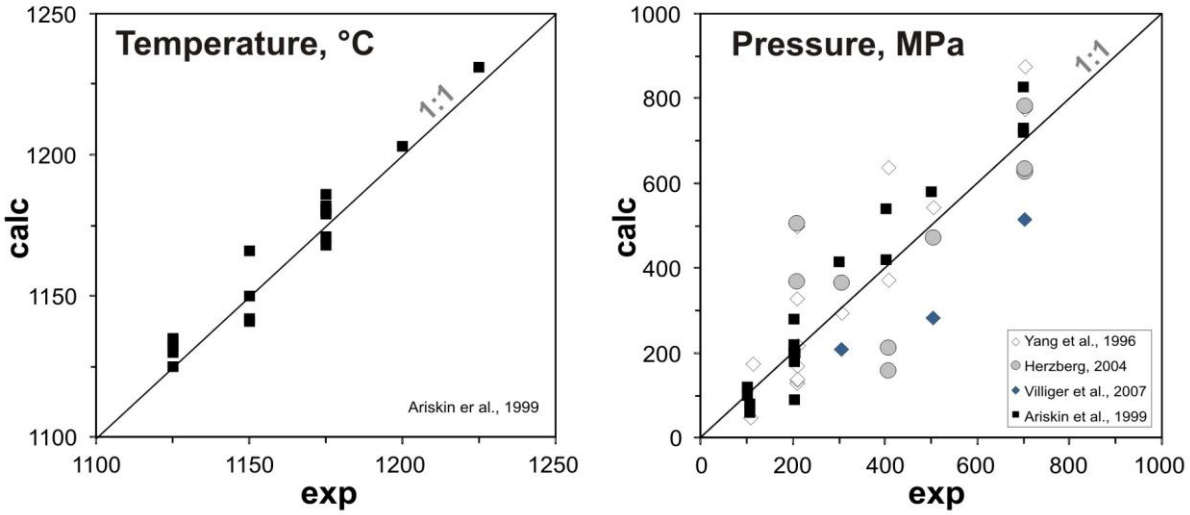

Figure 4: The calculated pressures and temperatures of Ol+Plag+Cpx saturated melts observed in experiments and calculated by different models. The precision of the method using COMAGMAT is ±15°C and ±100 MPa.

The method used to calculate the pre-eruptive P-T conditions of the natural Shatsky Rise basalts, was also applied to reproduce experimental observations. The results of the calculations of the conditions multiple saturation are compared to those observed in experiments (Figure 4). Here it can be seen, that the error of those data is around ±15°C and ±100 MPa, which leads to a better accuracy compared to other barometers, which are also displayed in figure 4.

Conclusion and Future Plans

Our data imply typical MORB-like characteristics for the TAMU Massif basalts. The glass compositions of the samples from Site U1347 and U1350 are in the field of EPR MORB and follow a trend which fits to typical MORB-type tholeiitic LLDs. However, considered collectively, tholeiitic basalts from Shatsky Rise (U1347, U1350) demonstrate compositions slightly off the trend of typical MORB (low SiO_2, high FeO and low Na_2O). The results of geothermobarometry lead to the assumption that the magmas were stored at relatively low pressures (1atm-200 MPa). The mechanisms which led to the whole range of Shatsky Rise basalts cannot be attributed to fractional crystallization only. The presence of distinct groups of basalts, which differ in their geochemical characteristics implies the formation of individual magma batches, which were stored at different levels of the magma chamber. Our experimental results confirmed the assumption of low pressure fractionation causing the differentiation trend of the basaltic glass compositions of Sites U1347 and U1350. In a more detailed view, it was observed that the formation conditions of Tamu and Ori Massiv are slightly different. Additionally the composition of melt inclusions found in the core of Site U1349, which are expected to be representatives of the source of the Shatsky Rise lavas, cannot produce the whole range of glass compositions via isobaric fractionation.

Noting that the H_2O concentrations in the previous experiments were very small (<0.2 wt%), it is planned to conduct a second set of *hydrous* experiments using the same set of starting compositions. Here the H_2O concentrations will be slightly higher (~0.5 wt%). The results of those experiments can be used 1.) to test the effect of H_2O on phase stabilities and thus melt differentiation and 2.) for the evaluation of the accuracy of thermodynamic models (MELTS, COMAGMAT, PETROLOG) in predicting conditions of multiple satuation in the presence of small amounts of H_2O.

References:

Almeev, R., F. Holtz, et al. (2008). "Depths of partial crystallization of H2O-bearing MORB: Phase equilibria simulations of basalts at the MAR near Ascension Island (7-11 degrees S)." Journal of Petrology 49(1): 25-45.

Ariskin, A.A. (1999). "Phase equilibria modeling in igneous petrology: use of COMAGMAT model for simulating fractionation of ferro-basaltic magmas and the genesis of high-alumina basalt." Journal of Volcanology and Geothermal Research, 90(1-2), 115-162.

Herzberg, C. (2004). "Partial crystallization of mid-ocean ridge basalts in the crust and mantle." Journal of Petrology, 45(12), 2389-2405.

Sano, T., Shimizu, K., Ishikawa, A., Senda, R., Chang, Q., Kimura, J.I., Widdowson, M., and Sager, W.W. (2012) Variety and origin of magmas on Shatsky Rise, northwest Pacific Ocean. Geochemistry Geophysics Geosystems, 13, 25.

Scientists, E. (2010). "Testing plume and plate models of ocean plateau formation at Shatsky Rise, northwest Pacific Ocean." IODP Prel. Rept, 324.

Stolper, E. (1982). "Water in silicate glasses: An infrared spectroscopic study." Contributions to Mineralogy and Petrology, 81(1), 1-17.

Villiger, S., Muentener, O., and Ulmer, P. (2007). „Crystallization pressures of mid-ocean ridge basalts derived from major element variations of glasses from equilibrium and fractional crystallization experiments." Journal of Geophysical Research-Solid Earth, 112(B1).

Yang, H.J., Kinzler, R.J., and Grove, T.L. (1996). "Experiments and models of anhydrous, basaltic olivine-plagioclase-augite saturated melts from 0.001 to 10 kbar." Contributions to Mineralogy and Petrology, 124(1), 1-18.

IODP

Evaluation of controlling factor of calcium isotope fractionation in *Porites* corals

M. INOUE[1,2], N. GUSSONE[1], Y. KOGA[3], A. IWASE[3], A. SUZUKI[4], K. SAKAI[3], H. KAWAHATA[2]

[1] Institute für Mineralogie, Universität Münster, Corrensst. 24, D-48149 Münster, Germany
[2] Ocean Research Institute, The University of Tokyo, 1-15-1 Minamidai, Nakano, Tokyo 164-8639, Japan
[3] Sesoko Station, Tropical Biosphere Research Center, University of the Ryukyus, 3422 Sesoko, Motobu, Okinawa 905-0227, Japan
[4] Geological Survey of Japan, National Institute of Advanced Industrial Science and Technology (AIST), 1-1-1 Higashi Tsukuba, AIST Tsukuba Central 7, Ibaraki 305-8567, Japan

Geochemical tracers such as $\delta^{18}O$ and Sr/Ca ratios in the skeleton of massive *Porites* coral have been well known as environmental proxies for sea surface temperature and/or salinity changes though time. For instance paleoclimate during the last glacial termination has been reconstructed using fossil *Porites* corals collected from Tahiti by IODP Exp. 310 (e.g., Felis et al., 2012). Although Sr/Ca-thermometer is robust for modern *Porites* corals, application for fossil corals might be vulnerable due to diagenesis and the change of Sr/Ca in seawater particularly during the LGM. Therefore, the development of new temperature proxies which could be used in combination with Sr/Ca for *Porites* coral would be important to reconstruct paleoenvironments more accurately. In addition, the conceptual understanding of proxy signal formation in relation to biomineralization processes is of special relevance. Although a weak but significant relationship between temperature and $\delta^{44}Ca$ in *Acropora* coral has also reported (Böhm et al., 2006), little has been revealed for *Porites* coral. In this study, we cultured multiple colonies of *Porites* coral under temperature, pH and light controlled environments and investigated the relationship between $\delta^{44}Ca$ in skeleton grown during the cultured period and each environmental parameters. On the other hand, to understand the mechanism of skeletal growth of *Porites* coral is crucial for the use of geochemical tracers as precise environmental proxy. Variation of fractionation pattern of $\delta^{44}Ca$ in skeleton of different colonies growing under different environments would reveal information to understand coral biomineralization.

Culture experiments on *Porites* coral have been conducted at Sesoko Station, Tropical Biosphere Research Center, University of the Ryukyus, Okinawa, Japan. Temperature and pH controlled experiments were conducted inside for 6 and 3 months, respectively and settings of water temperature and pH were, 21, 23, 25, 27, 29˚C and 7.4, 7.6, 8.0, respectively. Light experiment was conducted in an outdoor tank of Sesoko Station for 18 months and light levels were maintained with high, middle and dark adjusted by partial shading with a sun-screen mesh. For temperature, pH and light experiments 3, 2 and 1 parallel colonies were analysed, respectively. Skeletal samples grown during the culture experiment, mostly < 1 mm from the surface of each colony, were taken after the experiments using a micro-milling. For isotope measurements, 300-400 ng Ca were loaded on Re-single filaments with a tantalum activator after addition of a ^{42}Ca-^{43}Ca double spike. Calcium isotope ratios were determined on Finnigan TRITON TI TIMS follwing the method described in Gussone et al. (2011). The isotope values are expressed relative to NIST SRM 915a as $\delta^{44}Ca=((^{44}Ca/^{40}Ca)_{sample}/(^{44}Ca/^{40}Ca)_{SRM915a}$ -1) x 1000.

As a result of culture experiments, skeletal growth rate varied with the variation of each environmental parameter, typically higher growth rate at higher temperature, pH and light conditions with a colony-specific variations especially in the temperature experiment. However, $\delta^{44}Ca$ showed negligible variation related to these variations of growth rate generated by differences of pH and light level, indicating there are little or no relationships between pH and light and $\delta^{44}Ca$ in *Porites* coral. A trend of positive correlation between temperature and $\delta^{44}Ca$ was found and its temperature dependence was 0.019 ‰/˚C which is similar with previous report on different coral species (Böhm et al., 2006).

The observation that different dominant aragonitic reef coral species show similar Ca isotope fractionation behaviour, is of great relevance for understanding the seawater calcium isotope evolution during the Phanerozoic. In particular for the effect of changing calcite and aragonite seas (Farkas et al. 2007, Blättler et al., 2012) is critical to understand the fractionation behaviour of marine calcifying organisms in response to changing environmental conditions. As calcium isotope data of the dominant reef coral *Porites* spp. have been very limited, the present data of coral skeleton based on precise culture experiments contributes to the better understanding of their biomineralization and to define the average isotope composition of the the oceanic Ca sink.

References:

Blättler, C.L., Henderson, G.M., Jenkyns, H.C. (2012) Explaining the Phanerozoic Ca isotope history of seawater. Geology doi: 10. 1130/G33191.1

Böhm, F., Gussone, N., Eisenhauer, A., et al. (2006) Calcium isotope fractionation in modern Scleractinian corals. Geochim. Cosmochim. Acta 70, 4452–4462.

Farkas, J., Böhm, F., Wallmann, K., et al. (2007) Calcium isotope record of Phanerozoic oceans: Implications for chemical evolution of seawater and its causative mechanism: Geochim. Cosmochim. Acta 71, 5117–5134.

Felis, T., Merkel, U., Asami, R., et al. (2012) Pronounced interannual variability in tropical South Pacific temperatures during Heinrich Stadial 1. Nat. Commun. 3:965, doi: 10.1038/ncomms1973.

Gussone, N., Nehrke, G., Teichert, B.M.A. (2011) Calcium isotope fractionation in ikaite and vaterite. Chem. Geol. 285, 194–202.

IODP

Transient paleoceanographic events of Danian-Selandian age: first micropaleontological results for the Latest Danian Event at Shatsky Rise

S. JEHLE[1], A. BORNEMANN[1], A. DEPREZ[2], R.P. SPEIJER[2]

[1] Institut für Geophysik und Geologie, Universität Leipzig, Talstr. 35, 04103 Leipzig, Germany
[2] Department of Earth and Environmental Sciences, KU Leuven, Celestijnenlaan 200E, 3001 Leuven, Belgium

The marine ecosystem has been severely disturbed by several transient (<200 ky) paleoenvironmental events during the early Paleogene, from which the Paleocene-Eocene Thermal Maximum (PETM, ~56 Ma) is the most prominent one. During these events the injection of isotopically light carbon into the ocean/atmosphere system resulted in a >1‰ negative carbon isotope excursion (CIE), a substantial temperature rise, biotic responses, and ocean acidification. Apart from an expected global temperature rise, future ecosystem threats include a re-organization at the base of the food web, mostly affecting primary producers. Specifically, consumers low in the food chain like planktic foraminifera are prone to environmental stress by a future global warming and decreasing calcification rates of marine calcifiers as a consequence of ocean acidification. Therefore, the detailed study of such events helps to understand if and how (fast) the biota may be affected during these relatively short-lived events. Several similar events to the PETM – also named hyperthermals – of Eocene age have been studied over the last decade, but little is known about those in the Paleocene. Two of the earliest events, the "Latest Danian Event" ("LDE", ~61.75 Ma; Bornemann et al., 2009; Westerhold et al., 2011) and the "Early-Late Paleocene Event" (ELPE, 58.9 Ma; Petrizzo, 2005), have rarely been studied in deep-sea sites.

The LDE or Top Chron 27n Event is characterized by a prominent negative CIE (up to 2‰) in various sections in Egypt, which has been correlated to carbon isotope shifts in Zumaia, the Wombat Plateau in the Indian Ocean (ODP 761B) and the deep-sea Pacific ODP Site 1209 (Bornemann et al., 2009; Westerhold et al., 2008, 2011). The LDE is also characterized by the most negative carbon isotope values for the entire Paleocene representing thereby an extreme position in the secular changes of the global cycle (Westerhold et al., 2011). Due to the supra-regional nature of the LDE and the associated paleoenvironmental changes that resemble those of the PETM in Egypt (Bornemann et al., 2009; Schulte et al. 2013) it has been hypothesized that the negative CIE may represent an additional Paleocene hyperthermal. Recently, Westerhold et al. (2011) documented a distinct 2°C bottom water temperature rise during this event at ODP Site 1209 (Shatsky Rise) providing additional evidence for the hyperthermal hypothesis based on benthic foraminiferal oxygen isotope data. In the deep-sea this event is marked by two prominent peaks in Fe intensities from XRF scanning and magnetic susceptibility at various ODP sites, and it stratigraphically correlates with an increase of both oceanic spreading rates and volcanic activity at the SE Greenland margin (Westerhold et al., 2008).

By contrast no temperature anomaly has been reported for the ELPE yet. The event has been unequivocally identified in Zumaia (Spain), Shatsky Rise (ODP Leg 198), Walvis Ridge (ODP Leg 208) and the western North Atlantic (Blake Nose – ODP Leg 171B; Newfoundland – IODP Expedition 342), but detailed data are only available from Zumaia and Shatsky Rise so far. At Shatsky Rise and on Walvis Ridge the event bed is characterized by a clay-rich layer and a major increase in igorinid abundance (Zachos et al., 2004; Petrizzo, 2005), and has been interpreted as a dissolution horizon resulting from lysocline shoaling. At Zumaia no dissolution has been reported, however, major biotic changes in planktic foraminifera and calcareous nannofossils are documented.

In this project we will primarily investigate the response of the planktic ecosystem to these perturbations. We will test whether these events are represented on a global scale. Planktic foraminiferal assemblages from several (I)ODP sites covering both the North and South Atlantic (IODP Site U1407, ODP Site 1262), the Pacific (ODP Site 1209/1210) and the Indian (ODP Site 761B) oceans will be quantitatively assessed and statistically analyzed. Faunal analyses are supplemented by foraminiferal stable isotope studies (carbon and oxygen isotopes) to reconstruct the prevailing paleoceanographic conditions. Moreover, clay mineralogy is expected to indicate climate driven changes in weathering conditions on the adjacent continent and inorganic geochemistry will be used to detail changes in the redox state of the oceans accompanying the studied events. The project will be carried out in close co-operation with the KU Leuven, where the benthic ecosystem represented by benthic foraminifera is studied on the same samples to assess the impact of these events on the entire water column. A first planktic and benthic foraminiferal faunal record for the LDE at Shatsky Rise is currently under preparation and will be presented on this meeting.

References

Bernaola, G. et al., 2007. Geol. Soc. Am. Bull. 119, 785-795.
Bornemann, A.et al., 2009. J. Geol. Soc. 166, 1135-1142.
Petrizzo, M.R., 2005. Proc. Ocean Drill. Program Sci. Res. 198, doi:10.2973/odp.proc.sr.2198.2102.2005.
Schulte, P. et al., 2013. Palaeogeogr. Palaeoclimatol. Palaeoecol. 371, 9-25.
Westerhold, T. et al., 2008. Palaeogeogr. Palaeoclimatol. Palaeoecol. 257, 377-403.
Westerhold, T. et al., 2011. Paleoceanography 26, doi: 10.1029/2010PA002092.
Zachos, J.C.et al., 2004. Proc. Ocean Drill. Program Sci. Res. 208, 1-112.

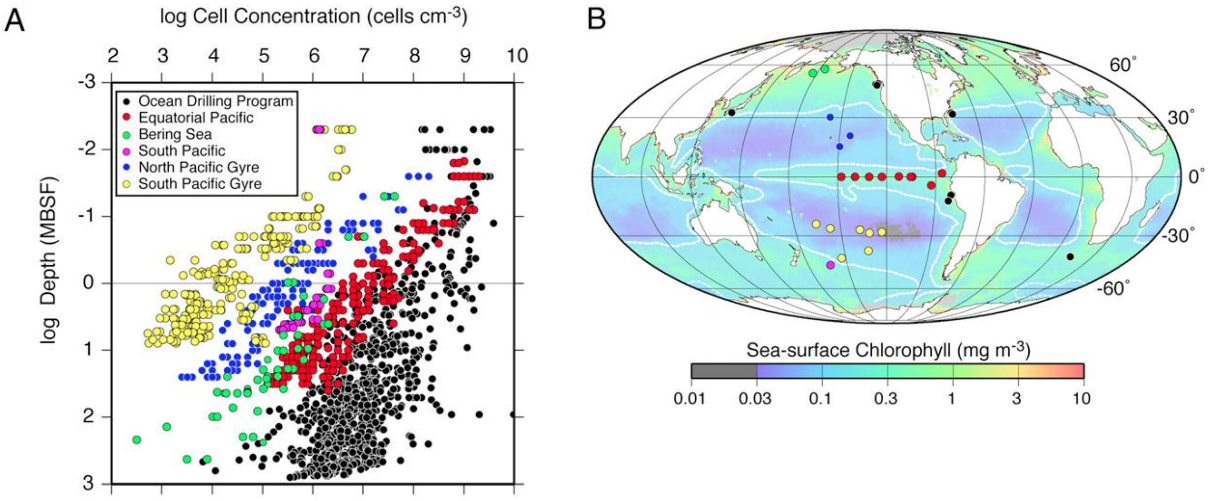

Fig. 1. Subseafloor sedimentary cell counts used for this study. (A) Counted cell concentration vs. depth (mbsf) for the sites used in this study. (B) Site locations overlain on a map of time-averaged sea surface chlorophyll-a.

IODP

Global Distribution of Microbial Abundance and Biomass in Subseafloor Sediment

JENS KALLMEYER[1], ROBERT POCKALNY[2], RISHI R. ADHIKARI[3], DAVID C. SMITH[2], STEVEN D'HONDT[2]

[1] GFZ Potsdam, Sektion 4.5, Geomikrobiologie, Telegrafenberg, 14473 Potsdam, kallm@gfz-potsdam.de
[2] Graduate School of Oceanography, University of Rhode Island, Narragansett, RI 02882, USA
[3] Universität Potsdam, Institut für Erd- und Umweltwissenschaften, Karl-Liebknecht Str. 25-27, 14476 Potsdam

Previously published cell counts were mostly from sites with high primary productivity, such as ocean margins and the eastern equatorial Pacific. Cell counts from these environments are generally similar from site to site and decrease logarithmically with sediment depth, although there can be sharp peaks of high cell densities in zones of anaerobic methane-oxidation. Recent cell counts from much more oligotrophic areas like the South Pacific Gyre and the North Pacific Gyre are several orders of magnitude lower and show a more rapid decrease with depth than all previously published datasets. With these new data available, total microbial cell abundance in subseafloor sediment varies between sites by ca. five orders of magnitude.

The differences between cell counts from ocean margins and upwelling areas and cell counts from oceanic gyres raise three questions. First, how does the abundance of microbes in subseafloor sediment vary throughout the world ocean? Second, what property or properties are likely to control that variation? Third, how does this variation affect estimates of total subseafloor sedimentary biomass and Earth's total biomass?

To address these questions, we compiled our cell counts from the South Pacific Gyre, the North Pacific Gyre and the eastern equatorial Pacific Ocean with previously published counts and parameterized the cell distribution at each site and determined two parameters, (i) cell concentration at 1 mbsf and (ii) rate of decrease in cell counts with depth. Calculating the correlations between both parameter and several oceanographic parameters that vary strongly between ocean margins and mid-ocean gyres identified possible causes of geographic variation in subseafloor sedimentary cell abundance. Best correlations were found with mean sedimentation rate and distance to shore.

Based on these correlations, we estimate global subseafloor sedimentary microbial abundance to be $2.9*10^{29}$ cells (corresponding to 4.1 Pg C and ~0.6% of Earth's total living biomass). This estimate of subseafloor sedimentary microbial abundance is roughly equal to previous estimates of total microbial abundance in seawater and total microbial abundance in soil. It is much lower than previous estimates of subseafloor sedimentary microbial abundance. In consequence, we estimate Earth's total number of microbes and total living biomass to be respectively 50% to 78% and 10% to 45% lower than previous estimates.

References:

Kallmeyer, J., Pockalny, R., Adhikari, R.R., Smith, D.C., D'Hondt, S., 2012. Global distribution of microbial abundance and biomass in subseafloor sediment. Proceedings of the National Academy of Sciences of the United States of America 109, 16213-16216.

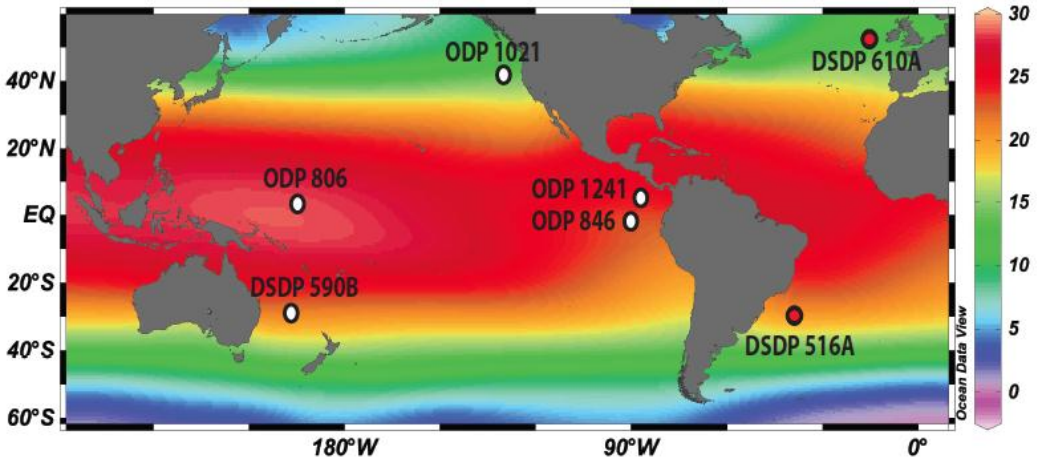

Figure 1. Hydrographic chart showing SST at 30 m water depth (WOA 2009). ODP/DSDP core sites are indicated. Paleoceanographic proxy data were generated for DSDP sites 516A and 610A (red).

IODP

Synchronous cooling of mid-latitude oceans during the early Pliocene and its implications for the Panama hypothesis

C. KARAS[1,2], J.O. HERRLE[1,2], D. NÜRNBERG[3], R. TIEDEMANN[4], A. BAHR[1]

[1] Goethe-University Frankfurt, D-60438, Frankfurt, Germany
[2] Biodiversity and Climate Research Centre (BIK-F), D-60325, Frankfurt, Germany
[3] Helmholtz Centre for Ocean Research Kiel (GEOMAR), D-24148 Kiel, Germany
[4] Alfred Wegener Institute for Polar and Marine Research, D-27568 Bremerhaven, Germany

We focus our studies on the paleoceanographic effects of the constriction of the Central American Seaway (CAS) on the North and South Atlantic Ocean during the early Pliocene. Based on paleoceanographic studies from either side of Panama it was assumed that the constriction of the CAS reached a critical threshold during ~4.8-4 Ma with distinct effects on the ocean circulation and climate. Through this tectonic closure model simulations predicted a significant increase of the Atlantic meridional overturning circulation leading to higher sea surface temperatures (SST) and sea surface salinities (SSS) of up to 7°C and 3 psu in the Northern Atlantic Ocean, while the entire Southern Hemisphere would experience cooling and freshening through "heat piracy" of the Northern Hemisphere.

To test this "Panama hypothesis" during ~4.8-4 Ma we selected DSDP core sites 516A (30°17'S; 35°17'W) from the South Atlantic and 610A (53°13'N; 18°53'W) from the North Atlantic which are sensitive to the proposed interhemispheric changes in SST and SSS (Fig. 1). We here used the combined measurement of Mg/Ca and $\delta^{18}O$ from planktic foraminifera *G. sacculifer* and *G. bulloides* to reconstruct sea surface temperatures and changes in salinities. However, our results are in contrast to the "Panama hypothesis": We find a sea surface freshening and a distinct cooling of up to ~4°C during ~4.6-4 Ma at both hemispheres in the Atlantic Ocean without any climatic effects from the constriction of the CAS (Fig. 2). In combination with other SST reconstructions these data indicate a global cooling of the mid-latitude oceans of both hemispheres. We interprete this global cooling due to solar forcing with important implications for the depth of the thermocline in the equatorial eastern Pacific. Our data point to a mechanism that cooling of surface waters of the mid-latitude oceans led to a cooling/shoaling of the equatorial eastern Pacific thermocline (Fig. 2; Harper, 2000) and presents for the first time an alternate interpretation for the cooling/shoaling of the East equatorial Pacific thermocline which started to terminate permanent El Niño-like conditions (seen by an increasing West-East Pacific SST gradient) during the early Pliocene.

References:

Harper, S., 2000. Thermocline ventilation and pathways of tropical–subtropical water mass exchange. Tellus, 52A, 330-345.

Karas, C., Nürnberg, D., Tiedemann, R., Garbe-Schönberg, D., 2011. Pliocene climate change of the Southwest Pacific and the impact of ocean gateways. Earth Planet. Sci. Lett., 301, 117-124.

LaRiviere, J. P., Ravelo, A. C., Dekens, P. S., Ford, H. L., Lyle, M., Wara, M. W., 2012. Late Miocene decoupling of oceanic warmth and atmospheric carbon dioxide forcing. Nature, 486, 97-100, doi:10.1038/nature11200.

Laskar, J., Robutel, P., Joutel, F., Gastineau, M., Correia, A.C.M, Levrard, B., 2004. A long term numerical solution for the insolation quantities of the earth. A&A, 428, 261-285, doi:10.1051/0004-6361:20041335.

Lawrence, K. T., Liu, Z., Herbert, T. D., 2006. Evolution of the eastern tropical Pacific through Plio-Pleistocene glaciation. Science 312, 79-83.

Steph, S., Tiedemann, R., Groeneveld, J., Sturm, A., Nürnberg, D., 2006. Pliocene changes in tropical east Pacific upper ocean stratification: response to tropical gateways? In Proc. ODP, Sci. Results, 202 Tiedemann, R., Mix, A.C., Richter, C., Ruddiman, W.F. (Eds.) (College Station, TX 2006) pp. 1–51.

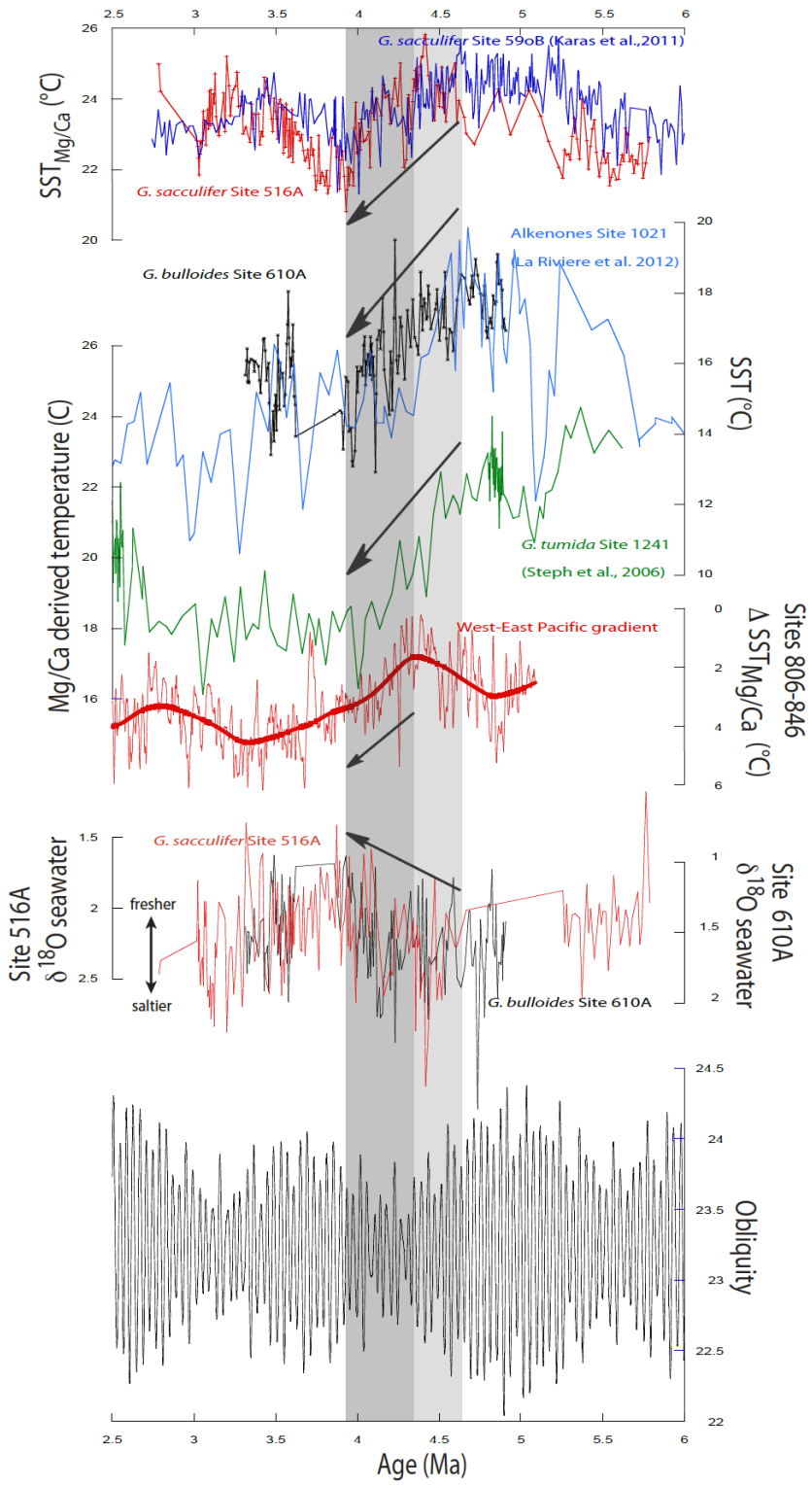

Figure 2. Pliocene paleoclimate conditions. (A) *G. sacculifer* SSTMg/Ca records from sites 516A (red; this study) and 590B (blue; Karas et al., 2011). (B) *G. bulloides* SSTMg/Ca record from Site 610A (black; this study) and alkenone derived SST from Site 1021 (light blue; LaRiviere et al., 2012). (C) *G. tumida* subsurface Mg/Ca derived temperatures from Site 1241 (green; Steph et al., 2006). (D) West-East Pacific gradient in SST (red; Site 806 $SST_{Mg/Ca}$- Site 846 alkenone derived SST; thick line is a 10% weighted smooth). Data from Wara et al. (2005) and Lawrence et al. (2006). (E) Surface water $\delta^{18}O_{seawater}$ calculations from sites 516A (red; *G. sacculifer*) and 610A (black; *G. bulloides*). (F) Obliquity of the earth calculated with the orbital solution of Laskar et al. (2004).

IODP

Micromorphological techniques and glaciogenic sediments – tool for analysis of soft-rock core samples?

M. KENZLER[1], M. MESCHEDE[1]

[1] University of Greifswald, Institute of Geography and Geology, Fr.-L.-Jahn Str. 17a, D-17487-Greifswald, edekenzler@web.de

Micromorphological techniques were first used by the pedologists Kubiëna in the 1930s. This approach produced a enormous growth in knowledge about the classification of different soil types. Since the last 25 years the micromorphology has also arrived the Quaternary Science. Especially the glacial geology is using the new important scientific achievements of this method (VAN DER MEER 1987, CARR et al. 2000, MENZIES et al. 2010).

The focus of the micromorphology rests on the microscopic dimension of, for example, sedimentological or deformation structures in different kinds of sediments. Therefore, it is necessary to produce thin sections. The preparation technique is in general similar to the technique used for hard rocks. But there are also significantly differences in detail: The collection of a sample in the field can be very difficult because of their mostly unconsolidated character. Thus, it is important to stabilize the sample with a so called Kubiëna tin. The next step is careful sample drying to prevent artefacts. Also the impregnation with resin can be delicate. A special oil is used as refrigerant for the sawing, grinding and polishing of the thin section blank. This prevents the swelling of clay minerals and the development of unwanted artefacts. After finishing the production process, the thin section is analysed with a polarising microscope.

The successful application of the mircomorphology technique takes place on sediments for example glacial-, periglacial-, lacustrine-, fluvial-, marine- and volcanic facies. Since 2009 our workgroup is also experimenting with the preparation and analysis of such thin sections under guidance of Jaap van der Meer, Simon Carr (Queen Mary University London) and Peter Kühn (University Tübingen). We are concentrating on the glacial and periglacial deposits at cliff outcrops of the Island of Rügen (SW Baltic Sea coast) with deposits of Saalian to Weichselian age. The first results are very encouraging. Consequently, we can present some examples of our research.

Due to the IODP Mission Specific Platform Expedition 347 Baltic Sea Paleoenvironment in the year 2013, it is possible to transfer our knowledge about micromorphology to the drilling cores. The proposed sites – especially Hanö Bay and Bornholm Basin – show a similar sequence like the cliff sections on Rügen (cp. ANJAR et al. 2012 and KENZLER et al. 2012). Therfore, a micromorphological comparision of the deposits of the cliff outcrops of Rügen on one side and the IODP drilling cores of the Baltic Sea Basin on the other side seem to be worthwhile. A more detailed look to the encountered tills and lacustrine clay units can help with the interpretation and reconstruction of the palaeomilieu.

The preparation of thin sections out of drilling cores of unconsolidated sediments is feasible like VAN DER MEER (1990) and CARR et al. (2000) demonstrated. This method can be a supporting tool to evaluate difficult sedimentary depositional setting.

References:

ANJAR, J.; ADRIELSSON, L.; BENNIKE, O.; BJÖRCK, S.; FILIPSSON, H. L.; GROENEVELD, J.; KNUDSEN, L. K.; KROG LARSEN, N. & MÖLLER, P. (2012): Palaeoenvironments in the southern Baltic Sea Basin during Marine Isotope Stage 3: a multi-proxy reconstruction

CARR, S. J.; HALFIDASON, H. & SEJRUP, H. P. (2000): Micromorphologcial evidence suppoerting Late Weichselian glaciation of the Northern North Sea. – Boreas **29**, 315-328, Oslo.

KENZLER, M.; MENG, S. & HÜNEKE, H. (2012): The MIS 3 at the cilff of Kluckow (Jasmund / SW Baltic Sea coast). – Betzler, C. & Lindhorst S.: Internatinal Conference of the Geologische Vereinigung and SEDIMENT Sep. 23rd-28th, 2012, Hamburg, Germany, Abstract Volume, 139, Hamburg.

MENZIES, A. D.; VAN DER MEER, J. J. M.; DOMACK, E. & WELLNER, J. S. (2010): Micromorphology: as a tool in the decetion, analyses and interpretation of (glaical) sediments and man-made materials. – Proceedings of the Geologists' Association **121**, 281-292.

VAN DER MEER, J. J. M. (1987): Micromorphology of glacial sediments as a tool in distinguishing genetic varieties of till. – Geological Survey of Finnland, Special Paper **3**, 77-89.

VAN DER MEER, J. J. M. (1990): Micromorphology of some North Sea till samples, a pilot study. – Journal of Quternary Science **5**(2), 95-101.

IODP

New Project: Reconstruction of changes in Mediterranean Outflow Water of the past 4 Myr applying neodymium isotopes (IODP Exp. 339)

N. KHÉLIFI[1], M. FRANK[1]

[1]GEOMAR Helmholtz-Zentrum für Ozeanforschung Kiel, Deutschland (nkhelifi@geomar.de)

Mediterranean Outflow Water (MOW) contributes significantly to the overturning circulation and climate in the North Atlantic through its salt supply. The strength of MOW depends on changes in the hydrological regime of the Mediterranean Sea, which is predicted to be strongly affected by anthropogenic climate change. A significant increase in salt supply by MOW has, therefore, been predicted to partly compensate for an expected decrease in the North Atlantic salinity budget that may lead to a reduced meridional overturning circulation in the near future. To test these model predictions, it is the aim of this project to reconstruct changes in the flow and strength of MOW over the global warmth of the Pliocene, a potential analogue for future global climatic conditions, after the onset of major northern hemisphere glaciation 2.7 million years ago (Ma), and through the mid-Pleistocene transition (~1.2–0.5 Ma).

On the basis of core material recently recovered by IODP Expedition 339 in the Gulf of Cádiz (Shipboard Scientific Party, 2012), we propose (1) to constrain major events in MOW strength, (2) to understand better its climatic forcings, and (3) to assess its effects on North Atlantic circulation and climate from the final opening of the Strait of Gibraltar gateway and the onset of the deep flow of MOW at about 4.2 Ma to the present. This systematic approach will be addressed by applying radiogenic neodymium (Nd) isotopes in order to reconstruct past Mediterranean/Atlantic water mixing and MOW throughflow rates. The seawater Nd isotope signature (ε_{Nd}) will be extracted from ferromanganese (Fe-Mn) coatings on foraminifera and bulk sediments applying established leaching techniques. Grain-size distributions

will be also used to explore past changes in the strength and speed of MOW. This qualitative approach will be supplemented by a quantitative reconstruction of past changes in MOW activity based on a compilation of more other geochemical proxies.

First ε_{Nd} results of bottom water from Fe-Mn coatings on bulk sediments at IODP Site U1387 (558 m water depth) in the Gulf of Cádiz show that (upper) MOW experienced a long-term gradual decrease of ~1-ε_{Nd} unit from a value of –8.5 near 4.0 Ma after the final opening of the Strait of Gibraltar to –9.5 at ~3.3 Ma providing strong evidence for a key change in Mediterranean climate. Apparently, the ε_{Nd} shift was linked to a gradual increase in atmospheric inputs from the Sahara (today ε_{Nd} –13; Henry et al., 1994) as a result of major aridification in the Mediterranean region. For this period, pollen records from the Gulf of Lions also document a distinct shift to more steppic vegetation (Fauquette et al., 1998) and salinity/density records show enhanced Mediterranean deep-water convection and increased MOW flow (Khélifi et al., 2009). Low ε_{Nd} values of MOW prior to 3.5 Ma reflect most likely less Saharan dust input and humid Mediterranean climates, further corroborating the major freshening recorded in the western Mediterranean by extremely low sea surface and bottom water salinities during that time (Khélifi et al., 2009). In total a ε_{Nd} record of ~300 data points will be generated for the past 4.2 Ma at three IODP sites in the Gulf of Cádiz along the flowpath of upper and lower cores of MOW in order to achieve the main objectives of this project.

References:

Fauquette, S., J. Guiot, and J.-P. Suc, 1998: A method for climatic reconstruction of the Mediterranean Pliocene using pollen data, Palaeogeography, Palaeoclimatology, Palaeoecology, 144, 183–201.

Henry, F., C. Jeandel, B. Dupré, and J.-F. Minster, 1994: Particulate and dissolved Nd in the Western Mediterranean Sea: Sources, fate and budget, Mar. Chem., 45, 283–305.

Khélifi N., M. Sarnthein, N. Andersen, T. Blanz, M. Frank, D. Garbe-Schönberg, B. A. Haley, R. Stumpf, and M. Weinelt, 2009: A major and long-term Pliocene intensification of the Mediterranean Outflow, 3.5–3.3 Ma ago, Geology, 37, 811–814.

Shipboard Scientific Party, 2012, Environmental significance of the Mediterranean Outflow Water and its global implications, Integrated Ocean Drilling Program Expedition 339 Preliminary Report, 97 pp.

IODP

Climate Evolution and Deep Sea Changes During the initial Cainozoic glaciation at 34 Ma

G. KNORR[1], G. LOHMANN[1], M. WERNER[1]

[1] Alfred-Wegener-Institut Helmholtz-Zentrum für Polar- und Meeresforschung, Bussestr. 24, 27570 Bremerhaven

The long-term evolution from hothouse to icehouse conditions during the Cainozoic (last ~65 Ma) is characterized by step-like glaciations of the high latitudes that represent the initial roots for our present climate with bi-polar glaciation and large equator-to-pole temperature differences. Although evidence for the onset of Antarctic glaciation at the Eocene/Oligocene transition (E/O) at ~34 Ma is commonly accepted, a large degree of uncertainty in the understanding of the associated environmental changes remains. A fundamental reason is related to the interpretation of an oxygen isotope shift in the benthic isotope record that reflects both, temperature changes and changes in the isotopic signature of sea water, which is influenced by continental ice volume changes and changes in hydrology.

During the last decade several model studies have investigated the E/O. Nevertheless it remains a major challenge to provide a coherent explanation for the recorded changes and hence, potential thresholds with respect to atmospheric CO_2, ice volume changes and potential glaciation outside Antarctica have been discussed controversially. So far, an investigation of the climate dynamics of the E/O, with a fully coupled model including the atmosphere/ocean/ice-sheet system has not been performed. Therefore, a deeper understanding of the impact and interaction between the various sub-systems requires a comprehensive modelling approach. In this project we will apply a state-of-the art atmosphere/ocean/ice-sheet model, including a stable oxygen isotope module. The explicit modelling of isotopes in different climate components will be used to explain the climate signature in proxy data. This approach aims to close a fundamental gap to understand the evolution of glacial conditions during the E/O in time and space. We aim to differentiate between classic hypotheses for Antarctic glaciations that involve tectonic/gateway alterations and associated changes in ocean circulation or declining atmospheric CO_2 in combination with changes in the earth orbital configuration. The mechanistic and process based investigations of E/O climate dynamics are complemented by an examination of changes in the spatial signature of stable water isotopes in the coupled atmosphere/ocean/ice-sheet system to disentangle individual contributions to the isotopic changes in the benthic record.

These investigations not only aim to gain a deeper understanding of the E/O, but also provide the basis for new insights in how far current climate models are capable to reproduce climate states and climate changes as recorded in the geological record. The integration of an isotope module in the coupled system will provide a frame for a critical data-model comparison, which has been identified as a key requirement for the relevance of paleoclimate modelling in the context of future assessment reports of the Intergovernmental Panel on Climate Change.

IODP

Early Pleistocene glacial-interglacial changes of North Atlantic intermediate-water masses

M. C. KOCH[1], O. FRIEDRICH[1], P. WILSON[2], M. COOPER[2]

[1] Institut für Geowissenschaften, Goethe-Universität Frankfurt, Altenhöferallee 1, 60438 Frankfurt, Germany

[2] Southampton Oceanography Centre, School of Ocean and Earth Science, European Way, Southampton SO14 3ZH, UK

Cooling on a global scale resulted in a major expansion of Arctic ice sheets from ~ 3 Ma onwards leading to the so-called intensification of Northern Hemisphere glaciation (iNHG) and a permanent bipolar glaciation.

To explain the intensification of the NHG, three main hypothesis have been put forward: First, an intensified North Atlantic Current (NAC) has been proposed [*Haug and Tiedemann*, 1998]. An increased northward heat and moisture transport and thus increased NAC as a consequence of the closure of the central American seaway and thus an increasing production of NADW after 3 Ma

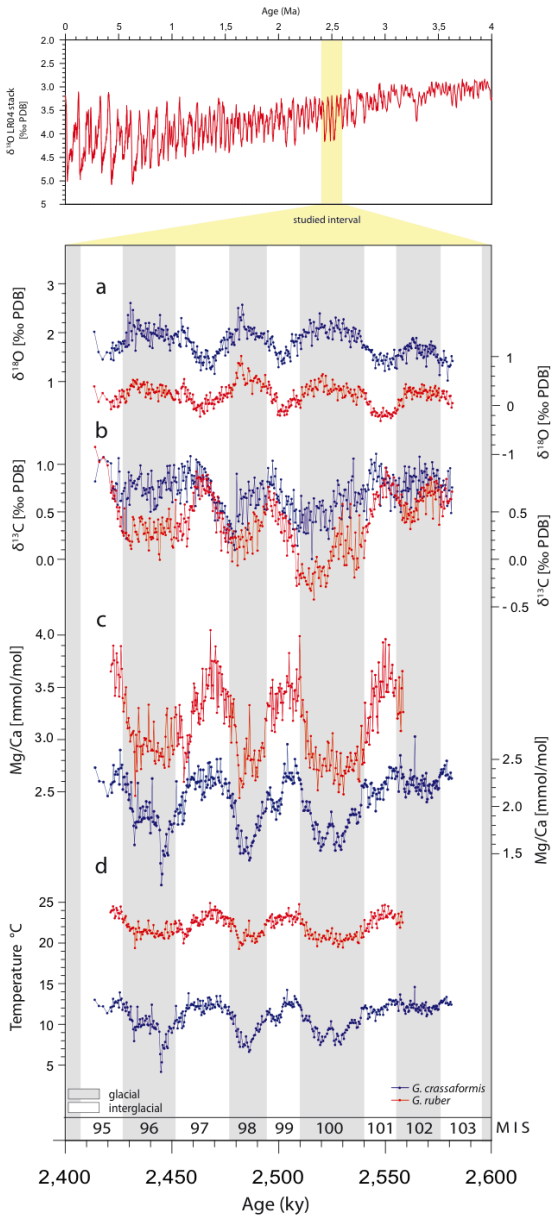

Figure 1: Top panel: Global benthic $\delta^{18}O$ stack (LR04) [*Lisiecki and Raymo*, 2005]. Bottom panel: Proxy records of *G. crassaformis* (blue, this study) and *G. ruber* [red, *Friedrich et al.*, subm.] tuned to the LR04 stack from Site U1313 for the time interval MIS 103 to 95 (2.6 to 2.4 Ma) following *Bolton et al.* [2010]. (a) $\delta^{18}O$ [‰ PDB] of *G. crassaformis* (this study) and *G. ruber* [*Friedrich et al.*, subm.]. (b) $\delta^{13}C$ [‰ PDB] of *G. crassaformis* (this study) and *G. ruber* [*Friedrich et al.*, subm.]. (c) Mg/Ca in mmol/mol for *G. crassaformis* (this study) and *G. ruber* [*Friedrich et al.*, subm.]. (d) Mg/Ca-derived temperatures for *G. crassaformis* (this study) and *G. ruber* [*Friedrich et al.*, subm.]. Glacials are highlighted in grey, interglacials in white. MIS = marine isotope stage.

has been proposed [*Haug and Tiedemann*, 1998]. Other studies and model experiments, however, indicate a decreased northward heat transport due to a south- and westward movement of the NAC, thus facilitating the built-up of ice sheets in the northern hemisphere [*Lunt et al.*, 2008]. As a second hypotheses, an observed increase in the amplitude of Earth's orbital obliquity at around 3.1 Ma has also been proposed to explain the intensification of the NHG [*Haug and Tiedemann*, 1998]. The third hypothesis suggests a significant decrease in atmospheric pCO_2 as driving mechanism for the iNHG [*Lunt et al.*, 2008] and it has been shown that atmospheric CO_2 decreased both at the start and during the iNHG [*Bartoli et al.*, 2011].

To understand the climatic evolution of the latest Pliocene–early Pleistocene and the underlying mechanisms responsible for the intensification of the NHG, it is crucial to precisely reconstruct North Atlantic hydrology.

Here we present stable oxygen and carbon isotope and Mg/Ca records measured on the deep–dwelling planktic foraminifera *Globorotalia crassaformis*, which is from Integrated Ocean Drilling Program (IODP) Site U1313 (North Atlantic, 41°N) covering marine oxygen isotope stages MIS 103 to 95 (early Pleistocene, 2.6 to 2.4 Ma). These new data are compared to existing data from the surface–dwelling planktic foraminifera *Globigerinoides ruber* analysed on the same samples.

For the interpretation of the *G. crassaformis* records of Site U1313, different intermediate water masses have to be considered. Today, MOW constitutes a warm, highly saline and nutrient depleted influence on intermediate waters in this part of the North Atlantic [*Loubere*, 1987]. Within the northeast Atlantic Ocean, MOW is generally thought to warm a water mass by up to 3–4 °C [Loubere, 1987]. It is highly saline, nutrient depleted and shows high $\delta^{13}C$ values [*Schönfeld and Zahn*, 2000]. During the LGM, MOW is relocated towards greater depth by more than 700 m [*Schönfeld and Zahn*, 2000; *Rogerson et al.*, 2005]. This deeper position of the MOW is most probably below the depth habitat of *G. crassaformis* and therefore a strong influence of MOW on our glacial *G. crassaformis* records can be neglected, resulting in smaller surface to intermediate water gradients. During glacial times, in contrast, the cold and less saline GNAIW is proposed to influence intermediate waters around and above 1000 m water depth in the northeast Atlantic [*Oppo and Lehman*, 1993; *Miller et al.*, 2012]. Our data show strong decrease in glacial salinity, temperature and $\delta^{13}C$ at around 600–1000 m, which cannot be found in surface waters (Figs. 1, 2). This can be attributed to the removed influence of MOW during glacial times. Additionally, GNAIW should influence the deeper water mass properties not only towards stronger cooling, but it should also be characterized by lower salinities and higher $\delta^{13}C$ values than compared to surface waters. $\delta^{18}O_{ivc\text{-}seawater}$ and temperature of *G. crassaformis* show a sharp decrease during early Pleistocene glacials MIS 100, 98 and 96, which is less pronounced in the *G. ruber* record (Fig. 1b).

Additionally, we calculated the $\delta^{18}O$, $\delta^{13}C$, temperature and salinity gradients between *G. ruber* (surface water) and *G. crassaformis*, representing intermediate waters at around 500–1000 m water depth [*Anand et al.*, 2003]. This enables us to reconstruct glacial–interglacial stratification changes, as a weaker stratification and a stronger mixing of the upper 1000 m would result in smaller temperature and salinity gradients. On the other hand, a stronger stratification would result in a distinct gradient in temperature and salinity as a consequence of weaker mixing. The calculation of $D\delta^{18}O_{icv\text{-}seawater}$ reveals a trend towards a lower $D\delta^{18}O_{icv\text{-}seawater}$ during interglacials and a higher gradient during glacials (Fig. 2c). The same pattern holds true for the calculated gradient of the Mg/Ca-derived temperature record (Fig. 2f). Increasing temperature and salinity gradients during glacial cooling periods point

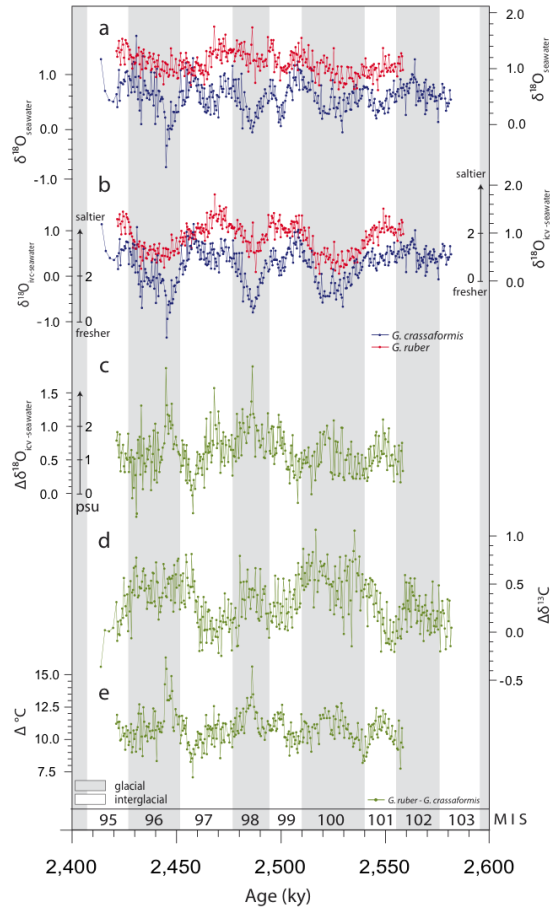

Figure 2: (a) $\delta^{18}O_{seawater}$ calculated by using $\delta^{18}O$ and Mg/Ca-derived temperatures of *G. crassaformis* and *G. ruber*, respectively [for details see *Shackleton*, 1974]. (b) Ice volume corrected (ivc) $\delta^{18}O_{seawater}$ of *G. crassaformis* and *G. ruber*, which is assumed to represent water salinity. Fresher water has lower $\delta^{18}O_{ivc\text{-}seawater}$ values, and vice versa. Relative psu changes are indicated next to the $\delta^{18}O_{ivc\text{-}seawater}$ scale. It is assumed that 1‰ change in $\delta^{18}O_{ivc\text{-}seawater}$ represents 2 psu change in salinity [after *Broecker*, 1989]. For more details see text. (c) Gradient between $\delta^{18}O_{ivc\text{-}seawater}$ of *G. ruber* and *G. crassaformis*. (d) Gradient between $\delta^{13}C$ of *G. ruber* and *G. crassaformis*. (e) Temperature gradient of *G. ruber* and *G. crassaformis* based on Mg/Ca-derived temperature estimates. Glacials are highlighted in grey, interglacials in white. MIS = marine isotope stage.

towards the establishment of a strong stratification of the upper water column in the earliest Pleistocene North Atlantic.

References:

Anand, P., H. Elderfield, and M. H. Conte (2003), Calibration of Mg/Ca thermometry in planktonic foraminifera from a sediment trap time series, *Paleoceanography*, *18*(2), 1050.

Bartoli, G., B. Hönisch, and R. E. Zeebe (2011), Atmospheric CO_2 decline during the Pliocene intensification of Northern Hemisphere glaciations, *Paleoceanography*, *26*(4), PA4213.

Bolton, C. T., P. A. Wilson, I. Bailey, O. Friedrich, C. J. Beer, J. Becker, S. Baranwal, and R. Schiebel (2010), Millennial-scale climate variability in the subpolar North Atlantic Ocean during the late Pliocene, *Paleoceanography*, *25*(4), PA4218.

Broecker, W. (1989), The salinity contrast between the Atlantic and Pacific Oceans during glacial time, *Paleoceanography*, *4*(2), 207-212.

Friedrich, O., P. A. Wilson, C. T. Bolton, C. J. Beer, and R. Schiebel (subm.), Millennial-scale sea-surface temperature variability in the late Pliocene to early Pleistocene North Atlantic

Haug, G. H., and R. Tiedemann (1998), Effect of the formation of the Isthmus of Panama on Atlantic Ocean thermohaline circulation, *Nature*, *393*, 673.

Lisiecki, L. E., and M. E. Raymo (2005), A Plio-Pleistocene stack of 57 globally distributed benthic $\delta^{18}O$ records, *Paleoceanography*, *20*, 522-533.

Loubere, P. (1987), Changes in mid-depth North Atlantic and Mediterranean circulation during the late Pliocene – Isotopic and sedimentological evidence, *Marine Geology*, *77*(1), 15-38.

Lunt, D. J., P. J. Valdes, A. Haywood, and I. C. Rutt (2008), Closure of the Panama Seaway during the Pliocene: implications for climate and Northern Hemisphere glaciation, *Climate Dynamics*, *30*(1), 1-18.

Miller, M., J. Adkins, D. Menemenlis, and M. Schodlok (2012), The role of ocean cooling in setting glacial southern source bottom water salinity, *Paleoceanography*, *27*(3), PA3207.

Oppo, D., and S. Lehman (1993), Mid-depth circulation of the subpolar North Atlantic during the last glacial maximum, *Science*, *259*(5098), 1148.

Rogerson, M., E. Rohling, P. Weaver, and J. Murray (2005), Glacial to interglacial changes in the settling depth of the Mediterranean Outflow plume, *Paleoceanography*, *20*(3), PA3007.

Schönfeld, J., and R. Zahn (2000), Late Glacial to Holocene history of the Mediterranean Outflow. Evidence from benthic foraminiferal assemblages and stable isotopes at the Portuguese margin, *Palaeogeography, Palaeoclimatology, Palaeoecology*, *159*(1), 85-111.

Shackleton, N. (1974), Attainment of isotopic equilibrium between ocean water and the benthonic foraminifera genus Uvigerina: isotopic changes in the ocean during the last glacial, *Colloq. Int. Cent. Natl. Rech. Sci.* , *219*, 203-209.

IODP

Oligocene, Miocene, and Pleistocene vegetation and climate development on the Atlantic Coastal Plain (IODP Expedition 313)

U. KOTTHOFF[1], F.M.G. MCCARTHY[2], D.R. GREENWOOD[3], S.P. HESSELBO[4]

[1] Department of Geosciences, Hamburg University, Bundesstraße 55, D-20146 Hamburg, Germany; e-mail: ulrich.kotthoff@uni-hamburg.de; phone: ++49 (0)40 42838 5009

[2] Department of Earth Sciences, Brock University, 500 Glenridge Avenue, St. Catharines, Ontario, L2S 3A1, Canada

[3] Department of Biology, Brandon University, 270 18th Street, Brandon, MB Manitoba, R7A 6A9, Canada

[4] Department of Earth Sciences, University of Oxford, South Parks Road, Oxford, OX1 3AN, United Kingdom

The major aims of IODP Expedition 313 are estimating rates, amplitudes, and mechanisms of sea-level change and the evaluation of sequence stratigraphic facies models that predict depositional environments, sediment compositions, and stratal geometries in response to sea-level change. Cores from three Sites (313-M0027, M0028, and M0029; 45 to 67 km off the coast) from the New Jersey shallow shelf (water depth approximately 35 m) were retrieved using an ECORD "mission-specific" jack-up platform. The recovery rate for the three sites exceeded 80%; in total, more than 1300 m core length were achieved. The oldest sediments were recovered from Hole M0027A, and dated as late Eocene/early Oligocene according to biostratigraphy, sequence-stratigraphy, and Sr-isotopy-based age estimates.

We have investigated the palynology of sediment cores from Sites M0027 and M0029. The cores examined span ~33 to ~11 million years before present. This time interval was analyzed in a temporal resolution of ~200 000 years. We have furthermore analyzed samples from the upper cores of Site M0027 in order to compare Miocene with Pleistocene conditions. The palynological results were complemented with pollen-based quantitative climate reconstructions using bioclimatic analysis, a mutual climate range NLR approach.

Until the middle Miocene, the hinterland vegetation of the New Jersey shelf was characterized by oak-hickory

forests in the lowlands and conifers in the highlands. The Oligocene witnessed several downward expansions of conifer forest, probably related to cooling events. The pollen-based climate data reveal a temperature increase during the Rupelian and at the Chattian-Aquitanian transition, with mean annual temperatures surpassing 15 °C. During the subsequent Miocene stages, mean annual temperatures varied around ~13.5°C. Generally, the ecosystem in the hinterland of the New Jersey shelf did not show significant changes for most of the Oligocene and the Miocene. We conjecture that the Miocene uplift of the Appalachian Mountains led to the proliferation of mountainous taxa and thus to an increase of related pollen taxa in the palynological record. This explains the comparatively low annual temperatures reconstructed for this time interval. The vegetation changed after the Miocene, with increasing conifers, and understorey and swamp taxa. A Miocene to Pleistocene expansion of grasslands is not evident for the hinterland of the New Jersey shelf.

The pollen-based annual temperature curve shows general agreement with global oxygen isotope data; however, there seems to be a shift to younger ages in the dataset from the New Jersey shallow shelf; thus for some time intervals, regional terrestrial temperature may have been decoupled from marine conditions. Transport-caused bias of the pollen assemblages was identified via the analysis of the terrestrial/marine palynomorph ratio and these were considered when interpreting palaeo-vegetation and climate from the pollen data.

IODP

NW African vegetation and climate variability: Plant-wax signals during the Pliocene-Pleistocene

R.R. KUECHLER[1], L. DUPONT[1], E. SCHEFUß[1]

[1] MARUM – Center for Marine Environmental Sciences, University of Bremen, D-28359 Bremen, Germany

Pliocene reconstructions of NW African biomes and climate variability revealed a more expanded vegetation cover under generally warmer and wetter conditions compared to today (e.g., Leroy & Dupont, 1994). Monsoonal activity was found to have been mainly controlled by orbitally induced insolation changes in the absence of large Northern Hemisphere ice sheets (deMenocal 2004; Trauth et al., 2009). Important steps in hominin evolution are generally linked to high-amplitude environmental variations, but it is still a controversy whether evolutionary changes are triggered by increased aridity (deMenocal, 2004) or humidity (Trauth et al., 2009).

For a better evaluation of paleoenvironmental changes during the Pliocene, we first focused on the last climatic (glacial) cycle (last 130 ka) as analog for 'modern' glacial/interglacial conditions under the influence of large Northern Hemisphere climate changes (Kuechler et al., in prep.). For the last 130 ka, three distinct wet intervals, i.e., the Holocene African Humid Period, a period within Marine Isotope Stage (MIS) 3 and the early MIS 5, were inferred to have experienced much wetter conditions than the present (Castañeda et al., 2009; Niedermeyer et al., 2010). It has been proposed that these humid periods reflected favorable conditions for mammalian and hominin migrations out of Africa (Osborne et al., 2008; Castañeda et al., 2009). Moreover, it has been shown that these humid events were coupled to maximum summer insolation in the northern low-latitudes causing strong monsoonal rainfall with additional influence of high-latitude climate variability (Tjallingii et al., 2008). In particular, the Atlantic meridional overturning circulation (AMOC) and the associated heat transport appear to be of main importance for controlling vegetation distributions (e.g., Castañeda et al., 2009) and triggering millennial-scale droughts in the Sahel (Mulitza et al., 2008). During the Pliocene, the mid Piacenzian warm period (MPWP, 3.3 - 3.0 Ma) is seen as the result of redirected ocean currents and the associated heat transport due to the closure of the Central American Seaway (CAS), enhancing AMOC strength (e.g., Dowsett et al., 2010).

Most findings derive, for instance, from dust, pollen and isotopic records and allow for only indirect inferences about the continental paleo-hydrologic regime. Hence, one main purpose of this study is to decipher rainfall variability over NW Africa with a molecular isotopic approach by using hydrogen (δD) and carbon ($\delta^{13}C$) isotopes of terrestrial plant waxes. Furthermore, we compare conditions before (5 - 4.6 Ma) and during (3.6 - 3.0 Ma) the CAS closure to investigate the impact of AMOC formation on NW African biomes and climate. For this, the stable carbon isotopic composition of benthic foraminifera is used as indicator for AMOC strength (Tiedemann et al., 1994), as well as sea-surface temperature (SST) estimates derived from the alkenone unsaturation index $U^{k'}_{37}$.

Compounds were obtained from marine sediments, which were retrieved from the deep-sea Cape Verde Plateau off Mauritania at ODP Site 659. This site is located right beneath the NE Atlantic dust plume fed by the Saharan Air Layer (SAL, also called the African Easterly Jet) and the North-East Trade Winds (NETW), which carry terrestrial material from the Sahara-Sahel-transition westwards onto the Atlantic Ocean (e.g., Huang et al., 2000). In total, 43 samples from the last glacial cycle and 232 samples from the Pliocene intervals were selected for organic-geochemical analyses, corresponding to a temporal resolution of about 3 ka. We additionally measured the distribution of major elements via XRF-scanning. The Al XRF-counts (Fig.), a proxy for terrigenous input (e.g., Prospero, 1996), consistently parallels the dust (%) record from ODP 659 (Tiedemann et al., 1994) and is also reflected in the XRF data of the neighboring MD03-2705 core (Jullien et al., 2007). The latter core was used for fine-tuning of the ODP 659 age model for the last 130 ka, due to its better resolution including eight AMS-^{14}C ages. The Pliocene age model of ODP 659 is based on isotope stratigraphy (Sarnthein & Tiedemann, 1989; Tiedemann et al., 1994). The alkenone-based SST record of ODP 659 shows the typical decrease during the last glacial cycle with values between 18.6 and 29 °C ($U^{k'}_{37}$ values between 0.66 and 1). Only 56% of the Pliocene alkenone samples yielded sufficient material for SST estimates and show a less pronounced variability between 22.7 and 29 °C ($U^{k'}_{37}$ values between 0.79 and 1). Sedimentary concentrations of long-chain C_{27-35} *n*-alkanes from the last glacial cycle range between 0.08 to 1.84 (average 0.46) μg g^{-1} dry weight (Fig.) and display typical plant wax signatures with carbon

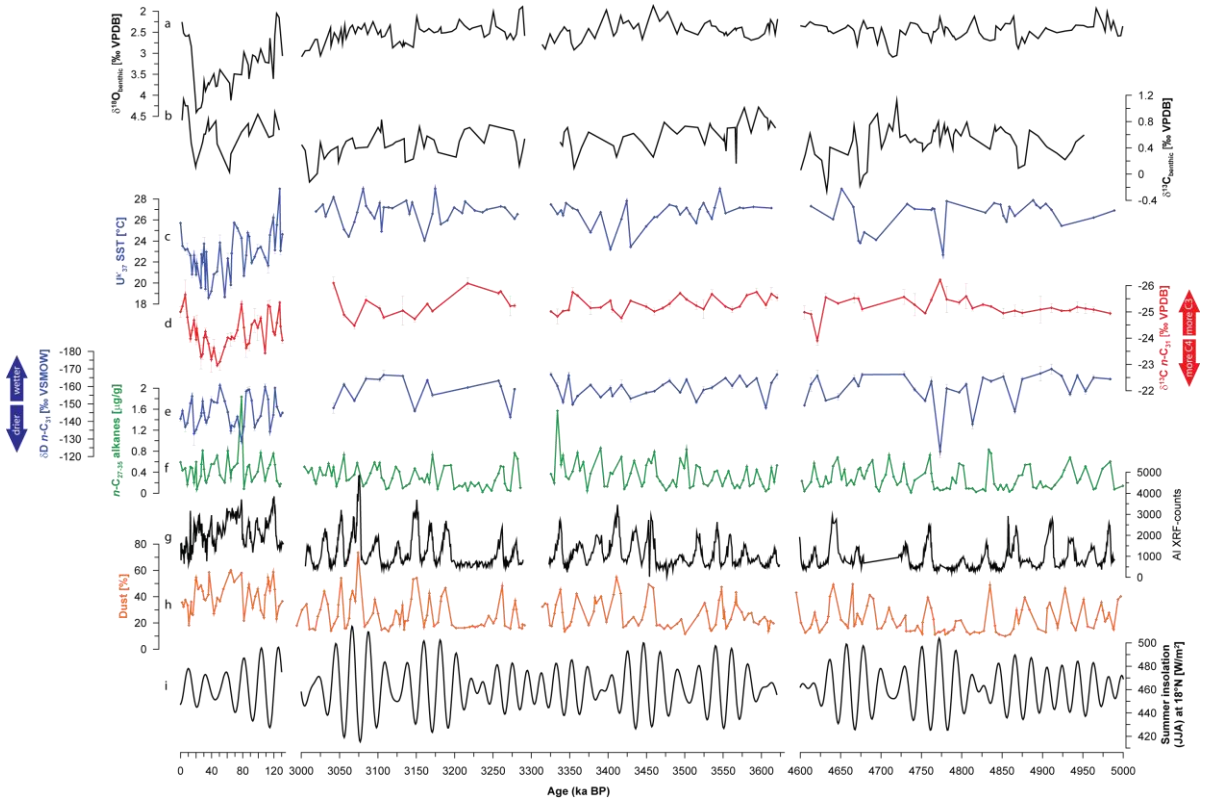

Figure: data compilation from ODP 659: (a) $\delta^{18}O$ and (b) $\delta^{13}C$ of benthic foraminifera (Tiedemann et al., 1994); (c) alkenone-derived SST estimates; (d) $\delta^{13}C$ and (e) δD of the n-C_{31} alkane; (f) concentrations of long-chain $C_{27\text{-}35}$ n-alkanes; (g) Al XRF-counts; (h) dust % (Tiedemann et al., 1994); (i) summer insolation (JJA) at 18 °N (Berger, 1978).

preference-indices (CPI) between 2.7 and 7.1 (average 4.9). Pliocene plant-wax concentrations vary between 0.01 and 1.57 (average 0.31) µg g^{-1} dry weight with CPI values between 2.27 and 8.73 (average 5.45). *n*-Alkane concentrations are mainly coupled to dust pulses, according to the model of dust generation during humid-arid climate transitions, accompanied by a strong export of plant material during aridification events (e.g., Trauth et al., 2009). The hydrogen isotopic composition (δD) of land-derived *n*-alkanes is used as proxy for past rainfall variability (Sachse et al., 2012 and references therein). Additionally, the $\delta^{13}C$ signature of the same compounds serves to reconstruct variations in vegetation composition (C_3/C_4 plants). The isotopic records obtained from the *n*-C_{29}, *n*-C_{31} and *n*-C_{33} alkanes agree well with correlation coefficients $r_{29/31}$ of 0.78 and $r_{31/33}$ of 0.73 for δD, and $r_{29/31}$ of 0.82 and $r_{31/33}$ of 0.79 for $\delta^{13}C$. For further interpretations we focused on the *n*-C_{31} alkane as the most abundant homologue in all samples. The δD_{C31} record is corrected for changes in the global δD pool due to ice volume fluctuations throughout the last glacial cycle. The correction is based on the sea level record of Waelbroeck et al. (2002) and shows the highest shift of about -8.3‰ corresponding to the Last Glacial Maximum (18-23 ka). For the last glacial cycle, δD_{C31} values range between -160.6‰ and -128.7‰ and $\delta^{13}C_{C31}$ values between -25.6‰ and -23‰ (Fig.). Pliocene plant-wax isotopes are generally more depleted, with δD_{C31} values between -170‰ and -138.5‰ (one value up to -122.8‰) and $\delta^{13}C_{C31}$ values between -26.2‰ and -23.9‰. Varying contributions from C_3 and C_4 plants were calculated with a binary mixing model using isotopic end-members for C_3 and C_4 plants derived from a data compilation by Castañeda et al. (2009) with averaged $\delta^{13}C_{C31}$ values of -35.2‰ and -21.7‰ for C_3 and C_4 plants, respectively. The $\delta^{13}C_{C31}$ record shows a predominance of drought-adapted C_4 plants with contributions between 70% and 90% during the last glacial cycle and 67% and 84% during the Pliocene. The high $\delta^{13}C_{C31}$ values are consistent with high C_4 plant contributions found in dust samples (Schefuß et al., 2003) and surface sediments (Huang et al., 2000) off the C_4 plant dominated Sahel. High δD_{C31} values are correlated to dust pulses, indicating arid conditions in NW Africa. In contrast, a shift in the δD_{C31} signature towards more negative values is seen as the result of intensified precipitation during the growing (summer) season. The ODP 659 record displays pronounced δD_{C31} variability during the last 130 ka with a range of about 32‰ between humid and arid periods, resembling signals detected off Senegal for the last 44 ka (Niedermeyer et al., 2010).

Strikingly, the glacial δD_{C31} and $\delta^{13}C_{C31}$ records are significantly anti-correlated, pointing to higher C_4 plant contributions (higher $\delta^{13}C_{C31}$) during humid periods (lower δD_{C31}). Usually, higher contributions of drought-adapted C_4 plants are expected under more arid conditions and vice versa (Ehleringer and Cerling, 2002). Considering the specific core location and the corresponding catchment areas for plant-wax supply, this can be described according to Zhao et al. (2003): We infer a combination of (1) sensitive responses of the vegetation cover to precipitation changes in the Sahel region, accompanied by (2) varying contributions from C_3-dominated biomes north of the Sahara by NETW. During arid phases, when the tropical rain belt was restricted to lower latitudes, especially the

Sahel experienced crucial water stress (higher δD_{C31}), resulting in a pronounced contraction of the vegetation cover (low *n*-alkane concentrations), which is mostly made up of C_4 plants (e.g., Still & Powell, 2010). The corresponding increase in NETW strength during dry glacial periods further promotes a more pronounced C_3-plant-wax signal (lower $\delta^{13}C_{C31}$) derived from the northern C_3 biomes. During humid interglacial periods, indicated by low δD_{C31} values, the C_4-dominated Sahelian environments spread northward into the Saharan realm (high *n*-alkane concentrations and $\delta^{13}C_{C31}$), in association with lower NETW inputs of C_3 plant waxes. In order to unravel the drivers of environmental changes detected in the ODP 659 records during the last glacial cycle, we investigated their relationship to external forcing factors, like SST, AMOC and solar insolation. Our results do not support a tight link to AMOC variations and rather point to a shift from strong orbital insolation forcing with high amplitudes in variability (MIS 4/5) to SST forcing during low-amplitude insolation changes (MIS 3 and early MIS 2) and a move back to insolation-coupled hydro-variability (MIS 1/2).

A comparison of the preliminary plant-wax isotopic records from the Pliocene (so far, 74 samples) with those of the last glacial cycle revealed remarkable differences: The variability is much more reduced in the Pliocene records, pointing to more stable conditions. Generally higher contributions of C_3 plants and overall wetter conditions are in accordance with previous pollen studies (Leroy & Dupont, 1994). In contrast, there are almost no differences between the Pliocene intervals, i.e., before and during the CAS closure. Additionally, the typical pattern of anti-correlating plant-wax isotopes during the last glacial cycle is not observed in the Pliocene data sets. This can be explained by the lack of glacial/interglacial modulations of the generally weak NETW during the Pliocene (Leroy & Dupont, 1994). Thus, relatively higher contributions of C_3 plants, reflected in lower $\delta^{13}C_{C31}$ values, have to be derived from the Sahel, in contrast to the last glacial cycle. Interestingly, the time between 3.6 and 3.3 Ma, prior to the MPWP, appears even more stable indicated by consistently low δD_{C31} values and slightly higher *n*-alkane concentrations. So far, the Pliocene results do neither support a link to AMOC variations, nor to SST changes and, according to previous studies (deMenocal, 2004; Trauth et al., 2009), rather show a coupling of paleohydrologic conditions in NW Africa to low-latitude insolation intensities.

References:

Berger, A.L., 1978. Long-term variations of daily insolation and Quaternary climatic changes. J. Atmos. Sci. 35, 2362-2367.

Castañeda, I.S., Mulitza, S., Schefuß, E., Lopes dos Santos, R.A., Sinninghe Damsté, J.S., Schouten, S., 2009. Wet phases in the Sahara/Sahel region and human migration patterns in North Africa. Proc. Natl. Acad. Sci. USA 106(48), 20159-20163.

deMenocal, P., 2004. African climate change and faunal evolution during the Pliocene-Pleistocene. Earth and Planetary Science Letters 220, 3-24.

Dowsett, H.J., Robinson, M., Haywood, A.M., Salzmann, U., Hill, D., Sohl, L., Chandler, M., Williams, M., Foley, K., Stoll, D., 2010. The PRISM3D paleoenvironmental reconstruction. Stratigraphy 7, 123-139.

Ehleringer, J.R., Cerling, T.E., 2002. C_3 and C_4 Photosynthesis. In: T. Munn (Ed.), Encyclopedia of Global Environmental Change 2, pp. 186-190, John Wiley & Sons, Ltd, Chichester.

Huang, Y., Dupont, L., Sarnthein, M., Hayes, J.M., Eglinton, G., 2000. Mapping of C_4 plant input from North West Africa into North East Atlantic sediments. Geochim. Cosmochim. Acta 64, 3505-3513.

Jullien, E., Grousset, F., Malaize, B., Duprat, J., Sanchez-Goni, M.F., Eynaud, F., Charlier, K., Schneider, R., Bory, A., Bout, V., Flores, J.A., 2007. Low-latitude "dusty events" vs. high-latitude "icy Heinrich events". Quaternary Research 68(3), 379-386.

Kuechler, R.R., Beckmann, B., Dupont, L., Schefuß, E., in prep. Plant-wax-specific hydrogen and carbon isotopes link NW African hydrology, vegetation and provenances during the last glacial cycle (130 ka).

Leroy, S., Dupont, L., 1994. Development of vegetation and continental aridity in northwestern Africa during the Late Pliocene: the pollen record of ODP Site 658. Palaeogeogr., Paleoclimatol., Paleoecol. 109, 295-316.

Mulitza, S., Prange, M., Stuut, J.B., Zabel, M., von Dobeneck, T., Itambi, A.C., Nizou, J., Schulz, M., Wefer, G., 2008. Sahel megadroughts triggered by glacial slowdowns of Atlantic meridional overturning. Paleoceanography 23(4), doi:10.1029/2008PA001637.

Niedermeyer, E.M., Schefuß, E., Sessions, A.L., Mulitza, S., Mollenhauer, G., Schulz, M., Wefer, G., 2010. Orbital- and millennial-scale changes in the hydrologic cycle and vegetation in the western African Sahel: insights from individual plant wax δD and $\delta^{13}C$. Quat. Sci. Rev. 29(23-24), 2996-3005.

Osborne, A.H., Vance, D., Rohling, E.J., Barton, N., Rogerson, M., Fello, N., 2008. A humid corridor across the Sahara for the migration of early modern humans out of Africa 120,000 years ago. Proc. Natl. Acad. Sci. USA 105, 16444-16447.

Prospero, J.M., 1996. Saharan dust transport over the North Atlantic Ocean and Mediterranean: an overview. In: S. Guerzoni, R. Chester (Eds.), The Impact of Desert Dust Across the Mediterranean, Kluwer Academic Publishers, Netherlands, pp. 133-151.

Sachse, D., Billaut, I., Bowen, G.J., Chikaraishi, Y., Dawson, T.E., Feakins, S.J., Freeman, K.H., Magill, C.R., McInerney, F.A., van der Meer, M.T.J., Polissar, P., Robins, R.J., Sachs, J.P., Schmidt, H.-L., Sessions, A.L., White, J.W.C., West, J.B., Kahmen, A., 2012. Molecular Paleohydrology: Interpreting the hydrogen-isotopic composition of lipid biomarkers from photosynthesizing organisms. Annu. Rev. Earth Planet. Sci. 40, 221-249.

Sarnthein, M., Tiedemann, R., 1989. Towards a high-resolution stable isotope stratigraphy of the last 3.4 million years: Sites 658 and 659 off Northwest Africa. In: W. Ruddiman, M. Sarnthein, et al. (Eds.), Proceedings of the Ocean Drilling Program, Scientific Results 108, pp. 167-185.

Schefuß, E., Ratmeyer, V., Stuut, J.-B.W., Jansen, J.H.F., Sinnighe Damsté, J.S., 2003. Carbon isotope analyses of *n*-alkanes in dust from the lower atmosphere over the central eastern Atlantic. Geochim. Cosmochim. Acta 67, 1757-1767.

Still, C.J., Powell, R.L., 2010. Continental-Scale Distributions of Vegetation Stable Carbon Isotope Ratios. In: J.B. West, G.J. Bowen, T.E. Dawson, K.P. Tu (Eds.), Understanding movement, pattern, and process on Earth through isotope mapping. Springer.

Tiedemann, R., Sarnthein, M., Shackleton, N.J., 1994. Astronomic timescale for the Pliocene Atlantic $\delta^{18}O$ and dust flux records of Ocean Drilling Program site 659. Paleoceanography 9(4), 619-638.

Tjallingii, R., Claussen, M., Stuut, J.-B.W., Fohlmeister, J., Jahn, A., Bickert, T., Lamy, F., Röhl, U., 2008. Coherent high- and low-latitude control of the northwest African hydrological balance. Nat. Geosci. 1(10), 670-675.

Tipple, B.J., Pagani, M., 2007. The early origins of terrestrial C_4 photosynthesis. Annu. Rev. Earth Sci. 35, 453-461.

Trauth, M.H., Larrasoaña, J.C., Mudelsee, M., 2009. Trends, rhythms and events in Plio-Pleistocene African climate. Quat. Sci. Rev. 28(5-6), 399-411.

Waelbroeck, C., Labeyrie, L., Michel, E., Duplessy, J.C., McManus, J.F., Lambeck, K., Balbon, E., Labracherie, M., 2002. Sea-level and deep water temperature changes derived from benthic foraminifera isotopic records. Quat. Sci. Rev. 21, 295-305.

Zhao, M., Dupont, L., Eglinton, G., Teece, M., 2003. *n*-Alkane and pollen reconstruction of terrestrial climate and vegetation for N.W. Africa over the last 160 kyr. Org. Geochem. 34, 131-143.

ICDP

Tiefbohrung zur Untersuchung der Wechselwirkung tiefer und flacher Fluidströme in Sedimentbecken

N. KUKOWSKI[1], K.U. TOTSCHE[1], M. ABRATIS[1], C. AUGUSTSSON[1], A. GOEPEL[1], A. HABISREUTHER[1], T. WARD[1] & INFLUINS-WORKING GROUP

[1] Friedrich Schiller Universität Jena, Institut für Geowissenschaften, Burgweg 11, 07749 Jena

Sedimentbecken sind nicht nur die Träger wirtschaftlich relevanter Rohstoffvorkommen vor allem von Kohlenwasserstoffen, sondern insbesondere die wichtigsten Reservoire für Trinkwasser. Vor diesem Hintergrund ist es das Hauptziel von INFLUINS, einem Projektverbund der ProSin-Initiative, am Beispiel des Thüringer Beckens ein vertieftes quantitatives und prozessorientiertes Verständnis der Wechselwirkungen zwischen oberflächennahen und tiefen Fluidsystemen mit einem Multimethoden-Ansatz zu erlangen. Daher sind an INFLUINS neben mehreren geologische Disziplinen (Sedimentologie, Hydrogeologie, Strukturgeologie), Geophysik (Seismik, Potentialverfahren, Aeromagnetik, Bohrloch- und Gesteinsgeophysik) und Mineralogie auch Fernerkundung, Mikrobiologie, Mikrometeorologie und numerische Modellierung beteiligt. Wesentlich ist hierbei die Rekonstruktion und Projektion der Fluidbewegung, des Wärmetransports und des gelösten wie auch kolloidalen Stofftransports auf verschiedenen raumzeitlichen Skalen sowohl in Teilgebieten als auch im gesamten Becken.

Eine zentrale Komponente von INFLUINS ist eine Tiefbohrung im Zentrum des Thüringer Beckens nahe Erfurt, mit deren Hilfe die triassischen Sedimente des Thüringer Beckens und ihre Fluide beprobt werden sollen. Nach etwas eineinhalbjähriger Vorbereitung wurde die Bohrung im Oktober 2012 genehmigt und die Vorbereitung des Bohrplatzes soll ab Februar dieses Jahres erfolgen woran sich eine etwa dreieinhalb Monate lange Bohrphase anschließen wird. Während der Bohrung sind bohrlochgeophysikalische Arbeiten, die Gewinnung von Kernstrecken sowie Pumptests geplant. Im Mittelpunkt dieses Beitrags soll daher vor allem ein tagesaktueller Bericht über den Stand der Bohrtätigkeit stehen. Informationen zur Bohrung bietet auch die INFLUINS-Webseite: www.influins.de. Sedimentbecken werden auch im Mittelpunkt der vom INFLUINS-Team organisierten internationalen Tagung “Sedimentary Basins Jena 2013” stehen, deren Webseite unter www.sedbas2013.uni-jena.de über die Themen und Termine informiert.

ICDP

Paleoclimate of the Lake Van region (Eastern Anatolia) in the period 20-15 ka BP

G. LANDMANN[1], S. KEMPE[1]

[1] Institut für Angewandte Geowissenschaften, TU-Darmstadt, Schnittspahnstr 9, 64287 Darmstadt

Lake Van is particularly suitable for paleoclimate studies. This is due to several factors: (i) the lake level is highly sensitive to climatic changes because Lake Van is lacking an outlet and therefore reacts to changes in the regional hydrologic regime; (ii) long sections of the sediment column are annually laminated and thus ideal for high resolution studies; and (iii) it is located at the junction of the Subtropical Jet Stream and the northern branch of the Subtropical High controlling the extension of dry continental air masses of northeastern Europe and Asia.

In our previous studies of Lake Van sediments we reconstructed lake level changes of the past 21 ka (Fig. 1). The curve is based on an evaluation of laminated lake bottom sediments for the past 15 ka and of laminated terrace sedimentes 55 m above the present lake level near River Engil. The terrace yielded a floating varve chronology of 606 years fixed by ^{14}C-dating of plant debris to the period 20.1-20.7 cal. ka BP (Kempe et al., 2002). This varve section has an average accumulation rate of 0.9 cm a^{-1}, which is 18 times higher than in sedimnets cored in the main basin.

There is a gap of about 5 ka between the floating chronology and the oldest sediments sampled in cores recovered in 1990. Changes in the aragonite to calcite ratio within these cores, the presence of protodolomite and magnesite in certain profile sections, the long-term record of the annual accumulation rate, the water and pollen content of the sediment, the concentration of clastics, organic carbon, and opal as well as the texture of the sediment provide the basis to reconstruct the lake level history (Fig. 1). Sediments of the lowest section of the two longest cores are not varved, contain a high content of dolomite and protodolomite, ooids, rounded pumice pieces and ostracods of the genus *Limnocythere*, all interpreted to reflect a lake level regression by at least of 428 m (Landmann et al., 1996). This interpretation is supported by the salinity of pore water which increases with sediment depth, reflecting upward diffusion of salts (Fig. 2; Reimer et al., 2009). The concentration gradients of pore water differ between cores and depend on the water depth of the core recovery. Cores from the deep basin show higher gradients because the salinity of lake water intruding into the sediment increase in the course of the regression.

At around 15 ka the lake level had dropped to at least 428 m (Landmann et al., 1996). This conclusion was questioned by other investigators. To estimate the salinity reached during this minimum lake stage, the upward transport of salt from the sediment pore space was calculated. The model considers two processes of salt transport: diffusion and compaction caused by the ongoing sedimentation. Input parameters are an initial chloride concentration, a diffusion coefficient of 5.9 10^{-10} m^2s^{-1} (Li & Gregory, 1974), a porosity profile ($\Phi=0.5+0.48e^{-0.08depth}$) and an average sedimentation rate of 0.64 mm a^{-1} (average of core K10, 420 m water depth, for the time period 0-8.8

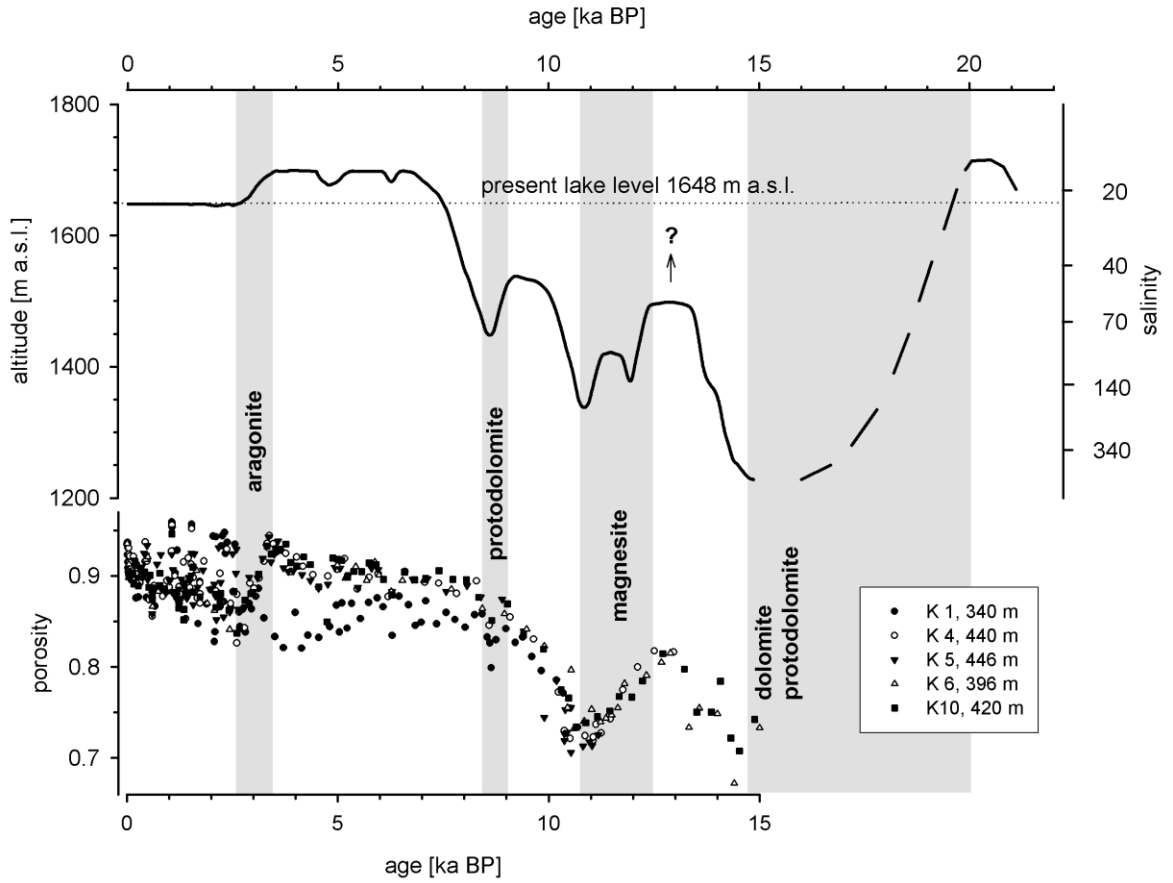

Fig. 1. Lake level fluctuations of Lake Van in the past 21 ka and sediment porosity versus age (from Reimer et al., 2009). Shaded areas mark periods with a negative water balance that is accompanied by mineral formation. Ongoing evapo-ration leads to an increase of dissolved ion concentrations within the lake water until supersaturation is reached and minerals precipitate. During these periods, the porosity is reduced suggesting that at least part of the minerals form during early diagenesis. The difference of porosity between core K1 (340 m water depth) and cores from the deeper basin, notably in the period 9-3.5 ka BP, is most likely caused by the stratification of the lake. The remarkably high variability of porosity in the sediments younger than 3.5 ka BP is connected to alternating light and dark brown bands with lower and higher content of organic matter, respectively; this may reflect a change of mixing behavior of the lake since that time. Taking into account the current total salt content of the lake (i.e., 1.3 x 10^{13} kg, Reimer, 1995), NaCl should start precipitating once the lake volume is reduced to a depth less than 80 m. However, salt will be removed by brine convection into the pore spaces of older sediments (see Fig. 2) allowing further lake level lowering without a salinity crisis. Thus, the lake level has dropped by at least 428 m within the period of about 20-15 ka BP. Note: The scale of the salinity axis is not linear.

ka including tephra layers, turbidites and slumps). A good fit between the measured Cl-concentration of the deep basin cores and the model data is obtained by running the time loop for 15 ka (corresponding to 9.6 m of sedimentation), starting with an initial Cl-concentration of 3000 mol m^{-3} in the pore water equivalent to a NaCl-salinity of 175 g l^{-1} (Fig. 3).

The model results reveal that most of the recent chloride mass in the water of Lake Van is brought from below by upward diffusion from the sediments. When the lake started refilling, it was therefore low in Cl-contration explaining the occurence of well-preserved ostracodes shells of four unknown species of the family *Limnocytheridae* within the lowermost sediment of core K10. Recent ostracodes of the family *Limnocytheridae* are found in habitats having a salinity of 0-10 ppt (Ian Boomer, University Birmingham, personal communication). The model explains also the long-lasting stratification of Lake Van in the period 10.7-3.7 ka BP because loss of salt from the lower water body at the pycnocline was replenished at the sediment water interface by upwards diffusion (Reimer et al., 2009).

Sedimentary features like the lack of lamination, large clasts, the presence of ooids, the formation of secondary minerals and the presence of iron oxide schlieren, can all be explained by assuming a playa stage prevailing during the deposition of the lowest sediment section of core K10. Occasionally appearing floods (caused by rare torrential rains or rapid snowmelt events) could be strong enough to transport the observed clasts into the main basin. During dry stages, capillary ground water can transport ions into the oxygenated horizon. This may explain the formation of dolomite, iron oxide and secondary minerals. At around 14.7 ka BP, marked by the sand layer, a more permanent water body provided suitable conditions for ooide formation. Soon after the lake became deep enough to allow the formation and preservation of varves (Landmann et al., 1996). During that stage accumulation rates of 10.8 mm a^{-1}, that is about 20 times higher than for the recent deep lake, were reached.

This scenario of a shallow lake before 15 ka is supported by geochemical and mineralogical evidence and by pollen data (Reimer et al., 2009; Litt et al., 2009). Parameters indicating terrigenous contribution (like Fe, Ti, quartz) show maxima in the lowermost core section while

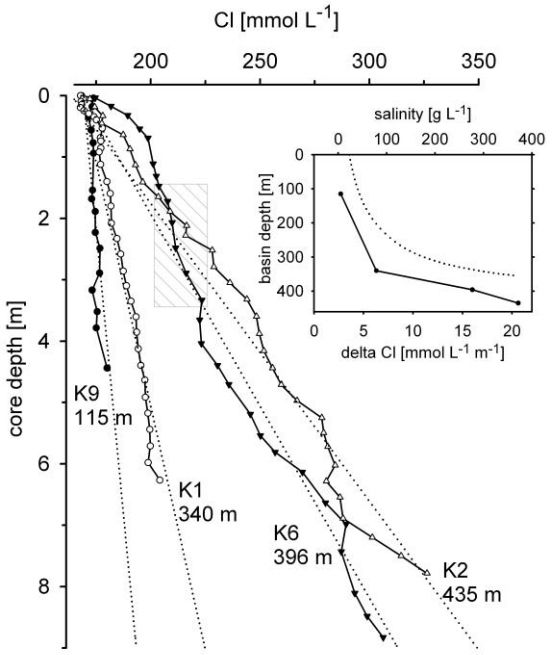

Fig. 2. Chloride concentration of pore water of cores from different water depths. The dotted lines give the linear regressions. The shaded area marks a section of core K6 that was replaced by older slump sediments. Inset: the solid line shows the Cl-gradient (lower X-axis) versus basin depth. The dotted line provides the salinity increase (upper X-axis) during a lake level decrease by keeping the total salt amount constant. Similarity in shape of the curves suggested that the salt was deposited during a strong lake level regression.

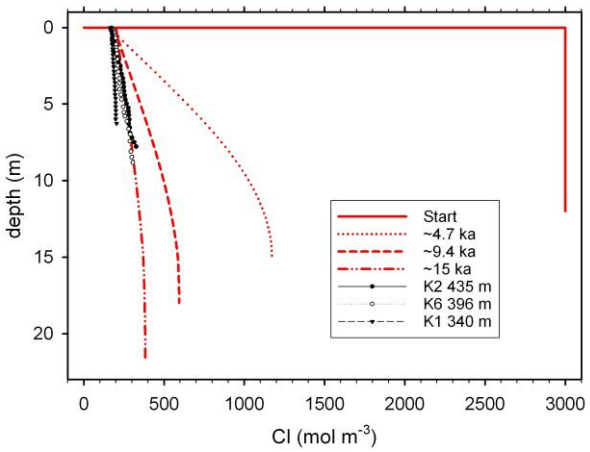

Fig. 3. Chloride concentration measured in pore water of cores from different water depths (black, see Fig. 2) and calculated for several time periods by considering upward transport of chloride caused by diffusion and compaction (red). The calculations start with an initial chloride concen-tration of 3000 mol m^{-3} at the sediment-water interface with a deposit of 12 m pore water with this concentration. Because the model simulates the ongoing sedimentation process, curves reach higher depth with increasing time loops.

those representing riverine input (aragonite, Ca and Sr) have minima. A drop of Lake Van level of about 500 m within a period less than 5 ka is a pronounced climate event that may have teleconnections because it is also recorded in the central Sahara (e.g., Maley, 2000) and in the Dead Sea record (e.g., Landmann et al., 2002). However, sharp lake level regressions allow not directly to differentiate between a reduced precipitation or an enhanced evaporation. More detailed quantification of those parameters can be obtained by water (or energy) balance modelling. We therefore suggest to study the pore water chemistry and the mineralogy of sediment deposited in the period 20-15 ka BP which will allow to improve the quality of our models. Even though the extent of Lake Van level recovery during the Allerød Interstadial is not exactly known (see Fig. 1), most likely the period of drought from 20-15 ka was stronger than that marking the Younger Dryas.

References:

Kempe, S., Landmann, G. & Müller, G., 2002: A floating varve chronology from the Last Glacial Maximum terrace of Lake Van/Turkey. – Zeitschr. Geomorphol., Supplem. 126 Research in Mountains and Deserts of Africa and Central Asia, 97-114.

Landmann, G., 1996: Van See/Türkei: Sedimentologie, Warvenchronologie und regionale Klimageschichte seit dem Spätpleistozän. - Dissertation, Facul. Geosci. Univ. Hamburg, Selbstverlag, 123 pp.

Landmann, G., Reimer, A. & Kempe, S., 1996: Climatic induced lake level changes of Lake Van/Turkey during the transition Pleistocene/ Holocene. - Global Biogeochemical Cycles 10(4), 797-808.

Landmann, G., Abu Qudaira, G. M., Shawabkeh, K., Wrede, V. & Kempe, S., 2002: Geochemistry of Lisan and Damya Formation in Jordan and implications on palaeoclimate. – Quaternary Intern. 89/1, 45-57.

Li, Y.-H. & Gregory, S., 1974: Diffusion of ions in seawater and in deep-sea sediments. Geochim. Cosmochim. Acta 38, 703-714.

Litt, T., Krastel, S., Sturm, M., Kipfer, R., Örcen, S., Heumann, G., Franz, S.O., Ülgen, U.B. & Niessen, F., 2009: 'PALEOVAN' International continental scientific drilling program (ICDP): site survey results and perspectives. - Quaternary Science Reviews 28, 1555-1567.

Maley, J., 2000: Last Glacial Maximum lacustrine and fluviatil formations in the Tibesti and other Saharan mountains, and large-scale climatic teleconections linked to the activity of the Subtropical Jet Stream. - Global and Planetary Change 26, 121-136.

Reimer, A., Landmann, G. & Kempe, S., 2009: Lake Van, Eastern Anatolia, hydrochemistry and history. - Aquatic Geochem. 15, 195-222

IODP

Cenozoic marine planktic diatom evolution controlled by climate change: implications for future extinction risk

D. LAZARUS[1], J. BARRON[2], J. RENAUDIE[1], A. TÜRKE[3], P. DIVER[4]

[1] Museum f. Naturkunde, Invalidenstrasse 43, 10115 Berlin. david.lazarus@mfn-berlin.de
[2] United States Geological Survey, Menlo Park, CA 94025 USA. jbarron@usgs.gov
[3] Department of Geosciences, Klagenfurter Strasse, D-28359 Bremen, Germany. atuerke@uni-bremen.de
[4] Divdat Consulting, 1392 Madison 6200, Wesley, Arkansas, 72773 USA. divdat@aol.com

The excellent Cenozoic deep-sea microfossil record provides a unique opportunity to study basic mechanisms of evolution, e.g. how diversity is related to causal factors such as environmental change. Changing diversity affects ecosystem functioning; while extinction permanently removes components from the system, reducing its ability to adapt (on human timescales) to future environmental change. The siliceous marine plankton are in many respects (ecology, geochemical role, preservation, evolutionary behavior) complementary to carbonate-shelled plankton and of equal importance to understanding evolution and future plankton response to climate change: diatoms in particular are key components of the carbon pump and affect it quite differently than coccolithophores, their carbonate-shelled counterpart. Despite this importance, surprisingly little is yet known about extinction risk from climate change in the living marine plankton, with most studies so far only modeling possible shifts in species ranges or changes in export productivity, implicitly assuming no extinctions that would affect model calibrations. Studies of carbonate microfossils have found significant, if complex and intermittent control of diversity by environmental factors, but only two larger syntheses of fossil marine diatom diversification have been published and they disagree (both from the Neptune database: Spencer-Cervato 1999 'SC'; Rabosky and Sorhannus 2009 'RS'), making correlation to environmental change uncertain. We have been able to resolve these discrepancies and create a first reasonably robust estimate

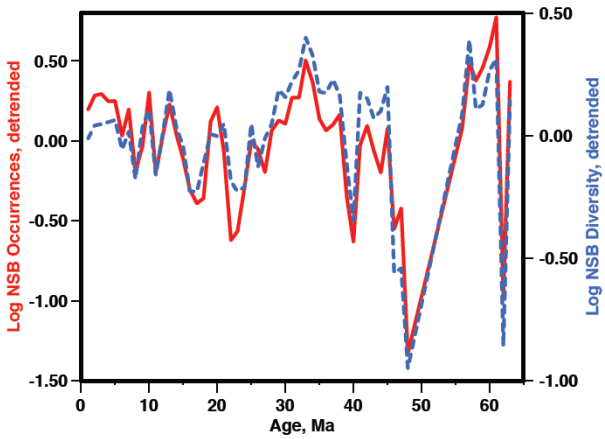

Figure 1 - Diversity of diatoms (blue dotted line) and number of occurrences (1 occurrence=1 species in 1 sample) in the NSB database (red line) over the Cenozoic. Both time series linearly detrended and normalized. Log scale to remove near geometric increase vs time in both data sets.

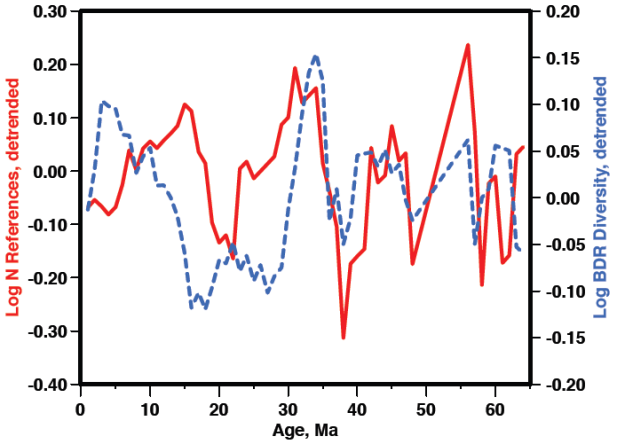

Figure 2 - Diversity of diatoms (blue dashed line) and number of publications (red line) in the Barron catalog over the Cenozoic. Both time series linearly detrended and normalized. Log scale to remove near geometric increase vs time in both data sets.

of global Cenozoic diatom diversity history. We also show that diatom diversity is strongly correlated to changing global climate over the Cenozoic, and discuss implications for diatom diversity due to future global warming.

Reconstructing diversity from the fossil record is challenging: compilations of diversity are usually strongly affected by, among other factors, the number of observations. The initial SC study, which found a strong increase in diversity over time, did not rigorously control for this. Assuming such a bias existed in the Neptune data, the RS study applied standardized subsampling methods, and found instead little diversity increase over the Cenozoic. Using a new version of this database (NSB, hosted at the MfN Berlin) we indeed find a very strong correlation between numbers of observations and diversity (figure 1). However, we did not confirm the RS result of little or no net diversity increase. Our study instead made use of both new data, and new methods applied to the NSB data, to reach a different conclusion.

Our new data consists of an as yet unpublished, fairly comprehensive listing of marine planktonic diatom microfossil species ranges, compiled from the literature over a period by one of us (Barron). This list, or catalog, also gives for each species a biogeographic assignment (most are one of Tropical, Southern Ocean, North Pacific). Diversity from such catalogs can also be biased by numbers of observations, either by different numbers of source publications used per time interval, or systematic differences in the numbers of samples examined per paper. For DSDP-ODP data the latter seems unlikely; and we do not find a correlation to numbers of papers used either, at least for the Oligocene-Recent (figure 2). We therefore expect that diversity, particularly Neogene diversity, as calculated from this list to be a sample size unbiased estimate of true diversity.

Our NSB analyses employed two new methods, neither employed earlier studies. We used SQS subsampling (Alroy 2010), which modifies sample sizes as needed to compensate for changing patterns of geographic endemism over time. This is substantial in Cenozoic diatom

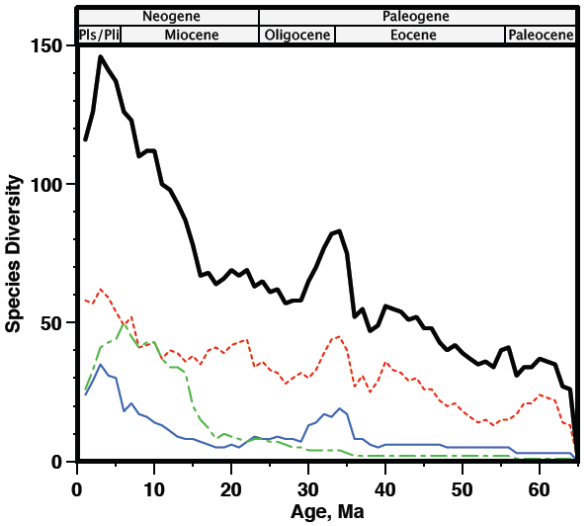

Figure 3 - Summary of diatom diversity change over the Cenozoic according to the Barron catalog. Black thick - total diversity, Red dotted - tropical, Green dashed - North Pacific, Blue - Southern Ocean. Based on best estimates for species ranges from DSDP, ODP and other literature.

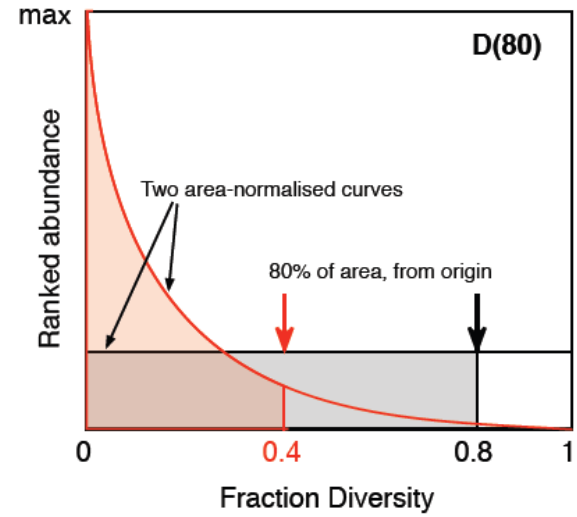

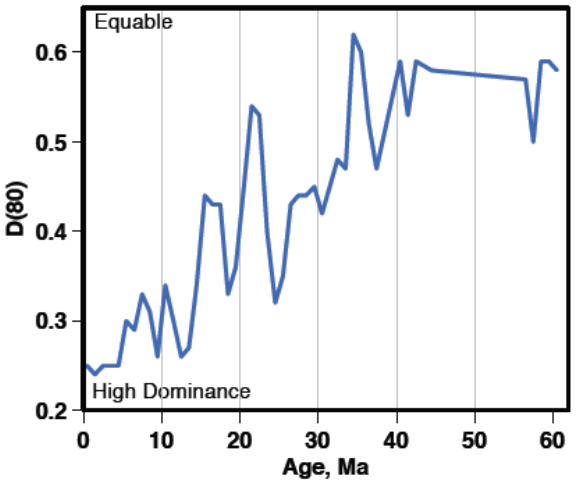

Figures 4, 5. 4 - Simple metric D(80), defined as fraction of total diversity at 80% of total data in ranked relative abundance data curve. 5 - D(80) of Cenozoic diatoms in NSB database, showing dramatic drop in equability beginning near the E/O boundary.

evolution, as can be seen from the Barron catalog data itself (figure 3).

Secondly, we calculated the equability of the NSB data in each time interval, using a simple dimensionless metric we created: 'D(80)' (figures 4, 5). Low equability or 'high dominance' populations have a very large number of individuals of only a few species, and many species with only a few individuals. Subsampling procedures are influenced by this, finding fewer species in samples of low equability than in same-diversity samples of higher equability (in low equability samples one mostly keeps sampling the same few common species, and rarely samples rare species). We calibrated the magnitude of this effect on the diatom data by subsampling two virtual populations, each with diversity of 100 (ca the average Cenozoic diversity in the Barron catalog), but with averaged Neogene or Paleogene equability. Over a wide range of subsampling sizes, lower Neogene equability (high dominance) causes a >50% underestimate of subsampled diversity (figure 6). From this we computed a correction factor as a linear function of D(80), and applied this to the NSB diversity data. We did not use the simple 'leave the most common taxon out' correction suggested by Alroy (2010) for equability as in our tests it was highly ineffective with the diatom data.

Lastly, we used the ratio of polar to tropical species in the Barron catalog to independently calculate the correction factor for geographic endemism. This served as a check on how well the SQS algorithm was performing.

The diatom diversity results for the Cenozoic are shown in figure 7. The 3 curves are: simple diversity from the Barron catalog ('BDC'), NSB diversity calculated with equability correction and SQS ('SQS'), and NSB diversity calculated with equability correction but geographic correction from the Barron catalog polar-tropical ratio ('PTR'). All three show remarkably similar features: overall increase in diversity over the Cenozoic, a brief latest Eocene-basal Oligocene peak, and rapid increase in the late mid Miocene-Recent.

This similarity, despite major differences in both data and methods, suggests that this is a robust result. We therefore calculated the mean of the 3 estimates for each time interval and compared this to the $\delta^{18}O$ curve (Zachos 2008), a commonly used proxy for global Cenozoic climate change (figure 8). There is a remarkably close correspondence between mean diatom diversity (thick blue line) and environmental change (red line) over time. The relationship between these variables can also be seen by plotting them directly against each other (figure 9). This shows the strong, but non-constant relationship.

Of particular interest is the change in system behavior in the late Neogene. While diatom diversity is almost insensitive to climate state in the Recent and Pliocene, 'warmer' climate states in the Miocene are associated with much lower diatom diversity - up to 30% vs modern diversity, using figure 7 as a calibration. The early Pliocene is a tipping point in system behavior. This is important in that the early Pliocene is the prior climate

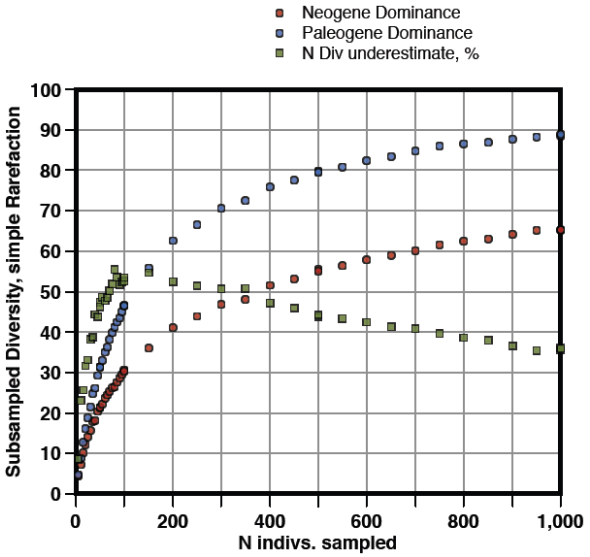

Figure 6 - effect on subsampling (simple rarefaction) of different equability distributions of occurrence frequences in two populations, each with 100 species. Equabilities set to those actually observed for Neogene and Paleogene diatoms in NSB database. Each dot represents average of 50 runs with sample size given. Diversity underestimate is Neogene vs. Paleogene.

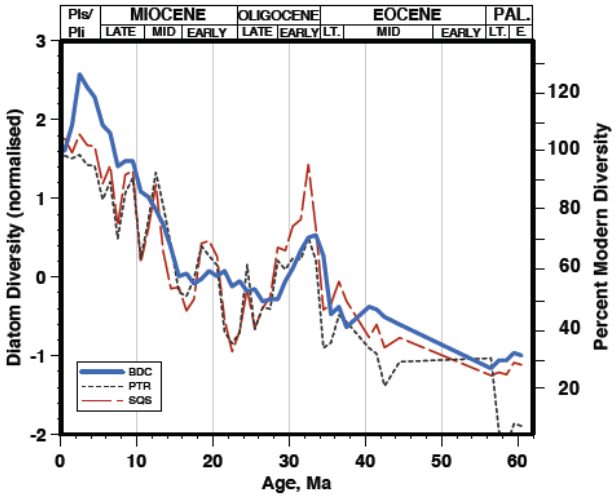

Figure 7 - Three differently calculated diversity estimates for Cenozoic diatoms. The SQS curve is based solely on NSB data; the BDC only on the Barron catalog; the PTR makes use of both. All three curves are normalised as subsampled curves (SQS and PTR) give relative diversity only.

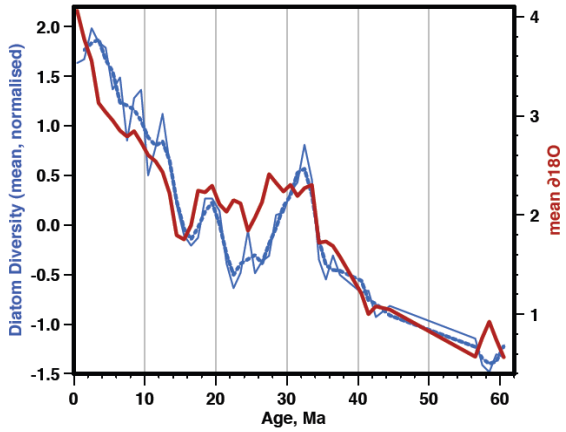

Figure 8 - Diversity of diatoms (mean of 3 estimates in figure 7, thin blue blue line, 3 point moving average, heavy dotted blue line) and global climate state ($\delta^{18}O$, Zachos et al. 2008, 1 my binned averages), both series normalized. Note inverted plotting vs convention for isotopes.

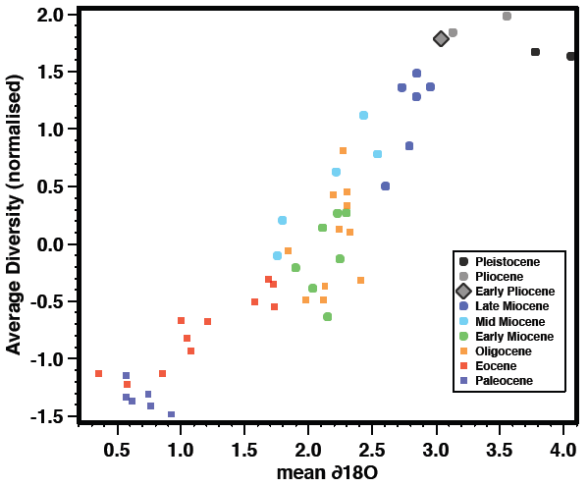

Figure 9 - Diversity of diatoms vs climate state ($\delta^{18}O$) over the Cenozoic, with different time intervals indicated by color/shape coding of points. Same data as in figure 8. Note location of early Pliocene is specially marked - see text.

state thought to be most similar to that predicted for our own future due to global warming. This has two implications: 1) if future global climates were to warm substantially beyond those levels thought to correlate to early Pliocene values, equilibrium diversity of diatoms in the oceans might be significantly lower than today, suggesting the risk of extinctions. 2) Models of ocean plankton response based on living species-ocean temperature relationships may not be valid if climate warming exceeds the early Pliocene level.

Our results are preliminary, and need better data. Past ocean environments are imperfect analogs for future ones, and thus may not be good predictors of future response. We particularly need a better understanding of the actual ocean parameters that regulated past ocean diversity, rather than generalized proxies such as global isotopic oxygen. Our results nonetheless suggest that the marine diatom plankton, and thus possibly the ocean's carbon pump, may be seriously adversely affected by future climate change, and in ways that are not easy to predict.

References:

Alroy, J. 2010. Fair sampling of taxonomic richness and unbiased estimation of origination and extinction rates. In: J. Alroy & G. Hunt, (Eds), Quantitative Methods in Paleobiology, The Paleontological Society, 55-80.

Rabosky, D. L. & Sorhannus, U. 2009. Diversity dynamics of marine planktonic diatoms across the Cenozoic. Nature, 247: 183-187.

Spencer-Cervato, C. 1999. The Cenozoic deep sea microfossil record: explorations of the DSDP/ODP sample set using the Neptune database. Palaeontologica Electronica, 2: web.

Zachos, J., Dickens, G. R. & Zeebe, R. E. 2008. An early Cenozoic perspective on greenhouse warming and carbon-cycle dynamics. Nature, 451: 279-283.

ICDP

The Siljan impact structure of central Sweden: an unique window into the geologic history of western Baltoscandia

O. LEHNERT[1,2], G. MEINHOLD[3], A. ARSLAN[4], U. BERNER[5], M. CALNER[2], W. D. HUFF[6], J. O. EBBESTAD[7], M. M. JOACHIMSKI[1], C. JUHLIN[8] & J. MALETZ[9]

[1] GeoZentrum Nordbayern, Lithosphere Dynamics, University of Erlangen-Nürnberg, Schloßgarten 5, D-91054, Erlangen, Germany; lehnert@geol.uni-erlangen.de, michael.joachimski@gzn.uni-erlangen.de

[2] Department of Geology, Lund University, Sölvegatan 12, SE-223 62 Lund, Sweden; mikael.calner@geol.lu.se

[3] Geowissenschaftliches Zentrum der Universität Göttingen, Abteilung Sedimentologie/Umweltgeologie, Goldschmidtstraße 3, D-37077 Göttingen, Germany; variscides@gmail.com

[4] Ulmenweg 2, D-37077 Göttingen, Germany; arzuarsl@gmail.com

[5] Bundesanstalt für Geowissenschaften und Rohstoffe, Stilleweg 2, D-30655 Hannover, Germany; ulrich.berner@bgr.de

[6] Department of Geology, University of Cincinnati, 500 Geology/Physics Building, Cincinnati, OH 45221-0013, USA; huffwd@ucmail.uc.edu

[7] Museum of Evolution, Uppsala University, Norbyvägen 16, SE 752 36 Uppsala, Sweden; Jan-Ove.Ebbestad@em.uu.se

[8] Department of Earth Sciences – Geophysics, Uppsala University, Villavägen 16, SE–752 36 Uppsala, Sweden; Christopher.Juhlin@geo.uu.se

[9] Institut für Geologische Wissenschaften, Freie Universität Berlin, Malteser Str. 74-100, Haus B, Raum 322, D-12249 Berlin, Germany; yorge@zedat.fu-berlin.de

Siljan is Europe's largest impact structure and preserves unique Lower Palaeozoic sedimentary successions in its ring-like depression around the central uplift. Outcrops are limited, but the Lower Palaeozoic stratigraphy investigated in three core sections provides new information revolutionizing the knowledge of the development of this area located at the western margin of Baltica. Effects of the Ordovician/Silurian foreland basin development and several facies belts can be observed in the sedimentary record of the area some 100 km away from the Caledonian front in the west (Fig. 1A). The Mora 001, Stumsnäs 1 and Solberga 1 cores (Fig. 1B) provided by the Swedish company Igrene AB comprise more than 1500 m of strata ranging from the late Tremadocian to Wenlock in age. The cores provide a complex dataset which is the basis for reconstructing shifts in palaeoclimate, sea-level, and changes in ecosystems. The volcanic record, expressed by Ordovician and Silurian K-bentonites, may be compared to occurrences of ash layers in other parts of Baltoscandia which serve as time-lines in a detailed stratigraphic framework including litho-, bio-, chemo- and sequence stratigraphic parameters. Well-defined carbon isotope excursions are additional pin-points within this framework.

The erosional unconformity and the hiatus spanning about 30 Ma between the Middle Ordovician Holen Limestone and early Silurian shales in the western Siljan Ring (i.e. Mora area) reflect the passage of the Caledonian peripheral forebulge due to tectonic loading by thrust sheets to the west (Lehnert et al. 2012b; Fig. 2).

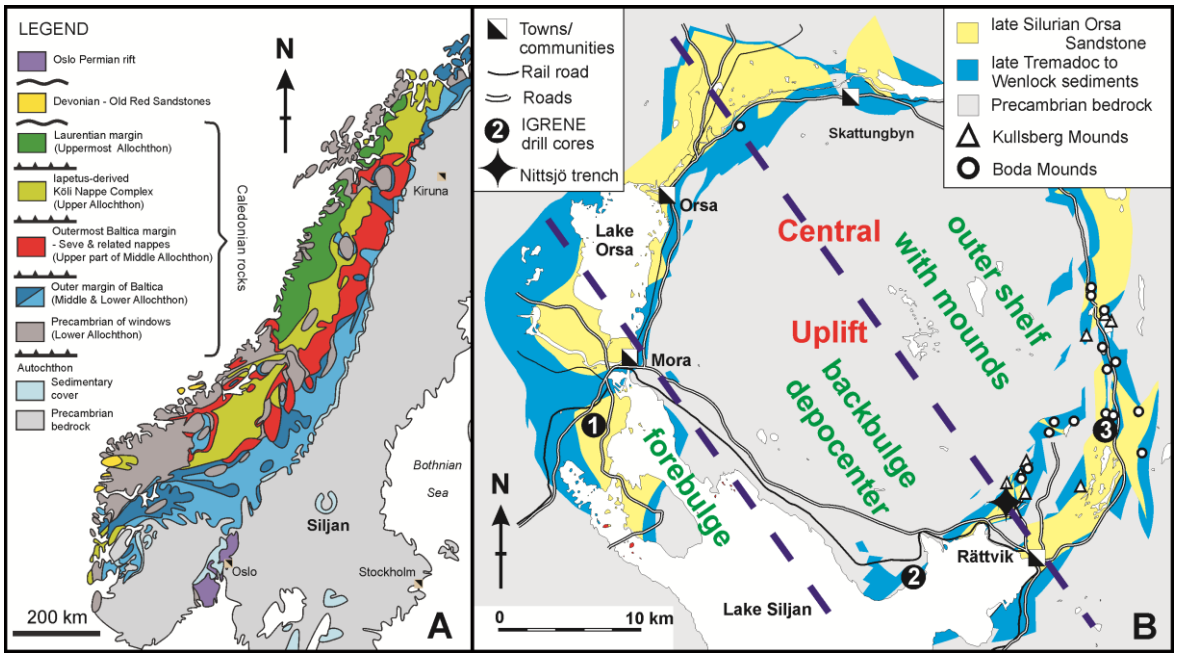

Figure 1: A- Location of the Siljan impact structure in relation to the Caledonian nappe system (modified from Gee et al. 2010); B - Simplified geological map of the Siljan district (modified from Ebbestad & Högström 2007) with locations of the Igrene AB drill sites (1 – Mora 001; 2 – Stumsnäs 1; 3 – Solberga 1) and the tentative position of late Ordovician facies belts.

In the Ordovician succession of the Stumsnäs 1 core (Fig. 1B), a previously unknown marly deeper water facies, time-equivalent to the uppermost Holen Limestone through upper Dalby Formation is observed (Fig. 2). The sediments display deposition in an area where backbulge basin and outer platform environments are interfingering (Fig. 1B). This backbulge depocenter presumably developed during late Middle Ordovician times when erosion started at the peripheral forebulge to the west (Lehnert et al. 2012b). During the time when erosion continued at the forebulge, large mud mounds developed on the outer shelf through the shelf to basin transition in the Upper Ordovician carbonate shelf succession (Kullsberg and Boda mounds). These ecosystems are characteristic for the eastern part of the impact structure (Fig. 1B). Due to westward movement of the forebulge during continuous crustal loading by the Caledonian nappes in the Silurian, the depocenter of an evolving shale basin also moved to the west where a thick siliciclastic succession was deposited in the western Siljan Ring (i.e. Mora and Orsa areas). The substantial thickness of the shale succession in the Orsa region can be deduced from two seismic lines studied in the northwestern part of the ring structure (Juhlin et al. 2012).

Within the upper part of the Silurian clastic succession in the Mora 001 core (Fig. 2) we observe the progradation of a delta system. The high influx of silt (‘tricolor member’) and proximal delta sands (‘sandstone member’) reflects a regression in an overall subsiding basin likely due to global sea-level drop during the Sheinwoodian (early Wenlock) glaciation.

The thick Silurian siliciclastic succession in the Mora 001 core as well as the shales of the early Silurian Kallholn Formation, the late Ordovician Fjäcka Shale and the early Ordovician Tøyen Formation have geochemically been investigated to support the view of a biotic origin of the oil and gas occurrences in the Siljan region (Fig. 2 – GC marked levels). This was necessary since some recent models favour an ‘abiotic deep source” in the mantle to explain the origin of the bulk of the hydrocarbons in that area. An interesting aspect of shale studies in the Siljan ring structure is that the Silurian ‘graptolitic shales’, usually interpreted as being fully marine deposits, show a deposition in lacustrine to brackish and marine environments (Berner et al., this volume). The data can explain the absence of marine fossils in large parts of the siliciclastic successions showing up only in periods of fully marine conditions. Similar geochemical data reflecting times of lacustrine to brackish conditions were obtained from one of the best source rocks of the Baltoscandian Basin, the late Ordovician Fjäcka Shale, showing intervals of reworked or land-plant derived hydrogen-lean organic matter in a basin flooded after the Katian ‘Slandrom Glaciation’. The geochemical data suggesting ‘lacustrine’ to brackish and marine palaeoenvironmental conditions are supported by biomarker studies from samples of crude oil and bitumen from the eastern Siljan Ring (i.e. Solberga area) (Ahmed et al. 2012).

The Katian ‘Slandrom Glaciation’ is reflected on Baltoscandia by a widespread palaeokarst surface (Calner et al. 2010a), and its prominent palaeokarst development is observed in cores (e.g. Solberga 1) and in outcrops (Calner et al. 2010b) in the eastern Siljan Ring. There, palaeokarst is developed in different Ordovician units in the shallower environments. Together with multiple karst horizons in the Cambrian–Silurian of other parts of Sweden widespread subaerial exposure surfaces are recognized at times of major regressions. These together with other sedimentary and biotic proxies of extremely shallow-water conditions challenge earlier ideas suggesting a tranquil, deep and stable basin (Lehnert et al. 2012a). However, the strata preserved in the Siljan impact structure provide not only the unique possibility to study sea-level changes but also shifts in palaeoclimate, and changes in

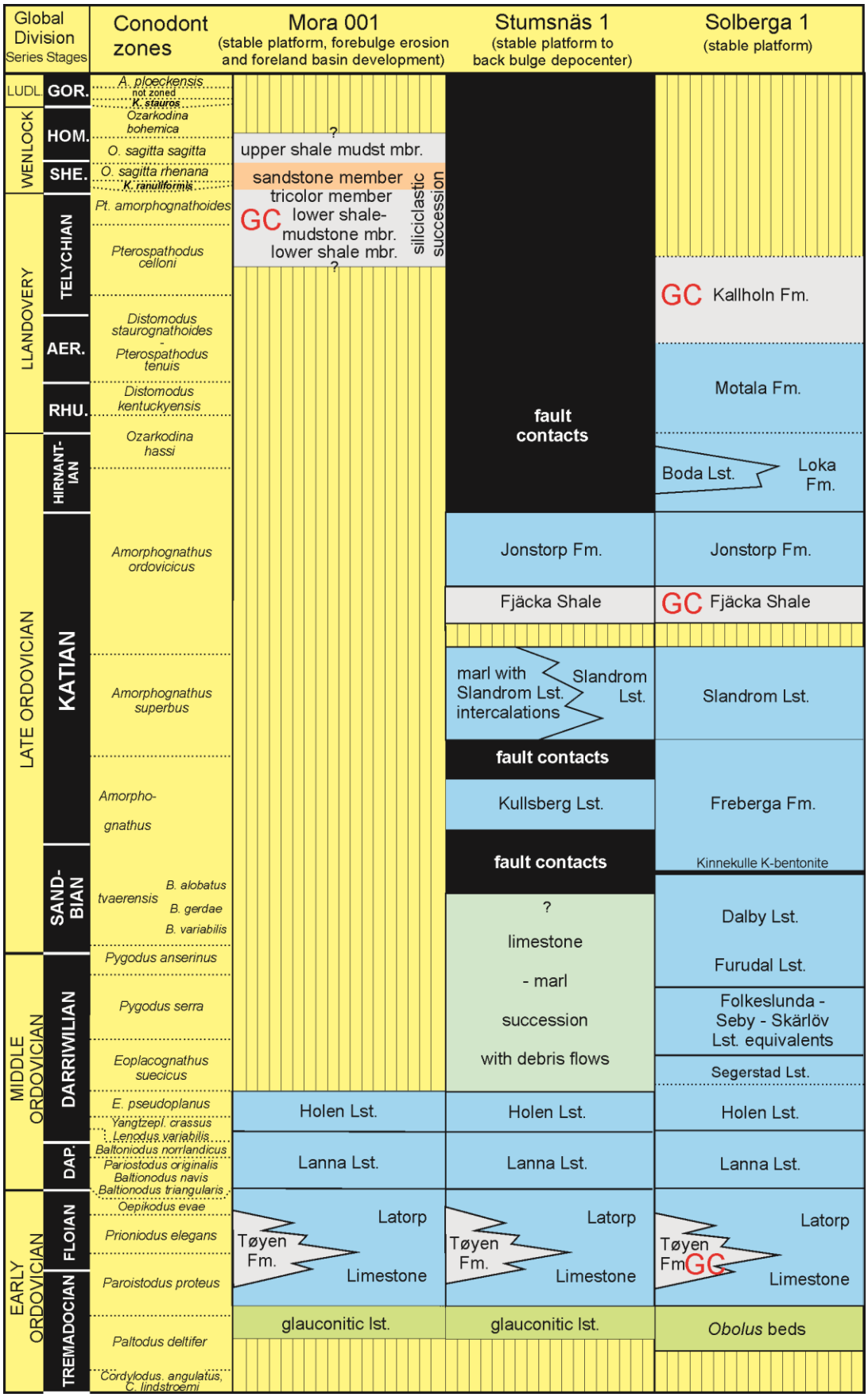

Figure 2: Preliminary lithostratigraphic correlation of the units recovered in the sedimentary successions of the Mora 001, Stumsnäs 1 and Solberga 1 core sections (Lehnert et al. submitted). The gaps shown in black are caused by faulting. The nomenclature follows Ebbestad & Högström (2007); GC marks shale units geochemically investigated for characterizing their potential for hydrocarbon generation.

palaeoenvironments and faunal communities in western Baltica where otherwise across long distances erosion cut down into the Precambrian basement rocks.

The most recently studied core is structurally highly complex and comes from the Stumsnäs 1 borehole (Arslan et al., this volume; Lehnert et al. submitted) (number 2 in Fig. 1B). Large parts of the Ordovician succession are cut out by faults. In the Stumsnäs 1 section and in other places of the southeastern ring structure, large slabs of granitic basement (up to 200 m in thickness) are lying on top of the Palaeozoic sedimentary succession. The impact-related thrusting of basement slivers over sedimentary strata caused folding and faulting of the underlying sediments and cutting out of weaker units such as the late Ordovician K-bentonites intercalated in marly limestones. An important goal of our future research is to relate the structural data from the core to the outcrop situation in the southern and southeastern part of the Siljan Ring. It is essential to determine transport directions in order to evaluate published impact models. The data collected so far are already in contradiction with these models and show the potential of a better understanding of impact dynamics by basic structural studies in the field in combination with high resolution shallow seismic research.

References:

Ahmed, M., Lehnert, O., Fuentes, D., Sestak, S., Meinhold, G. & Gong, S. (2012): Biomarker evidence for the origin of seep oil and solid bitumen from the Late Devonian Siljan impact structure, Sweden. In: Ahmed, M., Gong, S., Kotzakoulakis, K. & George, S.C. (Eds.): Biogeochemistry from Deep Time through Petroleum Resources to Modern Environments. 17th Australian Organic Geochemistry Conference, Program and Abstracts, 2–5 December 2012, Macquarie University, Sydney. CSIRO Report Number EP129608, 71-72.

Arslan, A., Meinhold, G. & Lehnert, O. (this volume): Tectonic structures in the Stumsnäs 1 core of the southern Siljan Ring, central Sweden.

Berner, U., Lehnert, O. & Meinhold, M. (this volume): Fluid migration in Ordovician and Silurian rocks of the Siljan impact structure (Sweden) – Insights from geochemistry.

Calner, M., Lehnert, O. & Nõlvak, J. (2010a): Palaeokarst evidence for widespread regression and subaerial exposure in the middle Katian (Upper Ordovician) of Baltoscandia: Significance for global climate. Palaeogeography, Palaeoclimatology, Palaeoecology 296, 235-247.

Calner, M., Lehnert, O. & Joachimski, M. (2010b): Carbonate mud mounds, conglomerates, and sea-level history in the Katian (Upper Ordovician) of central Sweden. Facies 56, 157-172.

Ebbestad, J. O. R. & Högström, A. E. S. (2007): Ordovician of the Siljan district, Sweden. In Ebbestad, J.O.R., Wickström, L.M. & Högström, A.E.S. (eds.) WOGOGOB 2007. 9th meeting of the Working Group on Ordovician Geology of Baltoscandia. Field guide and Abstracts. SGU Rapporter och meddelanden 128, 7-26.

Gee, D. G., Juhlin, C., Pascal, C. & Robinson, P. (2010): Collisional Orogeny in the Scandinavian Caledonides (COSC). GFF 132, 29-44.

Juhlin, C., Sturkell, E., Ebbestad, J. O. R., Lehnert, O., Högström, A. E. S. & Meinhold, G. (2012): A new interpretation of the sedimentary cover in the western Siljan Ring area, central Sweden, based on seismic data. Tectonophysics 860, 88-99.

Lehnert, O., Calner, M., Ahlberg, P. & Harper, D. A. (2012a): Multiple palaeokarst horizons in the Lower Palaeozoic of Baltoscandia challenging the dogma of a deep epicontinental sea. Geophysical Research Abstracts 14, EGU 2012-11362-1.

Lehnert, O., Meinhold, G., Bergström, S. M., Calner, M., Ebbestad, J. O. R., Egenhoff, S., Frisk, Å. M., Hannah, J. L., Högström, A. E. S., Huff, W., Juhlin, C., Maletz, M., Stein, H. J., Sturkell, E. & Vandenbroucke, T. R. A. (2012b): New Ordovician–Silurian drill cores from the Siljan impact structure in central Sweden – an integral part of the Swedish Deep Drilling Program. GFF 134, 87-98.

Lehnert, O., Meinhold, G., Arslan, A., Calner, M. & Ebbestad, J. O. R. (submitted): The Stumsnäs 1 core from the southern Siljan Ring in central Sweden. GFF.

ICDP

Tectono-stratigraphic interpretation of sediments within Lake Ohrid (Albania/Macedonia) for the SCOPSCO ICDP campaign

K. LINDHORST[1], S. KRASTEL[1], T. SCHWENK[2], B. WAGNER[3]

[1] Christian-Albrechts-Universität zu Kiel, Institut für Geowissenschaften, Abteilung Geophysik, Otto-Hahn-Platz 1, 24118 Kiel

[2] Fachbereich Geowissenschaften, Universität Bremen, Germany

[3] Institute für Geologie und Mineralogie, Universität Köln, Germany

Ancient Lake Ohrid is probably the oldest existing lake in Europe. It is located on the Balkan Peninsula within the Dinaride-Albanide-Hellenide mountain belt, and is often referred to as a hotspot of endemic biodiversity (Albrecht and Wilke, 2008). This study sheds light on the tectonic and sedimentary evolution of Lake Ohrid based on newly-acquired hydro-acoustic and seismic data sets. It testifies the importance of Lake Ohrid as a valuable archive susceptible to provide a continuous sediment record within the scope of the SCOPSCO project within the International Continental Drilling Program (ICDP) campaign. Drilling is now scheduled for April 2013.

Intensive work has been done in the last couple of years resulting in a better understanding with respect to the

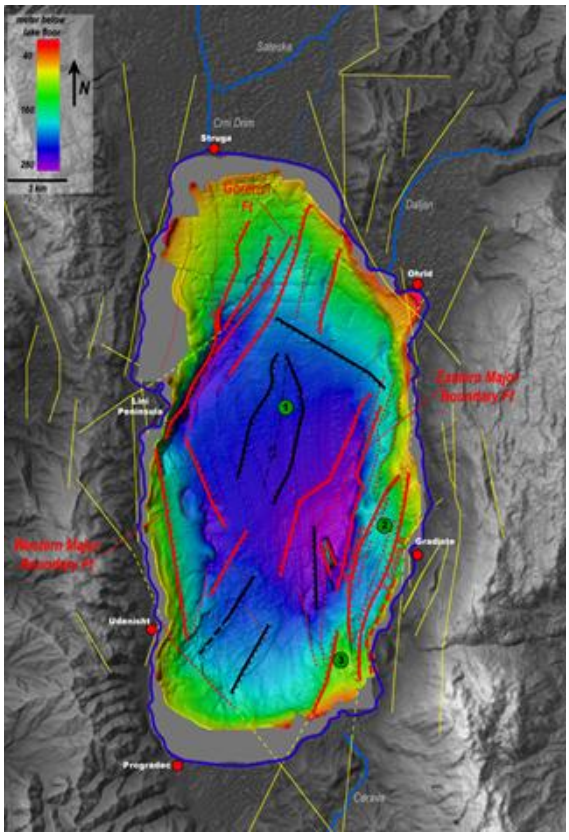

Figure 1: Compilation of bathymetric map and topography of the surrounding area at Lake Ohrid. Red lines are major active normal faults. Thick black lines are inactive faults. Dashed lines are inferred faults. Yellow lines are faults described onshore (Hoffmann et al. 2010). Green dots are proposed drill sites (1: DEEP, 2: Gradiste, 3: Cerava).

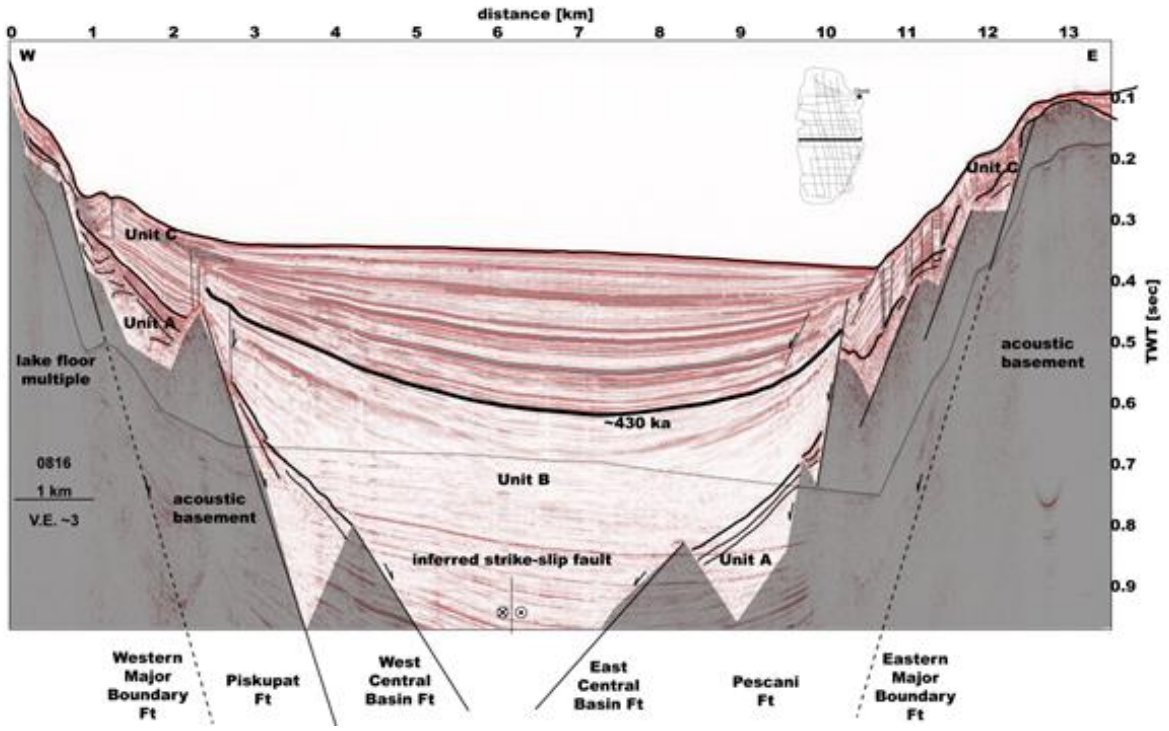

Figure 2: Seismic cross section illustrating the internal structure and sediment filling within the central part of Lake Ohrid. Major seismic units (acoustic basement – oldest to Unit B,C – youngest successions) are marked. The reflector interpreted as 430 ka years old is marked as a thick black line.

initial opening of the basin, the subsequent tectonic and sedimentary evolution, and its role within the present geodynamic regime of the surrounding region. Interpretation of multichannel seismic cross sections and bathymetric data reveals that Lake Ohrid formed in two main deformation phases: (1) a transtensional phase resulted in an opening of a pull-apart basin probably in Late Miocene; and (2) an extensional phase since the Pliocene to recent that led to the present geometry of Lake Ohrid. For the purpose of reconstructing the initial opening of the basin we mapped the acoustic basement on all seismic lines resulting in a grid of the host rock underlying the sediments. The so-called early stage geometry of the basin resembles a rhomboidal shape in the center bounded by four major normal faults (Fig. 1). The location of the basin initiation coincides with the greatest depth of the acoustic basement; nowadays a thick succession of undisturbed sediments is found in this area. En-enchelon faults are observed in the north and southern continuation (Fig. 1). Furthermore we interpreted seismic cross section and found that they show a symmetrical graben structure with an inferred strike-slip fault in the center pointing to an opening as a pull-apart basin in a short transtensional phase during the Late Miocence (Fig. 2, Rahe et al. 1998, Lindhorst et al. in review).

Since Miocence times the area around Lake Ohrid is affected by an E-W extension caused by a slab roll back of the Hellenic subduction slab which lead to the formation of N-S trending sedimentary basins that are progressively younging toward the west. Lake Ohrid basin and its sister Lake Prespa are the youngest of these sedimentary basins. Neotectonic activity since the Pliocene takes place along the roughly N-S directed Eastern and Western Major Boundary Normal faults that are partly exposed at the lake . Numerous faults are present in the northern area offsetting syn-tectonic sediments, thus confirming the hypothesis that Lake Ohrid Basin is still experiencing extension. Furthermore, the active Gorenci sinistral strike slip Fault is most likely responsible for the opening of the Struga Graben detectable at the lake floor as a NE-SW directed elongated graben structure.

A first chronological model was developed using the seismic characteristic of thick undisturbed sediments along a 2 km transect within the deepest part of Lake Ohrid. This model give a first estimation of reflectors up to an age of 430 ka (Fig 2). Based on that model we calculated an 0.43 mm/yr as average sedimentation rate for the entire sedimentary filling. Applying this number to older reflectors we estimate an minimum age of ~2 Ma years for the oldest sediments Stacked clinoforms indentified on seismic lines in the southern area indicate significantly lower lake levels prior to MIS 6. This period is also characterized by a progressive rise of water level with intermittent stillstands since its existence as water-filled body, which might have favored expansion of endemic species within Lake Ohrid. Significant lake level fluctuations with prominent lowstands of ca. 60 and 35 m below the present water level occurred during MIS 6 and 5, respectively. The effect of these lowstands on the biodiversity along most of the coasts of the lake is probably negligible, due to only small changes in lake surface area, coastline, and habitat. In contrast, the biodiversity in shallow-lacustrine areas was more severely affected due to disconnection of sublacustrine springs from the main water body (Lindhorst et al. 2010).

Other interesting features in Lake Ohrid are mass movement deposits that are widespread within the basin and have been mapped at different stratigraphic levels of the basin. A cluster of slide deposits around Magic Mountain (a prominent basement high in the central basin)

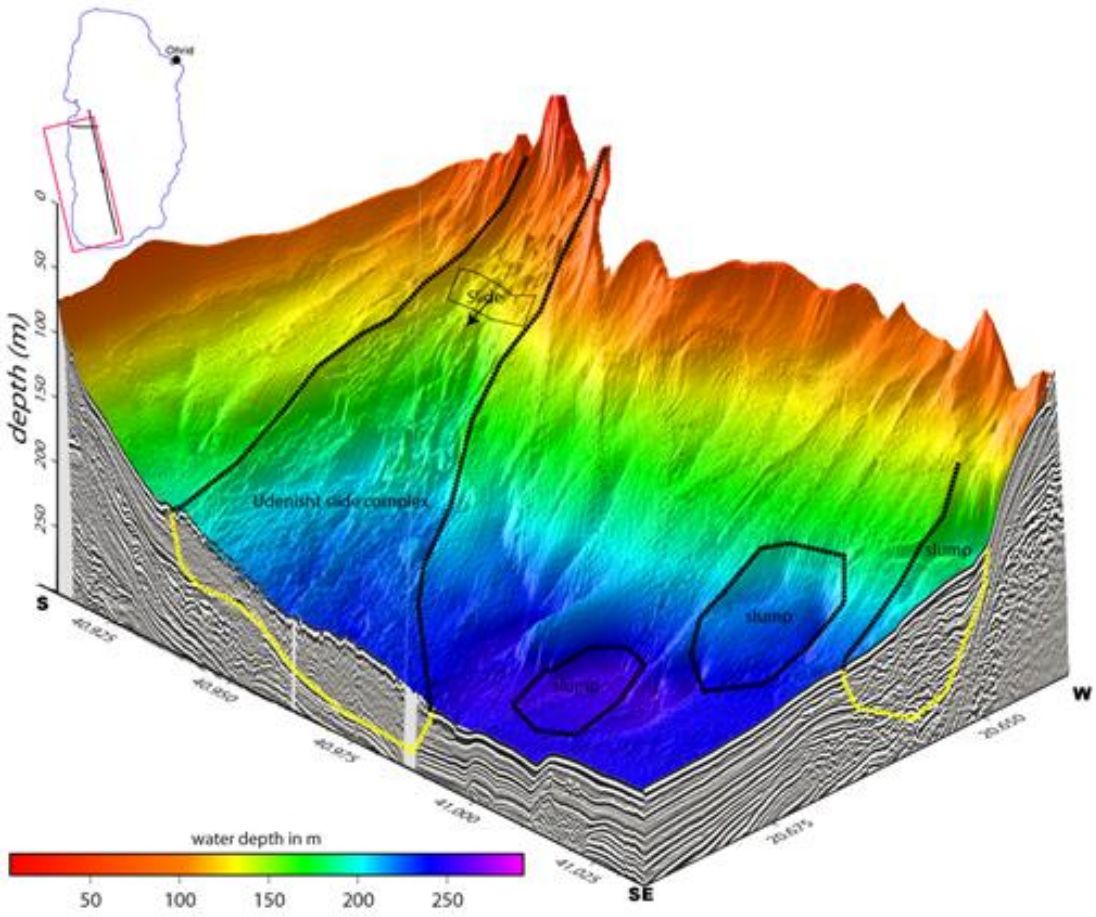

Fig. 3: A 3D bathymetric map of the southwestern area of Lake Ohrid. Dashed lines mark mass movement deposits (black – at the surface, yellow - in the subsurface.

indicates a relationship between mass movement events and the activation of faults that bound the intrabasinal high. In general slides are present adjacent to major fault structures such as the Lini fault, the Eastern and Western Major Boundary faults, and the Udenisht fault in the south suggesting that they are seismically triggered. The Udenisht slide complex in the southwestern part of the lake is by far the largest mass failure event within the basin (Fig. 3). The slide deposits cover an area of ~27 km², are up to 50 m thick, and sum up to a volume of ~0.11 km³. First age estimations suggest that the Udenisht Slide is less than 1,500 years old. Because the volume of the Udenisht slide is well within the range of landslide volumes capable to trigger tsunamis we have evaluated the potential tsunami hazard within Lake Ohrid basin by simulating a wave generated by an underwater slump located on the upper slope of the Udenisht slide with a similar shape to the slump in the north (Fig. 3). Our model suggests that mass movements in Lake Ohrid have a low tsunamigenic potential. We calculated an initial tsunami wave with a wavelength of 500 m and a waveheight of 5.20 m which propagates within 10 min across the entire lake. Nevertheless the wave heights in Struga and Ohrid in the north are negliglible small. We obtained the maximum tsunami amplitude of 120 cm and a run-up height of 142 cm off the monastry Sveti Naum.

Based on these new insigths in the tectono-stratigraphic evolution of Lake Ohrid and the morphological analysis of the basin by means of high bathymetric data we selected three potential drill sites for the ICDP campaign. The main site (DEEP , Fig. 1) has been chosen in the central part as the most promising drill site for the purpose of collecting an almost 700 m-long core because we find no indications for a hiatus or major mass transport deposits. A continuous record of paleoenvironmental history obtained from Lake Ohrid would provide an important database for historic climate changes within the northern Mediterranean region as well as for volcanic activity. Major objectives to be addressed with this site include the age and origin of the lake, its environmental and climatic history, tephra deposition, and the link between evolutionary changes and geological events. Two additional drill sites in proximity to the shore will shed light on (i) major changes of the hydrological regime, (ii) ages of ancient clinoforms that are linked to lake level fluctuations, as well as (iii) its neotectonic activity and associated mass wasting events.

References:

Albrecht, C. and T. Wilke (2008). "Ancient Lake Ohrid: biodiversity and evolution." Hydrobiologia 615: 103-140.

Lindhorst, K., S. Krastel, et al. (in review). "Tectonic and Sedimentary Evolution of Lake Ohrid (Albania/Macedonia)." Basin Research.

Lindhorst, K., H. Vogel, et al. (2010). "Stratigraphic analysis of lake level fluctuations in Lake Ohrid: an integration of high resolution hydro-acoustic data and sediment cores." Biogeosciences 7, (in: Evolutionary and geological history of Balkan lakes Ohrid and Prespa

Rahe, B., D. A. Ferrill, et al. (1998). "Physical analog modeling of pull-apart basin evolution." Tectonophysics 285(1-2): 21-40.

IODP

Reconstruction of the Atlantic Meridional Overturning Circulation applying sediment $^{231}Pa/^{230}Th$

JÖRG LIPPOLD[1], YIMING LUO[2], ROGER FRANCOIS[2], SUSAN E. ALLEN[2], JEANNE GHERARDI[3], SYLVAIN PICHAT[4], BEN HICKEY[5], HARTMUT SCHULZ[6]

[1] Institute of Environmental Physics, University of Heidelberg, 69120 Heidelberg, Germany
[2] Department of Earth and Ocean Sciences, University of British Columbia, Vancouver, British Columbia V6T 1Z3, Canada
[3] LSCE/IPSL Laboratoire CNRS/CEA/UVSQ, domaine du CNRS, 91190 Gif sur Yvette, France
[4] Ecole Normale Supérieure de Lyon, Université Claude Bernard and CNRS, 69364 Lyon, France
[5] Department of Earth Sciences, University of Oxford, Oxford, OX1 3AN, UK
[6] Institute for Geosciences, University of Tübingen, 72074 Tübingen, Germany

The Atlantic Meridional Overturning Circulation (AMOC) plays a key role in the climatic system of our planet by redistributing heat and carbon between the hemispheres and between low and high latitudes. During the last 100,000 years abrupt shifts as well as long-lasting evolutions of climatic modes have been linked to changes in the Ocean circulation. Using traditional geological and palaeontological methods these changes have been established. However, traditional methods predominantly work qualitatively only and are thus not capable of quantifying the oceanic transport. A new promising approach of measuring the ratio of the Uranium decay products $^{231}Pa/^{230}Th$ in marine sediments has been increasingly applied, but initially yielded contradicting results. Based on a huge new $^{231}Pa/^{230}Th$ data set build up with contributions from IODP/ODP and a model backed concept we constrained the AMOC during the Last Glacial Maximum (LGM) quantitatively.

The strength and geometry of the AMOC is tightly coupled to climate on glacial-interglacial and millennial timescales [Rahmstorf 2002], but has proved difficult to reconstruct, particularly for the LGM [Lynch-Stieglitz et al. 2007]. Today, the return flow from the northern North Atlantic to lower latitudes associated with the Atlantic meridional overturning circulation reaches down to approximately 4,000 m. In contrast, during the Last Glacial Maximum this return flow is thought to have occurred primarily at shallower depths [Curry and Oppo 2005; Sarnthein et al. 1994]. One promising proxy of paleocirculation is $^{231}Pa/^{230}Th$. The radioisotopes ^{231}Pa and ^{230}Th are constantly produced in seawater from the radioactive decay of dissolved uranium (^{235}U and ^{234}U) and are rapidly removed to the underlying sediment by adsorption on settling particles. Because ^{231}Pa is removed at a slower rate than ^{230}Th, a larger fraction of the ^{231}Pa produced in the Atlantic is exported to the Southern Ocean by North Atlantic Deep Water (NADW). The average $^{231}Pa/^{230}Th$ of modern Atlantic sediments is thus lower than the production rate ratio of the two isotopes (0.093) and varies with the rate of formation of NADW.

Measurements of sedimentary $^{231}Pa/^{230}Th$ have been used to reconstruct the strength of circulation in the North Atlantic Ocean [Marchal et al. 2000; McManus et al. 2004; Yu et al. 1996], but the effects of biogenic silica on $^{231}Pa/^{230}Th$ based estimates remain controversial [Keigwin and Boyle 2008]. Further, new $^{231}Pa/^{230}Th$ time series from different locations of the Atlantic Ocean display very different profiles and absolute values for specific time periods obviously not allowing a direct deduction of AMOC strength from $^{231}Pa/^{230}Th$ [Gherardi et al. 2009; McManus et al. 2004; Negre et al. 2010].

First, we found that the water depth of the sediment core is a crucial parameter on the measured $^{231}Pa/^{230}Th$. An

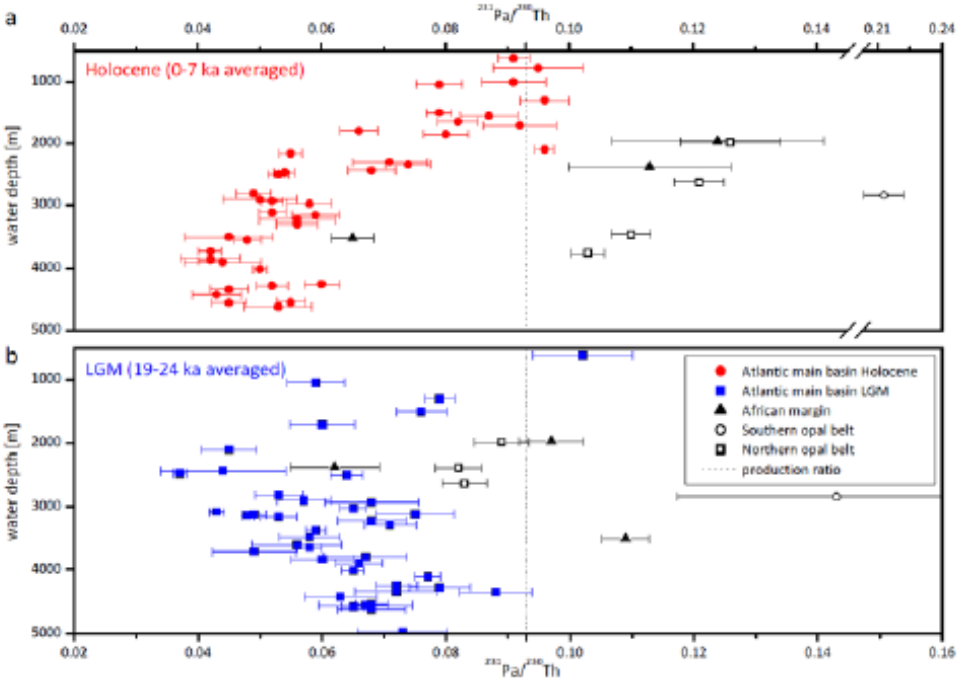

$^{231}Pa/^{230}Th$ versus water depth. **a:** Holocene sediment $^{231}Pa/^{230}Th$ generally decreases with water depth (red circles). **b:** LGM $^{231}Pa/^{230}Th$ in the main Atlantic basin (blue squares) decreases with depth down to 2,500m and then increases in deeper waters. Values deviating from these general trends are from regions with very high opal flux (open symbols) or from the African margin (black triangles).

anti-correlation of water depth with $^{231}Pa/^{230}Th$ has been reported before [Gherardi et al. 2009; Scholten et al. 2008], but it was only after comparing a new increased data base with the output of a two-dimensional scavenging model [Luo et al. 2010] that predominantly the AMOC strength controls this anti-correlation [Lippold et al. 2011].

Further, we used measurements of $^{231}Pa/^{230}Th$ ratios and biogenic silica in Holocene-aged Atlantic sediments and the two-dimensional scavenging model to demonstrate that the geometry and strength of the AMOC are the primary controls of $^{231}Pa/^{230}Th$ ratios in modern Atlantic sediments [Lippold et al. 2012]. The role of biogenic silica is subordinate only up to a certain level.

Repeating this approach for the LGM a simulation of Atlantic overturning with a shallow, but vigorous circulation and bulk water transport at around 2,000 m depth best matched observed glacial Atlantic $^{231}Pa/^{230}Th$ values. We estimate that the transport of intermediate water during the Last Glacial Maximum was at least as strong as deep water transport today [Lippold et al. 2012].

References:

Curry, W. and D. Oppo, 2005. Glacial water mass geometry and the distribution of $\delta^{13}C$ of CO_2 in the western Atlantic Ocean. Paleoceanography. 20: PA1017.

Gherardi, J., L. Labeyrie, S. Nave, R. Francois, J. McManus and E. Cortijo, 2009. Glacial-interglacial circulation changes inferred from $^{231}Pa/^{230}Th$ sedimentary record in the North Atlantic region. Paleoceanography. 24: PA2204.

Keigwin, D. and E. Boyle, 2008. Did North Atlantic overturning halt 17,000 years ago? Paleoceanography. 23: PA1101.

Lippold, J., J. Gherardi and Y. Luo, 2011. Testing the $^{231}Pa/^{230}Th$ paleocirculation proxy - A data versus 2D model comparison. Geophysical Research Letters. 38: L20603.

Lippold, J., Y. Luo, R. Francois, S. Allen, J. Gherardi, S. Pichat, B. Hickey and H. Schulz, 2012. Strength and Geometry of the glacial Atlantic Meridional Overturning Circulation. Nature Geoscience. 5: 813-816.

Luo, Y., R. Francois and S. Allen, 2010. Sediment $^{231}Pa/^{230}Th$ as a recorder of the rate of the Atlantic meridional overturning circulation: insights from a 2-D model. Ocean Science. 6: 381–400.

Lynch-Stieglitz, J., J. Adkins, W. Curry, T. Dokken, I. Hall, J. Herguera, J. Hirschi, E. Ivanova, C. Kissel, O. Marchal, T. Marchitto, I. McCave, et al., 2007. Atlantic Meridional Overturning Circulation During the Last Glacial Maximum. Science. 316: 5821.

Marchal, O., R. Francois, T. Stocker and F. Joos, 2000. Ocean thermohaline circulation and sedimentary $^{231}Pa/^{230}Th$ ratio. Paleoceanography. 15: 6.

McManus, J., R. Francois, J. Gherardi, L. Keigwin and S. Brown-Leger, 2004. Collapse and rapid resumption of Atlantic meridional circulation linked to deglacial climate change. Nature. 428: 834-837.

Negre, C., R. Zahn, A. Thomas, P. Masque, G. Henderson, G. Martinez-Mendez, I. Hall and J. Mas, 2010. Reversed flow of Atlantic deepwater during the Last Glacial Maximum. Nature. 468: 84 - 89.

Rahmstorf, S., 2002. Ocean circulation and climate during the past 120,000 years Nature. 419: 207-214.

Sarnthein, M., S. J. K. Winn, J. Duplessy, L. Labeyrie, H. Erlenkeuser and G. Ganssen, 1994. Changes in East Atlantic Deepwater Circulation over the last 30,000 years: Eight time slice reconstructions. Paleoceanography. 9(2)(209-267.).

Scholten, J., J. Fietzke, A. Mangini, D. Garbe-Schönberg, A. Eisenhauer, P. Stoffers and R. Schneider, 2008. Advection and Scavenging: Effect on ^{230}Th and ^{231}Pa distribution off Southwest-Africa. Earth and Planetary Science Letters. 271: 159-169.

Yu, E., R. Francois and M. Bacon, 1996. Similar rates of modern and last-glacial ocean thermohaline circulation inferred from radiochemical data. Nature. 379: 689-694.

IODP

New Proposal: Ocean circulation modes of the Glacial-Interglacial cycle - high resolution measurements of neodymium isotopes

JÖRG LIPPOLD[1], NORBERT FRANK[1], PATRICK BLASER[1], MARCUS GUTJAHR[2], YIMING LUO[3], JOHANNES REMPFER[4], HARTMUT SCHULZ[5]

[1] Institut für Umweltphysik, Universität Heidelberg, Germany
[2] GEOMAR, Helmholtz-Zentrum für Ozeanforschung, Kiel, Germany
[3] Department of Earth and Ocean Sciences, University of British Columbia, Vancouver, Canada
[4] Institut für Umweltphysik, Universität Bern, Switzerland
[5] Institut für Geowissenschaften, Universität Tübingen, Germany

One main focus in paleoclimatology has been put on the Atlantic Meridional Overturning Circulation (AMOC) as one of the key players in the climate system [Robinson and Siddall 2012]. It is supposed that long-lasting changes as well as short term excursions in global climate during the last glacial cycle were linked to changes in the strength and geometry of the AMOC [Rahmstorf 2002]. In a see-saw like interplay either the deep water production in the North Atlantic or in the Southern Ocean prevailed, having significant influence on the heat budget of the respective hemisphere [Barker et al. 2009]. The neodymium isotope ratio ($^{143}Nd/^{144}Nd$) can be used as an indicator of water mass provenance recorded in the ferromanganese oxyhydroxide fraction of marine sediments [Piotrowski et al. 2004, Gutjahr et al. 2008]. In a new comprehensive study we aim for reconstructing this interplay for the last glacial cycle and the last interglacial in order to disentangle the feedback system of AMOC and circum-Atlantic climate.

Although great efforts have been made to reconstruct the past circulation of the Atlantic Ocean, there is still no consensus on the role of the ocean circulation as cause or consequence of the in part dramatic climate fluctuations which have taken place in the past 150,000 years. Paleoceanographic approaches face two essential problems here: On the one hand, the methods used often have weaknesses and limited applicability, especially tracers, which take part in the nutrient cycle and/or are subject to diagenetic processes. On the other hand the temporal and spatial coverage of existing measurements allows only limited conclusions to be drawn, which may not easily be extrapolated from the local measured record to larger or even global scales [Robinson and Siddall 2012]. In order to gain more reliable conclusions about the past oceanic heat transport and the distribution of carbon and nutrients it is necessary to collect a high amount of data. The material provided from the IODP/ODP core repositories represents a perfect source for this work. In the younger past the measurement of the neodymium isotope ratio $^{143}Nd/^{144}Nd$ emerged as a unique method of choice. The distinct isotopic signatures of water masses originating in the Pacific and the North Atlantic Deep Water render neodymium a exceptional tracer for the ocean circulation in the Atlantic [Frank 2002, Rempfer et al. 2012]. The neodymium isotopic signature and with it the mixing ratio of the prominent water masses in the past is preserved in corals, foraminifera and authigenic Fe-Mn oxyhydroxide fractions in sediment [van de Flierdt and Frank 2010]. The approach of careful separation of these Fe-Mn oxyhydroxides from the bulk sediment and the subsequent

measurement of their neodymium isotopy serves as a methodology which is, applied on a large scale, uttermost promising [e.g., Gutjahr et al. 2007; 2010]. Reliable records can be retrieved in a variety of deep marine settings, it is readily and quickly measurable with modern mass spectrometers with high sample thoughput and the chemical treatment of the sample material is relatively fast and cost-efficient, as long as the respective experience and the knowledge of the chemical purification procedure is provided. Using about 10 selected IODP/ODP cores the question of the timing of water mass transitions in the Atlantic will be pursued. Particular focus will be placed towards identifying how fast these transitions took place and in which global climatological phase circulation changes were prominent. Supported by models and the comparison with further tracers (^{231}Pa/^{230}Th, δ^{13}C) a comprehensive picture of the past glacial-interglacial cycle will be drawn, allowing for the reconstruction of crucial feedback effects and interactions in the climate system, which are directly necessary for the improvement and validation of climate models.

References:

Barker, S., P. Diz, M. Vautravers, J. Pike, G. Knorr, I. Hall and W. Broecker, 2009. Interhemispheric Atlantic seesaw response during the last deglaciation. Nature. 457: 1097-1102.

Frank, M., 2002. Radiogenic isotopes: Tracers of past Ocean Circulation and erosional input. Reviews of Geophysics. 40(1).

Gutjahr, M., B. Hoogakker, M. Frank and N. McCave, 2010. Changes in North Atlantic Deep Water strength and bottom water masses during Marine Isotope Stage 3 (45-35 ka BP). Quaternary Science Reviews. 29(2451-2461).

Gutjahr, M., M. Frank, C. Stirling, L. Keigwin and A. Halliday, 2008. Tracing the Nd isotope evolution of North Atlantic Deep and Intermediate Waters in the western North Atlantic since the LGM from Blake Ridge sediments. Earth and Planetary Science Letters. 266: 61–77.

Piotrowski, A., S. Goldstein, S. Hemming and R. Fairbanks, 2004. Intensification and variability of ocean thermohaline circulation through the last deglaciation Earth and Planetary Science Letters. 225: 205-220.

Rahmstorf, S., 2002. Ocean circulation and climate during the past 120,000 years Nature. 419: 207-214.

Rempfer, J., T. Stocker, F. Joos and J.-C. Dutay, 2012A. On the relationship between Nd isotopic composition and ocean overturning circulation in idealized freshwater discharge events. Paleoceanography. 27(PA3211): doi:10.1029/2012PA002312, 2012.

Robinson, L. and M. Siddall, 2012. Palaeoceanography: motivations and challenges for the future. Philosophical Transactions of the Royal Society. 370(doi:10.1098/rsta.2012.0396): 5540–5566.

van de Flierdt, T. and M. Frank, 2010. Neodymium isotopes in paleoceanography. Queternary Science Reviews. 29(2439-2441).

IODP

Biogeochemistry of Phosphorus in Ultra-oligotrophic South Pacific Gyre Seafloor and Sub-seafloor Sediments (IODP Expedition 329)

J. MARSHALL[1], B. BRUNNER[1], T. GOLDHAMMER[2], R. MURRAY[3], A. SPIVACK[4], W. ZIEBIS[5], B. HOPPIE[6], F. INAGAKI[7], S.E. D'HONDT[4], AND T.G. FERDELMAN [1*]

[1] Max-Planck-Institute for Marine Microbiology, Bremen, Germany
[2] MARUM, University of Bremen, Bremen, Germany
[3] University of Boston, Boston, MA, USA
[4] Graduate School of Oceanography, University of Rhode Island, Kingston, RI, USA
[5] University of Southern California, Pasadena, CA, USA
[6] Department of Geology, Minnesota State University, Mankota, MN, USA
[7] Kochi Institute for Core Sample Research, JAMSTEC, Kochi, Japan
*corresponding author (tferdelm@mpi-bremen.de)

Over geological time scales, phosphorus (P) is considered to be the ultimate limiting nutrient in the ocean. Even in today's ocean, P may limit biological dinitrogen fixation and primary productivity in the ultra-oligotrophic waters of ocean gyre systems (Halm et al. 2012). Weathering and burial of P, especially in continental margin settings, exert a major influence on P fluxes. In contrast, open ocean settings are not considered to play a large role on the control on P fluxes. A major exception is the input and removal of P in the vicinity of active mid-ocean venting. These flux and budget calculations are based on relatively few data points; processes and fluxes are not well-constrained for the oligotrophic regions of the Ocean. Moreover, mechanisms for P cycling in such low activity, and dark pelagic environments are not well-studied.

Here we report on P distributions and fluxes in the sediments of the South Pacific Gyre (SPG). The ultra-oligotrophic SPG comprises not only the Earth's largest oceanic province, but represents the one of the largest scientifically unexplored regions of the seafloor. The SPG is farther from the continents than any other ocean gyre, surface chlorophyll concentrations and primary productivity are lower than any of the other regions of the world ocean, and it contains the world's clearest seawater (Morel et al., 2007). During IODP Expedition 329 (Pape'ete, French Polynesia, Oct. 9, 2010 to Dec. 13, 2010 Auckland, New Zealand), operations were conducted at seven sites (U1365 to U1371). The sites followed two transects from the edge to the center of the gyre, with the easternmost hinge-point in the center of the ultra-oligotrophic gyre. Water depths ranged from 3749 to 5707 meters below sea level. The dominant sediment lithology along the deep water sites (U1365 – U1367) was a zeolitic metalliferous clay. A shift to carbonate lithology was observed at the easternmost, shallowest water depths (Site U1368). The sediments underlying this gyre exhibit extreme lows in sedimentation rates and surface cell abundances. Dissolved oxygen was present at all and sediment depths (bar U1371), suggesting that the microbial activities in these sediments are persistently low (D'Hondt, Inagaki, Zarakian et al., 2012).

High resolution interstitial water phosphate concentrations determined onboard IODP Expedition 329, suggest that phosphate is being released in stoichiometric amounts with the degradation of marine organic matter in the near surface sediments. However, and distinctly unlike nitrate, phosphate concentrations decrease to 0.5 to 0.75 µM in the deeper reaches of the zeolitic, metalliferous pelagic clays. Even in the less oligotrophic "control" Site U1371, where the siliceous sediments became anoxic, a phosphate sink in the underlying pelagic clays is evident. We estimate diffusive fluxes of dissolved phosphate using a reaction-transport fittin routine (Wang et al. (2008). Upward fluxes of phosphate towards the sediment water interface in the southern transect (U1369 through U1371) range from 3.3 to 27.4 µmol P m^{-2} a^{-1} and 0.4 and 2.2 µmol P m^{-2} a^{-1} at Sites U1365 and U1366. In contrast, a downward flux of phosphate from sediment surface seawater and into the sediment is estimated for Sites U1367 and U1368 in the heart of the oligotrophic gyre. Downward fluxes of phosphate into the deeper sediments at the other sites are also in the range of 0.1 to 3.2 µmol P m^{-2} a^{-1}.

Mechanisms for removal of remineralized phosphate from the interstitial waters may include (a) adsorption onto metal (iron and manganese) oxide phases, (b) removal into phillipsites as Fe-Ca hydroxophosphates and eventual diagenetic decomposition to apatite, (c) microbial uptake, and (d) loss to basement processes.We explored these mechanisms by determining P concentrations and distributions in the solid phases of the sediment using X-ray fluorescence and a sediment extraction method (SEDEX). Total P contents measured with X-ray fluorescence typically are <50 µmol g^{-1} (<0.5 wt.% PO_4) in the siliceous sediments outside the SPG and in the surface sediments of the southern transect, but ranged from over 100 up to 500 µmol g^{-1} (ca. 5 wt.% PO_4) in the pelagic red clay sediments. SEDEX indicates that the largest fraction of solid phase P was present in the apatite/carbonate fraction, with the remainder associdated with iron oxides. In spite of low rates of sediment accumulation, burial fluxes of P (23 to 201 µmol P m^{-2} a^{-1}) are significantly greater than diffusive fluxes (with the exception of Site U1371). First estimates for total P burial for the entire SPG. The diffusive and burial fluxes of P in the SPG sediments do not, at first glance, appear large: 0.73 Gmol a^{-1}, or ~2.6% of total P burial in the ocean. Nonetheless, given the extensive area of seafloor lying under oligotrophic gyre systems (roughly 48% of the ocean seafloor), this deep sink of P may be significant for deep ocean nutrient chemistry than originally thought.

References:
Halm et al. (2012) *ISME J*, 6, 1238–1249.
D'Hondt, Inagaki, Zarakian and Expedition Scientists (2012) *Expedition Reports, Vol. 329 of Proc. IODP.*
Morel et al. (2007*) Limnol Oceanogr*. 52, 217-229.
Wang et a.,(2008) *Geochim. Cosmochim. Acta*, 72, 3279-348

ICDP

Simulating magma ascent: An experimental challenge

H. MARXER, P. BELLUCCI, S. ULMER, M. NOWAK

University of Tübingen, Department of Geosciences, Wilhelmstr. 56, 72074 Tübingen, Germany

Magma ascent is accompanied by physicochemical processes such as volatile exsolution and crystallization. These processes are triggered by changes in the *P-T* conditions during ascent and affect the viscosity and the density of the magma, controlling the ascent rate and the eruptive behavior (e.g. Gonnermann & Manga, 2007). This results in a broad range of natural decompression rates, comprising the beginning of magma ascent at depth as well as volcanic eruptions. The dynamic processes during magma ascent cannot be observed directly in nature. Nevertheless, they can be studied by the conduction of decompression experiments with volatile-bearing melts in a *HP-HT* laboratory. As part of experimental studies in the course of the Campi Flegrei Deep Drilling project, decompression experiments will provide information about the degassing behavior during magma ascent prior to eruptive events (see Preuss & Nowak, this colloquium).

Until now, the majority of experiments was performed with a stepwise decompression technique. Due to technical limitations, decompression was realized by the release of the pressure medium from the isothermally heated autoclave by opening a *HP* needle valve manually for a short time. This release caused a rapid pressure drop with 2.5-10 MPa·s^{-1} corresponding to unrealistic magma ascent velocities of 300-1200 km·h^{-1}. After the decompression step, the sample was held at lower pressure for a specific time to simulate a continuous decompression (CD) path, with a nominal interpolated decompression rate much lower than the rate of actual pressure drop. Target *P* was either adjusted immediately within one step (single-step decompression, SSD) or multiple pressure drops of equal Δ*P* (multi-step decompression, MSD). At target pressure the partially degassed melt was quenched to a vesiculated glass. Only few super-liquidus experiments were performed with CD to date, using a complex system of needle valves with different *HP* capillaries for continuous pressure medium bleed-off (Mangan & Sisson, 2000). Therefore, the knowlegde of dynamic processes related to magma ascent in deeper zones of volcanic systems is very limited, especially in terms of decompression induced degassing and crystallization in volatile-bearing magmas. In order to perform controlled decompression experiments with reasonable ascent rates, a novel type of *HP* valve was developed for experiments in an internally heated argon pressure vessel (IHPV) at *P* up to 500 MPa and *T* up to 1773 K (Nowak *et al.*, 2011). The valve system consists of a modified *HP* valve, driven by a piezoelectric nano-positioning system. The piezoelectric actuator facilitates either statical positioning of the needle on a nanometer scale for continuous argon gas bleed-off down to infinitesimally low decompression rates or complete opening and closing of the valve to achieve fast pressure drops limited by the diameter of the *HP* tubing.

Using this new valve, a series of super-liquidus decompression experiments with a H_2O-saturated

phonolitic melt (synthetic Vesuvius AD 79 “white pumice” composition) were performed to investigate the effect of decompression path on the degassing behavior. Results on the degassing behavior of this particular melt are relevant for Campi Flegrei, because recent sudies suggest a single magma pool beneath this caldera and Vesuvius (Pappalardo & Mastrolorenzo, 2012). The phonolitic melt was decompressed isothermally from 1323 K and 200 MPa to a final *P* of 75 MPa with 5 decompression rates in the range of 0.0028-4.8 MPa·s^{-1}, applying CD, MSD (ΔP steps of 10 MPa) as well as SSD for each rate. At target *P* the melt was quenched rapidly. The comparison of the vesiculated glass products in terms of number of nucleated bubbles, size distribution of bubbles and residual H_2O-content in the glass reveals a massive influence of the applied decompression path on the degassing behavior of the melt. In general, decompression of the H_2O-saturated melt induces a supersaturation with H_2O. At a certain supersaturation pressure, bubbles will nucleate homogeneously distributed within the melt and grow by H_2O diffusion towards the bubble to regain equilibrium. The extent of supersaturation is controlled by the actual decompression rate, because the diffusivity of H_2O is limited within a certain time. The experiments have shown that the number of nucleated bubbles increases with decompression rate, whereas average size decreases. At low CD rates <0.024 MPa·s^{-1} (<3 km·h^{-1}) only few bubbles nucleate in the melt, because the decompression rate provides suffient time for H_2O diffusion towards existing bubbles. Therefore, bubble growth is the predominant degassing process. MSD and SSD run products with nominally identical decompression rates feature smaller and more numerous bubbles. Decompression in a stepwise manner results in instantaneous supersaturation due to rapid pressure drop, which can only be reduced by a massive nucleation event. The differences between the three decompression techniques decrease with increasing nominal decompression rate, because the rapid pressure drop even at CD enhances bubble nucleation.

The stepwise deompression technique is not suitable to investigate the dynamic processes during continuous magma ascent. MSD may be appropriate to study magma ascent with intermediate storage on different volcanic levels, but not with decompression steps exceeding natural ascent rates. Fast CD is most certainly appropriate for the simulation of explosive volcanic eruptions. All kinds of natural decompression paths can be simulated with the novel valve construction. Future experiments will give new insights into the dynamic processes within ascending magma prior to eruption.

References:

Gonnermann, H.M. and Manga, M. (2007): The fluid mechanics inside a volcano. Annual Review of Fluid Mechanics, 39: 321-356.

Mangan, M. and Sisson, T. (2000): Delayed, disequilibrium degassing in rhyolite magma: Decompression experiments and implications for explosive volcanism. Earth and Planetary Science Letters, 183: 441-455.

Nowak, M., Cichy, S.B., Botcharnikov, R.E., Walker, N. and Hurkuck, W. (2011): A new type of high-pressure low-flow metering valve for continuous decompression: First experimental results on degassing of rhyodacitic melts. American Mineralogist, 96: 1373-1380.

Pappalardo, L. and Mastrolorenzo, G. (2012): Rapid differentiation in a sill-like magma reservoir: A case study from the Campi Flegrei caldera. Scientific Reports, 2: 1-10.

IODP

Four million years of phosphorus burial and diagenesis in the Bering Sea (IODP Site U1341, Bowers Ridge): Implications for the marine P cycle

C. MÄRZ[1, 2], S.W. POULTON[3], T. WAGNER[2], B. SCHNETGER[1], H.-J. BRUMSACK[1]

[1] Institut für Chemie und Biologie des Meeres (ICBM), Carl-von-Ossietzky University Oldenburg, Carl-von-Ossietzky-Strasse 9-11, 26129 Oldenburg, Germany (christian.maerz1@uni-oldenburg.de)

[2] School of Civil Engineering and Geosciences (CEGS), Newcastle University, Newcastle upon Tyne, NE1 7RU, United Kingdom

[3] School of Earth and Environment, University of Leeds, Leeds, LS2 9JT, United Kingdom

Phosphorus (P) is a key biolimiting nutrient that exerts a major control on marine primary productivity, which is, in turn, a key factor for the sequestration of CO_2 from the atmosphere into the ocean and further into the sediments. Therefore, the amount of bioavailable P in the photic zone may directly interact with Earth’s climate. An important factor in the global P cycle is its burial into marine sediments, which regulates the oceanic reservoir of potentially bioavailable (i.e., reactive) P. The oceanic P residence time is estimated to range from 8,800 to 36,000 years, (Ruttenberg, 1993; Wallmann, 2003). In these calculations, the burial rate of reactive P into marine sediments is a major uncertainty because reactive P phases are affected by various biogeochemical transformations. Under oxygen-depleted bottom water conditions, organic and Fe-bound P is recycled into the water column (Ingall et al., 1993), resulting in an overall reactive P depletion from the sediment. Also diagenetic processes (“sink switching”) affect the burial of reactive P by transferring P between different particulate forms within the sediments (Anderson et al., 2001). From labile, diagenetically reactive phases (e.g., adsorbed P, fish remains, Fe-bound P, organic P), P is transferred to diagenetically stable carbonate fluorapatite (CFA). This results in an increased reactive P burial efficiency, rather than loss of P by diffusion to the overlying water column (Delaney, 1998).

In this study we evaluate the P speciation in Plio- to Pleistocene sediments of the Bering Sea to show how depositional and diagenetic processes affected the speciation of P, and its long-term removal from the water column. We also show that our Bering Sea data have major implications for the way we apply sedimentary P records to reconstruct the past P cycle, and specifically for the calculation of the oceanic P residence time. To reconstruct the cycling of reactive (i.e., formerly bioavailable) P in the Bering Sea and its relationship to detrital and biogenic sediment input, major and trace element analysis by X-ray fluorescence (XRF) in combination with a sequential P extraction scheme were applied to a ~4 Ma sediment record recovered during Integrated Ocean Drilling Program (IODP) Expedition 323 at Site U1341 (Bowers Ridge) (Takahashi et al., 2011). The well-tested SEDEX scheme (Ruttenberg, 1992), modified after Schenau and De Lange (2000) and Latimer et al. (2006), differentiates between loosely adsorbed P, fish bones, P bound to Fe (oxyhydr)oxides, authigenic carbonate fluorapatite, detrital

fluorapatite, organic P, and biogenic opal-bound P. Thus, this extraction represents a unique method to quantify reactive P input, burial and diagenetic transformations in aquatic systems.

As shown in an earlier study by März et al. (in press), our XRF analysis provides the Al contents (proxy of fine-grained detrital material) and, after normalisation to Upper Continental Crust (Wedepohl, 1995), the excess Si (Si_{XS}) contents (proxy for biogenic opal) of the samples. While the excess silica record at Site U1341 (in conjunction with indepedent micropaleontological evidence) implies high biosiliceous productivity and biogenic matter deposition, it correlates negatively with the Al record due to dilution of these two main sediment components (März et al., in press).

Authigenic carbonate fluorapatite (CFA) and opal-bound P are the dominant P fractions at Site U1341. An overall increasing contribution of CFA to total P with sediment depth at Site U1341 documents that the typical gradual "sink switching" from more labile P fractions (e.g., fish bones, Fe-bound P, organic P) to stable authigenic CFA is taking place in these deposits. All these original, labile P fractions sampled the biologically available (i.e., reactive) marine P pool. As sedimentary CFA sensu Ruttenberg (1992) is considered as being exclusively derived from these labile fractions via "sink switching", it is usually defined as part of the reactive P pool as well. However, a positive correlation of the CFA record with Al contents (Fig. 1) implies that a significant part of the supposedly reactive CFA is non-reactive "detrital contamination" by eolian and/or riverine CFA. A number of studies discuss sources, transport, and deposition of terrigenous-sourced CFA in the marine environment. Zhang et al. (2010) found a CFA contribution of ~13 % of total P in surface sediments of the Bering Sea shelf that is most probably related to the weathering and erosion of CFA-rich sedimentary rocks in the Alaskan hinterland. This river/shelf-derived CFA could have been transported to Bowers Ridge as suspension load by currents or sea ice. Regarding potential eolian input of CFA to the North Pacific, Guo et al. (2011) found that in sediments of the Chinese Loess Plateau and Inner Mongolia, most P occurs as CFA. As dust from these Asian regions is dominantly delivered to the North Pacific, including the Bering Sea, eolian deposition may have contributed significantly to the CFA budget at Site U1341. In conclusion, it is a valid assumption that a significant portion of the CFA extracted from Site U1341 sediments has a terrigenous source, despite the open marine location of Bowers Ridge. While the idea of CFA reworking in continental shelf settings is by no means new, and is even seen as a prerequisite for the formation of major phosphorite deposits, our hypothesis also encompasses open marine environments.

In contrast to CFA, opal-bound P has rarely been studied in marine sediments. We find that at Site U1341, opal-bound P is a significant fraction of the total P pool and directly correlates with excess silica enrichments (Fig. 1), indicating that this P fraction was bioavailable to diatoms at the time of sediment deposition. Beyond the operational separation of the opal-bound P fraction, the precise nature of this biosilica-P coupling is unclear, but there are several

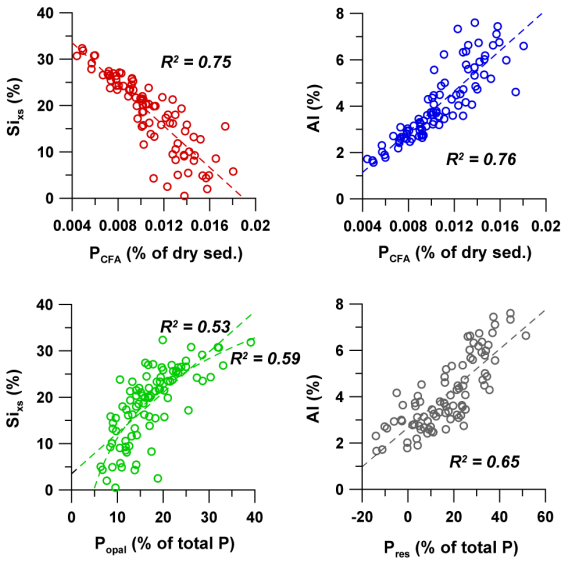

Figure 1: Scatter plots displaying relationships and respective correlation coefficients (R^2) between different geochemical parameters determined by XRF (Si_{xs}, Al) and sequential extraction (carbonate fluorapatite, opal-bound P, residual P).

possible explanations. First, P is incorporated into the opal frustules of diatoms as phospholipids and highly phosphorylated proteins (silaffins), which play a critical role in biosilica morphogenesis (Sumper and Kröger, 2004). Second, polyphosphate was recently discovered as a major and ubiquitous form of P within diatoms, incorporated into the opal frustules by a vital effect (Diaz et al., 2008). Third, biosilica-associated P might be organic P that was protected within the diatom frustules during organic P extraction, and was only released upon frustule dissolution. The third option is less likely because the opal-bound P contents would largely be a function of frustule preservation at the sea floor, which was low in the interval with highest opal-associated P (Aiello and Ravelo, 2012). We therefore assume that the opal-bound P is a structural component of the diatom frustules that still appears to be preserved in the deeper sediments at Site U1341, and contributes to the burial of reactive P in marine sediments.

Our study of Bering Sea sediments exemplifies how the input of detrital CFA and biosilica-bound P may affect sedimentary P records across wide areas of the world ocean (Fig. 2), and may consequently bias current estimates of the oceanic P residence time. These estimates are largely based on the assumption that the sedimentary CFA fraction represents a purely authigenic mineral phase, formed within the sampled sediment column by "sink switching" from labile P phases. As such, the CFA fraction is considered as part of the reactive P pool. However, if part of this CFA fraction did not precipitate within the sediments but was delivered from eroded sedimentary rocks on land, it was not bioavailable during deposition due to its low solubility under normal marine pH and temperature conditions (Guidry and Mackenzie, 2003). This terrigenous CFA should be treated as part of the non-reactive detrital apatite fraction. Consequently, defining the CFA fraction as being exclusively derived from the reactive P pool would lead to an overestimation of reactive P burial rates, and to an underestimation of the oceanic

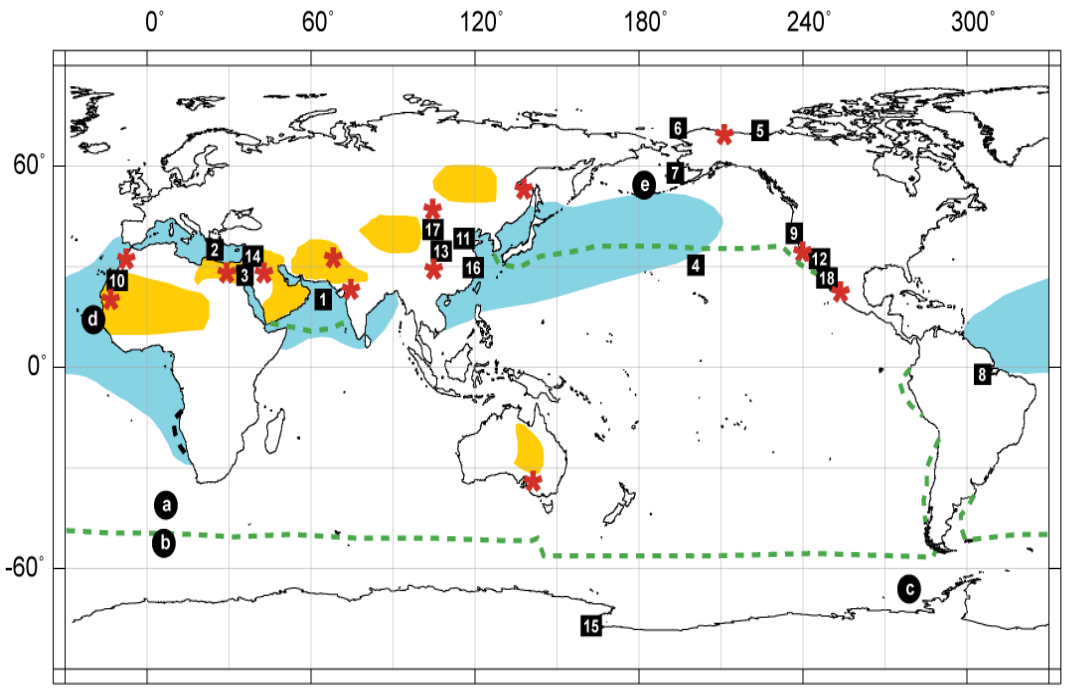

Figure 2: Global map with occurrences of terrestrial CFA in dust, rivers, marine particles and surface sediments (black squares); opal-associated P in marine sediments (black circles); phosphorite deposits in high-latitude/arid regions (red stars); major dust sources to the ocean (yellow); ocean regions potentially receiving CFA-rich dust (blue); boundaries of major biogenic opal depositional areas.

phosphate residence time (Compton et al., 2000). The "detrital contamination" of the CFA pool is strongest in regions that receive detritus from CFA-rich lithologies, and that are dominated by physical weathering (e.g., deserts or polar latitudes; Fig. 2) (Eijsink et al., 2000; Kraal et al., 2012). In open marine regions beyond the immediate influence of river-borne CFA, the deposition of eolian CFA plays a dominant role, especially within the Northern Hemisphere "dust belt" between ~10 and ~60° N (Prospero et al., 2002). In this region, large amounts of potentially CFA-rich dust are redistributed from the Inner Asian, Northern African and Arabian deserts across the North Pacific, Equatorial Atlantic and Arabian Sea, respectively (Fig. 2). In summary, "detrital contamination" of the authigenic CFA signal in marine sediments might be a major issue, and can only be overcome by distinguishing between truly authigenic and terrestrial CFA in marine sediments, which is not possible with the currently applied extraction methods.

While an uncritical interpretation of the sedimentary CFA record might lead to an overestimation of marine reactive P burial, excluding a significant reactive P fraction (i.e., opal-bound P) from the P budget will have the opposite effect. The relationship between biogenic opal contents and the opal-bound P record at Site U1341 implies that the amount of opal deposited/preserved at the sea floor has a direct impact on the removal of bioavailable P from the overlying water column, although the exact opal-P binding mechanism is unclear. This hypothesis was not taken into account in recent estimates of the marine P residence time. Doing so would result in shorter residence times of reactive P in the ocean due to its increased burial in marine settings dominated by biosiliceous producivity, i.e., the Southern Ocean, the North and Equatorial Pacific, and upwelling areas (Fig. 2) (Hüneke and Henrich, 2011). To date, our understanding of opal-bound P (e.g., occurrence, diagenetic reactivity) is too limited to establish any quantitative estimate of its contribution to global reactive P burial in marine sediments, and further studies into this direction are needed. However, it can be assumed that the contribution of this P fraction to total reactive P burial in marine sediments was particularly significant during times of wide-spread biogenic opal deposition like the Pliocene and Eocene.

References:

Anderson, L.D., Delaney, M.L., Faul, K.L., 2001. Carbon to phosphorus ratios in sediments: implications for nutrient cycling. Global Biogeochem. Cycles 15, 65-79.

Anderson, L.D., Faul, K.L., Paytan, A., 2010. Phosphorus associations in aerosols: what can they tell us about P bioavailability? Mar. Chem. 120, 44-56.

Compton, J., Mallinson, D., Glenn, C.R., Filippelli, G., Föllmi, K., Shields, G., Zanin, Y., 2000. Variations in the global phosphorus cycle, in: Glenn, C.R., Prévot-Lucas, L., Lucas, J. (Eds.), Marine Authigenesis: From Global to Microbial. SEPM Spec. Publ. 66, 21-33.

Delaney, M.L., 1998. Phosphorus accumulation in marine sediments and the oceanic phosphorus cycle. Glob. Biogeochem. Cycles 12, 563-572.

Diaz, J., Ingall, E., Benitez-Nelson, C., Paterson, D., de Jonge, M., McNulty, I., Brandes, J.A., 2008. Marine polyphosphate: A key player in geologic phosphorus sequestration. Science 320, 652-655.

Eijsink, L.M., Krom, M.D., Herut, B., 2000. Speciation and burial flux of phosphorus in the surface sediments of the Eastern Mediterranean. Am. J. Sci. 3000, 483-503.

Guidry, M.W., Mackenzie, F.T., 2000. Apatite weathering and the Phanerozoic phosphorus cycle. Geology 28, 631-634.

Guo, B., Yang, H., Li, Y., 2011. The speciation of phosphorus in the sand particles in western Inner Mongolia. Proceedings, Second International Conference on Mechanic Automation and Control Engineering (MACE), 2755-2757, doi:10.1109/MACE.2011.5987555.

Hüneke, H., Henrich, R., 2011. Chapter 4 – Pelagic sedimentation in modern and ancient oceans, in: Hüneke, H.,Mulder, T. (Eds.), Deep-Sea Sediments. Developments in Sedimentology 63, Elsevier, 215-351.

Ingall, E.D., Bustin, R.M., Van Cappellen, P., 1993. Influence of water column anoxia on the burial and preservation of carbon and phosphorus in marine shales. Geochim. Cosmochim. Acta 57, 303-316.
Kraal, P., Slomp, C.P., Reed, D.C., Reichart, G.-J., Poulton, S.W., 2012. Sedimentary phosphorus and iron cycling in and below the oxygen minimum zone of the northern Arabian Sea. Biogeosciences 9, 2609-2623.
Latimer, J.C., Filippelli, G.M., Hendy, I., Newkirk, D.R., 2006. Opal-associated particulate phosphorus: implications for the marine P cycle. Geochim. Cosmochim. Acta 70, 3843-3854.
März, C., Schnetger, B., Brumsack, H.-J., in press. Nutrient leakage from the North Pacific to the Bering Sea (IODP Site U1341) following the onset of Northern Hemispheric Glaciation? Paleoceanography.
Paytan, A., Faul, K.L., 2007. The oceanic phosphorus cycle. Chem. Rev. 107, 563-576.
Prospero, J.M., Ginoux, P., Torres, O., Nicholson, S.E., Gill, T.E., 2002. Environmental characterization of global sources of atmospheric soil dust identified with the Nimbus 7 Total Ozone Mapping Spectrometer (TOMS) absorbing aerosol product. Rev. Geophys. 40, 1002, doi:10.1029/2000RG000095.
Ruttenberg, K.C., 1992. Development of a sequential extraction method for different forms of phosphorus in marine sediments. Limnol. Oceanogr. 37, 1460-1482.
Ruttenberg, K.C., 1993. Reassessment of the oceanic residence time of phosphorus. Chem. Geol. 107, 405-409.
Schenau, S.J., De Lange, G.J., 2000. A novel chemical method to quantify fish debris in marine sediments. Limnol. Oceanogr. 45, 963-971.
Sumper, M., Kröger, N., 2004. Silica formation in diatoms: The function of long-chain polyamines and silaffins. J. Mater. Chem. 14, 2059-2065.
Takahashi, K., Ravelo, A.C., Alvarez Zarikian, C., Expedition 323 Scientists, 2011. Proc. IODP 323, Tokyo (Integrated Ocean Drilling Program Management International, Inc.), doi:10.2204/iodp.proc.323.105.2010.
Wallmann, K., 2003. Feedbacks between oceanic redox states and marine productivity: A model perspective focused on benthic phosphorus cycling. Global Biogeochem. Cycles 17, GB1084, doi:10.1029/2002GB001968.
Wallmann, K., 2010. Phosphorus imbalance in the global ocean? Global Biogeochem. Cycles 24, GB4030, doi:10.1029/2009GB003643.
Wedepohl, K.H., 1995. The composition of the continental crust (Ingerson Lecture). Geochim. Cosmochim. Acta 59, 1217-1232.
Zhang, J.-Z., Guo, L., Fischer, C.J., 2010. Abundance and chemical speciation of phosphorus in sediments of the Mackenzie River delta, the Chukchi Sea and the Bering Sea: importance of detrital apatite. Aquat. Geochem. 16, 353-371.

IODP

Regional differences in the chemical composition of surface sediments across the central Arctic Ocean

A.-K. MEINHARDT[1], T. MANDYTSCH[1], C. MÄRZ[1], H.-J. BRUMSACK[1]

[1] AG Mikrobiogeochemie, Institut für Chemie und Biologie des Meeres (ICBM), Postfach 2503, 26111 Oldenburg, Germany

With our study we provide the first high-resolution inorganic-geochemical data set of a sediment coring transect across the central Arctic Ocean (RV Polarstern cruises ARK-XXIII/3 and ARK-XXVI/3; Jokat et al., 2009; Schauer et al., 2012). The overall aim is to develop new, and improve existing paleoenvironmental proxies for tracing, e.g., the provenance of detrital sediments to various parts of the Arctic Ocean and to document the varying influence of surface currents and sea ice distribution. Major and trace elements were quantified by wavelength-dispersive X-ray fluorescence analysis (XRF) of surface sediments (0-2 cm depth) taken from representative parts of the Arctic Ocean. This geochemical approach will provide fundamental data that are crucial for provenance and paleoenvironmental studies in older Arctic Ocean sediments that will most likely by drilled during the next phase of IODP after 2013. We are planning to successively expand our study to deeper sediment layers (sampled by gravity coring) to check if the geochemical signals detected in the surface sediments are also discernible in the paleorecord. Additionally, the planned application of more advanced isotopic techniques (Nd, Sr) will provide further information about the variability of sea ice cover and currents in space and time.

In this contribution we present the distribution patterns of the elements Ca, Co, Fe, Mg, Mn, Mo, Sr and TIC (total inorganic carbon). We particularly focus on the association of Co and Mo with Mn and the input of Mn and Fe, whereas Ca, Mg, Sr and TIC are used to trace the input of carbonates.

Both Mn and Fe are predominantly delivered to the Arctic Ocean via rivers. Despite the similar biogeochemical behaviour of these two elements in fully oxic marine systems like the Arctic Ocean, their distribution patterns in Arctic surface sediments are different. At all sampling points, Mn is highly enriched compared to the background sediment composition (approximated by average shale (AS); Wedepohl, 1971, 1991). Generally speaking, Mn contents in the Amerasian Basin sediments are higher than in the Eurasian Basin. Highest Mn contents are found on the Lomonosov Ridge near the North Pole and on the Alpha Ridge, i.e., in areas dominated by severe sea ice cover. Four sediment samples along a transect in the Nansen Basin show decreasing Mn contents from the crest of the Gakkel Ridge towards the adjacent basin. This is in accordance with findings of hydrothermal activity at the Gakkel Ridge and the related release of Mn into the water column (Middag et al., 2011). The trace elements Co and Mo show similar distribution patterns with highest enrichments at the Gakkel Ridge crest and decreasing values towards the shelf. The similar distribution patterns of Mn, Co and Mo indicate a common source and/or a similar biogeochemical behaviour of these elements, presumably because Mn (oxyhydr)oxides scavenged Co and Mo. Iron is enriched in these samples as well, but to a lesser extent than Mn, Co and Mo. The enrichment factors (EF) relative to average shale fall into a narrow range, due to generally higher amounts of Fe in the background sediment compared to Mn. To compare enrichments of Fe and Mn relative to the local terrigenous input – which not necessarily has an AS composition - we defined the lowest values attained in the corresponding multicorer sediment cores as respective background values and calculated excess contents (Fe_{xs} and Mn_{xs}). The Fe_{xs} contents are slightly higher than the Mn_{xs} contents, but both are on the same order of magnitude and show the comparable enrichment of Fe and Mn in the investigated surface sediments. In the four sediment samples in the Nansen Basin, the Fe contents do not follow the decreasing spatial trend from the Gakkel Ridge towards the basin. This indicates a less important input of Fe via hydrothermal activity or different reactivities of these two elements in the water column.

Calcium, Mg, Sr and TIC show maximum values in the surface sediments from the Amerasian Basin, indicating the presence of detrital carbonates. The Canadian Arctic Archipelago has been identified as the source of carbonates, especially dolomite. Detrital carbonates are transported via the Beaufort Gyre across the Amerasian Basin and this circulation pattern is clearly visible in the distribution of carbonate-related elements, with highest concentrations at two locations near the Alpha-Mendeleev Ridge. Magnesium contents in detrital carbonate (dolomite)

are usually higher than in biogenic carbonate. In our samples, Ca and Mg show the highest EFs in sediments from the Alpha Ridge. This indicates the occurrence of dolomite at these locations. However, the EFs of Sr are comparably high, which points to the additional presence of biogenic carbonate, because Sr contents in biogenic carbonate are much higher than in dolomite.

References:
Jokat, W. (Ed.), 2009. The Expedition ARK-XXIII/3 of RV Polarstern in 2008. Reports on Polar and Marine Research, 597: 1-159.
Middag, R., de Baar, H.J.W., Laan, P. and Klunder, M.B., 2011. Fluvial and hydrothermal input of manganese into the Arctic Ocean. Geochimica Et Cosmochimica Acta, 75(9): 2393-2408.
Schauer, U. (Ed.), 2012. The Expedition of the Research Vessel "Polarstern" to the Arctic in 2011 (ARK-XXVI/3 - TransArc). Reports on Polar and Marine Research, 649: 1-203.
Wedepohl, K. H., 1971. Environmental influences on the chemical composition of shales and clays. In: Ahrens, L. H. Press, F., Runcorn, S. K., Urey, H. L. (Eds.), Physics and Chemistry of the Earth. Pergamon, Oxford, Sydney.
Wedepohl, K. H., 1991. The composition of the upper earth's crust and the natural cycles of selected metals. Metals in nature raw materials. Natural Resources. In: Merian, E. (Ed.), Metals and their compounds in the environment. VCH, Weinheim.

IODP

How kinetics of organic matter degradation controls the distribution of sulphate and methane in the deep biosphere

PATRICK MEISTER[1], BO LIU[1], ARZHANG KHALILI[1,2], TIMOTHY G. FERDELMAN[1], AND BO BARKER JØRGENSEN[1,3]

[1] Max Planck Institute for Marine Microbiology, Celsiusstrasse 1, 28359 Bremen, Germany; email: pmeister@mpi-bremen.de
[2] Earth & Space Sciences Program, School of Engineering and Science, Jacobs University, 28725 Bremen, Germany
[3] Center for Geomicrobiology, Aarhus University, Ny Munkegade 114, 8000 Aarhus, Denmark

An active sub-seafloor biosphere has been discovered and studied over the last decades, in particular by accessing deep habitats by Ocean Drilling. Nevertheless, how much sub-seafloor microbial activity contributes to the global biogeochemical cycles remains still largely un-assessed. Sub-seafloor microbial activity may provide a major feedback to organic carbon burial as major sink of atmospheric CO_2. Thereby, microbes mediate degradation and re-mineralization of organic matter to CO_2 through a cascade of redox processes. If all oxidants are consumed still organic matter is being fermented to methane and CO_2, whereby methane becomes mostly re-oxidized to CO_2 before it can escape into the water column. Hence, the

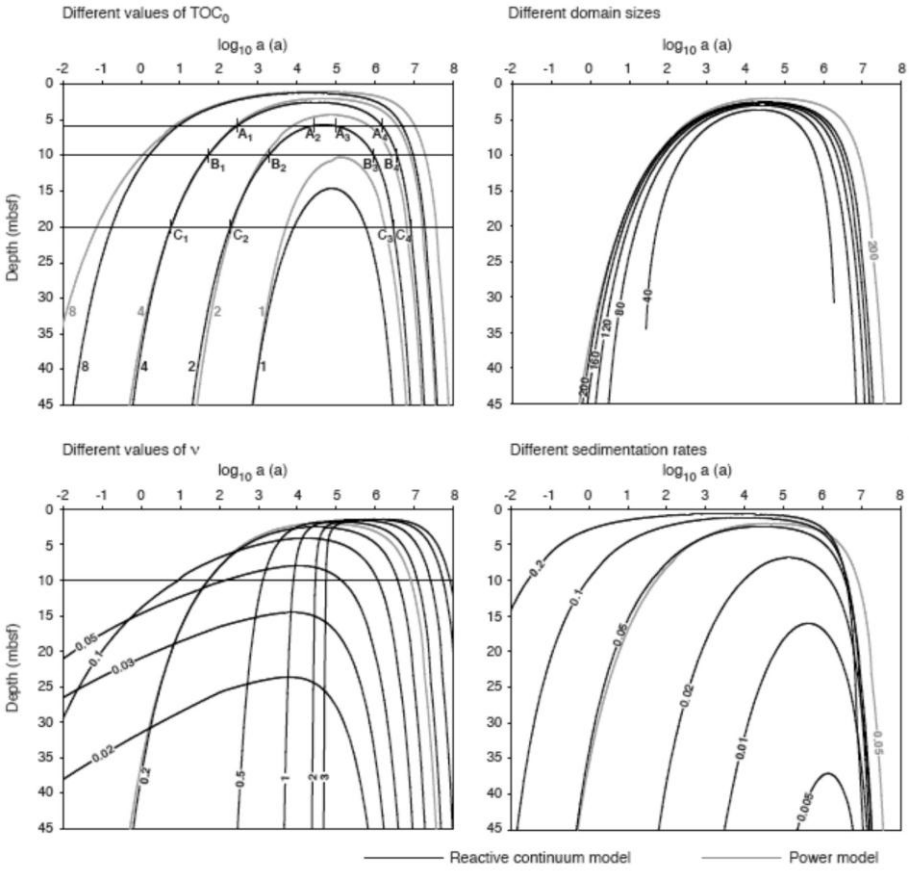

Depth of the sulphate methane interface as a function of organic matter reactivity parameters (initial age of organic matter), a_{RC} in the reactive continuum model (black lines) and a_P in the power model (grey lines), modified after Meister et al. (2013). (A) Contours of equal initial TOC (wt%; numbers in the plot). The sedimentation rate is 0.05 m/ka. The parameters a_{RC} and a_P have a similar effect on the z_{SMT} provided that ν is around 0.2 (a low ν indicates a low contribution of refractory compounds in the reactive continuum model). Letters A_1-A_4, B_1-B_4 and C_1-C_4 indicate cases of different a_{RC} but the same SMT depth. (B) Sensitivity test for different domain sizes (numbers on curves) using the same parameters as in (A). (C) Dependence of SMT depth on a_{RC} for different values of ν. The labels on the curves represent the dimensionless values of ν. TOC_0 is 2 wt%. (D) Dependence of the SMT depth on the sedimentation rate for an initial TOC of 2 wt% and ν = 0.2. The labels on the curves are sedimentation rates in (m/ka).

downward decrease of sulphate and the occurrence of methane in marine pore fluids are the most obvious features of ongoing biogeochemical activity. Therefore, porewater profiles are being analysed in marine sediments to locate and quantify ongoing metabolic processes involved in organic matter degradation. However, the interpretation of porewater profiles is controversial as the factors controlling the shapes of the profiles are not intuitively understandable.

In this study, we tried to reproduce sulphate and methane profiles as a result of degradation of different types organic matter. It is important to note that the amount of organic matter that is degraded not only depends on how much and how rapid the organic matter is buried below the seafloor, but also on the composition and reactivity. We used a reaction transport model to simulate diffusion and consumption of sulphate and production of methane coupled to different organic matter decay functions under steady state conditions. Several attempts have been made in past studies to describe degradation of organic matter. Single organic compounds may naturally decay with a first order kinetics therefore showing an exponential decrease over time of reaction. However, it was observed in many marine sedimentary settings that rates of microbial activity, which is essentially fuelled by mineralization of organic carbon, decrease as power law with increasing burial depth (e.g. Jørgensen et al., 1978). Middelburg (1989) suggested a power-law rate constant over time based on experimental results, whereas Boudreau and Ruddick (1991) treated organic matter as a pool of an infinite number of differently reactive compounds, the reactive continuum. An important factor is the initial age of organic matter, i.e. the apparent average age of the pool of organic matter at the time of deposition on the seafloor. It is understandable that younger organic matter decays more rapidly than old organic matter.

Our model results show that an organic matter pool with an initial age of less than 10^4 years shows a counter-intuitive relationship with the depth of the sulphate methane transition (SMT), i.e. a shallower SMT with higher initial age. However, the shallowest SMT depth is reached if the initial age is between 10^4 and 10^6 years, and the SMT becomes deeper if the initial age becomes larger than 10^6 years. As a consequence, for two entirely different reactivities in organic matter may lead to the same SMT depth. However, for the two identical SMT depths, the contributions of organoclastic sulphate reduction and anaerobic oxidation of methane are different. This can be derived from the shapes of the sulphate profiles, which are more curved if the organic matter is more reactive and more linear if organic matter is more refractory. This can be explained because more reactive organic matter decays rapidly at shallow burial depth in the sulphate reduction zone, and more refractory organic matter decays over a longer time period at greater depth in the methane zone.

In conclusion, the depth of the SMT depends in a counter-intuitive way on organic matter reactivity and cannot be used as a simple indicator for the organic carbon burial rate. Various shapes of sulphate and methane profiles in marine porewaters result from different kinetics of organic matter decay. This has to be taken into account for the interpretation of porewater profiles. In particular, curved sulphate profiles are to be expected in the case of relatively fresh organic matter if steady state conditions prevail. However, many sites are subject to non-steady state conditions. Future studies will have to address non-steady state conditions by modelling. For example a non-steady state upward/downward migration of the SMT has been modelled for ODP Site 1229 located on the Peru Margin. Future Ocean Drilling will be fundamental to provide high-resolution porewater profiles combined with high-resolution age dating in combination with new approaches to analyse complex organic mixtures and degradation pathways.

References:

Boudreau, B.P. and Ruddick, B.R. (1991) On a reactive continuum representation of organic matter diagenesis. *American Journal of Science* 291, 507-538.

Jørgensen, B.B. (1978) A comparison of methods for the quantification of bacterial sulfate reduction in coastal marine sediments. *Geomicrobiology* 1, 11-64.

Meister, P., Liu, B., Ferdelman, T.G., Jørgensen, B.B. and Khalili, A. (2013) Control of sulphate and methane distributions in marine sediments by organic matter reactivity. Geochim. Cosmochim. Acta 104, 183-193.

Middelburg, J.J. (1989) A simple rate model for organic matter decomposition in marine sediments. *Geochim. Cosmochim. Acta* 53, 1577-1581.

Regnier, P., Dale, A.W., Arndt, S., LaRowe, D.E., Mogollón, J. and Van Cappellen, P. (2011) Quantitative analysis of anaerobic oxidation of methane (AOM) in marine sediments: a modeling perspective. *Earth Science Reviews* 106, 105-130.

IODP

Early diagenetic quartz formation at a deep iron oxidation front in the Eastern Equatorial Pacific

PATRICK MEISTER[1], BERNHARD CHAPLIGIN[2], AUDE PICARD[1,3,4], HANNO MEYER[2], CORNELIUS FISCHER[5], GEORG AMTHAUER[6], AND IVANO W. AIELLO[7]

[1] Max-Planck Institute for Marine Microbiology, Celsiusstrasse 1, 28359 Bremen, Germany; email: pmeister@mpi-bremen.de
[2] Alfred Wegener Institute for Polar and Marine Research, Unit Potsdam, Telegrafenberg A 43, 14473 Potsdam, Germany
[3] Geomicrobiology, Center for Applied Geoscience, Eberhard Karls University, Sigwartstrasse 10, 72076 Tübingen, Germany
[4] MARUM, Center for Marine Environmental Sciences, University of Bremen, Loebener Strasse, 28359 Bremen, Germany
[5] Department of Geosciences, University of Bremen, Klagenfurter Straße, 28359 Bremen, Germany
[6] Material Sciences, University of Salzburg, Hellbrunnerstrasse 34, 5020 Salzburg, Austria
[7] Moss Landing Marine Laboratories, 8272 Moss Landing Road, Moss Landing, CA 95039-9647, U.S.A.

The formation of quartz under low-temperature early diagenetic conditions and its mechanism are still poorly understood. Nevertheless, lithified chert consisting of microcrystalline quartz was recovered at ODP Site 1226 in the Eastern Equatorial Pacific (D'Hondt et al., 2003) near the base of a 420 m thick Miocene-Holocene sequence of nanofossil and diatom ooze. Palaeo-temperatures reconstructed from $\delta^{18}O$ values in the cherts in comparison with values in the porewater (Meister et al., 2009) are near to present temperatures at the depth of the cherts (between 370 and 400 m below seafloor; mbsf). Oxygen isotopes in adjacent semi-lithified chalk are negative indicating either a formation at elevated temperatures or in the presence of an altered fluid in the past. In both cases, low reconstructed palaeo-temperatures in the cherts imply that they formed recently. Also, a sharp depletion in dissolved silica around

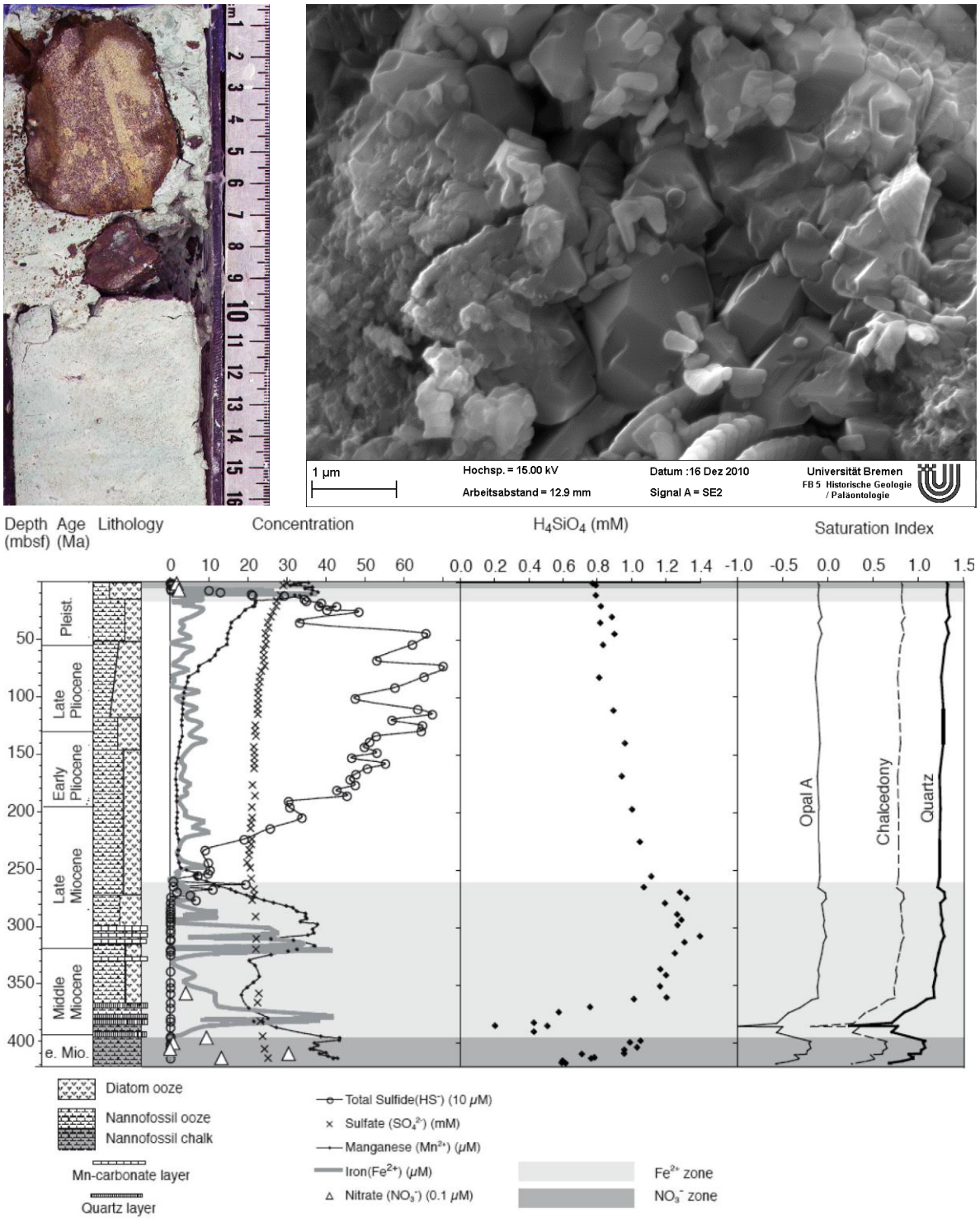

A. – top left. Core photograph showing fragment of diagnetic chert. Layers consist of microcrystalline quartz. B. – top right. Scanning electron microscope (SEM) photomicrographs of chert showing euhedral micron-scale quartz crystals and fragments of coccoliths. Well-preserved coccoliths are enclosed and cemented in chert. C. – bottom. Lithostratigraphic column at ODP Site 1226 (Eastern Equatorial Pacific), porewater chemistry, dissolved silica and saturation indices (SI) for opal A, chalcedony and quartz.

385 mbsf indicates that silica precipitation is still ongoing. As quartz is supersaturated throughout the drilled sequence – while silica concentration is buffered by opal-A dissolution – the sharp depletion of silica to concentrations at which quartz is just about saturated suggests that supersaturation could not have been the cause of silica precipitation.

It is known that newly-precipitated, poorly crystallized iron oxyhydroxides show a high affinity to silica, and quartz has been experimentally precipitated in the presence of amorphous oxyhydroxides (Harder and Flehmig, 1970). Furthermore, it is often observed that quartz precipitation is mediated by bacteria with the simultaneous formation of oxyhydroxides (Ferris et al., 1986; Konhauser et al., 1996). Indeed, a deep iron oxidation front occurs at 400 mbsf, which is caused by upward diffusing nitrate from an oxic seawater aquifer in the underlying oceanic crust (D'Hondt et al., 2003). Sequential iron extraction showed a higher content of the adsorbed iron hydroxide fraction in the chert compared to adjacent nanofossil and diatom ooze. Further analysis of the X-ray absorption near-edge structure (XANES) of bulk chert samples revealed that iron in the cherts predominantly occurs as illite and amorphous iron, whereas iron in the nanofossil and diatom ooze occurs mainly as smectites. Mössbauer spectroscopy confirmed that the amorphous iron in the cherts is largely oxidized.

Two possible mechanisms may be operative during early diagenetic chert formation at iron oxidation fronts: (1) quartz precipitation may be catalyzed by adsorption to freshly precipitated iron oxide surfaces, as observed in several experiments. (2) Also, during iron oxidation, the porewater pH is locally dropped. A slight decrease in pH may be sufficient to induce silica precipitation. We suggest that the formation of early-diagenetic microcrystalline chert at iron oxidation fronts is an important process in suboxic zones of silica-rich sediments. However, incipient chert formation may often be disturbed by bioturbation, and hard layers may only develop if the redox front is deep. The largest iron oxidation front ever, occurred when Earth's atmosphere changed from an anoxic to an oxic state – the great oxidation event – during the Palaeoproterozoic era (ca. 2.5-1.6 Ga). During this time large amounts of banded chert and iron formations were deposited.

References:

D'Hondt, S., Jørgensen, B.B., Miller, J. and ODP Leg 201 Shipboard Scientific Party (2002) Controls on microbial communities in deeply buried sediments, Eastern Equatorial Pacific and Peru Margin, Sites 1225-1231. Proc. ODP, Init. Repts. 201, College Station, TX (Ocean Drilling Program).

Ferris, F.G., Beveridge, T.J. and Fyfe, W.S. (1986) Iron-silica crystallite nucleation by bacteria in a geothermal sediment. Nature 320, 609-611.

Harder, H. and Flehmig, W. (1970) Quarzsynthese bei tiefen Temperaturen. Geochim. Cosmochim. Acta 34, 295-305.

Konhauser, K.O. and Ferris, F.G. (1996) Diversity of iron and silica precipitation by microbial mats in hydrothermal waters, Iceland: Implications for Precambrian iron formations. Geology 24, 323-326.

Meister, P., Bernasconi, S.M., Aiello, I.W., Vasconcelos, C. and McKenzie, J.A. (2009) Depth and controls of Ca-rhodochrosite precipitation in bioturbated sediments of the Eastern Equatorial Pacific, ODP Leg 201, Site 1226 and DSDP Leg 68, Site 503. Sedimentology 56, 1552-1568.

IODP

Episodes of intensified biological productivity during the termination of the Middle Eocene Climatic Optimum

I. MOEBIUS[1], O.FRIEDRICH[1], K.M.EDGAR[2], P.F.SEXTON[3]

[1] Institut für Geowissenschaften, Goethe-Universität Frankfurt, Altenhöferallee 1, 60438 Frankfurt, Germany
[2] School of Earth and Ocean Sciences, Cardiff University, Cardiff CF10 3AT, UK
[3] Department of Earth and Environmental Sciences, The Open University, Milton Keynes MK7 6AA, UK

The Eocene (55 to 34 Ma) is characterized by significant global climate change. Following the greenhouse climate of the Cretaceous, a warm climate was sustained during the Palecene-Eocene Thermal Maximum (PETM) and Early Eocene, culminating in the Early Eocene Climatic Optimum (EECO, 52-50 Ma). Thereafter, a gradual cooling took place during the middle and late Eocene (49-34 Ma) that eventually resulted in the growth of the first continental-scale ice caps on Antarctica during the Eocene-Oligocene-transition (Miller et al., 1991; Zachos et al., 1996). Superimposed on the long-term Eocene cooling trend are a series of transient global warming events as well as longer-lived warming events like the Middle Eocene Climatic Optimum (MECO; e.g. Bohaty and Zachos, 2003; Bohaty et al., 2009). The latter is a prominent ~650 kyr long warming event that interrupts the middle to late Eocene cooling at ~40 Ma. Bulk and benthic foraminiferal carbonate $\delta^{18}O$ values indicate a gradual 1.0 – 1.5 ‰ decrease during the MECO. Assuming an absence of significant continental ice sheets at this time (Bijl et al., 2010; Bohaty et al., 2009; Burgess et al., 2008; Edgar et al., 2007), this $\delta^{18}O$ excursion likely corresponds to a temperature increase of 4 – 6 °C in surface and intermediate deep waters (Bohaty and Zachos, 2003; Bohaty et al., 2009; Edgar et al., 2010). This inferred warming culminates in a $\delta^{18}O$ minima for ~50 kyrs at ~40 Ma (MECO peak warming). The MECO is also accompanied by a transient increase in atmospheric pCO_2 (~2000 to 3000 ppmv; Bijl et al., 2010) as well as a brief, global shoaling of the Carbonate Compensation Depth (CCD) on the order of 500 to 1500 m (Bohaty et al., 2009; Pälike et al., 2012). The termination of the MECO is marked by an inferred abrupt increase in $\delta^{18}O$ values and inferred cooling of up to 6°C in surface and intermediate deep waters to return to the pre-MECO long-term cooling trend. This is accompanied by a global deepening of the CCD and a proposed rapid decrease in pCO_2 (Bijl et al., 2010; Bohaty et al., 2009). The rapid nature of the cooling suggests enhanced organic carbon burial as the most likely driver for pCO_2 drawdown, while increased silicate weathering rates at this time as a possible additional (smaller) contributor (Pälike et al., 2012).

Immediately following the MECO, Spofforth et al. (2010) and Luciani et al. (2010) describe two intervals of organic-rich sediments (ORG1 and ORG2) in the Alano section (Italy) characterized by high TOC contents (2.5 – 3 %) relative to background values (0.1%), coincident with peaks in Al concentration and elevated $\delta^{13}C$ values (Spofforth et al., 2010). At the same time, Luciani et al. (2010) noted a pronounced increase in the relative abundance of the cool water, eutrophic favoring planktic foraminifera *Subbotina*, in the absence of evidence for

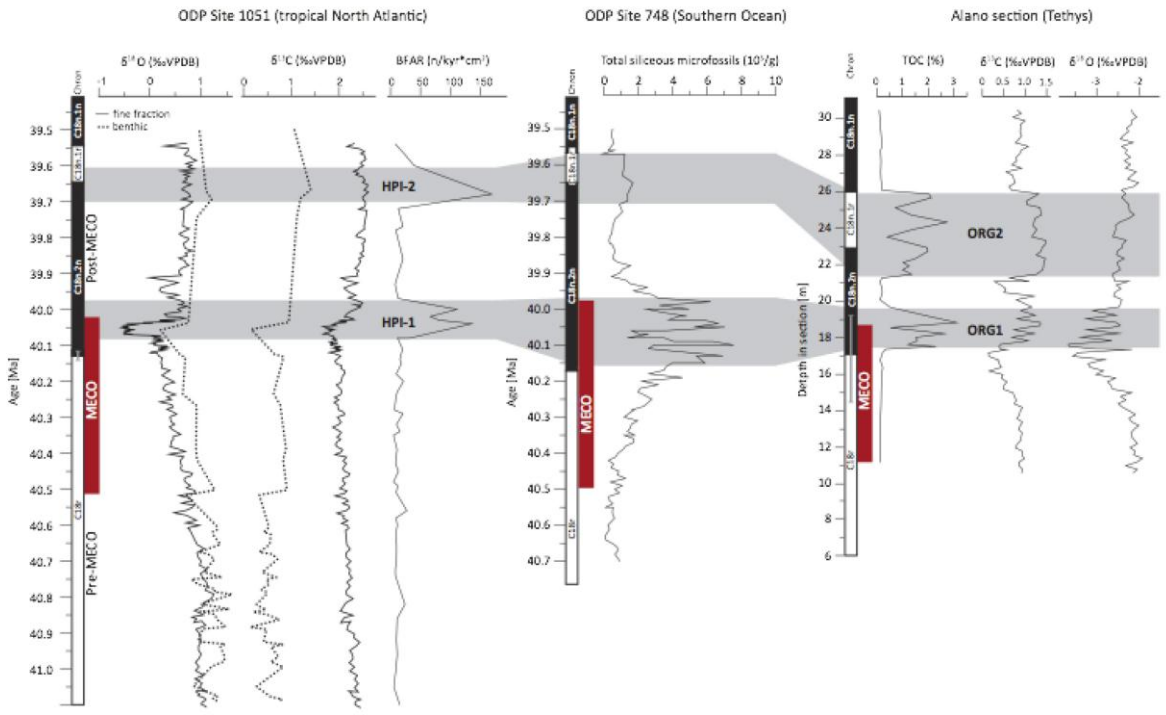

Fig. 1:. Stable isotope records (Fine-fraction isotope data (solid line) from Bohaty et al. (2009), benthic foraminiferal isotope data (dotted line) are from Edgar et al. (2010)) and benthic foraminiferal accumulation rates from ODP Site 1051 (left), total siliceous microfossil content from ODP Site 748 (Witkowski et al., 2012) (middle) and stable isotope and TOC record from Alano Section (Spofforth et al., 2010) (right). Highlighted in grey is the infered correlation of maxima in BFARs (HPI-1 and HPI-2) with total siliceous microfossil content and maxima in TOC (ORG1 and ORG2) highlighted in gray), suggesting that these events are local manifestations of a global eutophication event associated with an enhanced hydrological cycle. Differences in duration of the high-productivity intervals are most likely due to the comparison of different proxies and ocean basins and uncertainties of the placement of the boundary between Chron C18r and C18n.2n (Error-bar given in gray, for the other boundaries the error is below the detection limit).

cooling likely indicating more eutrophic surface waters in agreement with the increasing number of siliceous microfossils (Toffanin et al., 2011). To explain these observations, a regionally enhanced hydrological cycle and increased productivity subsequent to the MECO is proposed (Spofforth et al., 2010) that led to enhanced organic carbon burial in the Alano section. However, these authors suggest that the identified ORG layers may only represent a local response to a global signal associated with the termination of the MECO.

To date, the sapropel-like organic-rich sediments documented at Alano are the only such layers known from the MECO, calling into question the veracity of the organic carbon burial hypothesis as a driver for the termination of the MECO. To test this hypothesis, we investigate any evidence for an increase in ocean trophic state and associated biological productivity during the MECO from a more open-ocean setting.

For this purpose we present new benthic foraminiferal assemblage data from ODP Site 1051 (Blake Plateau, 30°N) in the western North Atlantic. The investigated record spans the Middle Eocene Climatic Optimum (MECO) and post-MECO interval (41.1 to 39.5 Ma). Within this succession, 52 samples were analyzed with respect to benthic foraminiferal assemblages and benthic foraminiferal accumulation rates (BFARs) based on the >125 µm size fraction. Classification was carried out to the species level whenever possible mainly following Bolli et al. (1994) and Tjalsma and Lohman (1983). Benthic foraminifera accumulation rates (BFAR) were calculated following Herguera and Berger (1991) and are calculated by assuming that sedimentation rates remained constant between magnetochron datums. The age model employed in this study is based on the revised ODP Site 1051 magnetostratigraphy by Edgar et al. (2010). All ages are reported on the timescale of (Cande and Kent, 1995).

The goals of this study are to (1) document changes in the benthic foraminifera assemblages associated with the MECO, (2) determine whether there is any evidence in the North Atlantic Ocean for ‘high-productivity’ events at the peak and following the MECO, (3) to test whether TOC pulses at Alano are indeed productivity (rather than preservation) controlled, (4) to constrain the age and duration of these events and (5) ultimately evaluate competing hypotheses for the termination of the MECO.

We find that benthic foraminiferal assemblages at ODP Site 1051 are diverse and preservation is typically sufficient to identify foraminifera to the species level. A total of 48 benthic foraminiferal taxa were identified, with 20 genera having an average relative abundance of >1% in the samples. Across the investigated 2 million year long time interval, benthic foraminiferal assemblages are typical of tropical Eocene environments and notably show only minor changes in species composition and/or abundance during the MECO. The muted biotic response implies that benthic foraminifera were relatively insensitive to the environmental changes that were occurring during the MECO. This may imply that the gradual rate of environmental change that accompanied the MECO allowed benthic foraminifera to adapt. However, there are

pronounced changes in the accumulation of benthic foraminifera during and after the MECO (Fig. 1). BFARs are generally very low (on average 23 n/cm^2/kyr) throughout the studied section, partially due to dilution by abundant siliceous microfossils (Edgar et al., 2010; Norris et al., 1998, qualitative observation on the analysed samples). However, during two short-lived intervals between 40.07 to 39.98 Ma and 39.70 to 39.62 Ma, BFARs increase by an order of magnitude (110-130 n/cm^2/kyr). BFARs are traditionally employed as an indicator of export productivity from surface waters with high BFAR values reflecting enhanced food availability (e.g. Herguera and Berger, 1991; Jorissen et al., 2007; Van der Zwaan et al., 1999). Therefore, we interprete these two transient intervals of elevated BFARs during the final stages of and following the MECO as intervals of increased of productivity.

The onset of the first inferred high-productivity interval (HPI-1) is synchronous with a significant decrease in $\delta^{18}O$ values thought to correspond to the rapid warming at the peak of the MECO and extends ~20 kyrs after the MECO. Notably, at 40.02 Ma, BFARs briefly decrease (but do not return to background values) contemporaneous with the rapid increase in $\delta^{18}O$ and inferred ocean cooling marking the end of the MECO. The second high-productivity interval (HPI-2) occurs ~300 ka later than HPI-1 (Fig. 3) and ~100 kyrs after the MECO. Benthic foraminiferal assemblage data tentatively suggest that HPI-1 and HPI-2 are associated with slightly reduced bottom-water oxygenation relative to background values. Benthic indicators of dysoxia or anoxia are, however, absent in the assemblages.

Several mechanisms could be responsible for the proposed increase in surface- and corresponding bottom-water productivity: (1) a change in ocean circulation, (2) upwelling of nutrient-rich waters, and (3) increasing continental runoff. While a change in ocean cirulation in not likely due to the lack of response of the benthic foraminiferal assemblage composition, it is not possible to distinguish between an upwelling or run-off driven hypothesis for an increase in productivity at ODP Site 1051 from our data set alone. Therefore, it is crucial to compare our results with near-shore sites in other settings to ascertain whether this change in productivity in a local (controlled by upwelling or run-off) or a global signal (run-off controlled).

It appears that our HPIs can be correlated with the organic-rich layers termed ORG1 and ORG2 identified in the Alano section in northern Italy (Luciani et al., 2010; Spofforth et al., 2010) that are characterized by significant increases in TOC. Increases in surface and export productivity have been invoked to explain these organic-rich intervals (Spofforth et al., 2010). Similar intervals of relative eutrophication are also reported from the Kerguelen Plateau in the Southern Ocean (Witkowski et al., 2012), who found that siliceous microfossil abundances reached maxima during the MECO peak warming (40.15 – 39.97 Ma) and between 39.7 – 39.55 Ma, indicative of enhanced surface water productivity and broadly correlative with our HPI-1 and HPI-2 intervals (Fig. 1).

Due to the occurrence of both of our high productivity events (HPI-1 and 2) in different oceanographic settings and ocean basins (e.g., proximal and distal to continent and in the Southern, Tethyan Oceans and Atlantic Ocean, respectively), we suggest that these productivity events are of global significance. Thus, localized changes in the position or intensity of upwelling are unlikely to be responsible for a global increase in productivity. Therefore, we suggest in accordance with Spofforth et al. (2010) an enhanced hydrological cycle as the driver of a global increase in surface water productivity. Parallel to MECO peak warming, continental precipitation might have increased, leading to enhanced runoff and nutrient availability.

In order to explain the abrupt cooling at the end of the MECO at ~40.03 Ma and a coincident global deepening of the CCD, a distinct drawdown in pCO_2 has been suggested for the termination of the MECO (Bohaty et al., 2009; Pälike et al., 2012). The hypothesis that an increase in the burial of organic carbon could cause a decrease in pCO_2 is, at least in part, supported by the discovery of TOC-enriched horizons following the MECO in the Alano section (Spofforth et al., 2010). Our new evidence highlighting the potentially global occurrence of high-productivity events associated with the termination of the MECO provides further support for the organic carbon burial hypothesis as a viable mechanism for pCO2 drawdown suggested by Bohaty et al. (2009) and Spofforth et al. (2010). Additionally, the good magnetostratigraphy at Site 1051 enables us to refine the dating of these events to 40.07 – 39.98 Ma (HPI-1) and 39.70 – 39.62 Ma (HPI-2), suggesting durations of ~90 and ~80 kyrs, respectively.

References:

Bijl, P.K., Houben, A.J.P., Schouten, S., Bohaty, S.M., Sluijs, A., Reichart, G.-J., Sinninghe Damsté, J.S., Brinkhuis, H., 2010. Transient Middle Eocene Atmospheric CO2 and Temperature Variations. Science 330, 819-821.

Bohaty, S.M., Zachos, J.C., 2003. Significant Southern Ocean warming event in the late middle Eocene. Geology 31, 1017.

Bohaty, S.M., Zachos, J.C., Florindo, F., Delaney, M.L., 2009. Coupled greenhouse warming and deep-sea acidification in the middle Eocene. Paleoceanography 24, PA2207.

Bolli, H.M., Beckmann, J.P., Saunders, J.B., 1994. Benthic foraminiferal biostratigraphy of the south Caribbean region. Cambridge Univ Pr.

Burgess, C.E., Pearson, P.N., Lear, C.H., Morgans, H.E.G., Handley, L., Pancost, R.D., Schouten, S., 2008. Middle Eocene climate cyclicity in the southern Pacific: Implications for global ice volume. Geology 36, 651-654.

Cande, S.C., Kent, D.V., 1995. Revised calibration of the geomagnetic polarity timescale for the Late Cretaceous and Cenozoic. Journal of Geophysical Research: Solid Earth 100, 6093-6095.

Edgar, K., Wilson, P., Sexton, P., Gibbs, S., Roberts, A., Norris, R., 2010. New biostratigraphic, magnetostratigraphic and isotopic insights into the Middle Eocene Climatic Optimum in low latitudes. Palaeogeography, Palaeoclimatology, Palaeoecology, 670–682.

Edgar, K.M., Wilson, P.A., Sexton, P.F., Suganuma, Y., 2007. No extreme bipolar glaciation during the main Eocene calcite compensation shift. Nature 448, 908-911.

Herguera, J.C., Berger, W., 1991. Paleoproductivity from benthic foraminifera abundance: Glacial to postglacial change in the west-equatorial Pacific. Geology 19, 1173-1176.

Jorissen, F.J., Fontanier, C., Thomas, E., 2007. Chapter Seven Paleoceanographical Proxies Based on Deep-Sea Benthic Foraminiferal Assemblage Characteristics. Developments in Marine Geology 1, 263-325.

Luciani, V., Giusberti, L., Agnini, C., Fornaciari, E., Rio, D., Spofforth, D.J.A., Pälike, H., 2010. Ecological and evolutionary response of Tethyan planktonic foraminifera to the middle Eocene climatic optimum (MECO) from the Alano section (NE Italy). Palaeogeography, Palaeoclimatology, Palaeoecology 292, 82-95.

Miller, K.G., Wright, J.D., Fairbanks, R.G., 1991. Unlocking the Ice House: Oligocene-Miocene Oxygen Isotopes, Eustasy, and Margin Erosion. J. Geophys. Res. 96, 6829-6848.

Norris, R.D., Kroon, D., Klaus, A., 1998. Initial report Site 1051. Proceedings of the Ocean Drilling Program 171B.

Pälike, H., Lyle, M.W., Nishi, H., Raffi, I., Ridgwell, A., Gamage, K., Klaus, A., Acton, G., Anderson, L., Backman, J., 2012. A Cenozoic record of the equatorial Pacific carbonate compensation depth. Nature 488, 609-614.

Spofforth, D.J.A., Agnini, C., Pälike, H., Rio, D., Fornaciari, E., Giusberti, L., Luciani, V., Lanci, L., Muttoni, G., 2010. Organic carbon burial

following the middle Eocene climatic optimum in the central western Tethys. Paleoceanography 25, PA3210.
Tjalsma, R.C., Lohmann, G., 1983. Paleocene-Eocene bathyal and abyssal benthic foraminifera from the Atlantic Ocean. Micropaleontology Pr.
Toffanin, F., Agnini, C., Fornaciari, E., Rio, D., Giusberti, L., Luciani, V., Spofforth, D.J.A., Pälike, H., 2011. Changes in calcareous nannofossil assemblages during the Middle Eocene Climatic Optimum: Clues from the central-western Tethys (Alano section, NE Italy). Marine Micropaleontology 81, 22-31.
Van der Zwaan, G., Duijnstee, I., Den Dulk, M., Ernst, S., Jannink, N., Kouwenhoven, T., 1999. Benthic foraminifers: proxies or problems?:: A review of paleocological concepts. Earth-Science Reviews 46, 213-236.
Witkowski, J., Bohaty, S.M., McCartney, K., Harwood, D.M., 2012. Enhanced siliceous plankton productivity in response to middle Eocene warming at Southern Ocean ODP Sites 748 and 749. Palaeogeography, Palaeoclimatology, Palaeoecology 326, 78-94.
Zachos, J.C., Quinn, T.M., Salamy, K.A., 1996. High-Resolution (104 Years) Deep-Sea Foraminiferal Stable Isotope Records of the Eocene-Oligocene Climate Transition. Paleoceanography 11, 251-266.

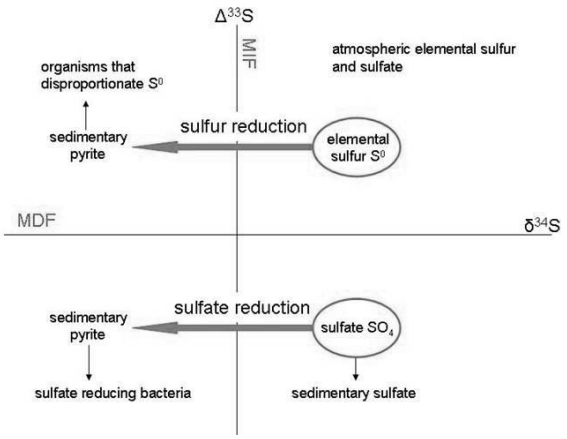

Fig. 1 Two metabolic pathways followed by early organisms.

ICDP

Peering into the Cradle of Life:

multiple sulfur isotopes reveal insights into environmental conditions and early sulfur metabolism some 3.5 Ga ago

A. MONTINARO[1], H. STRAUSS[1], P. MASON[2]

[1] Institut für Geologie und Paläntologie, Westfälische Wilhelms-Universität Münster, Münster, Germany
[2] Department of Earth Science, Utrecht University, Utrecht, The Netherlands

During the early stages of Earth's evolution, environmental conditions were much different from today. Early Earth was characterized by a predominance of oceanic over continental crust, more vigorous mantle convection and presumably warmer surface temperatures (Knauth, 2005). The early atmosphere was reducing with abundant carbon dioxide and methane but largely devoid of oxygen ($<10^{-5}$ PAL – present atmospheric level), while the ocean was anoxic (Holland, 2002). Hence, life emerged and evolved under seemingly inhospitable environmental conditions. The low oxygen concentration in the atmosphere ended with the Great Oxidation Event at 2.4–2.3 Ga (Pufahl and Hiatt, 2012). Apart from more classical petrographic evidences for an anoxic atmosphere (e.g., the occurrence of detrital reduced minerals) a key observation is the presence of mass-independent fraction of sulfur isotopes (MIF-S) preserved in terrestrial rocks. The preservation of distinctly different $\Delta^{33}S$ signals in the sedimentary realm is possible only under anoxic atmospheric conditions, with a maximum level of atmospheric oxygen of 10^{-5} PAL (Pavlov and Kasting, 2002), thus, anoxic conditions of Earth's atmosphere.

Indications for early life on Earth derives from different proofs: microfossils, stromatolites and chemofossils, i.e. chemical and isotopic signatures related to metabolic pathways. In particular, the stable isotopes of key elements of life, i.e. C, N and S have been utilized successfully for tracing life in Earth's respective archive, i.e. the sedimentary rock record. One of the most intriguing questions in Earth and Life Sciences is where, when and under what conditions life emerged on our planet.

This multinational and multidisciplinary ICDP project aims at investigating which environmental conditions existed when life emerged and evolved on our planet.
A systematic and comprehensive multiple sulfur isotope (^{32}S, ^{33}S, ^{34}S, and ^{36}S) study is being pursued for understanding the early sulfur cycle, prevailing overall environmental and redox conditions in particular, as well as for tracing life on Earth (Fig. 1). The minor isotopes ($\Delta^{33}S$, $\Delta^{36}S$) identify an atmospheric source of sulfur compounds whereas the traditional $\delta^{34}S$ values reflect microbial sulfur metabolism. As a matter of fact, generally, bacteria prefer the lighter isotope for their metabolism, allowing the precipitation of ^{34}S-depleted pyrite.

However, sulfur fractionation is not constant through Earth's history. The present day sulfur cycle is deeply different from the Archean cycle, with the latter being dominated only by volcanogenic input and not by oxidative

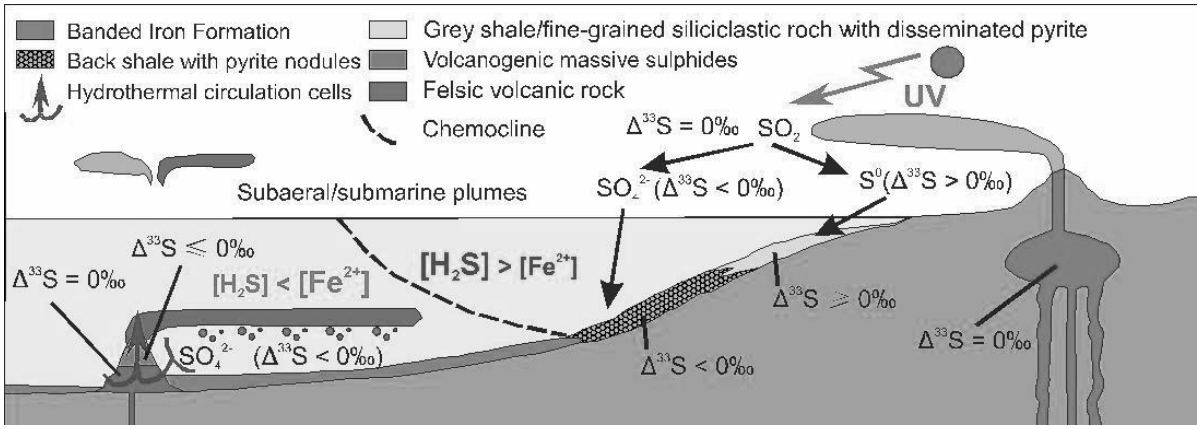

Fig.2 Sulfur isotope composition of depositional environments influenced by mass independent fractionation in the Archean anoxic ocean and atmosphere (Bekker et al., 2009, modified).

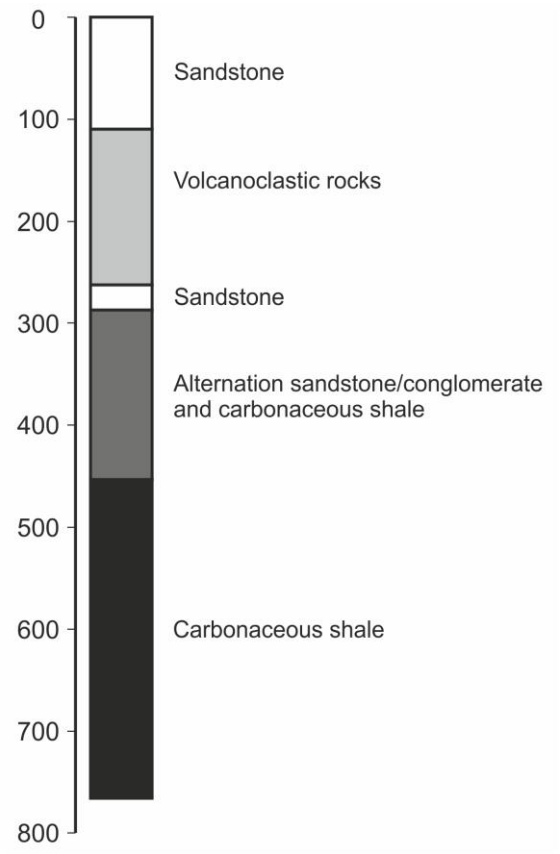

Fig. 3 Main lithologies in BARB5.

continental weathering. The volcanogenic emissions of SO_2 and H_2S are characterized by a $\Delta^{33}S$ value of 0‰. Ultraviolet photolysis of volcanogenic SO_2 generates elemental sulfur (reduced to sulfide) with positive $\Delta^{33}S$ and sulfate (dissolved in the ocean) with negative $\Delta^{33}S$ values, i.e. clearly mass-independently fractionated sulfur compounds (Bekker et al, 2009). Both products are being transferred to Earth surface environments, thereby delivering distinctly different sulfur isotope signals (Fig. 2).

This study focuses on the 3.55–3.23 billion years old Barberton Greenstone Belt in South Africa as one of the oldest well preserved rock successions from the earliest part of Earth history. This greenstone belt is characterized by a sequence of volcanic and sedimentary rocks. The latter have archived environmental conditions prevailing at the surface of our young planet.

Specifically, ICDP drill core BARB5 was obtained from the Barite Syncline, and preliminary results are reported for samples from the Mapepe Formation, Fig Tree Group. The lowest part is mostly composed of carbonaceous shale, the middle part of sandstone and conglomerate intercalated with carbonaceous shale while the upper part comprises volcanoclastic rocks. The uppermost sandstone is mostly alterated and weathered. Total core length is 763.23 m (Fig. 3).

From powdered bulk samples total carbon (TC), total sulfur (TS) and total inorganic carbon (TIC) were measured via IR spectroscopy of CO_2 and SO_2 using a CS-MAT 5500 instrument.

Isotope analyses, acid-volatile sulfide (AVS) and chromium-reducible sulfur (CRS) were extracted from bulk rock and precipitated as silver sulfide (Ag_2S). Resulting silver sulfides are then subjected to multiple sulfur isotope measurements (^{32}S, ^{33}S, ^{34}S, ^{36}S), performed using a ThermoFinnigan MAT 253 following the fluorination of sulfide precipitates (international reference material: IAEA-S1).

Total sulfur abundance ranges between 0.01 and 3.03 wt.% (avg. 0.29 wt.%; n=92), while total carbon bundances vary between 0.15 and 10.29 wt.% (avg. 2.98 wt.%; n=92). In addition, total inorganic carbon varies between 0.03 and 8.82 wt.% (avg. 1.98 wt.%; n=58). Thus, total organic carbon ranges from 0.12 to 2.28 wt.% (avg. 1.30 wt.%; n=58). (Fig. 4).

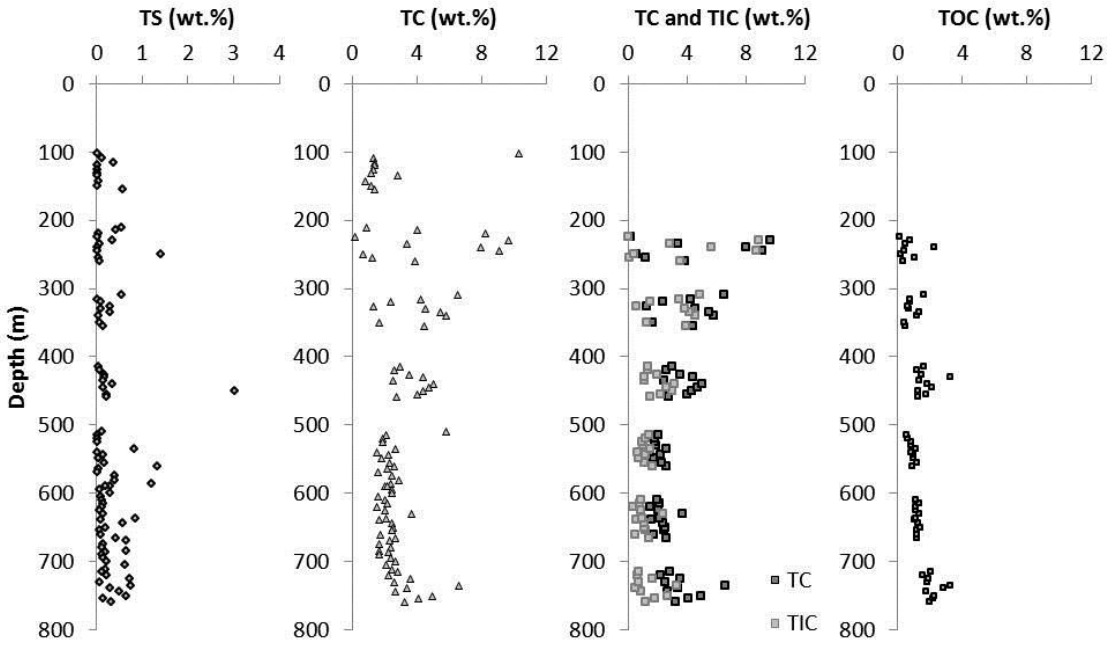

Fig. 4 Total sulfur, total carbon, differences between total carbon and total inorganic carbon and total organic carbon for BARB5 samples

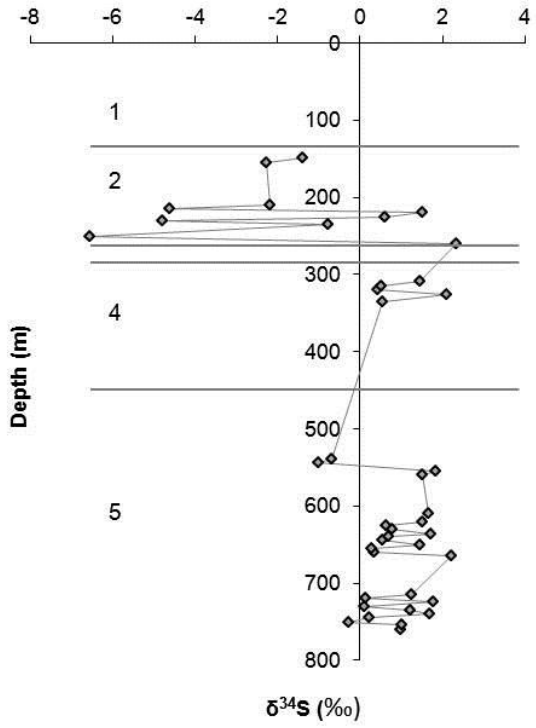

Fig. 5 $\delta^{34}S$ values of BARB5 samples plotted again depth. 1: sandstone; 2: volcanoclastic rocks; 3: sandstone; 4: alternation of sandstone/conglomerate and carbonaceous shale; 5: carbonaceous shale.

The carbonaceous shale displays a sulfur isotopic composition ($\delta^{34}S$) between -0.09 and 2.21‰ (avg. 0.88‰; n=33) (Fig. 5 number 5); volcanoclastic rocks show $\delta^{34}S$ values ranging from -6.57 to 2.32‰ (avg. -2.19‰; n=9) (Fig. 5 number 2); sandstone and conglomerate are characterized by a $\delta^{34}S$ composition between 1.51 and 2.11‰ (avg. 1.84‰; n=3) (Fig. 5 number 3 and 4).

Similar to $\delta^{34}S$, $\Delta^{33}S$ values are different for each lithofacies. Samples from the carbonaceous shale yielded a range between 0.41 and 2.33‰ (avg. 0.97‰, n=33), so values are positive, while volcanoclastic rocks show values between -0.32 and 0.20‰ (avg. -0.10‰, n=9) and sandstone and conglomerate between 0.14 and 0.61‰ (avg. 0.50‰, n=3) (Fig. 6). Furthermore, samples reveal a linear negative correlation between the $\Delta^{33}S$ and $\Delta^{36}S$ with a slope of -0.8, typical for Archean sedimentary sulfides (Fig. 6 B).

Some preliminary conclusions can be drawn from these first results of ICDP BARB5 core. Each lithofacies is characterized by a different isotopic composition. Clearly, $\Delta^{33}S$ values in carbonaceous shale reflect mass-independent sulfur isotope fractionation, hence an atmospheric signal, while volcanoclastic rocks display a strong mass-dependent fractionation. This could represent a biotic signal, but alternatives have been proposed, i.e. a fractionation of the sulfur isotopic signal related to the volcanic activities (Philippot et al., 2012).

Acknowledgements: Financial support from the Deutsche Forschungsgemeinschaft (DFG Str 281/36) is gratefully acknowledged.

References:

Bekker, A., Barley, M.E., Fiorentini, M. L., Rouxel O.J., Rumble, D., Beresford, S.W., 2009. Atmospheric sulfur in Archean Komatiite-hosted Nickel deposits. Science 326, 1086-1098.

Holland, H.D., 2002, Volcanic gases, black smokers, and the Great Oxidation Event. Geochim. Cosmochim. Acta 66: 3811-3826.

Knauth, L.P., 2005. Temperature and salinity history of Precambrian ocean: implications for the course of microbial evolution. Palaeogeogr. Palaeclimat. Palaeoecol. 219: 53-69.

Pavlov, A.A., and Kasting, J.F., 2002. Mass-independent fractionation of sulphur isotopes in Archaean sediments: strong evidence for an anoxic Archaean atmosphere. Astrobiology 2: 27-41.

Philippot et al 2012. Variations in atmospheric sulphur chemistry on early Earth linked to volcanic activity. Nature Geoscience: Volume 5, Pages 668-674

Pufahl, P., Hiatt, E., 2012. Oxygenation of the Earth's atmosphere-ocean system: A review of physical and chemical sedimentologic responses. Marine and Petroleum Geology, 32:1–20.

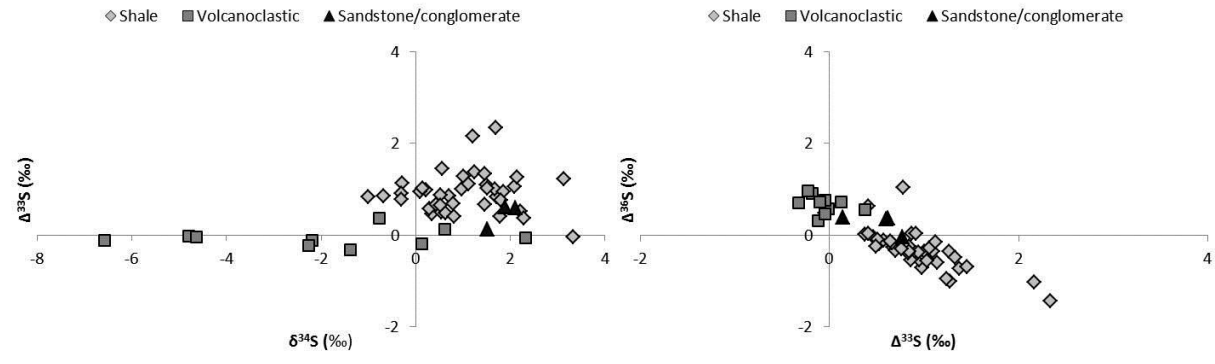

Fig. 6 Multiple sulfur isotopes for the three main lithologies in BARB5 samples

ICDP

3-D velocity structure of upper crust beneath NW Bohemia/Vogtland

S. MOUSAVI[1], M. KORN[1], K. BAUER[2] , D. RÖßLER[3]

[1] Institut für Geophysik und Geologie, Universität Leipzig, Talstraße 25, 04103 Leipzig
[2] Deutsches Geoforschungszentrum Helmholtz-Zentrum Potsdam
[3] DTU Space, Technical University of Denmark, 2800 Kgs. Lyngby, Dänemark

We present preliminary results from a travel time tomography investigation of the upper crust beneath west Bohemia/Vogtland region which is characterized by a series of phenomena like occurrence of repeated earthquake swarms, surface exhalation, CO2 enriched fluids, mofettes, mineral springs and enhanced heat flow. This region is an excellent location for an ICDP drilling project targeted to a better understanding of the crust in an active magmatic environment.

The data set were taken from permanent and temporary seismic networks in Germany and Czech Republic from 2000 to 2010, as well as active seismic experiments like Celebration 2000 and quarry blasts. Seismic Handler was applied for picking P and S wave arrival times. Before travel time inversion, we selected 399 events which were recorded by 9 or more stations and azimuthal gap < 160◦.

In the first step a simultaneous inversion of P and S wave 1-D velocity models together with relocations of hypocenters and station corrections was performed. To test the reliability of earthquake locations we performed two experiments: first relocation of randomly perturbed earthquakes in the preferred 1-D velocity model, second mislocations of shots to check the accuracy of the earthquake positions.

In the next step, 3-D tomography was performed. The obtained minimum 1D velocity model was used as starting model for the 3-D Vp and Vp/Vs velocity models. P and S wave travel time tomography employs damped least-square method and ray tracing by pseudo-bending algorithm. For model parametrization different cell node spacings have been tested to evaluate the resolution in each node. Synthetic checkerboard tests have been done to check the structural resolution. Then Vp and Vp/Vs in the preferred 3D grid model have been determined. Earthquakes locations in iteration process change till the hypocenter adjustments and travel time residuals become smaller than the defined thereshold criteria. Finally the analysis of the resolution depicts the well resolved features for interpretation. We observed lower Vp/Vs ratio in depth of 5-10 km close to the foci of earthquake swarms and higher Vp/Vs ratio is observed in Saxoturingian zone and surrounding area.

ICDP

Formation processes of fast-spreading oceanic crust: Evidence from the "Wadi Gideah" cross section in the Oman Ophiolite

T. MÜLLER[1], J. KOEPKE[1], D. GARBE-SCHÖNBERG[2], P.E. WOLFF[1], H. STRAUSS[3]

[1] Institut für Mineralogie, Leibniz Universität Hannover, Germany (t.mueller@mineralogie.uni-hannover.de)
[2] Institut für Geowissenschaften, Christian-Albrechts-Universität zu Kiel, Germany
[3]Institut für Geologie und Paläontologie, Westfälische Wilhelms-Universität Münster, Germany

Ocean crust formed at fast-spreading rates is known to display relatively uniform seismic stratigraphy. In contrast to oceanic crust generated at slow-spreading ridges, it is regarded as layered and relatively homogeneous. Therefore theoretical models on magma accretion of oceanic crust, thermal models, general alteration models and mass balance calculations for complete oceanic crust are only existent for fast-spreading systems. Due to the poor access to deeper parts of the oceanic crust of fast-spreading systems, as well as the general lack of drill sections reaching the deep basement of fast-spread crust, most models for this are not tested by using natural samples. Ophiolites, like the Oman Ophiolite, representing ancient oceanic crust obducted on continents, offer a possibility for complementary studies and play a vital role in developing crucial paradigms for understanding sea floor spreading.

We undertook three detailed field campaigns in the Wadi Gideah, which is located in the Wadi-Tayin Massif in the southern part of the Oman Ophiolite, sampling a complete section through oceanic crust. The southern massifs of the Oman Ophiolite are regarded as the best area for studying primary “normal” fast-spreading ridge processes with so-called “late-stage magmatism” being widely absent. Our profile contains 223 samples representing mantle peridotite, gabbro, dikes and lavas. Therefore, we assume that this profile is representative for fast-spread oceanic crust in terms of completeness of the crust-forming structural components as well as coherence of geochemical and petrological data to be obtained. Thus it´s well suited for shedding light on accretion processes and the evolution of primary and secondary geochemical cycles of fast-spreading oceanic crust.

We follow the concept of performing all analytical investigations, like analyses of major- and trace elements and isotopes, on the same samples to create data sets as coherent as possible. At the same time considerable effort is made to optimize procedures for sample preparation and ultra-trace analysis. With our study we follow the initial approach of an US-working group in the 1970´s to obtain a complete compositional profile through the Oman Ophiolite (Pallister & Hopson, 1981) in the same Wadi.

Here we present our data obtained so far focusing on first geochemical and petrological logs of the Wadi-Gideah section. The main interest of the project is to focus on mineral chemical- as well as bulk major/trace element compositional evolution with profile depth.

With the structural data obtained during the field campaigns we reconstructed the layered stratigraphy of a virtually undeformed oceanic crust with a thickness of approximately 6 km. We identified pillow lavas (600 m), sheeted dikes (1300 m), varitextured gabbros (400 m),

foliated gabbros (1600 m) and layered gabbros (2200 m) as main lithologies from top to bottom (estimated thickness in parenthesis), resting upon a very thin MOHO transition zone (<50 m) on the mantle sequence.

First results based on electron microprobe analyses of the constituent mineral phases of the gabbroic section reveal compositions of XMg (Mg/(Mg+Fe) of olivine molar from 0.76 to 0.82, XMg clinopyroxene from 0.82 to 0.91 and An% plagioclase from 79 to 85 mol% for the layered gabbro sequence. Foliated gabbros display more scattering in the mineral data, and show slightly more evolved compositions of XMg olivine from 0.65 to 0.74, XMg clinopyroxene from 0.74 to 0.87 and An% plagioclase from 62-82 mol%. Compositions of varitextured gabbros seem to be more evolved as displayed by An% plagioclase from 60 to 85 mol%. These general trends in mineral chemistry are also discernable in bulk rock major and trace element data. While layered gabbro cumulates show only minor variability for most elements over the entire thickness systematic trends in La/Sm, La/Yb, Zr/Hf, Nb/Ta, Cr/Zr etc. can be observed in the transition from foliated gabbros and varitextured gabbros towards sheeted dikes and basalts. This bulk rock data will be complemented by trace element micro analytical data for the different minerals. Supplementary data for strontium, hafnium, neodymium, and sulfur isotopic composition will be generated in near future.

Our comprehensive compositional data set forms a sound basis for testing the existing conceptual models for the accretion of fast-spreading oceanic crust. Far reaching goals include to elaborate a complete mass balance for fast-spreading oceanic crust and to establish the hydrothermal alteration cycles for deep fast-spread oceanic crust. In addition, the obtained reference profile will provide scientific support for the “Oman Ophiolite Drilling Project” (full proposal submitted 15. Jan. 2013; lead PI: Peter Kelemen) within the ICDP (Integrated Continental Drilling Program) and also for IODP (Integrated Oceanic Drilling Program) drilling at Site 1256 (equatorial pacific) where a complete section from lavas through sheeted dikes down to the uppermost gabbros is available as well as for IODP Drilling 345 Hess Deep, where deep layered gabbros were recently drilled.

IODP

The development of the Western Boundary Undercurrent (WBUC) in a changing climate since the beginning of the Miocene

A. MÜLLER-MICHAELIS[1], G. UENZELMANN-NEBEN[1]

[1] Alfred-Wegener-Institut Helmholtz-Zentrum für Polar- und Meeresforschung, Am Alten Hafen 26, 27568 Bremerhaven

The present deep Western Boundary Undercurrent (WBUC) at the Eirik Drift off the southern tip of Greenland is mainly fed by the overflows over the Greenland-Scotland ridge (GSR), the Denmark Strait Overflow Water (DSOW) and Iceland-Scotland Overflow Water (ISOW), respectively (Fig. 1). Interactions of the atmosphere with the warm and saline Atlantic surface inflow to the Norwegian-Greenland Sea (NGS) yield in convective mixing and the production of these dense overflow water masses *(Van Aken, 2007)*. Therefore, the WBUC at the Eirik Drift is sensitive to changes in the deep-water formation and hence, to climate changes. Changes in the WBUC will, in turn, affect the world's climate. The WBUC is the main contributor to the lower branch of the North Atlantic Thermohaline Circulation (THC). The upper counterpart of the THC is responsible for the global redistribution of heat and freshwater via the surface ocean.

The Eirik Drift has been shaped by the WBUC since the Miocene. It therefore archives information of changes in depositional processes and hence, changes in the pathways and strength of the WBUC.

The high-resolution multichannel seismic reflection data network collected during RV *Maria S. Merian* cruise MSM 12/2 crossed ODP Leg 105 Site 646 and IODP Expedition 303 Sites U1305, U1306, and U1307 (Fig. 1). Thus, the seismic reflection data could be incorporated with geological information from the ODP and IODP sites *(Channell et al., 2010; Srivastava et al., 1989)* to deduce information on the development of the WBUC and a much clearer understanding of the evolution of the climate in the northern North Atlantic during the Neogene.

Synthetic seismograms based on density and P-wave velocity data from ODP Leg 105 Site 646 and IODP Expedition 303 Sites U1305, U1306, and U1307 were correlated with the processed seismic reflection data. We identified four seismic units and the reflectors defined by *Arthur et al. (1989)* and refined the stratigraphy by horizons A1 (0.8 Ma), A2 (1.4 Ma) and A3 (19-17 Ma) (Table 1).

We tracked the reflectors and seismic units from ODP Leg 105 Site 646 over our complete study area. The erosional and depositional centers of each (sub)unit were interpreted with respect to the prevailing deep current activity. The shapes and locations of the depocenters of the seismic (sub)units as well as the internal structure and reflection characteristics are used to decipher the changes in the WBUC's pathways and intensity in the study area. In sediment drifts deposited under the influence of along-slope processes, unit thinning, converging internal reflections and reflector truncations indicate the erosional centers of deep current cores. In the Northern Hemisphere, the depocenters with diverging internal reflections are found to the right of the deep current flow *(Faugères et al., 2008; Faugères et al., 1999; Nielsen et al., 2008)*. The location and orientation of the depocenters as well as the morphology of the basal horizons help to connect the erosional centers to pathways over the study area as contour currents follow certain depth ranges. We observe shifts in the location and orientation of the depocenters and crest migrations among the seismic subunits. This indicates a highly variable deep current activity at the Eirik Drift. The interpretation of our data leads to a model of the paleocirculation at the Eirik Drift with pathways and intensity of the WBUC. Here, the observations in every (sub)unit and their interpretations are discussed with respect to the evolution of deep currents, shifts in deep water formation regions and climate changes in the northern North Atlantic.

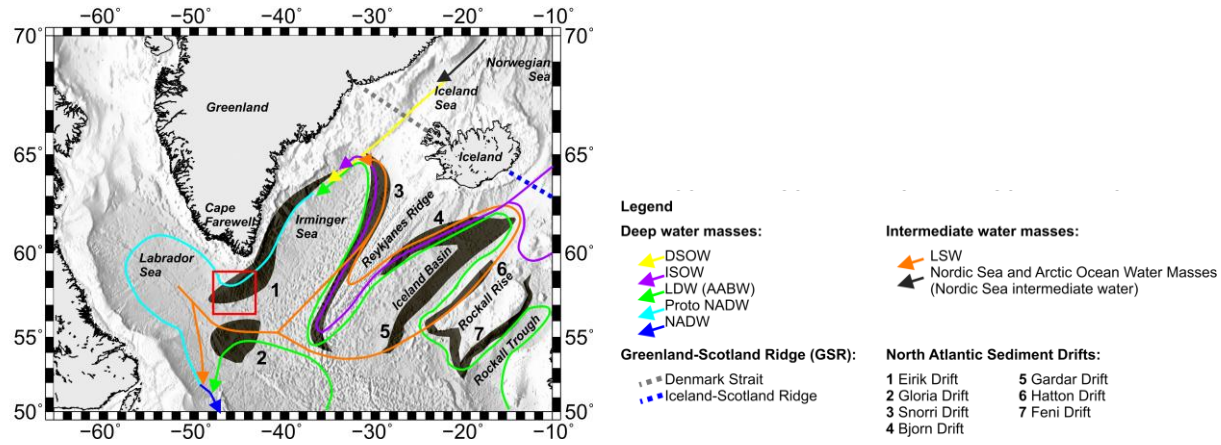

Figure 1: Satellite bathymetry map (*Smith and Sandwell*, 1997) including basins, ridges, sediment drifts and the prevailing current system of the North Atlantic. The present WBUC at the Eirik Drift transports mainly North Atlantic Deep Water (NADW), which consist of Denmark Strait Overflow Water (DSOW), Iceland-Scotland Overflow Water (ISOW), Lower Deep Water (LDW; also: modified Antarctic Botom Water (AABW)) and Labrador Sea Water (LSW). The red box shows the location of our seismic profiles and of ODP Leg 105 Site 646 and IODP Exp. 303 Sites U1305, U1306 and U1307 at the Eirik Drift south of Cape Farewell and is enlarged in the upper left corner.

The various depocenters of subunit SUIV-c (~40-19 Ma; Table 1) are interpreted as an infill and drape of the hummocky basement (~60-40 Ma) in a tranquil environment at the Eirik Drift (*Mueller-Michaelis et al., 2012 (submitted)*). Not surprisingly, no WBUC is observed at the Eirik Drift as the GSR has not reached the critical level to allow NCW overflow until early Miocene *(Vogt, 1972)*. But still there is an indication for existing NCW deep circulation in the NE North Atlantic within this time interval observed with a major increase in drift accumulation at the Feni Drift *(Wold, 1994)* (~35-33 Ma; Fig. 1). This NCW flow is found southward directed from the Rockall Trough to the North Atlantic (Fig. 2a). Two possible deep-water formation regions have been hypothesized to be responsible for that: South of the GSR in the Rockall Trough *(Stoker, 1998)* or north of the sill in the SE Norwegian Sea with an open gateway at the distal eastern end of the GSR via the Faroe-Shetland basin *(Davies et al., 2001)*. Indications for the latter are also documented in the Faroe Drift NE of the GSR *(Davies et al., 2001)* and therefore seems more likely than the Rockall Trough theory.

We observe the onset of WBUC activity at ~19 Ma at the Eirik Drift. A widespread erosional event in the North Atlantic in the early Miocene accounts also for the onset of drift building at horizon A3 (~19-17 Ma, Table 1) *(Mueller-Michaelis et al., 2012 (submitted))*. This event is also observed in Bjorn, Gardar and Feni Drifts (Fig. 1) *(Miller and Tucholke, 1983)*. We suggest the deep-water formation region in the NGS and the onset of NCW overflows following the subsidence of the GSR in early Miocene *(Vogt, 1972)*. The NCW flow remained intense at the Eirik Drift until ~15 Ma, but was depleted between 15-12.5 Ma *(Mueller-Michaelis et al., 2012 (submitted))*. This is in accordance to the general observation of low NCW flux between ~16 to 12.5 Ma *(Woodruff and Savin, 1989; Wright et al., 1992)*. We suggest that the onset of the NCW overflows and intensification of the deep-water formation reinforced the Miocene warming phase with an intensified northward transport of warm and saline Atlantic surface water. Increased freshwater input to the Nordic Seas towards the mid Miocene Climatic Optimum may then have yielded in a strong, stable ocean stratification with a freshwater-barrier-layer, which inhibited deep convection in the Nordic Seas. The decrease in NCW formation, in turn, accounted for a decrease in northward heat transport to high latitudes and assisted the cooling of the mid Miocene Climate Transition (~14 Ma). We expect this climate cooling to have resulted in increasing instability of the surface ocean stratification due to heat loss and salt input at the oceans surface. This yields a renewed NCW production and thus, a renewed onset of WBUC has been observed at ~12.5 Ma at the Eirik Drift with the formation of horizon R5 (~12-10 Ma; Table 1). The renewed NCW production is also documented in increased accumulation observed at Snorri, Bjorn, Gardar and Hatton Drift (Fig. 1) between 13 and 10 Ma *(Wold, 1994)*.

Between ~10 and 8.1 Ma we observe a shallower WBUC than between 19 and 15 Ma at the Eirik Drift. The shallower WBUC is interpreted as the result of less dense and thus, weaker NCW flow. With our knowledge of the present WBUC at the Eirik Drift, we would expect a strong WBUC along with higher NCW production and vice versa. Higher NCW production, in turn, is expected in a cool regime, as surface cooling and salt input due to formation of sea-ice increase the ocean surface density and thus, the deep-water production *(Van Aken, 2007)*. However, we observe a decrease in WBUC intensity along with the ongoing Miocene cooling phase. The WBUC transports lower (DSOW) and upper (ISOW) NCW in different core depths. It is possible that we only observe one of the two different cores at the Eirik Drift region. As we observe a shallowing and thus weakening during a cold phase, we interpret the observed NCW flow as the upper NCW (ISOW), which more likely weakened and shallowed in a cooling regime. We suggest that the lower NCW (DSOW) flowed at larger depths outside of our study area (Fig. 2b).

At 8.1 and 7.5 Ma the reflector doublet R3/R4 was formed by NCW pulses with inhibited NCW flow at 9 Ma and 7 Ma *(Mueller-Michaelis et al., 2012 (submitted))*. We suggest short-term temperature fluctuations to result in strong NCW pulses with similar pathways like between 12 and 8 Ma (Fig. 2b). During the following deposition of subunit SUIII-b (7.5-5.6 Ma) the observed WBUC influence at the Erik Drift further weakened. The WBUC here was presumably too weak to (re)deposit sediments on top of the piled drift axis. We address this weakening to the ongoing climate cooling, resulting in an intensification of a deeper, denser lower NCW (DSOW) flow outside of our study area, and a weakening of the observed upper NCW

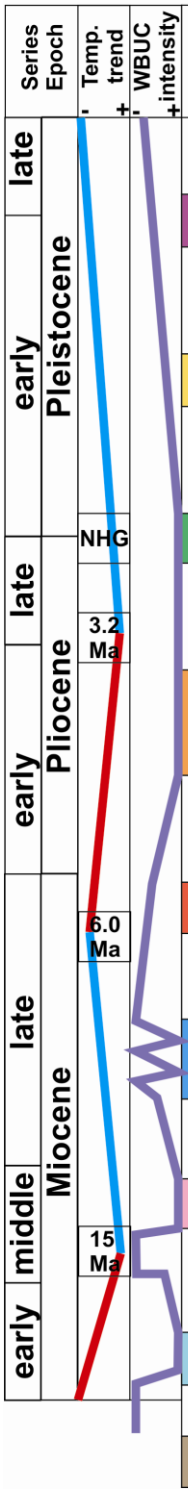

Age [Ma]	Reflector/ unit name	Depth at ODP 646 [ms TWT]	Thickness (min/max) [ms TWT]	Seismic characteristic
	SUI-a		0/170	continuous high amplitude reflctions, parallel to subparallel to seafloor
0.8	A1	456		High-amplitude reflector
	SUI-b		0/150	continuous to discontinuous, narrowly-spaced, parallel medium amplitude reflections
1.4	A2	470		High-amplitude reflector
	SUI-c		50/440	wide-spaced, continuous to discontinuous, parallel to subparallel reflections, upward increase in amplitudes
2.5	R1	490		Medium- to high amplitude reflector
	SUII		50/720	narrowly-spaced, continuous high-amplitude reflections unit rises from W to E
4.5	EU	500		Erosional unconformity high-amplitude reflector reflector truncation
	SUIII-a		50/580	upward increase in amplitudes and reflector spacing unit thickens from W to E
5.6	R2	510		Medium-amplitude reflector
	SUIII-b		0/430	narrowly-spaced, parallel to subparallel, low-amplitude reflections
7.5/ 8.1	R3/ R4	540/ 545		medium- to high-amplitude reflector doublet
	SUIV-a		0/940	parallel to subparallel, low-amplitude reflections
10-12	R5	570		band of 3-4 high-amplitude reflections
	SUIV-b		0/900	converging, low- to medium-amplitude reflections unit thins from W to E
17-19	A3	580		High-amplitude reflector
	SUIV-c		0/380	almost acoustically transparent
40-60	basement	590		irregular basement topography

Table 1: Refined seismic stratigraphy following *Arthur et al.* (1989). At the left the climatic conditions (warming phase=red, cooling phase=blue) are indicated as well as the inferred trends in intensity of the WBUC at the study area (purple).

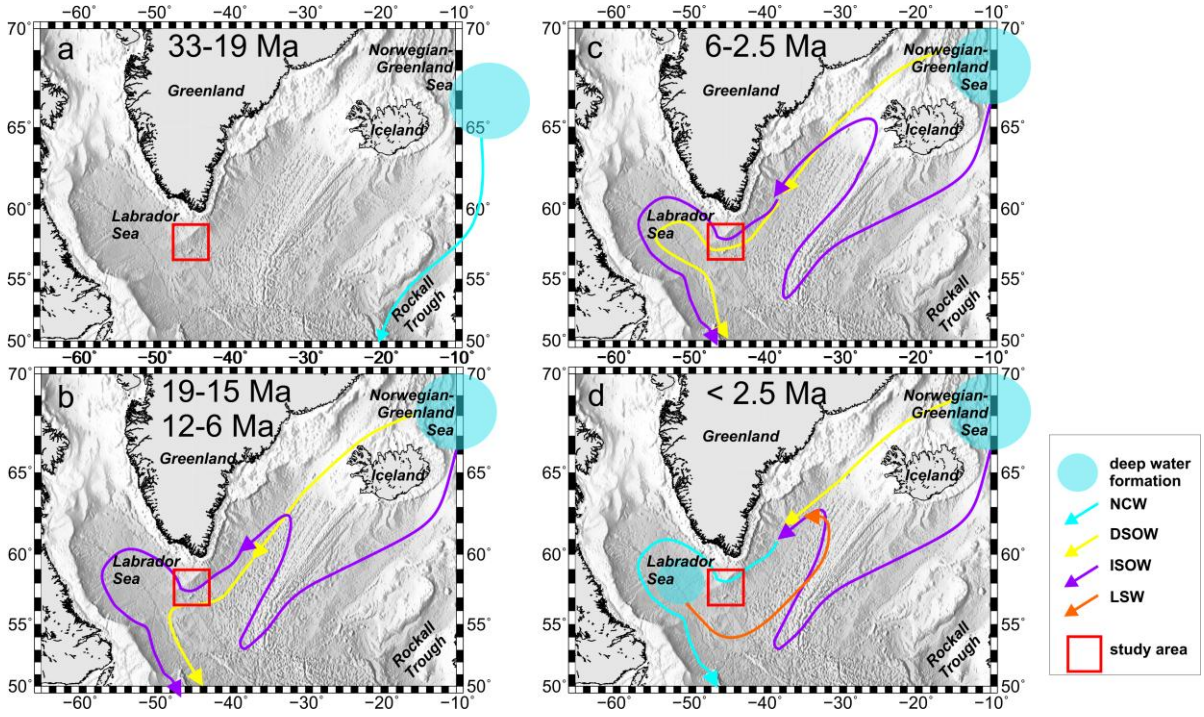

Figure 2: Schematic maps of deep-water formation regions and simplyfied deep current activity in the northern North Atlantic.

(ISOW) flow. Thus, the WBUC at the Eirik Drift stayed weak until the climate started to warm again at ~6 Ma with an increase in WBUC activity in the study area observed at reflector R2 (5.6 Ma).

Between 5.6-4.5 Ma we observe an increasing WBUC at the Eirik Drift with its maximum intensity leading to the formation of the erosional unconformity at ~4.5 Ma (Table 1) (*Kaminski et al., 1989)* along with climate warming. For the first time, we observe two branches of NCW flow at the Eirik Drift. The lower branch flows over ODP Leg 105 Site 646 and was identified as rather DSOW (lower NCW) then ISOW (upper NCW) *(Kaminski et al., 1989)*. We therefore conclude that the upper branch transported ISOW (upper NCW). The two branches of WBUC at the Eirik Drift are of maximum intensity observed here. Nevertheless, we interpret this observation as a shallowing and weakening of the NCW flow system in the northern North Atlantic during warming climate. During the preceding cool phases the one observed branch is assumed to transport ISOW (upper NCW) and the flow of DSOW (lower NCW) is suggested to proceed at greater depth and/or different pathways outside of our study area. Along with the climate warming the WBUC system shallows and hence, the intense deep branch of NCW flow lies within our study area. The DSOW (lower NCW) flow during this warming period is, even though it is assumed to have shallowed and weakened, still of higher intensity than the upper NCW (ISOW) flow during the cold phases.

With the end of mid Pliocene warmth cooling started again at ~3.6 Ma, and the WBUC intensity of DSOW and ISOW flow remained strong and the pathways almost the same until ~2.5 Ma. The onset of drift building at the Gloria Drift (Fig. 1) at ~4 Ma *(Wold, 1994)* indicates the onset of deep-water formation in the Labrador Sea along with the Pliocene cooling (Fig. 2c). Entrainment of less dense LSW to the dense overflows may explain why we do not observe intensification and deepening of the WBUC system during Pliocene cooling.

At 2.5 Ma the intensification of Northern Hemisphere Glaciation (NHG) is documented in the sedimentary record of ODP Leg 105 Site 646 *(Arthur et al., 1989)*. We observe a gradual shallowing and deepening of 2 WBUC branches after 2.5 Ma at the Eirik Drift NHG. The expanded Nordic ice shields isolate the surface ocean from exchanges in heat, freshwater and momentum with the overlying atmosphere and might have shifted the deep water formation region to the south. This southward shift possibly account for less dense overflow waters even in a cold regime. Also the changes of NCW composition due to the entrainment of LSW should be considered.

Based on our data and the geological records at the ODP/IODP sites at the Eirik Drift, we deciphered parts of the complex interplay of changes in the NCW flow and climate in the northern North Atlantic.

References:

Arthur, M.A., Srivastava, S.P., Kaminski, M., Jarrard, R.D., Osler, J., 1989. Seismic Stratigraphy and History of Deep Circulation and Sediment Drift Development in Baffin Bay and the Labrador Sea, in: Srivastava, S.P., Arthur, M., Clement, B., et_al. (Eds.), Scientific Results. Ocean Drilling Program, College Station, pp. 957-988.

Channell, J.E.T., Sato, T., KANAMATSU, T., STEIN, R., Alvarez Zarikian, C.A., 2010. Expedition 303/306 synthesis: North Atlantic climate, in: Channell, J.E.T., KANAMATSU, T., Sato, T., STEIN, R., Alvarez Zarikian, C.A., Malone, M.J., Scientists, a.t.E. (Eds.), Proceedings of the Integrated Ocean Drilling Program. Integrated Ocean Drilling Program, College Station, TX.

Davies, R., Cartright, J., Pike, J., Line, C., 2001. Early Oligocene initiation of North Atlantic Deep Water formation. Nature 410, 917-920.

Faugères, J.C., Stow, D.A.V., Camerlenghi, M.R.a.A., 2008. Chapter 14 Contourite Drifts: Nature, Evolution and Controls, Developments in Sedimentology. Elsevier, pp. 257, 259-288.

Faugères, J.C., Stow, D.A.V., Imbert, P., Viana, A.R., 1999. Seismic Features Diagnostic of Contourite Drifts. Marine Geology 162, 1-38.

Kaminski, M.A., Gradstein, F.M., Scott, D.B., Mackinnon, K.D., 1989. NEOGENE BENTHIC FORAMINIFER BIOSTRATIGRAPHY AND DEEP-WATER HISTORY OF SITES 645, 646, AND 647, BAFFIN BAY AND LABRADOR SEA, in: Srivastava, S.P., Arthur, M., Clement, B., et_al. (Eds.), Scientific Results. Ocean Drilling Program, College Station, pp. 731-756.

Miller, K.G., Tucholke, B.E., 1983. Development of Cenozoic Abyssal Circulation south of the Greenland-Scotland Ridge, in: Bott, M.H.P., Saxov, S., Talwani, M., Thiede, J. (Eds.), Structures and Development of the Greenland-Scotland Ridge - New Methods and Concepts. Plenum Press, New York and London, pp. 549-589.

Mueller-Michaelis, A., Uenzelmann-Neben, G., Stein, R., 2012 (submitted). Onset of drift building at the Eirik Drift during the Miocene: Evidence from high-resolution seismic reflection data. Marine Geology.
Nielsen, T., Knutz, P.C., Kuijpers, A., Camerlenghi, M.R.a.A., 2008. Chapter 16 Seismic Expression of Contourite Depositional Systems, Developments in Sedimentology. Elsevier, pp. 301-321.
Smith, W.H.S., Sandwell, D.T., 1997. Global Sea Floor Topography from Satellite Altimetry and Ship Depth Soundings. Science 277, 1956-1962.
Srivastava, S.P., Arthur, M.A., Clement, B., et_al_(eds.), 1989. Proceedings ODP, Scientific Results, 105. ODP, College Station, TX (Ocean Drilling Program).
Stoker, M.S., 1998. Geological Processes on Continental Margins, in: Stoker, M.S., Evans, D., Cramp, A. (Eds.), Geological Processes on Continental Margins. Geological Society, London.
Van Aken, H.M., 2007. The Oceanic Thermohaline Circulation. Springer, New York.
Vogt, P.R., 1972. The Faroe-Iceland-Greenland aseismic ridge and the western boundary undercurrent. Nature 239, 79-81.
Wold, C.N., 1994. Cenozoic Sediment Accumulation on Drifts in the Northern North Atlantic. Paleoceanography 9, 917-941.
Woodruff, F., Savin, S., 1989. Miocene deepwater oceanography. Palaeogeography 4, 87-140.
Wright, J.D., Miller, K.G., Fairbanks, R.G., 1992. Early and middle Miocene stable isotopes: implications for deepwater circulation and climate. Paleoceanography 7, 357-389.

ICDP

Reflection seismic investigation of the geodynamically active West - Bohemia/Vogtland region

N. MULLICK[1,2], S. BUSKE[1], S. SHAPIRO[2], P. WIGGER[2]

[1] Institute of Geophysics and Geoinformatics,TU Bergakademie Freiberg
[2] Institute for Geological Sciences, FU Berlin

The West Bohemia-Vogtland region in central Europe attracts much scientific interest due to recurrent earthquake swarms and continuous exhalation of CO2 dominated fluid from the subsurface. Seismological and geochemical studies reveal (1) significant upper mantle derived content of the emitted fluid (Weinlich et al., 1999), (2) an updoming of the MOHO below that area (Geissler et al., 2005) (3) possible existence of a magmatic fluid reservoir in the upper mantle (Weinlich et al., 1999) and (4) fluid activity as a possible trigger for the swarm earthquakes (Horalek and Fischer., 2008). In this study the subsurface structure beneath the region is investigated by reprocessing the deep reflection seismic profile 9HR, which runs almost directly across the swarm area (Figure 1).

The migrated image (Figure 2) confirms the upwelling of the MOHO known from receiver function studies. Directly below one of the major gas escape centers, channel like fault structures are observed (Figure 3) which

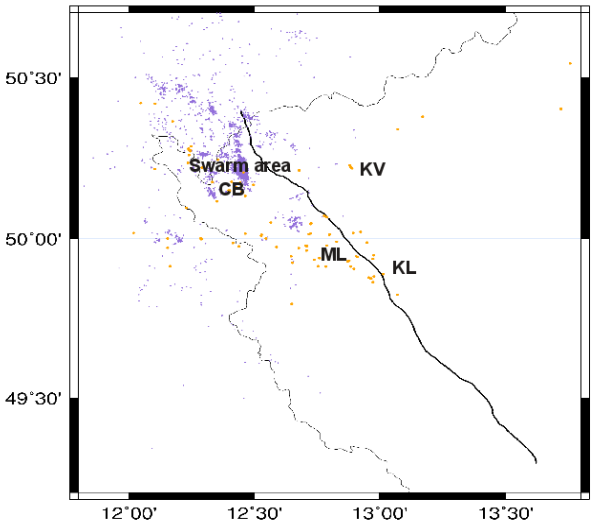

Figure 1. 9HR profile along with regional seismicity (purple dots) and fluid escape points (orange dots) in the West Bohemia-Vogtland region. The major gas escape centers are designated as CB (Cheb Basin), ML (Marianske Lazne), KV (Karlovy Vary) and KL (Konstantinovy Lazne).

seem to have their roots at the Moho. They may represent deep reaching degassing channels that allow direct transport of mantle-derived fluid/gas.

The middle and lower crust appears highly reflective and therefore likely fractured below the swarm area (Figure 3). This may allow mantle fluid/gas to ascend through the crust and then getting blocked at some barrier in the upper crust. Such blockage could result in building up of an over-pressured fluid zone at the bottom of near surface rocks. After a critical state is reached, the over-pressured fluid may have sufficient energy to force its way above into near surface rocks and to trigger seismicity. Since the swarm seismicity is found to be restricted along a plane only (Figure 3), such intrusion might have taken place along a semi-permeable zone that extends from the fractured lower crust into the near surface rocks. The bright spot defining the upper boundary of the swarm seismicity could then be identified as boundary of this semi-permeable zone.

A comparison of the spatio-temporal evolution of the recent swarms in the years 2000 and 2008 with the subsurface reflectivity (Figure 4) shows that in both cases the swarm activity initiates at the upper edge of a highly diffuse reflectivity zone, moves upward, bends at a bright spot above and finally stops after travelling a few kilometers along the bright spot. This correlation indeed

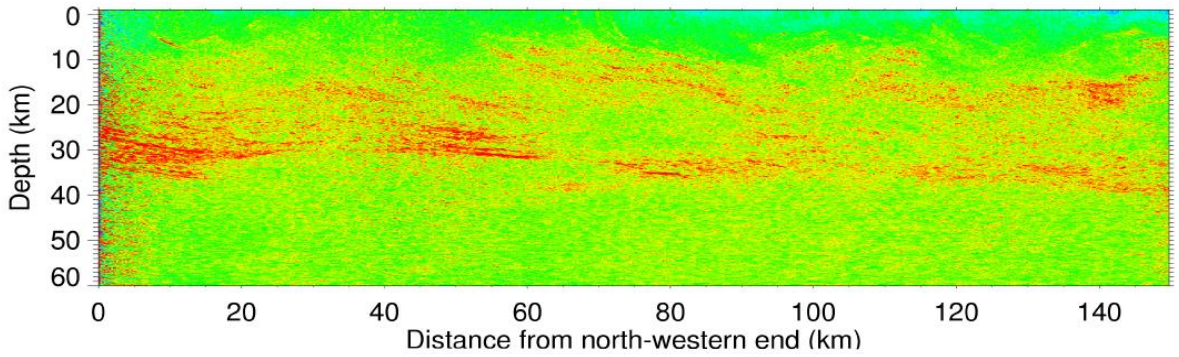

Figure 2: Migrated section of 9HR profile.

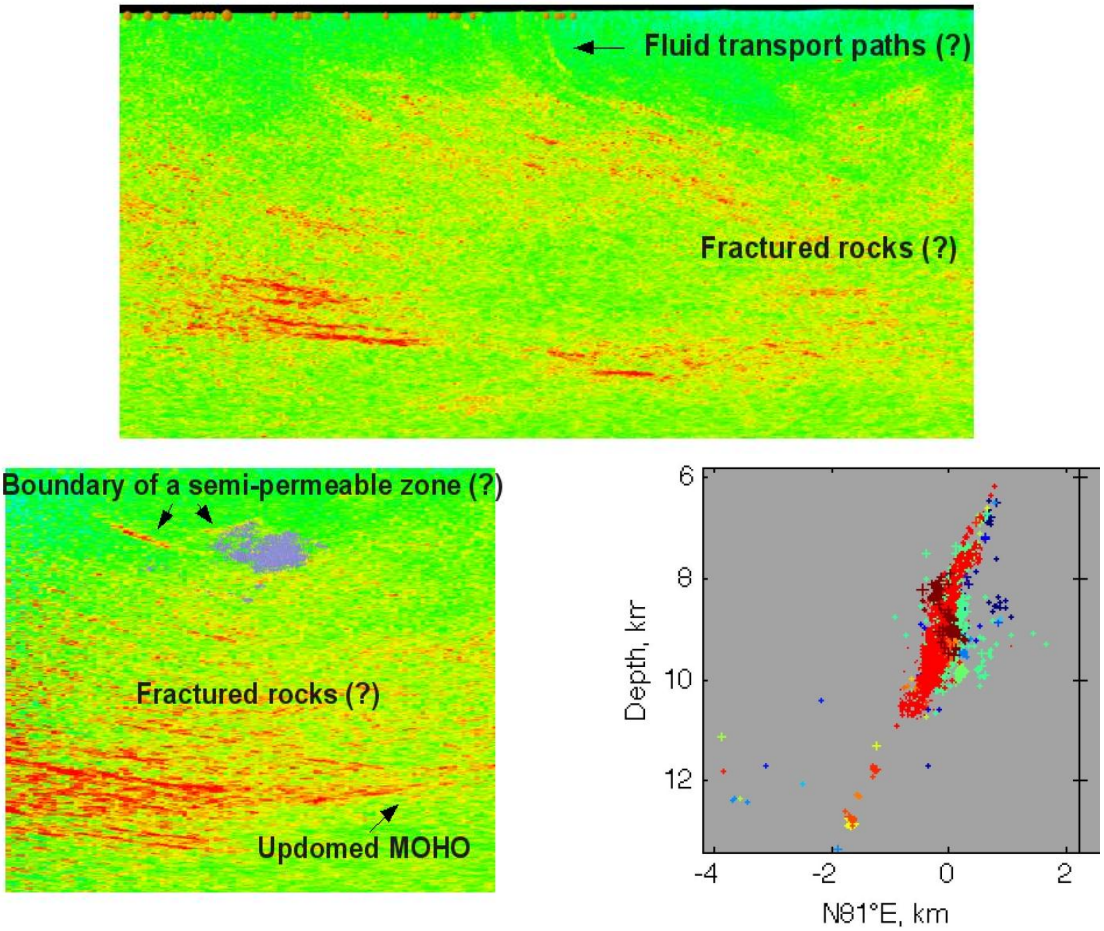

Figure 3. (Top) The fluid emission points of Marianske Lazne and Konstantinovy Lazne gas escape centers (orange dots) against the subsurface reflectivity image of Figure 2. The 9HR profile runs through these centers (Figure 1). (Bottom left) The seismicity of the swarm area from year 1991 to 2011 (purple dots) plotted against the subsurface reflectivity image of Figure 2. (Bottom right) Side view of the main cluster of swarm seismicity distributed along a near-vertical plane (Horalek and Fischer, 2008).

resembles movement of an overpressured trapped fluid forcing its way into a less permeable volume above it and thereby generating a swarm of earthquakes.

These observations and in particular their joint interpretation give new insight into the causes and driving mechanisms of the West Bohemia-Vogtland earthquake swarms.

References:

Geissler,W.H., Kämpf, H., Kind, R., Bräuer, K., Klinge, K., Plenefisch, T., Horalek, J., Zednik, J., Nehybka, V., 2005. Seismic structure and location of a CO2 source in the upper mantle of the western Eger (Ohre) Rift, central Europe. Tectonics 24 (TC5001).

Horalek, J., Fischer, T., 2008. Role of crustal fluids in triggering thewest Bohemia/Vogtland earthquake swarms: just whatwe know (a review). Studia Geophysica et Geodaetica 52, 455–478.

Weinlich, F., Bräuer, K., Kämpf, H., Strauch, G., Tesa, J., Weise, S. (1999) An active subcontinental mantle volatile system in the western Eger Rift, Central Europe: Gas flux, isotopic (He, C, and N) and compositional fingerprints. Geochim Cosmochim Acta 63:3653-3671.

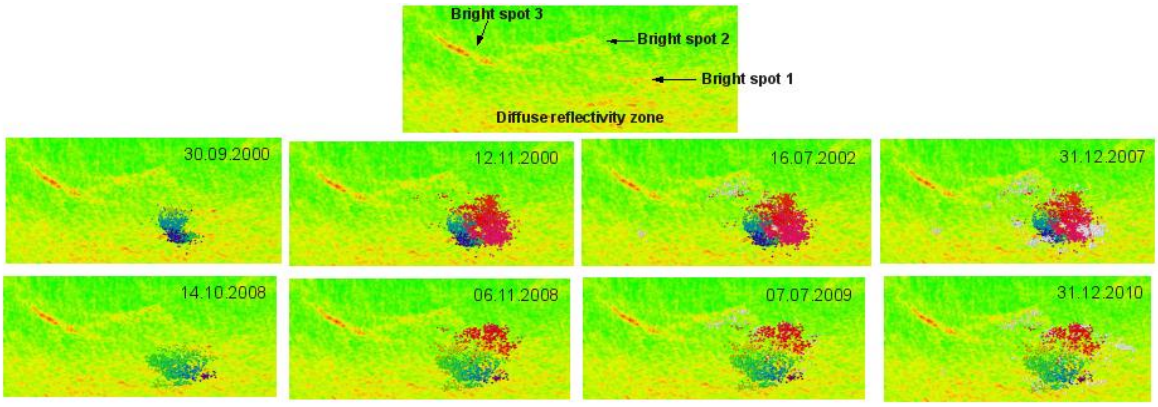

Figure 4. (Top) Close-up view of the subsurface reflectivity image of Figure 2 within which the swarm activity is confined. (Middle) Snapshots of spatio-temporal evolution of year 2000 swarm, (Bottom) Snapshots of spatiotemporal evolution of year 2008 swarm.

IODP

Massive surge of the Laurentide ice sheet during the Younger Dryas

B.D.A. NAAFS[1], J. HEFTER[2], J.E.T. CHANNELL[3], AND R. STEIN[2]

[1] Organic Geochemistry Unit, School of Chemistry, University of Bristol, Cantock's Close, BS8 1TS Bristol, United Kingdom (david.naafs@bristol.ac.uk)
[2] Alfred Wegener Institute for Polar and Marine Research, Department of Marine Geology and Paleontology, D-27568 Bremerhaven, Germany
[3] Department of Geological Sciences, University of Florida, Gainesville FL 32611, USA

The overall consensus is that the Younger Dryas (YD) cold event, between 12.9 and 11.7 thousand years ago, was the response to a slowdown in Atlantic Meridional Overturning Circulation (AMOC) and associated feedback mechanisms due to meltwater discharge. However, the origin of this meltwater flux and thus the mechanisms behind the YD are still subject to intense debate. Based on marine sediment cores from the Labrador Sea and North Atlantic, here we provide novel results which indicate that during the YD a massive surge from the Laurentide ice sheet (LIS), similar in origin and magnitude to the most recent Heinrich Events, took place. We speculate that this instability of the LIS and surges through the Hudson Strait, analogous to the Heinrich Events, provided an additional source of meltwater to suppress AMOC during the YD. These results challenge the classical and prevailing theory which attributes the source of meltwater to drainage of Lake Agassiz alone.

ICDP

Reconstructing climate in an extreme lacustrine environment – The Dead Sea sediment record

I. NEUGEBAUER[1], A. BRAUER[1], M.J. SCHWAB[1], P. DULSKI[1], U. FRANK[1] AND DSDDP SCIENTIFIC PARTY*

[1] GFZ German Research Centre for Geosciences, Section 5.2 Climate Dynamics and Landscape Evolution, Telegrafenberg, D-14473 Potsdam, Germany
*The complete list of scientists involved in the DSDDP can be found at http://www.icdp-online.org

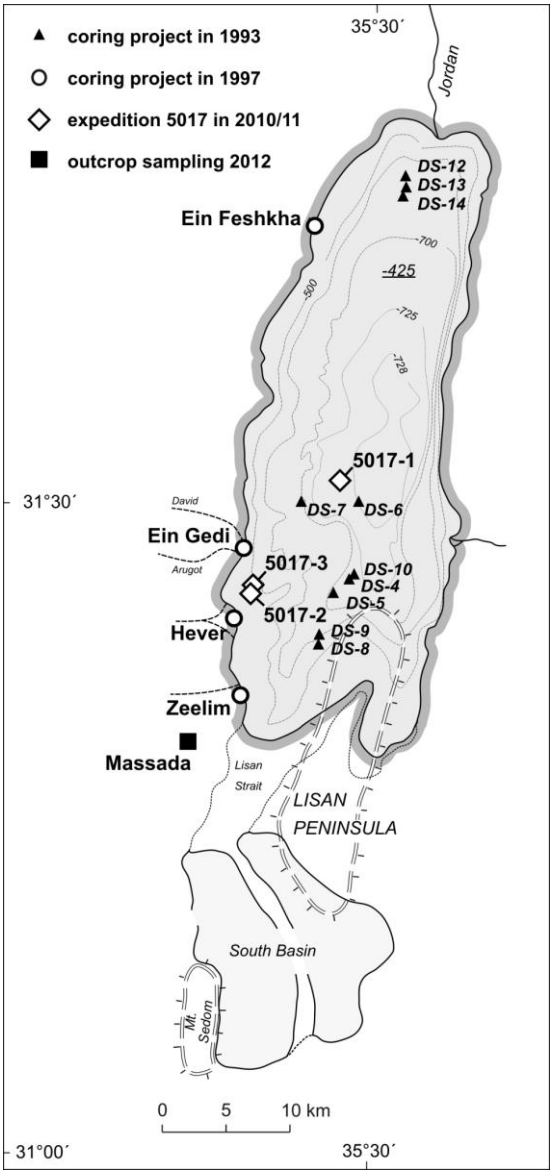

Figure 1: Drilling locations from the deep northern basin in 1993 (Heim et al., 1997), from the western shore of the Dead Sea in 1997 (Migowski et al., 2004, 2006), the ICDP Dead Sea Deep Drilling Project (expedition 5017 in 2010/2011) and the Massada outcrop sampling location 2012.

Introduction

The Mediterranean is one of the vulnerable regions, where it is expected to get more and more dry in the future. But to develop reliable climate scenarios for the future, it is necessary to understand the past climate dynamics. Concerning this, lake sediments from the Dead Sea and its Pleistocene precursors provide important and high-resolution information about climatic and environmental changes in the eastern Mediterranean region. With a current lake level of ~427 m below mean sea level the hypersaline Dead Sea is situated at the deepest point on continents. The steep escarpments to the east and west of the pull-apart basin, the tectonic activity as well as the explicitly dry climate and high evaporation further strengthen the extreme character of the Dead Sea environment. Moreover, the deposition of sediments in the Dead Sea basin (DSB) reacts extremely sensitive to climatic changes, which is expressed in drastic lake level fluctuations. Earlier reconstructions of past lake levels and hence climate were mainly based on exposed sediments and paleoshorelines (e.g. Bookman et al., 2004; Migowski et al., 2006, Fig. 1). However, depositional gaps are recognised during dry periods, when no sediments have been deposited at the margin of the lake. A first drilling attempt in the deep basin has been performed in 1993 by Heim et al. (1997, Fig 1), depicting the climatic and environmental history of the last ~2500 years.

Dead Sea Deep Drilling Project

Through the ICDP-based deep drilling in the northern basin of the Dead Sea, scientists from several institutions in Israel, Germany, Switzerland, the US and Japan intended to recover a continuous high-resolution sediment record of the Dead Sea basin for the past several glacial-interglacial

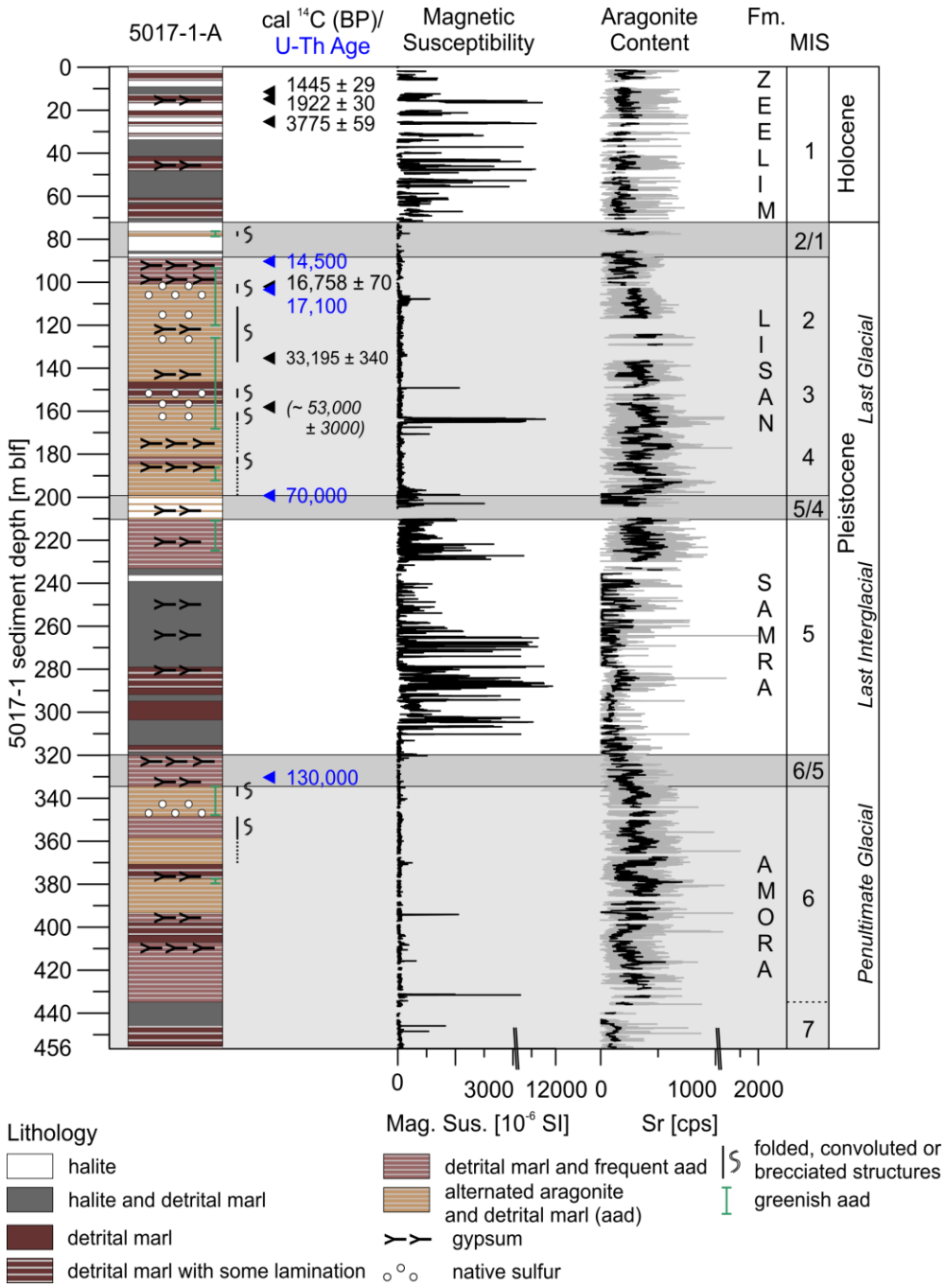

Figure 2: Major lithology and stratigraphy of core 5017-1-A from the deep drilling location (water depth ~300 m), first radiocarbon and U-Th ages, magnetic susceptibility data of the scanned core sections (resolution 1 mm) and strontium values from continuous µXRF element scanning (grey: 1 mm resolution, black: 10 cm running means), indicating aragonite that is mainly enhanced during glacials. Fm. – Dead Sea sediment formation; MIS – marine isotope stage, assumed from sediment stratigraphy.

cycles. Main research goals of the project include reconstructing the environmental, climatic, seismic, tectonic and magnetic history of the region. Another focus is set on the study of physical and chemical properties of the Dead Sea sediments, especially salt sequences and earthquake-triggered intraclast-breccias. High-resolution chronologies are being established by AMS radiocarbon and U-series dating, supported by varve counting in selected intervals.

The drilling in the deep northern DSB took place from November 2010 to March 2011. About 720 meters of sediment cores have been obtained from three drilling sites (Fig.1). At the priority site 5017-1 (coordinates for hole 1-A: N 31°30'28.98", E 35°28'15.60") about 485 meters were recovered from one deep (5017-1-A) and several short cores at a water depth of 297 meters, which is close to the deepest point of the basin. From a water depth of 11.42 m, ~19 m have been drilled and ~11 m recovered from site 5017-2 (N 31°25'13.998", E 35°23'38.4"). The third drilling location (N 31°25'22.74", E 35°23'39.58"), close to the second, revealed one long (5017-3-C) and two short cores from 2.12 m water depth with a recovery of ~237 m.

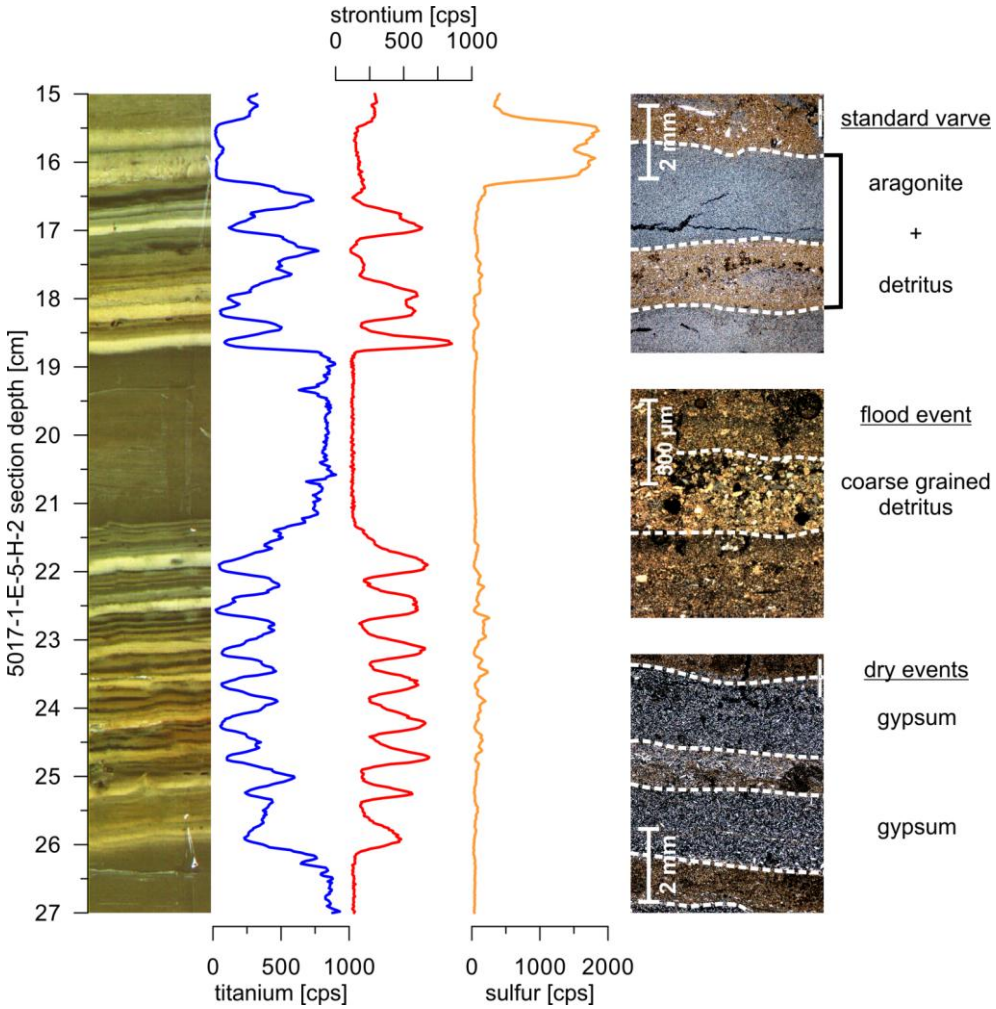

Figure 3: An example of seasonal deposition in the Dead Sea basin and event layers. On the left side a 12 cm section of typical Holocene laminated detrital marl, aragonite and gypsum sediments is shown with according high-resolution µXRF values (200 µm resolution) of Ti (indicating detrital layers, deposited by winter flash floods), Sr (proxy for aragonite layers, precipitated in the water column due to evaporation during summer) and S (indicating gypsum layers, precipitated during lake level lowering and mixing of the water body).On the right side microscopic photos from petrographic thin sections show a standard aragonite-detritus varve and examples for flood and drought event layers that can form additionally or replace the standard laminae.

Sediment record

Due to the sediment stratigraphy and interpretation of petrophysical data of the longest core 5017-1, a first estimate yields an age of this core of ~220,000 years, which is confirmed by first radiocarbon and U-Th ages (Fig 2). Hence, this record covers the last two glacial-interglacial cycles including the Holocene Zeelim formation, the last glacial Lisan (Stein, 2001), the last interglacial Samra (Waldmann et al., 2009) formation and the later part of the Amora formation (penultimate Glacial; Torfstein et al., 2009). The glacial Lisan and Amora deposits are mainly composed of alternated primary aragonite and detrital marl layers representing annual layer couplets that formed under humid climate conditions in the Levant. Prominent up to 15 cm thick gypsum layers indicate major lake level decline (Torfstein et al., 2008). During interglacial dry climatic conditions (Zeelim and Samra formations) mainly salt has been deposited in the DSB, but also homogeneous and laminated detrital marl is found. Magnetic susceptibility strongly fluctuate during the Interglacial intervals, while constantly low values have been measured in the Glacial sequences (Fig. 2).

Combining high-resolution µXRF element scanning and micro-facies analysis

High-resolution studies of small-scale climate variability have a great potential to characterise abrupt climate change and natural decadal-scale variabilities in the Mediterranean region. Furthermore, we want to better understand and document the frequencies of extreme events, like floods and droughts, during warmer climatic conditions in the past. A new methodological approach has been applied, where high-resolution µXRF element scanning (step-size 200 µm) is combined with micro-facies analysis on petrographic thin sections to understand the seasonal deposition of sediments. Some elements can be used as a proxy for different types of laminae, which in turn reflect different climatic conditions or extreme events, respectively (Fig. 3). Micro-facies analysis allows defining the mineral components, layer/varve thickness, grain size, possible grading and other characterisation of the evaporite (aragonite, gypsum, halite) and detrital layers (Fig. 3) as well as earthquake-triggered structures.

From the deep core 5017-1 a micro-facies inventory of the sediments is being established that can be used as a

climate proxy. Therefore, a prerequisite is the general relation of the sediment depostion in the DSB to precipitation (Enzel et al., 2008). Evaporites reflect dry climatic conditions during interglacials, while alternated aragonite-detritus (aad facies) deposition is favoured during glacial lake level high-stands. Two intervals have been further chosen for establishing time-series of extreme events and analysing dynamics of abrupt climate change: 1) the middle to late Holocene from 4 to 2 ka BP, where a major lake level drop of more than 40 meters has occurred (e.g. Migowski et al., 2006) and 2) the lateglacial period from 17 to 14.5 ka BP that represents an extreme lake level decline of more than 100 meters (e.g. Bartov et al., 2003). Both intervals are compared regarding sedimentation processes in the deep basin from core 5017-1 with its shallow-water counterparts (Holocene Ein Gedi core

(DSEn) and lateglacial outcrop Massada (MAZ), see Fig. 1). First results reveal that we are able to improve the existing lake level and climate reconstructions.

Outlook

Within the ICDP Dead Sea Deep Drilling Project analyses of the sedimentation processes in the deep and shallow-water environment of the Dead Sea during late Holocene and Lateglacial times are ongoing. Furthermore, stable oxygen and carbon isotope meaurements on aragonite layers will complement the micro-facies and µXRF dataset. This offers a great potential for developing high-resolution timeseries of climatic fluctuations, depicting single extreme events like floods, droughts and dust storms and moreover understanding abrupt climate change in the eastern Mediterranean.

References:

Bartov, Y., Goldstein, S.L., Stein, M., Enzel, Y., 2003. Catastrophic arid episodes in the eastern Mediterranean linked with the North Atlantic Heinrich events. Geology 31, no. 5, 439-442.

Bookman (Ken-Tor), R., Enzel, Y., Agnon, A., Stein, M., 2004. Late Holocene lake levels of the Dead Sea. GSA Bulletin 116, no. 5/6, 555-571.

Enzel, Y., Amit, R., Dayan, U., Crouvi, O., Kahana, R., Ziv., B., Sharon, D., 2008. The climatic and physiographic controls of the eastern Mediterranean over the late Pleistocene climates in the southern Levant and its neighboring deserts. Global and Planetary Change 60, 165-192.

Heim, C., Nowaczyk, N.R., Negendank, J.F.W., Leroy, S.A.G., Ben-Avraham, Z., 1997. Near East Desertification: Evidence from the Dead Sea. Naturwissenschaften 84, 398-401.

Migowski, C., Agnon, A., Bookman, R., Negendank, J.F.W., Stein, M., 2004. Recurrence pattern of Holocene earthquakes along the Dead Sea transform revealed by varve-counting and radiocarbon dating of lacustrine sediments. Earth Planet. Sci. Lett. 222, 301-314.

Migowski, C., M. Stein, S. Prasad, Negendank, J.F.W., 2006. Holocene climate variability and cultural evolution in the Near East. Quaternary Research 66(3), 421-431.

Stein, M., 2001. The sedimentary and geochemical record of Neogene-Quaternary water bodies in the Dead Sea basin – inferences for the regional paleoclimatic history. J. Paleolimnol. 26, 271-282.

Torfstein, A., Gavrieli, I., Katz, A., Kolodny, Y., Stein, M., 2008. Gypsum as a monitor of the paleo-limnological-hydrological conditions in Lake Lisan and the Dead Sea. Geochimica et Cosmochimica Acta 72, 2491-2509.

Torfstein, A., Haase-Schramm, A., Waldmann, N., Kolodny, Y., Stein, M., 2009. U-series and oxygen isotope chronology of the mid-Pleistocene Lake Amora (Dead Sea basin). Geochimica et Cosmochimica Acta 73, 2603-2630.

Waldmann, N., Stein., M., Ariztegui, D., Starinsky, A., 2009. Stratigraphy, depositional environments and level reconstruction of the last interglacial Lake Samra in the Dead Sea basin. Quaternary Research 72, 1-15.

IODP

Reconstruction of the Timing of Water Mass Exchange during Progressive Closure of the Central American Seaway in the Pliocene

A. OSBORNE[1], M. FRANK[1], R. TIEDEMANN[2]

[1] GEOMAR Helmholtz Centre for Ocean Reseach Kiel, Wischhofstr. 1-3, 24148 Kiel

[2] AWI Alfred Wegner Institute for Polar and Marine Research, Columbusstr., 27568 Bremerhaven

The closure of the Central American Seaway caused a major reorganisation of ocean circulation. Competing hypotheses claim that the disconnection of the Pacific and Atlantic at low latitudes contributed to either a warming or a cooling of global climate. A further hypothesis suggests that an increase in moisture supply to the northern hemisphere resulting from the closure was necessary for the development of Northern Hemisphere Glaciation. A well-defined timeframe is central to understanding the direct and indirect consequences of the closure of this major ocean gateway. Here we use radiogenic isotopes of Nd and Pb in early diagenetic ferromanganese sediment coatings to reconstruct the history of intermediate and deep water connections between the Caribbean Sea and the eastern Equatorial Pacific Ocean from 5.0 to 2.0 million years ago. Surface water exchange will be characterised using the Nd isotope composition of planktonic foraminiferal calcite.

During the first 14 months of the project the validity of our approach was tested and established by the analysis of core top samples from the proposed study areas (Figures 1 and 2) and by down core comparisons between different leaching methods. A complete dataset of leachate Nd, Pb and Sr isotope data spanning the key period of CAS closure was produced for two ODP Sites (1241 and 999) and Nd and Sr isotope data for a third ODP Site (1000) (Nd isotope data shown in Figure 3). Full procedural blanks were simultaneously processed and measured and column chemistry was recalibrated using certified standards.

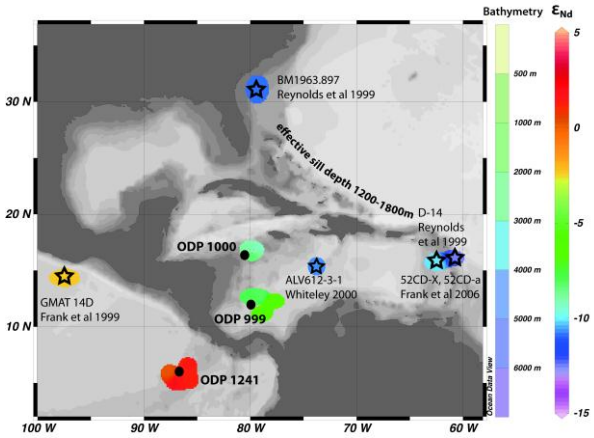

Figure 1 Locations of ODP sites 999, 1000 and 1241 (closed circles), with colour shading indicating the ε_{Nd} signatures of coretop sediment leachates. Stars and associated shading mark the ε_{Nd} signature of ferromanganese crusts for comparison.

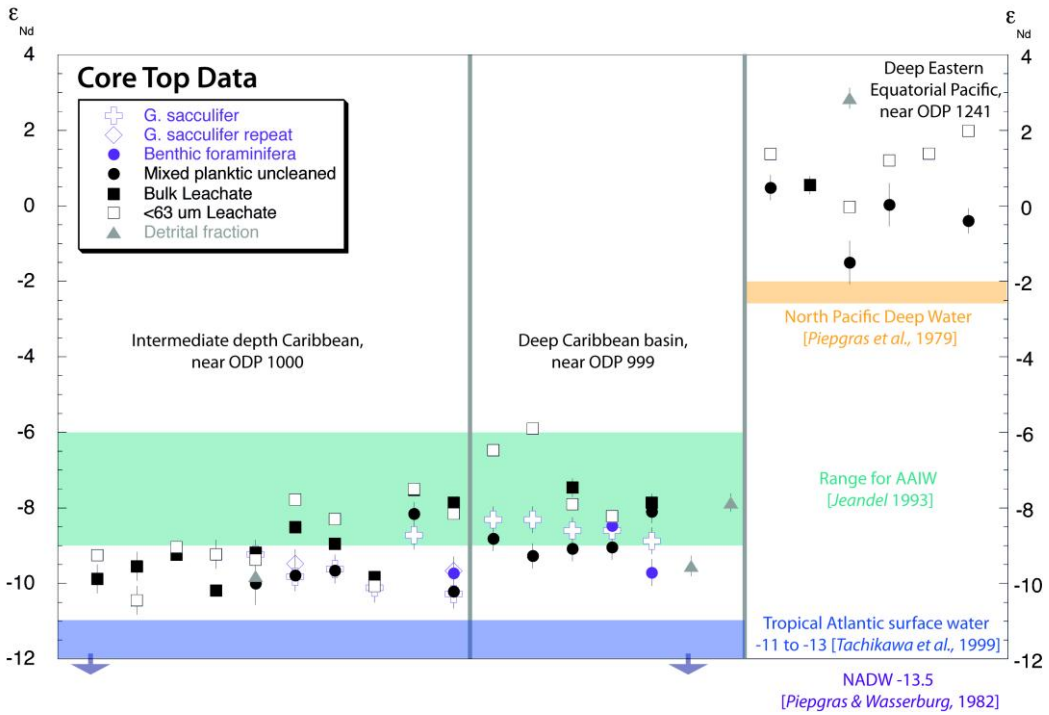

Figure 2. ε_{Nd} of different sediment components to test whether both a surface water (*G. sacculifer* calcite) and bottom water (benthic foraminifera, coatings of bulk and <63 µm sediment and uncleaned foraminifera) signal was recorded. Insufficient amounts *of G. sacculifer* were available for the Pacific samples.

The coretop survey confirmed that there is a large difference in the seawater ε_{Nd} between the eastern Equatorial Pacific and the Caribbean (Figures 1 and 2), as extracted by leaching of authigenic ferromanganese coatings [*Gutjahr et al*, 2007]. This feature will be used to study the closure history of the CAS to deep and intermediate water. Downcore samples were subjected to a number of tests, following observations in other study areas that a two-step leaching, in which the carbonate fraction is first removed by buffered acetic acid solution, exposes not only the REEs and trace metals contained in the coatings but also attacks the detrital material, in particular in the presence of volcanic glasses. There was no significant offset in Nd, Pb or Sr isotopic composition of the solutions produced by the two-step leach, the acetic-acid only leach or the hydroxylamine only leach. Furthermore, seawater Sr isotope compositions were obtained for the leach fraction and the Sr isotope composition of the detrital fraction was significantly different for both coretop and downcore samples.

Published stable carbon and oxygen isotope and Mg/Ca data from planktonic foraminifera indicate a divergence in surface water properties on either side of the CAS from 4.7 to 4.2 Ma [*Haug et al.*, 2001; *Steph et al.*, 2006; *Groeneveld et al.*, 2008]. These changes may have occurred without complete closure of the seaway. It is expected that a surface water Nd isotope record will allow to precisely determine the timing of the final separation of the Pacific and Atlantic oceans, which is a central goal of this project.

The suitability of planktonic foraminiferal calcite as a carrier of the surface water ε_{Nd} signal was recently called into question [*Roberts et al.*, 2010]. To address this issue, a comparison was made between redox cleaned and uncleaned coretop samples (Figure 2). In most cases the results were within error of each other. This could mean that a) redox cleaning does not sufficiently remove the authigenic coatings [*Roberts et al.*, 2010], b) the Nd concentration in foraminiferal calcite is much higher than that of the coatings and therefore dominates the signal [*Martínez-Boti et al.*, 2009], or c) the ε_{Nd} signature of surface and deep waters is the same.

It is possible that the normal 'batch' redox cleaning process used so far has not successfully removed ferromanganese coatings from the foraminifera. Additional unforeseen efforts are required to process further core top samples and, depending on the outcome, further downcore samples, applying a flow-through cleaning [*Haley et al.*, 2005] in order to determine which method is most suitable to produce foraminiferal records of past surface water Nd isotope compositions. This will be the main priority of the proposed third year of the project.

Having established that a seawater signal can be obtained from sediment leachates, the Nd, Pb and Sr isotope composition of samples spanning 5.5 to 2.2 Ma were analysed from ODP sites 999, 1000 and 1241 at a temporal resolution of 100 Kyr or higher. The seawater ε_{Nd} signal obtained from eastern Equatorial Pacific Site 1241 (2027 mbsl) showed a remarkably narrow range during the Pliocene (-0.03 ± 0.24 to 1.45 ± 0.16 ε_{Nd}) (Figure 3). The core top composition also falls within this range (0.55 ± 0.24 ε_{Nd}). Fish teeth records from the same core (representing deep water signatures) showed similar values during the Miocene, with the exception of a single outlier [*Newkirk and Martin*, 2009]. Pb isotope data from the leachates (not shown) exhibit some covariance with ε_{Nd}

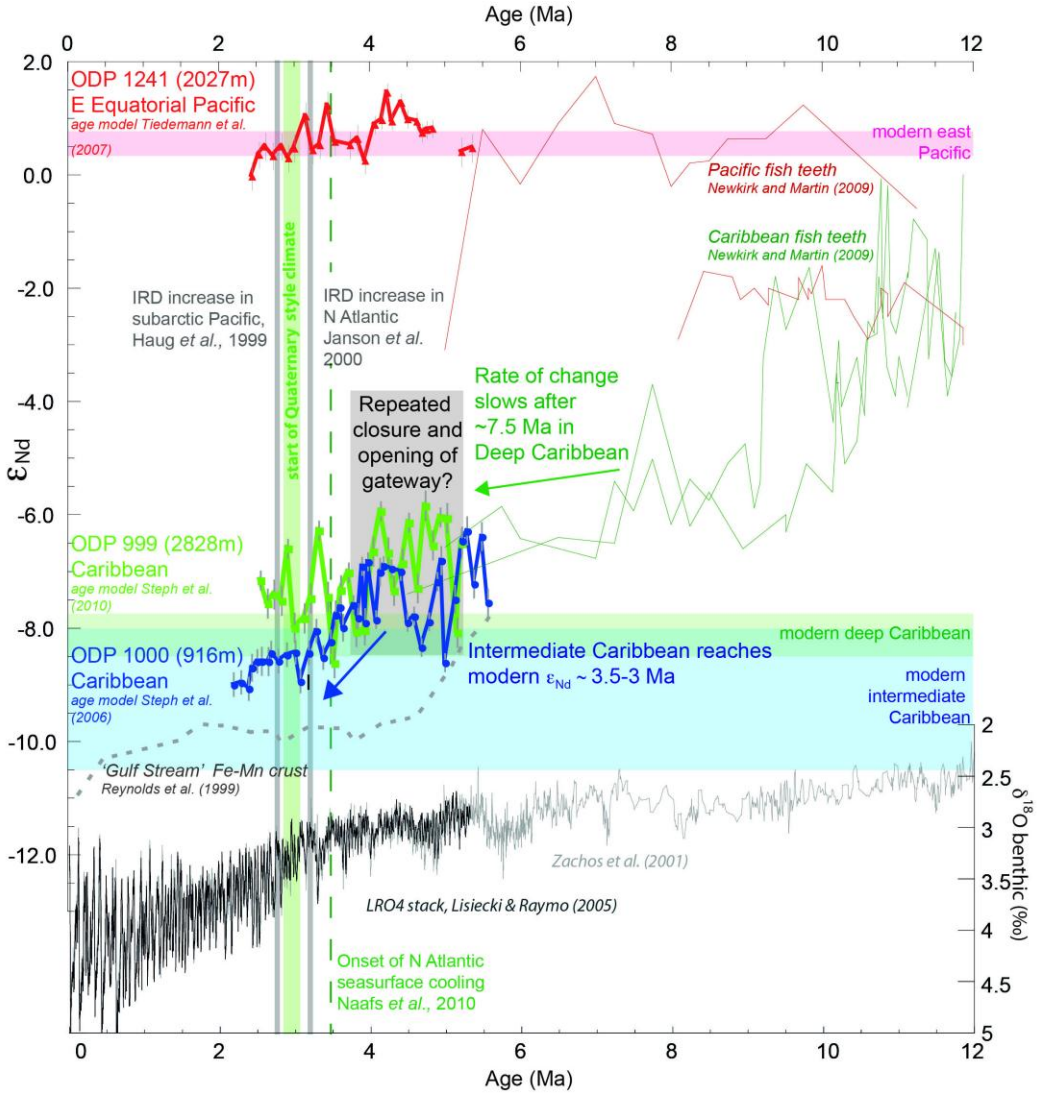

Figure 3. Comparison of sediment leachates from the three ODP sites with published fish teeth data [*Newkirk and Martin*, 2009] and ferromanganese crust data [*Reynolds et al*., 1999]. Also shown are stacked benthic foraminiferal $\delta^{18}O$ [*Lisiecki and Raymo*, 2005; *Zachos et al*., 2001], showing global trends in temperature and ice volume, with a vertical green bar showing the onset of Quaternary style climate . Vertical dashed green line corresponds to the onset of sea surface cooling of the N Atlantic current [*Naafs et al*., 2010]. Vertical grey bars indicate increases in ice rafted debris in the northern hemisphere [*Haug et al*., 1999; *Jansen et al*., 2000].

(R^2=0.38 for ε_{Nd} and $^{206}Pb/^{204}Pb$). Given that Pb has a much shorter residence time in the oceans than Nd, this suggests that there was influence from local, terriginous inputs. There is no evidence from the ε_{Nd} data that there was a significant contribution of unradiogenic Atlantic water to the eastern Equatorial Pacific during the last 11 Ma. This is consistent with a dominant Pacific to Atlantic flow across an open CAS, as simulated by a number of different 3-D ocean circulation models.

Early Pliocene leachate ε_{Nd} signatures of deep Caribbean Site 999 (2828 mbsl) are in good agreement with fish teeth data published by Newkirk and Martin [2009] (Figure 3). The extension of the deep Caribbean record into the Pliocene demonstrates that the rate of change towards less radiogenic seawater ε_{Nd} compositions decreased from ~7.5 Ma onwards. Seawater ε_{Nd} signatures display significant variability throughout the Pliocene. When compared with benthic $\delta^{13}C$ from the same site [*Haug and Tiedemann*, 1998], there is a hint that periods of increased ventilation are associated with lower ε_{Nd} values, which would be consistent with an increased influence of NADW. Some of the maxima and minima were also reflected by the Pb isotopic compositions until 3.1 Ma when the records were decoupled and the $^{206}Pb/^{204}Pb$ ratio started to increase, similar to the timing of changes in the $\delta^{18}O$ record [*Haug and Tiedemann*, 1998] and changes in deep Atlantic Pb isotope compositions as recorded in ferromanganese crusts [*O'Nions et al.*, 1998], both thought to respond to an increased supply of incongruently weathered Pb since the onset of northern hemisphere glaciation. Site 999 will be resampled to produce a higher resolution leachate record to test the robustness of the relationship between the radiogenic and stable isotope records. This additional information will help to precisely establish when the deep Caribbean became isolated from the Pacific at low latitudes.

The main feature of the Pliocene record from the intermediate depth Caribbean (Site 1000) is a trend towards

less radiogenic seawater ε_{Nd} between 3.9 and 3.2 Ma, from -7 to -8.5 ε_{Nd} (Figure 3). No such change has been recorded in the "Blake" ferromanganese crust, taken from a downstream location at similar depth in the western North Atlantic [*Reynolds et al.*, 1999], thus arguing against a change in the composition of the intermediate depth Atlantic circulation during this time. It thus appears that the intermediate Caribbean continued to be affected by radiogenic Pacific waters until 3.2 Ma. This is similar in timing to North Atlantic sea surface cooling [*Naafs et al.*, 2010] and a major increase in ice rafted debris deposition [*Jansen et al.*, 2000], although still earlier than the onset of major Northern Hemisphere Glaciation at ~ 2.7 Ma [*Shackleton et al.*, 1984].

In summary, the work scheduled for the first 14 months of the original proposal has been successfully completed and it is anticipated that the remaining goals will be reached within the next 10 months of the current proposal and a further 12 months requested. An additional 12 months are needed to address unforeseen complications in the cleaning of planktonic foraminifera, essential for producing a reliable surface water ε_{Nd} record for the final stages of CAS closure, as well as to extend the intermediate water record at Site 1000 back into the Miocene and to investigate changes in REE concentrations on the same samples as used for Nd isotope analyses of the Pliocene.

References

Frank, M., *et al.* (1999) *Geology*, *27*(12), 1147-1150. Frank, M., *et al.* (2006) *G*^{3}, *7*. Groeneveld, J., *et al.* (2008) *G*^{3}, *9*. Gutjahr, M., *et al.* (2007) *Chem. Geol.*, *242*(3-4), 351-370. Haley, B. A., *et al.* (2005) *EPSL*, *239*(1-2), 79-97. Haug, G. H., and R. Tiedemann (1998) *Nature*, *393*(6686), 673-676. Haug, G. H., *et al.* (2001) *Geology*, *29*(3), 207-210. Haug, G. H., *et al.* (1999) *Nature*, *401*(6755), 779-782. Jansen, E., *et al.* (2000) *Paleoceanography*, *15*(6), 709-721. Jeandel, C. (1993) *EPSL*, *117*(3-4), 581-591. Lisiecki, L. E., and M. E. Raymo (2005) *Paleoceanography*, *20*(1). Martinez-Boti, M. A., *et al.* (2009) *G*^{3}, *10*. Naafs, B. D. A., *et al.* (2010) *EPSL*, *298*(3-4), 434-442. Newkirk, D. R., and E. E. Martin (2009) *Geology*, *37*(1), 87-90. O'Nions, R. K., *et al.* (1998) *EPSL*, *155*(1-2), 15-28. Piepgras, D. J., and G. J. Wasserburg (1982) *Science*, *217*(4556), 207-214. Piepgras, D. J., *et al.* (1979) *EPSL*, *45*(2), 223-236. Reynolds, B. C., *et al.* (1999) *EPSL*, *173*(4), 381-396. Roberts, N. L., *et al.* (2010) *Science*, *327*(5961), 75-78. Shackleton, N. J., *et al.* (1984) *Nature*, *307*(5952), 620-623. Steph, S., R. *et al.* (2006) *Paleoceanography*, *21*(4). Steph, S., *et al.* (2010) *Paleoceanography*, *25*. Tachikawa, K., C. *et al.* (1999) *EPSL*, *170*(4), 433-446. Tiedemann, R., *et al.* (2007) *Proc. ODP, Sci. Res. 202*, 1-69. Whiteley, N. (2000) PhD Thesis Zachos, J., *et al.* (2001) *Science*, *292*(5517), 686-693.

IODP

Using coupled Fe-Mg chemical and isotopic diffusion profiles to model magma residence times of crystals

M. OESER[1], S. WEYER[1], R. DOHMEN[2], I. HORN[1]

[1] Leibniz Universität Hannover, Institut für Mineralogie, Callinstr. 3, 30167 Hannover

[2] Ruhr-Universität Bochum, Institut für Geologie, Mineralogie und Geophysik, Universitätsstr. 150, 44780 Bochum

Chemical zoning in minerals, such as Fe-Mg in olivine, can be the result of inter-diffusion driven by a chemical disequilibrium between a mineral and the surrounding melt. In this case, chemical zoning profiles (measured e.g. by electron microprobe analysis) can be used to constrain magma residence times of crystals by modeling such intra-mineral chemical gradients (e.g. [1, 2]). However, Fe-Mg zoning in olivine may also develop during olivine growth in an evolving magma without any diffusion-driven Fe-Mg exchange between olivine and melt. In this latter case, it provides no time information. The in situ analysis of stable metal isotope ratios in pheno- and xenocrysts may provide a powerful tool to distinguish between diffusion-driven- and growth zoning, as diffusive processes result in large kinetic isotope fractionation even at high temperatures (e.g. [3]). Accordingly, diffusion-generated Fe-Mg zoning in olivine should be coupled with Fe-Mg isotopic zoning. In contrast to diffusion associated with large kinetic isotope fractionations, diffusion-free crystal growth can be regarded to be an equilibrium process with only small isotope effects (e.g. [4]).

We investigated olivine grains in basaltic rocks from the Massif Central volcanic region (France) in order to test whether in situ analyses of Fe- and Mg isotopes provides a useful tool to identify diffusion-generated zoning in minerals. Large, chemically zoned olivines were analyzed by femtosecond laser ablation MC-ICP-MS. With this technique the internal precision that can routinely be achieved is ±0.05‰ (2σ) for both Fe and Mg.

Several of the investigated olivines (including both xeno- and phenocrysts) show significant Fe-Mg isotopic zoning (of up to 1.5‰ for δ^{56}Fe and up to 0.8 for δ^{26}Mg) that is coupled with the chemical zoning expressed as Mg#. Furthermore, the Fe-Mg isotopic zoning profiles are inverse, resulting in a negative correlation between δ^{26}Mg and δ^{56}Fe. This negative correlation is expected if the chemical zoning was generated by diffusion of Fe into and Mg out of the olivine that is driven by a chemical gradient between crystal and melt (e.g. [5]). Consequently, the clearly diffusion-generated chemical and isotopic zoning in such olivine crystals can be used to estimate the duration of chemical diffusion between crystal and melt. This duration can reflect the residence time of crystals in a magma chamber before an eruption [6]. Simplified and independent modeling of Fe- and Mg- chemical and isotopic zoning of the investigated olivines point to magma residence times between 1 and 10 years, which is similar to the short timescales determined by diffusion modeling of chemical gradients in olivines hosted in basaltic lava flows from the Chilean Andes and Mt. Etna [1, 2].

A major focus of our project is to apply our developed technique to olivine crystals in MORBs to improve our knowledge on magma evolution at mid-ocean ridge settings. Appropriate basalt samples were taken in drill cores from two DSDP holes (332A and 396B) at the slow-spreading Mid-Atlantic Ridge (MAR) and from one ODP hole (896A) at the intermediate-spreading Costa Rica Rift. Numerous samples host fresh olivine phenocrysts with sizes from 0.5 mm to 2 mm across. Our first electron microprobe analyses of olivines from the MAR reveal that the latter show both normal zoning and reverse zoning in terms of Fo content (up to 4 mole percent). The chemical zoning is up to 100 µm wide and thus large enough for the in situ analyses of Fe-Mg isotopes, given a laser ablation spot diameter of ~40 µm. Consequently, the Fe-Mg isotopic profiles will help to define the process that generated the chemical zoning and thus determine whether the chemical zoning can be used to model magma residence times of these olivines. Furthermore, some of the basalt samples contain glassy parts with unzoned olivine

phenocrysts. This may provide an opportunity to determine the (equilibrium) isotope fractionation between melt and olivine, as we can analyze the Fe-Mg isotopic composition of both glass and olivine in situ.

Our initial results show that in situ Fe- and Mg isotope analyses by femtosecond laser ablation MC-ICP-MS provide a powerful means to resolve small-scale isotopic variations in minerals and, therefore, allow to tracing diffusive processes that occur on the mineral scale during magma differentiation. Consequently, more reliable time information on the evolution of magma chambers can be obtained by performing diffusion modeling of chemical *and* isotopic profiles in minerals.

References:
[1] Costa, F., Dungan, M. (2005). Geology 33, 837–840.
[2] Kahl, M., et al. (2011). EPSL 308, 11–22.
[3] Richter, F.M., et al. (1999). GCA 63, 2853-2861.
[4] Davidson, J.P., et al. (2007). Annu. Rev. Earth Planet. Sci. 35, 273–311.
[5] Dauphas, N., et al. (2009). EPSL 288, 255–267.
[6] Costa, F., et al. (2008). Rev. Mineral. Geochem. 69, 545-594.

IODP

Fluctuations of Cenozoic oceanic Ca isotopic budget and environmental changes

ST. PABICH[1], N. GUSSONE[1], B.M.A. TEICHERT[2]

[1] Westfälische Wilhelms-Universität Münster, Institut für Mineralogie, Münster, Germany
[2] Westfälische Wilhelms-Universität Münster, Institut für Geologie und Paläontologie, Münster, Germany

One of the main aims in earth science is to reconstruct and understand the oceanic chemical and isotopical evolution over geologic time, to gain a better understanding of earth's climate changes. In this context Ca, as one of the major elements in the ocean, is especially vital because its temporal variations in concentration are controlled by weathering, carbonate sedimentation and thus related to the CO_2 concentration of the atmosphere. Imbalances in input and output of Ca to the ocean will cause a shift in the Ca isotopic composition (Farkas et al. 2007). Therefore, the Ca isotopic composition of paleo seawater, which is recorded in biominerals like foraminifers, is an ideal tool to study changes in Ca budget of the ocean. In this context, the Cenozoic is of special interest, as it is known for its times of extreme and rapid climate variabillity, expressed in a rapidly shifting carbonate compensation depth (CCD) (Zachos et al. 2001, Pälike et al. 2012).

The Pacific Equatorial Age Transect (PEAT) program was developed to achieve a Cenozoic age transect along the paleo-equatorial Pacific. IODP Expeditions 320 and 321 retrieved a well-preserved continuous Cenozoic carbonate record (Pälike et al. 2010, Lyle et al. 2010) which provides an archive of extreme Cenozoic climate variability and gives indications about the evolution of the equatorial Pacific and how it interacts with global climate. In this study we use this record to establish a reliable, high resolution $\delta^{44/40}$Ca paleo seawater record for the Late Paleogene between 45 and 23 Ma and model changes in the Ca budget through time in response to major paleoceanographic fluctuations in the global carbonate cycle, as expressed in dramatic CCD fluctuations.

The sediment samples were first characterised in terms of their calcareous microfossil content, in order to select the most appropriate Ca isotope archive for our seawater reconstructions. Based on occurrence, isotope fractionation behaviour and preservation, we chose the benthic foraminifers *Nuttalides* spp. (mainly *N. truempyi*), *Gyroidinoides* spp. (*G. soldanii* and *G. neosoldanii*) and *Cibicidoides* sp. (*C. grimsdalei*, *C. mundulus*, *C. subhaidingerii*) from size-fraction >63µm for $\delta^{44/40}$Ca measurements. Foraminifer tests were hand-picked under the binocular and cleaned individually following the method described in Gussone and Filipsson (2010). An aliquot of each sample was mixed with a ^{42}Ca/^{43}Ca double-spike, prior to the isotope analysis with a Thermofinnigan TRITON T1 thermal ionosation mass spectrometer, to correct isotope fractionation during measurements (Gussone et al. 2011).

Our first results suggest considerable differences in the Ca isotope record of benthic foraminifers during the Eocene and the Oligocene (Figure 1).

The Eocene is characterized by a succession of carbonate poor and rich sediments, reflecting a highly dynamic carbonate compensation depth (CCD) and strong

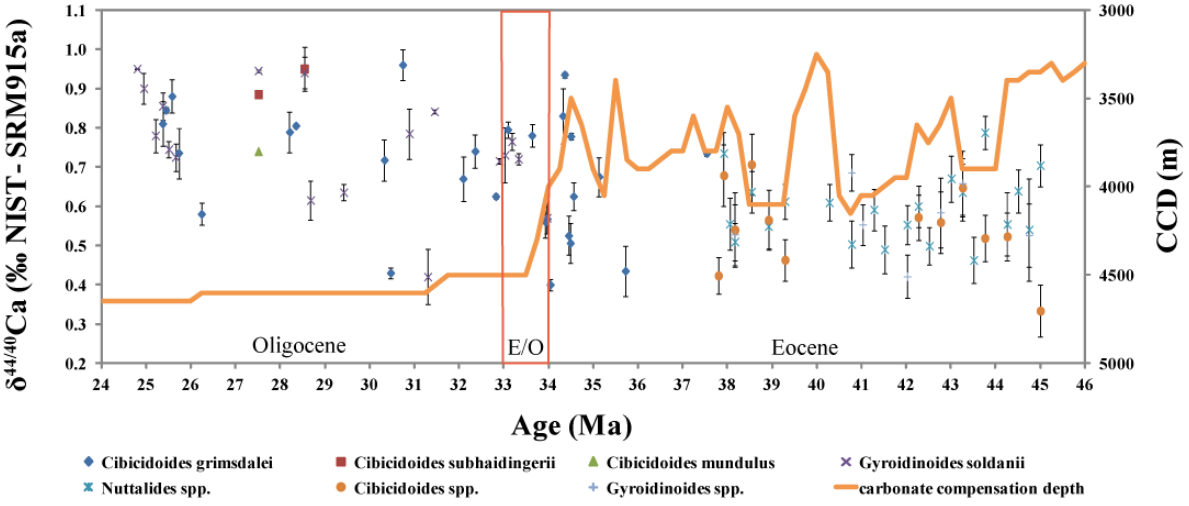

Figure 1: Eocene and Oligocene benthic foraminifer calcium isotope ratios. The red box marks the Eocene – Oligocene transition zone. The orange line illustrates the carbonate compensations depth (CCD) from Pälike et al. (2012). Error bars represent $2\sigma_{mean}$.

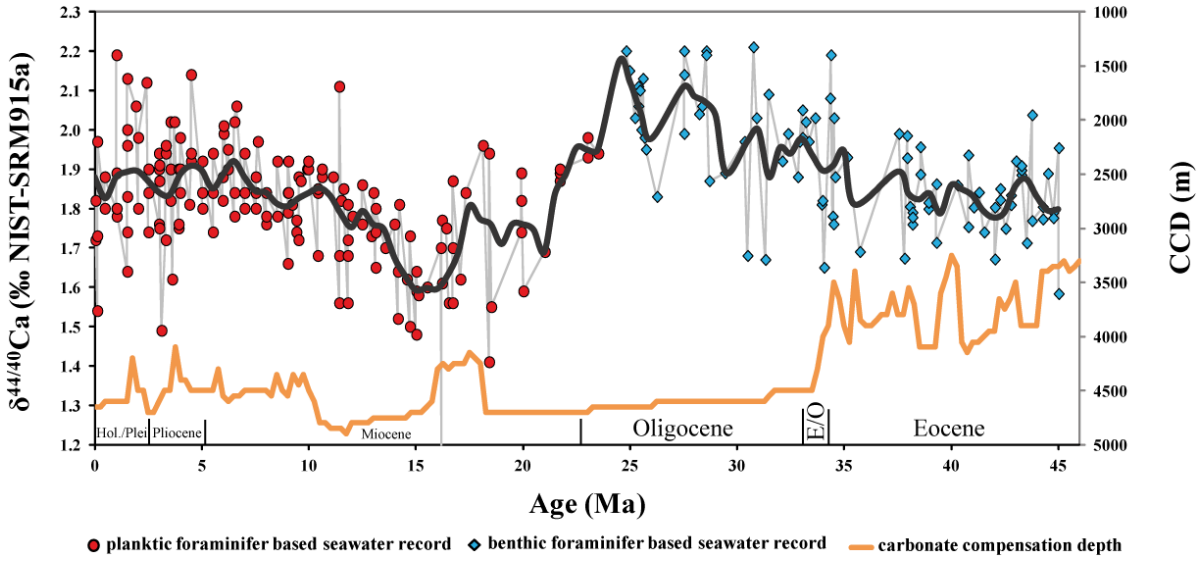

Figure 2: $\delta^{44/40}$Ca seawater record from the Eocene to present. The Neogene record is based on planktonic foraminifers (Heuser et al. 2005 and Sime et al. 2007), the Paleogene record is based on benthic foraminifers (this project). Black line: spline smoothed $\delta^{44/40}$Ca seawater reconstruction. Abbreviations are Hol, Holocene and Plei, Pleistocene.

changes in bottom water calcite saturation whereas the Oligocene shows a constantly deep CCD with carbonate rich sediments (c.f. Coxall et al. 2005, Pälike et al. 2010, Lyle et al. 2010, Pälike et al. 2012). Figure 1 shows the measured $\delta^{44/40}$Ca data of benthic foraminifers for the middle to upper Eocene and the Oligocene in comparison with the CCD (Pälike et al. 2012). In general, the values show little variation, with relatively constant values throughout the Eocene. In addition, the Eocene record shows no significant fluctuations in $\delta^{44/40}$Ca values during phases of large CCD fluctuations (short term). The lack of excursions to higher $\delta^{44/40}$Ca values during phases of low carbonate preservation (indicative for low calcite saturation of the bottom water) provides further evidence that at bottom water temperatures above 10°C, which are postulated for the Eocene, a bias of the Ca isotope fractionation of benthic foraminifers can be excluded. This is an important verification, as previous studies suggested that low calcite saturation in combination with low temperatures might result in anomal Ca isotope fractionation pattern (Gussone and Filipsson 2010). There is also no offset between the different species visible, consequently no species-specific fractionation factors need to be applied. In contrast to the Eocene, the Oligocene record indicates a long term trend with increasing $\delta^{44/40}$Ca towards the late Oligocene by ~0.3‰. The different Ca isotope trends seem to be related to differences in the oceanic Ca and C cycling, expressed in the carbonate preservation and CCD. While the Eocene sedimentation is characterised by a strong variability in CCD, leading to rapid changes in the carbonate content of the sediments and the occurrence of several carbonate accumulation events (CAE) (Pälike et al. 2012), the Oligocene sediments show uniformly high carbonate contents.

Past seawater $\delta^{44/40}$Ca was calculated from the benthic foraminifer record applying the calibration for *Gyroidinoides* spp. ($1000\ln\alpha = -1.25$ ‰) from Gussone and Fillipson (2010). The different analysed species reveal similar $\delta^{44/40}$Ca values, indicating that there is no species-specific offset in Ca isotope fractionation. Hence, we used this offset to reconstruct the $\delta^{44/40}$Ca seawater record (Figure 2). The Ca budget during the Eocene seems to be relatively constant and the short term CCD fluctuations seem to be to small to alter the isotopic Ca budget. The Oligocene on the other hand, is characterized by a general increase in values and a continuous deepening of the CCD and the isotopic composition of the paleo seawater shows a trend to heavier values. This is consistent with a massive long term (> 1 Ma) carbonate deposition and a decreasing Ca concentration in the ocean water. During carbonate formation, the lighter Ca isotopes are favoured over the heavier isotopes. As a consequence, the seawater isotopy will be depleted in light ^{40}Ca and the $\delta^{44/40}$Ca seawater increases. Combined with Neogene data from Heuser et al. (2005) and Sime et al. (2007) the data suggest an increase in values during the Oligocene with a maximum at the end of the Paleogene. A further mechanism that was proposed to potentially alter the seawater Ca isotope composition, is a change in the average fractionation of the marine carbonates, e.g. by the shift from a calcite to an aragonite ocean (Farkas et al. 2007). As Ca isotope fractionation in inorganic aragonite is stronger pronounced compared to calcite (Gussone et al. 2005), a shift from a calcitic to aragonitic ocean could also lead to a trend towards heavier seawater Ca isotope values during the Oligocene.

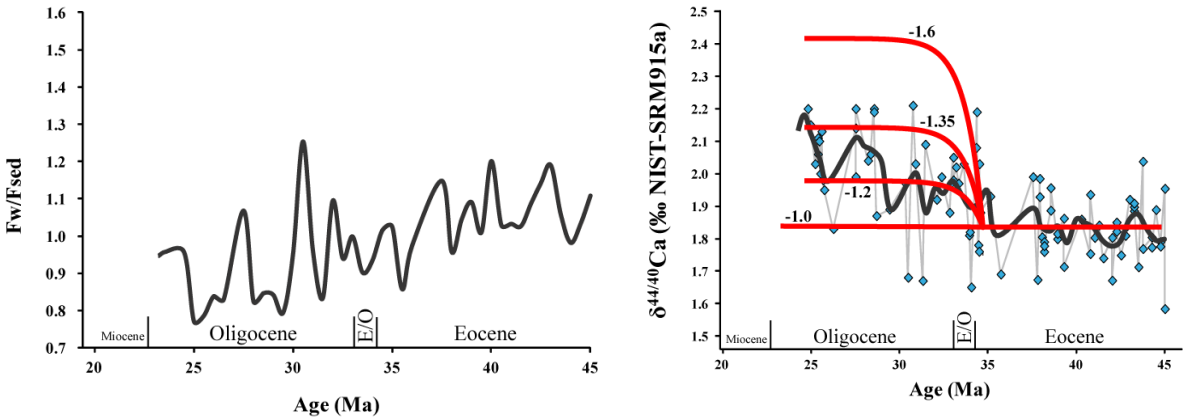

Figure 3 A: Oceanic Ca input/output model indicates increasing Ca sedimentation during the Oligocene and a decrease in Ca concentration of the ocean. Fw: weathering flux (input), Fsed: sedimentation flux (output). B: Effect of changing the isotope fractionation of the oceanic Ca sink on the $\delta^{44/40}$Ca seawater evolution.

Figure 3A shows a quantitative model of the Ca flux (input/output ratio) plotted against time with constant boundary conditions (todays isotope composition of oceanic Ca sources and fractionation factor of sink). At Fw/Fsed = 1 input and output are in equilibrium. Above this equilibrium the input is higher than the output and is compatible with carbonate dissolution, indicated by a shallower CCD. Beneath this equilibrium the output is higher than the input, which is consistent with a deeper CCD. In Figure 3B, we modeled the effect of changing the fractionation between seawater and marine Ca sink in response to the shift from a calcite to an aragonite ocean. The model starts with the assumption of constant conditions (input = output) and a Ca isotope fractionation of -1.0‰. A relative change in fractionation factor of about 0.35‰ in the Oligocene could explain the observed increase in the $\delta^{44/40}$Ca seawater values. The shift from calcite to aragonite is consequently not a likely mechanism for the $\delta^{44/40}$Ca increase in the Oligocene. Therefore, the Ca isotope record is most likely reflecting changes in the input/output ratio of Ca.

References:

Coxall H. K.,Wilson P. A., Pälike H. Lear C., and Backman J. (2005) Rapid stepwise onset of Antarctic glaciation and deeper calcite compensation in the Pacific Ocean. Nature 433, 53 – 57.

Farkas J., Böhm F., Wallmann K., Blenkinsop J., Eisenhauer A., van Geldern R., Munneke A., Voigt S., Veizer J. (2007) Calcium isotope record of Phanerozoic oceans: Implications for chemical evolution of seawater and its causative mechanisms. Geochimica et Cosmochimica Acta 71, 5117 – 5134.

Gussone N., Böhm F., Eisenhauer A., Dietzel M., Heuser A., Teichert B. M. A., Reitner J., Wörheide G., and Dullo W.-C. (2005) Calcium isotope fractionation in calcite and aragonite. Geochimica et Cosmochimica Acta 69, 4485-4494

Gussone N. and Filipsson H.L. (2010) Calcium isotope ratios in calcitic tests of benthic Foraminifers. Earth and Planetary Science Letters 290, 108 – 117.

Gussone, N., Nehrke, G. and Teichert, B.M.A. (2011) Calcium isotope fractionation in ikaite and vaterite. Chemical Geology 285, 194-202.

Heuser, A., Eisenhauer, A., Böhm, F., Wallmann, K., Gussone, N., Pearson, P.N., Nägler T.F. and Dullo, W.-C. (2005) Calcium Isotope ($\delta^{44/40}$Ca) Variations of Neogene Planktonic Foraminifera. Paleoceanography 20, PA2013, doi:10.1029/2004PA001048.

Lyle M., Pälike H., Nishi H., Raffi I., Gamage K., Klaus A. and the IODP Expeditions 320/321 Scientific Party (2010) The Pacific Equatorial Age Transect, IODP Expeditions 320 and 321: Building a 50-Million-Year-Long Environmental Record of the Equatorial Pacific Ocean. Scientific Drilling 9, 4 – 15.

Pälike H., Lyle M., Nishi H., Raffi I., Gamage K., Klaus A. and the IODP Expeditions 320/321 Scientists (2010) Expedition 320/321 summary. Proc. IODP, 320/321: Tokyo (Integrated Ocean Drilling Program ManagementInternational, Inc.)

Pälike H., Ridgwell A., and the Expedition 320/321 Scientists (2012) A Cenozoic record of the equatorial Pacific carbonate compensation depth. Nature 488, 609 – 615.

Sime N. G., De La Rocha C.L., Tipper E.T, Tripati A., Galy A., and Bickle M.J. (2007) Interpreting the Ca Isotope Record of Marine Biogenic Carbonates. Geochim. Cosmochim. Acta 71, 3979 – 3989.

Zachos J., Pagani M., Sloan L., Thomas E., Billups K. (2001) Trends, Rhythms, and Aberrations in Global Climate 65 Ma to Present. Science 292: 686 – 693.

ICDP

The first palynological results for the last glacial / interglacial cycle at Lake Van, Turkey

N. PICKARSKI[1,*], T. LITT[1] AND PALEOVAN SCIENTIFIC TEAM

[1] University of Bonn, Steinmann Institute, Nussallee 8, 53115, Bonn, Germany

* pickarski@uni-bonn.de

Lake Van is located on the Eastern Anatolia High Plateau in Turkey, between the eastern Taurus in south Turkey and the highlands of Ararat, close to the border to Iran. The Lake is surrounded by active volcanoes (Nemrut, Süphan) within a tectonically active and climatically sensitive region, at about 1,646 m above sea level. Therefore, it provides a key position for paleoclimate and paleoenvironmental reconstructions in the Near East. Lake Van is the greatest soda lake and the fourth largest hydrologically closed lake system on earth, with a surface area of 3,570 km² and a volume of 607 km³. In addition, the greatest extension of 130 km is located between Tatvan (WSW) and the mouth of the Bendimahi River (ENE). The maximum depth of Lake Van is about 460 m. The water chemistry of the lake is characterized by high salinity (22 ‰) and a high alkalinity with a pH reaching ~10. The recent vegetation is represented by the Irano-Turanian plant zone, whereby the precipitation distribution controls the vegetation in this region. The northeast of the lake is marked by steppe plants, which are mainly characterized by grasses, chenopods and Artemisia, whereas some oak-forest remnants can be observed in the southwest of Lake Van. We present a preliminary pollen record based on analyses of sediment cores obtained during a drilling campaign in summer 2010. The first palynological data suggest that the whole 220 m long sedimentary record encompasses c. 500,000 years. The major focus of the

study presented here is to identify and interpret the vegetation and the climatic oscillations during the last glacial-interglacial cycle in more detail. Therefore, we have generated a well-dated, millennial-scale resolution pollen record of the first 60 mcblf (meter composite below lake floor). Warmer environments are characterized by higher amount of thermophiles trees, especially by deciduous oak, whereas pollen of steppe elements and semi-desert plants like Artemisia, chenopods and grasses suggest periods with more arid, continental and probably colder climate. In this context, a complete glacial-interglacial sequence of lacustrine sediments can be unambiguously correlated with the MIS 1-5 (last 130 ka) by means of its pollen stratigraphy. The tentative chronology of the core is confirmed by tephrostratigraphy, oxygen isotope data, and by matching of the pollen record to the SPECMAP curve. Based on palynological data, we are able to identify warm intervals such as oxygen – isotope stages 5e, 5c, 5a and 3. Ongoing work is mainly focused on the identification of the Dansgaard-Oeschger events.

References:
Litt et al. (2012): 500,000 Years of Environmental History in Eastern Anatolia: The PALEOVAN Drilling Project, Scientific Drilling Journal, pp. 18-29.

IODP

Viruses in deep subseafloor sediments

F. PREUSS[1], T. ENGELHARDT[1], H. CYPIONKA[1], B. ENGELEN[1]

[1] Institut für Chemie und Biologie des Meeres, Carl-von-Ossietzky Universität Oldenburg, Carl-von-Ossietzky Straße 9-11, D-26111 Oldenburg, Germany, www.pmbio.icbm.de

Viral infections as a controlling factor for the deep biosphere. The overall goal of our project is to understand the impact of phages on biogeochemical cycling, microbial abundance and diversity within the marine deep biosphere. Due to the absence of grazers, viruses might be the main predators in highly compacted and mostly anoxic subsurface sediments. The integration of the viral component into the biogeochemical model for subsurface sediments is important to understand the recycling of labile organic matter within this habitat. We hypothesise that viruses might be one controlling factor for the abundance and diversity of indigenous microorganisms.

Bacteriophages were shown to be present in high numbers in deep marine sediments obtained during ODP Leg 201. Direct counting of virus-like particles has shown that their number typically exceeds total cell counts. Furthermore, the virus-to-cell ratio increased with depth, indicating ongoing viral production in these sediments. To get a better understanding of the origin of these viruses and their influence on the microbial life in the marine subsurface, we started investigations on phage-host systems.

Quantification of Rhizobiophages and associated host populations in subsurface sediments of ODP Leg 201. Populations of *Rhizobium radiobacter* were used to analyse viral communities in marine deep sediments. For ODP Leg 201 sediments, this species contributed up to 7.5% to the total bacterial community. Our culture collection from these sediments comprises 36 different strains of *R. radiobacter*. Genome fingerprints by ERIC-PCR have shown that *R. radiobacter* forms site-specific subpopulations. We were able to induce prophages in all 36 strains indicating their lysogenic nature. Analysis of the phage genomes by pulsed-field gel electrophoresis indicated that two different phages were present in the analyzed host population. The genome sizes were determined to be 52kb and 34kb, respectively. Several strains occurred to have multiple prophage infections. Thus, lysogeny appears to be a typical feature of the deep subsurface isolates of *R. radiobacter*.

Both isolated Rhizobiophages were subjected to whole-genome sequencing. Based on the genome information of Rhizobiophage RR1-A, primer sets targeting the

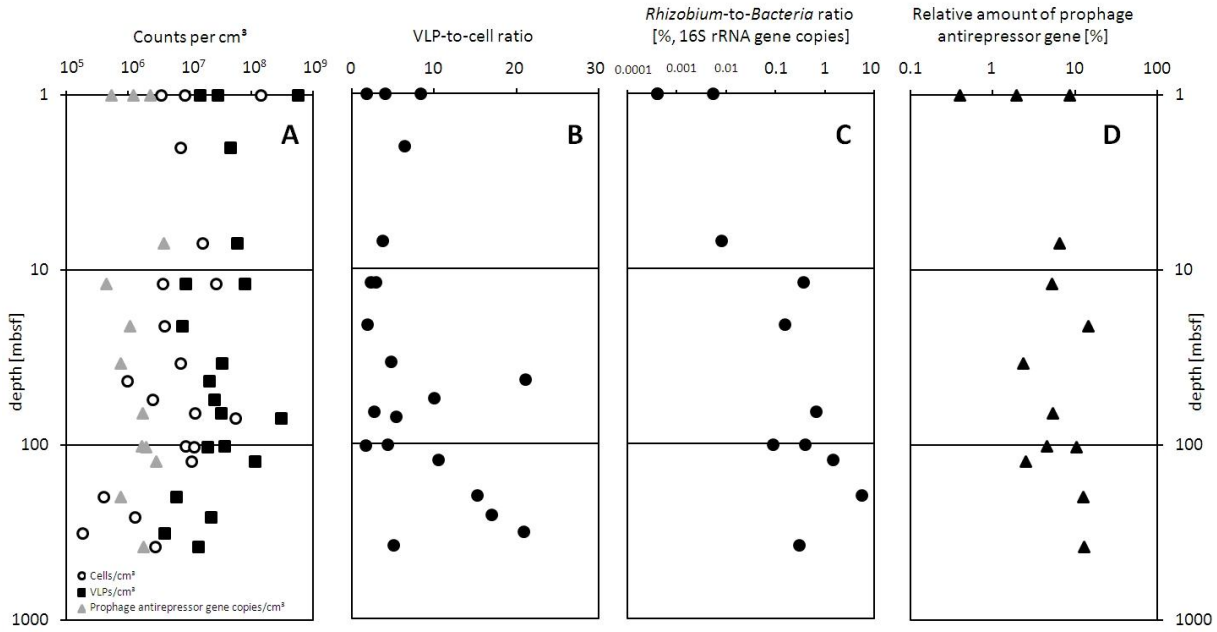

Figure 1. (a) Cellcounts per cm^3 (open circles), number of virus-like particles; VLP per cm^3 (squares) and copies of the prophage antirepressor gene (gray triangles) within ODP Leg 201 sediments. (b) VLP-to-cell ratio. (c) Relative amount of *R. radiobacter* compared with total Bacteria based on 16S rRNA gene copies. (d) Relative amount of prophage antirepressor gene copies compared to the total viral abundance.

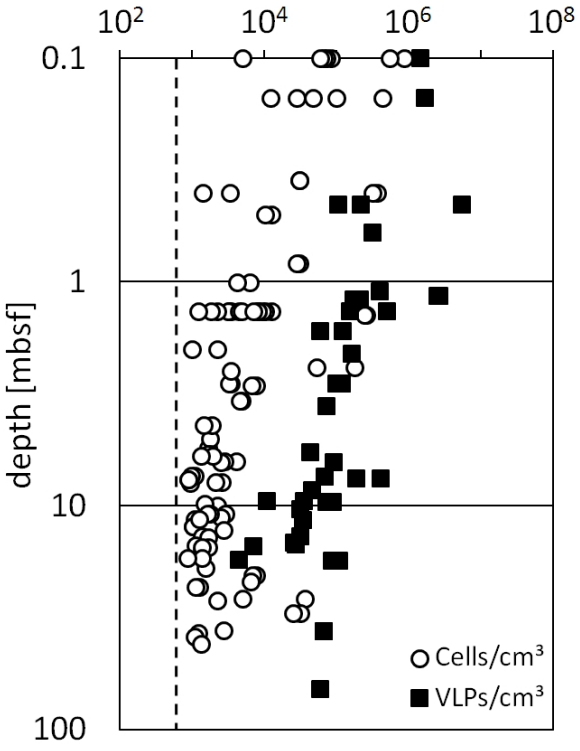

Figure 2. Cell numbers and virus counts from subsurface sediments of IODP Exp. 329 (IODP sites U1365 – U1369). The dashed line indicate the detection limit for the cell counts of 2.8 x 10^2 cells/cm^3.

antirepressor gene were developed. This gene is involved in the switch between lysogeny and the lytic cycle and is indicative for temperate phages. Quantitative PCR was applied to purified viral DNA extracts obtained from various sites and depths to quantify the number of antirepressor gene copies in these sediments. Gene copy numbers of prophage antirepressor gene accounted for 10^5 to 10^6 genes cm^{-3} of sediment. Phages containing the targeted antirepressor gene contributed up to 14.3% (ODP site 1225, 198 mbsf) to the total virus abundance.

The occurrence of lysogeny as a typical characteristic of *R. radiobacter* is reflected by the high number of temperate Rhizobiophages found in the investigated deep subsurface sediments. Furthermore, an ongoing production of phages can be assumed due to the generally high number of phages in deeper sediment layers. As the mobility of phages and host cells is limited in highly compacted sediments, it appears unlikely that lytic viral reproduction is a dominant mechanism for viral proliferation. Furthermore, the host cell density might be too low to support a lytic phage reproduction. Thus, the production of phages may result more likely from natural induction of prophages, which is strongly supported by the presence of the high amount of temperate phages in subsurface sediments. Our results show that phages are an active component in marine deep sediments and indicate lysogeny as an important feature of microbial communities in the marine subsurface.

Viruses in extremely nutrient-depleted sediments of the South Pacific Gyre (IODP Exp. 329). While sub-seafloor life has mostly been studied at continental margins, mid-ocean gyres are rather unexplored, so far. Mid-ocean gyres represent the most oligotrophic marine ecosystems comprising about 42% of the world´s oceans. An extremly low primary productivity leads to extremly low cell numbers and diminished microbial activities within the water column and the sediments below. The

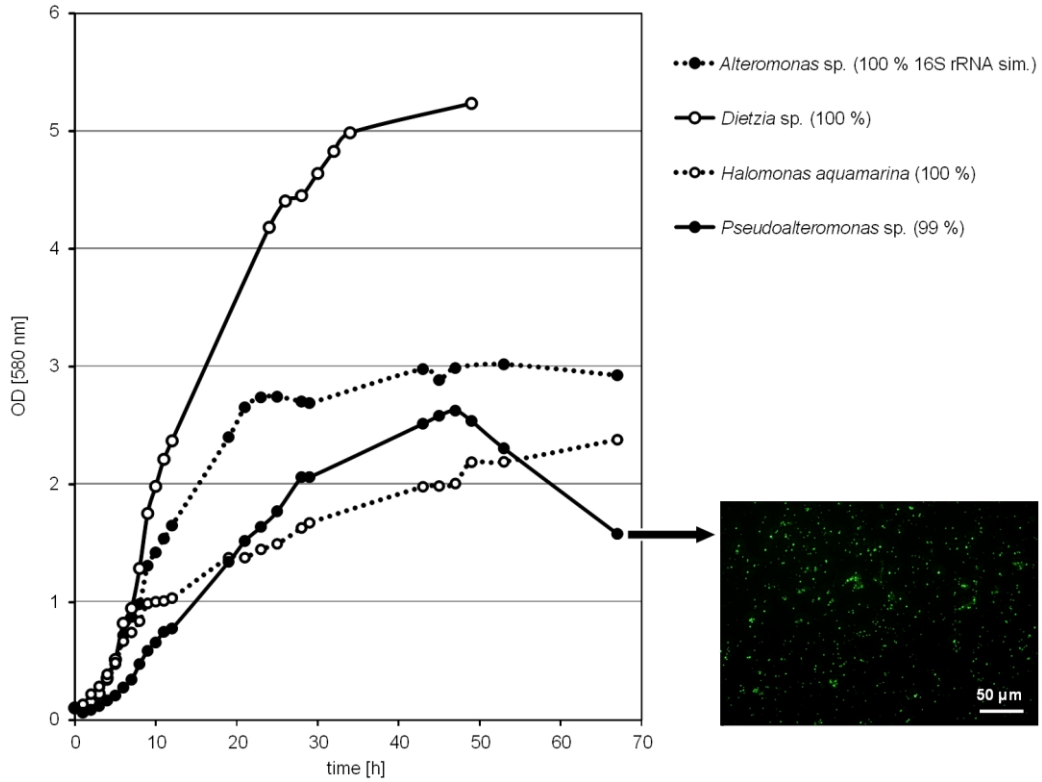

Figure 3. Growth curves of the first SPG isolates prior to phage induction experiments (left:). The decrease in the optical density of the *Pseudoalteromonas* culture at the end of the growth experiment indicate the presence of temperate phages. The image (right) shows large bacterial cells and small viruses after SYBR Green staining of this culture.

largest of these oceanic provinces, the South Pacific Gyre (SPG), was now investigated during IODP Exp. 329.

First, viral counts were determined on SPG sediments to calculate their distribution within the subsurface. In comparison to our previous studies on benthic viruses from continental margin sites (Engelhardt et al., 2011 and 2013), we will obtain more realistic estimates for the viral loop as a factor for sustaining the deep biosphere. Our results from the SPG indicate that the number of viruses always exceeded those of prokaryotic cells with an increasing virus-to-cell ratio with depth (Fig. 2).

The diversity of viruses within the SPG sediments will be analysed by applying a novel approach using whole genome amplification. This technique is needed to enhance the amount of viral DNA in sediments with an extremly low abundance of viruses. Subsequently, other molecular down stream applications such as RAPD-PCR will be used to analyse virus diversity patterns of the different sites.

In our cultivation-based approach, we have started to isolate subseafloor microorganisms from the SPG to identify prophages within their genomes. Sediment samples that were recovered from different sites and sediment horizons were directly transferred into three different media onboard the JOIDES Resolution. Two media containing a mix of several monomers as substrates were used to target either aerobic or anaerobic heterotrophs. For the enrichment of autotrophs, cultures were set up in artifical seawater medium (without any organic substrate) and flushed with hydrogen/carbon dioxide.

Due to the slow growth of indigenous microorganisms, we have now obtained the first isolates from a limited number of oxic enrichments from site U1371 (3.7 mbsf, 122 mbsf, 127 mbsf). Those are affiliated to *Nocardioides basaltis* (99% 16S rRNA sim.), *Halomonas aquamarina* (100%), *Erythrobacter vulgaris* (99%), *Pseudoaltoromonas* sp. (99%), *Alteromonas* sp. (100%), and *Dietzia* sp. (100%). Their presence was already detected by molecular screening of the cultures by DGGE. First growth experiments with these isolates indicated the presence of temperate phages within their genomes (Fig. 3).

When the process of strain purification is completed, we will start to induce the prophages within their genomes. The morphologic and phylogenetic diversity of these phages will be analysed in detail. Concerning our culture collection, we will then identify if the percentage of infected cells that are under severe starvation is different to those isolated from “high activity sites”.

References:

Engelhardt T, Sahlberg M, Cypionka H, Engelen B (2011) Induction of prophages from deep-subseafloor bacteria. Environm Microbiol Rep 3:459–465

Engelhardt T, Sahlberg M, Cypionka H, Engelen B (2013) Biogeography of Rhizobium radiobacter and distribution of associated temperate phages in deep subseafloor sediments. ISME J 7: 199–209

ICDP

Simulation of magma ascent prior to the high risk caldera forming eruptions of Campi Flegrei: first results

O. PREUSS[1], M. NOWAK[1]

[1] Eberhard Karls Universität Tübingen, Department of Geoscience, Wilhelmstraße 56, 72074 Tübingen, Germany

The dynamic magmatic processes beneath Campi Flegrei, occurring during magma ascent, cannot be observed directly in nature. Nevertheless, these processes may lead to potentially catastrophic eruptions threaten millions of people in and around Naples (Italy). Therefore, the Campi Flegrei Deep Drilling Project (CFDDP) offers a unique opportunity to sample a substantial sequence of volcanic rocks and ashes of the restless Campi Flegrei caldera. The textural and structural analysis of drilled natural samples will be compared with experimental results achieved in this study. Experimental simulations of Campanian Ignimbrite (CI) magma storage and ascent will give insight to the mechanisms of the Campanian Ignimbrite super eruptions, thus providing tools for volcanic hazard assessment at the high risk Campanian Volcanic District and other comparable volcanic systems.

The Campanian Volcanic District is located in the middle-southern part of the Campanian plain with the Campi Flegrei (CF) Volcanic Field and the Monte Somma-Vesuvio strato-volcano (Mastrolorenzo and Pappalardo 2006). CF is an active volcanic field characterized by mainly explosive activity, both hydromagmatic and magmatic, and few effusive episodes. The main structural feature is a nested caldera that formed during two main collapse episodes, related to the two most powerful eruptions, the 39 ka Campanian Ignimbrite (CI) and the 14 ka Neapolitan Yellow Tuff events. This project focuses on the CI super-eruption yielding > 200-300 km^3 dense rock equivalent of trachytic-phonolitic material, distributed over ~30,000 km^2 synchronous with significant climate changes (De Vivo 2010).

A pressure decrease during ascent accompanied with fluid oversaturation in the melt initiates bubble nucleation, growth, coalescence and segregation, which leads to a substantial density decrease and a change in viscosity in the ascending magma. These processes may act as driving forces for increased ascent rates and may lead to different eruption styles (e.g. Gonnermann & Manga, 2007).

Discrepancies of previous studies demonstrate that the P-T-t conditions and volatile contents (H_2O, CO_2, Cl) of the primitive melt prior to the eruption, generating the CF volcanic products are not well constrained. The determination of these conditions at which differentiation occurred to produce the CF phonolites and trachytes is necessary and is the main focus of the coordinated project of Behrens and Botcharnikov (BE 1720/28-1) in Hannover. In coordination with this project, our study is focused on the conduction of continuous decompression experiments to gain insight into dynamic degassing processes like bubble nucleation, bubble growth and decompression induced partial crystallization. To investigate these processes occurring during magma ascent, a trachytic CI composition (Civetta et al. 1997) is used. The same composition is also used for the investigation of phase relations by the coordinated project in Hannover.

First decompression experiments are performed inside an Internally Heated Pressure Vessel (IHPV) using a starting pressure of 200 MPa and H_2O content of 5 wt%, close to saturation (S. Fanara, pers. communication). Up to now, H_2O is the only added volatile to the system to keep the identification of occurring processes simple. Series of experiments with four different decompression rates (0,0028, 0,024, 0,17 and 1,7 MPa s^{-1}) and two different types of sample material (glass cylinders / glass powder) are used. Prior to the decompression, the samples are equilibrated at 1300°C for 96 hours for the cylinders and 24 hours for the powder. The comparison between glass cylinder and powder is necessary to test for possible heterogeneous bubble nucleation on former grain boundaries inside the powder sample that may distort the results. The isothermal decompression takes place above the liquidus at 1050°C to ensure a crystal free melt and a homogenous bubble nucleation. The continuous pressure decrease to 75 MPa is realized by a novel high P low-flow metering valve equipped with a piezoelectric nano-positioning system (for technical details see Marxer et al., this colloquium). After isobaric rapid quench at 75 MPa, the samples are analyzed by a scanning electron microscope (SEM). The resulting BSE-images provide information on the bubble number density, bubble distribution and bubble sizes in the quenched melts.

Based on a phonolitic composition, Marxer et al. (this colloquium) demonstrate that changes in decompression rate and style lead to a different degassing behavior of the magma. Analytical investigations using near infrared (NIR) spectroscopy for determining the residual H_2O content indicate that an increase in decompression rate results in higher H_2O contents in the residual melt. As a consequence, for the trachytic CI melt similar processes are expected. In future experiments, additional volatiles (CO_2, Cl) will be added to simulate conditions closer to the CF volcanic system. To investigate heterogeneous bubble nucleation caused by decompression induced crystallization processes, experiments will be performed at lower temperatures below the liquidus.

References:

Civetta et al. (1997) - Geochemical zoning, mingling, eruptive dynamics and depositional processes - The Campanian Ignimbrite, Campi Flegrei caldera, Italy. Journal of Volcanology and Geothermal Research, 75(3-4): 183-219.

De Vivo et al. (2010) - Research progress in volcanology in the Neapolitan area, southern Italy: a review and some alternative views. Miner Petrol, 99(1-2): 1-28.

Gonnermann, HM and Manga M (2007) - The fluid mechanics inside a volcano. Annu. Rev. Fluid Mech, 39: 321-356.

Mastrolorenzo, G. and Pappalardo, L. (2006) - Magma degassing and crystallization processes during eruptions of high-risk Neapolitan-volcanoes: Evidence of common equilibrium rising processes in alkaline magmas. Earth and Planetary Science Letters, 250(1-2): 164-181.

IODP

Rare earth elements in scleractinian cold-water corals: New insights from the Challenger Mound (IODP Site 1317), NE Atlantic

JACEK RADDATZ[1], ED HATHORNE[1], MARTIN FRANK[1], VOLKER LIEBETRAU[1], ANDRES RÜGGEBERG[1,2] AND WOLF-CHRISTIAN DULLO[1]

[1] GEOMAR Helmholtz Zentrum für Ozeanforschung Kiel, Wischhofstr. 1-3, 24148 Kiel

[2] Renard Centre of Marine Geology, Ghent University, Krijgslaan 281, S8, B-9000 Gent, Belgium.

In 2005 the IODP Expedition 307 retrieved for the first time complete records through the entire sediment body of the 155 m high Challenger Mound (CM) in the Porcupine Seabight, NE Atlantic (~ 800 m below sea level). These sediment cores contained mainly the scleractinian cold-water coral (CWC) *Lophelia pertusa*. First studies could show that the initiation of the CM coincided with the intensification of the Mediterranean Outflow Water (MOW) and the onset of the Northern Hemisphere Glaciation (NHG) at ~ 3 Ma. (Kano et al. 2007; Raddatz et al., 2011). As the main builder of carbonate mounds CWCs serve as an unique archive for geochemical proxies (e.g Mg/Li, Sr/Ca, $\delta^{88/86}$Sr Raddatz et al., under review, a) to reconstruct intermediate water mass dynamics. Hence, CWCs from the CM provide the unique opportunity for MOW reconstruction over last 3 Myrs (Raddatz et al., under review, b)

Here, we investigate the potential of CWCs skeletons to archive Rare Earth Elements (REE) and their isotopes. The REEs and their isotopes have a great potential to trace continental input, particle scavenging and the oxidation state of seawater and were shown to provide an independent water-mass mixing proxy. Here we show that, these REE are recorded in the skeleton of the cosmopolitan cold-water coral *Lophelia pertusa*. In particular, we use an online preconcentration ICP-MS method (Hathorne et al. 2012) to measure REE concentrations in seawater and associated cold-water coral carbonates in order to investigate their seawater origin. Scleractinian cold-water corals were collected *in-situ* and alive and with corresponding seawater samples covering the entire European Continental Margin. The seawater REE patterns are characterized by the typical negative cerium anomaly of seawater, but are distinct for the northern Norwegian Margin and the Oslo Fjord, probably related to continental input. Initial results for the corresponding coral samples suggest that these distinct REE patterns of ambient seawater are recorded by coral skeletons. although some fractionation during incorporation into the aragonite occurs. This indicates that scleractinian cold-water corals can serve as a valuable archive for seawater derived REE signatures, as well radiogenic Neodymium (Nd) isotope compositions.

However, in a second step we analysed fossil coral samples from various locations, which were oxidatively and reductively cleaned prior to analysis. Initial results reveal that sediment-buried fossil (early Pleistocene to Holocene) coral samples from the Norwegian Margin and the Porcupine Seabight (Challenger Mound, IODP Site 1317) do not show the expected seawater REE patterns. In particular, the fossil coral-derived REE patterns lack a

negative cerium anomaly suggesting that fossil coral-REE patterns do not represent ambient seawater. Thus, we suggest that the oxidative-reductive cleaning method widely used for cleaning of marine carbonates such as foraminifera prior to measurements of seawater-derived trace metal and isotope compositions are not sufficient for REE and Nd isotopes in sediment-buried coral-water corals and require alternative or additional approaches.

References:
Hathorne, E.C., B. Haley, T. Stichel, P. Grasse, M. Zieringer, and M. Frank (2012). Online preconcentration ICP-MS analysis of rare earth elements in seawater, Geochem. Geophys. Geosyst.,13, Q01020, doi:10.1029/2011GC003907.
Kano, A., Ferdelman, T.G., Williams, T., Henriet, J.-P., Ishikawa, T., Kawagoe, N., Takashima, C., Kakizaki, Y., Abe, K., Sakai, S., Browning, E.L., Li, X., IODP Expedition 307 Scientists, 2007. Age constrains on the origin and growth history of a deep-water coral mound in the northeast Atlantic drilled during Integrated Ocean Drilling Program Expedition 307. Geology 35, 1051-1054.
Raddatz, J., Rüggeberg, A., Margreth, S. und Dullo, W. C. and the IODP Expedition 307 Scientific Party, 2011. Paleoenvironmental reconstruction of Challenger Mound initiation in the Porcupine Seabight, NE Atlantic. Marine Geology 282, 79-90. doi:10.1016/j.margeo.2010.10.019
Raddatz, J., Liebetrau, V., Rüggeberg, A., Hathorne, E., Krabbenhöft, A., Eisenhauer, A, Böhm, F, Vollstaedt, H, Fietzke, J, López Correa, M, Freiwald, A and W.- Chr. Dullo. Environmental influences on the stable Sr-isotope, Sr/Ca, Mg/Ca, Li/Ca and Mg/Li ratios in the scleractinian cold-water coral Lophelia pertusa (under review, a, Chemical Geology)
Raddatz, J., Rüggeberg, A. Liebetrau, V., Foubert, A., Hathorne, E., Fietzke, J., Eisenhauer, A. and W.-Chr. Dullo. Environmental boundary conditions of cold-water coral mound growth over the last 3 Million years in the Northeast Atlantic (under review, b, Deep-Sea Research Part II - Proceedings of ISDSC 5)

ICDP

PGE and Re-OS in organic rich shales: optimisation of sample preparation protocols for measurement by isotope dilution ICP-MS

P. RAMMENSEE[1], S. AULBACH[1], D. GUDELIUS[1], G. BREY[1]

[1] Goethe-Universität Frankfurt, Altenhöferallee 1, 60438 Frankfurt am Main

Platinum-group elements (PGE) and Re-Os isotopes, which are variably redox-sensitive and fluid-soluble, have potential as proxies for the oxygenation of the atmosphere and oceans (e.g. [1]). However, analysis of these elements in organic rich shales (ORS) is challenging due to abundances of <1 ng/g and the presence of interfering isotopes or molecules of matrix elements. Furthermore, PGE-ReOs systematics in detrital and hydrogenous components may vary, and the choice of digestion parameters (reagents, temperature and pressure) during decomposition of rock powder affects the ratio of digested components [2,3]. Additional treatment to remove the matrix and pre-concentrate PGE-Re by column chromatography is necessary to minimise the effects of interfering elements, but presents its own challenges.

We are in the process of conducting variations of acid digestion and column chromatographic protocols on reference sample SDO-1 (Devonian Ohio Shale, USGS). We aim to identify the optimum protocol to investigate PGE-Re-Os systematics of ORS that were sampled as part of the Barberton Drilling Project BARB5 drill core, in order to constrain the changes in detrital and hydrogenous contributions to the sediment with time, to assess the extent of euxinity in the sedimentary basin and to look for evidence of transient "whiffs of oxygen" [1]. The following digestion methods were tested: (1) 4h acid digestion in High Pressure Asher (HPA) apparatus with reverse aqua regia at 300°C and 130 bar (only this digestion allows extraction of volatilised Os in $CHCl_3$ followed by HBr); (2) 3h reverse aqua regia digestion in centrifuge vials on hotplate at 80°C; (3) 48h reverse aqua regia digestion in closed Teflon beakers on hotplate at 140°C followed by a HF/HNO_3 digestion step; (4) 48h HF/HNO_3 digestion of ashed sample powder in closed Teflon beaker at 140°C on hotplate followed by an aqua regia digestion step. Column chromatographic approaches to decrease the concentrations of interfering elements (Y, Zr, Mo, Cd, Hf, Hg) include the use of cation- and anion-resins, and variations of the molarity and composition of the eluent.

Preliminary results show that digestion method (1) leaves behind small amounts of presumably PGE-free silica gel; (2) yields consistently higher Re concentrations with an expectedly large amount of solid residue; (3) produces an insoluble sludge; (4) allows complete digestion, but precludes the collection of Os. Column calibrations show the best recovery of PGE-Re in cation resin using 0.2 mol/l HCl as eluent, but intolerably high ratios of interfering over elements of interest, whereas the best matrix separation is achieved using 0.05 mol/l HCl as eluent, but is accompanied by low PGE-Re yields presumably due to the instability of Cl complexes in this medium. They also show that U elutes separately from PGE-Re in 6 mol/l HCl and could be collected with a view to analysing U isotopes as an additional redox proxy. Further tests will be carried out using alternative high-pressure digestion systems.

References:
[1] Anbar, et al. (2007) Science 317:1903-1906
[2] Meisel et al. (2003) JAAS 18:720-72
[3] Xu et al. (2012) CG 324:132-147

ICDP

Petrography of the impact breccias and their melt particles from the ICDP-El´gygytgyn drill core, NE Russia

U. RASCHKE[1], W. U. REIMOLD[1,2] AND R. T. SCHMITT[1]

[1] Museum für Naturkunde, Leibniz-Institut für Evolutions- und Biodiversitätsforschung, Invalidenstraße 43, 10115 Berlin, Germany (e-mail: ulli.raschke@ mfn-berlin.de)
[2] Humboldt-Universität zu Berlin, Unter den Linden 6, 10099 Berlin, Germany

Introduction: The El´gygytgyn crater located in the Ochotsk-Chukotsky Volcanic Belt of the Chukotka Peninsula (Northeast Russia) [1-2] is a 18-km-diameter complex impact structure [3] of 3.6 Ma [4] age. It is one of the rare terrestrial cases of an impact crater in a volcanic target material (Fig. 1). A 170 m deep, circular lake largely covers the interior of the impact structure and is somewhat offset with respect to the crater center. In 2008/2009 an ICDP (International Continental Scientific Drilling Program) drilling campaign [5] obtained a ~520 m long drill core (D1c) from the northeast part of the lake, comprising ~318 m of lake sediments and ~202 m of impactites [5]. During an expedition to the crater in July 2011 occurrences of target rocks were mapped and sampled, resulting in a new geological map [6] comprising all available literature data and our new field observations.

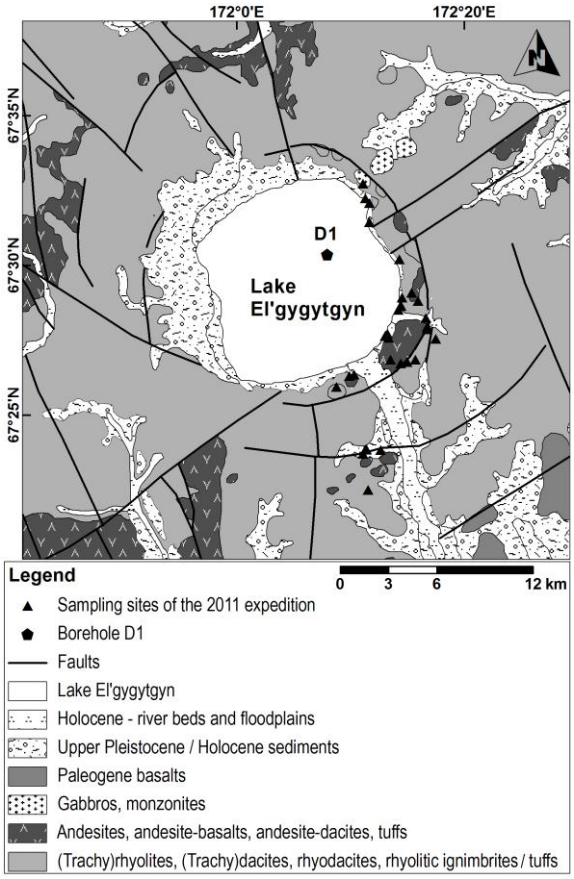

Fig. 1. Simplified geological sketch map of the El´gygytgyn impact structure based on the Russian geological map [11, 12].

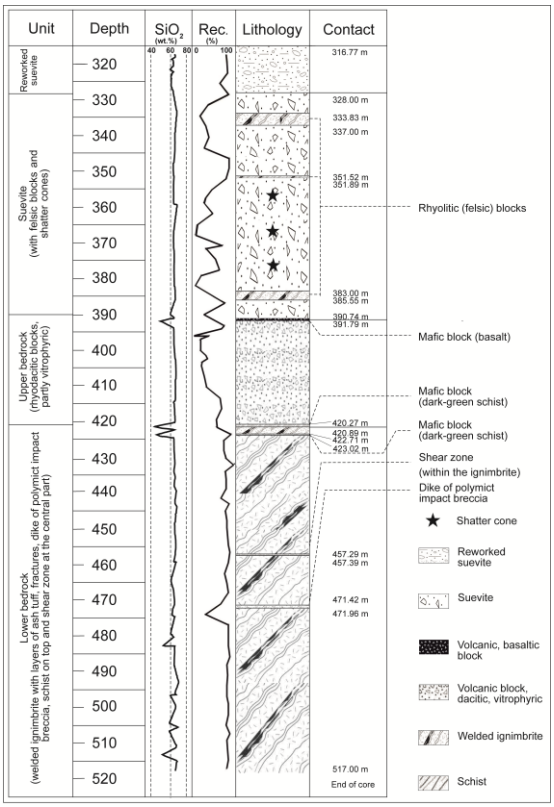

Fig. 2. Schematic stratigraphic column of the impactite sequence of the El´gygytgyn ICDP drill core. The abbreviation "Rec." means "core recovery.

Here, we present an overview of the impact rocks - with a special focus on the nature of impact melt particles.

Results: We studied the impactite sequence with respect to their petrographic and geochemical character [7-8]. This sequence can be subdivided into four different units (Fig. 2): (1) ***Lower bedrock unit*** (520-423 mblf, m below lake floor): A welded ignimbrite that has been brecciated to a monomict impact breccia. Brownish, elongated and flattenend, cm-sized pumice fragments ("fiamme") are typical for this unit. At 471 mblf a half meter wide dike of polymict impact breccia occurs in this lower, ignimbritic bedrock. (2) ***Upper bedrock unit*** (423–390 mblf): A heterogeneous, dacitic, partly vitrophyric, ignimbrite with some intercalations of <1 m wide mafic blocks. Lowermost shock metamorphic effects (planar deformation features - PDF) were noted at 391.72 mblf. (3) ***Polymict impact breccia*** (~390 - 328 mblf), interpreted as suevite due to the occurrence of impact melt particles: This suevitic breccia consists of a very melt-poor clast-dominated matrix and rock fragments that represent the entire range of volcanic target rocks known from the El'gygytgyn area and environs. All stages of shock metamorphism have been observed in lithic clasts and mineral fragments, covering the shock pressure range from unshocked to highly (> 50 GPa, impact melt clasts) shocked. We found three shatter cones at 376.20, 368.32 and 351.79 mblf, which are meso- to macroscopic features representing low to moderate shock metamorphism [9]. (4) ***Reworked suevite*** (~328 - 318 mblf): The uppermost ~10 m of the impactite sequence is considered a reworked suevite, with comparatively more, and, on average, stronger, shocked minerals than found in the underlying main suevite body. This includes quartz crystals with three or more sets of PDF, mosaicism, and diaplectic glass. There is a distinct component of glass spherules occuring within this unit.

One important topic during our study of the polymict impact breccias is the differentiation between volcanic and impact-generated melt particles. The recognition of impact-generated melt particles is not only important for the genetic interpretation of these breccias, because these

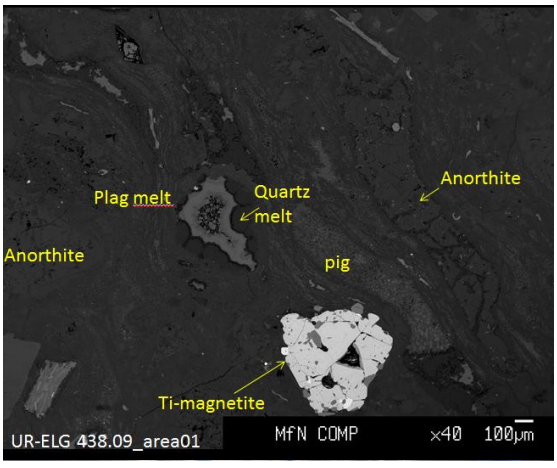

Fig. 3. Pumice fragment (lower bedrock unit, 438.09 mblf) with heterogeneous melts after quartz or plagioclase, and with plagioclase and anorthite as well as pigeonite clasts.

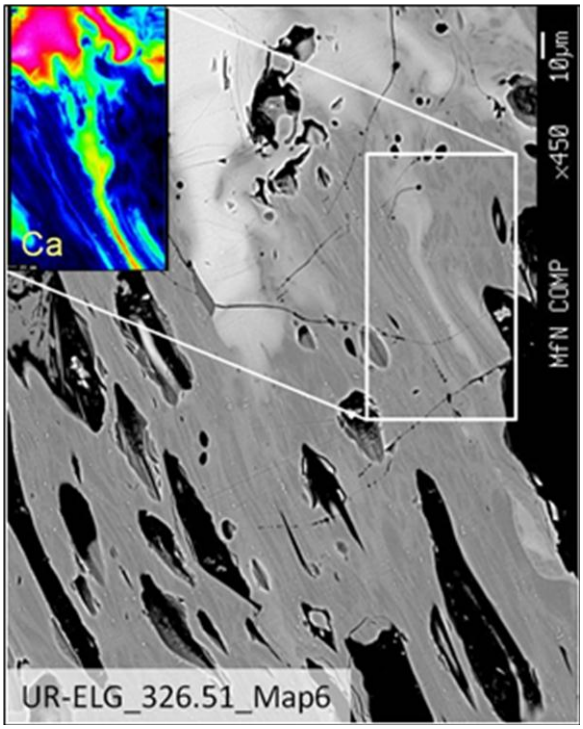

Fig. 4. Intricately banded impact melt particle with "schlieren" of lechatelierite and various feldspathic com-positions, and melts of combinations of these precursor components. Insert map: Ca distribution by EMPA, dark color = low concentration, green and red = high concentration. Reworked suevite, 326.51 mblf.

particles reflect the highest degree of shock metamorphism, but also for the classification of the impactites, as the distinction between polymict impact breccias and suevite is based on the occurence of impact melt [10]. Therefore, we have carried out first scanning electron micoscopy (SEM) and electron microprobe analysis (EMPA) studies of the different melt and glass particles:

(i) ***Volcanic melt particles***: The volcanic melt particles occurring in the lower bedrock unit include ignimbrite pumice fragments, and in the upper bedrock unit basaltic lava and pyroclastic glass shards of felsic to basaltic composition. The brownish pumice fragments ("fiamme") consist of euhedral phenocrysts (mostly feldspars) in a crystalline to aphanitic groundmass. Ore minerals (Fe-–Ti oxides) are widespread in the matrix (Fig. 3). Pumice may include black glass shards. Such volcanic melt particles occur together with clasts of all target lithologies, also within the suevite and reworked suevite.

(ii) ***Accretionary lapilli***: Rare particles are found in the upper bedrock, but were not observed within the suevite and reworked suevite.

(iii) ***Impact-generated melt particles***: In addition to the above described volcanic melt particles we found in the suevite intricately banded melt particles that contain "schlieren" of lechatelierite or of various feldspathic compositions, and melts of a range of combinations of different precursor components (Fig. 4). Such melt particles with micro-schlieren were not observed in the volcanic bedrock and are, therefore, interpreted as impact-generated melts.

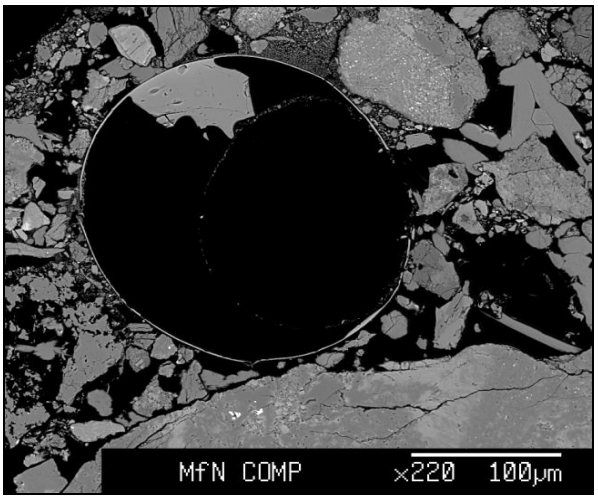

Fig. 5. Remnant of a glass spherule with a feldspatic rim and relict of SiO_2-rich glass fill. Reworked suevite, 318.13 mblf.

(iv) ***Glass spherules***: The glass spherules are relatively enriched in the reworked suevite in the depth interval from 318 to 322 mblf. For the mainly hollow spherules we could identify feldspathic compositions for the translucent glass rims. Small patches of glass may occur inside such rims and can be relatively enriched in SiO2, up to 89 vol.% (Fig. 5). Another type of spherule is completely filled with melt and then lacks a clear rim or quench margin. Sometimes the melt is devitrified and contains Mg-rich orthopyroxene or feldspar quench crystals (Fig. 6). Some spherules are partially replaced by secondary carbonate. Due to the similarities with glass sherules observed in other impact craters these spherules here were also interpreted as impact-generated, most likely derived from the ejecta plume.

Discussion: Discrimination of volcanic and impact melt particles is highly complicated and will need further investigations. At this time some trends for the distinction of different melt particles can be proposed. The volcanic melts have a finest-grained to aphanitic flow texture with a heterogeneous composition ranging from basaltic to rhyolitic, very similar to the respective host rock compositions. They include euhedral phenocrysts of feldspar, quartz and accessory ore minerals. No intricate schlieren texture at the µm-scale was observed. In contrast, the impact melt particles show intricate schlieren structures with little evidence of devitrification. The heterogeneous chemical composition is silica- and/or feldspar dominated. No phenocrysts occur in the groundmass, but moderately to strongly shocked quartz grains may occur. Disseminated Fe, Mg, Ti-oxides appear only in brownish schlieren of feldspathic composition with small Fe and/or Mg contributions. The wide variety of impact melt compositions is consistent with findings on impact melts in suevites from the Bosumtwi and Chesapeake Bay drill cores that were also obtained through ICDP projects.

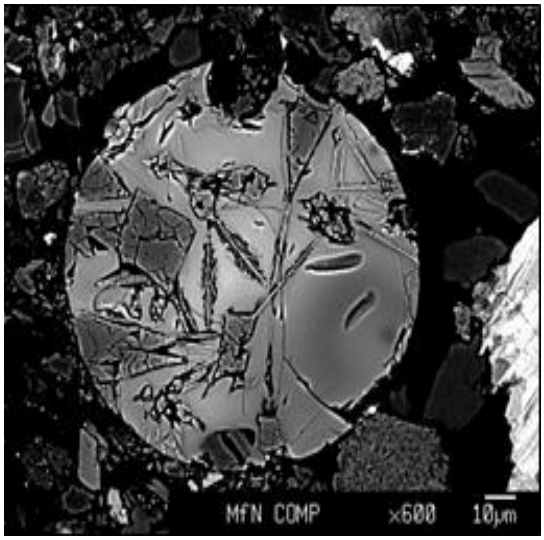

Fig. 6. Glass spherule with feldspathic melt and pyroxene quench crystals. Reworked suevite, 318.13 mblf.

Acknowledgment: This work is supported by DFG grant RE 528/10-2 to WUR and RTS.

References**:**

[1] Gurov E. P., Valter A. A. Gurova E. P., and Kotlovskaya F. I. 1979. El'gygytgyn impact crater, Chukotka: Shock metamorphism of volcanic rocks (abstract). *Lunar and Planetary Science Conference* 10:479–481; [2] Gurov E. P., and Gurova E. P. 1991. Geological structure and rock composition of impact structures. *Naukova Dumka Press.* 160 p. In Russian; [3] Gurov E. P., Koeberl C., and Yamnichenkov A. 2007. El'gygytgyn impact crater, Russia: Structure, tectonics, and morphology. *Meteoritics and Planetary Science* 42:307–319; [4] Layer P. W. 2000. ^{40}Argon/^{39}Argon-age of the El'gygytgyn event, Chukotka, Russia. *Meteoritics and Planetary Science* 35:591–599.; [5] Melles M., Brigham-Grette J., Minyuk P., Nowaczyk N. R., Wennrich V.,DeConto R. M., Anderson P. M., Andreev A. A., Coletti A., Cook T. L., Haltia-Hovi E., Kukkonen M., Lozhkin A. V. Rosen P., Tarasov P., Vogel H. and Wagner B. 2012. 2.8 Million Years of Arctic Climate Change from Lake El'gygytgyn, NE Russia. *Science* 337:315-320;. [6] Raschke U., Zaag P., Reimold W. U. and Schmitt R. T. 2013. A new geological map of the El´gygytgyn impact structure, NE Russia. *Lunar and Planetary Science Conference* 44, in press; [7] Raschke U., Reimold W. U., Zaag P. T., Pittarello L., and Koeberl C. 2013. Lithostratigraphy of the impactite and bedrock section in ICDP drill core D1c from the El´gygytgyn impact crater, Russia. *Meteoritics and Planetary Science*, in press; [8] Raschke U., Schmitt R. T. and Reimold, W. U. 2013. Petrography and geochemistry of the impactites and volcanic bedrock of the ICDP drill core D1c from Lake El´gygytgyn, NE Russia. *Meteoritics and Planetary Science*, in press; [9] Dietz, R.S., 1968. Shatter cones in cryptoexplosion structures. In: French, B.M., Short, N.M. (Eds.), *Shock Metamorphism of Natural Materials.* Mono Book Corp, Baltimore, MD, pp. 267–285; [10] Stöffler D., and Grieve R. A. F. 2007. 11. Impactites - A proposal on behalf of the IUGS Subcommission on the Systematics of Metamorphic Rocks: In *Metamorphic rocks – a classification and glossary of terms*, edited by Fettes D. and Desmons J. Cambridge: Cambridge University Press. pp. 82-92; [11] Raevsky F. B. and Potapova E. P. 1984. Geological map of the Anadyr region, sheet Q-59-III, IV. In: Official geological map of the USSR. Eds: Ministry of Geology, USSR. In Russian; [12] Zheltovsky V. G. 1985. Geological map of the Anadyr region, sheet Q-59-V, IV. In: *Official geological map of the USSR.* Eds: Ministry of Geology, USSR. In Russian.

IODP

Carbonate veining in rocks from the Louisville seamount chain

S. RAUSCH[1], W. BACH[1], A. KLÜGEL[1]

[1] Geoscience Department, University of Bremen, Germany; srausch@uni-bremen.de / wbach@uni-bremen.de / akluegel@uni-bremen.de

Intense circulation of seawater through the oceanic crust changes physical properties of the rocks and is the most important reason for chemical exchange between lithosphere and hydrosphere (e.g. Alt and Teagle, 2003, Bach et al. 2003). While it ages, the oceanic crust accumulates carbonates, which precipitate in veins and vesicles and form the matrix of breccias. Recent work has shown that carbonates formed at mid-ocean ridge flanks can be used to examine the chemical exchange between seawater and crust and as an archive for ancient seawater composition (Coggon et al. 2010, Rausch et al. 2013). The precipitation of carbonates also acts as a major sink for CO_2 in the Earth system; the estimated CO_2 uptake associated with carbonate precipitation in fractures and void space of crust at mid-oceanic ridge flanks is about 10^{12} mol/yr. The timing of carbonate formation during the lifespan of ocean crust is not known very well. Upon ageing, the oceanic crust becomes covered with sediments of increasing thickness. These sediments will ultimately inhibit seawater-crust exchange and the related carbonate precipitation. However, in old crust seamounts can act as breathing holes (Fisher et al., 2003), which allow for prolonged fluid circulation and carbonate formation. To examine the importance of seamounts for seawater-crust chemical exchange and carbon fixation, we study samples from the Louisville seamount chain.

The Louisville seamount trail is a 4300 km long seafloor morphological expression of a late Cretaceous to Cenozoic hotspot. The seamounts are located on the Pacific plate north east of New Zealand (Fig. 1). During IODP expedition 330 five seamounts were drilled along this chain, with the goal of investigating the evolution and relative movement of the Louisville hotspot (Koppers et al. 2012). Our first dataset of void filling carbonates includes

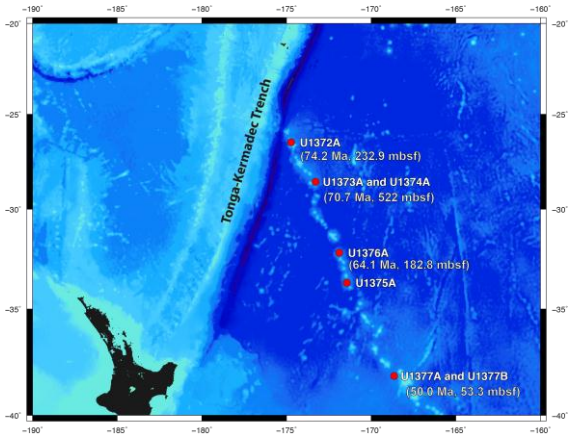

Fig. 1: Section of the Louisville Seamount Trail northwest of New Zealand. The five seamounts drilled during Expedition 330 are indicated by pink circles.

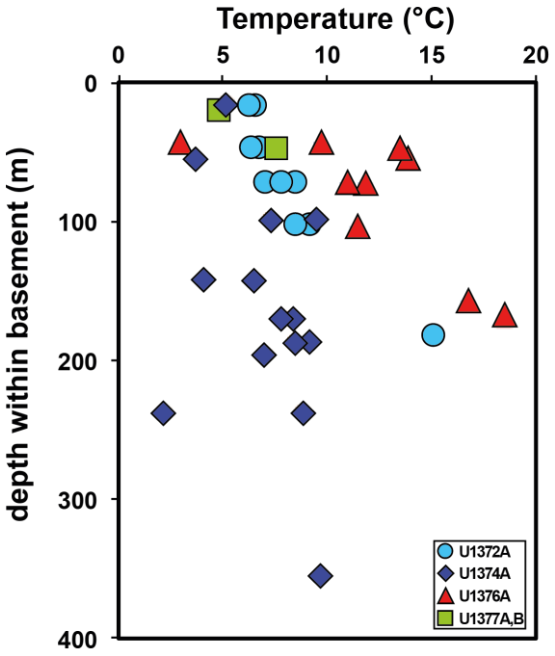

Fig. 2: Carbonate formation temperature calculated from $\delta^{18}O$ values for calcites and aragonites versus depth within basement.

four seamounts: Canopus (74.2 Ma, hole U1372A, 232.9 mbsf), Rigil (70.7 Ma, hole U1374A, 522 mbsf), Burton (64.1 Ma, hole U1376A, 182.8 mbsf) and Hadar (50.0 Ma, holes U1377A and B, 53.3 mbsf). The sampled carbonates form veins within the host rock or the matrix of breccias. Especially in hole U1372A and U1374A most of the cores were made up by volcanic breccia, because they were drilled at the flank of the volcano. In these holes calcite is the most common carbonate phase, but Mg-rich carbonate and Fe-/Mn-rich carbonate (siderite, Fe-/Mn-rich calcite) were also found. U1376A is characterized by aragonite precipitation, and U1377A and B show Mn- and Fe- rich calcite.

Stable isotope ($\delta^{18}O$ and $\delta^{13}C$) analyses of drilled material reveal that most of the carbonate samples lie in the common range of marine carbonates (0.1 to 2.62 ‰ VSMOW; -1.2 to 3.4 ‰ PDB), except for U1376A, which tends to have slightly lower $\delta^{18}O$ values (0.5 to -0.65 ‰) and clearly lower $\delta^{13}C$ (-1.0 to -8.9 ‰). The formation temperature was calculated from oxygen isotopic ratios and lies in the range of 2.2 to 18.4 °C. A slight downhole increase in temperature is observed in holes U1372A and U1376A, the latter being shifted to slightly higher temperatures (Fig. 2). On the other hand, U1374A shows a temperature range from 3.0 to 9.7°C with no systematic downhole trend. $^{87}Sr/^{86}Sr$ ratios range from 0.70508 to 0.70812 and show a decrease with increasing sample depth. An exception are samples from Hole U1374A, which encompass a narrow $^{87}Sr/^{86}Sr$ range of 0.70750 to 0.70812 that does not correlate with depth, even though it is the deepest hole drilled during Leg 330.

Estimates of the formation ages of carbonate veins, breccia cements and void filling carbonates were done by relating the Sr isotope data to the Sr seawater evolution curve from McArthur and Howarth (2004). In holes U1372A and U1374A carbonate precipitated shortly (a few million years) after seamount formation, whereas the younger samples (U1376A and U1377A, B) show evidence

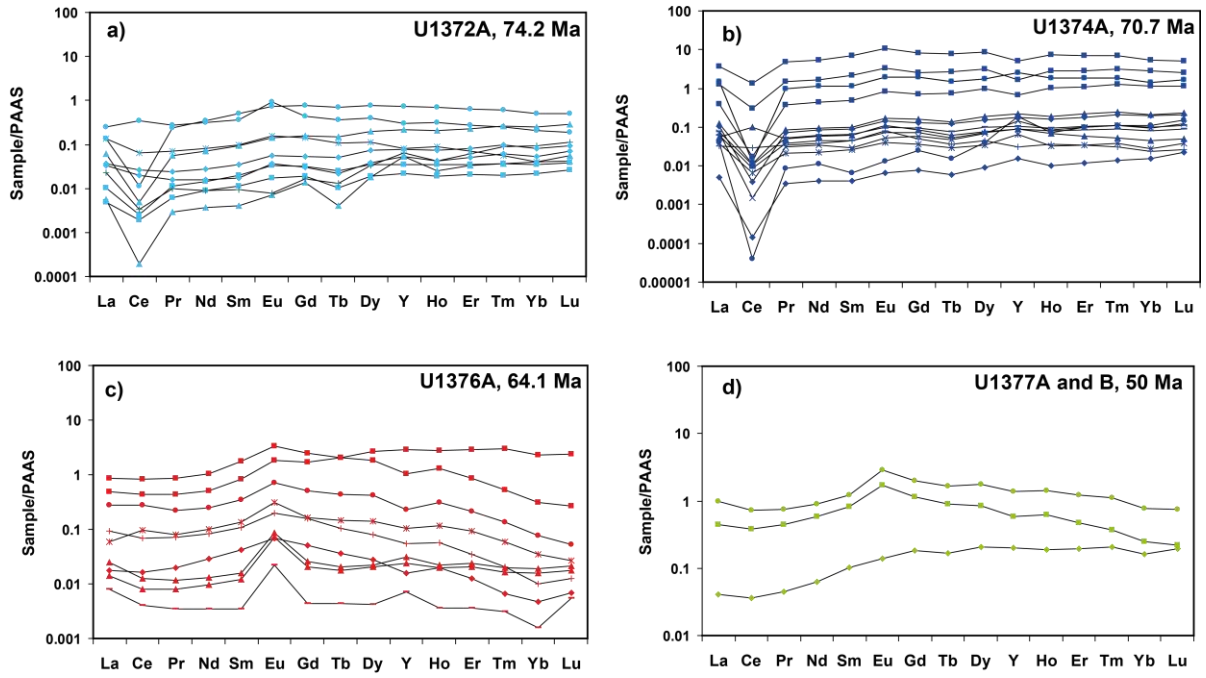

Fig. 3: Shale-normalized (PAAS = Post-Archean Australian Shale; Taylor and McLennan, 1985) REE+Y spectra of investigated carbonates indicate different stages of seawater–crust (hydrothermal fluid) interaction.

for prolonged precipitation from a fluid that had exchanged Sr with the basement to variable degrees.

Highly variable extents of fluid-basement interaction are also shown by the trace-element compositions of carbonate samples obtained by solution ICP-MS analyses. The rare-earth element (REE) spectra of carbonates from the two older seamounts (U1372A and U1374A) are characterized by pronounced negative Ce-anomalies and positve Y-anomalies (Fig.3 a and b), which may indicate precipitation from pristine seawater. In contrast, the two younger seamounts (U1376A and U1377A,B) show REE patterns that lack these seawater-signatures and show subtle positive Eu anomalies (Fig.3 c and d), indicative of enhanced exchange with basement.

We derived the compositions of circulating seawater-derived fluids from seamount carbonate samples, using carbonate compositions and temperature estimates. For the samples lacking Sr isotope evidence for exchange with basement, these values provide insights into the compositions of past seawater. The data from the Louisville carbonate samples allow us to fill the critical data gap between 74 Ma and 50 Ma from earlier publications (Coggon et al. 2010; Rausch et al, 2013). The recalculated Mg/Ca ratios (1.93-2.04 mol/mol) of past seawater corroborate values derived from carbonate samples retrieved from ridge flank crust of corresponding age (Fig. 4). The new seamount samples reveal no increase of Mg/Ca before 50 Ma. The Neogene increase in Mg/Ca ratio did therefore not start in late Cenozoic when global ocean crust production rate dropped. Our data show that seawater composition remained unchanged throughout the Paleogene, confirming previous evidence for a 40 Myrs long time lag between apparent tectonic forcing (slowdown of ocean crust production) and ocean chemistry response.

The data collected thus far in this ongoing study indicate that the carbonate archive in the Louisville seamount chain appears to provide a rather sparse record of seawater compositional change. Instead, the extent of seawater-basement interaction was much greater than anticipated, and most of the carbonates could not be age-dated with confidence due to Sr isotope leaching from basement. The large spread in compositions and temperatures displayed in the carbonate data provides an unanticipated opportunity to learn about seawater-basement exchange during the ageing of seamount basement. The magnitude and direction of this exchange is strongly controlled by temperature. The isothermal gradient displayed by carbonates from Hole 1374A may suggest recharge of cold seawater deep into the basement, making the Canopus Seamount a possible paleo-seawater-recharge site. In contrast, the linear O isotope trends observed in carbonates from U1372A and U1376A may suggest roughly steady-state thermal gradients of 50°C/km, corresponding to a conductive heat flow of around 150 mW/m^2.

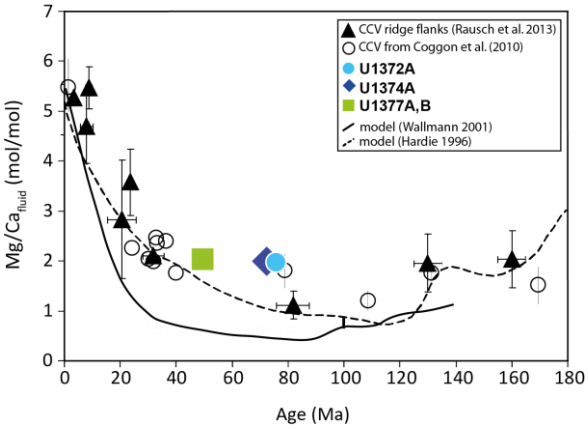

Fig. 4: Reconstructed Mg/Ca ratio in seawater from carbonate formed within ocean crust through time. Also shown are computational model trends from Wallmann (2001; solid line) and Hardie (1996; dashed line).

Ongoing work is devoted to assigning compositional trajectories to these depth-temperature relations, hoping to establish common ratios for the flux of heat and elements. If successful, this approach would provide novel insights into the role of seamounts in ocean-crust exchange budgets. We also investigate bulk rock alteration budgets for two selected seamounts to assess chemical fluxes from a rock geochemical mass balance perspective.

References:

Alt, J.C. and Teagle, D.A.H. 2003. Hydrothermal alteration of upper oceanic crust formed at a fastspreading ridge: mineral, chemical, and isotopic evidence from ODP Site 801. Chemical Geology, 201:191-211.

Bach, W., Peucker-Ehrenbrink, B., Hart, S.R. and Blusztajn, J.S., 2003. Geochemistry of hydrothermally altered oceanic crust: DSDP/ODP Hole 504B – Implications for seawater-crust exchange budgets and Sr- and Pb-isotopic evolution of the mantle. Geochem. Geophys. Geosys., 4(3): 10.1029/2002GC000419.

Coggon, R. M., Teagle, D. A. H., Smith-Duque, C. E., Alt, J. C., and Cooper, M. J., 2010, Reconstructing past seawater Mg/Ca and Sr/Ca from mid-ocean ridge flank calcium carbonate veins. Science, 327: 1114-1117.

Fisher, A. T. et al., 2003. Hydrothermal recharge and discharge across 50 km guided by seamounts on a young ridge flank. Nature, 421: 618-821.

Hardie, L.A., 1996. Secular variation in seawater chemistry: An explanation for the coupled secular variation in the mineralogies of marine limestones and potash evaporites over the past 600 m.y. Geology, 24(3): 279-283.

Koppers, A. A.P., Yamazaki, T., Geldmacher, J., Gee, J. S., Pressling, N., Hoshi, H., at al. 2012, Limited latitudinal mantle plume motion for the Louisville hotspot. Nature Geoscience, 5: 911-917.

McArthur, J.M., Howarth, R.J., 2004. Strontium isotope stratigraphy. In: Gradstein F., Ogg J., A., S. (Eds.), A Geologic Time Scale. Cambridge University Press, Cambridge, pp. 96-105.

Rausch, S., Böhm, F., Bach, W., Klügel, A., Eisenhauer, A., 2013. Calcium carbonate veins in ocean crust record a threefold increase of seawater Mg/Ca in the past 30 million years. Earth and Planetary Science Letters, 362(0): 215-224.

Taylor, S.R., McLennan, S.M., 1985. The continental crust: Its composition and evolution. Blackwell Scientific Publications, Oxford, 328 pp.

Wallmann, K., 2001. Controls on the cretaceous and cenozoic evolution of seawater composition, atmospheric CO2 and climate. Geochimica et Cosmochimica Acta, 65(18): 3005-3025.

IODP

Early Cretaceous bathyal holothurians from the western North Atlantic Ocean (Blake Nose, ODP Leg 171B)

M. REICH[1,2], A.S. GALE[3], N. SCHLÜTER[1,2], B. THUY[1,2], F. WIESE[2,4]

[1] Georg-August University of Göttingen, Geoscience Museum, Goldschmidtstr. 1-5, 37077 Göttingen, Germany; mreich@gwdg.de
[2] Georg-August University of Göttingen, Geoscience Centre, Dept. of Geobiology, Goldschmidtstr. 3, 37077 Göttingen, Germany
[3] School of Earth and Environmental Sciences, University of Portsmouth, Burnaby Building, Burnaby Road, Portsmouth, PO1 3QL, UK
[4] Georg-August University of Göttingen, Courant Research Centre Geobiology, Goldschmidtstr. 3, 37077 Göttingen, Germany

Sediments recovered from the lower bathyal ODP Leg 171 at Site 1049 on the Blake Nose escarpment (western North Atlantic) offer an opportunity to study well-preserved fossil deep-sea echinoderms, including sea cucumbers. Among echinoderms, holothurians are the most common megafaunal elements in the deep sea, from bathyal to hadal depths. Today, several holothurian groups are unique in being confined to the deep sea, including members of the Laetmogonidae (Elasipodida), Synallactidae (Aspidochirotida), and Myriotrochidae (Apodida). While there is some knowledge on shelf-sea holothurian records, deep-sea taxa are virtually unknown. Thus, the Blake Nose records provide insight into deep-sea assemblage structures and enable a first assessment of possible depth gradients among early Cretaceous holothurian groups.

Here we present the first detailed analysis of early Cretaceous holothurian assemblages from Blake Nose. The fauna consists of dissociated ossicles and other skeletal elements, dominated by members of the Laetmogonidae and Myriotrochidae; representatives of the Chiridotidae are less frequent. Laetmogonid holothurians are surface-dwelling species and predominantly bathyal, represented within our material by diagnostic body wall ossicles only. Myriotrochid and chiridotid sea cucumbers live in large aggregations in soft sediments, documented in the present material by distinct body wall ossicles and calcareous ring elements. All these fossil species are closely related to modern representatives, like *Pannychia* (Laetmogonidae), *Myriotrochus* (Myriotrochidae) and *Chiridota* (Chiridotidae).

This is the first report of a fossil holothurian species closely related to a laetmogonid genus other than *Laetmogone* representing also the first elasipodid taxon ever recorded from the Early Cretaceous. The discovery of a middle to lower bathyal holothurian community of nearly modern composition of early Cretaceous age implies that at least a significant part of the modern deep-sea fauna is much older than previously assumed.

References:
Reich, M.; Gale, A.S.; Schlüter, N.; Thuy, B. & Wiese, F. subm. Early Cretaceous holothurians in the western North Atlantic Ocean (Blake Nose, ODP Leg 171B): Faunal composition, origin and implications for modern zoogeography. *Marine Micropaleontology*.
Thuy, B.; Gales, A.S.; Kroh, A.; Kucera, M.; Numberger-Thuy, L.D.; Reich, M. & Stöhr, S. 2012. Ancient Origin of the Modern Deep-Sea Fauna. *PLoS ONE* **7** (10), 1–11. [e46913]

IODP

Toward an high resolution stratigraphy for Antarctic Neogene radiolarians

J. RENAUDIE[1], D. LAZARUS[1]

[1] Museum für Naturkunde, Leibniz-Institut für Evolutions- und Biodiversitätsforschung, Invalidenstraße 43, 10115 Berlin. johan.renaudie@mfn-berlin.de

Introduction

Cenozoic climate evolution is directly linked to the paleoceanographical evolution of the Southern Ocean. However the current accuracy of the available geochronological framework hinders the understanding of this evolution. Because of the peculiar sedimentary conditions of the Neogene Southern Ocean that prevents the reliable use of calcareous microfossils for biostratigraphy and because of the widespread hiatuses and the poor paleomagnetic polarity record in many sections, the Antarctic Neogene stratigraphic framework relies heavily on siliceous microfossils.

Current radiolarian biostratigraphy for the Antarctic Neogene is based on a total of 40 species for the all Neogene. However, ca. 500 species are present in the Neogene Southern Ocean: the radiolarian fossil record for this time interval and that region has a huge potential that previous studies didn't make use of.

The aim of this preliminary study was to uncover this potential by using a full fauna dataset in the context of a quantitative biostratigraphic analysis. Although still preliminary, this study underlines the feasibility of improving biostratigraphic analysis using whole fauna data.

Using a whole-fauna dataset to increase stratigraphic resolution

Eighty-three samples from six of the studied sites were considered for this study: ODP Leg 113 Sites 689 (11 samples), 690 (10 samples) and 693 (10 samples), ODP Leg 120 Sites 747 (15 samples) and 751 (24 samples) and ODP Leg 183 Site 1138 (13 samples). These sites cover the late Miocene to Pliocene sequence.

The stratigraphic analysis was conducted using Constrained Optimization (CONOP, Kemple et al. 1995; Sadler 2007) methodology. The CONOP analysis consists in finding the optimal sequence of events such as all observed co-occurrences are respected and the misfit between the observed range of each species on each site

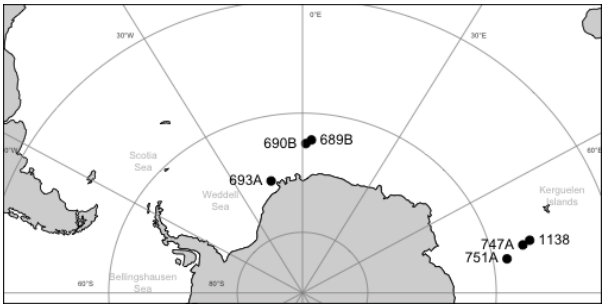

Figure 1 – Map of the sites used for the biostratigraphic analysis.

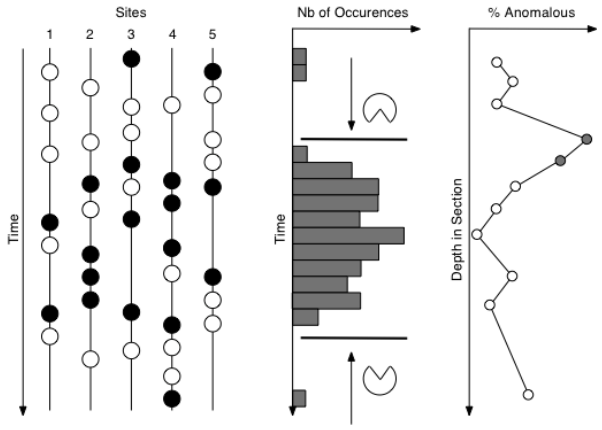

Figure 2 – Illustration of the pacman profiling concept.
Left panel: Occurences of a given species in several sites (white: absent; back: present).
Middle panel: Compilations of occurences on all sites. Pacman routine flags a given percentage of occurences at the top and the bottom of the species range as anomalous.
Right panel: Anomalous data for all species are compiled for each sites and problematic samples are hence spotted. (redrawn after Lazarus et al. 2012)

and that on the composite sequence is minimized.

Given the nature of the abundance distributions of species in a given ecosystem, using the full number of species in the fauna means adding mostly rare species to the analysis. Species scarcity combined to the incompleteness of the fossil record produces truncated local ranges and therefore using a full fauna dataset should be more a source of noise than a tool for increasing resolution. However, even if the probability of finding a non-truncated range for a rare species in any given section is low, the first (FO) and last occurrences (LO) for a section still help constraining the true solution for the "line of correlation". Furthermore, the co-occurrences of species (rare or abundant) with other species are additional constraints that narrow the field of possible solutions.

Instead of eliminating rare species, we chose to reduce the stratigraphic noise by finding and weighting down the outlying data: highly diachronic events were detected using a preliminary raw CONOP run; species with inconsistent ranges were detected using a Gap ratio analysis and samples with probable reworking were flagged using pacman profiling (Lazarus et al. 2012; Fig. 2).

The composite sequence of events resulting from the CONOP analysis was then calibrated using the few reliable magnetostratigraphic and diatom data from sites 689, 690 (Censarek & Gersonde 2002) and 1138 (Bohaty et al. 2003) in order to yield a first estimate for the age scale.

Results

The resulting sequence of events is composed of 605

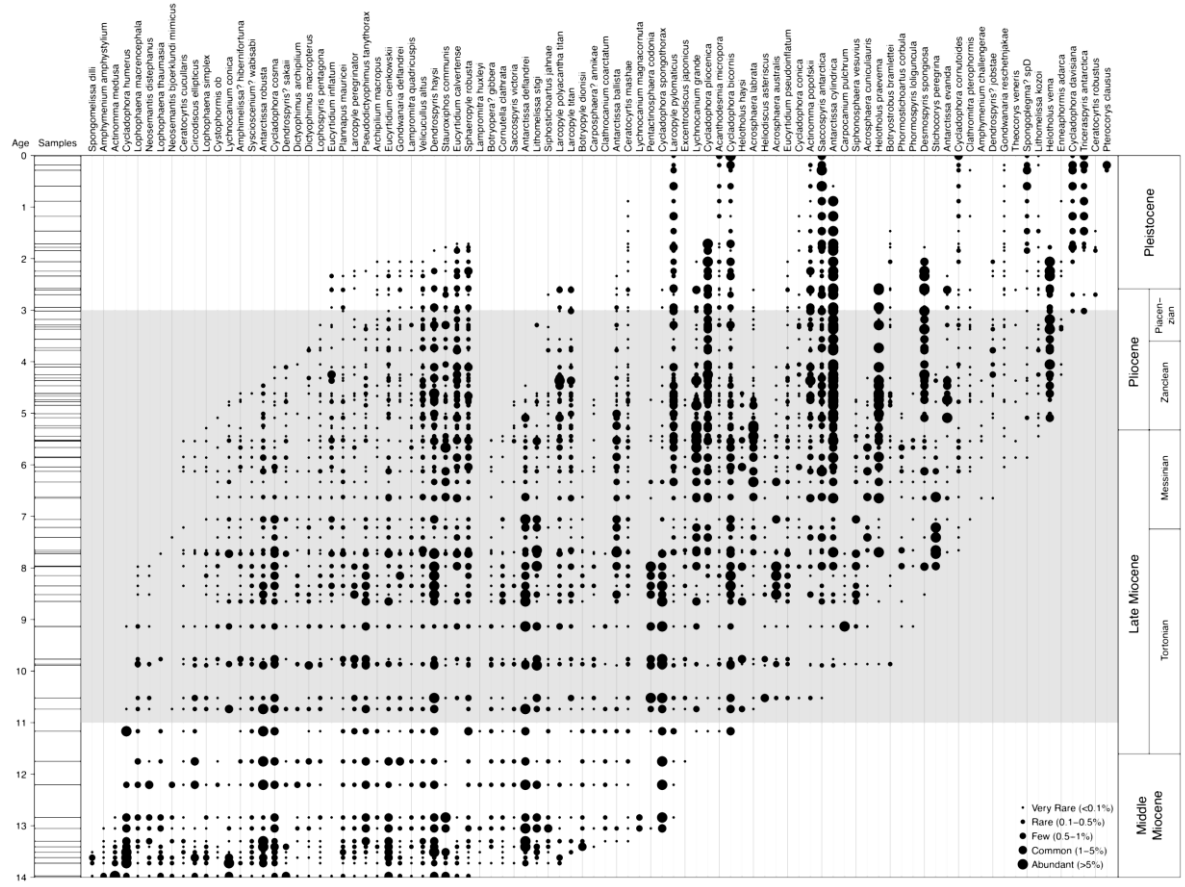

Figure 3 - Range-chart for a small selection of Late Miocene - Early Pliocene composite occurrence data. Occurrences of each species in samples (represented on the composite sequence of event on the side) by a black dot whose size increases with abundance (categorical; see legend). Taxa are arranged in order of first appearances.

events aggregated in 78 well defined levels. The mean misfit is of 0.696 level (i.e. sample) per observed event.

If we select only the events that are observable on the majority of sites, that have robust ranges (i. e. that are continuous, without trailing range ends) and a very low mean misfit (see Fig. 3 for a selection of these events), 94 events (87 LOs and FOs and 7 abundance-based events) seems reliable enough to use as biostratigraphic markers.

Additionally, although those results are still very preliminary, age models for each sites were improved: the difference between the published age model and the new age model developed in this study is in half of the samples greater than 0.6 My. A fair number of samples are between 1 and 2 My younger in the new model than in the old one: it is presumably due, in the original age model, to a difficulty to interpret the paleomagnetic signal (see Fig. 4 for one such example).

Reassessment of classically used bioevents also showed that out of the 20 FO and LO used classically for the Late Miocene- early Pliocene sequence, only 2 of these events are completely inconsistent with our new stratigraphic scale: the FO and LO of *Amphymenium challengerae* lie at, respectively, 4.3 and 5.5 Ma instead of the published ages of 6.1 and 6.7 Ma. If confirmed, this is an interesting preliminary result considering this species' range defines the *A. challengerae* zone and is critical for age models crossing the Miocene-Pliocene boundary. It would reinforce similar tentative inferences from stratigraphic studies of other sites (e.g. Lazarus 2001) and support a substantial re-calibration of many Southern Ocean age-models near the Miocene-Pliocene boundary.

Outlook

The biostratigraphy presented in this study, though promising, is still largely preliminary: heavy sampling is still required in order to develop a high resolution radiolarian biostratigraphy in the late Neogene.

Additionally, the 6 sections covered in this study were primarily chosen for their good coverage of the entire Neogene and their better, continuous preservation of the radiolarian fauna. There were not however optimal for calibrating high resolution stratigraphy, since the best paleomagnetic stratigraphy sites are either high sedimentation rate hemipelagic sites near the continent with partially only moderate radiolarian preservation, or Subantarctic sites with partially non-Antarctic radiolarian faunas.

Calibrating our new radiolarian biostratigraphy to GPTS using such sites and integrating it to the recently-revised diatom biostratigraphy (Cody et al. 2008) will be the subject of a new proposal that we submitted this year.

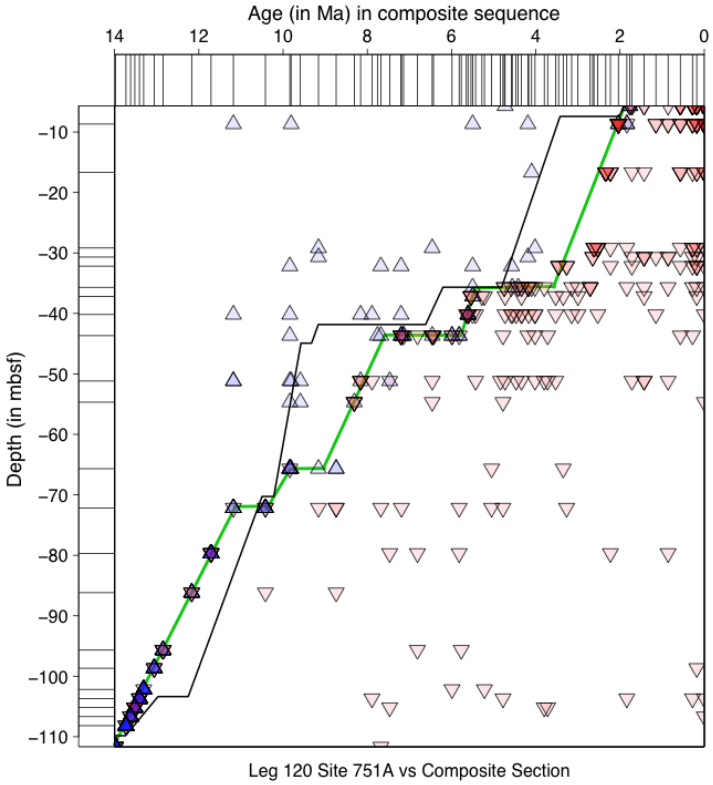

Figure 4 – Age-Depth plot for Leg 120 site 751. Lines on the left side represent the samples. Lines on the upper side represent each level of the composite sequence. Blue triangles are observed FO of radiolarian species while red ones are observed LO of radiolarian species. The intensity of the color is linked to the number of LO or FO present on this sample at this level.. Bold black line is the former age model for the site (Harwood et al. 1992) while the green bold line is the age model deriving from the CONOP analysis. The published age model is based on a few magnetostratigraphic data however the actual polarity signal for this interval is in reality rather poor (see Figs 3 & 5 in Heider et al. 1992) and, from our new radiolarian results, may not be reliable. The ambiguous, poorly resolved paleomagnetic polarity pattern between ca. 35 and 40 mbsf (Heider et al. 1992) would, based on our initial results probably better be assigned, not to C3A but to the lower normal events in C3.

References:
Bohaty, S. M., S. W. Wise Jr, R. A. Duncan, C. L. Moore & P. J. Wallace. 2003. Neogene diatom biostratigraphy, tephra stratigraphy, and chronology of ODP Hole 1138A, Kerguelen Plateau. In F. A. Frey et al. (Eds), Proceedings of the Ocean Drilling Program, Scientifc Results, College Station ,TX (Ocean Drilling Program), 183: 53pp.
Censarek, B. & R. Gersonde. 2002. Miocene diatom biostratigraphy at ODP Sites 689, 690, 1088, 1092 (Atlantic sector of the Southern Ocean). Marine Micropaleontology, 45: 309-356.
Cody, R., R. H. Levy, D. M. Harwood & P. M. Sadler. 2008. Thinking outside the zone: High-resolution quantitative diatom biochrnology for the Antarctic Neogene. Palaeogeography, Palaeoclimatology, Palaeoecology, 260: 92-121.
Harwood, D. M., D. B. Lazarus, A. Abelmann, M.-P. Aubry, W. A. Berggren, F. Heider, H. Inokuchi, T. Maruyama, K. McCartney, W. Wei & S. W. Wise Jr. 1992. Neogene integrated Magnetobiostratigraphy of the central Kerguelen Plateau, leg 120. In S. W. Wise Jr et al. (Eds), Proceedings of the Ocean Drilling Program, Scientific Results, College Station, TX (Ocean Drilling Program), 120: 1031-1052.
Heider, F., B. Leitner & H. Inokuchi. 1992. High Southern latitude magnetostratigraphy and rock magnetic properties of sediments from sites 747, 749 and 751. In S. W. Wise Jr et al. (Eds), Proceedings of the Ocean Drilling Program, Scientific Results, College Station, TX (Ocean Drilling Program), 120: 225-245.
Kemple, W. G., P. M. Sadler & D. J. Strauss. 1995. Extending graphic correlation to many dimensions: stratigraphic correlation as constrained optimization. In K. O. Mann & H. R. Lane (Eds), Graphic correlation, Special Publications of the Society of Economic Paleontologists and Mineralogists, 53: 65-82.
Lazarus, D. B. 2001. Late Miocene to Early Pliocene radiolarians from glaciomarine drift deposits, ODP Leg 178, Hole 1095B (Bellinghausen Basin, Antarctic Ocean). In P. F. Barker et al. (Eds), Proceedings of the Ocean Drilling Program, Scientific Results, 178: 22pp.
Lazarus, D. B., M. Weinkauf and P. Diver. 2012. Pacman profiling: a simple procedure to identify stratigraphic outliers in high-density deep-sea microfossil data. Paleobiology, 38(1): 858-875.
Sadler, P. M. 2007. CONOP9 version 7.43

IODP

Eocene and Oligocene geochemical records from the Wilkes Land Margin, Antarctica

U. RÖHL[1], P. K. BIJL[2], F. JIMÉNEZ[3], S. PASSCHIER[4], J. PROSS[5] AND IODP EXPEDITION 318 SCIENTISTS

[1] MARUM - Center for Marine Environmental Sciences, University of Bremen, Bremen, Germany
[2] Utrecht University, Utrecht, The Netherlands
[3] University Granada, Spain
[4] Montclair State University, Montclair, New Jersey, USA
[5] University of Frankfurt, Germany

Expedition 318 operated at seven sites in direct proximity to the Antarctic continent and resulted in the recovery of ~2000 m of upper Eocene to Holocene sediments. Site U1356 was drilled at the transition between the Wilkes Land rise and the abyssal plain at 3992 meters below sea-level. During the early Eocene Hole U1356A was situated in a mid-shelf setting and cored to 1006 meters below seafloor (mbsf) encompassing the past ~53 m.y. of Antarctic history. These cores document the evolution of the Wilkes Land margin from an ice-free greenhouse Antarctica to the present-day icehouse conditions, including the onset and erosional consequences of the first glaciation and the subsequent dynamics of the waxing and waning ice sheets.

The Paleogene section is characterized by a superb magnetostratigraphy and also got a robust biostratigraphic age control (dinocysts/pollen/calcareous nannofossils) (Tauxe et al., 2012). For our multi-proxy analysis approach we have chosen the moderately to strongly bioturbated claystones and calcareous claystones of Eocene and Oligocene age by the rate of core recovery that consistently improves starting at 640 mbsf. Our investigation includes X-ray fluorescence (XRF) core scanning and collection of bulk geochemical data via ICP-MS and discrete sample XRF analysis, as well as bulk organic carbon isotope ratios ($\delta^{13}C_{org}$) in combination with the concentration of the total organic carbon (TOC). Two time intervals are of major interest for our project: the early Eocene (lower Ypresian, ~52 to 54 Ma) and the upper Oligocene (Chattian, ~24 to 28 Ma) intervals.

The **early Eocene** at Site U1356 consists of well developed cyclic claystones that span the interval of magnetochron C24 which is ideal to re-evaluate the early Eocene part of the Geomagnetic Polarity Time Scale (GPTS) and to provide new insights into the environmental responses as well as orbital configuration of early Eocene climatic cycles.

The early Eocene Greenhouse interval (~56–49 Ma) was punctuated by a number of transient global warming events, or hyperthermals – the most prominent of which was the Palaeocene-Eocene Thermal Maximum (PETM). Additional thermal maxima identified in Eocene records exhibit negative carbon isotope excursions (CIEs), carbonate dissolution horizons, and biotic perturbations, although of reduced magnitude and duration relative to the PETM (Zachos et al., 2010). It is unclear, however, which of these events are normal carbon-cycle variations that occurred at orbital frequencies and which are exceptional events outside the normal range of Eocene carbon-cycle variability. An essential prerequisite for deciphering the origin and nature of hyperthermals is placing them within the exact temporal context of short- and longer-term variations in climate and the global carbon cycle. However, climatic conditions of the early Eocene greenhouse world are poorly constrained in critical regions, particularly the Antarctic continent (Pross et al., 2012). The U1356 record provides a key section from the Antarctic margin for this critical time interval.

We would like to address critical questions through detailed investigation of the early Eocene strata recovered at Site U1356. Several lines of investigation on the Wilkes Land cores are ongoing (e.g., Pross et al., 2012; Tauxe et al., 2012) and a sampling sharing scheme between several labs in Germany, UK, The Netherlands, and USA, was developed. The 32-m long early Eocene record from Site U1356 consists of about 600 individual data points for each parameter and these high-resolution datasets exhibit several variations in the record. Namely, the about 1.2 m $\delta^{13}C_{org}$ cycles are well pronounced and the excursions have amplitudes of up to -26 (in one case -25) ‰. The wavelengths of these cycles are in the order of 100 kyr as estimated from the number of cycles in relation to the duration of magnetochrons, e.g., subchron C25n.3n (~ 525 kyr, Westerhold & Röhl, 2009). Notably, the variations in $\delta^{13}C_{org}$ are accompanied by oscillations in XRF intensity (e.g., Ca, Fe), γ-ray (NGR), and TOC data, as well as in variations in the occurrence of the dinoflagellate cyst *Apectodinium* spp.. This suggests that variations in $\delta^{13}C_{org}$ are influenced by climatic cycles expressed by fluctuating terrigenous input into the marine domain. The average $\delta^{13}C_{org}$ values of ~26 to ~28 ‰ are typical for terrestrial organic matter (Hayes, 1993). The cyclicity in the $\delta^{13}C_{org}$ record is more pronounced in the lower part of the studied section, where TOC values are high enough (0.5 – 1.2 wt

%) to provide excellent data quality. In the upper part of the early Eocene section, TOC contents are on average not higher than 0.5 wt %, which yields a lower fidelity of the $\delta^{13}C_{org}$ signal (higher degree of noise). From detailed investigation and interpretation of all these data we now know that the early Eocene record of Site U1356, starting at 53.6 Ma, is ~1.3 Myr long and exhibits a temporal resolution of at least 100 kyr; it provides new key information necessary to identify the relationships between the origin of carbon cycle excursions and related climate changes.

New records from Wilkes Land **Oligocene** cores (a ~400 m sequence is constrained by magnetostratigraphy and partially by dinocyst and nannofossil data) are characterized by a typical hemipelagic sedimentation with variable bottom current and gravity flow influence. Microfossil contents, sedimentology, and geochemistry of the Oligocene sediments from Site U1356, at present occupying a distal setting (i.e., lowermost rise-abyssal plain), unequivocally reflect icehouse environments with evidence of iceberg activity (dropstones) and at least seasonal sea ice cover. The cyclic sediments as well as biota, indicate deeper water settings relative to the underlying Eocene sediments. Combined paleoenvironmental data also indicate significantly cooler, high-productivity, and sea ice–influenced surface waters, with only occasional incursions of warmer conditions (Escutia et al., 2011). Due to the presence of diamictite the upper ~205 meters of the Oligocene record (from ~434 to 640 mbsf) are only poorly recovered. Therefore, our study focusses on the interval between 640 to ~875 mbsf with good recovery although only a single hole available. XRF core scanning data (especially Ca intensities and Zr/Al ratios) in line with grain size variations cleary exhibit the alternation of bioturbated mudstones (pelagic sedimentation) with laminated silty claytones (contour current sedimentation) in high-resolution. Our working model for interpreting these very regular alternations is that shifting current patterns controlled by wind-driven systems that respond to orbitally forced changes in ice volume. At this moment we are working on an increase the resolution of grain size and dinoflagellate data for carefully selected, representative intervals as this information will be needed to validate our hypothesis in detail. Another important ongoing effort is trying to integrate the U1356 record characterized by a superb, unambiguous magnetostratigraphy for this time interval (Tauxe et al., 2012) with orbitally-tuned Equatorial Pacific records as well as with records from the Tasman Sea.

References:

Escutia, C., Brinkhuis, H., Klaus, A., and the Expedition 318 Scientists (2011) Wilkes Land Glacial History. Proc. IODP, 318: Tokyo (Integrated Ocean Drilling Program Management International, Inc.). doi:10.2204/iodp.proc.318.2011

Hayes, J.M., Factors controlling 13C contents of sedimentary organic compounds: Principles and evidence, Marine Geology, 113, 111-125, 1993.

Pross, J., Contreras, L. Bijl, P.K., Greenwood, D.R., Bohaty, S.M., Schouten, S., Bendle, J.A., Röhl, U., Tauxe, L., Raine, J.I., Huck, C.E., van der Flierdt, T., Jamieson, S.S.R., Stickley, C.E., van de Schootbrugge, B., Escutia, C., Brinkhuis, H. & IODP Exp. 318 Scientists (2012) Persistent near-tropical warmth on the Antarctic continent during the early Eocene epoch, Nature, 488, 73–77, doi:10.1038/nature11300

Röhl, U. Bijl, P.K., Jiménez, F., Pross, J., Contreras, L, Tauxe, L., Bohaty, S.M., Bendle, J.A., and IODP Exp. 318 Scientists (2011) Early Eocene cyclicity at the Wilkes Land Margin, Antarctica: Orbital forcing and environmental response, Abstract PP33B-1938 presented at 2011 Fall Meeting, AGU, San Francisco, Calif., 5-9 Dec.

Tauxe, L., Stickley, C.E., Sugisaki, S., Bijl, P.K., Bohaty, S., Brinkhuis, H., Escutia, C,, Flores, J.A., Iwai, M.,, F. Jiménez-Espejo, McKay, R., Passchier, S., Pross, J., Riesselman, C., Röhl, U., Sangiorgi, F., Welsh, K., Klaus, A., Fehr, A., Bendle, J.A.P., Dunbar, R., Gonzalez, J., Hayden, T., Olney, M.P., Pekar, S.F., Shrivastava, P.K., van de Flierdt, T., Williams, T., Yamane, M. (2012) Chronostratigraphic framework for the IODP Expedition 318 cores from the Wilkes Land Margin: constraints for paleoceanographic reconstruction, Paleoceanography, 27, PA2214, doi:10.1029/2012PA002308

Westerhold, T. and Röhl, U.: High resolution cyclostratigraphy of the early Eocene – new insights into the origin of the Cenozoic cooling trend, Clim. Past, 5, 309-327, 2009.

Zachos, J. C., McCarren, H.K., Murphy, B., Röhl, U., Westerhold, T. (2010): Tempo and scale of late Paleocene and early Eocene carbon isotope cycles: Implications for the origin of hyperthermals, Earth Planet. Sci. Lett. (299 (2010) 242–249, doi:10.1016/j.epsl.2010.09.004.

IODP

Cold-water coral mound development related to INtermediate WAter DEnsity gradient (INWADE)

A. RÜGGEBERG[1,2,3], W.-CHR. DULLO[1]

[1] GEOMAR | Helmholtz Center for Ocean Research Kiel, Wischhofstr. 1-3, D-24148 Kiel, Germany
[2] RCMG, Department of Geology and Environmental Sciences, Ghent University, Krijgslaan 281, S8, B-9000 Gent, Belgium
[3] Present Address: Department of Geology and Paleontology, University of Fribourg, Chemin du Musée 6, CH-1700 Fribourg, Switzerland

Cold-water corals occur along the European continental margin and form large reefs and mound structures. Recent studies underline the environmental control on the growth and development of these reefs. DFG-project INWADE concentrates on the new observation indicating that the density of seawater may be a prerequisite environmental control factor for the Northeast Atlantic coral reefs (Dullo et al. 2008). Another study (White and Dorschel 2010) proposed that the position and stability of the thermocline is likely the key in providing favourable conditions over long time scales allowing mounds to grow through sediment baffling processes. However, from a paleoceanographic point of view, both findings are very important and interesting and the possibility to reconstruct paleo-densities and paleo-temperatures gives us the opportunity to determine past environmental water mass characteristics related to cold-water coral growth and carbonate mound development. A compilation of existing (and new) stable isotope data from DSDP, ODP and IODP sites combined with existing (and new) data from short sediment cores will provide the basis of this study (Fig. 1a). Three depth-transects at 37°N, 51°N and 65°N cross the European continental slope down to 3000 m water depth and show except for the latter good coverage of drill cores (Fig. 1b). Along these transects paleo-densities and paleo-temperatures will be calculated for important time periods during the past 3 million years and compared to the history of settlement and development of cold-water coral reefs.

References:

Dullo, W.-Chr., Flögel, S., Rüggeberg, A., 2008. Cold-water coral growth in relation to the hydrography of the Celtic and Nordic European Continental Margin. Marine Ecology Progress Series 371: 165–176.

White, M., Dorschel, B., 2010. The importance of the permanent thermocline to the cold water coral carbonate mound distribution in the NE Atlantic. Earth and Planetary Science Letters 296: 395–402.

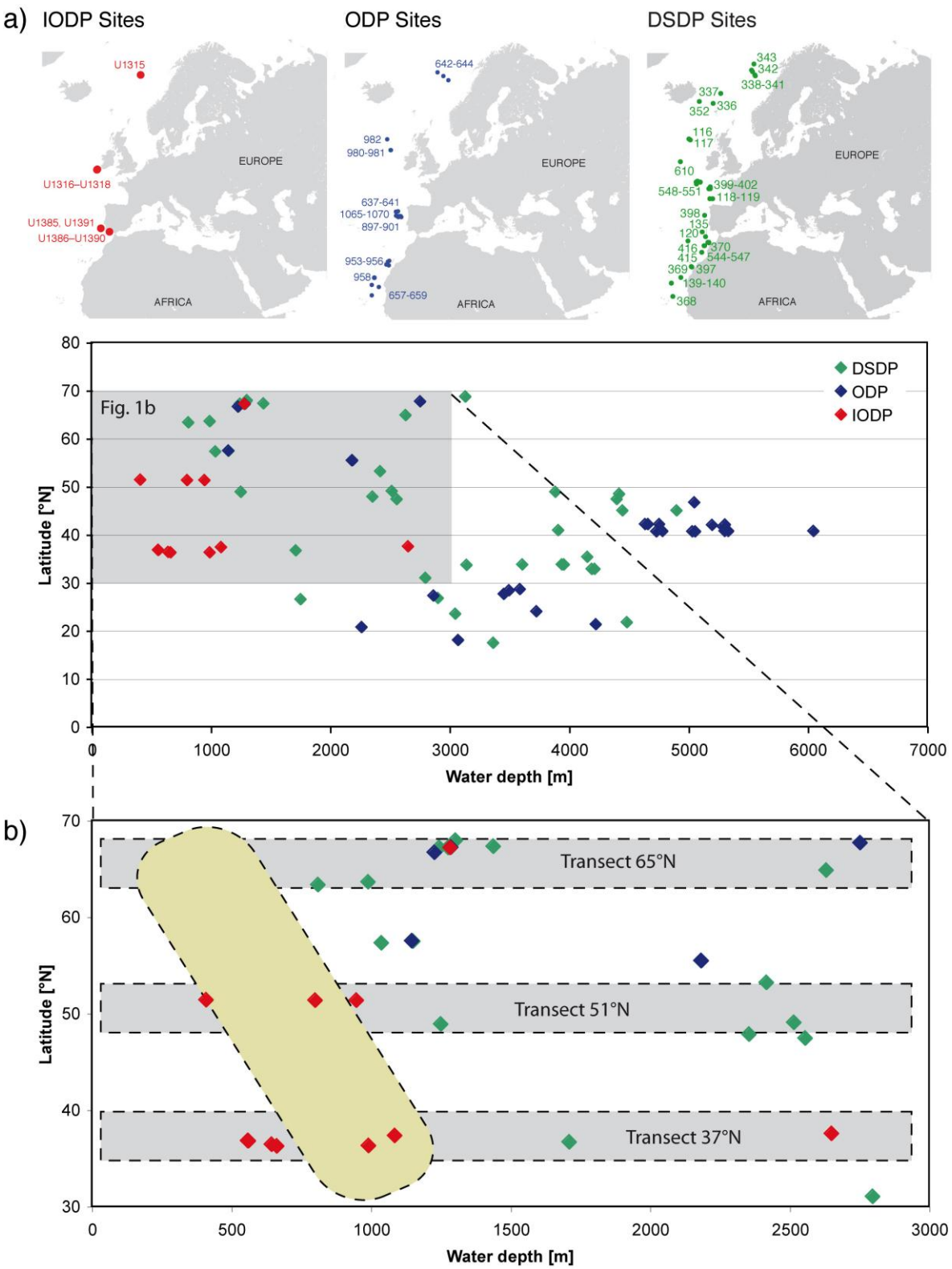

Fiure 1. a) Drill cores of DSDP (green), ODP (blue) and IODP (red) initiatives along the NE Atlantic margin plotted in a latitude–water depth diagram. b) Three latitudinal transects at 37°N, 51°N and 65°N: Beige area indicates cold-water coral reef belt along the European margin. Shallow areas along the Norwegian margin lack drill sites – here other sediment cores will provide Late Pleistocene data.

ICDP

Timing and Significance of Mass Movement Events for the 3.6 Ma Sediment Record of Lake El'gygytgyn, Far East Russian Arctic

M. SAUERBREY[1], C. GEBHARDT[2], O. JUSCHUS[3], V. WENNRICH[1], N.R. NOWACZYK[4], M. MELLES[1] AND EL'GYGYTGYN SCIENTIFIC PARTY

[1] University of Cologne, Institute of Geology and Mineralogy, Cologne, Germany (maaret.kukkonen@uni-koeln.de)
[2] Alfred Wegener Institute for Polar and Marine Research, Bremerhaven, Germany
[3] Eberswalde University of Sustainable Development, Faculty of Landscape Management and Nature Conservation, Eberswalde, Germany
[4] Helmholtz Center Potsdam, GFZ German Research Centre for Geosciences, Potsdam, Germany

The sediment archive of Lake El'gygytgyn has been intensively studied since 2009 for past environmental and climate changes. These studies concentrate on the pelagic sediment that was settled continuously over long periods of time from allochtonous and autochtonous supply. The sediment record has revealed new insights into Quaternary and Pliocene environments in the high Arctic (Melles et al. 2012, Brigham-Grette et al. in review). Additionally to the pelagic sediment, various short-lived mass movement sediments have deposited in Lake El'gygytgyn throuhout the lake's existence and comprise 35 % of the recovered sediment record (Sauerbrey et al. 2013). In the scope of this study, the nature of the mass movement deposits (MMDs) is investigated.

The 320-m long sediment record from ICDP Site 5011 at Lake El'gygytgyn (67° 30‘ N, 172° 5‘ E; Fig. 1) recovered in winter/spring 2009 from the 3.6 Ma old impact crater, consists of three parrallel partly overlapping cores (Melles et al. 2011, 2012). The lake is situated 492 m above sea level and has a diameter of 12 km. The drill site, with a water depth of 170 m, is located in the deepest part of the lake, where a pre-site survey indicated undisturbed and layered sediments. In the lake marginal areas, seismic survey and pilot cores have revealed thick erosive debris flows (3–20 m) thinning toward the lake centre, where several turbidites can be found. (Niessen et al. 2007, Juschus et al. 2009). The slopes are deepest in the eastern and northern parts of the lake, with inclinations between 15-30°. The highest slopes of greater than 40° can be found in the east, where bedrock outcrops into the lake. The southern and western shores are characterised by lower inclinations of 5-15°. In the investigations of the drill cores five different types of MMDs were identified: turbidites, debrites, slumps, slides and grain flows (Sauerbrey et al. 2013). In the Quaternary sediments, which comprise the uppermost 123 m of the record and were recovered nearly perfectly, a total of 238 mass movement events have been discovered, consisting 37 % of the record. In the Pliocene sediments, which are between 123 and 320 m and were recovered by only 52 %, another 185 events have occurred. MMDs comprisise 32 % of the Pliocene recovered sediments. The lower percentage of MMDs in the Pliocene may be partly explained by the lower recovery.

Turbidites in Lake El'gygytgyn are normally graded from sand or silt to clay and have thicknesses between 2 mm and 95.3 cm. They have sharp lower boundaries, and most of of them show clear intra-bed boundaries between grain sizes, whilst some have more diffuse boundaries between grain sizes. Grain flow deposits are massive sands and silts with sharp contacts to underlying sediment. Their thicknesses vary between 3.3 and 26.2 cm. These deposits are very rare in the sediment record and occur only 8 times. Debrites are poorly sorted greyish fine gravels and sands in a silty to clayey matrix, whose thicknesses vary between 30 cm and 3 m. They occasionally have clasts of finer, deformed sediment in their upper parts and are capped by a turbidite. Slumps are folded and deformed pelagic sediments or event layers (tephras, turbidites), where the facies of the source sediment is still widely identifiable. The thicknesses vary between 44 and 380 cm and they can be overlain by turbidites. Slides consist of slightly deformed dupli- or multiplicated sequences of fine sediment or event layers. They have thicknesses between 160 and 275 cm and they may be overlain by turbidites.

More than 420 identified events contribute significantly to the sediment thickness in Lake El'gygytgyn. 91 % of the number of events are turbidites, but their portion of the recovered sediment thickness is only 14.5 %. This reflects the generally thin nature of turbidites at the lake center, with a mean thickness of 8.6 cm. The rest of the MMD types, i.e. debrites, grain flows, slides and slumps contribute only 9 % of the number of MMDs but to 20 % of the total sediment thickness.

Most of the Pliocene sediments were recovered only in one drill hole (5011-1C). The lack of a parallel core below 150 m composite depth (cd) hinders the identification of some MMDs, in particular slides, thus leading to an underestimation of the event layers. Interrestingly, both twist-offs in holes 1A (149 m cd) and 1B (115 m cd) occurred in debrites (D279 & D221, respectively). In hole 1A the lower boundary, and in hole 1C the upper boundary of D221 as well as D279 were not recovered at all, suggesting that the twist-offs as well as the core gaps can be related to coarser grained mass movement deposits. Therefore, the amount of MMDs in the Pliocene could have been significantly higher.

Based on the findings in the drill cores, a simplified illustration of the mass movement evolution in Lake El'gygytgyn was developed (Fig. 2). We suppose that the formation of MMDs is associated with an initial sediment failure in the upper slope that advances deeper towards the lake floor. Depending on the characteristics of the source material three possible scenarios can explain the findings in the lake center. A) When the sediment failure occurs in deltaic environments, where the source material is well-sorted, the mass movement takes place as a mainly laminar grain flow. Grain flows are slightly erosive and have rarely reached the lake center. B) When the sediment failure takes place outside the deltas, in shallow water depths, where coarser grained sediments are available, the failure develops into a debris flow. Debris flows are the coarsest sediments found in the lake center. During their advance on the lake slope, debris flows deform previously deposited sediments that become partly disintegrated. The debris flow becomes partly diluted and sediment is brought into suspension. A turbidity flow is formed on top and in front of the debris flow. A normally graded turbidite is deposited in the lake basin, and is more widely distributed than the debris flow. Debrites have reached the lake center 10 times during the lakes history and are often associated with folded and deformed pelagic sediment clasts in their upper parts, as well as overlain by a turbidite. Slump deposits, without an underlying debrite, have reached the lake center 16 times. Since the facies of the source material is still clearly identifiable, the deformation and transportation of slump deposits is limited. C) In a few cases, slide deposits

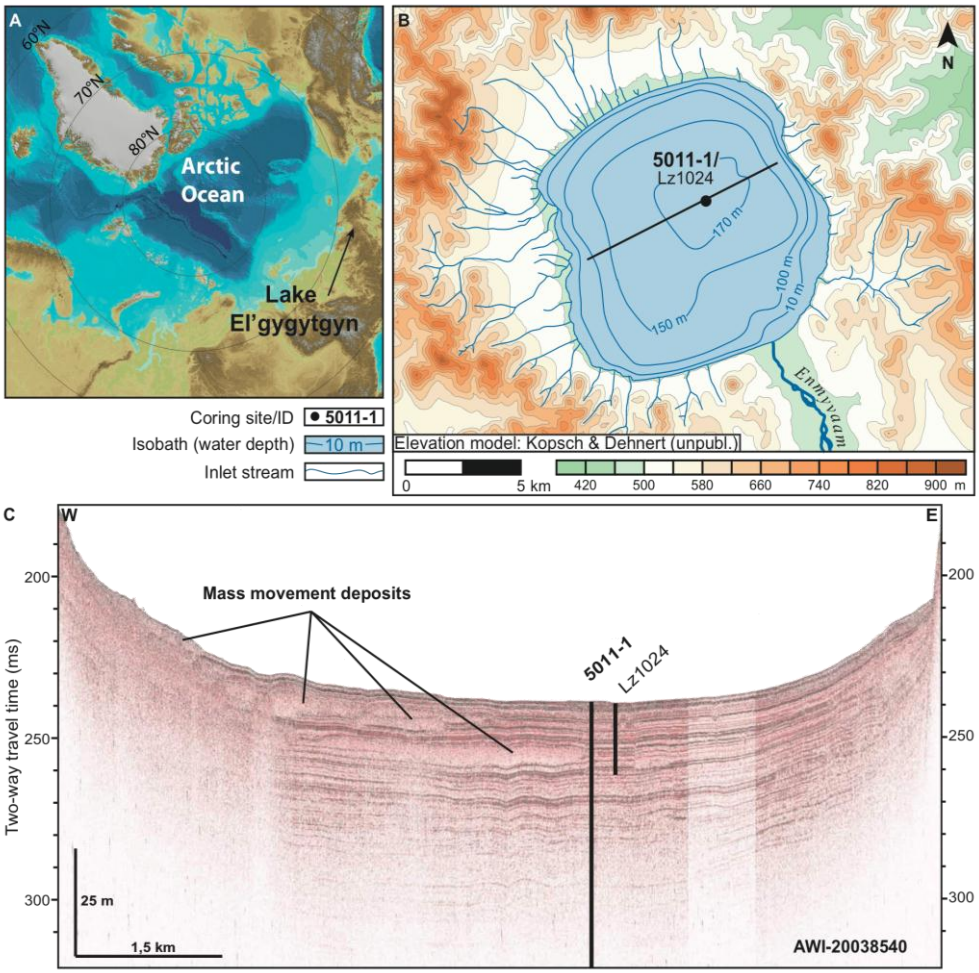

Fig. 1. A) Location of Lake El'gygytgyn in Far East Russian Arctic. B) Position of the drill site 5011-1 and pilot core Lz1024 as well as seismic profile (black line) AWI-20038540. Digital elevation model ist after Kopsch (2005) and lake bathymetry after Belyi (2001). C) Sediment echosounder profile AWI-20038540 (3.5 kHz) in a WSW-ENE direction crossing the coring site ans showing multiple mass movement deposits as acoustically transparent units in the western slope ans lake floor.

are found in the lake center, in which specific sediment sections are multiplicated but not folded. They could be formed when a debris flow deforms more rigid sediments, displacing sediments along small thrust faults. Another possible explanation is retrogradation of an initial sediment failure on the lake slope that leads to instability and failure in the neighbouring areas (Mulder and Cochonat, 1996). However, as this would occur on the lake slope, which is several kilometers away from the lake center, it is unlikely that the sediments would have reached the coring site as undeformed as they have. Additionally, the lake slopes are characterised by coarser grained sediments than at the lake floor. Slide deposits are encountered only four times at the drill site.

Several processes can trigger mass movement, such as earthquakes, considerable lake-level changes, sediment overloading, delta collapses and extreme flooding events. Evidence of syncronious events within the lake basin points at a regional triggering mechanism, such as seismic shaking or lake-level changes rather than local sediment failures due to overloading on the lake slope. At Lake El'gygytgyn extreme flooding events as the cause of MMDs can be considered minimal, as the precipitation and water discharge from the inlet creeks is small (Fedorov et al. 2012). Additionally, the internal structure of the majority of the turbidites does not suggest formation by hyperpycnal flows, where the deposit would have a basal coarsening upward unit overlain by a fining upward unit.

In the deep lake basin, the accumulated sediments are fine grained (Wennrich et al. 2013, Francke et al. 2013), suggesting that the coarser grained mass movements, in particular debrites, but also grain flows and turbidites, originate from shallow water depths, where such sediments are found (Juschus et al. 2011). The large alluvial fan and its subaquaous prologation in the western and northern lake catchment provide coarser grained sediments into the lake basin (Schwamborn et al. 2012) and delta collapses surely account for some of the mass movements encountered at the lake center.

Since the coarser grained sediments in the marginal lake areas resulted in poorer penetration in the seismic investigations, the seismic data cannot be used to identify precise source areas for the mass movements. However, the direction of their origin can be seen in the profiles. Mapping of debris flows in the seismic profiles is hampered in the proximal areas due to low penetration on the lake slope. Whilst most of the debris flows appear to be single events, they cover large areas of the lake (up to 50%) and have multiple lobes of several kilometers length. This suggests a more regional triggering mechanism, e.g. paleo-earthquakes or lake-level changes, at least for larger events. In fact, seismic surveys revealed small faults within the sediment column that might be related to the central uplift structure of the impact crater (Niessen et al. 2007). Although the faults did not penetrate the water-sediment interface, their existence shows that the area of Lake

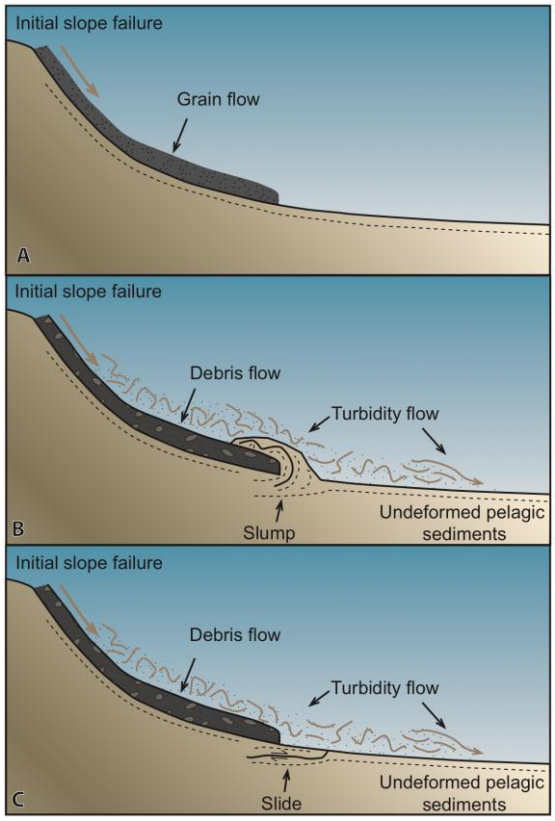

Fig. 2. Illustration of the evolution of mass movements in Lake El'gygytgyn. A) Delta collapses of well-sorted material result in grain flows where the sediment density and grain size is too high to support turbulence. B) Debris flow deforms pelagic sediments and creates co-generic turbidity current in front and on top of the debris flow. C) Slide deposits encountered at the lake center may be caused by debris flows.

El'gygytgyn is neotectonically active. In the southeastern catchment, a mercury survey of the soil air revealed elevated values also indicating ongoing activaty of the fault system (Fedorov and Kupolov 2005).

Lake-level changes are also a plausible triggering mechanism for mass movements in Lake El'gygytyn. The lake level is known to have fluctuated in the past, at least four former lake terraces are known with heights of 35–40 m, 9–11 m, 3–5 m and -10 m (Glushkova and Smirnov 2005; 2007, Juschus et al 2011). In general, higher lake levels are thought to correlate to warmer climate periods and lower terraces to colder stages (Juschus et al. 2011). Additionally, several pebble bars on the northern shore mark a gradual lake-level drop of 4 m during the Holocene (Schwamborn et al. 2008). Currently, paleo-earthquakes, lake-level changes as well as delta collapses and overloading of the slope sediment remain as plausible triggering mechanisms for mass movements at Lake El'gygytgyn.

Turbidites are found abundantly throughout the sediment record, intercalated in all pelagic sedimentary facies, reflecting their importance to the filling of the crater lake and sedimentation processes. Eventhough turbidites are generally thin, their high number ensures that a significant portion of the sediment thickness, in the Quaternary 11.7 % and in the Pliocene 18 % of the recovered sediments are turbidites. Other mass movement types occur exclusively during warm climate conditions, indicating that their occurrence might be dependent on climate conditions. In addition, the thickness of turbidites was detected to show differences depending on the facies association. Quaternary turbidites deposited during cold periods (facies A) have a mean thickness of 4.07 cm, whilst during warm stages (facies B) it was 7.35 cm. The warmer Pliocene is characterised by an increase in the mean thickness of turbidites to 11.3 cm from the 6.6 cm of the Quaternary mean, whilst the median thickness increases only slightly to 3.4 cm from 2.9 cm. However, the turbidite thickness as well as their frequency in the Pliocene may have been influenced by higher erosion rates in the young steep crater. The sedimentation rate was also higher during the Pliocene (15 cm ka^{-1}), especially during the first ca. 300 ka after the impact (45 cm ka^{-1}), compared to the Quaternary (4.7 cm ka^{-1}).

The influence of climate on mass movements in Lake El'gygytgyn is further supported by the absence of thicker MMDs (debrites, slides and slumps) during cold periods. The concentration of thicker MMDs to warm climates could be explained by a thicker active layer, enhanced erosion and transport as well as the generally slightly coarser grained sedimentation compared to cold stages (Francke et al. 2013), whereas the perennial ice cover of the lake during cold periods would largely hinder sediment transport into the lake.

References:

Brigham-Grette, J., Melles M., Minyuk, P., Andreev, A, Tarasov, P., DeConto, R., Koenig, S., Nowaczyk, N., Wennrich, V., Rosén P., Haltia-Hovi, E., Cook, T., Gebhardt, C., Meyer-Jacob, C., Snyder, J., and Herzschuh, U. (in review): Pliocene Warmth, extreme Polar Amplification, and Stepped Pleistocene Cooling recorded in NE Russia, *Science*, 2013.

Fedorov, G., Nolan, M., Brigham-Grette, J., Bolshiyanov, D., Schwamborn, G. and Juschus, O. (2012): Lake El'gygytgyn water and sediment balance components overview and its implications for the sedimentary record, *Clim. Past Discuss.*, 8, 3977–4001, doi:10.5194/cpd-8-3977-2012.

Fedorov, G. and Kupolov, A. (2005): Gas mercury survey in the El'gygytgyn crater. In: Melles, M., Minyuk, P., Brigham-Grette, J. and Juschus, O. (Eds): The Expedition El'gygytgyn Lake 2003 (Siberian Arctic), Rep. Polar Mar. Res, 509, 69-70,

Francke, A., Wennrich, V., Sauerbrey, M.A, Asikainen, C., Melles, M., and Brigham-Grette, J. (2013): Quaternary grain-size distribution of Lake El'gygytgyn, NE Siberia: statistic analysis and climate dependency, *Clim. Past Discuss.*, 9, 217–244, doi: 10.5194/cdp-9-217-2013.

Gebhardt, A. C., Francke, A., Kück, J., Sauerbrey, M. A., Niessen, F., Wennrich, V., and Melles, M. (2013): Petrophysical characterization of the lacustrine sediment succession drilled in Lake El'gygytgyn, Far East Russian Arctic, *Clim. Past Discuss.*, 9, 351–391, doi:10.5194/cpd-9-351-2013.

Glushkova, O.Y. and Smirnov, V.N.: Coastal Morphology. In: Melles, M., Minyuk, P., Brigham-Grette, J. and Juschus O. (Eds.): The Expedition El'gygytgyn Lake 2003 Siberian Arctic, Rep. Polar Mar. Res., 509, 104-108, 2005.

Glushkova, O.Y. and Smirnov, V.N.: Pliocene to Holocene geomorphic evolution and paleogeography of the El´gygytgyn Lake region, NE Russia. *Journal of Paleolimnology* 37, 37-47, 2007.

Juschus, O., Pavlov, M., Schwamborn, G., Preusser, F., Fedorov, G., and Melles, M. (2011): Late Quaternary lake-level changes of Lake El'gygytgyn, NE Siberia, *Quaternary Res.*, 76, 441–451, doi.10.1016/j.yqres.2011.06.010.

Juschus O., Melles M., Gebhardt A.C. & Niessen F. (2009): Late Quaternary mass movement events in Lake El´gygytgyn, north-eastern Siberia. *Sedimentology*, 56, 2155-2174. DOI: 10.1111/j.1365-3091.2009.01074.x

Melles, M., Brigham-Grette, J., Minyuk, P. S., Nowaczyk, N. R, Wennrich, V., DeConto, R. M., Anderson, P. A., Andreev, A. A., Coletti, A., Cook, T. L., Haltia-Hovi, E., Kukkonen, M., Lozhkin, A. V., Rose´n, P., Tarasov, P. E., Vogel, H., and Wagner, B. (2012): 2.8 Million Years of Arctic climate change from Lake El'gygytgyn, NE Russia, *Science*, 307, 315–310, doi:10.1126/science.1222135.

Melles M., Brigham-Grette J., Minyuk P., Koeberl C., Andreev A., Cook, T., Fedorov G., Gebhardt C., Haltia-Hovi E., Kukkonen M., Nowaczyk N., Schwamborn G., Wennrich V. and El'gygytgyn Scientific Party (2011). The El'gygytgyn Scientific Drilling Project – conquering Arctic challenges through continental drilling. *Scientific Drilling*, 11: 29-40. DOI: 10.2204/iodp.sd.11.03.2011.

Mulder, T. and Cochonat, P.: Classification of offshore mass movements. J. Sed. Res., 66, 43-57, 1996.

Niessen, F., Gebhardt, A.C., Kopsch, C. and Wagner, B. (2007). Seismic investigation of the El'gygytgyn impact crater lake Central Chukotka, NE Siberia: preliminary results. *J. Paleolimnol.*, 37, 49–63.

Sauerbrey, M.A., Juschus, O., Gebhardt, A.C., Wennrich, V., Nowaczyk, N.R. and Melles, M. (2013): Mass movement deposits in the 3.6 Ma sediment record of Lake El'gygytgyn, Far East Russian Arctic: classification, distribution and preliminary interpretation, Clim. Past Discuss., 9, 467-505, doi: 10.5194/cpd-9-467-2013.

Schwamborn, G., Fedorov, G., Schirrmeister, L, Meyer, H. and Hubberten, H.-W.: Periglacial sediment variations controlled by late Quaternary climate and lake level change at Elgygytgyn Crater, Artic Siberia. *Boreas*, vol. 37, pp. 55-65, 2008.

Schwamborn, G., Fedorov, G., Ostanin, N. Schirrmeister, L., Andreev, A. and the El'gygytgyn Scientific Party: Alluvial fan dynamics in the El'gygytgyn Crater: implications for the 3.6Ma old sediment archive, *Clim. Past*, 8, 1897-1911, doi:10.5194/cp-8-1897-2012, 2012.

Wennrich, V., Francke, A., Dehnert, A., Juschus, O., Leipe, T., Vogt, C.,Brigham-Grette, J., Minyuk, P., Melles, M., and El'gygytgyn Science: Modern sedimentation patterns in Lake El'gygytgyn, NE Russia, derived from surface sediment and inlet stream samples, *Clim. Past*, 9, 135-148, doi:10.5194/cd-9-135-2013, 2013.

IODP

Much older than expected – a view from recent into the bathyal atelostomate fossil record (Spatangoida, Holasteroida; irregular echinoids)

N. SCHLÜTER[1,2], F. WIESE[2], B. THUY[1] & M. REICH[1,2]

[1] Georg-August University of Göttingen, Geoscience Museum, Goldschmidtstr. 1-5, 37077 Göttingen, Germany; mreich@gwdg.de

[2] Georg-August University of Göttingen, Geoscience Centre, Dept. of Geobiology, Goldschmidtstr. 3, 37077 Göttingen, Germany

Atelostomate irregular echinoids (Holasteroida, Spatangoida) developed in the Lower Cretaceous and became essential parts of the Cretaceous shelf. While holasteroid echinoids are today restricted to the deep-sea, spatangoids are found in both deep sea and shelf habitats. The history and origin of deep-sea representatives of both groups is still unsettled. The earliest known records of a deep-sea spatangoid so far is from the Santonian, Upper Cretaceous (Smith 2013). The origin of deep sea atelostomates was inferred so far from combined analyses of morphologies and molecular clock studies, and it was inferred that spatangoid and holasteroid deep sea faunas are not older than 75 Myr (Stockley *et al.* 2005, Smith & Stockley 2005).

However, entire tests are often rare especially in deeper settings, while isolated plates and spines of irregular echinoids can be common to very abundant in washing residues of shelf and deep sea sediments together with ossicles of other echinoderms such as ophiuroids, crinoids and holothurians. The latter three can generally be identified with great confidence at genus to species level, enabling deep sea palaeobiogeographic research and the reconstruction of timing of deep sea colonization (Thuy *et al.* 2012). In contrast, there is only little knowledge on the morphology of atelostomate spines. Thus spines from irregular echinoids has largely been ignored by zoologists and palaeontologists for systematic issues and thus were not useful for any view on geological history. An actualistic approach of comparing microstructures in spines from holasteroid and spatangoid echinoids resulted in very well definable systematic differences in spines of both groups, which are detectable even in fragments.

By these results we can report the occurrence of both atelostomate groups in DSDP samples of Albian age (Site 327, Falkland Plateau). This indicates that the colonisation of the deep sea by the Atelostomata happened earlier than previously thought. Our data are in well accordance with the results of Thuy *et al.* (2012), who showed that the the origin of some of the modern deep sea echinoderm fauna dates back at least to the Early Cretaceous (Aptian, ~120 Myr).

Our results bear the large potential to trace back the origin of deep sea Atelostomata in time, and a careful re-assessment of the IODP/ODP/DSDP material might be the key to map the Atelostomata deep time from the inferred moment of its origin (estimated at ~145 Myr by Smith & Stockley 2005) to its dispersion into the depth.

References:

Schlüter, N.; Wiese, F.; Thuy, B. & Reich, M. subm. Systematic assessment of the Atelostomata (Spatangoida, Holasteroida; irregular echinoids) based on spine microstructures – a view from recent into the fossil record. *Zoological Journal of the Linnean Society*.

Stockley, B.; Smith, A.B.; Littlewood, T.; Lessios, H.A. & MacKenzie-Dodds, J.A. 2005. Phylogenetic relationships of spatangoid sea urchins (Echinoidea), taxon sampling density and congruence between morphological and molecular estimates. *Zoologica Scripta* **34** (5): 447–468.

Smith, A.B. 2013. Geological history of bathyal echinoid faunas, with a new genus from the late Cretaceous of Italy. *Geological Magazine* **150** (1): 177–182.

Smith, A.B. & Stockley, B. 2005. The geological history of deep sea colonization by echinoids: the roles of surface productivity and deep-water ventilation. *Proceedings of the Royal Society of London B* **272** (1565): 865–869.

Thuy, B.; Gales, A.S.; Kroh, A.; Kucera, M.; Numberger-Thuy, L.D.; Reich, M. & Stöhr,S. 2012. Ancient Origin of the Modern Deep-Sea Fauna. *PLoS ONE* **7** (10), 1–11. [e46913]

ICDP

Impact of volcanism on the evolution of Lake Van III: İncekaya - an exceptionally large magnitude (DRE > 1 km^3) subaqueous/subaerial explosive basaltic eruption

H.-U. SCHMINCKE[1], M. SUMITA[1], D. CUKUR[1], PALEOVAN SCIENTIFIC TEAM

[1] GEOMAR Helmholtz-Zentrum für Ozeanforschung Kiel , Wischhofstr. 1-3, 24148 Kiel, Germany

The morphologically prominent, horseshoe-shaped basaltic hyaloclastite İncekaya tephra ring rises ca. 400 m above the southwestern shore of Lake Van, 15 km east of Tatvan, the volcano extending to an unknown depth below lake level. The ca. 4 km wide tephra ring forms the seaward end of a 5 km long lithosphere fracture that propagated from south to north beginning at Dibekli scoria cone group. The central sector of the hyaloclastite edifice forms a lower massive to crudely banked core facies (stage 1) that collapsed and was subsequently mantled by a layered facies (stage 2) >50 m thick. The bedded, dominantly sideromelane tephra, alternating with beds of more vesicular and coarser-grained tachylite tephra forms a ca. 2 – 2.5 m thick deposit in outcrops 20 km east and 15 km northwest on land. A 2-m-thick basaltic tephra deposit was cored 27 km northeast of the eruptive center at Site 2 ca. 35 mblf (meter below lake floor) during the ICDP PaleoVan drilling. The well-preserved lithostratigraphy of the drilled section is remarkably similar to that of the main land section 10 km east of İncekaya cone, 20 km south of Site 2. Poorly recovered parts of the İncekaya tephra were drilled at Site 1 at 123 mblf. Major tephra units of the more than 20 fallout events that can be correlated between three holes (Sites 2B, 2D and 2E) and subaerial outcrops (Sumita

and Schmincke 2013, in press) must reflect an exceptionally high and broad eruption column. The sedimentation rate at the drill site must have been fast in order to preserve the integrity of structurally contrasting particle populations under water probably being supplied to the site at short intervals. The present water depth of the lake of 360 m at the drill site was much lower ~270 m at the time İncekaya erupted, probably ca. 80 ky ago as also indicated by other lines of evidence. The explosive energy for most of this large magnitude basaltic eruption was clearly supplied by the interaction of magma and lake water in which case the site of interaction (base of the cone) was likely >100 m below present lake level. The lacustrine İncekaya tephra unit forms the most widespread reflector in the lake Van sediments covering an area of > 1500 km^2, making the eruption one of the largest explosive basaltic eruption known worldwide (Constantini et al. 2009). The mildly alkalic (moderate K_2O concentrations of 0.6-0.8 wt. %) İncekaya basalt is a fractionated (6-7 wt. % MgO, low Cr and Ni) high alumina basalt (17.5-18 wt. % Al_2O_3) differing from other Nemrut-system related basalts in the area and qualifying more as a parental basalt to the more calcalkalic Süphan. Olivine and plagioclase microphenorysts and microlites make up < 1 vol %, clinopyroxene being absent. The minor rock fragments (<< 1 vol. %) in the hyaloclastite are dominantly metamorphic, locating the source vent in the Bitlis massif rocks. These must have extended to the southern shore of lake Van underneath a belt of marginal sedimentary rocks south of the coast. The İncekaya eruptive fissure system is impressive evidence for north-south lithosphere cracking. N-S-oriented fractures were also the pathways for the basalts of the historic 3 km fracture north of Nemrut caldera rim contrasting with the dominant SW-NE trending fractures in the area. This suggests that N-S fractures are particularly deep-reaching intersecting basaltic magma reservoirs where more primitive basalic magmas had started to fractionate. Dense shrub and tree vegetation below and above the İncekaya tephra section on land as well as underlying swamp deposits are powerful evidence for a warm and wet climate at ca. 80 ka at the time of the eruption, much prior to the Eemian. The areal distribution of İncekaya tephra deposits reflects dominantly south to southwest wind directions at the time resembling dominant wind directions for most larger rhyolitic to trachytic Nemrut tephra deposits.

References:

Constantini L, Bonadonna C, Houghton BF, Wehrmann H (2009) New physical characterization of the Fontana Lapilli basaltic Plinian eruption, Nicaragura. Bull Volc 71: 337-355

Sumita M, Schmincke H-U (2013) Impact of volcanism on the evolution of Lake Van II: temporal evolution of explosive volcanism of Nemrut Volcano (eastern Anatolia) during the past ca. 0.4 Ma. J Volcanol Geotherm Res 253: 15-34

Sumita M, Schmincke H-U (2013) Impact of volcanism on the evolution of Lake Van I: Evolution of explosive volcanism of Nemrut Volcano (eastern Anatolia) during the past ca. 0.4 Ma. Bull Volcanol (in press)

IODP

Synchrotron texture analysis of naturally and experimentally deformed clay-rich sediments from the Nankai Subduction zone

K. SCHUMANN[1], M. STIPP[1], B. LEISS[2], J. H. BEHRMANN[1]

[1] GEOMAR, Helmholtz Centre for Ocean Research Kiel, Wischhofstr. 1-3, 24148 Kiel, kaschumann@geomar.de, mstipp@geomar.de, jbehrmann@geomar.de

[2] GZG, University of Göttingen, Germany, Goldschmidtstr. 3, 37077 Göttingen, bleiss1@gwdg.de

Introduction

The Nankai Trough Seismogenic Zone Experiment (NanTroSEIZE) of the Integrated Ocean Drilling Program (IODP) was designed to drill, sample and monitor the Nankai trench system, located at the Pacific side of SW Japan. This tectonically highly active region is formed by the subduction of the Philippine Sea Plate beneath the Japanese islands Honshu and Shikoku (Eurasian plate). Earthquakes of Magnitude >8 repeatedly occurred in an interval of 100 to 200 years in historical times. Within the accretionary complex, several out-of-sequence thrust faults accommodate horizontal compressive deformation. NanTroSEIZE drilling focuses on the Kumano transect, south of Kii peninsula (Honshu island), located in the 1944 Tonankai earthquake rupture area. Normal to the trench, a drill transect of 13 drill locations (Sites C0001-C0012 and C0018) with multiple holes was drilled during several IODP cruises. This study focuses on sites drilled during Expedition 315 (Site C0001E, C0001F and C0001H), Expedition 316 (Site C0004C, C0006E, C0007C and C0008A), and Expedition 333 (Site C0011D, C0012C and C0012E). Both, Expeditions 315 and 316 investigated the accretionary prism, while Expedition 333 investigated incoming plate sediments. Recovered samples used for our study range in depths between 28.9 and 522.9 mbsf (meter below seafloor).

Along with tectonics, sediment characteristics directly control the frictional behaviour of faults in the accretionary prism and therefore, play a key role in earthquake rupture dynamics (Scholz, 2002). The initially unlithified sediments of the Philippine Sea plate are scraped off from the underlying oceanic crust and added to the accretionary prism. Clastic slope sediments from Japan and the overriding Eurasian plate lie on top of the accreted Philippine Sea Plate sediments. Due to compaction and dewatering caused by burial and tectonic stress, soft sediments become stiffer and are turned finally into rocks. This process is reflected in the variation of mechanical and petrophysical properties of the sediments and in crystallographic preferred orientations of mineral grains (texture). The texture development directly influences the macroscopic mechanical properties, which may be important for earthquake nucleation and rupture. Here we present a set of 24 texture measurements of polyphase clay-rich sediments from the incoming plate and the accretionary prism of the Nankai trench system carried out by hard x-ray synchrotron radiation.

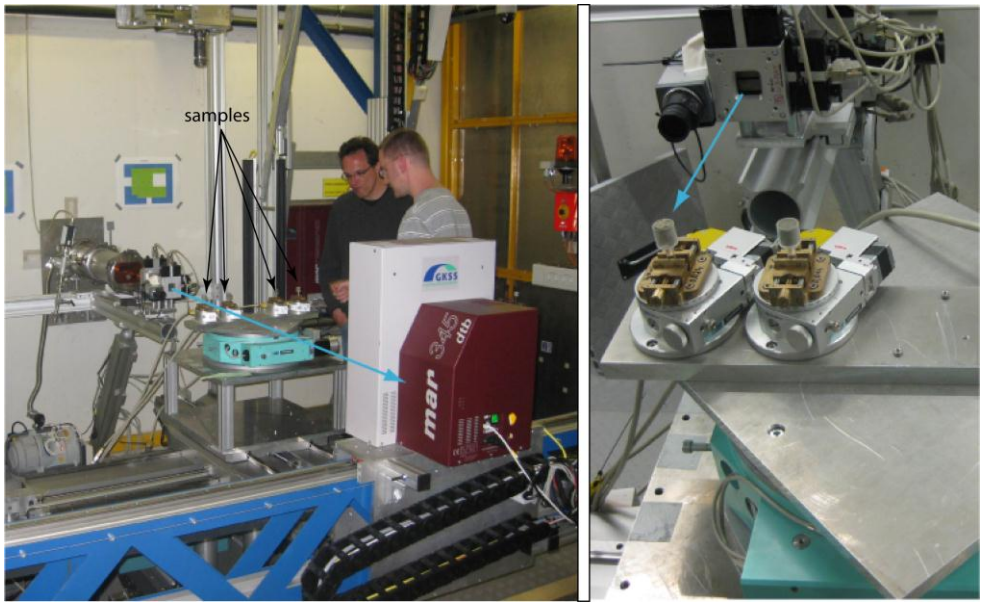

Figure 1: Measurement configuration at the Doris W2 beamline at DESY in Hamburg. The path of the synchrotron x-ray beam coming from the electron acceleration ring is indicated by blue arrows. The red box in the left picture is the MAR 345 plate detector mounted ~1.3 m behind the samples. The acrylic glass sample holders and their position in the x-ray beam can be seen in the right enlarged picture.

Methods

Synchrotron x-ray measurements were conducted at the HASYLAB x-ray wiggler hall of the Helmholtz-Zentrum Geesthacht, Centre for Materials and Coastal Research (GKSS, DORIS W2) of the German Electron Synchrotron source (DESY) in Hamburg. Cylindrical samples of 17 mm in diameter and ~18 mm in length were cut out without pre-treatment of the sample material. The samples were placed inside acrylic glass sample holders in the x-ray beam (Figure 1). The cylindrical sample shape ensures that the radiated sample volume is constant while rotating the samples in the x-ray beam. Otherwise, sample shape effects may cause variations in the diffraction intensity. The DORIS ring provides a monochromatic x-ray beam with a wavelength of ~0.12 Å and 100 keV energy. The x-ray beam of 1x1 mm was directed perpendicular to the axis of the drill cores which itself is parallel to the sample cylinder axis (Figure 1). Transmission diffraction patterns were recorded using a MAR 345 image-plate detector with 2000x2000 pixel resolution mounted ~1.3 m behind the samples. Since the reflection intensity of a textured sample depends on the sample orientation, samples were rotated in 5° steps from -90° to +90° around the core axis (ω) with 4 s counting time per step. The combination of 37 images (ω positions) resulted in 100% pole figure coverage.

Results

Existent textures can immediately be seen in plate detector images (Figure 2). We used the MAUD program package (Lutterotti et al. 1997) for mineral phase (Rietveld) and texture refinement. Results of the Rietveld refinement indicate sample compositions of quartz (16 to 42 %), albite (12 to 33 %), illite (3 to 34 %), kaolinite (7 to 30 %), calcite (2 to 23 %) and montmorillonite (2 to 16 %)

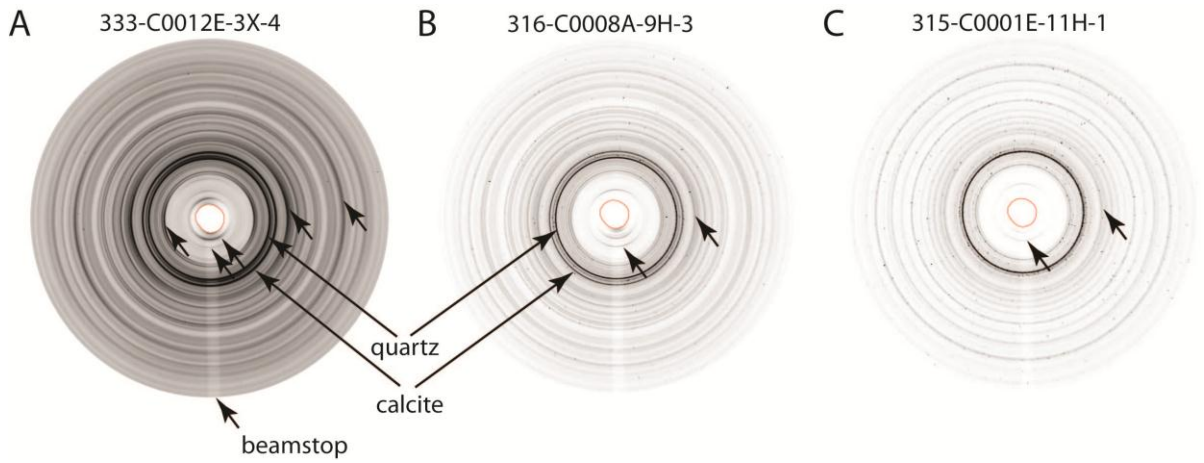

Figure 2: Plate detector images of the three different samples (333-C0012E-3X-4, 316-C0008A-9H-3 and 315-C0001E-11H-1). Variable Debye-Scherrer ring intensity shows textures (short arrows). Smooth rings are indicative for fine grained sample material (A), while spotty rings point on coarse grained samples, i.e. single crystal reflections (B and C). The position of the beam stop (a massive lead block) is indicated by red circles. A straight lighter line in the plate detector images is caused by the acrylic glass beam stop holder. Darkest rings can be related to quartz and calcite reflections, showing random distributions.

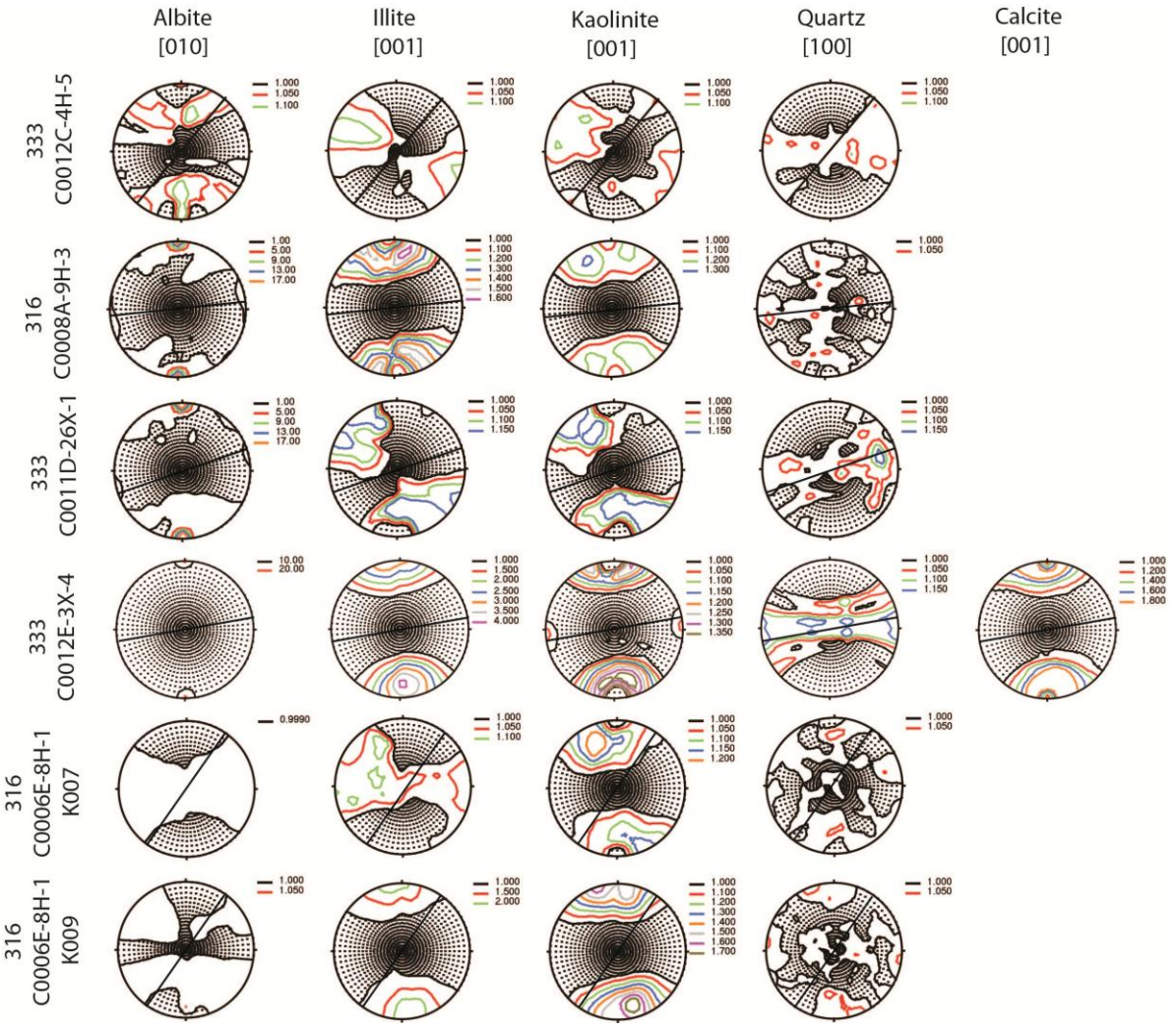

Figure 3: Pole figure plots of the samples. Core axis are directed N-S in all samples and the bedding plane is indicated by black lines. Samples 333-C0012C-4H-5 (28.9 mbsf), 316-C0008A-9H-3 (76 mbsf), 333-C0011D-26X-1 (206 mbsf) and 333-C0012E-3X-4 (522.9 mbsf) are experimentally undeformed samples from the incoming plate. Increasing texture strength with increasing burial depth can be derived from these samples. Sample 316-C0006E-8H-1 was drilled at the prism toe. Subsamples K007 and K009 are experimentally deformed (22% and 60% axial strain, respectively). The (001)- maxima of illite and kaolinite are increasingly oriented more parallel to the experimental compression direction with increasing strain.

and minor chlorite (up to 3 %). These results correspond to standard XRD data presented in the IODP reports (Kinoshita et al., 2009). The incoming plate sediments (Expedition 333) show slightly higher clay contents compared to the Expedition 315 and 316 samples from the accretionary prism.

The texture of the shallowly buried and experimentally undeformed samples ars expected to be weak and to increase with depth. In most samples, quartz and albite are randomly or close to randomly oriented (Figure 3). In some samples, especially 333-C0012E-3X-4 and 316-C0008A-9H-3 albite shows very strong (010) point maxima parallel to the core axis (Figure 3) between 17 and 20 mrd (multiples of random distribution). Illite and kaolinite pole figures of the experimentally undeformed samples (333-C0012C-4H-5, 333-C0011D-26X-1, 333-C0012E-3X-4 and 316-C0008A-9H-3) show preferred (001) orientation perpendicular to the bedding planes. The strength of the (001) illite pole figures increase with depth from 1.1 mrd (333-C0012C-4H-5, 28.9 mbsf) to 4.0 mrd (333-C0012E-3X-4, 522.9 mbsf, Figure 3).

In the experimentally deformed samples (316-C0006E-8H-1, experimental subsamples K007 and K009), we mostly observe random distribution or close to random distribution of albite and quartz (Figure 3). The (001) illite and kaolinite maxima are in most samples perpendicular to the bedding plane, except for sample 316-C0006E-8H-1 (subsample K007 and subsample K009, Figure 3).

Discussion

The observed texture strength increases of illite and kaolinite in the experimentally undeformed samples from the incoming plate (333-C0012C-4H-5 and 333-C0012E-3X-4) can be attributed to increasing burial depth and sample compaction (Figure 3). Illite and kaolinite (001)-maxima are oriented perpendicular to the bedding plane. Interestingly, also calcite (001)-maxima show a preferred alignment in the sample of greater burial depth. The albite texture might be due to a shape fabric of the grains and is affected by strong single crystal reflexes of coarser grains. A coarse grain size can be identified in the plate detector images by a “spotty” appearance (Figure 2). Also the

original samples from the accretionary prism (316-C0008A-9H-3) show a bedding-related texture, but the relation to sediment depth is not so clear. This has probably to do with the intense reworking of the accretionary prism sediments by slumping and maybe also by deformation, especially in the zone between the frontal thrust and the megasplay fault. The (001) kaolinite maxima of the experimentally deformed subsample K007 and the (001) illite and kaolinite maxima of subsample K009 (316-C0006E-8H-1) are increasingly more parallel to the experimental compression direction (Figure 3). While the low strain sample K007 (22% axial shortening strain) shows an illite (001)- maximum close to the normal of the bedding plane, the kaolinite (001)- maximum seems already being reorientated parallel to the experimental compression direction. The high strain sample K009 (60% axial shortening strain) shows both kaolinite and illite (001)- maxima parallel to the experimental compression direction (Figure 3). In addition, texture maxima increase from the low to the high strain sample from 1.1 to 2.4 mrd for illite and from 1.2 to 1.7 mrd for kaolinite. Hence, the two samples clearly show an ongoing rotation of the preferred mineral orientation and increasing texture intensity with increasing shear strain. Only quartz and albite, the minerals with isotropic or random sample shapes, are randomly oriented (Figure 3).

References:

Kinoshita, M., Tobin, H., Ashi, J.,Kimura, G., Lallemant, S., Screaton, E.J., Curewitz, D., Masago, H., Moe, K.T., and the Expedition 314/315/316 Scientists, Proc. IODP, 314/315/316: Washington, DC (Integrated Ocean Drilling Program Management International, Inc.).

Lutterotti, L.; Mathies, S.; Wenk, H.R.; Schultz, A.J.; Richardson, J. (1997): Texture and structure analysis of deformed limestone from neutron diffraction spectra. Journal of Applied Rhysics, Vol. 81, No. 2, 594-600

Scholz, C.H. (2002): The mechanics of earthquakes and faulting. Second edition. Cambridge. 466 pp.

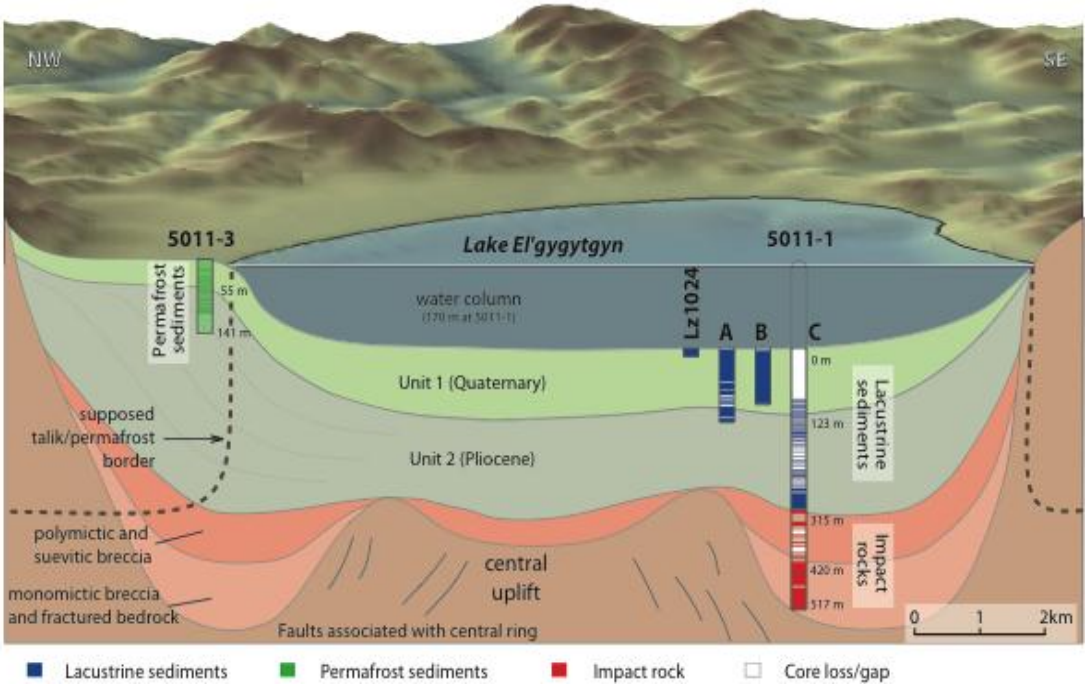

ICDP cores recovered from the permafrost (core 5011-3) and the lake deposits (5011-1) of the El'gygytyn Impact Crater, NE Russian Arctic (from: Melles et al., 2012).

ICDP

Permafrost-to-lake interaction in 3.6 Ma old El'gygytgyn Impact Crater

G. SCHWAMBORN[1], G.B. FEDOROV[2], L. SCHIRRMEISTER[1], H. MEYER[1], A. ANDREEV[3], D. MOTTAGHY[4], V. RATH[5]

[1] Alfred Wegener Institute for Polar and Marine Research, 14473 Potsdam, Germany
[2] Arctic and Antarctic Research Institute, Bering Street, 199397 St. Petersburg, Russia
[3] University of Cologne, Zülpicher Str. 49, 50674 Cologne, Germany
[4] Geophysica Beratungsgesellschaft mbH, Aachen, Germany
[5] Department of Earth Sciences, Astronomy and Astrophysics, Faculty of Physical Sciences, Universidad Complutense de Madrid, Madrid, Spain

After the recovery of 315 m core within the ICDP programme Lake El'gygytgyn now provides a continuous record from the Arctic spanning the the last 3.6 Ma. For much of this time the permafrost dynamics, lake level changes and the tectonical framework played a crucial role for sediment delivery to El'gygytgyn Crater Lake.

Our report provides an overview on how permafrost dynamics affected the lake archive based on multidisciplinary studies of cored deposits in and around the lake (see Figure below). The following questions are addressed:

- how did periglacial slope processes control the sediment transport and the frequent mass movement deposits in the lake
- how did lake level changes affect the permafrost build-up
- how thick is permafrost
- how old is permafrost

We conclude that (i) tectonics presumably caused extended alluvial fan inception in the catchment. (ii) The progradational sediment transport constantly delivers material to the lake basin. (iii) The slope inclination supports sliding events (Schwamborn et al., 2012). (iv) Times of higher relative lake levels during the Quaternary have induced permafrost thaw (i.e. talik) in the lake margin and have destabilized the slopes. (v) The permafrost thickness around the lake is about 330 to 360 m. (vi) The permafrost temperature measured in a 141 m deep borehole is not in equilibrium with the modern climatic conditions, but has inherited a temperature signal from the Last Glacial Maximum (Mottaghy et al., 2012). (vii) Cryogenic weathering (freeze-thaw weathering including ice in the deposits) favors the break-up of quartz particles and the enrichment of quartz in the silt fraction on the permafrost slopes. (viii) The permafrost is about 2.5 Ma old, this is the time when the cryogenic weathering became distinctly intense.

References:

Melles, M., Brigham-Grette, J., Minyuk, P.S., Nowaczyk, N.R, Wennrich, V., DeConto, R.M., Anderson, P.A., Andreev, A.A., Coletti, A., Cook, T.L., Haltia-Hovi, E., Kukkonen, M., Lozhkin, A.V., Rosén, P., Tarasov, P.E., Vogel, H., and Wagner, B.: 2.8 Million Years of Arctic climate change from Lake El'gygytgyn, NE Russia, Science, 307, 315–310, doi:10.1126/science.1222135, 2012.

Mottaghy, D., Schwamborn, G., and Rath, V.: Past climate changes and permafrost depth at the Lake El'gygytgyn site: implications from data and thermal modeling, Clim. Past, 9, 119-133, doi:10.5194/cp-9-119-2013, 2013.

Schwamborn, G., Fedorov, G., Ostanin, N., Schirrmeister, L., Andreev, A.: Depositional dynamics in the El'gygytgyn Crater margin: implications for the 3.6 Ma old sediment archive, Clim. Past, 8, 1897-1911, doi:10.5194/cp-8-1897-2012, 2012.

IODP

Potential drill sites for records of geohazards and monsoonal changes in the northern Bay of Bengal - Results from the Magellan+ workshop "Bay of Bengal Drilling", October 2012, Bremen

T. SCHWENK[1], V.SPIEß[1], H.R. KUDRASS[2], L. PALAMENGHI[1]

[1] Department of Geoscience, University of Bremen, Klagenfurter Str., D-28359 Bremen, Germany
[2] MARUM, University of Bremen, Klagenfurter Str., D-28359 Bremen, Germany

The Southeast Asian monsoon governs the seasonal heat and humidity transfer from sea to land, and precipitation drives huge sediment loads by Ganges and Brahmaputra into the Bay of Bengal. The rapidly accumulating sediments on shelf, slope and in a canyon contain a high-resolution record of Anthropocene, Holocene and late Pleistocene paleoclimatic changes and cyclonic episodes. The sediments have also recorded subsidence, sea-level changes and subduction-related earthquakes.

To develop and optimize an IODP drilling proposal and strategy, the multidisciplinary workshop "Records of Geohazards and Monsoonal Changes in the Northern Bay of Bengal - Preparation of an IODP Drilling Proposal" has been held in Bremen in October 2012. This workshop was funded by the ECORD Program "Magellan+" and co-funded by IODP-MI, and brought together 21 scientists from Bangladesh, China, Denmark, France, Germany, Spain, Switzerland, UK and USA. The workshop discussed six major topics: 1) Anthropocene environmental changes, 2) Late Holocene cyclone history, 3) Late Holocene subduction earthquakes, 4) Holocene paleoclimatic, paleoceanographic and paleoenvironmental changes, 5) Pleistocene sea level changes and subsidence and 6) Pleistocene paleoceanographic history.

All these objectives are highly ranked in the IODP Science Plan, and the unique opportunities from the rapidly accumulated canyon fill and shelf aggradation match goals proposed by the INVEST conference and by the recent IODP workshop in Goa. Parts of the thematic objectives, especially the cyclone history, were presented at both meetings and were highly appreciated. At this stage of IODP planning, the Goa workshop in October 2011 on Indian Ocean drilling revealed opportunities for mature Indian Ocean drilling proposals to replace Arabian drilling activity, which is on hold. Due to the readiness of site survey data for the Bay of Bengal, an excellent community proposal might receive immediate support for further Indian Ocean drilling. The development of a new IODP proposal as result of the workshop is in progress.

As one major topic of the workshop, locations of promising drill sites were discussed based on multichannel seismic data collected during the FS Sonne Cruise SO188, which was carried out in cooperation between the University of Bremen and the BGR, Hannover. With respect to the scientific hypotheses to be tested by a drilling in the northern Bay of Bengal, the workshop community identified potential drilling locations on the upper slope, at the shelf edge, in the shelf canyon "Swatch of No Ground" and within the submarine delta. On the poster, we will present the seismic data of each of these locations together with the corresponding aims of drilling.

IODP

Reconstruction and Modeling neogene Environments – Interim Results

PETER P. SMOLKA[1]

[1] University Muenster, 48149 Muenster, smolka@uni-muenster.de

Past project–phases focused on the reconstruction of neogene sea surface temperatures (SSTs) to assess environments that are characterized by different CO_2–levels and – as was the initial hypothesis – higher temperatures. Some of the results had been: A widespread pliocene El Nino (later confirmed by others with Ca/Mg SSTs) coexisted(!) with cold temperatures in high–latidues (Norwegian Sea, N Pacific), independently shown by IRD (such results differ from the project PRISM, see for pliocene IRD also Jansen et al., 1990 and Krissek 1989, 1995). Driving a climate model (ccm3.6) with these temperatures (4–5 m.y.) showed conditions overall comparable to today in summer (more moisture in the tropics) and extremely cold winter–conditions with large snowfall on the NH continents in winter. The winter 2010, with a mild El Nino, showed results (large NH snowfall, the large long–term "Low" over the Norwegian Sea) that had been a "mild" version of that. Reconstructions from the upper Miocene (5–6 m.y.) had even colder SSTs. If above–mentioned pliocene conditions re–appear again, in addition to climate change, heating–costs will become unaffordable.

To address such conditions (Smolka 2012 a,b), a new, cheap fast deep drilling–method (pat. pend., licensing ongoing) was developed (presented in the preceding IODP/ICDP colloquium and on the IGC in Brisbane, Symp. 6.2). This way climate change is – in the mid–range – no longer a problem.

The next project phase, ongoing, consists of accelerating the climate–model CESM such that, at a high resolution, long times can be simulated transiently and fully coupled such that the various reconstructions are met by the model, including, later, various time–series of SSTs. This means: Not driven by the reconstructed ocean, as was done before, but modeled fully coupled such, that reconstructions are met. Individual modules for acceleration have been tested. They are implemented into the model stepwise. The poster will show the current state as it will exist shortly before the colloquium. Following this data–gaps shall be filled by an IODP–Leg (preproposal 563Rev), either, financially, within the standard–system or paid by above–mentioned license–fees from the drilling–method.

As one sidetrack–well of above–mentioned "fast deep drilling" will, at 0.5 m diameter in hardrock, only cost below 300 000 Euros for 4 km, depending on the steel–costs, the method might also he useful for the ICDP: The "cutting–device" works inside the well, computers are actively cooled. A relay–system for core–segments of 120° each, in the form of pies, avoids a costly drillstring and enables synchronous upward and downward transport inside the well. The method is so fast (and so cheap) because only those few nuclear bonds are destroyed that

are needed to be destroyed (ring plus radii for the “pies”). Because geothermal electricity, at geothermal conditions of Germany, will be cheaper than eletricity by coal (below 3 Ct/kWh), changing old coal–powerstations to geothermal steam and raising respective funds for above–mentioned IODP–Leg, is realistical.

References:
Krissek, L.A., 1995. Late Cenozoic ice–rafting records from Leg 145 Sites in the North Pacific: Late Miocene onset, Late Pliocene Intensification and Pliocene–Pleistocene events. In: Rea, D.K., Bassov, I.A., Scholl, D.W., Allan, J.F. (Eds.), Proceedings of the Ocean Drilling Program, Scientific Results, Vol. 145, pp. 179–191.
Krissek, L.A., 1989. Late Cenozoic Records of ice–rafting at ODP Sites 642, 643, and 644, Norwegian Sea: Onset, chronology, and characteristics of glacial/interglacial fluctuations. In: Eldholm, O., Thiede, J., Taylor, E. et al. Proceedings of the Ocean Drilling Program, Scientific Results, Vol. 104, pp. 61–74.
Jansen, E., Sjoholm, J., Bleil, U., Erichsen, J.A., 1990. Neogene and Pleistocene Glaciations in the Northern Hemisphere and Late Miocene–Pliocene Global Ice Volume Fluctuations: Evidence from the Norwegian Sea. In: Bleil, U., Thiede, J. (Eds.), Geological History of the Polar Oceans: Arctic versus Antarctic. NATO ASI Series C: Math. And Phys. Sci., 308 (Kluwer Acad. Publishers).
Smolka 2012a. The End of the CO2–Age – with first Steps to Earthquake–Prevention as Side–Effect. Proc. 34th IGC.
Smolka 2012b. The End of the CO2–Age – to avoid Reoccurrence of unaffordable neogene Climates. Proc. 34th IGC.

IODP

Morphological variations in channel-levee complexes of the Magdalena Turbidite System, Colombia Basin, Caribbean Sea

D. SPERL[1], M. MESCHEDE[2], H. HÜNEKE[2]

[1] Univ. Köln, FB Geowissenschaften, Zülpicher Str. 49a/b, D-50674-Köln, daniel.sperl@yahoo.de
[2] Univ. Greifswald, Inst. f. Geographie und Geologie, Friedr.-Ludw.-Jahn-Str. 17a, D-17487 Greifswald, meschede@uni-greifswald.de / hueneke@uni-greifswald.de

In March and April 2010 RV Meteor cruise M81/2A and B "CLIP" (Origin of the Caribbean Large Igneous Province) performed bathymetric mapping (SIMRAD), sediment echosounding (PARASOUND), as well as magnetic profiling, hard rock sampling (ROV and dredging) in the Central Caribbean. Four north-south oriented magnetic profiles were taken in the Columbia Basin and during all of these profiles the bathymetry was mapped along these profile tracks. This bathymetric mapping combined with sediment echosounding delivered new, unique and high resolution sedimentological data of channel-levees of the southwestern part of the Magdalena Turbidite System.

Channel, as well as channel-levee structures of the Magdalena Turbidite System (MTS) could be identified at the southwestern margin of the Columbia basin, which is confined by the Hess Escarpment in the north and the continental margin of Panama and Columbia in the south. The analysis of bathymetric mapping and 3d-modelling is based on architectural element analysis. The two channels in the westernmost part of the Magdalena deep-see fan, which are in focus of this study, differ in their tectonic position and sedimentary regime. These documented channels are located in a water depth between 1350 and 3700 m, with a breadth between 2.5 km and 900 m and a channel depth between 20 m in case of the depositional and up to 100 m in case of the erosive channel.

The one in the upper part of the fan, with a meandering form, has a depositional character whereas the channel in the middle part of the fan, with a meandering form in the upper part and a sinuous form in the lower part, is clearly erosive. The main point of the study was a detailed analysis of morphological structures in the pathway of the channel. As a result of that, different types of meander-cutoff could be identified in a quick succession of the pathway ("normal" meander cut-off, a pseudo-cut-off and nested-levees) as well as channel-remnants, originated in channel-avulsion, could be detected and characterized concerning the activity of the MTS in this area.

As related to channel-evolution, two models could be established, primarily based on (1) changes in the inflow of sediment in case of the depositional channel and a subsequent development of a smaller channel in the older bigger one, and (2) meander-cutoffs and avulsions indicative for the erosive channel, which were crucial for shifting of the active channel.

Preliminary studies assume that channel-levee complexes in the western part should be the youngest and the active ones of the MTS. Detailed analyses of channels of this study didn´t show any implications for inactivity of these structures, as they were described for other channels more east of the MTS, like channel-fills etc.. These results suggest that the newly mapped channels should be the recent active channels of the MTS, which are responsible for the transport of sediment material into the deep-sea.

IODP

Last Glacial Maximum decadal- to millennial-scale ice-sheet fluctuations recorded in southeastern Weddell Sea sediment

D. SPRENK[1], M. E. WEBER[1], G. KUHN[2]

[1] University of Cologne, Institute of Geology and Mineralogy, Zuelpicher Straße 49a, 50674 Cologne, dsprenk@uni-koeln.de
[2] Alfred Wegener Institute for Polar and Marine Research, Helmholtz Association, Am Alten Hafen 26, 27568 Bremerhaven

High-resolution sediment records from the Southern Ocean covering the Last Glacial Maximum are very rare. Therefore there is only limited knowledge about short-term regional climate fluctuations and their global correlations. To gain insight into annual- to decadal-scale climate changes it is imperative to investigate varved archives. Here we present varved sediment records from the continental slope of the southeastern Weddell Sea. The cores originate from up to 300 m high and up to 100 km long sediment ridges, which are accompanied by channels on their southeastern side, located on a terrace in 2000 – 3000 m water depth.

During the Last Glacial Maximum, when the grounded East Antarctic Ice Sheet margin had advanced to the shelf break, coastal polynyas formed, supported by intensified katabatic winds. This led to increased sea-ice formation, which induced brine rejection. The produced dense, high-salinity water masses sank down the continental slope, reworked sediments and drained as contour currents into the channels. Seasonally variable

current velocities led to deposition of either a muddy or silty layer, forming an annual layer couplet, a siliciclastic varve. Accordingly, the varved sediment is indicative for ice-sheet advance. Occasional interruption by bioturbated sediments, which must have been deposited during open-water conditions with inactive thermohaline convection, points to ice-sheet retreat (Weber et al., 2011).

To distinguish and count the siliciclastic varves, we used the BMPix and PEAK tools (Weber et al., 2010a). Varve thickness varies quite strongly in time and between different core sites, with a mean thickness of 0.3 – 0.75 cm, hence a mean sedimentation rate of 3 – 7.5 m/kyr. Correlations of the sites using AMS ^{14}C ages and varve counts show that the facies changes from bioturbated to laminated sediment occurred around the same time, i.e., 23 ka, 21.5 ka, 20 ka, and 19 ka. Although the sites only describe about five millennia during the Last Glacial Maximum, the pacing of 1000 – 1500 years may correspond to the 1470-yr cycle (e.g., Bond et al., 1997) known from the Northern Hemisphere.

For further information on varve thickness variation we conducted bulk and evolutionary spectral analysis on laminated sections using the REDFIT (Schulz and Mudelsee, 2002) and ESALAB (Weber et al., 2010b) programs. All varved sediment sections show similar decadal-scale cyclic thickness variations, with a dominant 50 – 85-yr cyclicity. Evolutionary spectral analysis shows, that the 50 – 85-yr cycle appears to have been a rather robust feature during the Last Glacial Maximum. This frequency band could either relate to the Gleissberg cycle (Gleissberg, 1944) with an 87-yr cyclicity, and thus be of solar origin, or to the Atlantic Multidecadal Oscillation, a roughly 60 – 90-yr cyclic North Atlantic sea surface temperature fluctuation (e.g., Delworth & Mann, 2000), and thus relate to internal atmosphere-ocean interaction.

References:
Bond et al., 1997. A Pervasive Millennial-Scale Cycle in North Atlantic Holocene and Glacial Climates. Science 278, 1257-1266.
Delworth & Mann, 2000. Observed and simulated multidecadal variability in the Northern Hemisphere. Clim. Dyn. 16, 661-676.
Gleissberg W., 1944. A table of secular variations of the solar cycle. Terr. Magn. Atmos. Electr. 49, 243-244.
Schulz, M., and Mudelsee, M., 2002. REDFIT: estimating red-noise spectra directly from unevenly spaced paleoclimatic time series. Computer & Geosciences 28, 421-426.
Weber et al., 2011. Interhemispheric Ice-Sheet Synchronicity During the Last Glacial Maximum. Science 334, 1265-1269.
Weber et al., 2010a. BMPix and PEAK tools: New methods for automated laminae recognition and counting—Application to glacial varves from Antarctic marine sediment. Gcubed 11, 1-18.
Weber et al., 2010b. Lacustrine sediments document millennial-scale climate variability in northern Greece prior to the onset of the northern hemisphere glaciation. Paleo3 291, 360-370.

IODP

Formation of methane, ethane and propane in marine sediments of the New Jersey shallow shelf (IODP Exp. 313)

S. STADLER[1], R. VAN GELDERN[2], S. SCHLÖMER[1]

[1] Federal Institute for Geosciences and Natural Resources (BGR), Stilleweg 2, 30655 Hanover, Germany
[2] GeoZentrum Nordbayern, Schlossgarten 5, FAU Erlangen–Nürnberg, 91054 Erlangen, Germany

Three cores (27A, 28A and 29A) were recovered during IODP Expedition 313 that targeted Mioscene sedimentary sequences up to 67 km off the coast of New Jersey, USA, to investigate the timing and magnitude of global sea-level change (Mountain et al. 2010). Sediment and pore fluid samples were analyzed for their chemical composition and for stable isotopes. We analyzed δ^{13}C of dissolved inorganic carbon, organic matter, methane (C_1), and first data on ethane (C_2), propane (C_3) and butane (n-C_4) to understand processes related to gas geochemistry and carbon cycling in the investigated shallow shelf. Concentrations and stable carbon isotope compositions of C_1 to C_4 gases were analyzed by gas chromatography – isotope ratio mass spectrometry (GC-IRMS).

Methane starts to occur below ~250 mbsf and reachs concentrations of several thousand ppm in the lower core parts (see van Geldern et al., 2013). It appears to be formed from microbial degradation of organic matter as indicated by low $\delta^{13}C_{CH4}$ values between –73‰ and –87‰ and corresponding gas concentrations ratios (C_1/C_{2+}). The concentrations of ethane, propane and butane start rising below ~500 mbsf and are only present in the deeper core parts. Sedimentary organic matter revealed $\delta^{13}C_{org}$ values between –22‰ and –28‰ at all three sites. These values may indicate a mixture of marine with terrestrial organic matter whereas the latter is characterized by lower isotope values in case it originates from C_3-plant vegetation.

Stable carbon isotope data and $C_1/(C_2+C_3)$ ratios suggest a biogenic origin of methane from the decay and fermentation of organic matter, a process called methanogenesis. If methane is produced by a biogenic process this could be in principle also the case for C_{2+} gases (ethane, propane and butane). Based on gas isotope analysis from IODP drillings Hinrichs et al. (2006) proposed a mechanism for *in-situ* biogenic formation of C_{2+} gases in marine sediments. However, other studies attributed these gases to low temperature cracking of kerogen (cf. Rowe and Muehlenbachs, 1999).

A systematic offset to methane can be observed in the isotope values from IODP Expedition 313 with propane being enriched over ethane and butane. A plot of δ^{13}C values versus the reciprocal carbon number (natural gas plot) reveals a linear relation between C_2, C_3, and C_4 gases. However, C_1 isotope data deviates from this regression line and show ^{13}C-depleted values. Mechanisms to discuss from these first gas isotope results from the IODP Expedition 313 include mixing of thermogenic and microbial gas, microbial production of higher chain hydrocarbons, secondary modification during microbial oxidation and diffusive fractionation as well as mixing of multiple gas sources.

References:
Hinrichs, K.U., Hayes, J.M., Bach, W., Spivackl, A.J., Hmelo, L.R., Holm, N.G., Johnson, C.G. and Sylva, S.P. (2006): Biological formation of ethane and propane in the deep marine subsurface. - Proceedings of the National Academy of Sciences of the United States of America 103:14684-14689.
Mountain, G., Proust, J.-N., McInroy, D., Cotterill, C., and the Expedition 313 Scientists, 2010, Proceedings of the Integrated Ocean Drilling Program, Volume 313: Tokyo (Integrated Ocean Drilling Program Management International, Inc.).
Rowe, D., and Muehlenbachs, A. (1999): Low-temperature thermal generation of hydrocarbon gases in shallow shales. – Nature (London) 398:61-63
van Geldern, R., Hayashi, T., Böttcher, M. E., Mottl, M. J., Barth, J. A.C., Stadler, S. (2013): Stable isotope geochemistry of pore waters and marine sediments from the New Jersey shelf: Methane formation and fluid origin. – Geosphere 9(1):96-112. doi:10.1130/GES00859.1.

ICDP

FAR-DEEP: Tracing Early Earth's Oxygenation

H. STRAUSS

Institut für Geologie und Paläontologie, Westfälische Wilhelms-Universität Münster, Corrensstraße 24, 48149 Münster

During the Archean-Proterozoic transition and the early Paleoproterozoic (between 2.6 and 1.9 billion years ago), Earth witnessed profound changes in the environmental conditions at the Earth surface (e.g., Melezhik et al., 2005; 2012) that undoubtedly affected the evolution of life on this planet. Among these global perturbations was the first significant rise in atmospheric oxygen abundance (the so called Great Oxidation Event, cf. Holland, 2006) and respective consequences for the redox conditions in Earth's surface settings (e.g., Melezhik et al., 2005). Our understanding about this critical period in Earth history is largely based on geochemical and isotopic proxy signals that were archived in respective sedimentary rock successions at the time of sediment deposition. These changes in the environmental conditions that characterized Earth surface environments are discernible by studying the abundance and stable isotopic composition of selected redox sensitive elements (i.e., C, S, Fe; e.g., Farquhar et al., 2007; Kaufman et al., 2007; Scott et al., 2008; Guo et al., 2009; Reinhard et al., 2009; Kendall et al., 2010; 2011). In addition to more frequently applied redox proxies, multiple sulfur isotope measurements were performed in order to address changes in the atmospheric oxygen abundance (e.g., Farquhar et al., 2007; Guo et al., 2009).

The scientific focus of the Fennoscandian Arctic Russia – Drilling Early Earth Project (FAR-DEEP) was an improved understanding of causes and consequences of the first significant rise in atmospheric oxygen abundance some 2.4 Ga ago, commonly referred to as the "Great Oxidation Event" (cf. Holland, 2006). For this, 15 drill holes with a total length of 3650m were drilled and respective core material was recovered for a great diversity of research objectives. Cores straddle the Archean-Proterozoic transition and cover a time interval roughly between 2.6 and 1.9 billion years ago.

Multiple sulfur isotopes from the Seidorechka Formation (basal stratigraphic unit cored by FAR-DEEP), the underlying Kuksha Formation and the overlying Polisarka Formation (glacial unit equivalent to the early Palaeoproterozoic Huronian glaciation; Melezhik et al., 2012) record the decline in mass-independent sulfur isotope fractionation. As the mass-independent sulfur isotope fractionation (MIF-S signature) has been proposed to be dependent upon the atmospheric oxygen abundance (e.g., Farquhar et al. 2010, and references therein), this is interpreted to reflect the change in pO_2 from $<10^{-5}$ PAL (MIF-S) to $>10^{-2}$ PAL (non-MIF-S), following the modeling results of Pavlov and Kasting (2002). Thus, these sediments have archived one of the most profound change in environmental conditions at the Earth's surface, i.e. the onset of the oxygenation of Earth's atmosphere. A discussion of this subject (see also Fig. 1a) can be found in Reuschel et al. (2012a) and Strauss et al. (2012), and detailed results for the sedimentary succession on the Fennoscandian Shield are currently being prepared for publication.

The rise in atmospheric oxygen, commonly termed the Great Oxidation Event (cf. Holland, 2006), triggered the oxygenation of Earth's surface environments. With respect to the global sulfur cycle, this represents a change from a clear influence/input of photochemical reactions in the atmosphere to a modern-style sulfur cycle that is dominantly governed by oxidative continental weathering and the riverine delivery of dissolved sulfate into the ocean and its subsequent processing via bacterial sulfate reduction (e.g., Strauss et al., 2012). The latter could happen in an anoxic water column and/or in the anoxic part of the sedimentary column, as sulfate reducing bacteria are strictly anaerobic (e.g., Canfield, 2001). Consequently, the rise in atmospheric oxygen is paralleled by a rise in oceanic sulfate abundance (see Fig. 1d). Based on a detailed assessment of different sulfate minerals in the Tulomozero Formation and their sulfur isotopic composition determined by ex-situ (wet chemistry and EA-IRMS) and in-situ (using the NORDSim ion-probe facility) methods, Reuschel et al. (2012b) clearly demonstrated the existence of a sizeable sulfate reservoir (around 2,5 mM) already 2.1 Ga ago.

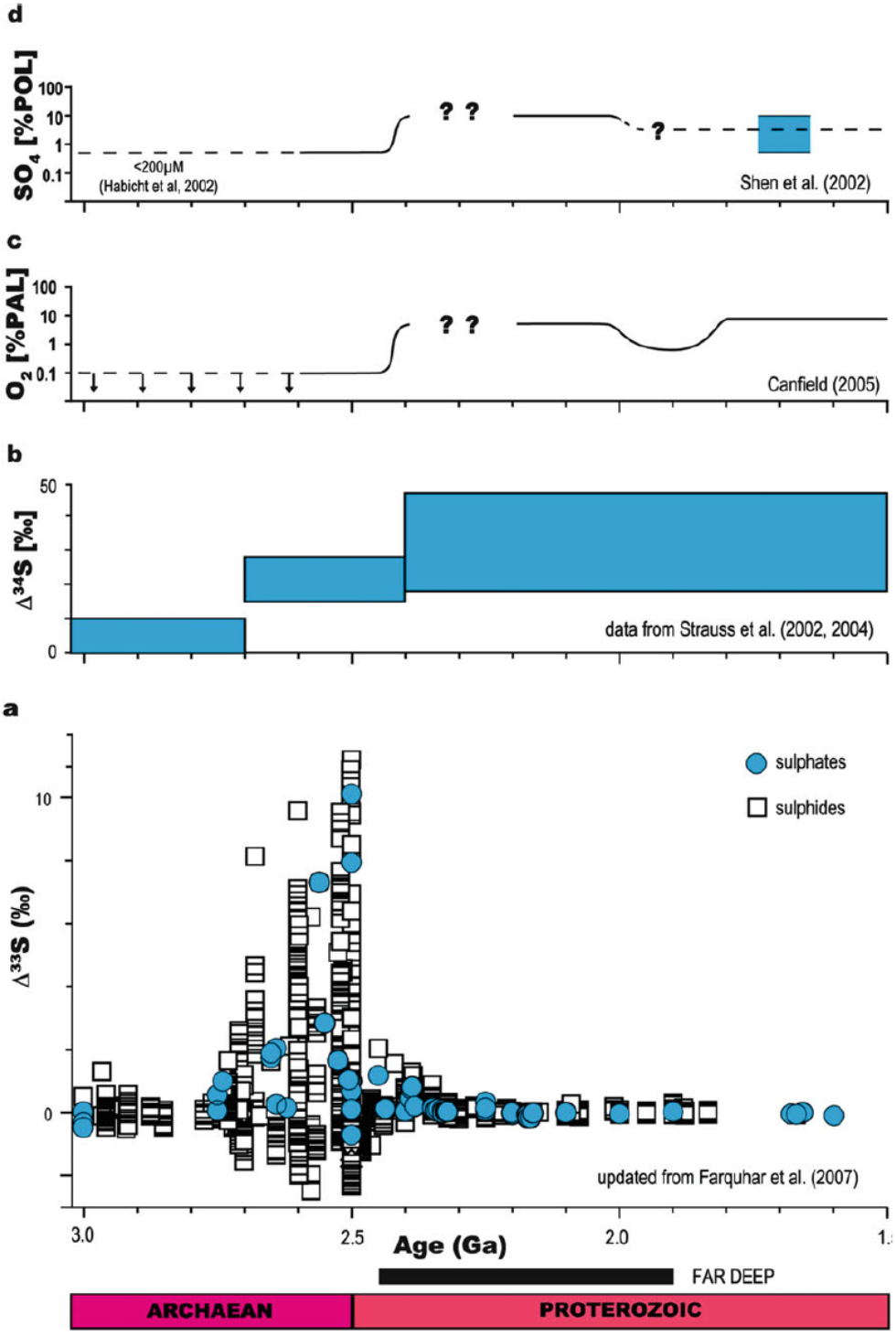

Fig. 7.52 Geochemical proxy signals showing (a) the termination of mass-independent sulphur isotope fractionation, (b) a change in magnitude in isotope fractionation between sulphate and sulphide, (c) the temporal evolution of atmospheric oxygen abundance as percent of present atmospheric level (PAL), and (d) the temporal change in seawater sulphate concentration as percent of present oceanic level (POL)

Figure reproduced from Strauss et al. (2012).

The increasing availability of oceanic sulfate in the aftermath of the Great Oxidation Event likely stimulated bacterial sulfate reduction in the marine realm. Under oxygenated bottom water, this process is restricted to the anoxic part of the sedimentary column as sulfate reducing bacteria are strictly anaerobic (e.g., Canfield, 2001). However, current thoughts about the oxygenation of the marine deep water reservoir Earth's evolution (e.g., Canfield et al., 2008) suggest a period of anoxic if not euxinic bottom water conditions in the early Paleoproterozoic, preceded and followed by anoxic, yet ferruginous (containing dissolved iron but not dissolved sulfide) conditions. Organic- and sulfide-rich sediments from the 2.0 Ga old Pilgujärvi Formation were studied by

Reuschel et al. (2012c) for their sulfur (abundance and isotopic composition) and iron (Fe speciation) geochemistry in order to determine the geochemical conditions prevailing during the deposition of the Pilgujärvi sediments. The detailed study by Reuschel et al. (2012a) revealed transient euxinic bottom water conditions during deposition of the Pilgujärvi sediments. Furthermore, bacterial sulfate reduction under changing availabilities of pore water sulfate is indicated by distinct sulfur isotope variations. An ongoing detailed study of the correlative 2.0 Ga old Zaonega Formation provides further details.

Acknowledgments

Funding by the Deutsche Forschungsgemeinschaft is gratefully acknowledged. This study benefited greatly from valuable discussions with colleagues from the ICDP FAR-DEEP initiative, most notably its principal investigator Prof. Victor Melezhik, Norwegian Geological Survey (NGU), Trondheim, Norway. Research results were generated during the Ph.D. thesis of Dr. Marlene Reuschel at the Institut für Geologie und Paläontologie, Universität Münster (finished in 2011).

References:

Canfield, D.E. (2001) Biogeochemistry of sulfur isotopes. In: J.W. Valley and D.R. Cole (Eds.) Stable Isotope Geochemistry. Reviews in Mineralogy and Geochemistry, Vol. 43, Min. Soc. Amer., p. 607–636.

Canfield, D.E., Poulton, S.W., Knoll, A.H., Narbonne, G.M., Ross, G., Goldberg, T., Strauss, H. (2008) Ferruginous conditions dominated later Neoproterozoic deep water chemistry. Science 321: 949-952.

Farquhar, J., Zerkle, A.L., Bekker, A. (2010) Geological constraints on the origin of oxygenic photosynthesis. Photosynth. Res. 107: 11-36.

Farquhar, J., Peters, M., Johnston, D.T., Strauss, H., Masterson, A., Wiechert, U., Kaufman, A.J. (2007) Isotopic evidence for Mesoarchaean anoxia and changing atmospheric sulphur chemistry. Nature 449, 706-710.

Guo, Q., Strauss, H., Kaufman, A.J., Schröder, S., Gutzmer, J., Wing, B., Baker, M.A., Bekker, A., Jin, Q., Kim, S.-T., Farquhar, J. (2009) Reconstructing Earth's surface oxidation across the Archean-Proterozoic transition. Geology 37, 399-402.

Holland, H.D. (2006) The oxygenation of the atmosphere and oceans. Phil. Trans. Roy. Soc. Biol. Sci. B 361: 903-915.

Kaufman, A.J., Johnston, D.T., Farquhar, J., Masterson, A.L., Lyons, T.W., Bates, S., Anbar, A.D., Arnold, G.L., Garvin, J., Buick, R. (2007) Late Archean Biospheric Oxygenation and Atmospheric Evolution. Science 317: 1900-1903.

Kendall, B., Gordon, G.W., Poulton, S.W., Anbar, A.D. (2011) Molybdenum isotope constraints on the extent of late Paleoproterozoic ocean euxinia. Earth Planet. Sci. Lett. 307: 450-460.

Kendall, B., Reinhard, C.T., Lyons, T.W., Kaufman, A.J., Poulton, S.W., Anbar, A.D. (2010) Pervasive oxygenation along late Archaean ocean margins. Nature Geosci. 3: 647-652.

Melezhik, V.A., Fallick, A.E., Hanski, E.J., Kump, L.R., Lepland, A., Prave, A.R., Strauss, H. (2005) Emergence of the aerobic biosphere during the Archean-Proterozoic transition: challenges of future research. GSA Today 15: 4-11.

Melezhik, VA., Kump, L.R., Hanski, E.J., Fallick, A.E., Prave, A.R. (2012) Tectonic Evolution and Major Global Earth-Surface Palaeoenvironmental Events in the Palaeoproterozoic. In: Melezhik, V.A.; Prave, A.R.; Hanski, E.J.; Fallick, A.E.; Lepland, A.; Kump, L.R.; Strauss, H. (Eds.) Reading the Archive of Earth's Oxygenation. Volume 1: The Palaeoproterozoic of Fennoscandia as Context for the Fennoscandian Arctic Russia - Drilling Early Earth Project. Springer, p. 3-24.

Pavlov, A., Kasting, J. (2002) Mass-independent fractionation of sulphur isotopes in Archean sediments: strong evidence for an anoxic Archean atmosphere. Astrobiology 2: 27–41.

Reinhard, C.T., Raiswell, R., Scott, C., Anbar, A.D., Lyons, T.W. (2009) A late Archean sulfidic sea stimulated by early oxidative weathering of the continents. Science 326: 713-716.

Reuschel, M., Strauss, H., Lepland, A., Prave, A. (2012a) The End of Mass-Independent Fractionation of Sulphur Isotopes. In: Melezhik, V.A.; Prave, A.R.; Fallick, A.E.; Kump, L.R.; Strauss, H.; Lepland, A.; Hanski, E.J. (Eds.) Reading the Archive of Earth's Oxygenation. Volume 3: Global Events and the Fennoscandian Arctic Russia - Drilling Early Earth Project. Springer, p. 3-12.

Reuschel, M., Melezhik, V.A., Whitehouse, M.J., Lepland, A., Fallick, A.E., Strauss, H. (2012b) Isotopic evidence for a sizeable seawater sulfate reservoir at 2.1 Ga.Precambrian Research 192-195: 78-88.

Reuschel, M., Strauss, H., Melezhik, V.A. (2012c) Insights into the sulfur cycle at 2.0 Ga ago-preservation of sedimentary monosulfides and transient euxinia. Precambrian Research 196-197: 193-203.

Scott, C., Lyons, T.W., Bekker, A., Shen, Y., Poulton, S.W., Chu, X., Anbar, A.D. (2008) Tracing the stepwise oxygenation of the Proterozoic ocean. Nature 452: 456-459.

Strauss, H., Melezhik, V.A., Reuschel, M., Fallick, A.E., Lepland, A., Rychanchik, D.V. (2012) Abundant Marine Calcium Sulphates – Radical Change of Seawater Sulphate Reservoir and Sulphur Cycle. In: Melezhik, V.A.; Prave, A.R.; Fallick, A.E.; Kump, L.R.; Strauss, H.; Lepland, A.; Hanski, E.J. (Eds.) Reading the Archive of Earth's Oxygenation. Volume 3: Global Events and the Fennoscandian Arctic Russia - Drilling Early Earth Project. Springer, p. 123-148.

IODP

Future Polar Research Capacities:

Science Strategies and Management Support Systems for a Multi-National Research Icebreaker and Drilling Vessel

JØRN THIEDE[1], LESTER LEMBKE-JENE[2], VERONICA WILLMOTT[2], OLAV ELDHOLM[3], NICOLE BIEBOW[2], LAURA DESANTIS[4]

[1] Faculty of Geography and Geoecology, SPbGU,St. Petersburg, RF
[2] Alfred Wegener Institute for Polar and Marine Research, Bremerhaven, Germany
[3] Department of Earth Science, University of Bergen, Norway
[4] Istituto Nazionale di Oceanografia e di Geofisica Sperimentale – OGS, Trieste, Italy

Despite significant advances in Antarctic marine science over the past years, the polar Oceans remain a formidable frontier due to challenging technical and operational requirements. Thus, key data and observations from these important regions are still missing or lack adequate lateral and temporal coverage, especially from time windows outside optimal weather seasons and ice conditions. These barriers, combined with the obligation to efficiently use financial resources and funding for expeditions, call for new approaches to create optimally equipped, but cost-effective maritime infrastructures. These must serve the international science community in a dedicated, long-term operation mode and enable researchers to participate in multi-disciplinary expeditions based on transparent, secured access modalities

The "European Research Icebreaker Consortium" (ERICON-AB) project with 19 partners from eleven nations was funded through the 7th Framework Programme of the European Commission. It was tasked with preparing all necessary frameworks and documents for policymakers, funding entities and stakeholders to decide on the future implementation of a multi-national research icebreaker and deep-sea drilling vessel for the international science community. Results from the ERICON-AB project are being published and comprise reports on the long-term strategic science and operational planning objectives, proposals for on- and offshore science support infrastructures, recommended scientific governance modes, as well as financial engineering, cost calculations and the legal aspects of operating a multi-national marine research infrastructure.

The high operational performance capacity of the planned icebreaking vessel Aurora is conceptually integrating today still separately operating national science programmes into a joint development of long-term research

missions with international cooperation both in the Arctic and Polar Southern Ocean. The icebreaker is planned to enable – as a worldwide first – autonomous year-round operations in the central Arctic and polar Southern Ocean. This includes severest ice conditions in winter, serving all polar marine disciplines. It will facilitate the implementation of atmospheric, oceanographic, cryospheric or geophysical observatories for long-term monitoring of the polar environment. Access to the biosphere and hydrosphere e.g. beneath ice shelves or in remote regions is made possible by acting as advanced deployment platform for instruments, robotic and autonomous vehicles and ship-based air operations.

The strategic Science Plan documents the scientific priorities for the first fifteen operational years of such a vessel. It explains the long-term scientific rationale and roadmap for international use of the vessel, and is based on the scientific excellence as well as on the integration of the European Countries' polar capacities and perspectives. The science planning process was achieved through meetings at national and international level, through liaison with International polar projects, networks and organizations, including relevant ESFRI infrastructures, and through international ERICON-AB conferences and initiatives.

IODP

A bathyal echinoderm assemblage from the Albian of the Falkland Plateau (South Atlantic): endorsing the ancient origin of the modern deep-sea fauna

B. THUY[1], N. SCHLÜTER[1,2], F. WIESE[2,3] & M. REICH[1,2]

[1] Georg-August University of Göttingen, Geoscience Museum, Goldschmidtstr. 1-5, 37077 Göttingen, Germany; mreich@gwdg.de
[2] Georg-August University of Göttingen, Geoscience Centre, Dept. of Geobiology, Goldschmidtstr. 3, 37077 Göttingen, Germany
[3] Georg-August University of Göttingen, Courant Research Centre Geobiology, Goldschmidtstr. 3, 37077 Göttingen, Germany

An extraordinary inisght into the geological history of the modern deep-sea fauna was recently discovered in the subtropical North Atlantic in the form of an echinoderm assemblage retrieved from latest Aptian bathyal sediments drilled at ODP Site 1049. The assemblage in question provided the first fossil-based evidence suggesting that much of the modern deep-sea fauna was significantly older than previously assumed. It thus challenged many of the inference-based hypotheses arguing for a latest Mesozoic or even Cenozoic origin of the modern deep-sea fauna. As a single data point, however, the North Atlantic echinoderm assemblage is legitimately vulnerable to the objection that at least part of the evidence is only valid for the North Atlantic.

Here we describe a second bathyal echinoderm assemblage of Early Cretaceous age. It was retrieved from sediments drilled at DSDP Site 327, Falkland Plateau, high-latitude South Atlantic, and dated to the Albian. As in the North Atlantic equivalent, it consists in numerous excellently preserved, dissociated plates of all five extant echinoderm classes, including highly diagnostic and thus taxonomically assessable remains. The crinoid material is all assignable to the extinct pelagic roveacrinids, providing no insights into the geological history of deep-sea benthos. The other four classes are represented by members of extant families typically occurring in present-day deep-sea settings. The Falkland Plateau assemblage thus can be considered as a modern-type deep-sea echinoderm fauna.

Comparison with the North Atlantic equivalent reveals that some aspects of the faunal spectra are shared by both assemblages, in particular the family-level composition of the holothuroids (laetmogonids, chiridotids and myriotrochids) and the ophiuroids (ophiacanthids, ophiurids, ophiolepidids and ophiomycetids). The asteroid faunal spectra, however, differ fundamentally. In fact, the Falkland Plateau assemblage includes remains of the extant typical deep-sea family Goniopectinidae, which failed to be recovered from the North Atlantic assemblage. On genus level, some forms occur in both assemblages, including the ophiuroids *Ophiomusium*, *Ophiozonella*, *Ophiolimna* and the peculiar, typical deep-sea genus *Ophiotholia*. Others, however, are unique to the Falkland Plateau. Among these is the extant ophiacanthid genus *Ophiocamax*. Intriguingly, the last known occurrence of this genus from shelf depths dates to the Late Jurassic, thus excluding the possibility of a later reinvasion of the deep sea.

The here described South Atlantic bathyal echinoderm assemblage endorses the hypothesis that modern-type echinoderm communities were distributed globally in the Early Cretaceous rather than restricted to the North Atlantic. It furthermore suggests that at least part of the South Atlantic assemblage were not immigrants from the slightly older North Atlantic analogue but had a different origin. The presence of a deep-sea taxon lacking pre-Aptian/Albian shelf occurrences furthermore endorses the hypothesis, derived from the North Atlantic fauna, that the last major reorganisation of the deep-sea fauna must have taken place prior to the Aptian.

IODP

Aptian brittle-star (Echinodermata: Ophiuroidea) remains from an ancient southwest Pacific seamount: implications for the evolution of the modern deep-sea fauna

B. THUY[1], N. SCHLÜTER[1,2], F. WIESE[2,3] & M. REICH[1,2]

[1] Georg-August University of Göttingen, Geoscience Museum, Goldschmidtstr. 1-5, 37077 Göttingen, Germany; mreich@gwdg.de
[2] Georg-August University of Göttingen, Geoscience Centre, Dept. of Geobiology, Goldschmidtstr. 3, 37077 Göttingen, Germany
[3] Georg-August University of Göttingen, Courant Research Centre Geobiology, Goldschmidtstr. 3, 37077 Göttingen, Germany

Seamounts and other oceanic submarine highs can alter ocean circulation patterns, producing local upwelling and turbulent mixing, which enhances local productivity. As a result, seamounts often harbour extraordinary densities and diversities of benthic organisms in the otherwise sparsely populated slopes and abyssal plains. Higher faunal densities combined with the relatively shallow depths, commonly rising well above the calcite compensation depth, make seamounts and other oceanic submarine highs particularly interesting for palaeontology. In fact, they are among the very few settings in which remains of ancient deep-sea large benthos has a slightly higher chance to be fossilised and discovered.

Here we report on an assemblage of brittle stars, retrieved from sediments drilled at DSDP Site 317, central part of the southwest Pacific Manihiki Plateau, and dated to the late Aptian. The area near the drillsite is of volcanic origin, raised into relatively shallow depths and was associated with considerable topography as suggested by turbiditic deposits. At the time of deposition, the area was a submarine high, most probably a now levelled seamount. The material is very sparse and poorly preserved but taxonomically assessable and thus insightful. The faunal spectrum comprises an ophiacanthid, two ophiolepidids and a probable ophioleucinid, identified on the basis of the diagnostic, spine-bearing lateral arm plates. The ophiacanthid-ophiolepidid-ophioleucinid association reflects a typical modern deep-sea ophiuroid fauna, and is strikingly reminiscent of a coeval assemblage recently discovered in middle bathyal sediments of the subtropical North Atlantic.

Since modern seamount ophiuroid assemblages have been shown to generally reflect the neighbouring slope assemblages at similar depths, it can be assumed that the here described fossil assemblage provides a representative insight into the southwest Pacific bathyal ophiuroid fauna in the Aptian. As such, it suggests that modern-type bathyal ophiuroid assemblages had established globally by the Aptian.

IODP

Tectonic and climatic control on water mass exchange between high and low latitudes in the eastern South Atlantic over the past 45 million years

G. UENZELMANN-NEBEN[1], M. FRANK[2]

[1] Alfred-Wegener-Institut für Polar und Meeresforschung, Am Alten Hafen 26, 27568 Bremerhaven
[2] GEOMAR, Wischhofstr. 1-3, 24848 Kiel

The Agulhas Ridge forms a topographic anomaly within the Agulhas Falkland Fracture Zone, South Atlantic, and in this way represents a barrier to the exchange of water masses and hence energy and salt between high and low latitudes. This exchange has played a critical role for the stability and variability of the global oceanic circulation and thus has a strong impact on climate. Variations in the local ocean circulation of the past, mainly Circumpolar Deepwater and Agulhas Rings, are archived in the structure and distribution of the corresponding sedimentary deposits, as well as their geochemical composition. In this project we propose to reconstruct palaeocirculation in the study area based on high-resolution multichannel seismic reflection data of these deposits acquired during RV *Maria S. Merian* cruise MSM 19/2 in October/November 2011 coupled with reconstructions of water mass mixing and major changes in the provenance of water masses based on radiogenic Nd and Hf isotope compositions of past seawater extracted from the sediments of ODP Leg 177 Sites 1088, 1089, and 1090. This is the first time that combined seismic data and analyses of radiogenic isotopic compositions will be used to reconstruct changes of palaeo-environment and –circulation together with sedimentation processes in the Southern Ocean from the Neogene to the Quaternary. This project and the period of time to be investigated covering all major oceanographic and climatic transitions of the past 45 million years including the opening of the Drake Passage, global Neogene cooling, and the onset of Antarctic and Northern Hemisphere glaciation, will allow new insights into causes and consequences of these crucial changes.

IODP

Pliocene vegetation and climate changes in north-west Africa

F.VALLÉ[1], L. M. DUPONT[1], S.A.G. LEROY[2], C.O.C. AGWU[3], E. SCHEFUß[1]

[1] MARUM - Center for Marine Enivironmental Sciences, University of Bremen, Leobener Strasse 28359, Bremen
[2] Brunel University, London, United Kingdom
[3] Department of Biological Sciences, Kogi State University, Nigeria

The Pliocene Epoch (5.33-2.58 Ma) was characterized by a global climate warmer and wetter than today, in which ice sheets were considerably reduced and sea level was up to 25 m higher (Dowsett et al., 1994). The shoaling of the Central American Seaway (CAS) starting around 4.6 Ma (Haug and Tiedemann, 1998) increased North Atlantic Deep Water (NADW) formation and strengthened the Atlantic meridional overturning circulation (AMOC) (Bartoli et al., 2005). Thus, warm and salty waters could be transported from the tropical West Atlantic into the North Atlantic bringing heat and moisture to northwest Europe. Models suggest that precipitation also increased at low latitudes, e.g. in Northern Africa (Contoux et al., 2012). The mid-Pliocene warm period (MPWP) defined between 3.29 and 2.97 Ma (Dowsett et al. 1999) is thought to have been substantially warmer than today, although the global oxygen isotope record is highly variable during that period (Lisiecki and Raymo, 2005), and is considered an analogue for future warm climate scenarios. Data-model comparisons of the MPWP vegetation suggest that in Northern Africa woodlands and tropical savannahs extended northwards far into today's arid regions as a result of more humid conditions (Salzmann et al., 2008).

Many studies have been published about Pliocene climate variability on the African continent, the information about the development of the vegetation and the different paleohydrological conditions are, however, scarce. Data about the possible link between the African continental climate and the oceanographic conditions during the Pliocene are lacking, especially data considering the effects of differences in AMOC strength before and after the closure of the CAS. For the Quaternary, it has been suggested that climate variability in West Africa is driven by changes in the AMOC (Mulitza et al., 2008). To test this hypothesis for the Pliocene, we are investigating the vegetation and climate changes in tropical West Africa for two periods; the mid-Pliocene (3.6-2.5 Ma, including the MPWP), when the AMOC was enhanced by the final steps of the closure of the CAS, and for the Early Pliocene between 4.9 and 4.6 Ma, when the CAS was still relatively deep and the AMOC not so strong.

We study Pliocene sediments from two sites offshore West Africa; one is ODP Site 659 located at 18°05'N 21°02'W and 3071 m water depth and the other is ODP Site 959 located at 3°38' N, 2°44' W and 2100 m water depth.

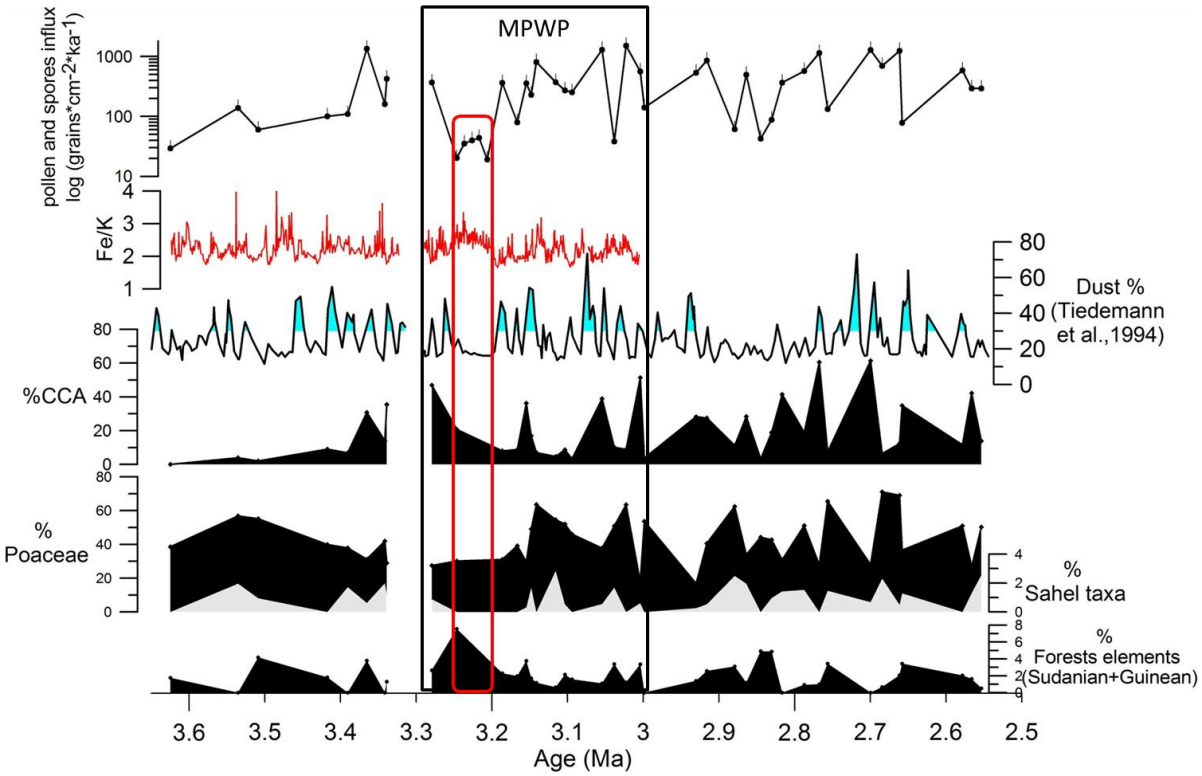

Figure 1: ODP Site 659, comparison of terrestrial proxies for the interval 3.6-2.5 Ma. Top to bottom, the pollen and spores influx on a logarithmic scale, the elemental Fe/K ratio, the dust percentages (Tiedemann et al, 1994), relative abundances (%) of the main pollen taxa, CCA (Chenopodiaceae, Caryophyllaceae, Amaranthaceae), Poaceae (grass), Sahel taxa and Forests elements. The Mid Pliocene Warm Period (3.29-2.97 Ma) is denoted by the black rectangle. Within the red rectangle is indicated the short wetter interval.

We analyse pollen, spores, and dinoflagellate cysts in order to reconstruct the vegetation and climate changes on the African continent and in the surface waters of the east Atlantic. Moreover, we use X-ray (XRF) scanning to obtain element ratios of titanium (Ti) over calcium (Ca), iron (Fe) over calcium, iron over potassium (K), and aluminium (Al) over potassium as indicators of terrestrial input and continental humidity.

Here, we present palynological results and element ratios obtained for ODP Site 659 located outside the upwelling area and directly under the main stream of the African Easterly Jet (AEJ), which is strongest in summer. The site is also reached by the northeast trade winds, which are strong in winter. Both wind systems carry dust, pollen, spores, and plant waxes out of the African continent to the site. During the last 4 Ma, the AEJ is assumed to have been latitudinally stable (Tiedemann et al. 1989) blowing between ~22° and ~16°N. However, Mulitza et al. (2008) and Bouimetarhan et al. (2012) inferred that the AEJ intensified and extended southwards during periods of the last glacial when the AMOC was reduced. We compare our results with other proxies such as the dust percentages (Tiedemann et al., 1994) as an indicator of wind intensities and with the pollen record of ODP Site 658 (Leroy and Dupont, 1994) located northeast of the study site.

At ODP Site 659, the terrestrial input is mainly aeolian as the large distance to the shore of the site precludes riverine input. High ratios between the terrigenous Ti and Fe and the marine Ca indicate more terrestrial input in the sediment. As the coating of dust particles is an important source of terrestrial elements Ti/Ca and Fe/Ca ratios correlate well with the published dust record (Tiedemann et al., 1994). The Al/K and Fe/K ratios indicate the degree of chemical weathering on the continent associated with humid conditions (Mulitza et al. 2008). Maxima in these ratios occurred when the Ti/Ca and Fe/Ca ratios are low suggesting little dust mobilisation and deposition during relative wet periods. Dust maxima suggesting dry and windy conditions are slightly more frequent between 3.6 and 3 Ma that between 4.9 and 4.6 Ma.

The part between 4.9 and 4.6 Ma is almost barren in pollen and spores, albeit the dust record indicates that aeolian transport from the continent was not significantly lower. The dinoflagellate cyst record of this part suggests strong degradation of palynomorphs. At this stage, we can only speculate about the reason of the bad preservation. We hypothesize that ODP Site 659 was bathed in more corrosive waters before the deep-water circulation changed in relation with the closure of the CAS. For the younger part of our study preservation of pollen and spores at ODP Site 659 is better although the sediments are still poor. The pollen and spore influx of the interval 3.6-2.5 Ma fluctuates between 20 and 1535 grains·cm-2·ka-1 (Fig. 1). Maxima in pollen and spore influx are found when dust percentages are high indicating that also pollen and spore influx rates strongly depend on the wind transport efficiency.

The vegetation of West Africa is distributed in zones following the rainfall distribution, from the Sahara desert of arid mid-latitudes to the rain forest of the equatorial latitudes. The source areas of modern pollen in our marine site are mainly the desert and the savannah and dry forest (woodlands) from the Sahara and the Sahelian and Sudanian vegetation. High relative abundance of Poaceae (grass) pollen in marine sediments traces savannahs and open woodland on the adjacent continent (Hooghiemstra et al., 2006). The maxima of Poaceae pollen percentages align

with those of a group of pollen taxa from plants nowadays growing in the Sahel and are interpreted as the spread of savannah and open bushland. In “Forest elements” pollen from trees and shrubs from the Sudanian and Guinean vegetation zones are grouped together. Increasing pollen percentages of the “forest elements” indicate an expansion of dry and wet forests. Pollen from Chenopodiaceae, Caryophyllaceae, Amaranthaceae are grouped as CCA. Source areas of CCA pollen grains are the desert and most probably sandy and salty soils and high percentages might have originated from dried up lake beds.

The more abundant pollen taxa in the mid-Pliocene sediments of ODP Site 659 are Poaceae, represented by an average percentage value of 43 % and CCA with an average value of 20 %. During the MPWP (3.29-2.97 Ma; Fig.1) the relative abundances of the different taxa show a higher degree of variability, compared to the interval of 3.6-3.4 Ma. Also the dust record is highly variable (Tiedemann et al., 1994). Only between 3.25 and 3.2 Ma an extended humid phase occurred with increased chemical weathering indicated by the Fe/K ratios (Fig. 1). Low dust input and low pollen concentration during this period of ca. 50 ka probably indicate decreased windiness. Similar large climate variability has been recorded at ODP Site 658 offshore Cape Blanc (Leroy and Dupont, 1994). These records challenge the idea of a stable warm climate during the MPWP.

We use data from ODP Site 959 (equatorial East Atlantic) for comparison to a more equatorial site. To get a better age control of the samples taken from ODP Site 959, we use the XRF element data to build up a composite record of the time interval of this study, including 7 cores from Hole A, 9 cores from Hole B, and 8 cores from Hole C. We construct an age model by tuning the Ti/Ca record to the eccentricity curve of Laskar et al. (2004). The scanned interval ranges from 2.08 Ma to 6.28 Ma. Preliminary results show a major change in the elemental record just after 2.7 Ma, when the Al/K ratio strongly decreased. We interpret this as a change in the clay mineral composition of the sediment containing more kaolinite relative to feldspars indicating reduced chemical weathering on the continent under drier conditions after 2.7 Ma (Schneider et al., 1997). We analyse a selection of samples for pollen and spores, transported to the site probably both fluvially and aeolian. Pollen assemblages turn out to be highly diverse representing forest and wooded savannah rather than the open savannah growing at latitudes further north. We hope that the dinoflagellate cysts analysis will give new insight into the oceanic circulation in the Gulf of Guinea during the Pliocene.

References:

Bartoli, G., Sarnthein, M., Weinelt, M., Erlenkeuser, H., Garbe-Schönberg, D., Lea, D.W., 2005. Final closure of Panama and the onset of northern hemisphere glaciation. Earth and Planetary Science Letters, 237, 33-44.

Bouimetarhan, I., Prange, M., Schefuß, E., Dupont, L., Lippold, J., Mulitza, S., Zonneveld, K., 2012. Sahel megadrought during Heinrich Stadial 1: evidence for a three-phase evolution of the low- and mid-level West African wind system. Quaternary Science Reviews, 58, 66-76.

Contoux C., Ramstein, G., Jost A., 2012. Modelling the mid-Pliocene Warm Period climate with the IPSL coupled model and its atmospheric component LMDZ5A. Geoscientific Model Development, 5, 903–917.

Dowsett H.J, Thompson R., Barron J., Cronin T., Fleming F., Ishman S., Poore R., Willard D., Holtz T. Jr, 1994. Joint investigations of the Middle Pliocene climate I: PRISM paleoenvironmental reconstructions. Global and Planetary Change 9, 169-195.

Dowsett, H.J., Barron, J.A., Poore, R.Z., Thompson, R.S., Cronin,T.M., Ishman, S.E., Willard, D.A., 1999. Middle Pliocene paleoenvironmental reconstruction: PRISM2. USGS Open File Report 99-535.

Haug, G.H., Tiedemann, R., 1998. Effect of the formation of the Isthmus of Panama on AtlanticOcean thermohaline circulation. nature, 393, 673-676.

Laskar, J., Robutel, P., Joutel, F., Gastineau, M., Correia, A.C.M., Levrard, B., 2004. A long-term numerical solution for the insolation quantities of the Earth. Astronomy & Astrophysics, 428, 261-285.

Leroy S., Dupont L.M., 1994. Development of vegetation and continental aridity in northwestern Africa during the Late Pliocene: the pollen record of ODP Site 658. Paleogeography, Paleoclimatology, Palaeocology, 109, 295-316.

Lisiecki, L.E., Raymo, M.E., 2005. A Pliocene-Pleistocene stack of 57 globally distributed benthic δ18O records. Paleoceanography, 20, PA1003, 1-17.

Mulitza, S., Prange, M., Stuut, J-B., Zabel, M., Von Dobeneck, T., Itambi, A.C., Nizou, J., Schulz, M., & Wefer, G., 2008. Sahel megadrougths triggered by glacial slowdowns of Atlantic meridional overturning circulation. Paleoceanography, 23, PA4206: 1-11.

Salzmann, U., Haywood, A.M., Lunt, D.J., Valdes, P.J., Hill, D.J., 2008. A new global biome reconstruction and data-model comparison for the Middle Pliocene. Global Ecology and Biogeography, 17, 432–447.

Salzmann, U. Williams M., Haywood A.M., Johnson A.L.A., Kender S., Zalasiewicz, J., 2011. Climate and environment of a Pliocene warm world. Paleogeography, Paleoclimatology, Palaeocology, 309: 1-8.

Schneider R.R., Price B., Müller P.J., Kroon D., Alexander I., 1997. Monsoon related variations in Zaire (Congo) sediment load and influence of the fluvial silicate supply on marine productivity in the east equatorial Atlantic during the last 200.000 years. Paleoceanography, 12, 463-481.

Tiedemann R., Sarnthein M., Stein R., 1989. Climatic changes in the western Sahara: aeolo-marine sediment record of the last 8 million years (SITE 657-661). Proceedings of the Ocean Drilling Program, Scientific Results, vol 108.

Tiedemann R., Sarnthein M., Shackleton N.J, 1994. Astronomic timescale for the Pliocene Atlantic δ18O and dust flux records of Ocean Drilling Program site 659. Paleoceanography, 9, 619-638.

IODP

Palynological analysis of the Cretaceous-Palaeogene boundary in cores from the New Jersey margin

B. VAN DE SCHOOTBRUGGE[1], J. VELLEKOOP[2], S. SCHOUTEN[3], J.S. SINNINGHE DAMSTE[3], J. BROWNING[4], K.G. MILLER[4], H. BRINKHUIS[2], A. SLUIJS[2], J. PROSS[1]

[1] Goethe University Frankfurt, Altenhöferallee 1, 60438 Frankfurt am Main, Germany
[2] Utrecht University, Budapestlaan 4, 3584 CD, Utrecht, The Netherlands
[3] NIOZ, Landsdiep 4, NL-1797 SZ 't Horntje (Texel) The Netherlands
[4] Rutgers University, 610 Taylor Road, Piscataway, NJ 08854-8066, United States

The Cretaceous-Palaeogene boundary (K/Pg; 65.0 Ma) mass-extinction event is one of the so-called Big Five extinctions that led to major faunal and floral overturn in marine and terrestrial ecosystems. In terrestrial floras the K/Pg boundary event is expressed by the extinction of angiosperms and the proliferation of pioneer plants, such as ferns, that likely dominated worldwide for several thousand years after the impact of a bolide at Chicxulub (Mexico). Alternatively, it has been suggested that volatile release from the Deccan Traps in India was a major driving force behind pulses of latest Maastrichtian warming, contributing to the collapse of ecosystems at the K/Pg boundary. Vegetation reconstructions of the Maastrichtian based on high-resolution palynological analyses could provide important information about the intensity, duration, and causes of environmental changes prior to the extinction event. A series of cores drilled along an onshore-offshore transect on the New Jersey margin drilled in the framework of ODP Leg 174AX and the Continental Dynamics Program provide an unique archive to study Maastrichtian to Danian vegetation changes. In particular, the set of core material allows to make land-sea correlations by incorporating the terrestrial data in a high-resolution biostratigraphic framework based on organic-walled dinoflagellate cysts, and to compare vegetation changes with sea surface temperature reconstructions based on the TEX_{86} proxy. Here, we present preliminary high-resolution pollen and spore data for the immediate boundary interval from the Fort Monmouth, Search Farm and Meirs Farm boreholes in combination with palaeotemperature data.

IODP

Carbonate diagenesis in the sediments from the Pacific Equatorial Age Transect (PEAT)

J. VOIGT[1], E. HATHORNE[1], M. FRANK[1], H. VOLLSTAEDT[1], A. EISENHAUER[1]

[1] GEOMAR Helmholtz-Zentrum für Ozeanforschung Kiel, Wischhofstraße 1-3, 24148 Kiel, Germany

The elemental and isotopic composition of microfossils incorporated in marine carbonate sediments are widely used to reconstruct oceanic and climatic conditions in the past. However, ancient microfossils are normaly altered after deposition by a process where the original biogenic calcite is replaced by secondary (inorganic) calcite. Therefore, it is important to quantify changes in the elemental and isotopic composition of the microfossils caused by this recrystallisation process and thus the reliability of the proxy data. Although, bulk carbonate diagenesis has been successfully modelled to fit pore water Sr profiles at different locations (Richter and DePaolo 1987, 1988; Richter and Liang 1993, Fantle and DePaolo

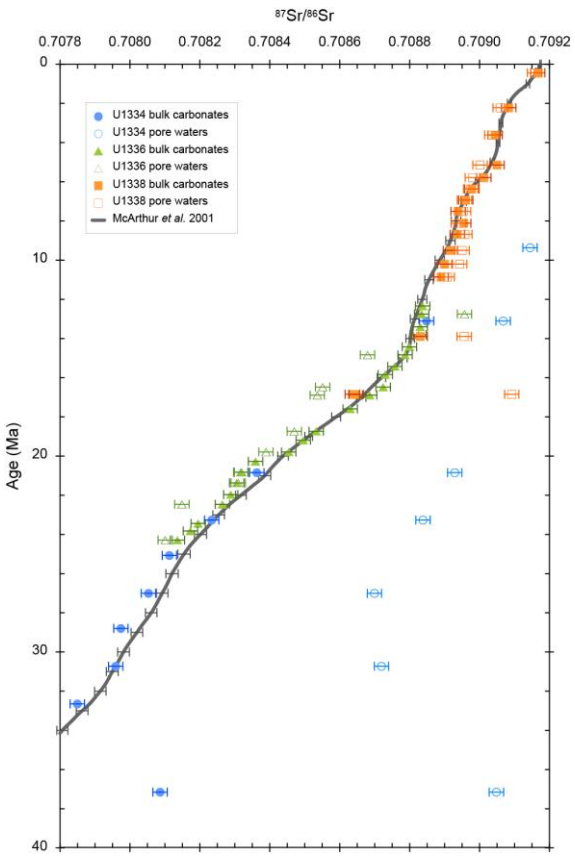

Figure 1. Sr isotope ratios, obtained by MC-ICP-MS, for Sites U1334, U1336, and U1338 plotted against age. Open symbols are pore water samples and filled symbols are bulk carbonates (0.1M acetic acid leach). The age model was used for PEAT Sites from the Initial Reports (Pälike *et al.* 2010). Error bars represent 2σ standard deviation of repeated measurements of IAPSO seawater. Samples were corrected to Sr Standard NBS 987 = 0.71025. The McArthur *et al.* (2001) curve (LOWESS fit, version 3) represents the contemporary seawater composition based on a compilation of 13 published sources for shown numerical ages.

2006) our new data reveal some additional complexity. Here, we present results from a multi-component study of recrystallisation in sediments from the IODP Expedition 320/321 Pacific Equatorial Age Transect (PEAT). This natural diagenesis laboratory, where sediments of similar age and initial composition have been subjected to different diagenetic histories, is ideal for the study of recrystallisation.

Radiogenic Sr ($^{87}Sr/^{86}Sr$) isotope ratios of bulk carbonate leachates and the associated pore waters generally suggest recrystallisation occurred relatively quickly (within 1.5 Myrs) as values are indistinguishable (within 2σ uncertainties) from the contemporaneous seawater (McArthur *et al.* 2001, LOWESS fit version 3) (Figure 1). All PEAT Sites investigated, except Site U1336 where the lower section was not sampled for pore waters, show circulation of relatively modern seawater in the basement as the $^{87}Sr/^{86}Sr$ signal of the pore waters increases towards present-day values with depth. Here, data are only shown for Sites U1334, U1336, and U1338 for clarity (Figure 1). Site U1338 pore water $^{87}Sr/^{86}Sr$ ratios are close to contemporaneous seawater in sediments younger than 9.5 Ma. In sediments older than 9.5 Ma the Sr isotope signal increases with depth from the upward diffusion of relatively modern seawater circulating in the basement (Pälike *et al.* 2010). Pore waters of Site U1336 exhibit lower $^{87}Sr/^{86}Sr$ ratios than contemporaneous seawater (McArthur *et al.* 2001) in sediments older than 14.8 Ma. These lower ratios likely result from the upward diffusion of Sr from older carbonates recrystallised deeper in the section. In sediments older than 20.3 Ma the carbonate $^{87}Sr/^{86}Sr$ ratios of Site U1336 exhibit lower values than contemporaneous seawater indicating the incorporation of Sr dissolved from older carbonates (Figure 1). The deepest bulk carbonate sample from Site U1334 appears to have incorporated some Sr from the relatively modern seawater circulating in the basement, as the $^{87}Sr/^{86}Sr$ ratio is much higher than contemporaneous seawater, suggesting persistent diagenetic alteration (Figure 1).

Some recrystallisation models (for example Richter and Liang 1993, Fantle and DePaolo 2006) state that diagenetic changes in the $^{87}Sr/^{86}Sr$ ratio of bulk carbonates should not be detectable as they would be smaller than the uncertainty of the measurements (between 10 and 20 ppm). However, recrystallisation is apparent in the deepest bulk carbonate sample from Site U1334 as well as the bulk carbonates and associated pore waters of Site U1336 older than 20 Ma (Figure 1). Furthermore, such models point out that recrystallisation rates decrease exponentially with age or depth (for example Richter and Liang 1993). However, it seems that the recrystallisation rate at Site U1336 increases around 20 Ma (Figure 1) and may still be ongoing in these depths as changes in the Sr concentration of the pore waters also suggest. These changes towards higher Sr concentrations could result from an interval of decreased porosity (Pälike *et al.* 2010). This interval of lower porosity indicates an aquitard which restricts the diffusive exchange of the pore water below and above (Rudnicki *et al.* 2001). Today, Site U1336 is below the carbonate compensation depth resulting in the dissolution of carbonate sediments younger than 12 Ma. In general, recrystallisation modelling at other locations produce the highest reaction rates for the uppermost 200 m (Fantle and DePaolo 2006). At Site U1336 bulk carbonate $^{87}Sr/^{86}Sr$ ratios do not deviate from contemporaneous seawater in the upper 100 m (rmcd) but in deeper sediments older than 20 Ma. This suggests a later phase of recrystallisation at this more reactive Site which probably has an enhanced thermal gradient (Pälike *et al.* 2010).

Sr/Ca ratios of bulk carbonates have been used to assess re-precipitation processes as well as paleo-climate variations (Delaney and Linn 1993). The Sr/Ca ratio is species-specific (Delaney 1989) and thus bulk Sr/Ca ratios reflect a mixture of the main carbonate constituents. The ratio of different species is different because of distinct calcification rates and crystal growth mechanisms (Elderfield *et al.* 1982). Recent foraminifera exhibit values of 1-2 mmol/mol (Rosenthal *et al.* 1999) whereas coccoliths have Sr/Ca ratios from 1.9 to 3.2 mmol/mol (Stoll *et al.* 2002).

The generally lower Sr/Ca ratios of bulk carbonates from Site U1336, compared to the other PEAT Sites, suggest more extensive diagenetic alteration as less Sr is incorporated into secondary calcite (Baker *et al.* 1982, Delaney 1989) (Figure 2). ODP Site 807 exhibits comparably low Sr/Ca ratios and is reported to be heavily recrystallised (Delaney and Linn 1993) and it is suggested that this Site approaches equilibrium between pore waters and carbonates (Fantle and DePaolo 2006). The Sr/Ca ratios of Sites U1335, U1337, and U1338 fluctuate around 2 mmol/mol with an increase at about 8.7-11.3 Ma at Sites U1337 and U1338 (Figure 2). There are no significant changes in the sedimentation rates at either Site during this interval. This increased Sr/Ca could be related to high

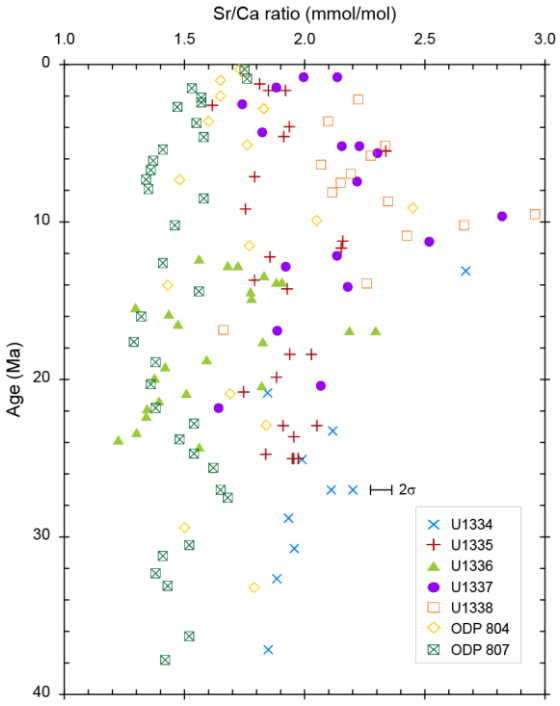

Figure 2. Bulk carbonate leachates (0.1M acetic acid leach) Sr/Ca ratios plotted against age. The error bar shown for Sites U1334-U1338 was estimated by replicate leaches and analyses. Data for ODP Sites 804 and 807 are from Delaney and Linn 1993.

productivity events as Site U1337 shows extensive diatom mats within this interval and Site U1338 exhibit diatom-rich sediments (Pälike *et al.* 2010). These blooming events led to extensive degradation of organic material resulting in reducing sediments which caused the dissolution of carbonates (Lyle *et al.* 1995). This in turn is also supported by the absence of planktonic foraminifera and a low carbonate content (< 1 wt %) during this interval at about 9.5 Ma at Site U1337 (Pälike *et al.* 2010). This high productivity event could be the late Miocene carbonate crash which was more pronounced in the eastern Pacific (Lyle *et al.* 1995). This Sr/Ca increase was also found at ODP Site 804 (Delaney and Linn 1993) (Figure 2). A smaller positive Sr/Ca excursion is also observed at Site U1335, which however occurred earlier in between 11.2 and 11.7 Ma (Figure 2). Similarly, this interval also exhibits diatom-rich sections (Pälike *et al.* 2010). The highest Sr/Ca value of Site U1338, of nearly 3 mmol/mol, coincides with the maximum in the pore water Sr concentration possibly indicating some of the carbonates recrystallised from the Sr-enriched pore waters.

Biogenic carbonates and contemporaneous seawater have the same radiogenic Sr isotope composition due to the neglect of isotope fractionation processes inherent to the radiogenic isotope systematics. Recently, stable Sr isotope fractionation has been investigated for biogenic carbonates and inorganic calcite (for example Böhm *et al.* 2012). Here, we present the first data for stable Sr isotopes from carbonate rich deep sea sediments.

Nine bulk carbonate and associated pore water couplets were chosen for measurement of $\delta^{88/86}Sr$ because their $^{87}Sr/^{86}Sr$ ratios either deviated from the seawater Sr curve or there was a difference in $^{87}Sr/^{86}Sr$ between pore water and bulk carbonate. The analysed pore waters of Site U1338 and the shallowest sample of U1336 are relatively close to modern seawater values whereas the analysed pore waters of Sites U1334, U1336 (except the shallowest sample), and U1337 exhibit higher or heavier $\delta^{88/86}Sr$ values compared to modern seawater ($\delta^{88/86}Sr_{IAPSO}$ = 0.381 ± 0.045 ‰, n = 8) (Figure 3). The pore water of Site U1334, the deepest sample analysed (see also Figure 1), also shows high $\delta^{88/86}Sr$ values despite the incorporation of Sr ($^{87}Sr/^{86}Sr$) from relatively modern seawater from the basement. Generally, the $\delta^{88/86}Sr$ values of U1336 pore waters increase with depth/ age (Figure 3). The $\delta^{88/86}Sr$ values of the bulk carbonates show more uniform values ranging from 0.211 to 0.249 ‰ and are similar to the modern carbonate JCp-1 (coral reference material, $\delta^{88/86}Sr$ = 0.202 ± 0.034 ‰, n = 17) (Figure 3). The bulk carbonates of Site U1336 do not show a trend with depth or age like the pore waters (Figure 3).

Furthermore, the pore water $\delta^{88/86}Sr$ values certainly do not derive from basalt or hydrothermal sources as this would result in lower values in $\delta^{88/86}Sr$ (Krabbenhöft *et al.* 2010). These results suggest that the recrystallisation of carbonates is associated with a fractionation process that enriches the pore waters with ^{88}Sr. This ^{88}Sr enrichment of the pore waters could indicate that, although less Sr is incorporated into secondary calcite during recrystallisation, lighter Sr isotopes (^{86}Sr) are incorporated preferably leaving heavy pore waters behind. The pore waters of Site U1336 become continously fractionated with depth but show similar $^{87}Sr/^{86}Sr$ values compared to the associated

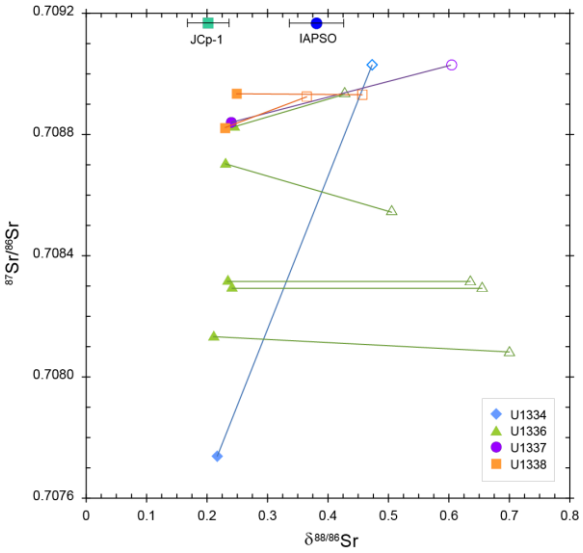

Figure 3. $\delta^{88}/^{86}Sr$ of bulk carbonate leachates and associated pore water couplets plotted against the $^{87}Sr/^{86}Sr$ ratio of these samples. Measurements were carried out using TIMS and a double-spike technique (Krabbenhöft *et al.* 2009). Open symbols represents pore waters and filled symbols are bulk carbonate leachates. Bulk carbonate samples and the associated pore waters are linked by coloured lines. Error bars represent 2σ standard deviation of repeated measurements of standard seawater IAPSO and coral reference material JCp-1. $^{87}Sr/^{86}Sr$ ratios were normalised to Sr Standard NBS 987, $^{88}Sr/^{86}Sr$ = 8.375209 (Nier 1938).

carbonates which suggests the same Sr source for pore waters and carbonates indicating a more or less closed system. The $\delta^{88/86}Sr$ values of the carbonates do not seem to change noticably with depth/ age since the carbonates have much higher concentrations of Sr than pore waters (by a factor of > 100, see Richter and DePaolo 1988) meaning pore waters are much more sensitive to fractionated Sr compared to the carbonates. Although, more measurements are required to verify these data our first results indicate that stable Sr isotopes have a great potential to identify diagenetic altered sediments by their pore water signals.

The next phase of the project and ongoing work will focus on the preservation of geochemical proxies in the shells of foraminifera which are the foundation of palaeoceanography.

References:

Baker P.A., Gieskes J.M., and Elderfield H. (1982) Diagenesis of carbonates in deep-sea sediments-evidence from Sr/Ca ratios and interstitial dissolved Sr^{2+} data. *Journal of Sedimentary Petrology* **52**, 71-82

Böhm F., Eisenhauer A., Tang J., Dietzel M., Krabbenhöft A., Kisakürek B., and Horn C. (2012) Strontium isotope fractionation of planktic foraminifera and inorganic calcite. *Geochimica et Cosmochimica Acta* **93**, 300–314

Delaney M.L. (1989) Temporal changes in interstitial water chemistry and calcite recrystallization in marine sediments. *Earth and Planetary Science Letters* **95**, 23-37

Delaney M.L. and Linn L.J. (1993) Interstitial water and bulk calcite chemisty, Leg 130, and calcite recrystallization. In: Berger, W.H., Kroenke, L.W., Janecek, T.R., *et al.* (Eds.), *Proc. ODP. Sci. Results* 130, 561–572

Elderfield H., Gieskes J.M., Baker P.A., Oldfield R.K., Hawkesworth C.J., and Miller R. (1982) $^{87}Sr/^{86}Sr$ and $^{18}O/^{16}O$ ratios, interstitial water chemistry and diagenesis in deep-sea carbonate sediments of the Ontong Java Plateau. *Geochimica et Cosmochimica Acta* **46**, 2259-2268

Fantle M.S. and DePaolo D.J. (2006) Sr isotopes and pore fluid chemistry in carbonate sediment of the Ontong Java Plateau: Calcite recrystallization rates and evidence for a rapid rise in seawater Mg over the last 10 million years. *Geochimica et Cosmochimica Acta* **70**, 3883-3904

Krabbenhöft A., Fietzke J., Eisenhauer A., Liebetrau V., Böhm F., and Vollstaedt H. (2009) Determination of radiogenic and stable strontium

isotope ratios ($^{87}Sr/^{86}Sr$; $\delta^{88/86}Sr$) by thermal ionization mass spectrometry applying an $^{87}Sr/^{84}Sr$ double spike. *Journal of Analytical Atomic Spectrometry* **24**, 1267–1271

Krabbenhöft A., Eisenhauer A., Böhm F., Vollstaedt H., Fietzke J., Liebetrau V., Augustin N., Peucker-Ehrenbrink B., Müller M.N., Horn C., Hansen B.T., Nolte N., and Wallmann K. (2010) Constraining the marine strontium budget with natural strontium isotope fractionations ($^{87}Sr/^{86}Sr^*$, $\delta^{88/86}Sr$) of carbonates, hydrothermal solutions and river waters. *Geochimica et Cosmochimica Acta* **74**, 4097–4109

Lyle M., Dadey K.A., and Farrell J.W. (1995) The late Miocene (11-8 Ma) eastern Pacific carbonate crash: Evidence for reorganization of deep-water circulation by the closure of the Panama Gateway. In: Pisias N.G., Mayer L.A., Janecek T.R., Palmer-Julson A., and van Andel T.H. (Eds.), *Proc. ODP. Sci. Results* 138

McArthur J.M., Howarth R.J., and Baily T.R. (2001) Strontium isotope stratigraphy: LOWESS version 3: best fit to the marine Sr-isotope curve for 0-509 Ma and accompanying look-up table for deriving numerical age. *The Journal of Geology* **109**, 155-170

Nier A.O. (1938) The isotopic constitution of strontium, barium, bismuth, thallium and mercury. *Physical Review* **5**, 275–278

Pälike, H., Lyle, M., Nishi, H., Raffi, I., Gamage, K., Klaus, A., and the Expedition 320/321 Scientists (2010) Proc. IODP, 320/321: Tokyo (Integrated Ocean Drilling Program Management International, Inc.)

Richter F.M. and DePaolo D.J. (1987) Numerical models for diagenesis and the Neogene Sr isotopic evolution of seawater from DSDP Site 590B. *Earth and Planetary Science Letters* **83**, 27-38.

Richter F.M. and DePaolo D.J. (1988) Diagenesis and Sr isotopic evolution of seawater using data from DSDP 590B and 575. *Earth and Planetary Science Letters* **90**, 382-394.

Richter F. M. and Liang Y. (1993) The rate and consequences of Sr diagenesis in deep-sea carbonates. *Earth and Planetary Science Letters* **117**, 553-565

Rosenthal, Y., Field M.P., and Sherrell R.M. (1999) Precise determination of element/calcium ratios in calcareous samples using sector field inductively coupled plasma mass spectrometry. *Analytical Chemistry* **71**, 3248–3253

Rudnicki M.D., Wilson P.A., and Anderson W.T. (2001) Numerical models of diagenesis, sediment properties, and pore fluid chemistry on a paleoceanographic transect: Blake Nose, Ocean Drilling Program Leg 171 B. *Paleoceanography* **16**, 563-575

Stoll, H.M., Rosenthal Y., and Falkowski P. (2002) Climate proxies from Sr/Ca of coccolith calcite: Calibrations from continuous culture of Emiliania huxleyi. *Geochimica et Cosmochimica Acta* **66**, 927–936

IODP

Hadley Cell dynamics and Cretaceous black shale sedimentation in the low latitude Atlantic Ocean: Validation against DSDP/ODP core data

THOMAS WAGNER[1,*], PETER HOFMANN[2], SASCHA FLÖGEL[3]

[1] School of Civil Engineering and Geosciences, Newcastle University, U.K.. * thomas.wagner@ncl.ac.uk
[2] Department of Geology and Mineralogy University of Cologne, Germany
[3] GEOMAR, Kiel, Germany

A central question for understanding small-scale heterogeneities in marine black shale, affecting quantity and quality of sedimentary organic matter, is the linkage between marine productivity, redox conditions and large scale atmospheric circulation patters, such as Hadley Cell dynamics in the subtropical-tropical zone. The Hadley Cells and the Intertropical Convergence Zone (ICZ) are major components of the global atmospheric circulation that exert control on continental climate via the trade wind and monsoonal systems, and ocean processes.

Black shale sedimentation occurred when sea surface temperatures in the Cretaceous equatorial region were extremely high. Consequences of a superheated tropical zone is a vigorous atmospheric circulation and an intensified hydrological cycle. The critical role of this connection has been instrumental in the formation of black shale off tropical Africa where nutrient, (clay) mineral and freshwater from runoff led to short periods of oxygen deficiency and exceptionally enhanced organic carbon storage.

Fluctuations of the ITCZ and the Headley Cells also control marine upwelling via the trade winds, adding a second powerful mechanism to force anoxia and enhanced marine organic carbon burial. Since both mechanisms are directly linked, upwelling and runoff occur in different areas at the same time. Understanding these large scale and temporal relationships is of importance to better understand and potentially also predict the quality of oil prone source rocks in areas where no well data exist.

Short-term fluctuations in climate can produce pronounced variations in the composition of black shales at the sub-meter to cm scale, including those in grain size, mineral composition, and early diagenetic overprint, in combination determining variations in porosity and permeability. From a petroleum systems aspect it is important to predict if thick black shale sections are likely to be composed of uniform units with similar OC richness and quality, or of variable units with alternations of OC-rich and OC-poor beds.

Combining conceptual ideas with geological evidence from three different time intervals of the Cretaceous - the Albian, the Cenomanian-Turonian, and the Coniacian-Santonian – we discuss the mechanistic and temporal relationships of black shale formation and Hadley Cell dynamics.

IODP

Antarctic Ice Sheet deglaciation revised – the dynamic record of Iceberg Alley

M.E. WEBER[1], G. KUHN[2], P.U. CLARK[3], A. TIMMERMANN[4], G. LOHMANN[2], R. GLADSTONE[4], D. SPRENK[1]

[1] Institute of Geology and Mineralogy, University of Cologne, Cologne, Germany
[2] Alfred Wegener Institute for Polar and Marine Research, Helmholtz Association, Bremerhaven, Germany
[3] College of Earth, Ocean, and Atmospheric Sciences, Oregon State University, Corvallis, OR, USA
[4] International Pacific Research Center, University of Hawaii at Manoa, Honolulu, HI, USA
[5] Arctic Centre, University of Lapland, Rovaniemi, Finland

Reconstruction of the last global sea level rise faces uncertainties because only a few robust data evidences are available for Antarctic ice sheets. Deglacial dynamics have mostly been inferred from shallow-water cores on the shelf, where decisive changes are either erased by grounding ice or occur in condensed, lithologically complex successions with partially reversed and generally unreliable ^{14}C ages. Modeling studies reconstruct a late ice-sheet retreat starting around 12 ka BP and ending around 7 ka BP with a large impact of an unstable West Antarctic Ice Sheet (WAIS) and a small impact of a stable East Antarctic Ice Sheet (EAIS). However, new findings from two deep-sea cores from the Scotia Sea challenge these reconstructions and call for a principal revision of the Antarctic deglacial history with an impact on projections on future sea-level rise as well.

The well-dated sites (*Weber et al., 2012*) provide the first integrative and representative record of Antarctic Ice Sheet instability. They are located in the central transport route of virtually all Antarctic icebergs, the so-called Iceberg Alley, and demonstrate a highly dynamic

Antarctic Ice Sheet during the last deglaciation with eight distinct phases of enhanced iceberg routing, dubbed Antarctic Ice Sheet Events (AIE), in contrast to existing models of a late and monotonous ice-sheet retreat which implied only little contribution to the last, natural, sea-level rise 19,000 to 9,000 years ago. Ice-sheet retreat signals detected in the Weddell Sea at 19 ka and 16 ka (*Weber et al., 2011*) are recorded as peaks in iceberg-rafted debris in the Scotia Sea during AIE 1 and 2. In addition, we found the first direct evidence for an Antarctic contribution to Meltwater Pulse 1A in the flux rates of iceberg-rafted debris during AIE3. The Soctia Sea sites are thus instrumental to decipher Antarctic ice-sheet dynamics as well as the deglacial record of ice-sheet instability. Therefore, we are currently putting together a pre-proposal, which should be submitted to IODP before April 1st, 2013, to obtain two deep drillings.

Using an ensemble of transient deglacial model simulations we could show that increased export of warmer Circumpolar Deep Water towards Antarctica contributed to Antarctic Ice Sheet melt by enhanced ocean thermal forcing (*Weber et al., in review*). These new findings hold the potential to substantially revise and improve our understanding of the transient response of the ice sheet to external and internal forcings, and the contributions to the postglacial isostatic adjustment as well as to the last, natural, sea-level rise. Our results will also help improving projections of future sea-level rise.

References:
Weber, M.E., Clark, P. U., Ricken, W., Mitrovica, J. X., Hostetler, S. W., and Kuhn, G. (2011): Interhemispheric ice-sheet synchronicity during the Last Glacial Maximum. – *Science*, 334, 1265-1269, doi: 10.1126:science.1209299

Weber, M.E., Kuhn, G., Sprenk, D., Rolf, C., Ohlwein, C., and Wicken, W. (2012): Dust transport from Patagonia to Antarctica – a new stratigraphic approach from the Scotia Sea and its implications for the last glacial cycle. – *Quaternary Science Reviews*, doi: 10.1016/j.quascirev.2012.01.016.

Weber, M. E., Clark, P. U., Kuhn, G., Timmermann, A., Sprenk, D., Gladstone, R., Zhang, X., Lohmann, G., Menviel, L., Chikamoto, M., Friedrich, T. (in review): Millennial-scale variability of the Antarctic Ice Sheet throughout the last deglaciation. – *Science*.

IODP

En route for a complete early Paleogene Geochronology

T. WESTERHOLD[1], U. RÖHL[1]

[1] MARUM - Center for Marine Environmental Sciences, University of Bremen, 28359 Germany

To decipher the driving mechanisms of Earth system processes including the climate dynamics expressed by paleoceanographic events we need a very accurate and high-resolution stratigraphy. Geologic time scale construction has been undergoing a revolution during the past decade as radioisotopic instrumentation enables ultra-high precision dating and solar system dynamics have been deciphered with incredible precision. In addition, especially astronomical tuning, the correlation of cyclic variations in the geological record to astronomical computations of the insolation quantities on Earth, has revolutionized the age calibration of the Neogene part of the geological time scale (Shackleton et al. 1990, Lourens et al. 2004, Hilgen 2010). Numerous studies documented the major advantage of astronomical tuning: its potential to provide very accurate geological ages and durations of periods in time.

Astronomical tuning relies on the progressive models of solar-system dynamics through time. Due to the chaotic motion of planets in the inner Solar System the orbital solution of Laskar et al. (2004) is valid up to 40 Ma only. Nevertheless, basic orbitally tuned chronological frameworks were established by tuning to the stable long eccentricity cycle (405-kyr) resulting in floating time scales in the context of absolute time. Uncertainties in radioisotopic age constraints (Min et al. 2000, Schoene & Bowring 2006) prevented the intercalibration of radioisotopic and astronomical dating techniques to anchor the floating time scale in order to extend the astronomically calibrated time scale into the early Paleogene. To overcome these problems, Kuiper et al. (2008) intercalibrated high-precision radioisotopic and astronomical tuning ages in Neogene geological successions to recalibrate the age of the Fish Canyon sanidine standard for $^{40}Ar/^{39}Ar$ dating. This new standard values imply that all previously published $^{40}Ar/^{39}Ar$ ages must be shifted 0.65% older, synchronizing them with previously diachronous U/Pb ages.

Detailed examination, analysis and astronomical tuning of ocean-drilling cores from the Pleistocene (Channell et al. 2010) and the Paleocene to early Eocene (Westerhold et al. 2012) reach a different, very controversial conclusion – the ages of the $^{40}Ar/^{39}Ar$ standards should indeed be younger, not older. These studies point to intrinsic problems with the available decay constants and/or standard ages used in $^{40}Ar/^{39}Ar$ dating, and possible biasing of the U/Pb clock in zircon crystals due to the memory of pre-eruption crystallization of magma, or both. If this is the case then the synchronization of $^{40}Ar/^{39}Ar$ and U/Pb radioisotopic clocks as proposed by Kuiper et al. (2008) is quite problematic. In turn, the orbital solution used in the early Paleogene study (Laskar et al. 2011) might not be correct in all details back to 54 Ma as suggested by the comparison to geological data (Westerhold et al. 2012). Here we will give an overview of the state of the art, provide possible options for solving this controversy, and discuss implications for the application of recent time scales. The desired options need to be independent from both the eccentricity pattern of the orbital solution back in the early Paleogene and radioisotopic ages to avoid circular reasoning. We are very close to unravel the controversy that most lilkely will lead to the establishment of a complete and accurate early Paleogene astronomically tuned time scale in the very near future.

References:
Channell, J. E. T., D. A. Hodell, B. S. Singer, and C. Xuan (2010), Reconciling astrochronological and $^{40}Ar/^{39}Ar$ ages for the Matuyama-Brunhes boundary and late Matuyama Chron, G-cubed, 11, Q0AA12.

Hilgen, F. J. (2010), Astronomical dating in the 19th century, Earth-Science Reviews, 98 (1-2), 65-80.

Kuiper, K. F., A. Deino, F. J. Hilgen, W. Krijgsman, P. R. Renne, and J. R. Wijbrans (2008), Synchronizing Rock Clocks of Earth History, Science, 320 (5875), 500-504.

Laskar, J., P. Robutel, F. Joutel, M. Gastineau, A. Correia, and B. Levrard (2004), A long-term numerical solution for the insolation quantities of the Earth, Astronomy and Astrophysics, 428, 261-285.

Laskar, J., M. Gastineau, J. B. Delisle, A. Farrés, and A. Fienga (2011), Strong chaos induced by close encounters with Ceres and Vesta, Astronomy and Astrophysics, 532, L4.

Lourens, L. J., F. J. Hilgen, J. Laskar, N. J. Shackleton, and D. Wilson (2004), The Neogene Period, in A Geological Timescale 2004, edited by F. Gradstein, J. Ogg and A. Smith, pp. 409-440.

Min, K., R. Mundil, P. R. Renne, and K. R. Ludwig (2000), A test for systematic errors in 40Ar/39Ar geochronology through comparison

with U/Pb analysis of a 1.1-Ga rhyolite, Geochimica et Cosmochimica Acta, 64(1), 73-98.
Schoene, B., and S. A. Bowring (2006), U-Pb systematics of the McClure Mountain syenite: thermochronological constraints on the age of the Ar-40/Ar-39 standard MMhb, Contributions to Mineralogy and Petrology, 151(5), 615-630.
Shackleton, N. J., A. Berger, and W. R. Peltier (1990), An alternative astronomical calibration of the lower Pleistocene timescale based on ODP Site 677, Transactions of the Royal Society of Edinburgh: Earth Sciences, 81, 251-261.
Westerhold, T., U. Röhl, and J. Laskar (2012), Time scale controversy: Accurate orbital calibration of the early Paleogene, Geochem. Geophys. Geosyst., 13, Q06015.

IODP

Orbital Pacing of the Middle to Late Eocene Equatorial Pacific Carbonate Compensation Depth

T. WESTERHOLD[1], U. RÖHL[1], K. EDGAR[2], M. LYLE[3], H. PÄLIKE[4,1], R. WILKENS[5], P. WILSON[4], J. ZACHOS[6]

[1]MARUM - Center for Marine Environmental Sciences, University of Bremen, 28359 Germany
[2]Cardiff University, UK
[3]Texas A&M Univ., USA
[4]National Oceanography Centre, Southampton, UK
[5]Univ. Hawaii, Honolulu HI 96822, USA
[6]University of California, Santa Cruz, California, USA

Critical high fidelity records that are providing new insight into the dynamics of the middle to late Eocene climate development are from depth transects retrieved by ODP Leg 199 (Lyle et al. 2002; Lyle and Wilson 2006) and IODP Expedition 320/321 (Lyle et al. 2010; Pälike et al. 2010) in the equatorial Pacific. IODP Expedition 320/321 recovered high-quality sedimentary sequences at several sites (U1331-U1334) that span key horizons of the greenhouse to icehouse transition, including the Eocene/Oligocene transition, an expanded middle to upper Eocene succession, and the Middle Eocene Climate Optimum (MECO). Within this transect Sites U1333 and U1334 records are particularly well suited for constraining the timing and extend of middle to late Eocene carbon cycle dynamics.

In the middle to late Eocene of the equatorial Pacific surprisingly large and geologically rapid fluctuations in the depth of calcium carbonate accumulation have been documented (Lyle et al., 2005; Pälike et al. 2012). Earlier studies based on ODP Sites 1218 and 1219 identified seven Carbonate Accumulation Events (CAEs), with each characterized by high-carbonate burial, a relatively deep Carbonate Compensation Depth (CCD), and oxygen isotope evidence of lower temperatures (Lyle et al. 2005). The individual events are separated by CCD excursions of up to 1200 - 1500 m. In contrast, Neogene CCD variations were only in the order of 200 m or less (Lyle et al. 2008). The CAEs have been linked to events of global cooling (Lyle et al. 2005, Tripati et al. 2005) that lead to elevated primary productivity and carbonate production in the equatorial region. The main driver for the strong CCD fluctuations was interpreted to represent different carbon reservoirs in the carbon cycle interacting with climate (Lyle et al. 2005). Due to the lack of evidence for large bi-polar fluctuations in ice volume (Edgar et al. 2007), changes in weathering and the mode of organic-carbon delivery have been identified using Earth system models as two key processes to explain these large-scale Eocene fluctuations of the carbonate compensation depth (Pälike et al. 2012). However, the data resolution was limited and a precise age model was still lacking both essential to unravel the ultimate causes of the CAEs as well as the potential relation of changes in the CCD to orbital cycles.

Our aim is to reconstruct the highly dynamic late Eocene carbon cycle at high resolution. Here we present Ca, Si, and Fe intensity data from XRF core scanning of more than 1200 meters of sediment from IODP Exp. 320 (Sites U1331-U1334) and ODP Leg 199 (Sites 1218-1220) spanning magnetic polarity chrons C13n to C21n (34 to 47 Ma). Prior to time series analysis XRF core scanning data, shipboard physical property and biomagnetostratigraphic data were correlated and integrated in detail (Westerhold et al. 2012). At Sites U1333 and U1334 we generated high-resolution bulk carbon and oxygen stable isotope data from 33 to 39 Ma to document the phase relationship to XRF core scanning data. We then used high-resolution XRF core scanning and bulk stable isotope data to establish a stratigraphic framework based on the identification of the stable long eccentricity cycle (405 kyr) and subsequently applied orbital tuning of the records. Our new time scale revises and refines the existing orbitally tuned age model (Pälike et al. 2006) from 31 to 41 Ma. The new astronomically tuned absolute age for the Eocene/Oligocene boundary (C13r.14) is 33.89 Ma, 100 kyr older than the age of Pälike et al. (2006), und thus validates the astronomical tuned age from the Massignano (Italy) global stratotype section and point (GSSP) by Brown et al. (2009).

Integration of calcium (Ca) intensity data from XRF core scanning of Leg 199 and Exp. 320 cores provide the ideal basis to reconstruct calcium carbonate records over a depth transect through time at unprecedented resolution. Ca elemental intensity data have been transferred into carbonate records using $CaCO_3$ values analyzed on discrete samples for calibration purpose. Amongst others, Fe and Si elemental intensity data have been quantified by calibrating normalized median-scaled (NMS, Lyle et al. 2012) XRF core scanning intensity data with ED-XRF analyses at 188 carefully chosen samples from Sites 1218, 1219, 1220, U1331, U1332, U1333, and U1334. For the calculation of mass accumulation rates we utilized the composite gamma-ray attenuation (GRA) density data corrected for moisture and the sedimentation rates based on the revised shipboard magnetostratigraphy (Westerhold et al. 2012).

Our data contribute to an improved spatial view of the CAEs in the equatorial Pacific. The CAEs are expressed as sharp carbonate concentration fluctuations at ~35, 37.5, 39, 41, 44, 46 Ma across Sites U1331-U1334 and 1218-1220, revealing a highly dynamic middle to late Eocene environment (Figure 1). The CAEs-bearing interval in the Eocene is followed by a sharp changeover to much higher carbonate accumulation rates in the Oligocene. Ignoring the effects of salinity and ice volume change, bulk stable oxygen isotope data show a long term warming of ~3°C from 38.5 to 35.2 Ma, a subsequent cooling of ~2°C till 34.8 Ma, and a strong warming of 6-7°C from 34.8 to 34.2 Ma. These trends are then followed by the stepped increase in bulk oxygen isotopes values at the EOT (Coxall et a. 2005). Bulk carbon stable isotopes show a long-term increase in values from 38.5 to 34.8 Ma, a subsequent strong decrease till 34.2 Ma, and the stepped increase in the EOT. Pronounced higher frequency variations in the data

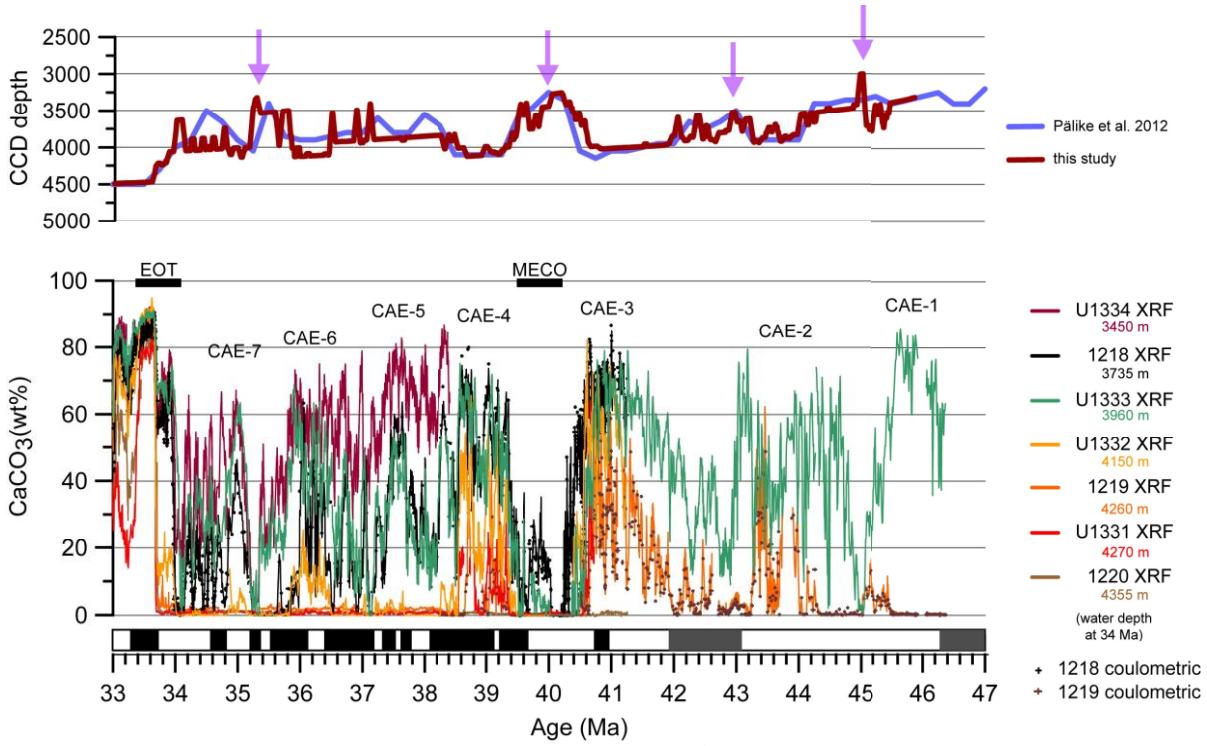

Figure 1. - CCD depth reconstruction and high-resolution $CaCO_3$ wt% records for reconstructing the middle to late Eocene carbon cycle dynamics from 33 to 47 Ma along a depth transect. Carbonate Accumulation Events (CAE1 - 7) from Lyle et al. (2005). Paleomagnetic reversal pattern plotted on the CK95 timescale. MECO = Middle Eocene Climate Optimum; EOT - Eocene/Oligocene Transition

are related to short (100kyr) and long (405 kyr) eccentricity cycles.

The phase relation between bulk isotopes and XRF data is not constant over time making the tuning process a bit more complicated. Lighter carbon and oxygen isotope values correspond to high carbonate and lower Fe as well as Si content in the middle to late Eocene until chron C15n (35 Ma). In the interval younger than chron C15n lighter carbon and oxygen isotope data correspond to lower carbonate and higher Fe as well as Si content. This switch in phase relation of isotopes vs carbonate content is very similar to the shift from the Atlantic type (high carbonate in interglacials) to Pacific-type (high carbonate in glacials) carbonate stratigraphy observed during the earliest Gauss Magnetic Chron (3.18 - 3.41 Ma) in equatorial Pacific sediment cores (Moore et al. 1982, Dunn 1982), close to the onset of northern hemisphere glaciation. We speculate that the shift in phase relation about 1 million years prior to the EOT could be related to a change in the deep and intermediate water circulation (Katz et al. 2011). This reorganization in ocean circulation probably affected the distribution of nutrients and also the response of the equatorial Pacific to orbital forcing. To understand the underlying processes modeling will be required.

Calibrated XRF core-scanning data enable us to reconstruct the middle to late Eocene equatorial Pacific sedimentation history over a depth transect at unprecedented resolution. For the first time we show that intervals of very shallow carbonate compensation depths in the Eocene equatorial Pacific are corresponding to very long eccentricity minima. This correlation in line with the pronounced orbital cyclicity in XRF data suggests that carbon cycle dynamics in the equatorial Pacific during the middle to late Eocene are driven by astronomical forcing. In more detail, our data show a repeating saw-tooth like pattern of a relatively abrupt rise in the CCD close to the very long eccentricity cycle minima and a gradually fall of the CCD afterward. During very long eccentricity minima Earth's orbit is almost circular. This might have diminished the amount of rainfall in tropical regions and thus the delivery of solutes to the oceans. Our data support the idea that changes in weathering rates might be responsible for the strong fluctuations of the carbonate compensation depth observed in the equatorial Pacific (Lyle et al., 2005; Pälike et al. 2012). To investigate to which extend changes in ocean circulation are involved, new high-resolution records with an orbitally tuned age model from the Atlantic Ocean are also needed.

References:

Brown, R. E., C. Koeberl, A. Montanari, and D. M. Bice (2009), Evidence for a change in Milankovitch forcing caused by extraterrestrial events at Massignano, Italy, Eocene-Oligocene boundary GSSP, in The Late Eocene Earth - Hothouse, Icehouse and Impacts: Geological Society of America Special Paper, edited by C. Koeberl and A. Montanari, pp. 119-137.

Dunn, D. A. (1982), Change from "Atlantic-type" to "Pacific-type" carbonate stratigraphy in the middle Pliocene Equatorial Pacific Ocean, Marine Geology, 50(1–2), 41-59, doi: http://dx.doi.org/10.1016/0025-3227(82)90060-3.

Edgar, K. M., P. A. Wilson, P. F. Sexton, and Y. Suganuma (2007), No extreme bipolar glaciation during the main Eocene calcite compensation shift, Nature, 448(7156), 908-911.

Katz, M. E., B. S. Cramer, J. R. Toggweiler, G. Esmay, C. Liu, K. G. Miller, Y. Rosenthal, B. S. Wade, and J. D. Wright (2011), Impact of Antarctic Circumpolar Current Development on Late Paleogene Ocean Structure, Science, 332(6033), 1076-1079, doi: 10.1126/science.1202122.

Lyle, M., J. Barron, T. J. Bralower, M. Huber, A. Olivarez Lyle, A. C. Ravelo, D. K. Rea, and P. A. Wilson (2008), Pacific Ocean and Cenozoic evolution of climate, Reviews of Geophysics, 46(RG2002)10.1029/2005RG000190.

Lyle, M., and P. A. Wilson (2006), Leg 199 synthesis: Evolution of the equatorial Pacific in the early Cenozoic, 39 pp.

Lyle, M., A. Olivarez Lyle, J. Backman, and A. Tripati (2005), Biogenic sedimentation in the Eocene equatorial Pacific - the stuttering greenhouse and Eocene carbonate compensation depth, in Proc. ODP,

Sci. Results, 199: College Station, TX (Ocean Drilling Program), edited by P. A. Wilson, M. Lyle and J. V. Firth, pp. 1-35.
Lyle, M., P. A. Wilson, T. R. Janecek, and et al. (2002), Proc. ODP, Init. Repts., 199: College Station, TX (Ocean Drilling Program).
Moore Jr, T. C., N. G. Pisias, and D. A. Dunn (1982), Carbonate time series of the Quaternary and Late Miocene sediments in the Pacific Ocean: A spectral comparison, Marine Geology, 46(3–4), 217-233, doi: http://dx.doi.org/10.1016/0025-3227(82)90081-0.
Pälike, H., et al. (2012), A Cenozoic record of the equatorial Pacific carbonate compensation depth, Nature, 488(7413), 609-614, doi: 10.1038/nature11360.
Pälike, H., H. Nishi, M. Lyle, I. Raffi, K. Gamage, A. Klaus, and the Expedition 320/321 Scientists (2010), Proc. IODP, 320/321: Tokyo (Integrated Ocean Drilling Program Management International, Inc.).
Pälike, H., R. D. Norris, J. O. Herrle, P. A. Wilson, H. K. Coxall, C. H. Lear, N. J. Shackleton, A. K. Tripati, and B. S. Wade (2006), The Heartbeat of the Oligocene Climate System, Science, 314(5807), 1894-1898, doi: 10.1126/science.1133822.
Tripati, A., and H. Elderfield (2005), Deep-Sea Temperature and Circulation Changes at the Paleocene-Eocene Thermal Maximum, Science, 308(5730), 1894-1898.
Westerhold, T., et al. (2012), Revised composite depth scales and integration of IODP Sites U1331-U1334 and ODP Sites 1218-1220, in Proc. IODP, 320/321: Tokyo (Integrated Ocean Drilling Program Management International, Inc.), edited by H. Pälike, M. Lyle, H. Nishi, I. Raffi, K. Gamage, A. Klaus and and the Expedition 320/321 Scientists.

ICDP

The Campi Flegrei Deep Drilling Project (CFDDP): Initial results from gas monitoring site surveys and drilling mud gas monitoring during the 500 m pilot hole drilling

T. WIERSBERG[1], J. ERZINGER[1], R. SOMMA[2], A. FEDELE[2]

[1] Deutsches GeoForschungsZentrum, Telegrafenberg, 14473 Potsdam, Germany
[2] Istituto Nazionale di Geofisica e Vulcanologia, Sezione di Napoli, Via Diocleziano 328, 80124 Napoli, Italy

Situated in the Campanian region (Italy), the Phlegraean Volcanic District is a densely populated active volcanic area, including the Campi Flegrei caldera, the islands of Procida and Ischia, and a number of submerged volcanoes. The understanding of mechanisms for volcanic unrest and eruptions of large calderas is crucial to mitigate volcanic hazards and to evaluate the influence of volcanic activity on the global environment. The Campi Flegrei Deep Drilling Project (CFDDP) was born to tackle these questions by scientific drilling of a 500 m pilot hole and a 3-4 km deep main hole.

The drilling of a pilot hole was successfully executed in late summer 2012 and late fall 2012, interrupted by three months of operational stop. In the first phase, a 12 ¼ inch hole was drilled to 222 m below ground level. In the second phase, the hole was deepened to 434 m (8 ¼ inch borehole diameter) and finally reached a depth of 501 m with 6 inch diameter. The hole was logged and cased at the end of each phase with exception of the lowermost 80 meter, where a slotted liner was installed to permit fluid flow from the formation into the well for future fluid and gas monitoring. Cuttings were separated from the drilling mud at the shale shakers, analysed in a field laboratory and sampled for further measurements. Two core runs at 438 m and 500 m yield only poor recovery.

On-line gas monitoring was carried out to gain new insights into the evolution of the fluid regime (drilling mud gas monitoring) and to understand the interplay between deep circulating fluids and volcanic/seismic processes. The only formation-derived gas extracted from the drilling mud during pilot hole drilling was CO_2 with concentrations lower than 0.1%. Preliminary data evaluation suggests that CO_2 concentrations vary with different lithology. The low gas concentrations identified by scientific mud gas monitoring and by commercial mud logging are most likely caused by heavy drilling mud that impedes the flow of gas from the formation into the drilling mud. In the future, water and gas will be sampled from the pilot hole by a modified U-tube technique.

Prior to drilling, two long-term gas monitoring site surveys were executed from January-Mai 2009 and from May-July 2012 at a Pisciarelli fumarole field at the eastern outer flank of the Solfatara volcano, 3.2 km away from the CFDDP drill site. The average composition (air-corrected) of fumarolic gas is as follows: CO_2 (98.4 vol.-%), H_2S (0.24 vol.-%), N_2 (1.13 vol.-%), CH_4 (65 ppmv), H_2 (0.089 vol.-%), and He (7.3 ppmv). Long-term and diurnal variations in the gas composition have been identified. Stable isotope and noble gas isotope analysis are planned on all types of gas samples.

ICDP

The role of bubble ascent in magma mixing

S. WIESMAIER[1], D. MORGAVI[1], D. PERUGINI[2], C. DE CAMPOS[1], K.-U. HESS[1], Y. LAVALLÉE[3], D. DINGWELL[1]

[1] Ludwig-Maximilians-Universität München, Earth and Environmental Sciences, Munich, Germany (sebastian.wiesmaier@min.uni-muenchen.de)
[2] Department of Earth Sciences, University of Perugia, Perugia, Italy
[3] School of Environmental Sciences, University of Liverpool, Liverpool, UK

Understanding the processes that affect the rate of liquid state homogenization provides fundamental clues on the otherwise inaccessible subsurface dynamics of magmatic plumbing systems. Compositional heterogeneities detected in the matrix of magmatic rocks represent the arrested state of a chemical equilibration. Magmatic homogenization is divided into a) the mechanical interaction of magma batches (mingling) and b) the diffusive equilibration of compositional gradients, where diffusive equilibration is exponentially enhanced by progressive mechanical interaction [1]. The mechanical interaction between two distinct batches of magma has commonly been attributed to shear and folding movements between two distinct liquids. A mode of mechanical interaction scarcely invoked is the advection of mafic material into a felsic one through bubble motion. Yet, experiments with analogue materials demonstrated that bubble ascent has the potential to enhance the fluid mechanical component of magma mixing [2].

Here, we present preliminary results from bubble-advection experiments. For the first time, experiments of this kind were performed using natural materials at magmatic temperatures. Cylinders of Snake River Plain (SRP) basalt were drilled with a cavity of defined volume and placed underneath cylinders of SRP rhyolite. Upon melting, the gas pocket (=bubble) trapped within the cavity, rose into the rhyolite, and thus entraining a portion of basaltic material in the shape of a plume trail.

These plume-like structures that the advected basalt formed within the rhyolite were characterized by microCT and subsequent high-resolution EMP analyses. Single protruding filaments at its bottom end show a composite structure of many smaller plume tails, which may indicate the opening of a preferential pathway for bubbles after a first bubble has passed. The diffusional gradient around the plume tail showed a progressive evolution of equilibration from bottom to top of the plume tail. Calculating the normalised variance provides an efficient statistical measure of the diffusion rate of cations at the interface of ambient rhyolite and basaltic plume tail.

Bubble ascent provides an efficient mechanism for advection of contrasting melt compositions, independent from Rayleigh-Taylor instabilities [cf. 2], or convection induced by overpressure of rising magma. Interaction of volatile-bearing magmas may thus be enhanced at saturation of one or two end-members by buoyant forces exerted from free fluid phases. Future strategies involve to hone down tolerances in the experimental setup to minimise extraneous bubbles, achieve fluid dynamical constraints on the ascent of bubbles in basalt.

References:
[1] De Campos, C., D. Perugini, W. Ertel-Ingrisch, D. Dingwell, and G. Poli (2011), Enhancement of magma mixing efficiency by chaotic dynamics: an experimental study, Contrib. Mineral. Petrol. , 161(6), 863-881.
[2] Thomas, N., S. Tait, and T. Koyaguchi (1993), Mixing of stratified liquids by the motion of gas bubbles: application to magma mixing, Earth Planet. Sci. Lett. , 115(1-4), 161-175.

IODP

Temperature and redox conditions in the conductive layer overlying a moving axial magma chamber: Constraints from granoblastic dikes at the IODP Site 1256

C. ZHANG, J. KOEPKE

Institut für Mineralogie, Leibniz Universität Hannover, Callinstr. 3, 30167 Hannover, Germany

Direct sampling of a whole column of upper oceanic crust down to fossilized magma chambers penetrating a mid-ocean ridge has been accomplished by the drilling program at the Integrated Ocean Drilling Program (IODP) Site 1256 (Leg 206, Expeditions 309, 312 and 335), located on the 15-Ma old superfast spreading crust at the East Pacific Rise (Wilson et al. 2006). As recovered from the drilled cores, two screens of plutonic gabbros were intruded into sheeted dikes. Ajdacent to the gabbroic screens, the sheeted dikes recrystallized to a granoblastic texture, and a dry high-temperature assemblage mainly consists of microcrystalline granular plagioclase, clinopyroxene, orthopyroxene and Fe-Ti oxides with minor sulfides, which indicates contact metamorphism induced by an axial magma chamber (Koepke et al. 2008). Fluid movements and related alteration/metamorphism, which can be traced by different types of amphibole-rich or sulfide-rich veins within granoblastic dikes, might have occurred in the intervals between high-temperature metamorphic events, i.e. between the upward and downward movements of the axial magma chamber. The recrystallized sheet dikes servered as a conductive boundary layer seperating the overlying hydrothermal system and the underlying aximal magma chamber (France et al. 2009), and thus can privide us insights into the mechanism of ocean crust creation from magmas at fast spreading mid-ocean ridges.

We have investigated some recrystallized sheeted dikes (i.e. granoblastic dikes) and associated plutonic rocks (i.e. crystallized aximal magma chamber and evolved magmatic veins) with mineralogical and geochemical approaches. Here we report the temperature and redox conditions constrained by applying the titanomagnetite-ilmenite thermo-oxybarometer (QUILF, Andersen et al. 1993) to the observed titanomagnetite-ilmenite pairs, and by using winTWQ (Berman 2007) to model the equilibrium conditions of coesting Fe-Ti oxides and sulfides.

Fe-Ti oxides

As illustrated in Fig 1, the recrystallizaiton temperature recorded by Fe-Ti oxides is ranging within 600-720 °C, and the estimated oxygen fugacities are mostly within NNO~NNO+1.5 buffers. These estimates cover the T-fO_2 condition derived from the sample directly above the

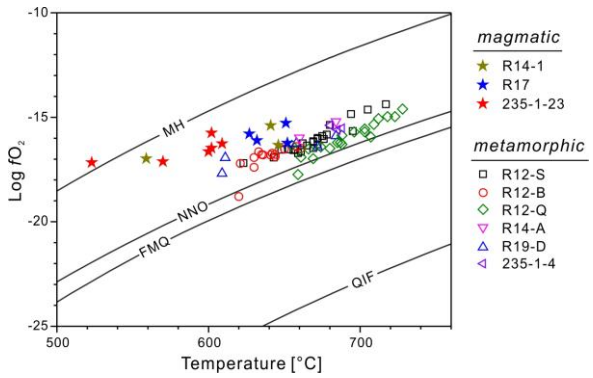

Fig 1. Estimated logfO_2-temperature conditions (at 500 bar) based on titanomagnetite-ilmenite pairs for granoblastic dikes (denotes as "metamorphic") and associated plutonic rocks (denoted as "magmatic").

contact to the gabbro (Koepke et al. 2008), but also indicate strong variations in temperature and redox conditions prevailing in the small scale. Differently, the magmatic rocks associated with the granoblasitc dikes show lower Fe-Ti oxides equilibrium temperatures below ~640 °C and higher oxygen fugacities within NNO+1.5~NNO+4 buffers. Furthermore, decreasing temperature tends to correspond to a more oxidized condition for the plutonic rocks, showing a variation trend not parallel to normal buffers, which might be related to increasing water activity with ongoing crystallization.

Since requilibrium of Fe-Ti oxides at low temperatures is highly promoted by slow cooling but suppressed by fast cooling, the large difference between two-pyroxene equilibrium tempeature (ca. 900-1000 °C) and Fe-Ti oxides equilibrium temperature indicate that the cooling process from peak contact metamorphism of granoblastic dikes cannot be very fast. As a result, a large magma chamber rather than a small melt lens underneath the sheeted dikes should be heat source of high-T metamorphism, consistent with the model proposed by Koepke et al. (2011).

Sulfides

Within an anhydrous vein, which is defined by linear distribution of secondary granular orthopyroxene and plagioclase, Fe-Ti oxides and sulfides are observed to be coexisting (Fig. 2a). The sulfides include pyrite, pyrrhotite and chalcopyrite. The distribution of pyrrhotite is much wider than pyrite, and overgrowth and replacement of pyrite by pyrrhotite can be observed, which indicate an incomplete transform from pyrite and to porrhotite. In addition, the distribution of pyrrhotite sometimes shows a characteristic feature indicative of growth during a sinistral shear movement. Except for large magnetite grains, tiny magnetite grains are usually distributed along the boundaries or fissures of the large ilmenite grains, which indicate that magnetite formed later than ilmenite. The relationship between ilmenite and magnetite observed in this case is distinctive from normal exsolution of ilmenite from ulvöspinel-rich magnetite which corresponds to reequilibrium at lower temperatures.

Thermodynamic modeling results show that the former low-temperature assemblage of pyrite+ilmenite corresponds to a redox condition near NNO buffer, while the later pyrrhotite+magnetite assemblage corresponds a temperature of above 700 °C and log$fO2$ of ca. -16 (NNO+2). Such a change in redox conditon reveals the prograde contact metamorphism of an anhydrous lithology induced by upmoving of the underlying axial magma chamber.

References:

Andersen, D., Lindsley, D., Davidson, P., 1993. QUILF: A pascal program to assess equilibria among Fe-Mg-Mn-Ti oxides, pyroxenes, olivine, and quartz. Computers & Geosciences 19, 1333-1350.

Berman, R.G., 2007. winTWQ (version 2.3): a software package for performing internally-consistent thermobarometric calculations. Geological Survey of Canada, Open File 5462, (ed. 2.32) 2007, 41 pages.

France, L., Ildefonse, B., Koepke, J., 2009. Interactions between magma and hydrothermal system in Oman ophiolite and in IODP Hole 1256D: Fossilization of a dynamic melt lens at fast spreading ridges. Geochemistry Geophysics Geosystems 10, Q10O19.

Koepke, J., Christie, D.M., Dziony, W., Holtz, F., Lattard, D., Maclennan, J., Park, S., Scheibner, B., Yamasaki, T., Yamazaki, S., 2008. Petrography of the dike-gabbro transition at IODP Site 1256 (equatorial Pacific): The evolution of the granoblastic dikes. Geochemistry Geophysics Geosystems 9, Q07O09.

Koepke, J., France, L., Müller, T., Faure, F., Goetze, N., Dziony, W., Ildefonse, B., 2011. Gabbros from IODP Site 1256, equatorial Pacific: Insight into axial magma chamber processes at fast spreading ocean ridges. Geochemistry Geophysics Geosystems 12, Q09014.

Wilson, D.S., Teagle, D.A.H., Alt, J.C. et al., 2006. Drilling to Gabbro in Intact Ocean Crust. Science 312, 1016-1020.

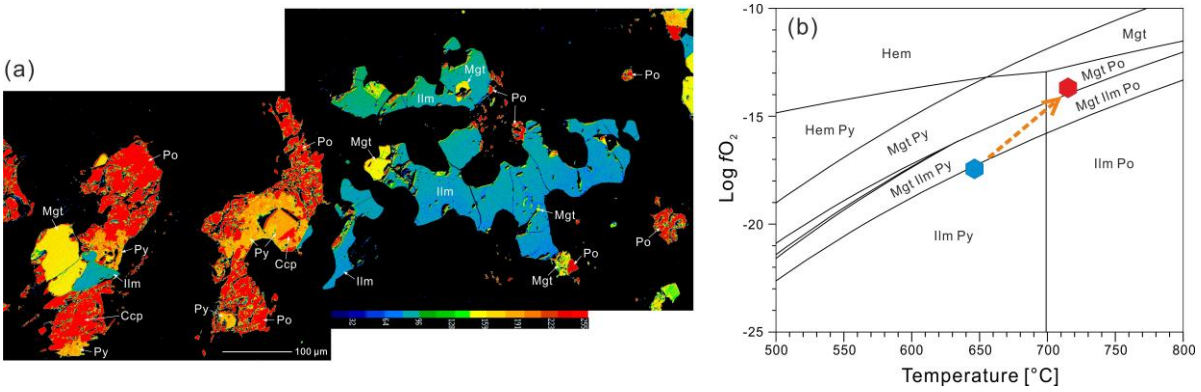

Fig 2. (a) BSE images showing the texture of coexisting Fe-Ti oxides and sulfides. (b) Modeled logfO_2-temperature conditions (at 500 bar). It is inferred that the incomplete-replacement texture and modeling record a temperature increase from below 700 °C to above 700 °C with a more oxidizing condition.

ICDP

Stable oxygen and carbon isotope records of aquatic moss cellulose from Laguna Potrok Aike in southern Patagonia

J. ZHU[1], A. LÜCKE[1], H. WISSEL[1], C. MAYR[2,3], C. OHLENDORF[4], B. ZOLITSCHKA[4] AND THE PASADO SCIENCE TEAM[5]

[1] Institute of Bio- and Geosciences, IBG-3: Agrosphere, Research Center Jülich, D-52428 Jülich, Germany,
[2] Institute of Geography, University of Erlangen-Nürnberg, D-91054 Erlangen, Germany,
[3] GeoBio-Center and Dept. of Earth and Environmental Sciences, University of Munich, D-80333 Munich, Germany,
[4] GEOPOLAR, Institute of Geography, University of Bremen, D-28359 Bremen, Germany,
[5] PASADO science team as listed at http://www.icdp-online.org/front_content.php?idcat=1494

Carbon and oxygen isotope analyses of lake sediment cellulose have shown a great potential to obtain paleohydrologic and paleoclimatic information (e.g. Wolfe et al., 2001 and 2007). An important assumption in the corresponding interpretation is the aquatic origin of the cellulose fraction analyzed. The culture experiment of aquatic moss cellulose (Sauer et al., 2001) and the previous field study in South Patagonia (Mayr et al., in review) have demonstrated that a strong linear correlation exists between the $\delta^{18}O$ of the submerged aquatic moss cellulose and the $\delta^{18}O$ of the respective host waters, where the mosses grow. Here we report the first results of the stable oxygen ($\delta^{18}O$) and carbon isotope ($\delta^{13}C$) records of the submerged aquatic moss from Laguna Potrok Aike (PTA), a southern Patagonian maar lake, in the framework of the ICDP-Project PASADO.

We analyzed around 400 samples containing available subfossil aquatic moss remains in order to measure the δ18O and δ13C values of aquatic moss bulk organic matter and extracted cellulose. The samples are from the sediment sections of the core (5022-2CP) within the composite depth from 30 to 10 m, covering the period between ca. 26,100 – 8400 cal. years BP, which includes the Last Glacial Maximum (LGM) and the last glacial-interglacial transition (Kliem et al., 2012).

Preliminary results of both moss organic matter and moss cellulose have shown that the samples from late Glacial and early Holocene have generally higher δ18O values and lower $\delta^{13}C$ values than the samples from the LGM. Our record displays a minimum shift of 1.5‰ of lake water $\delta^{18}O$ values inferred from moss $\delta^{18}O$ data during the last Glacial-Interglacial transition period in PTA. The strong correlation between the isotopic values ($\delta^{18}O$ and $\delta^{13}C$) of moss cellulose and of moss organic matter, which requests less material for the isotopic analyse, allows us to establish a high resolution aquatic moss isotopic record and to achieve a better understanding of terrestrial Glacial and Lateglacial climatic change in the southern hemisphere higher latitudes. The ongoing work extends the $\delta^{18}O$ and $\delta^{13}C$ moss records of the lake sediments from Laguna Potrok Aike back to 50,000 cal. years BP covering the first two warming events (A1 and A2) in Antarctica.

References:
Kliem, P., D. Enters, A. Hahn, C. Ohlendorf, A. Lisé-Pronovost, G. St-Onge, S. Wastegård, B. Zolitschka and the PASADO science team, 2012. Lithology, radiocarbon chronology and sedimentological interpretation of the lacustrine record from Laguna Potrok Aike, southern Patagonia. Quaternary Science Reviews, in press (available online, 10.1016/j.quascirev.2012.07.019).
Mayr, C., Lücke, A., Wagner, S., Wissel, H., Ohlendorf, C., Haberzettl, T., Oehlerich, M., Schäbitz, F., Wille, M., Zhu, J., Zolitschka, B., in review. Intensified Southern Hemisphere Westerlies as a Trigger for the last Deglaciation. Geology.
Sauer, P.E., Miller, G.H. & Overpeck, J.T. (2001): Oxygen isotope ratios of organic matter in arctic lakes as a paleoclimate proxy: field and laboratory investigations. – Journal of Paleolimnology, 25: 43-64.
Wolfe, B.B., Edwards, T.W.D., Elgood, R.J. & Beuning, K.R.M. (2001): Carbon and oxygen isotope analysis of lake sediment cellulose: methods and applications. In: Last, W. & Smol, J. (Ed.): Tracking environmental change using lake sediments, vol.2. Kluwer Academic Publications, 373-400.
Wolfe, B.B., Falcone, M.D., Clogg-Wright, K.P., Mongeon, C.L., Yi, Y., Brock, B.E., Amour, N.A.St., Mark, W.A. & Edwards, T.W.D. (2007): Progress in isotope paleohydrology using lake sediment cellulose. – Journal of Paleolimnology, 37: 221-231.

IODP

Mid-Oligocene high-resolution benthic foraminiferal productivity records from the Central Eastern Pacific Ocean (Site U1334, IODP Expedition 320)

J. ZIRKEL[1,2], J.O. HERRLE[1,2], H. PÄLIKE[3], C. KARAS[1,2], D. LIEBRAND[4]

[1] Goethe-University Frankfurt, Institute of Geosciences, D-60438 Frankfurt, Germany
[2] Biodiversity and Climate Research Centre (BIK-F), D-60325 Frankfurt, Germany
[3] MARUM/Center for Marine Environmental Sciences, University of Bremen, D-28359, Bremen
[4] School of Ocean and Earth Sciences, University of Southampton, SO14 3ZH, United Kingdom

The Oligocene is a critical epoch of the Cenozoic as it marks the onset of major Antarctic ice sheets and hence the first step into a “icehouse”world, which continues to the present day. To understand the evolution of the Antarctic ice sheet, it is fundamental to assess and quantify changes in the ocean circulation pattern and the intensity of Pacific equatorial upwelling (PEU) since the initiation of southern hemisphere ice caps during the Eocene-Oligocene transition.

It is well known that combined variations in the eccentricity, obliquity and precession of Earth´s orbit (Milankovitch cycles) influence long-term climate fluctuations, notably the build up and decay of ice volume. To unravel the importance of the orbital forcing on ice volume changes and to estimate its impact on paleoproductivity in the Central Eastern Pacific Ocean, we focused on the Oi-2b event about 26.8 Ma ago, being the most important glacial episode in the mid-Oligocene (Pälike et al., 2006).

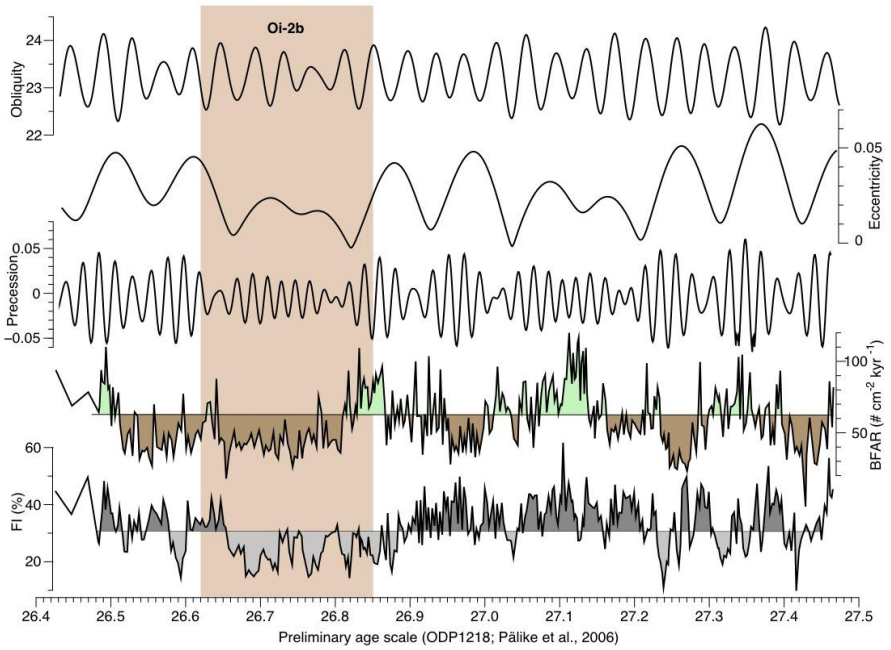

Fig. 1: Preliminary benthic foraminifera accumulation rates (BFAR) and planktic foraminifera fragmentation index (FI) as an indicator for dissolution of the Oi-2b maximum glaciation event of Site U1334 of 26.4 - 27.5 Ma. Higher BFAR values indicate increasing organic matter flux to the sea floor and thus higher surface water productivity. Values <60 % of the FI are interpreted as an indicator for good preservation of the carbonate fraction (see detailed discussion in the text). Filters are shown for the precession, eccentricity, and obliquity cycles calculated from BFAR values using the time series analyzing tool AnalySeries 2.0.4.2. The Oi-2b glacial event falls within a low-amplitude of precession, obliquity and minimum eccentricity. BFAR indicating a higher variability of productivity as previously suggested for the Oi-2b interval (Wade & Pälike, 2004). The FI indicates a slightly better preservation of the carbonate fraction during the Oi-2b interval. The brown interval indicates the duration of the Oi-2b maximum glaciation interval following (Wade & Pälike, 2004).

We calculated benthic foraminifer accumulation rates (BFAR) (Herguera & Berger, 1991) from the >150 µm size fraction to reconstruct organic matter flux to the sea floor and hence surface water productivity. BFAR were taken as a product of the number of benthic foraminifera per gram (NBF/g), the dry bulk density (DBD) and linear sedimentation rate (LSR) and they are reported as number of specimens/cm^2/kyr. Furthermore, to assess and differentiate between changes in productivity and dissolution, a planktic foraminifera-based fragmentation index (FI) was calculated by determining the ratio of whole planktic foraminiferal tests versus planktic foraminiferal test fragments.

BFAR values range between 19.5 and 118 NBF/cm^2/kyr (average: 63 NBF/cm^2/kyr). Increasing BFAR can be observed at about 26.43-26.51, 26.81-26.87, 27.10-27.16 and 27.31-27.39 Ma, indicating phases of higher supply of organic matter through the sea floor and thus enhanced surface water productivity (Fig.1). Following the assumption of Wade & Pälike (2004) that the Oi-2b glacial event represents the interval between 26.62 to 26.85 Ma, our BFARs indicate variable but generally lower productivity conditions during the glacial event compared to pre-Oi-2b conditions. However, the transition into the Oi-2b event is characterized by higher productivity accompanied by decreasing FI values between 26.81 to 26.87 Ma, which would support the assumption of increased productivity for the onset of Oi-2b based on $\Delta\delta^{13}C$ variations of planktic and benthic foraminifera from ODP Site 1218 (Wade & Pälike, 2004). In addition, both BFAR and FI records indicate that fluctuations of productivity changes as well as the preservation state are highly variable and do not change in concert during the mid-Oligocene.

Samples are characterized by a good preservation and only minimal signs of dissolution are observed based on scanning electron microscope (SEM) studies. The good preservation of the carbonate fraction is also documented in our FI record which varies between 9 % and 66 % (average: 31 %) with constant lower FI percentages during Oi-2b indicating less fragmented planktic foraminifera specimens and therefore a better preservation of the sample material. This assumption is also supported by the relatively high $CaCO_3$ content of >80 wt.% within the succession studied. Additionally, the low correlation coefficient between FI and BFAR (R^2 = 0.001) further support the assumption that our BFAR record is mostly unaffected by dissolution. Therefore, we suppose that fluctuations of the BFAR mainly reflect changes of organic matter flux and thus surface water productivity.

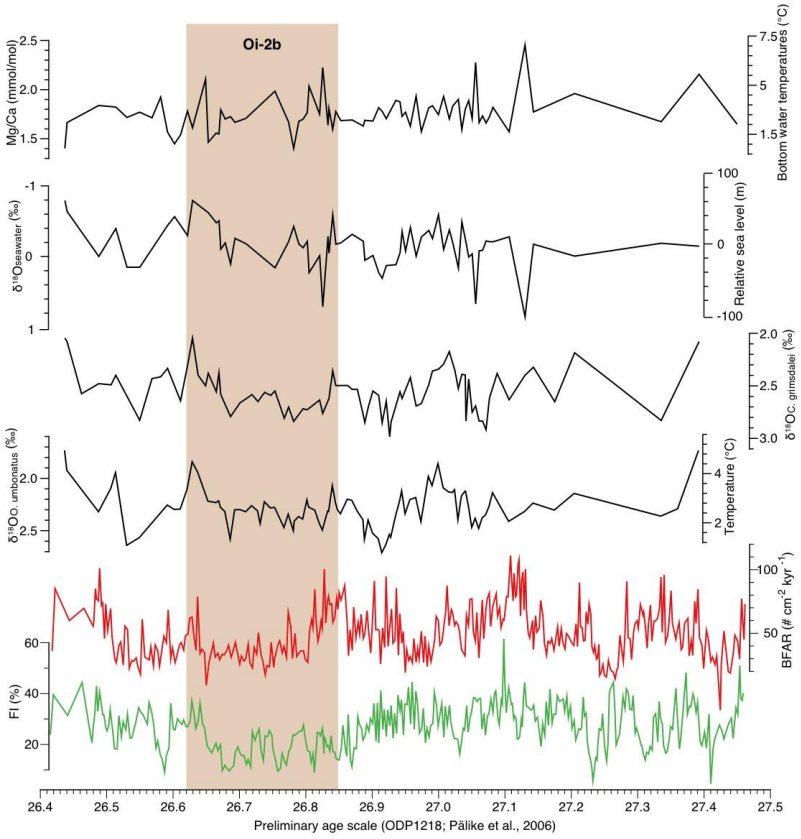

Fig. 2: Preliminary Mg/Ca paleotemperatures, $\delta^{18}O_{seawater}$ estimates and $\delta^{18}O$ records of *O. umbonatus* and *C. grimsdalei* of Site U1334 plotted against BFAR and FI between 26.4 – 27.5 Ma. Estimated variation in $\delta^{18}O_{seawater}$ composition, is calculated by substituting Mg-temperatures and benthic $\delta^{18}O$ of *O. umbonatus* data into $\delta^{18}O$ paleotemperature equation. The brown interval indicates the duration of the Oi-2b maximum glaciation interval following (Wade & Pälike, 2004).

So far, no astronomical tuned age model exists for Site U1334. However, to establish a preliminary age model for our studied interval of Site U1334, we used ODP Site 1218 as a reference site because this site is hitherto the most complete sedimentary succession for the Oligocene and provides an astronomical tuned oxygen and carbon isotope record (Pälike et al., 2006). As a first attempt, we used our preliminary age model to calculate spectral analyses of the BFAR record of Site U1334 to determine the presence of the main orbital parameters such as eccentricity, obliquity and precession (Fig.1). Cyclic variations are discernible during the whole record. Frequencies are most likely related to variations on eccentricity and precession forcing for the BFAR record. Surprisingly, high amplitude cyclic variations are recorded in the BFAR, which show a trend to precessional cycles, indicating short-term fluctuations of surface water productivity and thus a highly dynamic equatorial upwelling system during the mid-Oligocene. However, we have to extend our data set and conduct a more precise age model before we can interpret our data in a more conceptual model.

Enrichments in Oligocene benthic foraminiferal oxygen isotope records have been interpreted as significant increases in Antarctic ice volume and support the oscillation of ice volume and sea level throughout the Oligocene (e.g., Pekar & Miller, 1996; Miller et al., 2008). Our preliminary benthic foraminifera oxygen isotope measurements range between 1.65 ‰ and 2.63 ‰ (*O. umbonatus*) and 2.08 ‰ to 3.02 ‰ (*C. grimsdalei*) respectively (Fig. 2). These values are similar to previous benthic foraminiferal oxygen isotope measurements from the Central Pacific (Wade & Pälike, 2004). Heavier $\delta^{18}O$ values can be recognized during the Oi-2b interval with maximum peaks at about 26.79, 26.92 and 27.06 Ma. In order to assess preliminary sea level changes we combined our oxygen isotope record with Mg/Ca temperatures to calculate $\delta^{18}O_{seawater}$. The maximum change of $\delta^{18}O_{seawater}$ is about 1.3 ‰ during the Oi-2b glaciation event. If applying the Pleistocene sea-level/ $\delta^{18}O$ calibration of 0.11 ‰/10 m (Fairbanks & Matthews, 1978) the observed $\delta^{18}O_{seawater}$ excursion would represent an increase in sea level change of about 118 m. Similar estimates of about 100 m were calculated from simultaneous changes between benthic and planktic foraminifera oxygen isotope values as an indicator of eustatic sea level fluctuations from Site 1218 (Wade & Pälike, 2004). However, given an error of 0.2 mmol/mol for Mg/Ca ratios (±1.3°C) in bottom water estimation and an uncertainty of ~0.1 ‰ in $\delta^{18}O_{seawater}$ the maximum uncertainty of our sea level reconstruction is ±30 m.

By comparing our preliminary estimates with sea level changes derived from backstripping of the Oligocene from the New Jersey and Gippsland shelf of Antarctica, eustatic estimates must be multiplied by 1.48 to obtain ASL changes for comparison with ice volume variations and global oxygen isotope records (Pekar et al., 2002). Mean ASL estimates would correspond to a sea level change of about 45 m to 76 m following Miller et al. (2011) for the Oi-2b glaciation event estimated from the New Jersey margin. Similar lower sea level estimates have been recently calculated from the Gippsland shelf (Gallagher et

al., 2013). Thus, our results of 118 m (±30 m) might overestimate the sea level change compared with the backstripping results. However, the greatest uncertainty of the backstripping methods is that the onshore sites fail to capture the lowstands, and thus reflect minimal estimates of eustatic falls (e.g., Miller et al., 2008; Gallagher et al., 2013). Therefore, short-term glaciation events as already shown in our record of maximal sea level change have the greatest potential to either be not recorded or overlooked by backstripping methods. Thus, our micropaleontological and geochemical approach has the advantage to fully record glaciation cycles and provide maximal estimates in sea level change.

References:

Fairbanks, R.G., Matthews, R.K., 1978. The marine oxygen isotope record in Pleistocene coral, Barbados, West Indies. Quat. Res. 10, 181-196.

Gallagher, S.J.,Villa, G., Drysdale, R.N., Wade, B.S., Scher, H., Li, Q., Wallace, M.W., Holdgate, G.R., 2013. A near-field sea level record of East Antarctic Ice Sheet instability from 32 to 27 Ma. Paleoceanography 28, 1-13.

Herguera, J. C. and Berger, W. H., 1991. Paleoproductivity from benthic foraminifera abundance: Glacial to postglacial change in the west-equatorial Pacific, Geology 19;1173-1176.

Miller, K.G., Wright, J.D., Katz, M.E., Browning, J.V., Cramer, B.S., Wade, B.S., Mizintseva, S.F., 2008. A View of Antarctic Ice sheet Evolution from Sea-Level and Deep-Sea Isotope Changes During the Late Cretaceous-Cenozoic. In: Cooper, A.K., et al. eds. Antarctica: A Keystone in a Changing World. Proc. 10th Int. Symp. Antarctic Earth Sci. Washington, DC: Nat. Acad. Press, 55-70.

Miller, K.G., Mountain, G.S., Wright, J.D., Browning, J.V., 2011. A 180-million year record of sea level and ice volume variations from continental margin and deep-sea isotopic records. Oceanography 24(2): 40-53, doi:10.5670/oceanog.2011.26.

Pälike, H., Norris, R.D., Herrle, J.O., Wilson, P.A, Coxall, H.K., Lear, C.H., Shackleton, N.J., Tripati, A.K., Bridget, S.W., 2006. The heartbeat of the Oligocene climate system. Science 314, 1894-1898.

Pekar, S., and K. G. Miller, 1996. New Jersey Oligocene ''Icehouse'' sequences (ODP Leg 150X) correlated with global $\delta^{18}O$ and Exxon eustatic records, Geology 24(6), 567 -570.

Pekar, S.F., Christie-Blick, N., Kominz, M.A., Miller, K.G., 2002. Calibration between eustatic estimates from backstripping and oxygen isotope records for the Oligocene. Geology 30, 903-906.

Wade, B.S., Pälike, H., 2004. Oligocene climate dynamics. Paleoceanography 19, PA4019. doi:10.1029/2004PA001042.

ICDP

Late Pleistocene and Holocene hydrological variability in Argentinean Patagonia links to the Southern Hemispheric Westerlies (ICDP-project PASADO)

BERND ZOLITSCHKA[1] , A. CATALINA GEBHARDT[2], ANNETTE HAHN[1], STEFAN HÖLZL[3,4], PIERRE KLIEM[1], CHRISTOPH MAYR[3,5], MARKUS OEHLERICH[3], CHRISTIAN OHLENDORF[1], AND THE PASADO SCIENCE TEAM[6]

[1] Institute of Geography (Geopolar), University of Bremen, Germany – zoli@uni-bremen.de
[2] Alfred Wegener Institute of Polar and Marine Research, Bremerhaven, Germany
[3] Department of Earth and Environmental Sciences, University of Munich, Germany
[4] Rieskrater-Museum Nördlingen, Germany
[5] Institute of Geography, University of Erlangen-Nürnberg, Germany
[6] PASADO Science Team as cited at: http://www.icdp-online.org/front_content.php?idcat=1494

Semiarid conditions are prevailing at the site of Laguna Potrok Aike (52°S, 70°W; 116 m asl; diameter: 3.5 km, water-depth: 100 m), a currently terminal maar lake in the southern Patagonian steppe of Argentina. Depositional processes are strongly controlled by the inflow-to-evaporation ratio, a direct function of climatic variables. In this climatic setting it is expected that the lake underwent distinct hydrological changes from open to terminal lake conditions at glacial/interglacial temporal scales. This variability could have ranged from a freshwater lake with outflow to a subsaline lake in which dissolved loads and chemical precipitates accumulated over time. Such distinct changes in turn are reflected in the chemical composition of lacustrine sediments. Additionally, terminal lakes are characterized by rapid water-depth and shoreline fluctuations accompanied by variations in lake area and water volume. Four seismic surveys (Anselmetti et al., 2009; Gebhardt et al., 2011) and a stratigraphic record based on 51 AMS ^{14}C dates (Kliem et al., 2013a) provide a database to compare the 106 m composite profile from the lake centre with piston cores from the littoral zone and outcrops in the catchment area. Based on event correlation using distinct volcanic ash layers with unique geochemical composition (Wåstegard et al., 2013) and additional infrared-stimulated luminescence (IRSL) dates on feldspars (Buylaert et al., in prep.), all sediment records are firmly linked (Kliem et al., 2013b). Moreover, this approach allows to match the sediment record with the water level during the past ca. 50 ka providing evidence for lake-level variations up to 200 m. Seismic reflection data even points to very low lake levels before ca. 55 ka (Gebhardt et al., 2012). During the Late Pleistocene, sediment-facies are characterized by a clastic depositional system (high inflow). During the Late Glacial (13.5-11.5 kcal BP) carbonates are precipitated biologically (*Phacotus*), whereas at the transition to the early Holocene (11.5-9.3 kcal BP) clastic sediments regain dominance. Since 9.3 kcal BP intense carbonate precipitation (up to 35% calcite) is recorded indicating an end lake. These conditions continue until today with only one distinct interruption for the neoglacial "Little Ice Age" (Haberzettl et al., 2007).

The related hydrological variability is most likely caused by (1) changes in runoff due to permafrost sealing of the ground during the Pleistocene (Kliem et al., 2013b), (2) variations in precipitation and wind-induced evaporation linked to changes in intensity and position of the Southern Hemispheric Westerlies (SHW; Mayr et al., 2007; Ohlendorf et al., 2013) and (3) the Glacial-to-Holocene temperature increase (Toggweiler, 2009). Based on multiproxy evidence a lake-level record for the last 51 ka was reconstructed (Fig. 1) which is interpreted as the result of the SHW being in a much more northerly position during the Last Glacial and their southward movement with the onset of deglaciation since ca. 17 kcal BP. At 9.3 ka cal. BP the SHW reached the latitude of the study area (52°S) and caused a pronounced negative water balance with a lake-level decrease of more than 50 m. Two millennia later, the SHW intensity started to diminished and lake level rose in a step-like manner to a subsequent maximum during the "Little Ice Age". Since the 20th century, a strengthening of the SHW increased the evaporative stress resulting in a more negative water balance (Ohlendorf et al., 2013).

A comparison of our data with other hydrological fluctuations at a regional scale for south-eastern Patagonia (Ariztegui et al., 2010; Cartwright et al., 2011) indicates that the core of the SHW shifted southward and re-established in southern Patagonia during the early

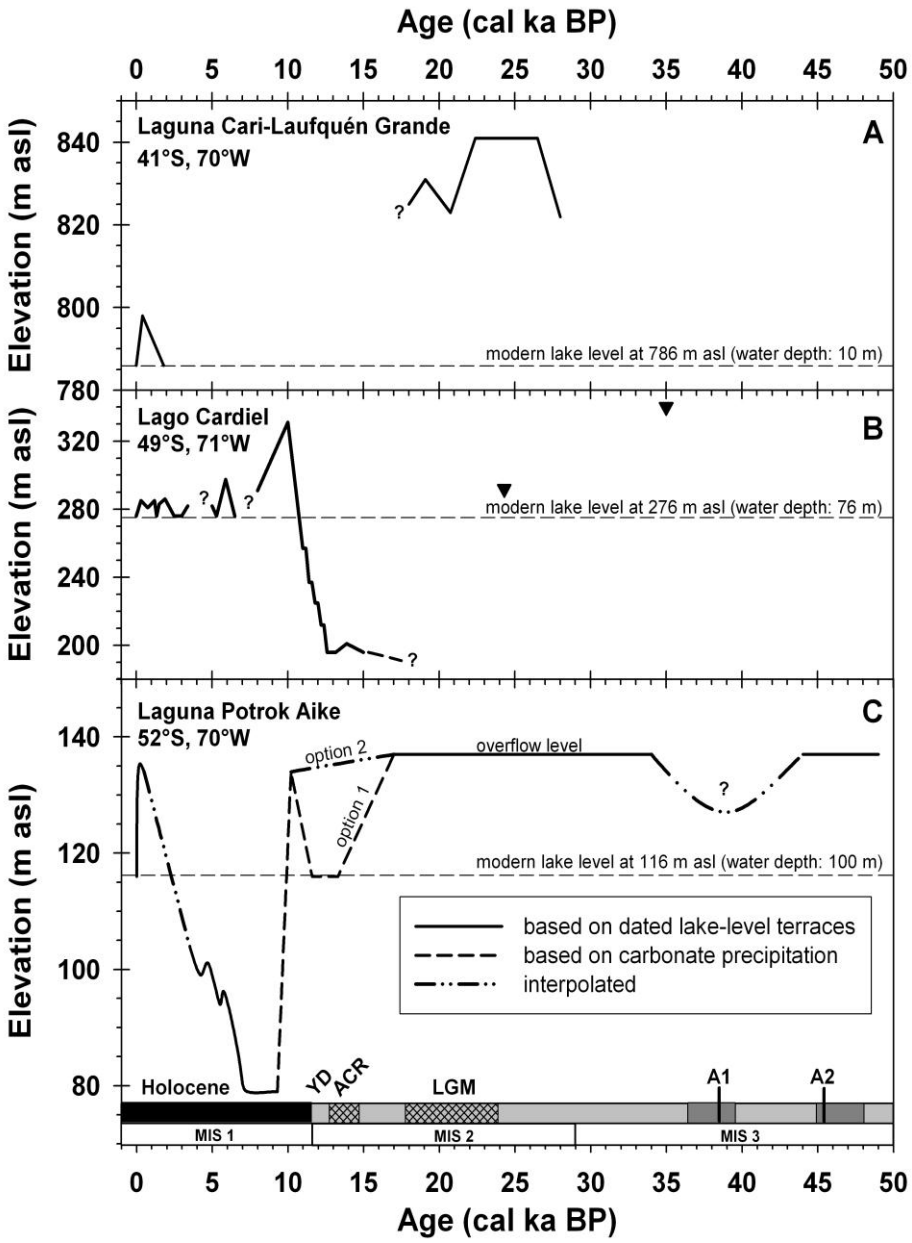

Fig. 1: Discontinuous lake-level histories from A) Laguna Cari-Laufquén (41°S; data from Cartwright et al., 2011) and B) Lago Cardiel (49°S; data from Ariztegui et al., 2010) with two last glacial lake level high stands (exposed transgressive units) indicated by black triangles (data from Stine & Stine, 1990) compared with the lake-level history of C) Laguna Potrok Aike (52°S; data from Anselmetti et al., 2009; Kliem et al., 2013b). For Laguna Potrok Aike two lake-level alternatives are shown for the time interval 17-10.5 ka cal. BP. Younger Dryas (YD), Antarctic Cold Reversal (ACR), Last Glacial Maximum (LGM) and peak warmth of Antarctic Warm Events (A1 and A2) are marked as well as marine isotope stages (MIS). Two periods with increased productivity as determined by Hahn et al. (2013) are coloured in dark grey (figure from Zolitschka et al., 2013).

Holocene. However, regional mid to late Holocene climate fluctuations in southern Patagonia appear to have occurred synchronously and thus seem to be related to intensity variations of the SHW (cf. Fletcher & Moreno, 2012). To improve our understanding of the past behaviour of the SHW, better chronologies and appropriate proxy parameters for high-resolution records of climate variability are indispensable. A first step into this direction is a new $^{87}Sr/^{86}Sr$ isotope record from lacustrine carbonates which is interpreted as varying input of allochthonous clastic material into the lake. These variations presumably are related to SHW intensity fluctuations and compared to the event-related and thus discontinous lake-level reconstruction.

Acknowledgements

This study was supported by the International Continental Scientific Drilling Program (ICDP) in the framework of the "Potrok Aike Maar Lake Sediment Archive Drilling Project" (PASADO, DFG grants MA 4235/4-1/2). Funding for drilling was provided by the ICDP, the German Science Foundation (DFG grants ZO-102/11-1,2), the Swiss National Funds (SNF), the Natural Sciences and Engineering Research Council of Canada

(NSERC), the Swedish Vetenskapsradet (VR) and the University of Bremen. For their invaluable help in field logistics we thank the staff of INTA Santa Cruz, the Moreteau family and the DOSECC drilling crew.

References

Anselmetti, F., Ariztegui, D., De Batist, M., Gebhardt, C., Haberzettl, T., Niessen, F., Ohlendorf, C., Zolitschka, B., 2009. Environmental history of southern Patagonia unraveled by the seismic stratigraphy of Laguna Potrok Aike. Sedimentology 56, 873–892. http://dx.doi.org/10.1111/j.1365-3091.2008.01002.x

Ariztegui, D., A. Gilli, Anselmetti, F.S., Goñi, R.A., Belardi, J.B., Espinosa, S., 2010. Lake-level changes in central Patagonia (Argentina): crossing environmental thresholds for Lateglacial and Holocene human occupation. Journal of Quaternary Science 25, 1092–1099.

Buylaert, J.P., Murray, A.S., Gebhardt C., Sohbati, R., Ohlendorf, C., Thiel, C., Zolitschka, B., in prep. Luminescence dating of the PASADO core 5022-1D from Laguna Potrok Aike (Argentina) using IRSL signals from feldspar. Quaternary Science Reviews.

Cartwright, A., Quade, J., Stine, S., Adams, K.D., Brocker, W., Cheng, H., 2011. Chronostratigraphy and lake-level changes of Laguna Cari-Laufquén, Río Negro, Argentina. Quaternary Research 76, 430-440.

Fletcher, M.-S., Moreno, P.I., 2012. Have the Southern Westerlies changed in a zonally symmetric manner over the last 14,000 years? A hemisphere-wide take on a controversial problem. Quaternary International 253, 32-46.

Gebhardt, A.C., M. De Batist, F. Niessen, F.S. Anselmetti, D. Ariztegui, C. Kopsch, C. Ohlendorf, B. Zolitschka, 2011. Origin and evolution of the Laguna Potrok Aike maar, Southern Patagonia. Journal of Volcanology and Geothermal Research 201, 357-363. http://dx.doi.org/10.1016/j.jvolgeores.2010.12.019

Gebhardt, A.C., C. Ohlendorf, F. Niessen, M. De Batist, F.S. Anselmetti, D. Ariztegui, B. Zolitschka, 2012. Seismic evidence of a highly dynamic lake development in Southeastern Patagonia during the Late Pleistocene. Sedimentology 59, 1087-1100. http://dx.doi.org/10.1111/j.1365-3091.2011.01296.x

Haberzettl, T., Corbella, H., M. Fey, S. Janssen, A. Lücke, C. Mayr, C. Ohlendorf, F. Schäbitz, G.-H. Schleser, E. Wessel, M. Wille, S. Wulf, B. Zolitschka, 2007. A continuous 16,000 year sediment record from Laguna Potrok Aike, southern Patagonia (Argentina): Sedimentology, chronology, geochemistry. The Holocene 17, 297-310.

Hahn, A., Kliem, P., Ohlendorf, C., Zolitschka, B., Rosén, P. and the PASADO science team, 2013. Climate induced changes in the content of carbonaceous and organic matter of sediments from Laguna Potrok Aike (Argentina) during the past 50 ka inferred from infrared spectroscopy. Quaternary Science Reviews, http://dx.doi.org/10.1016/j.quascirev.2012.09.015

Kliem, P., D. Enters, A. Hahn, C. Ohlendorf, A. Lisé-Pronovost, G. St-Onge, S. Wastegård, B. Zolitschka and the PASADO science team, 2013a. Lithology, radiocarbon dating and sedimentological interpretation of the 51 ka BP lacustrine record from Laguna Potrok Aike, southern Patagonia. Quaternary Science Reviews, http://dx.doi.org/10.1016/j.quascirev.2012.07.019

Kliem, P., Buylaert, J.P., Hahn, A., Mayr, C., Murray, A., Ohlendorf, C., Wastegård, S., Veres, D., Zolitschka, B. and the PASADO science team, 2013b. Magnitude, geomorphologic response and climate links of lake-level oscillations at Laguna Potrok Aike, Patagonian steppe (Argentina). Quaternary Science Reviews, http://dx.doi.org/10.1016/j.quascirev.2012.08.023

Mayr, C., M. Wille, T. Haberzettl, M. Fey, S. Janssen, A. Lücke, C. Ohlendorf, G. Oliva, F. Schäbitz, G.-H. Schleser, B. Zolitschka, 2007. Holocene variability of the Southern Hemisphere westerlies in Argentinean Patagonia (52°S). Quaternary Science Reviews 26, 579-584.

Ohlendorf, O., M. Fey, C. Gebhardt, T. Haberzettl, A. Lücke, C. Mayr, F. Schäbitz, M. Wille and B. Zolitschka, this issue. Mechanisms of lake-level change at Laguna Potrok Aike (Argentina) - Insights from hydrological balance calculations. Quaternary Science Reviews. http://dx.doi.org/10.1016/j.quascirev.2012.10.040

Stine, S., Stine, M., 1990. A record from Lake Cardiel of climate change in southern South America. Nature 345, 705-708.

Toggweiler, J.R. (2009). Shifting Westerlies. Science 323: 1434-1435.

Wastegård, S. Veres, D., Kliem, P., Ohlendorf, C., Zolitschka, B. and the PASADO science team, 2013. Towards a late Quaternary tephrochronological framework for the southernmost part of South America – the Laguna Potrok Aike tephra record. Quaternary Science Reviews, http://dx.doi.org/10.1016/j.quascirev.2012.10.019

Zolitschka, B., F. Anselmetti, D. Ariztegui, H. Corbella, P. Francus, A. Lücke, N. Maidana, C. Ohlendorf, F. Schäbitz, S. Wastegard, 2013. Environment and climate of the last 51,000 years – new insights from the Potrok Aike maar lake sediment archive drilling project (PASADO). http://dx.doi.org/10.1016/j.quascirev.2012.11.024